Universitat Autònoma de Barcelona

Photofunctional processes and materials based on molecular switches

Marc Villabona Pedemonte

Universitat Autònoma de Barcelona

Photofunctional processes and materials based on molecular switches

PhD Thesis

PhD in Chemistry

Departament de Química

2021

Marc Villabona Pedemonte

Directors: Dr. Jordi Hernando Campos
Dr. Gonzalo Guirado López

Index

Abbreviations

AcCl	Acetyl chloride
ACN	Acetonitrile
AcOH	Acetic acid
APCI	Atmospheric-pressure chemical ionization
ATR	Attenuated total reflection
B_2pin_2	bis(pinacolato)diboron
COSY	Correlation spectroscopy
CV	Cyclic voltamperometry
Cy	Cyclohexyl
DA	Diels Alder
DAE	Diarylethene
DBU	1,8-diazabicyclo(5.4.0) undec-7-ene
DCC	Dicyclocarboxyl carbodiimide
DIC	Diisopropyl carbodiimide
DMAP	4-(dimethylamino)pyridine
DMF	Dimethyl formamide
DMSO	Dimethyl sulfoxide
DTE	Dithienylethene
DTT	Dithiothreitol
EDG	Electrodonating group
EtOAc	Ethyl acetate
EtOH	Ethanol
ESI	Electrospray ionization
EWG	Electrowithdrawing group
FET	Field-effect transistors
HPLC	High pressure liquid chromatography
HSQC	Heteronuclear single quantum coherence spectroscopy
ICT	Internal charge transfer
iPr	*iso*-propyl
ITO	Indium tin oxide
KOAc	Potassium acetate
KSAc	Potassium thioacetate
LC	Liquid chromatography
LDA	Lithium diisopropyl amide
LED	Light emitting diode
LG	Leaving group
MeI	Methyl iodide
MeOH	Methanol
MS	Mass spectrometry
***n*BuLi**	n-butyllithium
NCS	*N*-chlorosuccinimide
NIR	Near infrared
NMP	1-methyl-2-pyrolidone
NMR	Nuclear magnetic resonance
***o*-DA**	*oxo*-Diels Alder
***o*-MBA**	*orto*-methylbenzaldehyde
***o*-QDM**	*orto*-quinodimethane
PDI	Perylene diimide

PET	Photoinduced-electron transfer
PMMA	Poly(methylmethacrylate)
PS	Polystyrene
PSS	Photostationary state
PVA	Polyvinyl alcohol
PyBOP	Benzotriazol-1-yloxytripyrrolidinophosphonium hexafluorophosphate
RET	Resonance energy transfer
SCE	Saturated calomel electrode
SN_{Ar}	Nucleophilic aromatic substitution
STED	Stimulated emission depletion
SZMC	Spirocyclic zwitterionic Meisenheimer compounds
TBAF	Tetrabutyl ammonium fluoride
TBAOH	Tetrabutylammonium hydroxide
TBDPS	*tert*-butyl diphenyl silyl
TBS	*tert*-butyl dimethyl silyl
***t*BuLi**	*tert*-butyl lithium
***t*BuOH**	*tert*-butanol
TEACN	Tetraethylammonium cyanide
TEAF	Tetraethylammonium fluoride
TFA	Trifluoroacetic acid
TFAA	Trifluoroacetic anhydride
THF	Tetrahydrofuran
TsOH	*p*-toluenesulfonic acid
UV	Ultraviolet
vis	Visible

Chapter I

Introduction

Light plays a crucial role in our lives. On one hand, it is one of the main sources of energy for living organisms, as beautifully illustrated by photosynthesis;[1] on the other hand, it is essential to the way humans interact with the environment, mainly through vision.[2] Importantly, none of these processes would be possible without molecules and materials that could interact with light, as it is the case of chlorophyll pigments in the photosynthetic complexes in plants and bacteria[3] or the rods and cones in our eyes.[2] Inspired by these examples found in Nature, the development of artificial photoactive systems for advanced light-based functions has become a very active area of research during the last decades. In fact, many of them are already used in our daily life, such as solar cells for the conversion of sunlight into energy,[4,5] photochromic lenses that adapt their transmittance to solar irradiation conditions,[6] photocurable resins for dental composites,[7] or pregnancy tests based on the visual inspection of color changes.[8]

In this thesis we aim to prepare new photofunctional processes and materials for application in a variety of areas, ranging from sensing to polymer network cross-linking. Despite their different potential uses, all of them share one feature in common: they are based on *molecular switches*, which allows the response of the systems developed to be controllable with one or more external stimuli.

I.1. MOLECULAR SWITCHES

Developing molecular compounds that reversibly change their physicochemical properties as a response to their environment has risen enormous interest in the recent years. These systems are often called molecular switches and their functioning both involves: (a) the application of an external stimulus that triggers the transformation of the switch between two (or more) stable states in a reversible way (*writing*); and (b) the detection of the state in which the switch lies by analysis of a certain physicochemical property (*reading*) (Figure I-1).[9,10]

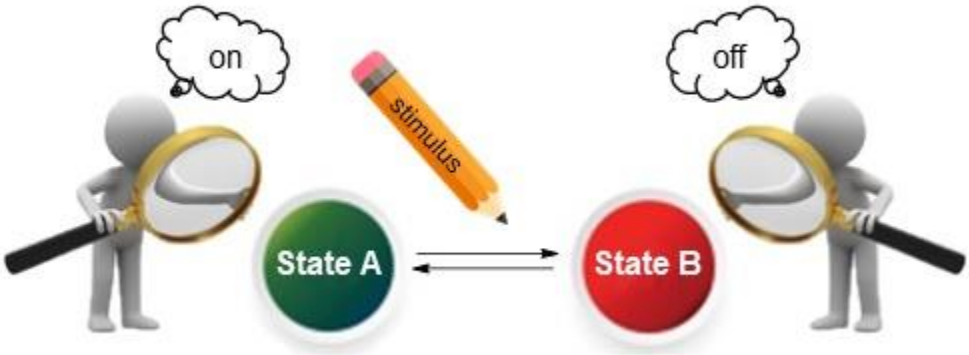

Figure I-1. Operation of a two-state molecular switch, whose states are often defined as “On” and “Off”. Reversible “On”-“Off” transformation is driven by an external stimulus (*writing*), while monitorization of the switch operation requires measuring the difference in properties between the two states (*reading*).

Because of the capacity of molecular switches to show a variety of changes in properties upon application of diverse stimuli, they have been proposed for a large number of applications in materials science,[11,12] chemistry,[13,14] physics[15] and biosciences.[16] A breakthrough in the recognition of the relevance of these systems occurred when the 2016 Nobel Prize in Chemistry was awarded to Jean-Pierre Sauvage, Sir J. Fraser Stoddart and Bernard L. Feringa for the preparation of molecular machines based on molecular switches,[17] which are capable of generating movement or mechanical forces when exposed to stimuli.[18] However, this is only one of the many types of responses that molecular switches can have; i.e., one of the many reading modes that they support. Changes in color,[19] reactivity,[13,14] fluorescence,[20] electronic properties[21] or even biological activity[22] are more examples of a longer list. Among them, chromic and fluorescent molecular switches that can be read via absorption and emission measurements are preferred in many occasions, as they are easy to monitor (even by naked eye), can be detected remotely with high sensitivity, and the color and/or emission variation that these systems experience can find application in a range of fields (e.g., (bio)sensing and (bio)imaging,[23] photoprotective coatings[6] and security inks).[12]

As for the writing modes of molecular switches, they are as well diverse. Thus, molecular switches have been described responding to thermal,[24] electronic,[25] optical,[9] magnetic,[26] chemical[27] or mechanical[28] stimuli, among others. However, none has gathered as much attention as light, which makes the preparation of photoresponsive molecules and materials one of the most common uses of molecular switches.[29] This is due to the several advantages that light provides as an external stimulus to trigger the operation of molecular systems: it is noninvasive and can be applied from afar with highly precise control over time (down to fs) and space (down to sub-μm).

Light is therefore often applied for the reading and writing processes of molecular switches, thus giving rise to a variety of photofunctional compounds and materials. This is also the case of this thesis, where both chromic, fluorescent and light-responsive molecular switches have been used.

I.1.1. Chromic and fluorescent molecular switches

Chromic and fluorescent molecular switches are defined as compounds capable of undergoing reversible transformations that induce a color or emission change, respectively. As a result, their operation can be monitored via absorption and emission measurements, i.e., with light, which as discussed above enables easy, remote, and noninvasive detection of the state of the switch with high sensitivity. The latter is especially true for fluorescent molecular switches, which can be ultimately detected on the single molecule level.[30]

Chromic molecular switches are much more abundant than fluorescent molecular switches, as most molecular switches experience a reversible variation of their absorption spectrum upon application of an external stimulus. These systems are generally classified on the basis of the class of stimulus that they react to.[31] Examples of such types are photochromic,[9,31–34] halochromic,[27,35–37] ionochromic,[27,31,38–40] solvatochromic,[31,32,41] electrochromic,[42,43] thermochromic[32,33,44,45] or mechanochromic[28,31,46,47] switches, which respond to light, pH, ions, solvent, redox potentials, temperature or mechanical forces, respectively (Figure I-2).

Although most chromic (and nonchromic) molecular switches are only sensitive to a single external stimulus, some of them are able to respond to more than one input signal. For instance, the chromic switch shown in Figure I-3 composed by the colorless spiropyran **SP1** and its colored zwitterionic **MC1** states presents multistimuli behavior, as it can modify its optical properties through two different mechanisms.[48] On the one hand, the equilibrium between these two isomers depends on solvent polarity. Thus, while the colorless **SP1** form is predominant in apolar solvents (e.g., hexane and petroleum ether), the zwitterionic **MC1** state becomes favored as polarity increases (e.g., in methanol and ethanol), therefore leading to colored solutions even in the dark. On the other hand, reversible **SP1**-**MC1** interconversion can also be promoted photochemically under ultraviolet (UV) and visible (vis) light irradiation, which allows obtaining fully colored and colorless solutions regardless of the solvent used.

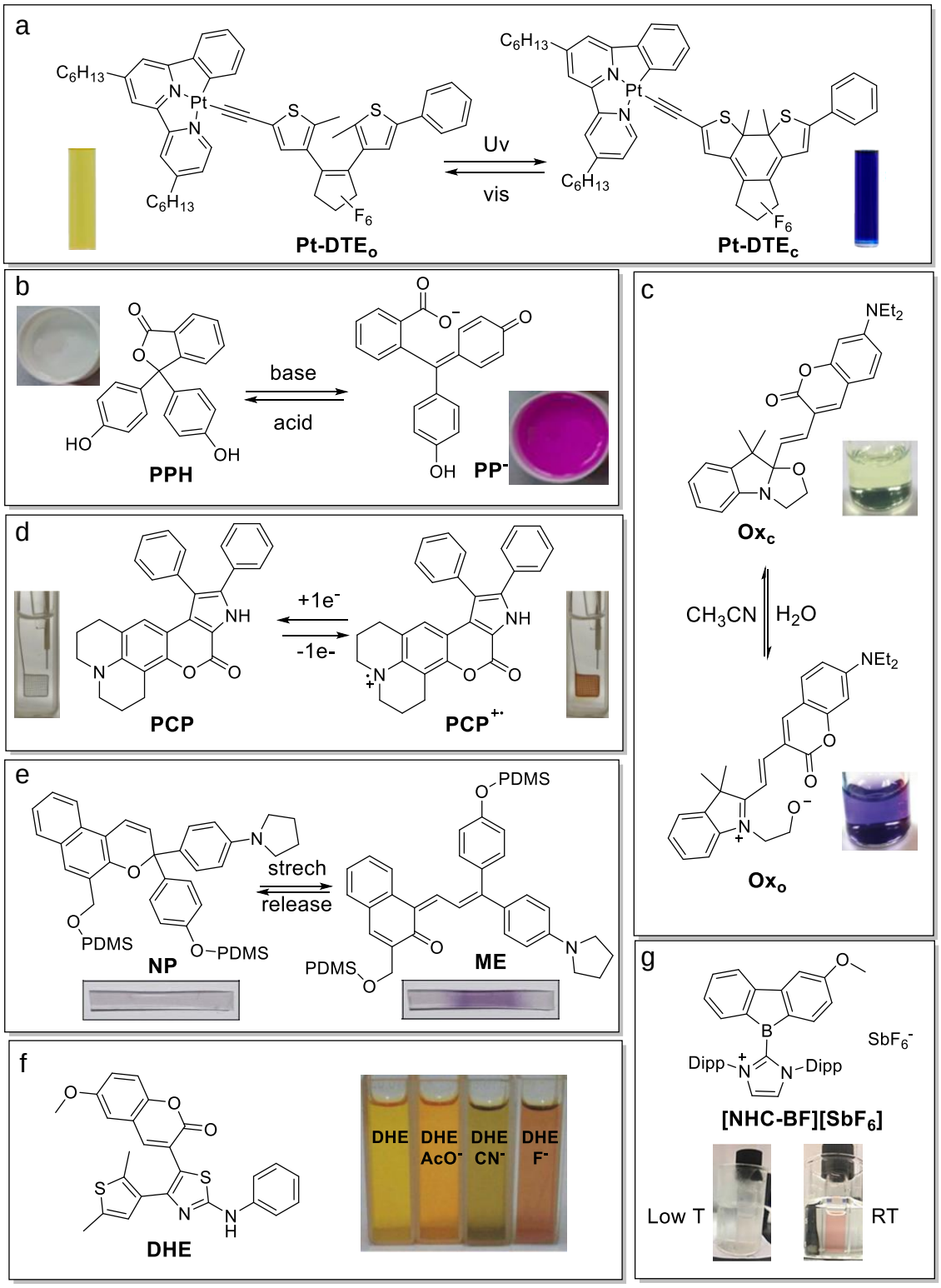

Figure I-2. Examples of chromic molecular switches responding to different stimuli: (a) photochromic dithienylethene is reversibly isomerized between the yellow **Pt-DTE$_o$** and blue **Pt-DTE$_c$** states upon UV and red light irradiation;[34] (b) halochromic phenolphthalein (**PP**) reversibly switches between the colorless **PPH** in neutral-acidic pH to the pink anionic form **PP$^-$** in basic pH;[37] (c) solvatochromic oxazine (**Ox**) that presents a solvent dependent tautomeric equilibrium between a colorless neutral **Ox$_c$** form, more favored in aprotic

solvents, and a purple zwitterionic **Ox_o** state, more stable in aqueous media; (d) electrochrome **PCP** is colorless but it can be reversibly oxidized to the red radical cation **$PCP^{+\cdot}$**;[43] (e) mechanochromic naphtopyran **NP** is colorless but when incorporated in poly(dimethylsilane) polymer films, its spirocyclic structure can be opened upon stretching to obtain the blue colored merocyanine **ME**;[47] (f) ionochrome dihetarylethene **DHP** color varies upon addition of different anions due to the H-bond interaction with the amine proton;[40] (g) thermochromic boron complex **[NHC-BF][PF_6]** is red in its monomeric form present at room temperature, but it dimerizes upon cooling to a colorless species by O-B coordination with the methoxy group.[45]

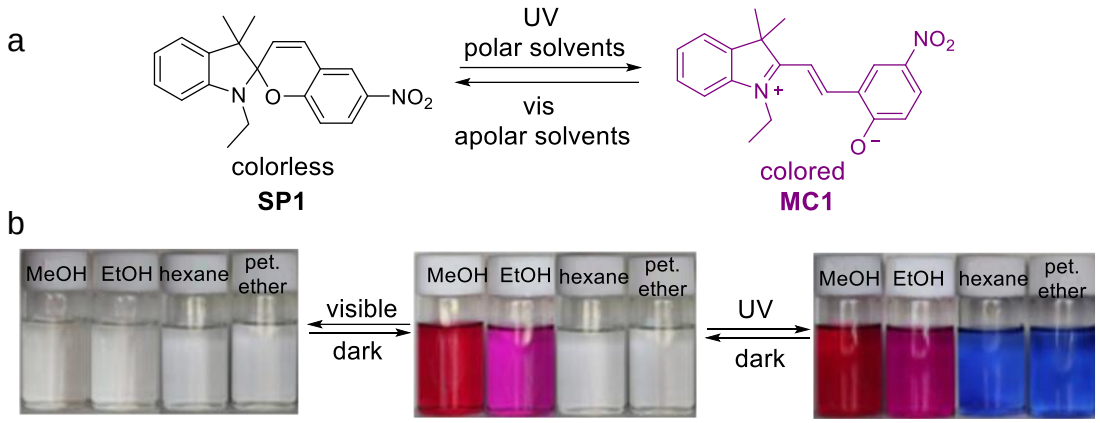

Figure I-3. (a) Scheme of the switching mechanisms between the **SP1** and **MC1** states of a nitrospiropyran derivative. (b) Photographs of solutions of **SP1**/**MC1** in methanol, ethanol, hexane and petroleum ether in the dark (center), after visible light irradiation (left), and after UV irradiation (right). Different colors are obtained for the **MC** solutions due to the effect of solvent polarity on the absorption spectrum of this isomer.[48]

Another advanced operating feature that some chromic (and nonchromic) molecular switches present is the capacity to interconvert between more than two states. As a consequence, the response of the so-called multistate molecular switches can be further tuned and exploited in applications requiring multiple readout signals. An example of this behavior is the electrochrome **Ec** designed by Fang and co-workers (Figure I-4).[49] This compound was synthesized by tethering an oxidation-active indolo[3,2-*b*]carbazole core to two redox-active benzo[*d*]thiazole and diphenylboron units. As a result, **Ec** could be interconverted between up to 5 different oxidation states by applying different potentials, each one of them with its own absorption spectrum and, therefore, particular color.

When stimuli-responsive chromic compounds are also intrinsically emissive, they can also behave as fluorescent molecular switches. This is the case of the isoquinoline chromophore **iQ** described by Ihmel and co-workers and shown in Figure I-5a, which absorbs and emits in the UV-visible region.[50] Interestingly, the optical properties of **iQ** are critically affected by tautomerization which can be controlled with solvent polarity. Indeed, polar protic solvents stabilize the green

emissive **iQ$_{lactam}$** form, while aprotic polar solvents favor the blue-emissive **iQ** isomer (Figure I-5b).

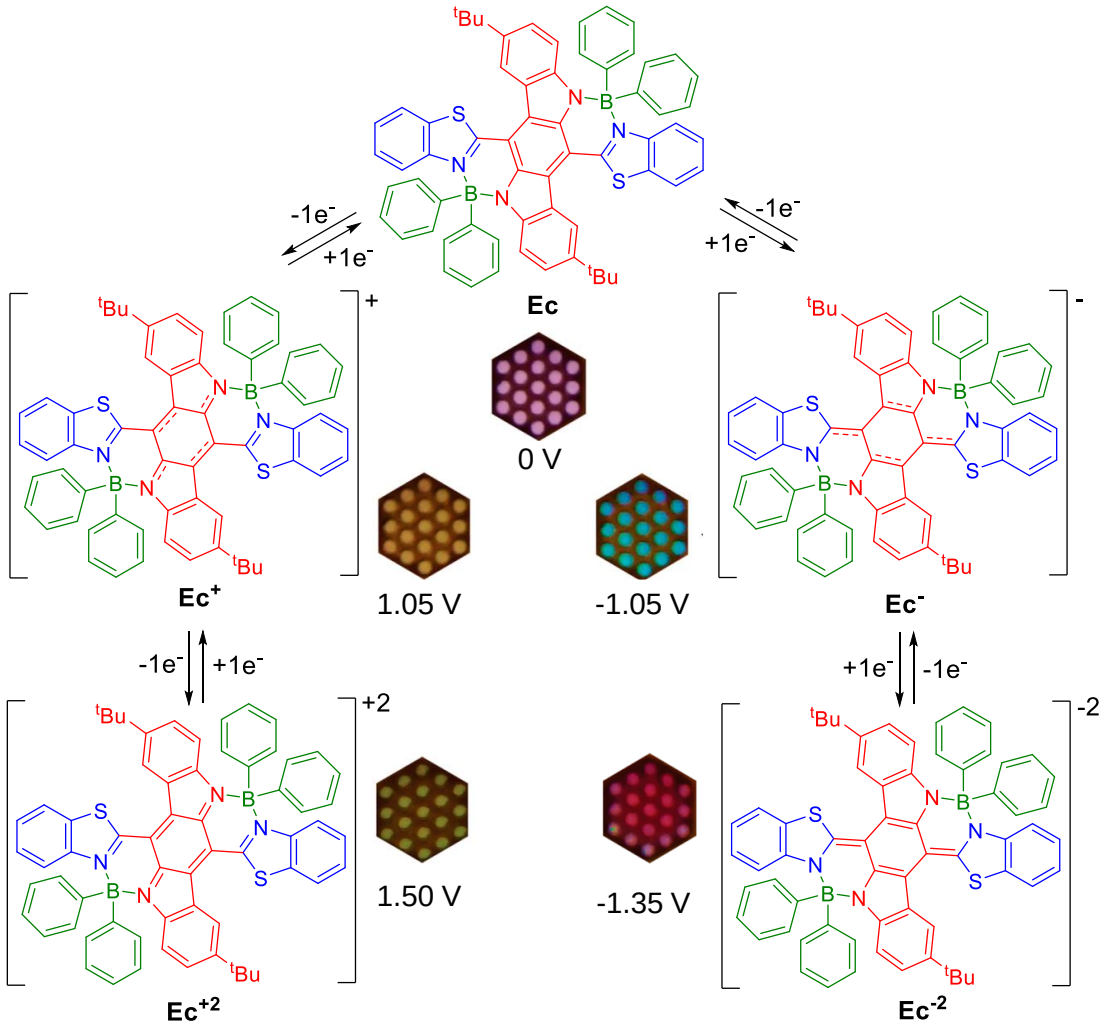

Figure I-4. Structure of the different redox states of electrochrome **Ec** and photographs of the color of these states in dichloromethane solution prepared upon application of defined electrochemical potentials (vs Ag/AgCl).[49]

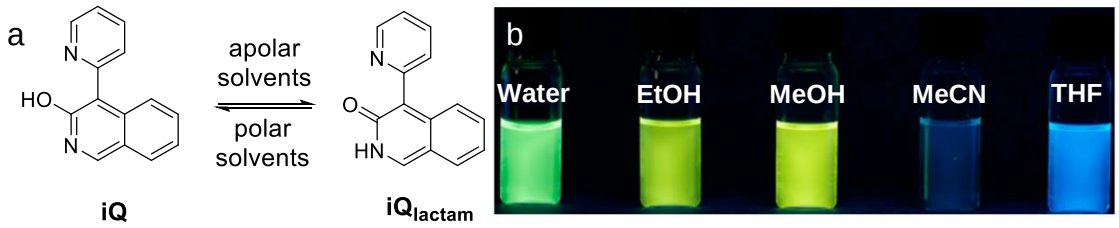

Figure I-5. (a) Structure of isoquinoline **iQ** and its tautomeric form **iQ$_{lactam}$**. (b) Solvent dependence of **iQ** fluorescence when irradiated at λ_{exc} = 420 nm.[50]

Although several intrinsic fluorescent molecular switches can be found in the literature, a different, more universal approach has been developed for the

preparation of these compounds that does not require the use of chromic systems. Instead, it relies on tethering two other functional units together: (a) a fluorophore that does not directly respond to external stimuli; and (b) a stimuli-switchable unit that selectively modifies the emission of the fluorophore in one of its states via engineered interactions (e.g., excited-state energy transfer and photoinduced electron transfer).[20] An example of this class of multicomponent fluorescent molecular switches is the anthracene-based fluorophore **AN** functionalized with a benzo-15-crown-5-ether shown in Figure I-6.[51] In this case **AN** fluorescence is quenched by photoinduced electron transfer (PET) between the anthracene unit and the ion-free crown ether moiety. When a sodium cation is recognized by the crown ether ligand, the PET process is inhibited and, therefore, the fluorescence of the system is enhanced.

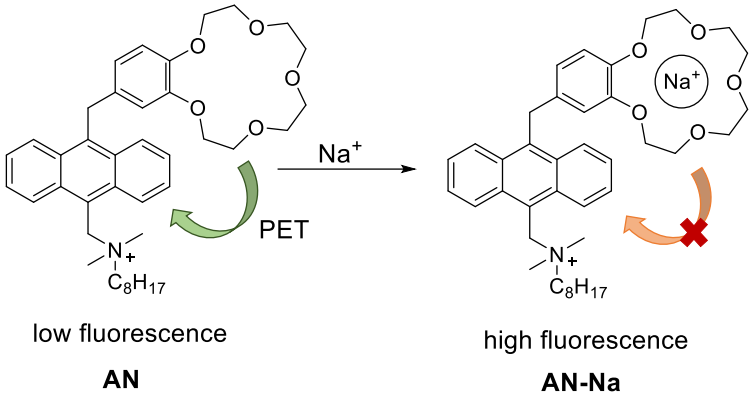

Figure I-6. Anthracene-based fluorophore **AN** tethering a benzo-15-crown-5 ether, whose fluorescence increases upon sodium ion coordination.[51]

In our group a new family of chromic and fluorescent molecular switches designed using a multicomponent approach has been developed during the last years.[52–55] These switches are based on spirocyclic zwitterionic Meisenheimer compounds (**SZMC**) and, as shown in Scheme I-1, they are multistate and respond to variate stimuli (pH, electrochemical potentials and temperature). In this thesis we have further investigated these systems with the aim of: (a) expanding the switching capabilities of SZMCs by adding new states and stimuli; and (b) preparing novel photofunctional materials based on SZMCs like sensors and displays.

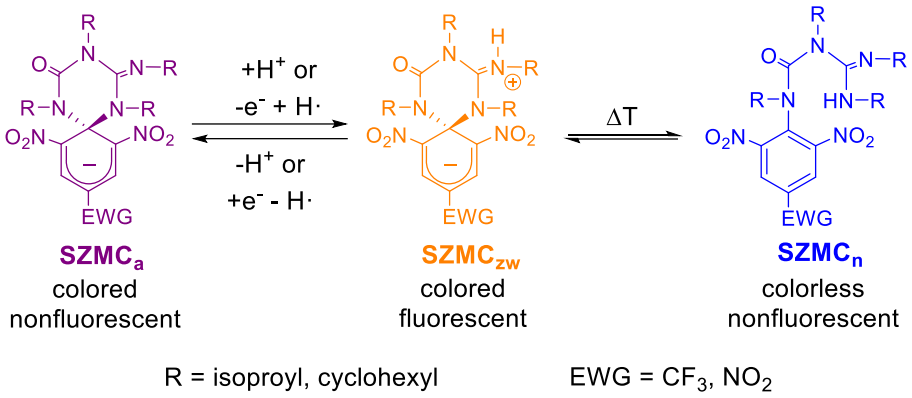

Scheme I-1. General scheme of the switching behavior of SZMC compounds described in our group before the start of this thesis.[55] They can be interconverted between colored fluorescent (**SZMC$_{zw}$**) and nonfluorescent (**SZMC$_a$**) states by pH variation or application of redox potentials, while transformation to the colorless form **SZMC$_n$** is accomplished thermally (see section III.1 for further details).

I.1.2. Photoresponsive molecular switches

As described above, light-responsive molecular switches (or molecular photoswitches) are compounds which interconvert between two (or more) states upon photon absorption. In most cases, they are based on photochromes; i.e., compounds that change their color upon irradiation.[31–34] Although some of the first examples of photochromism reported were based on light-induced bimolecular reactions, photochromes currently used for the preparation of molecular photoswitches operate under unimolecular photoisomerization processes.[56] These are isomerization reactions than do not proceed thermally through the ground electronic state of the system because of unfavorable kinetics; instead, they take place on an excited electronic state produced upon illumination, where no or very small energy barriers must be overcome for the system to isomerize (Figure I-7).

Photochromes and, therefore, the resulting molecular photoswitches are classified into two major groups on the basis of the thermal stability of the photochemically generated state. If it is thermally stable and can only be reverted back to the initial state via photoisomerization, photochromes are of P-type (*photochemically reversible type*). This is the case for diarylethenes,[9,19] stilbenes[57] and thiophenefulgides[58] (Figure I-8a). On the other hand, if the photoproduced state of the switches is thermally unstable and back-isomerization to the initial state can also occur spontaneously without light excitation, then they are of T-type (*thermally reversible type*).[59] Compounds such as azobenzenes,[60] donor-acceptor Stenhouse adducts[61] or spiropyrans[33,62] are examples of T-type molecular photoswitches (Figure I-8b).

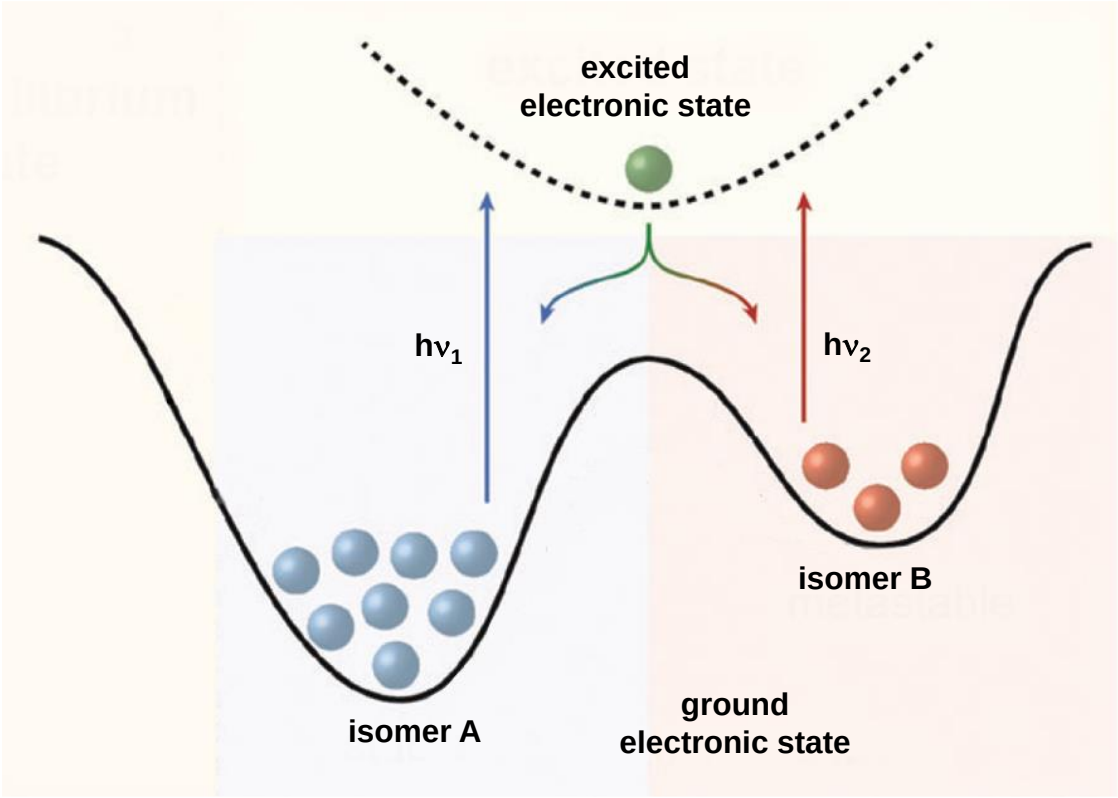

Figure I-7. General representation of the potential energy levels in a photoswitch isomerization process. The thermodynamically stable isomer **A** cannot overcome the isomerization energy barrier in the ground energy surface. Instead, isomerization takes place upon illumination when an excited state is created where there is none or a small energy barrier to yield the photoproduced isomer B after relaxation back to the ground electronic state. The back reaction can happen photochemically or thermally if the activation energy is low enough.

Several parameters are employed to evaluate the light-induced performance of molecular photoswitches. First, photoisomerization quantum yields are a measure of the efficiency of the process in the excited state, as they quantify how many molecules react per each photon absorbed and do not decay to the ground state by other processes (i.e., luminescence, internal conversion, …).[63] Second, the composition of the photostationary states (PSS) indicate the conversion of the photoreaction, as they correspond to the final equilibrium states reached under irradiation when the rates of the photoisomerization process and the back-reaction become equal.[64] PSSs are determined by the absorbance of the two isomers at the irradiation wavelength, their photoisomerization quantum yields and, for T-type photochromes, by the thermal lifetime of the photoinduced isomer and the irradiation intensity. Third, the fatigue resistance describes the loss of performance of the molecular photoswitch over repetitive photoisomerization cycles due to photodegradation.[65]

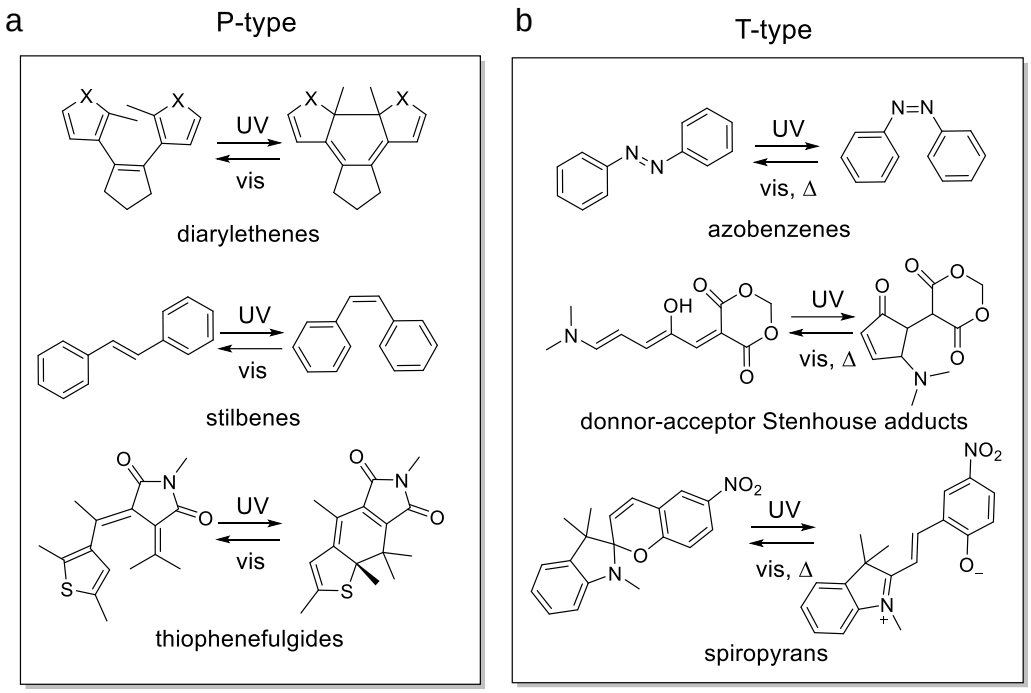

Figure I-8. (a) Examples of P-type photochromes: diarylethenes, stilbenes and thiophenefulgides. (b) Examples of T-type photochromes: azobenzenes, donor-acceptor Stenhouse adducts and spiropyranes.

As it can be noted from Figure I-8, most photochromes operate under *E*/*Z* and ring-opening/ring-closing photoisomerization reactions that induce a change in the electronic structure of the system and, as such, of its absorption spectrum. However, other molecular parameters are strongly modified upon photoswitching, such as geometry and polarity, which can be exploited to light-trigger advanced functions other than a simple color change. As a consequence, photochromic compounds can be used for the development of light-responsive processes and materials with applications in a variety of fields ranging from data storage[31] to photolithography,[66] catalysis,[13,67] photoprotective coatings[31] and photopharmacology.[22]

Although it is one of the most basic features of molecular photoswitches, changes in absorption are often used to derive light-controlled processes and materials. This is the case of the example shown in Figure I-9, where the emission from an anthracene fluorophore is regulated with a close-by photochrome to construct a fluorescent molecular memory.[30] For such a purpose, a molecular switch suffering a significant shift of the absorption upon photoisomerization was required, a feature presented by dithienylethenes (DTE). DTEs have two different isomers, a colorless open state and a colored closed state which interconvert upon UV and visible light irradiation, respectively.[19] Thus, the anthracene fluorophore of the dyad becomes selectively nonfluorescent when the DTE unit in **Ant-DTE** is photoisomerized to the closed state, as their respective emission and absorption spectra overlap, and the excited state of

the emitter can then decay nonradiatively by intramolecular resonance energy transfer (RET).

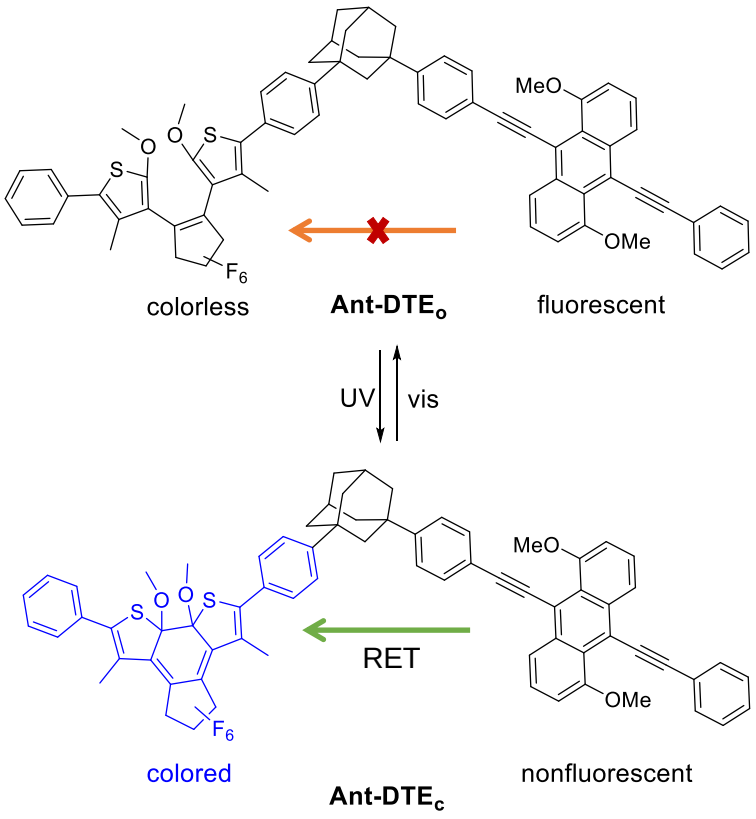

Figure I-9. Light-gated control over the luminescence of an anthracene fluorophore in the **Ant-DTE** dyad by photoisomerization of a nearby DTE moiety.[30]

Another feature widely exploited to realize light-controlled functions with molecular photoswitches is the geometry change between their two isomers, especially when it involves *E*/*Z* isomerization. In our group we have employed this principle to photocontrol the activity of neuronal glutamate receptors GluK1 and GluK2 through the *cis-trans* isomerization of the azobenzene-glutamate tether **Glu_brAzo** (Figure I-10).[68] In its thermodynamically stable *cis* isomer, the glutamate moiety of this compound is too sterically hindered as to permit interaction with the binding site of the receptors, thus inhibiting the agonist effect of the neurotransmitter. Such impediment is removed upon light-induced *Z*-to-*E* isomerization, which enables glutamate-receptor binding and, as a result, the opening of an ion channel through neuron membrane and the eventual firing of action potentials (Figure I-10b).

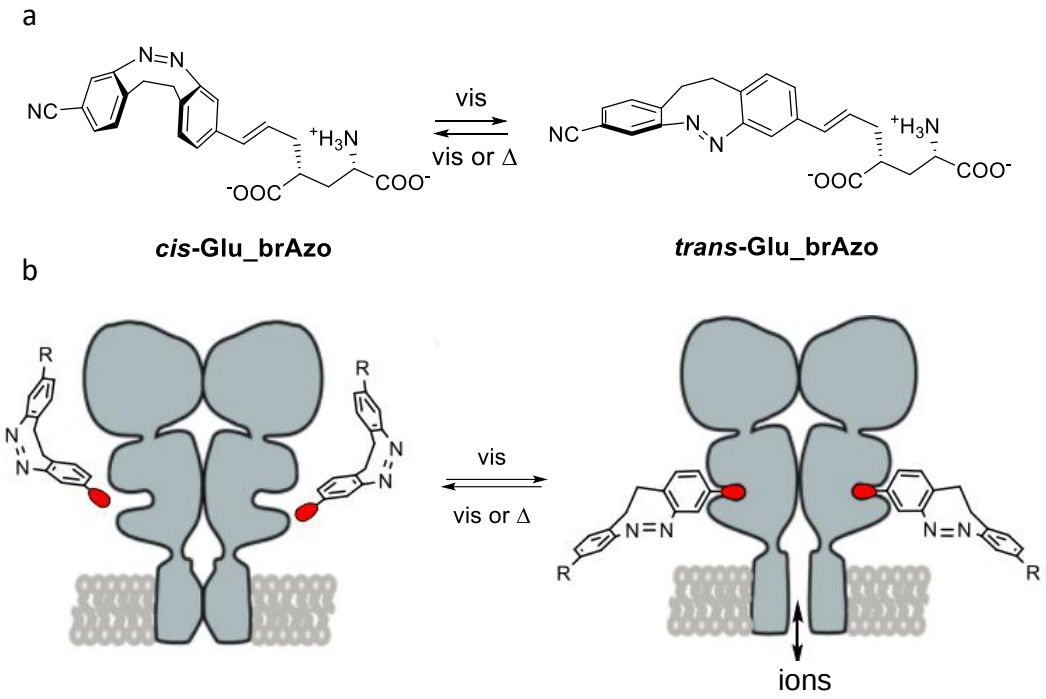

Figure I-10. (a) Structure of the two isomers of the photoresponsive ligand **Glu_brAzo**, which is composed of a glutamate neurotransmitter and a bridged azobenzene photochrome. (b) Light controlled activation/deactivation of neural membrane receptors GluK1 and GluK2 with **Glu_brAzo**.[68]

Photoisomerization can also trigger significant changes in the molecular switches' polarity, which can be further applied to light-control a variety of processes. This is the case of spiropyran switches, which reversibly interconvert from a neutral and nonpolar spirocyclic structure to a polar zwitterionic merocyanine structure under UV and visible light irradiation. This feature was exploited by Matyjaszewski and co-workers to photocontrol the formation of micelles using the block copolymer shown in Figure I-11.[69] This polymer presents two different types of domains: (a) a hydrophilic polyethylene glycol block, and (b) a hydrocarbon polymer block functionalized with spiropyran side groups, which switches from hydrophobic (**PEO-SP**) to hydrophilic (**PEO-MC**) upon photoisomerization. In this fashion, only in its **PEO-SP** state, the polymer is amphiphilic and, therefore, can form micelles; by contrast, after irradiation with UV light and formation of the open zwitterionic merocyanine units in **PEO-MC**, the polymer becomes hydrophilic and the micelles dissolve.

In this thesis it is a different property of molecular photoswitches that has been exploited to derive advanced light-regulated functions: the variation in the electronic properties of the functional groups appended to a photochrome upon photoisomerization. In this way, we aimed at reversibly modulating their reactivity with light to develop new photocontrolled processes. To reach this goal, we focused

our attention on dithienylethenes,[9,19] a well-known class of diarylethene photochromes that are further described in section IV.1.2.

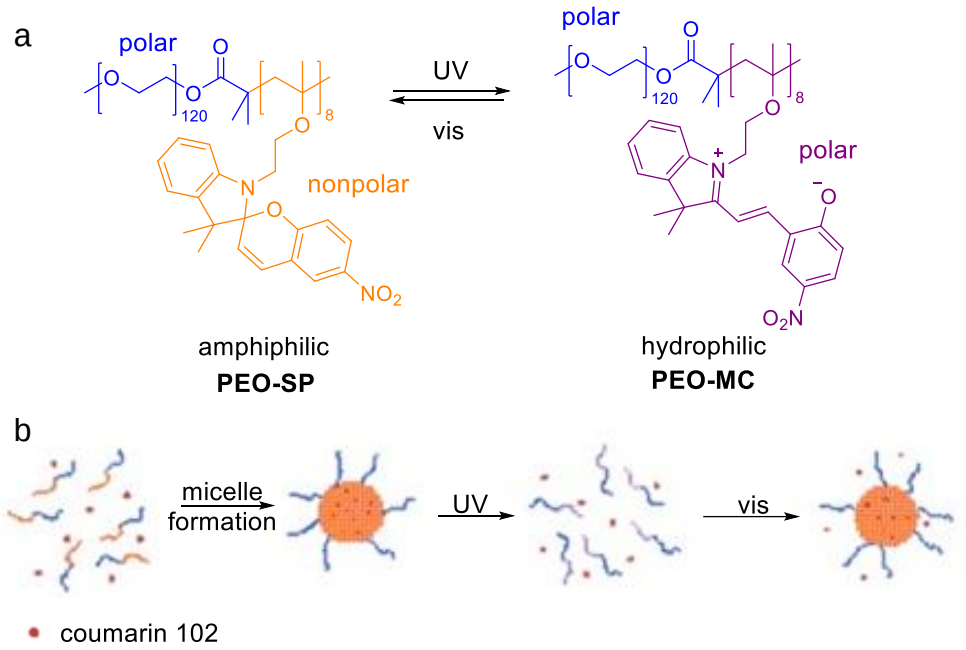

Figure I-11. (a) Light-induced polarity switch of the block copolymer **PEO-SP** by photoisomerization of its spirocyclic units to their merocyanine isomers in **PEO-MC**. (b) Schematic representation of the light-reversible formation of micelles employing **PEO-SP** to trap a hydrophobic molecule as coumarin 102 and release by photoconversion into **PEO-MC**.[69]

I.2. References

1 J. Barber, *Chem. Soc. Rev.*, 2009, **38**, 185–196.

2 B. A. Wandell, *Foundations of Vision*, Sinauer, 1995.

3 T. Mirkovic, E. E. Ostroumov, J. M. Anna, R. Van Grondelle, Govindjee and G. D. Scholes, *Chem. Rev.*, 2017, **117**, 249–293.

4 Y. Lin, Y. Li and X. Zhan, *Chem. Soc. Rev.*, 2012, **41**, 4245–4272.

5 Y. Zhao and K. Zhu, *Chem. Soc. Rev.*, 2016, **45**, 655–689.

6 H. Kuroiwa, Y. Inagaki, K. Mutoh and J. Abe, *Adv. Mater.*, 2019, **31**, 1805661.

7 F. A. Rueggeberg, *Dent. Mater.*, 2011, **27**, 39–52.

8 F. S. Ligler and J. J. Gooding, *Anal. Chem.*, 2019, **91**, 8732–8738.

9 M. Irie, *Chem. Rev.*, 2000, **100**, 1685–1716.

10 B. L. Feringa and W. R. Browne, *Molecular Switches*, Wiley-VCH, 2nd edn.,

2011.

11 T. J. Kucharski, Y. Tian, S. Akbulatov and R. Boulatov, *Energy Environ. Sci.*, 2011, **4**, 4449–4472.

12 M. I. Khazi, W. Jeong and J. M. Kim, *Adv. Mater.*, 2018, **30**, 1705310.

13 V. Blanco, D. A. Leigh and V. Marcos, *Chem. Soc. Rev.*, 2015, **44**, 5341–5370.

14 M. Kathan and S. Hecht, *Chem. Soc. Rev.*, 2017, **46**, 5536–5550.

15 F. Gallego-Gómez, F. Del Monte and K. Meerholz, *Nat. Mater.*, 2008, **7**, 490–497.

16 S. Mura, J. Nicolas and P. Couvreur, *Nat. Mater.*, 2013, **12**, 991–1003.

17 G. Ertl, Press release: The Nobel Prize in Chemistry 2016, https://www.nobelprize.org/prizes/chemistry/2016/press-release/.

18 T. Kudernac, N. Ruangsupapichat, M. Parschau, B. MacIá, N. Katsonis, S. R. Harutyunyan, K. H. Ernst and B. L. Feringa, *Nature*, 2011, **479**, 208–211.

19 M. Irie, T. Fukaminato, K. Matsuda and S. Kobatake, *Chem. Rev.*, 2014, **114**, 12174–12277.

20 I. Yildiz, E. Deniz and F. M. F. M. Raymo, *Chem. Soc. Rev.*, 2009, **38**, 1859–1867.

21 L. Hou, T. Leydecker, X. Zhang, W. Rekab, M. Herder, C. Cendra, S. Hecht, I. McCulloch, A. Salleo, E. Orgiu and P. Samorì, *J. Am. Chem. Soc.*, 2020, **142**, 11050–11059.

22 K. Hüll, J. Morstein and D. Trauner, *Chem. Rev.*, 2018, **118**, 10710–10747.

23 M. Li, J. Zhao, H. Chu, Y. Mi, Z. Zhou, Z. Di, M. Zhao and L. Li, *Adv. Mater.*, 2019, **31**, 1804745.

24 J. R. Chen and D. Y. Yang, *Org. Lett.*, 2009, **11**, 1769–1772.

25 G. Guirado, C. Coudret, M. Hliwa and J. P. Launay, *J. Phys. Chem. B*, 2005, **109**, 17445–17459.

26 I. Dierking and S. E. San, *Appl. Phys. Lett.*, 2005, **87**, 233507.

27 J. F. Callan, A. P. De Silva and D. C. Magri, *Tetrahedron*, 2005, **61**, 8551–8588.

28 S. J. Yoon, J. W. Chung, J. Gierschner, K. S. Kim, M. G. Choi, D. Kim and S. Y. Park, *J. Am. Chem. Soc.*, 2010, **132**, 13675–13683.

29 H. Dürr and H. Bouas-Laurent, *Photochromism: Molecules and Systems*, Elsevier Amsterdam, 2001.

30 M. Irie, T. Fukaminato, T. Sasaki, N. Tamai and T. Kawai, *Nature*, 2002, **420**, 759–760.

31 P. Bamfield, *Chromic Phenomena: Technological Applications of Colour*

Chemistry, Royal Society of Chemistry, 2010.

32 V. I. Minkin, *Chem. Rev.*, 2004, **104**, 2751–2776.

33 L. Kortekaas and W. R. Browne, *Chem. Soc. Rev.*, 2019, **48**, 3406–3424.

34 J. Boixel, V. Guerchais, H. Le Bozec, D. Jacquemin, A. Amar, A. Boucekkine, A. Colombo, C. Dragonetti, D. Marinotto, D. Roberto, S. Righetto and R. De Angelis, *J. Am. Chem. Soc.*, 2014, **136**, 5367–5375.

35 S. Zheng, P. L. M. Lynch, T. E. Rice, T. S. Moody, H. Q. N. Gunaratne and A. P. De Silva, *Photochem. Photobiol. Sci.*, 2012, **11**, 1675–1681.

36 J. Ling, G. Naren, J. Kelly, T. S. Moody and A. P. De Silva, *J. Am. Chem. Soc.*, 2015, **137**, 3763–3766.

37 B. B. Rathod, S. Murthy and S. Bandyopadhyay, *J. Chem. Educ.*, 2019, **96**, 486–494.

38 O. A. Bozdemir, R. Guliyev, O. Buyukcakir, S. Selcuk, S. Kolemen, G. Gulseren, T. Nalbantoglu, H. Boyaci and E. U. Akkaya, *J. Am. Chem. Soc.*, 2010, **132**, 8029–8036.

39 A. Jiménez-Sánchez, N. Farfán and R. Santillan, *J. Phys. Chem. C*, 2015, **119**, 13814–13826.

40 E. N. Shepelenko, V. A. Podshibyakin, K. S. Tikhomirova, Y. V. Revinskii, A. D. Dubonosov, V. A. Bren and V. I. Minkin, *J. Mol. Struct.*, 2018, **1163**, 221–226.

41 M. M. A. Mazza, F. Cardano, J. Cusido, J. D. Baker, S. Giordani and F. M. Raymo, *Chem. Commun.*, 2019, **55**, 1112–1115.

42 G. Gunbas and L. Toppare, *Chem. Commun.*, 2012, **48**, 1083–1101.

43 C. K. Wu, Z. Weng and D. Y. Yang, *Org. Lett.*, 2019, **21**, 5225–5228.

44 A. Seeboth, D. Lötzsch, R. Ruhmann and O. Muehling, *Chem. Rev.*, 2014, **114**, 3037–3068.

45 W. Yang, K. E. Krantz, L. A. Freeman, D. A. Dickie, A. Molino, A. Kaur, D. J. D. Wilson and R. J. Gilliard, *Chem. Eur. J.*, 2019, **25**, 12512–12516.

46 T. Yang, Y. Wang, X. Liu, G. Li, W. Che, D. Zhu, Z. Su and M. R. Bryce, *Chem. Commun.*, 2019, **55**, 14582–14585.

47 B. A. Versaw, M. E. McFadden, C. C. Husic and M. J. Robb, *Chem. Sci.*, 2020, **11**, 4525–4530.

48 W. Tian and J. Tian, *Dyes Pigm.*, 2014, **105**, 66–74.

49 C. Zhu, X. Ji, D. You, T. L. Chen, A. U. Mu, K. P. Barker, L. M. Klivansky, Y. Liu and L. Fang, *J. Am. Chem. Soc.*, 2018, **140**, 18173–18182.

50 G. E. Gomez Pinheiro, H. Ihmels and C. Dohmen, *J. Org. Chem.*, 2019, **84**, 3011–3016.

51 S. Uchiyama, E. Fukatsu, G. D. McClean and A. P. DeSilva, *Angew. Chem. Int. Ed.*, 2016, **55**, 768–771.

52 R. O. Al-Kaysi, G. Guirado and E. J. Valente, *Eur. J. Org. Chem.*, 2004, 3408–3411.

53 R. O. Al-Kaysi, J. L. Bourdelande, I. Gallardo, G. Guirado and J. Hernando, *Chem. Eur. J.*, 2007, **13**, 7066–7074.

54 R. O. Al-Kaysi, I. Gallardo and G. Guirado, *Molecules*, 2008, **13**, 1282–1302.

55 I. Gallardo, G. Guirado, J. Hernando, S. Morais and G. Prats, *Chem. Sci.*, 2016, **7**, 1819–1825.

56 H. Bouas-Laurent and H. Dürr, *Pure Appl. Chem.*, 2001, **73**, 639–665.

57 F. D. Lewis and R. S. Kalgutkar, *J. Phys. Chem. A*, 2001, **105**, 285–291.

58 M. M. Krayushkin, V. A. Barachevsky and M. Irie, *Heteroat. Chem.*, 2007, **18**, 557–566.

59 A. Lennartson, A. Roffey and K. Moth-Poulsen, *Tetrahedron Lett.*, 2015, **56**, 1457–1465.

60 E. Merino, *Chem. Soc. Rev.*, 2011, **40**, 3835–3853.

61 M. M. Lerch, W. Szymański and B. L. Feringa, *Chem. Soc. Rev.*, 2018, **47**, 1910–1937.

62 R. Klajn, *Chem. Soc. Rev.*, 2014, **43**, 148–184.

63 E. Stadler, A. Eibel, D. Fast, H. Freißmuth, C. Holly, M. Wiech, N. Moszner and G. Gescheidt, *Photochem. Photobiol. Sci.*, 2018, **17**, 660–669.

64 J. W. Verhoeven, *Pure Appl. Chem.*, 1996, **68**, 2223–2286.

65 S. E. Braslavsky, *Pure Appl. Chem.*, 2007, **79**, 293–465.

66 J. Alves, S. Wiedbrauk, D. Gräfe, S. L. Walden, J. P. Blinco and C. Barner-Kowollik, *Chem. Eur. J.*, 2020, **26**, 809–813.

67 T. Imahori and S. Kurihara, *Chem. Lett.*, 2014, **43**, 1524–1531.

68 G. Cabré, A. Garrido-Charles, À. González-Lafont, W. Moormann, D. Langbehn, D. Egea, J. M. Lluch, R. Herges, R. Alibés, F. Busqué, P. Gorostiza and J. Hernando, *Org. Lett.*, 2019, **21**, 3780–3784.

69 H. Il Lee, W. Wu, J. K. Oh, L. Mueller, G. Sherwood, L. Peteanu, T. Kowalewski and K. Matyjaszewski, *Angew. Chem. Int. Ed.*, 2007, **46**, 2453–2457.

Chapter II

Objectives

The goal of this thesis is the development of photofunctional materials and processes based on molecular switches. In particular, attention has been focused on two main topics: (a) the use of spirocyclic zwitterionic Meisenheimer complexes for the preparation of multistimuli-responsive and multistate chromic and fluorescent materials; and (b) the application of dithienylethene switches to the modulation of chemical reactivity with light. A detailed description of both objectives is presented below.

II.1. STIMULI-RESPONSIVE CHROMIC AND FLUORESCENT MATERIALS BASED ON SPIROCYCLIC ZWITTERIONIC MEISENHEIMER COMPLEXES

Multistate and multiresponsive chromic and fluorescent materials are highly desirable for a wide range of applications. The family of SZMC switches introduced in our group a few years ago are excellent candidates to achieve this behavior. Actually, by the start of this thesis, they had already been demonstrated to present three different states and respond to three distinct type of stimuli (i.e., pH, redox and temperature). For this reason, in this work we aimed at (Figure II-1):

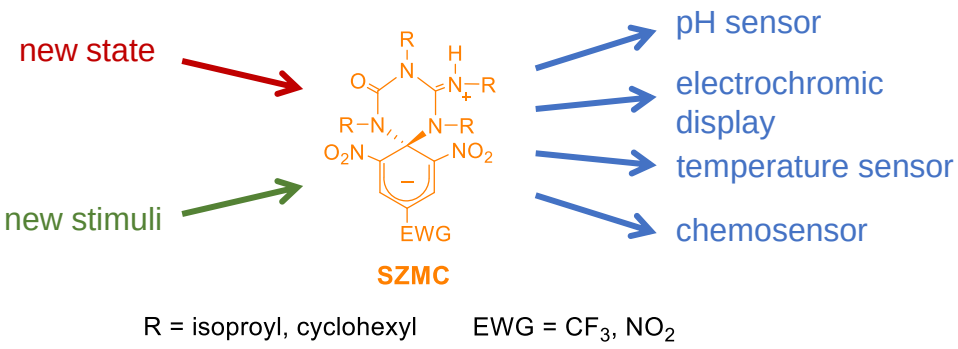

Figure II-1. By broadening the multistate and multistimuli-responsive behavior of **SZMC** switches, these systems were applied in this work to the preparation of different types of photofunctional materials.

- Broadening the multistate and multiresponsive character of SZMC switches, for which we investigated the formation of a new protonation state for these systems and their capacity to show solvato(fluoro)chromic properties.
- Exploiting the multistate and multiresponsive character of SZMC switches for the preparation of a variety of photofunctional materials: thermal sensors, wide-range pH detectors, electro(fluoro)chromic displays, and ionic and solvent sensors.

The results obtained for these objectives are described in Chapter III.

II.2. LIGHT-CONTROLLED REACTIVITY BASED ON DITHIENYLETHENE PHOTOSWITCHES

To reach accurate and remote control over where and when a chemical reaction occurs could be of great importance for many applications. In this thesis we pursued this goal by employing light as a trigger signal and dithienylethenes molecular photoswitches as photocontrollable reactants. Two main objectives were proposed in this area (Figure II-2):

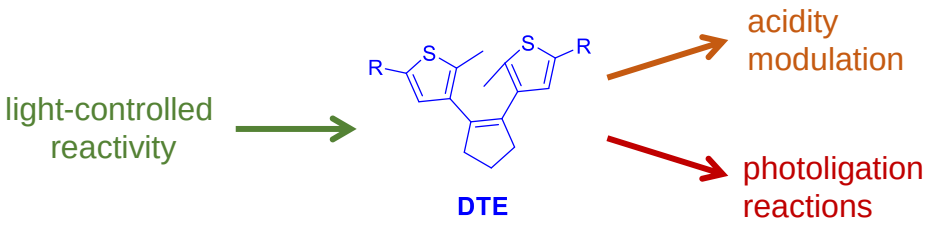

Figure II-2. DTE photoswitches were prepared in this work to achieve photocontrolled acidity and develop new photoligation reactions.

- To control the acidity of phenols attached to DTE upon photoisomerization. The results accomplished in this area are described in Chapter IV.
- To develop photoligation processes enabling light-controlled chemical functionalization of molecules and materials, for which we explored the use of DTE switches capable of undergoing light-gated amide bond formation reactions and Diels-Alder cycloadditions. The results obtained for these objectives are discussed in Chapters V and VI.

Chapter III

Stimuli-responsive chromic and fluorescent materials based on spirocyclic zwitterionic Meisenheimer complexes

In this chapter we explore new states and operating stimuli for the molecular switches based on spirocyclic zwitterionic Meisenheimer complexes as well as their use for the preparation of a variety of chromic and fluorescent materials.[a]

.

[a] The results described in this chapter have been published in: "Fluorescent "Turn-Off" Detection of Fluoride and Cyanide Ions Using Zwitterionic Spirocyclic Meisenheimer Compounds", M. Benet, M. Villabona, C. Llavina, S. Mena, J. Hernando, R. O. Al-Kaysi and G. Guirado, *Molecules* 2017, **22**. 1842; "New Smart Functional Fluorophores Based on Stable Spirocyclic Zwitterionic Meisenheimer Compounds", N. Sala, G. Prats, M. Villabona, I. Gallardo, T. Hamdan, R. O. Al-Kaysi, J. Hernando and G. Guirado, *Dyes Pigments* 2018, **153**, 160-171, and "Multistimuli-Responsive Fluorescent Switches Based on Spirocyclic Meisenheimer Compounds: Smart Molecules for the Design of Optical Probes and Electrochromic Materials" M. Villabona, M. Benet, S. Mena, R. O. Al-Kaysi, J. Hernando and G. Guirado, *J. Org. Chem.* 2018, **83**, 9166-9177

III.1. INTRODUCTION

III.1.1. Multiresponsive and multistate molecular switches

Multiresponsive molecular switches are compounds that can respond to two or more different external input signals. Having more than one stimulus at the system disposal enhances its performance, especially if they are orthogonal and can overcome the limitations of each other. For this reason, compounds with multistimuli-responsive behavior are highly desirable and have been exploited in complex logic-gate[1–3] and analog operations,[4] multimode information storage,[5] smart functional materials[6–10] or multiplexed sensing.[11,12]

A good example of the advantages of multistimuli-responsive switches is the compound **DBDCS** presented in Figure III-1.[13] In the solid state, **DBDCS** is a fluorophore with two different interconvertible crystalline phases, each one of them with distinctive emission and response to external stimuli: (a) a green-emissive G-phase that reacts to thermal changes, and (b) a blue-emissive B-phase sensitive to both organic vapors and pressure. Such behavior was exploited for the preparation of fluorescent optical displays which require of two basic functions: (a) writing, which should have good spatial resolution, and (b) erasing, which should be homogeneous. In the case of the G-to-B-phase transformation, temperature can be easily employed for both uses by either heating the whole sample for erasing or by using a hot object to write (i.e., a hot letter stamp, hot needle…). However, for the B-to-G-phase conversion, pressure is more suitable for writing as it is easier to be applied locally, while organic vapor annealing is preferred for erasing larger areas homogeneously. This is a clear demonstration that the use of multiple input signals when operating molecular switches allows for better performances, as the most appropriate stimulus can be selected for each application.

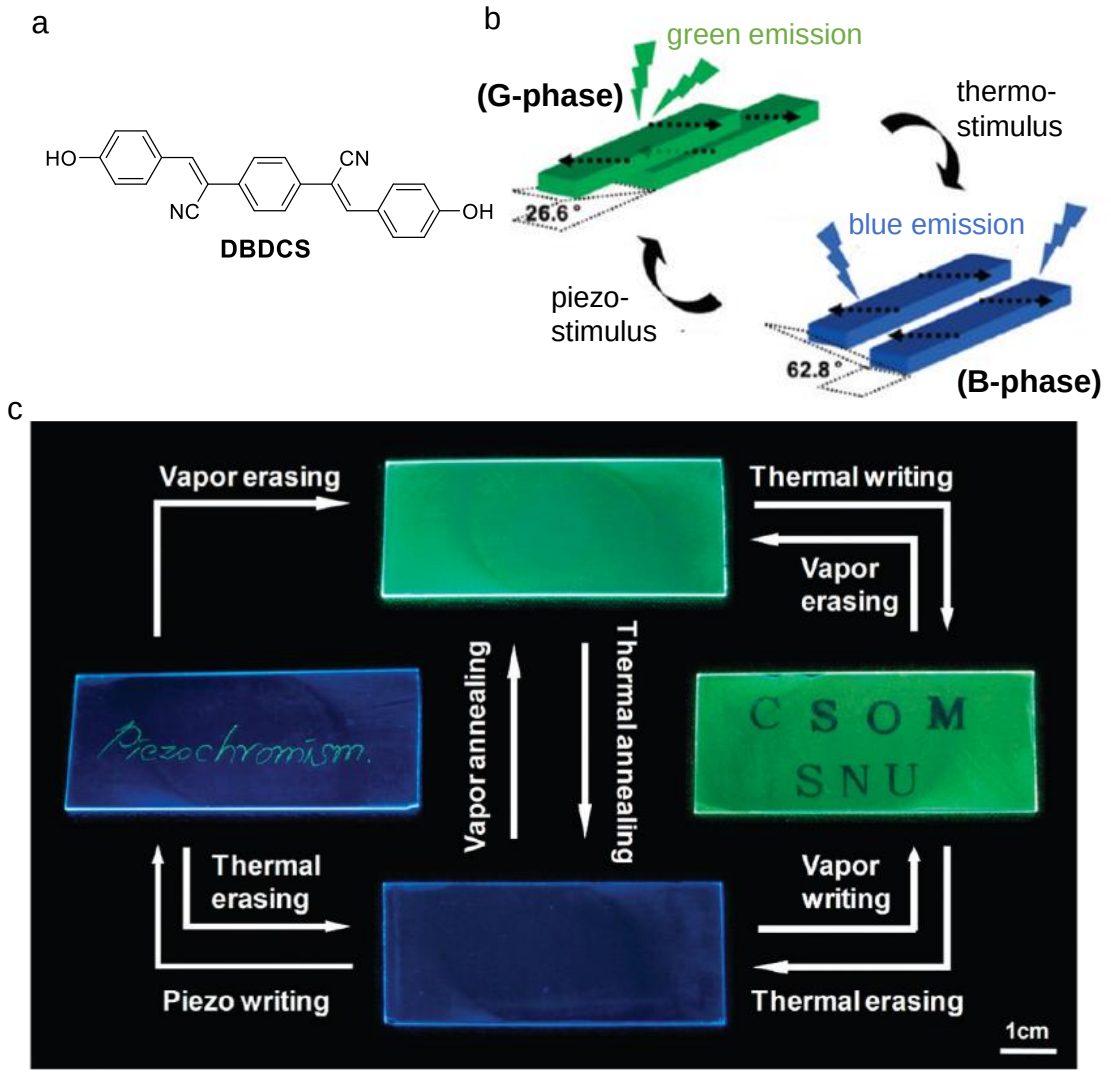

Figure III-1. (a) Structure of the dye **DBDCS.** (b) **DBDCS** fluorescent B and G crystalline phases that are interconvertible upon application of different stimuli. (c) Optical displays based on the reversible transformation between the green emissive G-phase and the blue emissive B-phase. The most suitable external stimuli for writing and erasing are indicated in each case.[13]

Memory systems are also benefited from the use of multistate switches, as they can overcome the binary code of 1s and 0s and, thus, exponentially increasing densities can be achieved for data storage.[14–18] An example of this is the polymerized ruthenium complex **Ru-poly** presented in Figure III-2, which was employed by Zhong and coworkers to prepare a ternary memory system.[18] This polymeric material has up to 4 oxidation states that could be selectively achieved electrochemically and easily differentiated by its characteristic absorption bands in the visible and near infrared (NIR) regions.

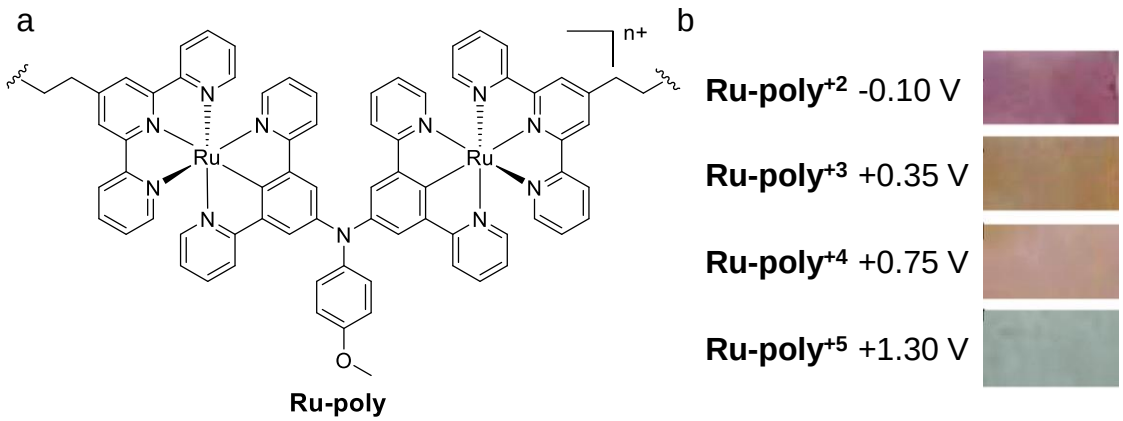

Figure III-2 (a) Structure of the multistate electrochrome **Ru-poly**. (b) Images of **Ru-poly** films electropolymerized over an indium thin oxide (ITO) plate after applying the corresponding potentials (vs Ag/AgCl) to switch between its 4 oxidation states.[18]

Although scarce, some chromic and fluorescent switches are both multistimuli-responsive and multistate, which allows combining the high degree of complexity of the former with the higher control that can be exerted over the latter. Some of these switches have been used for advanced applications in dynamic covalent chemistry,[19] nonlinear optics [20] or as logic gates.[21,22]

The most common strategy to prepare systems with multiresponsive and multistate behavior is the combination of two or more switching entities that respond to different stimuli. For instance, the compound **BodipyL3** in Figure III-3b is a multistate and multistimuli-responsive fluorescent switch composed of a Bodipy emitter and 3 selective cation binding sites: (a) a Zn^{2+} ligand dipicolylamine, (b) a Hg^{2+} selective thiaazacrown ether, and (c) an azacrown ether known for its complexing capacity of earth-alkaline cations such as Ca^{2+}.[23] In total, **BodipyL3** has up to 8 different states depending on 3 chemical stimuli (i.e., the distinct metal ions). The idea behind this system is to work as an AND logic gate which only gives a positive response (i.e., fluorescence) when two or more cations are present. This happens because the Bodipy core can undergo PET-based nonradiative relaxation pathways if any of the ligands is free; thus, only when all three cations are recognized, the complex is fully fluorescent.

Because of the multicomponent nature of most multistate and multistimuli-responsive switches, they are complex to prepare. However, in this thesis we will focus on SZMCs, a family of fluorescent switches developed in our group that combine the multistate and multistimuli-responsive properties in a single unit obtained through a facile one-step synthesis.

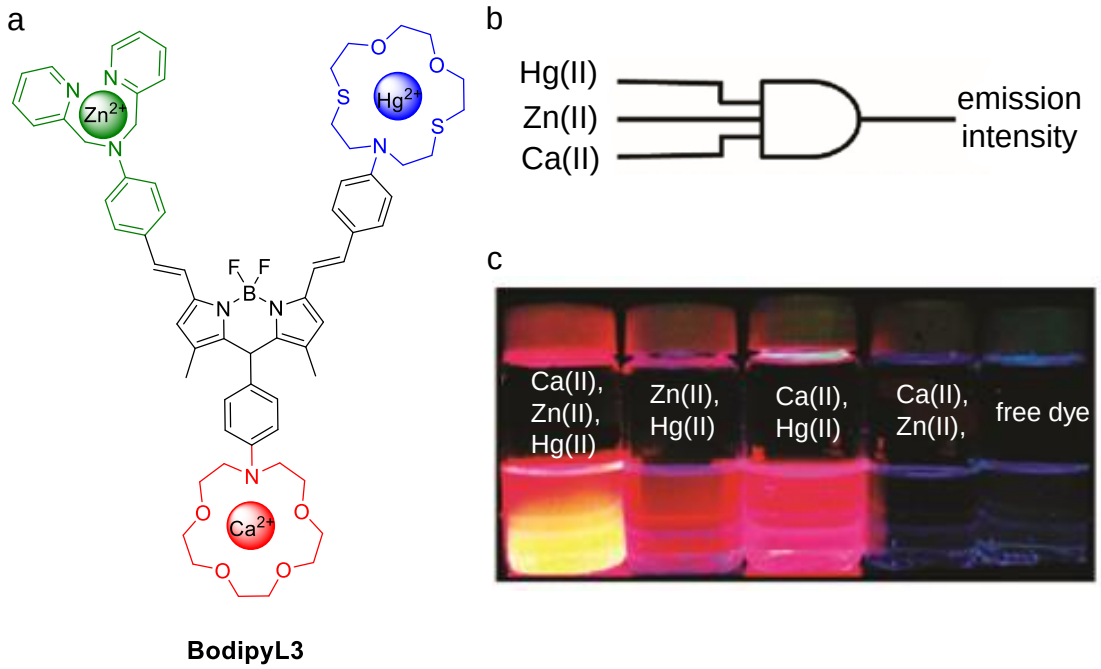

Figure III-3. (a) Structure of **BodipyL3** when coordinating Zn^{2+}, Hg^{2+} and Ca^{2+} ions. (b) AND logic gate operation of **BodipyL3**. (c) Fluorescence of **BodipyL3** acetonitrile solutions containing different combinations of ions.

III.1.2. Molecular switches based on spirocyclic zwitterionic Meisenheimer compounds

Meisenheimer complexes are a well-known intermediates of nucleophilic aromatic substitution reactions (SN_{Ar}) on electron-deficient arenes.[24] Several years ago our group reported that a particular class of stable zwitterionic Meisenheimer compounds behave as chromic and fluorescent molecular switches.[4,25–28] Their structure is spirocyclic and composed of two different structural motifs: (a) a colored and fluorescent cyclohexadienyl anion moiety bearing electron-withdrawing groups (EWGs) at positions 2, 4 and 6; and (b) a triazine ring which can be employed to modulate the emission and color of the cyclohexadienyl anion group (Scheme I-1). Therefore, SZMCs are an example of modular chromic and fluorescent switches, which, as previously discussed in Chapter I, are known to have applications in sensing,[23,29,30] imaging,[30] logic gates[23,31,32] and data storage[33–35], among others.

An important advantage of SZMCs over other multicomponent fluorescent switches is that they do not require long synthetic pathways. Instead, SZMCs can be obtained via a one-pot process from commercially available phenols in an excess of carbodiimide to yield the zwitterionic state of the target molecular switch (**$SZMC_{zw}$**) together with a by-product resulting from the complete SN_{Ar} reaction (compounds **5-8** in Scheme III-2a). By the start of this thesis, four different SZMC switches had been synthesized using this strategy (**SZMC1-4**), which differ in the nature of the EWG at

the 4 position of the cyclohexadienyl anion and the substituents of the triazine ring.[4,25,28,36] On one hand, **SZMC1** and **SZMC2** are derivatives of picric acid (**1**) that contain a 2,4,6-trinitrocyclohexadienyl anion fluorophore and isopropyl (iPr) or cyclohexyl (Cy) pending groups on their triazene moiety, respectively. When starting from 2,6-dinitro-4-trifluoromethylphenol (**2**), **SZMC3** and **SZMC4** are obtained, which also present the isopropyl or cyclohexyl substituents of the precursor diisopropylcarbodiimide (**3**) and dicyclohexylcarbodiimide (**4**). A plausible mechanism for the synthesis of these compounds is shown in Scheme III-2b,[36] which starts with the nucleophilic attack of the nitrogen atom of the carbodiimide to the phenolic carbon atom followed via migration of the hydroxyl group. The resulting intermediate **II** can easily evolve to the monosubstitution products **5**-**8** by tautomerization, whereas further reaction with a second carbodiimide molecule eventually generates the desired spirocyclic structure of the SZMC switches.

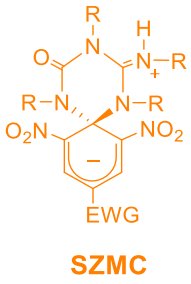

Scheme III-1. General structure of SZMC molecular switches.[4,25–28,36]

Owing to the presence of the spirocyclic cyclohexadienyl anion, the zwitterionic state of **SZMC1**-**4** shows strong absorption and emission in the visible region, which are significantly affected by the nature of the EWGs. Thus, while organic solutions of **SZMC1** and **SZMC2** are red-colored ($\lambda_{abs,max}$ = 408 and 528 nm in acetonitrile) and emit yellow light ($\lambda_{fl,max}$ = 570 in acetonitrile with fluorescence quantum yield (Φ_{fl}) around 0.5), those prepared from **SZMC3** and **SZMC4** present magenta color ($\lambda_{abs,max}$ = 564 nm in acetonitrile) and produce red emission ($\lambda_{fl,max}$ = 594 nm and Φ_{fl} ~ 0.75 in acetonitrile).[4,28,36,37] However, this behavior drastically changes in the absence of the guanidinium proton of the triazene ring, which can then transfer an electron to the photoexcited cyclohexadienyl anion fluorophore that quenches its emission. As a result, the anionic form of the complexes **SZMC$_a$** becomes nonfluorescent (Φ_{fl} < 0.01; Scheme III-3), though it retains the strong coloration of **SZMC$_{zw}$**. This opens the door to use **SZMC1**-**4** as fluorescent molecular switches that reversibly interconvert between emissive and nonemissive states by protonation-deprotonation of its triazene moiety upon acid-base addition.[4,27,37]

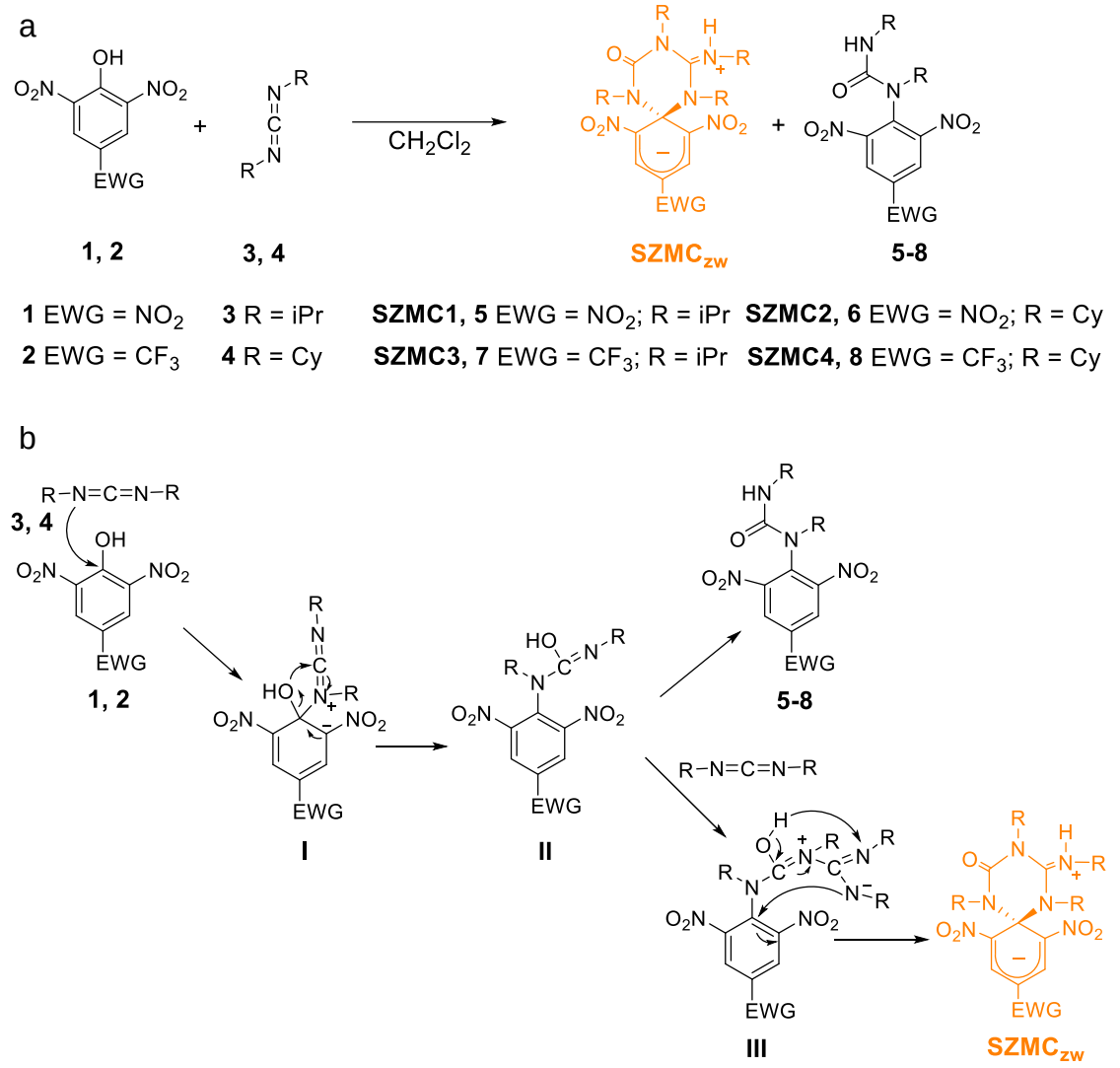

Scheme III-2. (a) General synthetic procedure for the preparation of SZMCs.[4,25,28,36] (b) Tentative mechanism proposed in the literature for the formation of **SZMC$_{zw}$** and its byproduct **5-8**.[36]

Interestingly, the transformation between the zwitterionic **SZMC$_{zw}$** and anionic **SZMC$_a$** forms of **SZMC1-4** is not only possible through acid-base treatment but also electrochemically. Thus, our group demonstrated that reduction of **SZMC$_{zw}$** followed by a hydrogen atom elimination yields **SZMC$_a$**, which in turn can be oxidized and abstract a hydrogen atom from the solvent to regenerate the initial zwitterionic state (Scheme III-3).[4,26,37] Therefore, this makes SZMCs multistimuli-responsive molecular switches.[4,27]

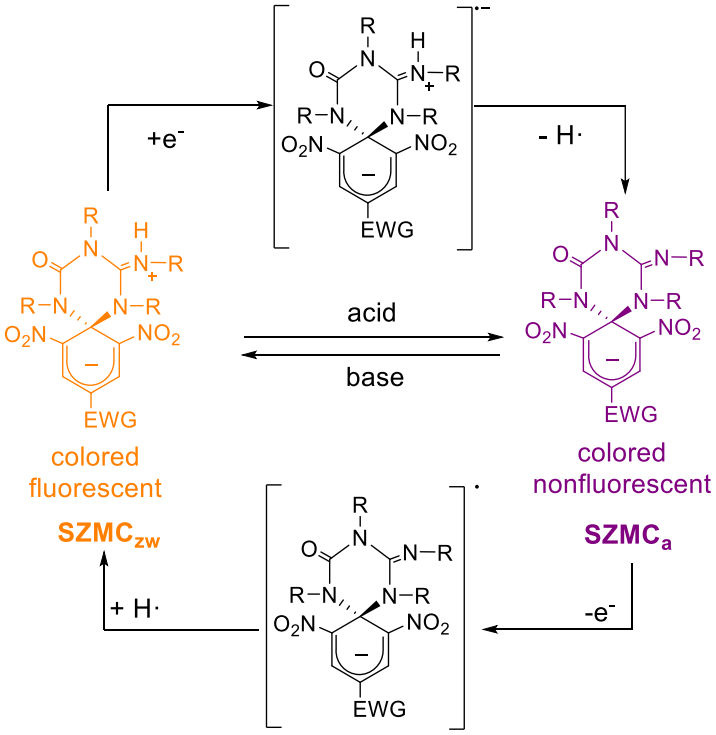

SZMC1 EWG = NO_2; R = *i*Pr **SZMC2** EWG = NO_2; R = Cy
SZMC3 EWG = CF_3; R = *i*Pr **SZMC4** EWG = CF_3; R = Cy

Scheme III-3. Acid-base and electrochemical switching mechanisms between **SZMC$_{zw}$** and **SZMC$_a$**.[4,26–28,37]

In addition, some SZMCs are known to be multistate molecular switches as well. Thus, our group reported that, while **SZMC1** and **SZMC2** spirocyclic structure is stable at room temperature, the zwitterionic form of **SZMC3** exists in equilibrium with a neutral aromatic tautomer (**SZMC3$_n$**; Scheme III-4).[4] This happens because the trifluoromethyl group lacks the mesomeric effect of the nitro substituents, which is critical to provide resonance stabilization of the anionic cyclohexadienyl fragment. Therefore, as the novel state resulting from the opening of the spirocyclic Meisenheimer complex does not present the fluorescent cyclohexadienyl anionic motif, **SZMC3$_n$** is colorless and nonfluorescent. Interestingly, the ratio between the two tautomers has been proven to be highly dependent on temperature, as the spirocyclic structure of **SZMC3$_{zw}$** becomes more stable upon cooling. This means that **SZMC3** does not only behave as a three-state switch, but also that its color and emission intensity can be tuned by an additional stimulus (i.e., temperature variations) to those previously described (i.e., pH and redox potentials).

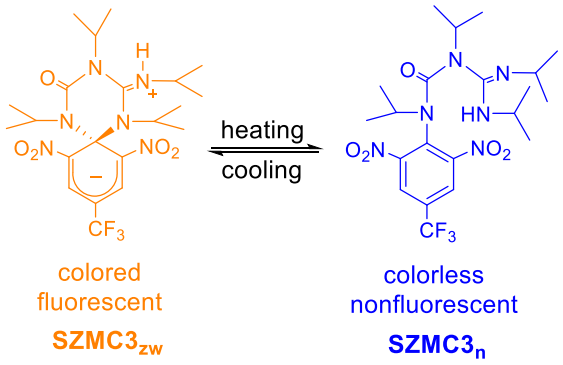

Scheme III-4. Thermal switching mechanism between the neutral states **SZMC3$_{zw}$** and **SZMC3$_{n}$**.[4]

This particular behavior of **SZMC3** has already been exploited for the preparation of functional materials. On one hand, the thermal switching between fluorescent **SZMC3$_{zw}$** and nonfluorescent **SZMC3$_{n}$** was employed in our group for the fabrication of color-tunable white-light-emitting materials.[38] To do so, two fluorophores with complementary emission colors were embedded within liquid-filled microcapsules: (a) 9,10-bis(phenylethynyl)anthracene (**BPEA**,Figure III-4a), a turquoise-emitting dye; and (b) **SZMC3$_{zw}$**, whose red emission intensity could be regulated by thermally varying the **SZMC3$_{zw}$**:**SZMC3$_{n}$** concentration ratio (Figure III-4b). Two advantages resulted from the use of this thermoresponsive molecule. First, color emission modulation from red at 244 K to blue at 348 K was achieved thanks to the transformation of **SZMC3$_{zw}$** into **SZMC3$_{n}$** when heating. Second, white light was generated at 288 K by finely tuning the red emission from **SZMC3$_{zw}$** as to properly complement **BPEA** turquoise fluorescence (Figure III-4).[38]

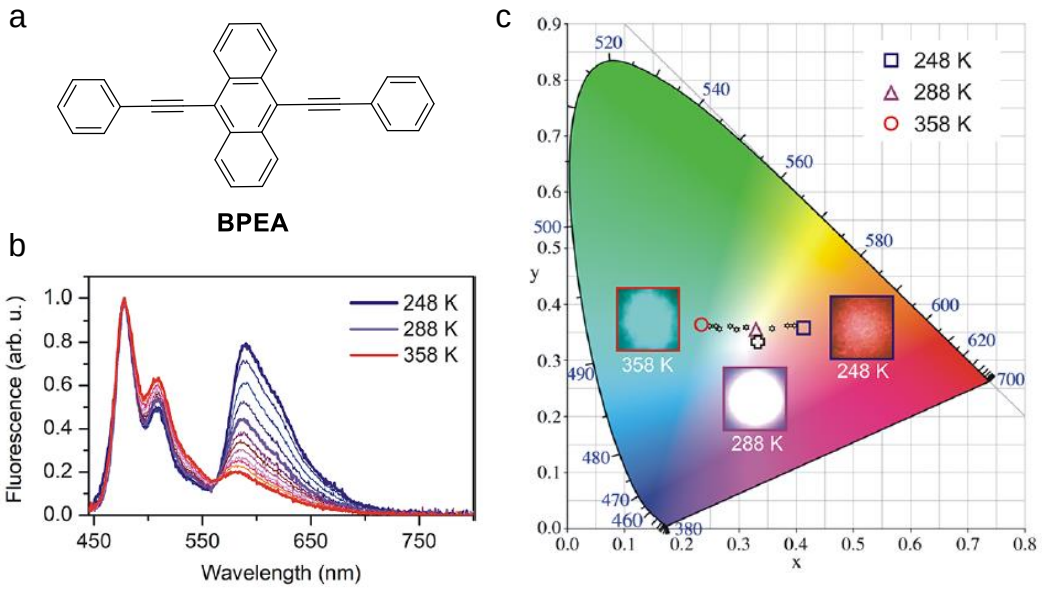

Figure III-4. (a) Structure of the turquoise-emissive fluorophore **BPEA**. (b) Temperature dependence of the emission spectra of microcapsules loaded with liquid solutions of

SZMC3$_{zw}$ and **BPEA** (λ_{exc} = 428 nm). (c) Temperature dependent chromaticity coordinates of the capsules emission in the CIE 1931 color space when heating from 248 K to 358K. The insets show photographs of the emission produced at 248, 288 and 358 K.[38]

The multistimuli-responsive and multistate properties of **SZMC3** have also been used to prepare molecular analogues of field-effect transistors (FETs), the most common type of transistors in current electronic systems (Figure III-5a).[4] To mimic this behavior, the nonfluorescent **SZMC3$_a$** compound was dissolved in an ionic liquid (1-ethyl-3-methylimidazolium bis(trifluorosulfonyl)imide), placed between a glass substrate and an ITO layer, and put in contact with a Pt and a saturated calomel (SCE) electrodes. Under the ITO layer, a hot plate was placed to modulate the temperature (Figure III-5b). In such fashion, the response of the transistor could be measured as a fluorescence increase when nonemissive **SZMC3$_a$** transformed into the emissive **SZMC3$_{zw}$** upon controlled electrolysis, whereas the amplitude of this response could then be regulated by heating the sample to modify the tautomeric equilibrium between **SZMC3$_{zw}$** and **SZMC3$_n$** (Figure III-5b).[4]

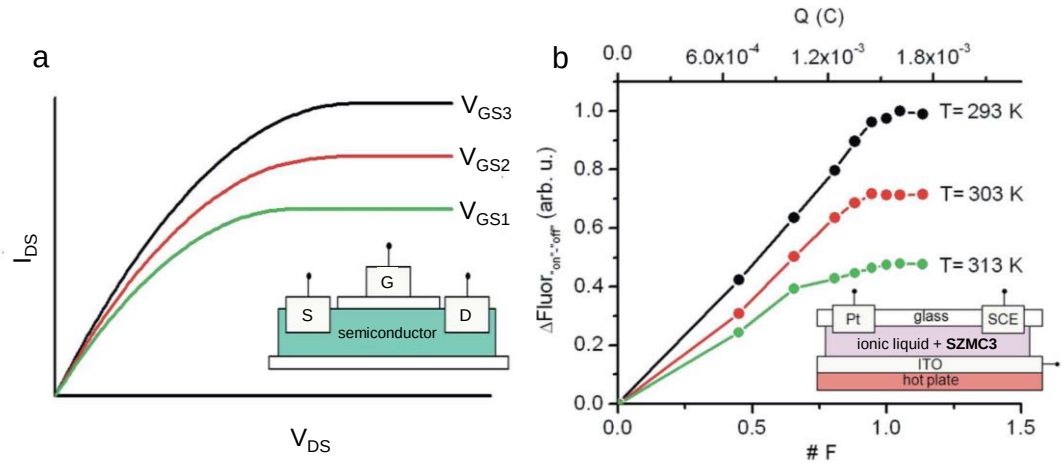

Figure III-5. (a) Example of the performance of a field-effect transistor where the source-to-drain current (I_{DS}) at a given voltage (V_{DS}) can be amplified by the application of a gate-to-source electric field (V_{GS}). (b) **SZMC3**-based molecular FET analogue where the fluorescence response is measured upon oxidation of **SZMC3$_a$** by applying an oxidative potential (E_{ap} = 1.3 V (vs SCE)) at different temperatures. The insets in each graphic show an schematic representation of (a) a FET and (b) the analogue **SZMC3** FET.[4]

Another example of the multistate behavior of SZMCs was more recently reported by Haldar and coworkers, who described an additional state obtained upon acid addition to **SZMC2$_{zw}$**.[39] The new form presented neither color nor fluorescence, thus suggesting the disappearance of the cyclohexadienyl anion chromophore. These authors proposed that this state arises from the protonation of the *para* position of the cyclohexadienyl anion moiety, thus resulting in the cationic structure shown in

Figure III-6a (**SZMC2'$_c$**). However, unequivocal experimental proofs for this elucidation were not provided. In spite of this, Haldar and coworkers demonstrated that transformation between the zwitterionic and cationic states of **SZMC2** was a reversible process accessible upon acid-base addition and they proposed interesting applications for such pH-dependent interconversion.[39] Firstly, it was used for ammonia sensing in the atmosphere, obtaining a response with concentrations as low as 0.1 ppm. The authors also explored a facile methodology to implement online analyte detection on a solid substrate by printing unreadable barcodes with the colorless cationic derivative of **SZMC2** on a cellulose paper. As soon as exposed to ammonia, **SZMC2$_{zw}$** was formed on the printed areas, thus revealing the barcode and allowing the measurement of the base concentration from the color intensity (Figure III-6b).[39] In a similar manner, they applied the same concept for the preparation of invisible security inks using the cationic state of **SZMC2** to print a message on a paper that could only be read when exposed to ammonia (Figure III-6c).[39]

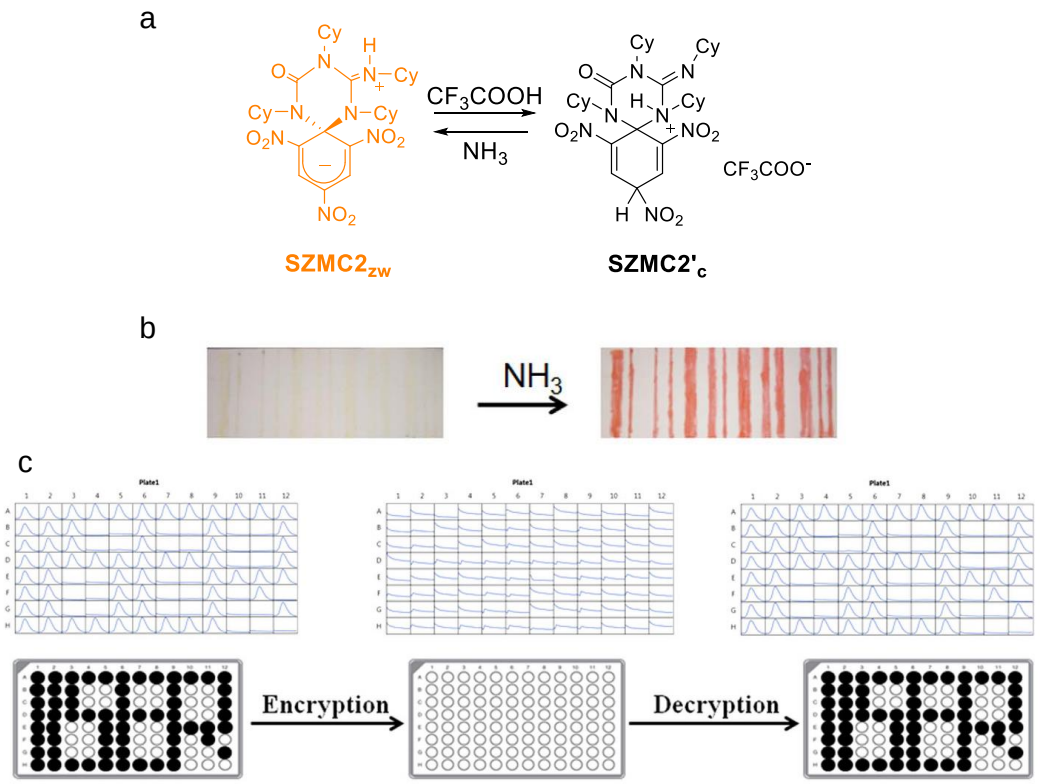

Figure III-6 (a) Acid-base switching reaction between **SZMC2$_{zw}$** and the proposed structure for the novel cationic state **SZMC2'$_c$**.[39] (b) **SZMC2'$_c$**-based barcode for ammonia detection and (c) halochromic security ink prepared from **SZMC2'$_c$**.[39]

III.2. OBJECTIVES

In light of these precedents on the multistimuli-responsive and multistate behavior of **SZMC1-4**, the following objectives were proposed for this part of the thesis (Scheme III-5):

- To investigate whether the *chromic and fluorescent thermal switching* mechanisms revealed for **SZMC3** could be expanded to the other SZMC switches.
- To explore if the *protonated* ***SZMC$_c$*** *state* could also be reversibly generated for other switches different from **SZMC2** and exploit this behavior and the already described **SZMC2$_a$-SZMC2$_{zw}$** interconversion to prepare *wide range pH sensors*. In addition, this would allow us to unambiguously elucidate the structure of **SZMC2$_c$** (and of the cationic state generated for other SZMCs) in order to assess the proposal from Haldar and coworkers.[39]
- To study if the transformation between the zwitterionic and cationic states of SZMC switches could be triggered *electrochemically*. This, in combination with the already reported redox switching between **SZMC1$_a$** and **SZMC1$_{zw}$**, could enable the preparation of *electrochromic and electrofluorochromic displays*.
- To analyze the effect of two new external stimuli for reversibly modulating the color and/or fluorescence of SZMC switches: (a) the *addition of anions*, and (b) the *variation of solvent nature*, which would open the door to use these molecular systems as *chemosensors*.

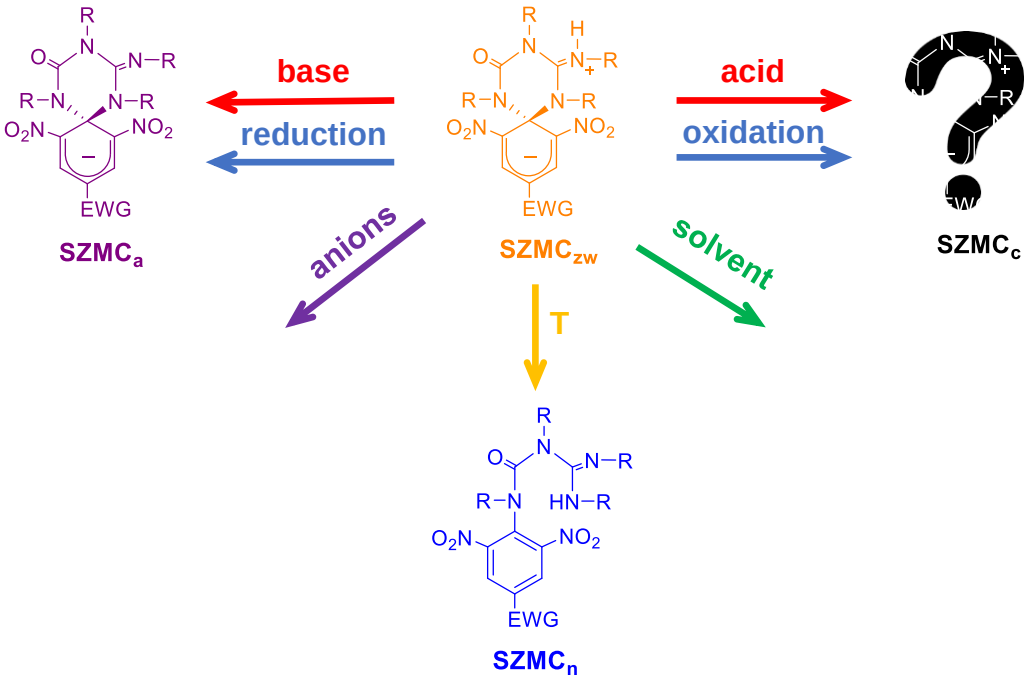

Scheme III-5. Schematic representation of the switching mechanisms that will be explored in this chapter for SZMCs, which will be then applied for the preparation of a variety of

functional materials: wide range pH detectors, electrochromic and electrofluorochromic displays, and chemical sensors.

III.3. Synthesis of spirocyclic zwitterionic Meisenheimer complexes SZMC1-4

In a first step, all the SZMC switches of interest in this work (i.e., **SZMC1**, **SZMC2**, **SZMC3** and **SZMC4**) were synthesized following the general procedure described in the literature (see Scheme III-2a).[36] **SZMC1** and **SZMC2** were obtained as a mixture of their zwitterionic state with the respective monosubstitution byproducts **5** and **6**, in a one-step synthesis from the commercially available picric acid (**1**) and an excess of diisopropyl carbodiimide (DIC, **3**) and dicyclohexyl carbodiimide (DCC, **4**), respectively. Although quantitative conversion of the starting phenols was observed, **5** and **6** were found to be the major products of the process and all the attempts to increase the selectivity towards the formation of the target SZMC switches failed. Actually, after purification by flash column chromatography, **SZMC1** and **SZMC2** could only be obtained in 35% and 22% yield, respectively, which is in good agreement with the precedents in our group[25,36] (Scheme III-6).

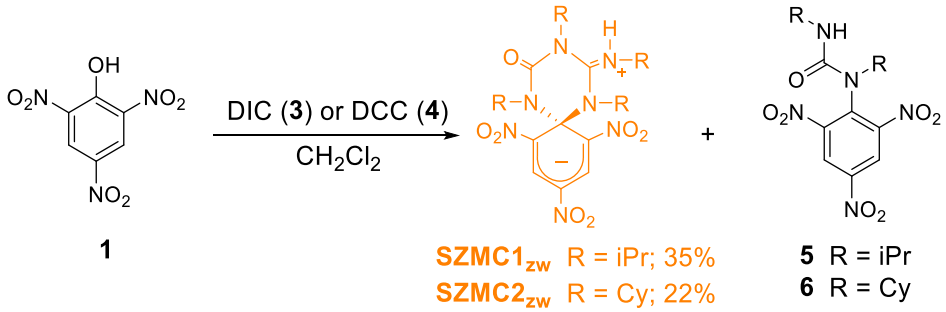

Scheme III-6: Synthesis of **SZMC1** and **SZMC2**.

The synthesis of **SZMC3** and **SZMC4** was carried out following the same procedure as for **SZMC1** and **SZMC2** but using commercially available 2,6-dinitro-4-(trifluoromethyl)phenol (**2**) as a precursor instead. As already described,[4,25] rather poor conversion to the desired switches was again observed that could not be further improved. After separation from the excess of carbodiimide and the monosubstitution byproducts **7** and **8** by flash column chromatography, **SZMC3** and **SZMC4** were indeed obtained in 26% and 11% yield, respectively (Scheme III-7). It must be noted that the pure zwitterionic state of the two SZMC switches could not be isolated in this case. Instead, they were produced as an irresoluble equilibrium tautomeric mixture of **SZMC$_{zw}$** and **SZMC$_n$**, as previously reported in our group.[4,25] The **SZMC$_{zw}$**:**SZMC$_n$** isomer ratio obtained in deuterated acetonitrile at room temperature was 24:76 and 6:94 for **SZMC3** and **SZMC4**, respectively.

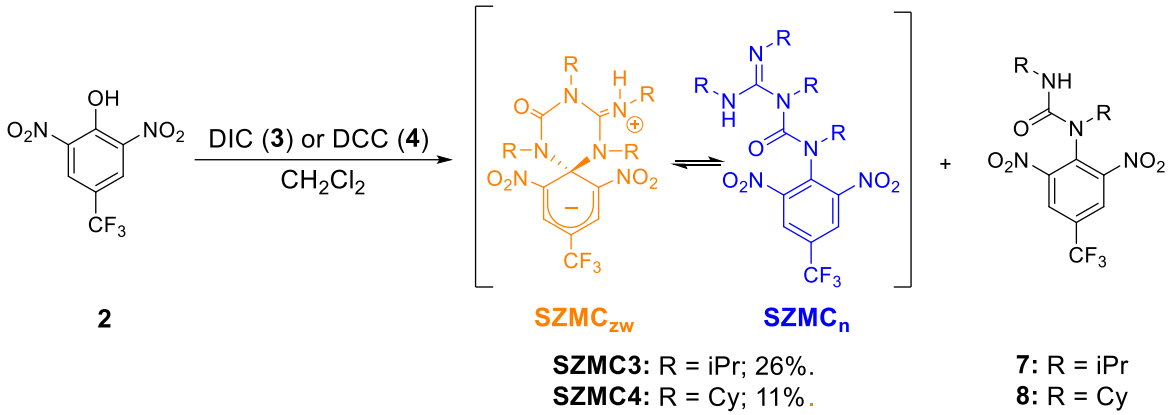

Scheme III-7: Synthesis of **SZMC3** and **SZMC4**.

III.4. Thermal switching of spirocyclic zwitterionic Meisenheimer compounds

III.4.1. SZMC1 and SZMC2

As previously explained in the introduction of this chapter, our group had reported that **SZMC3$_{zw}$** spirocyclic structure was not stable at room temperature due to the lower electron-withdrawing character of the trifluoromethyl group. Consequently, the neutral state of **SZMC3** is isolated as an equilibrium mixture of the spirocyclic zwitterionic **SZMC3$_{zw}$** state and the neutral aromatic form **SZMC3$_{n}$**, as just mentioned in section III.3.[4] Although this situation had not been observed for **SZMC1$_{zw}$** and **SZMC2$_{zw}$**, we hypothesized that it might also occur in a very low extent at room temperature that would not be detectable by ^{1}H-NMR spectroscopy. Based on our previous observation that the conversion of **SZMC3$_{zw}$** into **SZMC3$_{n}$** was favored upon heating, we then decided to investigate the stability of **SZMC1$_{zw}$** and **SZMC2$_{zw}$** at high temperatures, thus aiming to generate larger amounts of the neutral aromatic forms of these compounds. In pursue of this objective, we performed temperature variable ^{1}H-NMR experiments in deuterated dimethyl sulfoxide (DMSO-d_6), as it allowed us to reach temperatures as high as 400 K to test the thermal stability of **SZMC1$_{zw}$** and **SZMC2$_{zw}$**. It must be noted that such type of measurements had been previously used to investigate the **SZMC3$_{zw}$-SZMC3$_{n}$** equilibrium, as the interconversion between these two tautomers is slow enough as to be resolved by ^{1}H-NMR for a large thermal range.[4]

Figure III-7 shows the results obtained by ^{1}H-NMR spectroscopy when DMSO-d_6 solutions of **SZMC1$_{zw}$** and **SZMC2$_{zw}$** were heated up to 398 K. The appearance of a new set of resonances that could be directly assigned to the open aromatic form of these compounds was not observed in either case. However, a clear broadening of

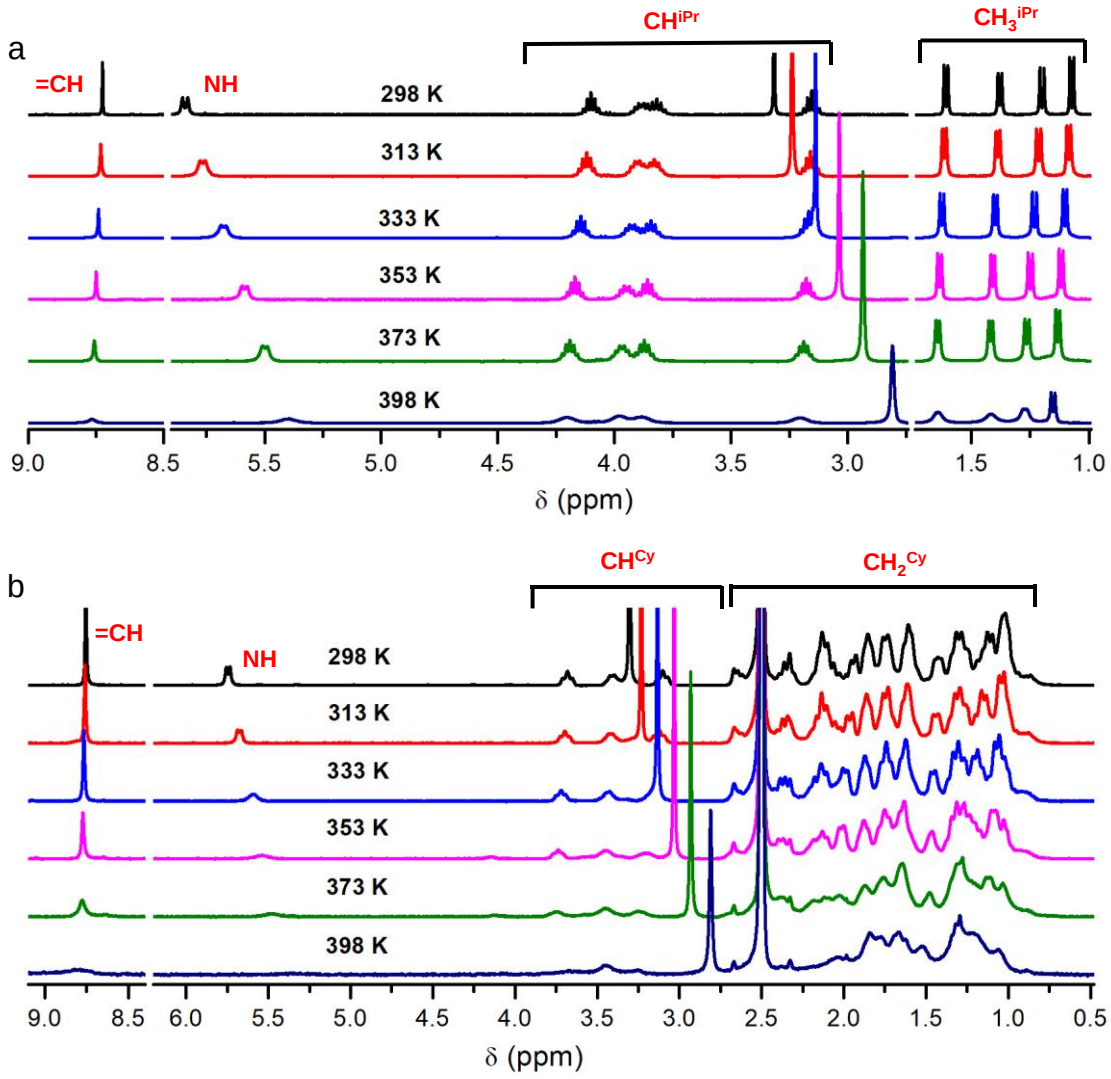

Figure III-7. Temperature variation of the ^{1}H-NMR spectra (400 MHz, DMSO-d_6) of (a) **SZMC1$_{zw}$** and (b) **SZMC2$_{zw}$**.

the narrow ^{1}H-NMR signals was registered at high temperatures, which is indicative of the occurrence of some dynamic process when heating. We ascribed this effect to the formation of the neutral aromatic tautomers **SZMC1$_n$** and **SZMC2$_n$**. Unfortunately, the tautomerization process is expected to take place at large rates at such high temperatures, which probably prevented us from resolving the two sets of signals for each of the isomeric species; instead, only broadened peaks were obtained. Interestingly, the onset temperature at which signal broadening (i.e., **SZMC$_{zw}$-SZMC$_a$** isomerization) occurred was 398 K for the isopropyl substituted **SZMC1$_{zw}$** (Figure III-7a) and 358 K for the cyclohexyl substituted **SZMC2$_{zw}$** (Figure III-7b). This suggests that steric hindrance from the pending alkyl chains also plays a role in the stability of the zwitterionic form of SZMC switches, as we further investigated for **SZMC4** (see below). In any case, because of the high temperatures required to trigger significant ring-opening of the spirocyclic structure of **SZMC1$_{zw}$** and **SZMC2$_{zw}$**,

the use of the thermally-induced chromic and fluorescent changes for these compounds should be of limited interest for practical applications.

III.4.2. SZMC4

As reported for **SZMC3**,[4] the trifluoromethyl-substituted spirocyclic structure of **SZMC4** also lacks the thermal stability observed for the trinitro derivatives **SZMC1** and **SZMC2**. Actually, this explains why **SZMC4** was isolated from the synthesis as an equilibrium mixture of **SZMC4$_{zw}$** and **SZMC4$_{n}$** (see section III.3). Therefore, **SZMC4** is a good candidate to show the thermoinduced chromic and fluorescent switching behavior already described for **SZMC3**.[4] In addition, because the nature of the pending alkyl groups of the triazene ring seems to affect the thermal stability of the spirocyclic structure of the zwitterionic state, **SZMC4** may show a different and complementary thermal response to **SZMC3**. For this reason, we investigated the thermal switching properties of **SZMC4**.

In a first step, we analyzed by ^{1}H-NMR spectroscopy the effect of temperature on the tautomeric equilibrium between **SZMC4$_{zw}$** and **SZMC4$_{n}$**. For this experiment, we chose deuterated acetonitrile as a solvent and focused our attention in two particular sets of ^{1}H-NMR signals: (a) the peak at δ = 8.20 ppm, which arises from the two equivalent protons of the cyclohexadienyl anion of **SZMC4$_{zw}$**; and (b) the peaks between 8.40 and 8.60 ppm, which are assigned to the two aromatic protons of **SZMC4$_{n}$** (Figure III-8). It must be noted that these nuclei become anisochronous below 288 K, probably due to the hindered rotation of the bulky urea substituent when cooling. As a consequence, a transition from a narrow single resonance to two different signals was observed for the aromatic protons of **SZMC4$_{n}$** when varying the temperature. In spite of this, the data in Figure III-8 clearly indicates that the **SZMC4$_{zw}$**:**SZMC4$_{n}$** concentration ratio changes with temperature and, as previously described for **SZMC3**,[4] that the stability of the spirocyclic structure of **SZMC4$_{zw}$** decreases when heating. This was confirmed by determining the composition of the tautomeric equilibrium mixture from 238 to 298 K using the area of the low-field ^{1}H-NMR peaks (Figure III-8). Unfortunately, this estimation was not possible for temperatures higher than 298 K due to two factors: (a) the low concentration of **SZMC4$_{zw}$** that may fall under the detection limit of the technique, and (b) the difficulty of resolving **SZMC4$_{zw}$** and **SZMC4$_{n}$** signals due to the faster interconversion rate when heating, as already observed for **SZMC1**-**2** (see section III.4.1). Indeed, the latter is corroborated by the broadening of the **SZMC4$_{zw}$** signal at temperatures higher than 288 K.

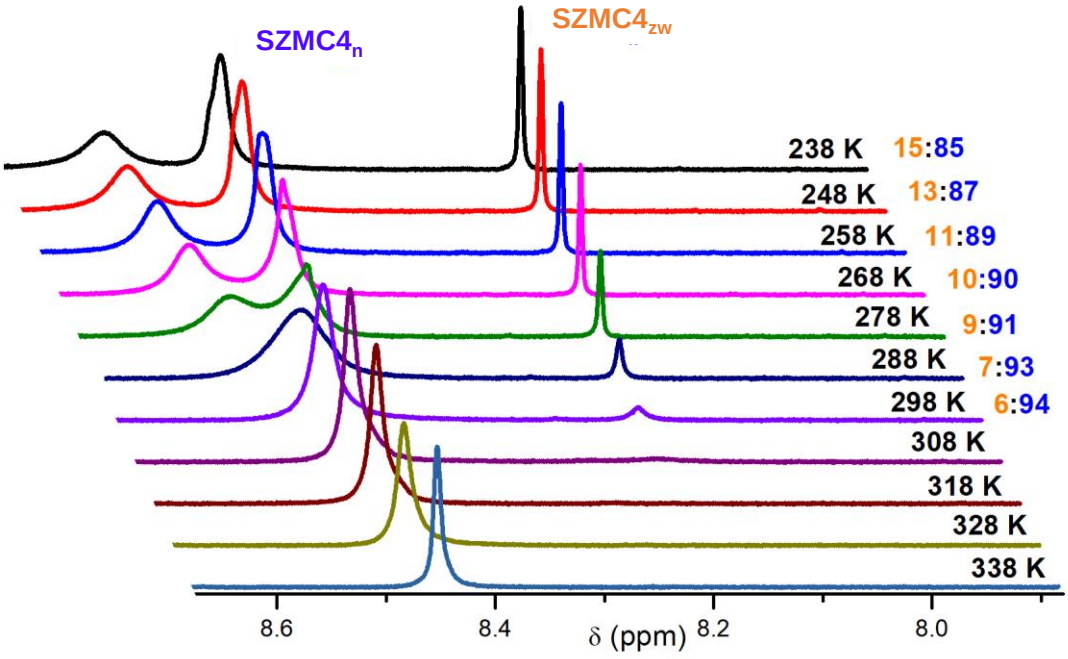

Figure III-8. Temperature variation of the ^{1}H-NMR spectrum (400 MHz, CD_3CN) of the equilibrium tautomeric mixture of **SZMC4$_{zw}$** and **SZMC4$_{n}$**.

As **SZMC4$_{n}$** does not contain the cyclohexadienyl anion fluorophore, the thermal variation of the **SZMC4$_{zw}$**:**SZMC4$_{n}$** concentration ratio should result in additional changes in absorption and emission. In fact, we observed a significant intensity loss of the absorption band in the visible region of **SZMC4$_{zw}$** upon temperature increase (Figure III-9a). This is in agreement with thermally-induced tautomerization towards the colorless isomer **SZMC4$_{n}$**, whose aromatic chromophore must only absorb in the UV region by analogy with similar compound **8** (Figure III-9a). However, some contribution to the visible absorption decrement may come from the thermal variation of the molar absorptivity of **SZMC4$_{zw}$**. To account for this effect, we basified a solution of the **SZMC4$_{zw}$**-**SZMC4$_{n}$** mixture and recorded the UV-vis absorption spectra of the resulting **SZMC4$_{a}$** anionic form for the same temperature range (Figure III-9b). It must be noted that **SZMC4$_{a}$** presents the same fluorophore as **SZMC4$_{zw}$** and, when analyzed by temperature-dependent ^{1}H-NMR spectroscopy, did not show transformation into a nonspirocyclic structure. Therefore, the small differences observed for the visible absorption band of **SZMC4$_{a}$** with temperature must be attributed to variation of molar absorptivity, which confirm that the larger changes measured for the **SZMC4$_{zw}$**-**SZMC4$_{n}$** mixture were mainly due to thermal interconversion between these two isomers. Actually, when correcting the absorption data for the **SZMC4$_{zw}$**-**SZMC4$_{n}$** sample taking into account the thermal variation of **SZMC4$_{a}$** absorption, we obtained absorption decrement values that correlate well

with ^{1}H-NMR data and, more importantly, we could estimate the composition of the equilibrium tautomeric mixture at temperatures higher than 298 K.

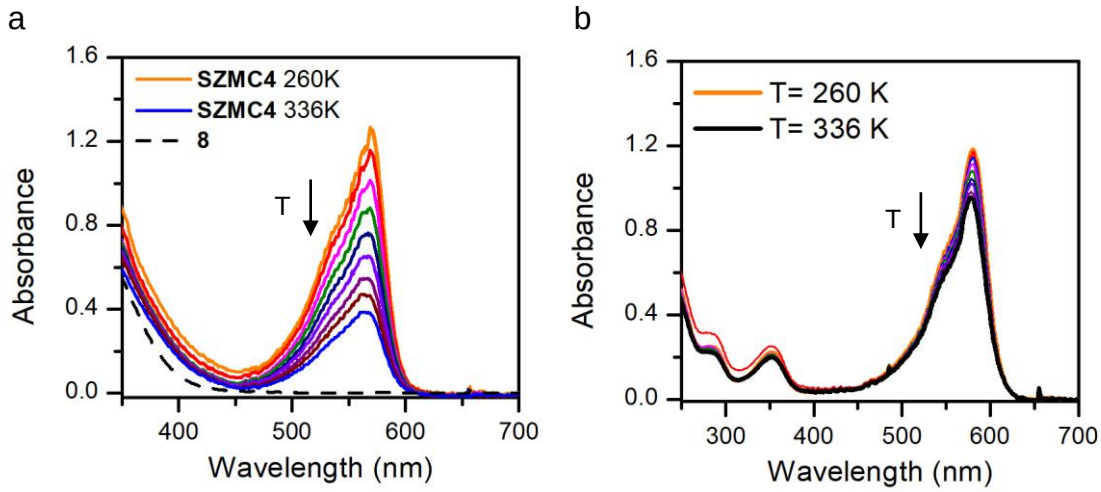

Figure III-9. Temperature variation of the UV-vis spectra of (a) the tautomeric mixture of **SZMC4$_{zw}$** and **SZMC4$_{n}$** (c_{SZMC4} = 8.2x10^{-4} M) and (b) **SZMC4$_{a}$** (c_{SZMC4} = 7.3x10^{-5} M) in acetonitrile. Spectra were measured at 260, 265, 272, 280, 288, 298, 307, 316, 326 and 336 K. In (a) the UV-vis spectrum of **8** at room temperature is also shown (c_{8} = 7.6x10^{-4} M), the monosubstitution byproduct of **SZMC4** synthesis that presents a very similar aromatic chromophore to that in **SZMC4$_{n}$** (see Scheme III-7).

Figure III-10b shows the thermal variation of the **SZMC4$_{zw}$** molar fraction ($\chi_{SZMC4_{zw}}$) in the neutral state of the switch obtained from the combined ^{1}H-NMR and colorimetric data, which is compared to that previously reported for **SZMC3$_{zw}$** (Figure III-10b).[4] Two main conclusions can be drawn from these results: (a) thermal variation of **SZMC4$_{zw}$** concentration follows a rather linear trend for most of the temperature range investigated; and (b) the amount of zwitterionic form determined for **SZMC4** is significantly lower than the reported value for **SZMC3** at the same temperature.[4] This confirms the previous observation made for **SZMC1**-**2** that the introduction of bulkier groups in the triazine ring of SZMCs (i.e., cyclohexyl instead isopropyl substituents) destabilizes their spirocyclic structure and favors tautomerization towards the neutral aromatic forms.

Thanks to the thermal control of the **SZMC4$_{zw}$**-**SZMC4$_{n}$** equilibrium and the different optical properties of these two isomers, the performance of **SZMC4** as a fluorescent switch could be modulated upon temperature variations. As shown in Figure III-10c, the amplitude of **SZMC4** emission modulation between its nonfluorescent anionic and fluorescent neutral states produced by acid-base titration can be tuned thermally by varying the **SZMC4$_{zw}$**-**SZMC4$_{n}$** concentration ratio. Thus, the *"On"*-"Off" fluorescence response of the system undergoes a 313% increase when cooling

down from 336 K to 260 K in acetonitrile. Therefore, **SZMC4** behaves as both a multistimuli-responsive and a multistate molecular switch, in a similar fashion to **SZMC3**.[4] However, because of the larger steric hindrance imparted by its cyclohexyl substituents, **SZMC4** shows a different thermal switching behavior than **SZMC3**, which makes it be better suited for applications where temperature control of fluorescence switching is required at very low temperatures.

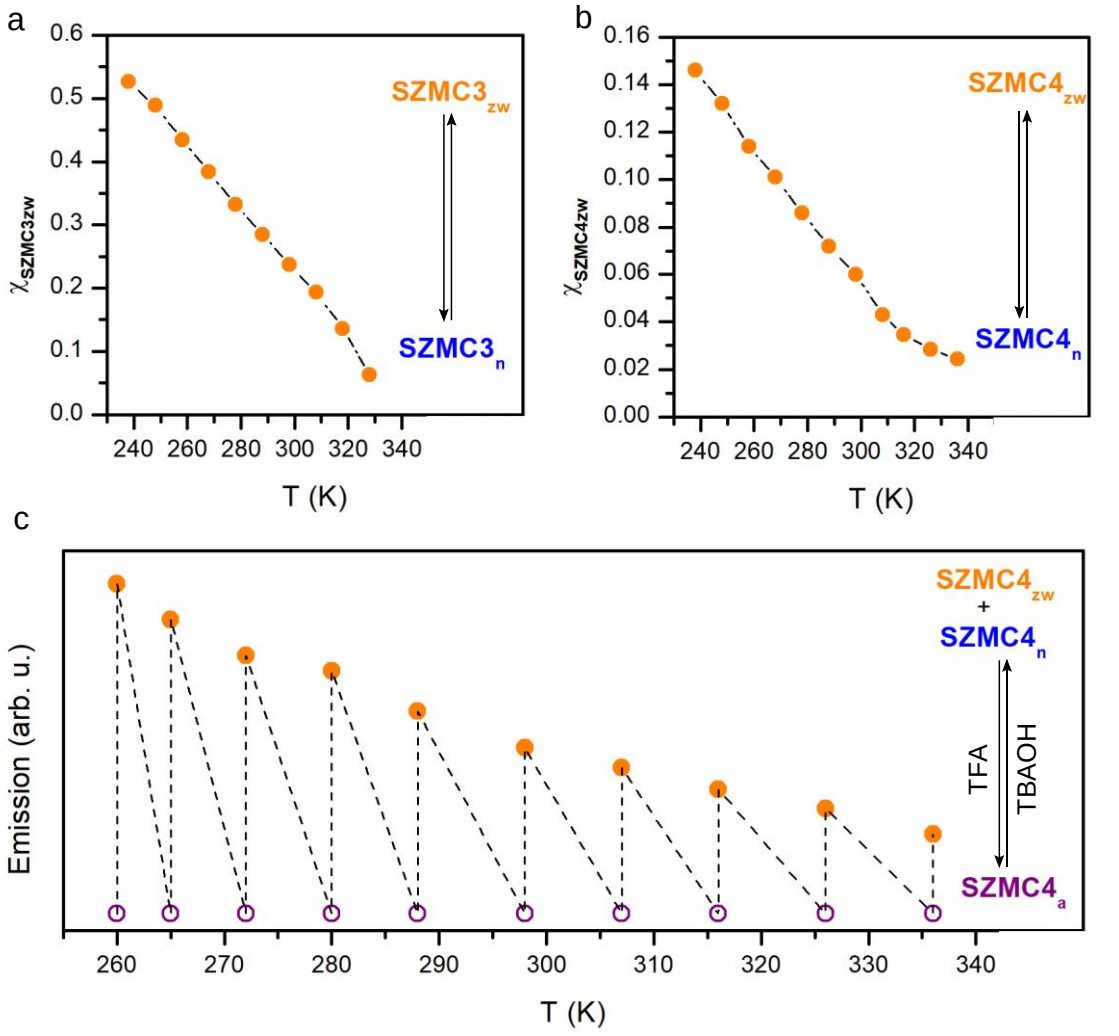

Figure III-10. Temperature variation of χ_{SZMCzw} in the neutral state of the switch for (a) **SZMC3**[4] and (b) **SZMC4** in acetonitrile. (c) Temperature dependence of the emission switching amplitude between the fluorescent $\mathbf{SZMC4_{zw}}$-$\mathbf{SZMC4_n}$ and nonfluorescent $\mathbf{SZMC4_a}$ states in acetonitrile (c_{SZMC4} = 1.2x10^{-4} M; λ_{exc} = 532 nm). Acetonitrile solutions of trifluoroacetic (TFA) and tetrabutylammonium hydroxide (TBAOH) were used to interconvert between the neutral and anionic forms of **SZMC4**.

III.5. ACID-BASE SWITCHING OF SPIROCYCLIC ZWITTERIONIC MEISENHEIMER COMPOUNDS

III.5.1. A novel cationic state for SZMC switches

By the beginning of this thesis, two protonation states with distinct optical properties had been described in our group for all the members of the SZMC family: a zwitterionic (**SZMC$_{zw}$**) and an anionic form (**SZMC$_{a}$**). In addition, a neutral aromatic state resulting from the thermally-induced aperture of the spirocyclic zwitterionic form had been reported for **SZMC3**[4] and subsequently observed for **SZMC1-2** (see section III.4.1) and **SZMC4** (see section III.4.2) in this work. It is the structure of this neutral aromatic form that inspired us to search for an additional protonation state for SZMCs, as the **SZMC$_{zw}$**-to-**SZMC$_{n}$** transformation converts an acidic guanidinium moiety into a basic guanidine group upon opening of the spirocyclic structure. Therefore, this newly formed guanidine substituent could be protonated by acid addition to achieve a cationic state with no fluorescence nor color due to the lack of the cyclohexadienyl chromophore (**SZMC$_{c}$**, Scheme III-8). It must be noted that such type of structure is in disagreement with the proposal made by Haldar and coworkers for **SZMC2$_{c}$** shortly after the start of this thesis (see Figure III-6a),[39] which further motivated us to unambiguously establish the existence and nature of a cationic state for SZMC switches.

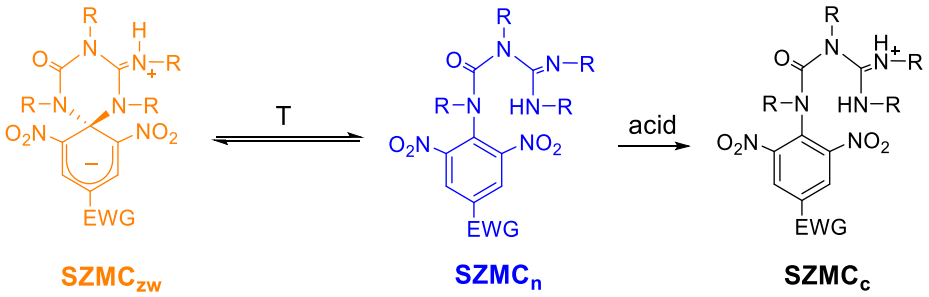

Scheme III-8: Proposed formation and structure of the cationic state **SZMC$_{c}$**.

III.5.1.a. SZMC1 cationic state

To test our hypothesis, we first focused on parent SZMC switch **SZMC1**. For this compound, we started by recording the absorption and emission spectra of **SZMC1$_{zw}$** in acetonitrile upon consecutive additions of trifluoroacetic acid. As expected if the proposed protonated structure **SZMC1$_{n}$** was formed, both the emission and absorption in the visible region disappeared after 1 equivalent of TFA was added (Figure III-11). As commented above, this is compatible with the loss of the spirocyclic cyclohexadienyl anion chromophore upon protonation, since the resulting trinitroaromatic group that would be generated resembles that of the

monosubstitution byproduct **5** of the synthesis of **SZMC1**, which has been reported to be colorless and nonfluorescent.[37]

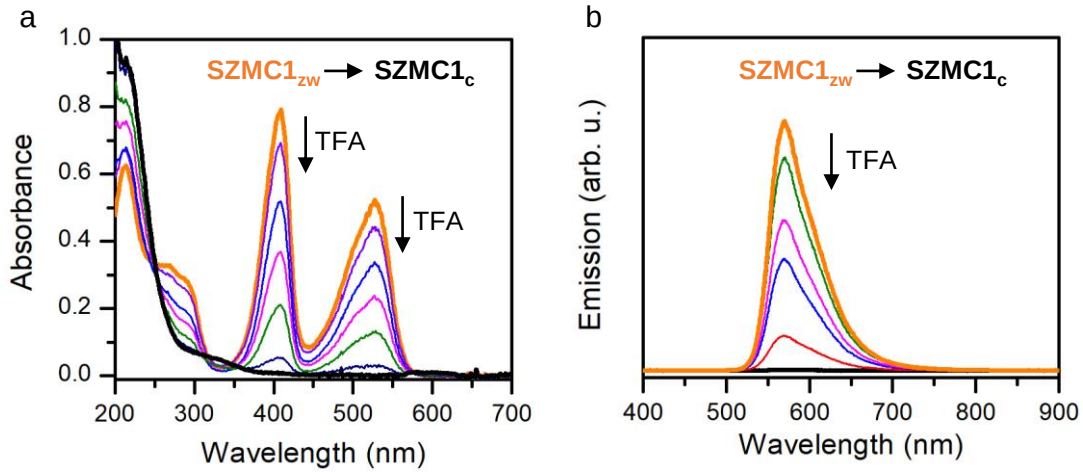

Figure III-11 Evolution of the (a) absorption ($c_{\mathbf{SZMC1}}$ = 6.0x10^{-5} M) and (b) emission spectra ($c_{\mathbf{SZMC1}}$ = 1.5x10^{-5} M; λ_{exc} = 473 nm) of **SZMC1$_{zw}$** upon titration with TFA in acetonitrile, which should generate the cationic state **SZMC1$_c$**.

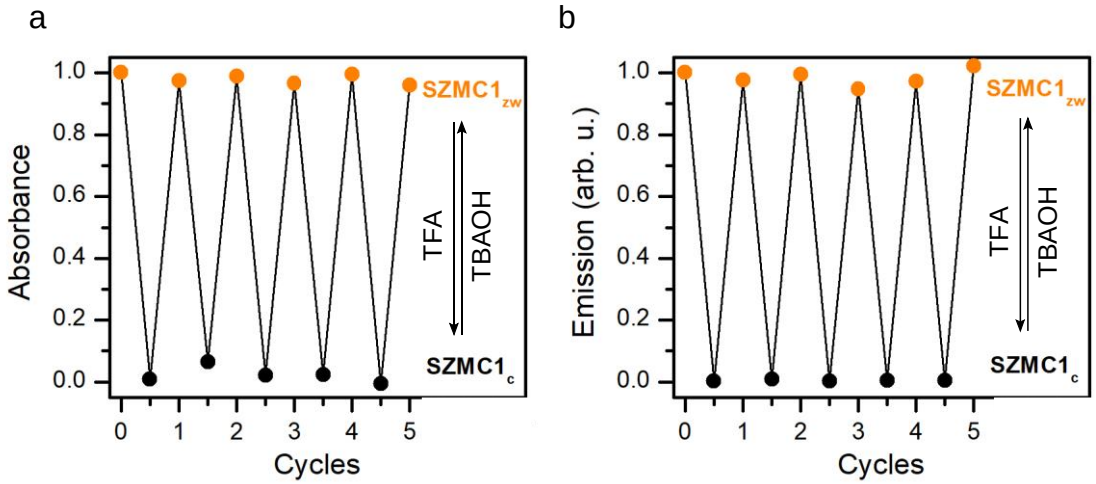

Figure III-12. Variation of **SZMC1** (a) absorbance ($c_{\mathbf{SZMC1}}$ = 6.0x10^{-5} M; λ_{abs} = 527 nm) and (b) emission ($c_{\mathbf{SZMC1}}$ = 1.5x10^{-5} M; λ_{exc} = 473 nm) in acetonitrile upon 5 cycles of acid-base titration with TFA and TBAOH to promote interconversion between the zwitterionic and cationic states of the switch. Absorption and emission values are referred to those measured for the initial **SZMC1$_{zw}$** solution. In all the cases, emission values were obtained by integrating over the fluorescence spectrum of the sample.

The next step was demonstrating the reversibility of the protonation process, a key aspect for any given switching mechanism. To do so, the recovery of the initial **SZMC1$_{zw}$** optical properties was tested upon base addition. Indeed, when 1 equivalent of TBAOH was added to a previously protonated solution of **SZMC1$_{zw}$,**

the original emission and color were restored. Actually, the reversible acid-base transformation between **SZMC1$_{zw}$** and **SZMC1$_{n}$** could be repeated up to 5 times with no significant alteration of the absorption and fluorescence signals measured (Figure III-12). Therefore, this confirmed the capacity to expand the switching operation of **SZMC1** to an additional protonation state, thus making this compound a multistate acid-base-responsive system.

It is worth mentioning that the loss of color and fluorescence observed for **SZMC1$_{zw}$** upon acid addition is not only compatible with the structure proposed by us for **SZMC1$_{c}$**, but also with the cationic structure suggested by Haldar and coworkers for the analogous switch **SZMC2**, where the spirocyclic backbone is preserved and protonation takes place at the 4 position of the cyclohexadienyl anion moiety.[39] To discriminate between these two possibilities, we followed the titration of **SZMC1$_{zw}$** with TFA by ^{1}H-NMR spectroscopy in deuterated acetonitrile. As shown in Figure III-13a, gradual disappearing of the characteristic signals of **SZMC1$_{zw}$** was observed after TFA addition, such as the signal at δ = 8.82 ppm corresponding to the cyclohexadienyl anion protons, the doublet at δ = 4.76 ppm assigned to the NH proton, the four isopropyl CH (CH^{iPr}) multiplets at δ = 4.21, 4.01, 3.87 and 3.22 ppm, and the four isopropyl methyl (CH_3^{iPr}) doublets at δ = 1.65, 1.39, 1.23 and 1.13 ppm. Interestingly, the resulting **SZMC1$_{c}$** spectrum showed less signals than **SZMC1$_{zw}$**, most notably a large singlet at δ = 9.07 ppm (2H), two CH^{iPr} multiplets at δ = 4.40 (1H) and 4.04 (1H) ppm, and two CH_3^{iPr} doublets at δ = 1.24 (6H) and 1.14 (6H) ppm. More intriguing were the three broad resonances found at δ = 7.25, 3.86 and around 1.23 ppm, which after integration were assigned to 2H, 2H and 12H, respectively (see the square-labeled signals in Figure III-13a(vi)). These findings strongly suggest that dynamic processes affect the ^{1}H-NMR spectrum of **SZMC1$_{c}$** at room temperature, thus leading to the coalescence of some separate signals for anisochronous nuclei. For this reason, we recorded the same spectrum at lower temperatures (Figure III-13b) and clearly observed that the signal at δ = 7.25 ppm split into two doublets (empty triangles in Figure III-13b), while the resonance at δ = 3.86 was separated into two multiplets (empty circles in Figure III-13b).

Based on these results, the structural elucidation of **SZMC1$_{c}$** was finally accomplished by analyzing the 2D ^{1}H-NMR COSY spectrum of this compound at 248 K (Figure III-14a), where two relevant sets of off-diagonal signals were observed. On one hand, strong correlation was found between two signals in the CH_3^{iPr} region and the two new peaks at δ = 3.88 and 3.68 ppm resolved at low temperatures (empty arrows in Figure III-14a). These resonances can therefore be assigned to the two other CH^{iPr} groups of **SZMC1$_{c}$**, which somehow become equivalent at 298 K. It must be noted that this is only possible if the spirocyclic structure of **SZMC1$_{zw}$** is opened upon protonation, as we propose. On the other hand, each of the doublets emerging

when cooling at δ = 7.39 and 7.19 ppm also showed correlation with the CH^{iPr} multiplets at δ = 3.88 and 3.68 ppm (full arrows in Figure III-14a). Hence, they must correspond to the initial NH nucleus of **SZMC1$_{zw}$** and the additional proton introduced in **SZMC1$_c$** upon TFA addition, both of which must lie next to isopropyl groups and be isochronous at sufficient high temperatures. Consequently, all these findings point to the structure proposed by us in Figure III-14b as the only possible for **SZMC1$_c$**, where protonation takes place on a nitrogen atom of the guanidine group.

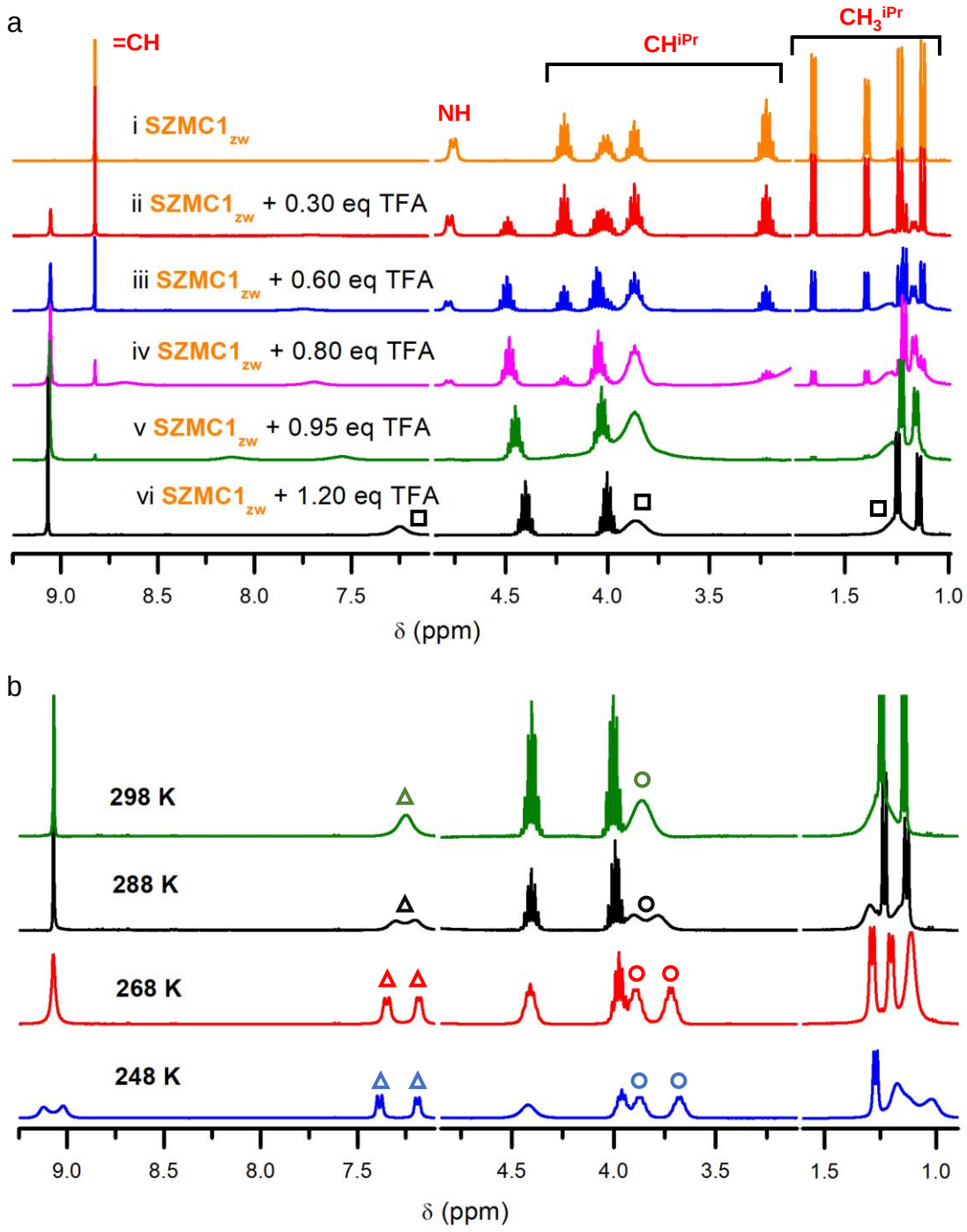

Figure III-13. (a) Variation of the ^{1}H-NMR (400 MHz, CD_3CN, 298K) spectrum of **SZMC1$_{zw}$** upon titration with TFA until **SZMC1$_c$** is formed (**SZMC1$_{zw}$** + 1.20 eq TFA). Empty squares

are used to denote the broad signals in the (vi) spectrum. (b) ^{1}H-NMR spectrum (400 MHz, CD_3CN) of **SZMC1$_c$** at 298, 288, 268 and 248 K. Empty triangles and empty circles indicate the newly formed signals arising from the splitting of the broad room temperature resonances at δ = 7.25 and 3.86 ppm signals upon cooling, respectively.

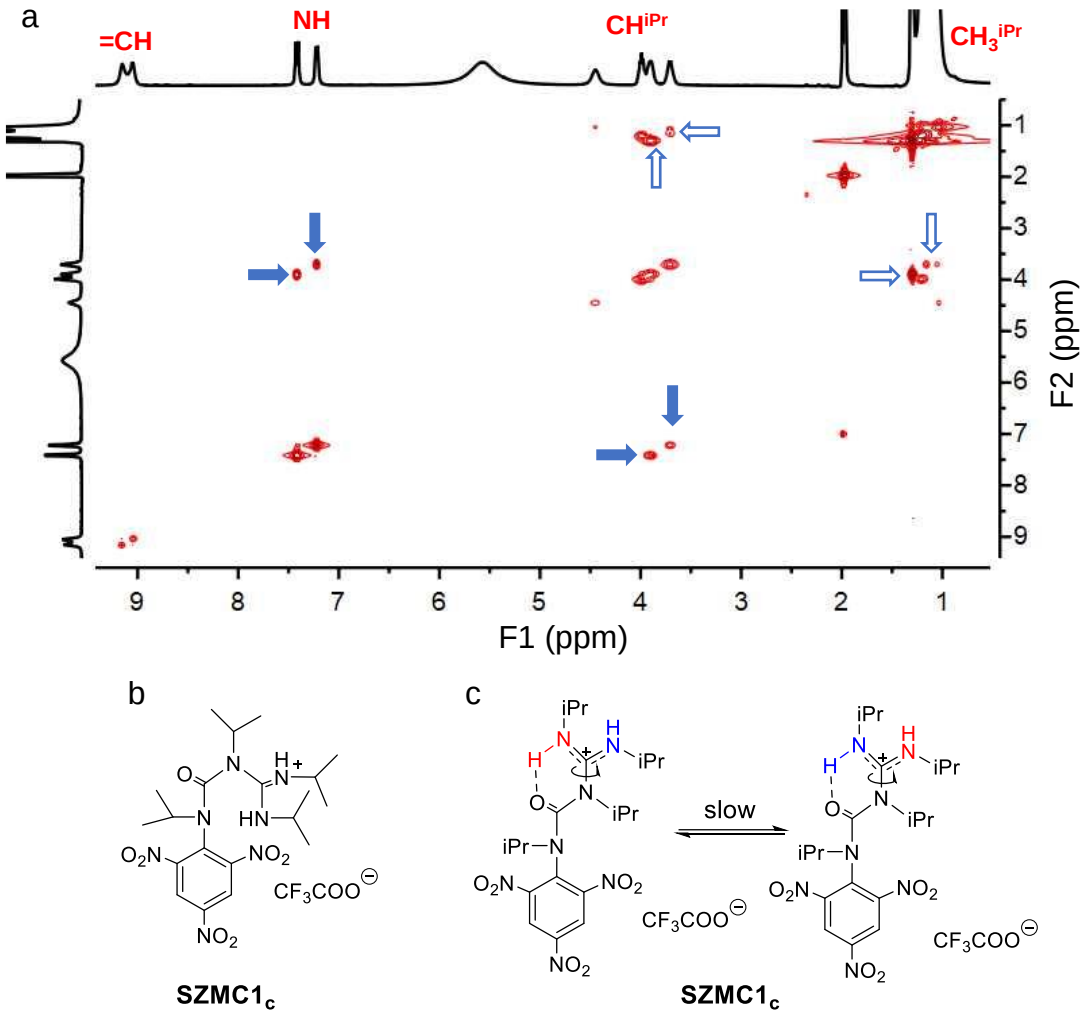

Figure III-14. (a) 2D ^{1}H-NMR COSY spectrum (400 MHz, CD_3CN) of **SZMC1$_c$** at 248 K, where full and empty arrows are used to indicate cross-peaks between NH and CH^{iPr} nuclei and CH^{iPr} and CH$_3$^{iPr} protons, respectively. (b) Proposed structure for **SZMC1$_c$** based on our spectroscopic measurements. (c) Possible mechanism for conformational rotation restriction around the N-C bond of the guanidinium group due to intramolecular H-bonding between the guanidinium protons and the urea carbonyl moiety.

Besides being consistent with the variation of the optical properties **SZMC1$_{zw}$** after acid addition, the structure proposed for **SZMC1$_c$** also provides an explanation for the temperature-dependent dynamic effects observed in the ^{1}H-NMR spectra of this compound. In the absence of processes that desymmetrize the structure of **SZMC1$_c$**, the two NH protons and the nearby isopropyl groups must be equivalent and give rise to only one set of ^{1}H-NMR resonances, as essentially observed at 298 K. However, those nuclei should be anisochronous and split into different groups of ^{1}H-

NMR signals if the formation of intramolecular H-bonding between the guanidinium protons and the urea carbonyl groups of **SZMC1$_c$** becomes of relevance and the exchange between the two structures shown in Figure III-14c sufficiently slows down. Most likely, this is what occurs when cooling, thus accounting for signal splitting in ^{1}H-NMR spectroscopy. Actually, because such intramolecular interaction must also hinder the rotation of the bulky urea substituent around the trinitrophenyl core, this might also contribute to make the aromatic protons of **SZMC1$_c$** separate into well-resolved resonances at 248 K (see Figure III-13b).

III.5.1.b. **SZMC2 cationic state**

Because of the discrepancy between the structure elucidated by us for **SZMC1$_c$** and that proposed by Haldar and coworkers[39] for the cationic state of **SZMC2** (Scheme III-9), we decided to also investigate the protonation process of **SZMC2$_{zw}$** by means of ^{1}H-NMR spectroscopy. In particular, we first monitored the titration of **SZMC2$_{zw}$** with TFA by ^{1}H-NMR spectroscopy and, once the protonated form was generated, temperature-dependent and correlation experiments were performed.

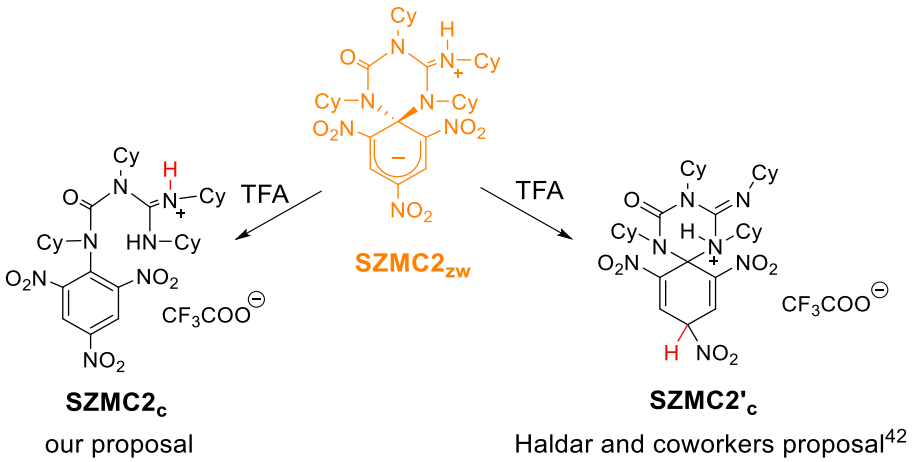

Scheme III-9 Structures proposed for the cationic state of **SZMC2** in the literature (**SZMC2'$_c$**)[39] and based on our elucidation of the analogous **SZMC1$_c$** compound (**SZMC2$_c$**). The hydrogen atom in red corresponds to the proton introduced in **SZMC2$_c$** and **SZMC2'$_c$** after treatment with TFA.

To establish which was the correct structure for the cationic state of **SZMC2**, we mainly focused our attention on the ^{1}H-NMR characterization of the two possible types of labile protons: (a) the two NH protons in **SZMC2$_c$**, both of which should show cross-correlation with the nearby isopropyl nuclei; and (b) the bisallylic proton in **SZMC2'$_c$**, which should couple to the cyclohexadienyl hydrogens. Unfortunately, the protonated state of **SZMC2$_c$** was not soluble enough to perform the experiments in deuterated acetonitrile, as previously done with **SZMC1**. On the other hand, no labile protons were seen by ^{1}H-NMR spectroscopy in deuterated chloroform, which would have prevented us to discriminate between **SZMC2$_c$** and **SZMC2'$_c$** structures. The

experiments were therefore carried out in deuterated dimethyl formamide (DMF), where the most characteristic ^{1}H-NMR signals of **SZMC2$_{zw}$** faded after TFA addition: the singlet at δ = 8.89 ppm for the cyclohexadienyl anion protons, the doublet at δ = 5.95 ppm for the NH group, and the multiplets at δ = 3.83, 3.58, 3.31 and 2.82 ppm for the cyclohexyl CH (CH^{Cy}) protons (Figure III-15). Simultaneously, several new resonances clearly appeared upon acid titration. Thus, three new signals emerged at δ = 4.33 (1H), 3.73 (2H) and 3.53 ppm (1H), which were attributed to the CH^{Cy} protons of the cationic state of **SZMC2**. Interestingly, this means that two of such groups became equivalent upon protonation, a feature only expected for our **SZMC2$_c$** structure due to the aperture of the spirocyclic backbone. In addition, four new downfield resonances at δ = 9.52 (1H), 9.33 (1H), 9.20 (1H) and 9.01 (1H) ppm were observed, which could only be ascribed to NH, aromatic or cyclohexandienyl protons due to their chemical shifts (Figure III-15). As one of such peaks should arise from the proton introduced upon TFA titration, it could hardly correspond to the bisallylic hydrogen in **SZMC2'c**, for which a much lower ^{1}H-NMR chemical shift value would be expected.

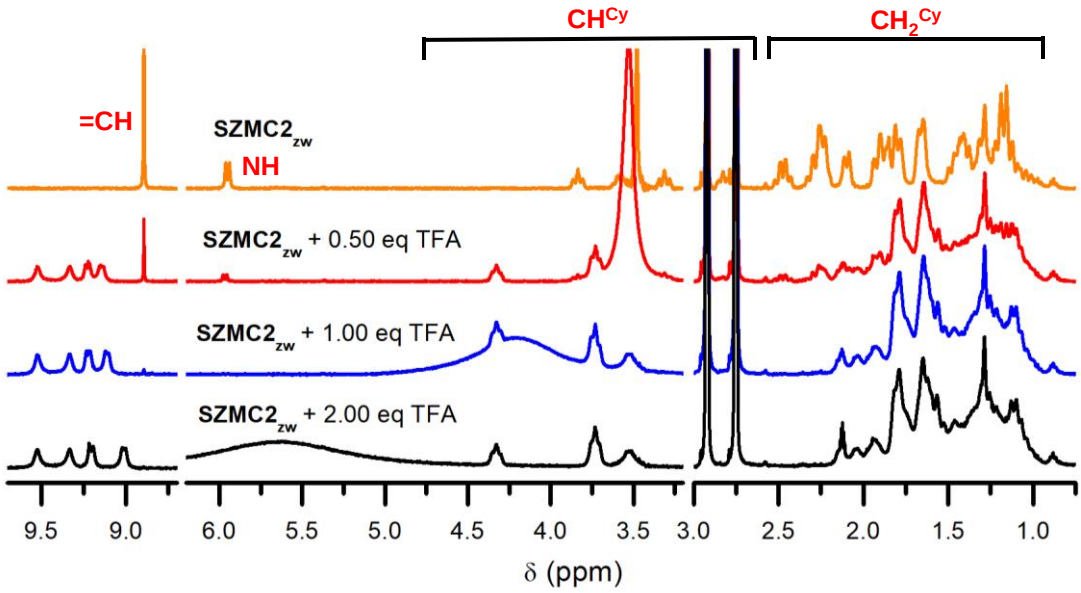

Figure III-15. Variation of the ^{1}H-NMR (400 MHz, DMF-d_7, 298K) spectrum of **SZMC2$_{zw}$** upon titration with TFA.

Next, temperature variable ^{1}H-NMR measurements were carried out for the protonated DMF-d_7 solution of **SZMC2** (Figure III-16a). These experiments showed that the peaks at δ = 9.52 and 9.33 ppm coalesced in a single signal when heated at 318 K (empty circles in Figure III-16a), which demonstrate the occurrence of conformational constraints that make the corresponding nuclei anisochronous at lower temperatures. Moreover, the signals at δ = 9.20 and 9.01 ppm could be identified as two doublets at 288 K, whose assignment to NH or cyclohexadienyl

protons would provide evidence for either **SZMC2$_c$** or **SZMC2'$_c$** structures, respectively (empty triangles in Figure III-16a). This was accomplished with the 2D ^{1}H-NMR COSY experiment shown in Figure III-16b that revealed cross-peaks between the signals at δ = 9.20 and 9.01 ppm with two CH cyclohexyl protons, as indicated with red arrows. Therefore, they must be attributed to the NH protons of the guanidinium group of **SZMC2$_c$**, which lie next to two cyclohexyl substituents. In addition, the resonances at δ = 9.52 and 9.32 ppm only showed cross-correlation

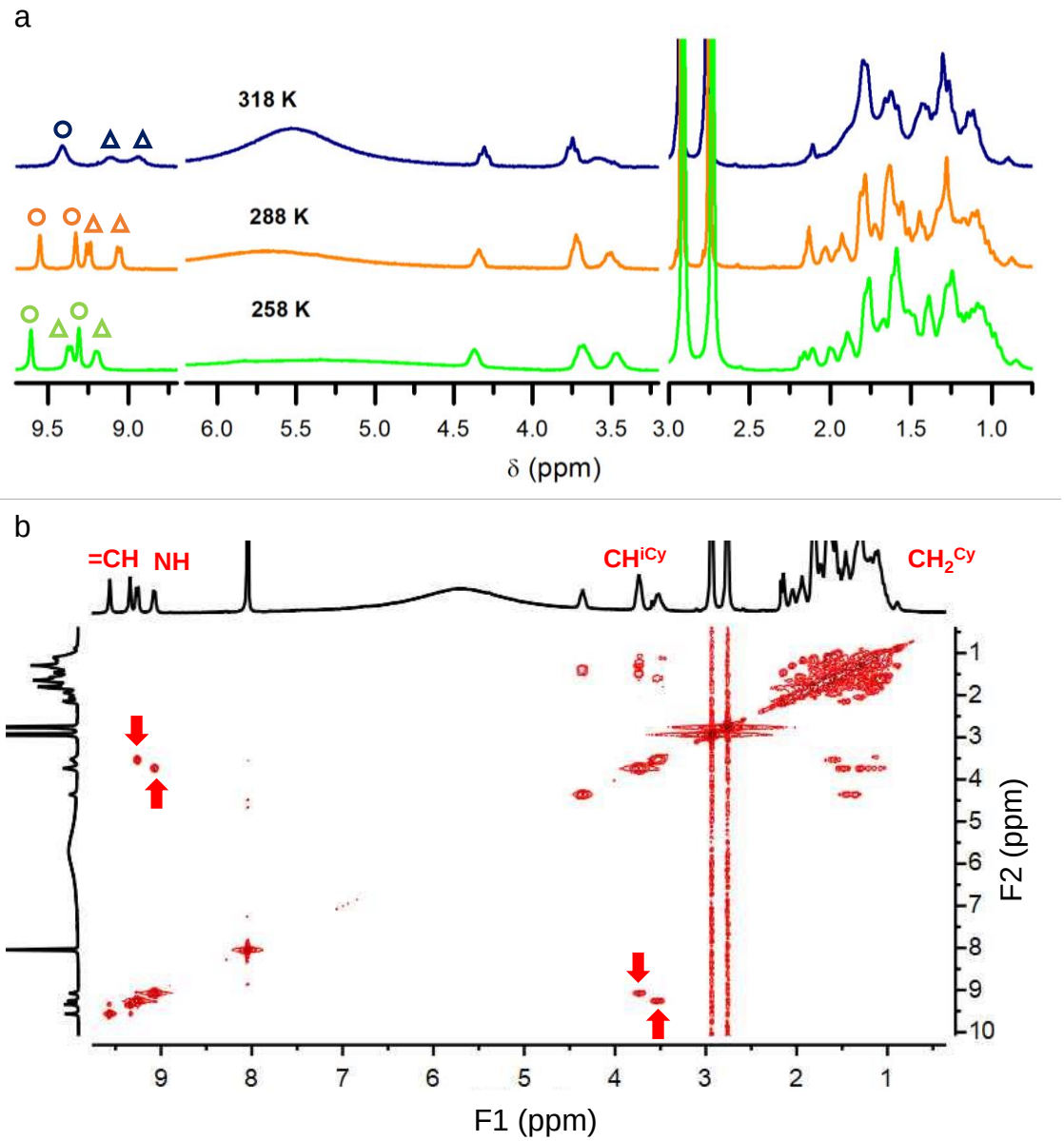

Figure III-16. (a) ^{1}H-NMR spectrum (400 MHz, DMF-d_7) of the cationic state of **SZMC2** at 318**,** 288 and 258 K. For sake of clarity, the aromatic signals that arise from the peak at δ = 9.41 ppm at 318 K are indicated with empty circles, while the two other resonances in the low-field region are labeled with empty triangles. (b) 2D ^{1}H-NMR COSY spectrum (400 MHz, DMF-d_7) of the cationic state of **SZMC2** at 288 K. Cross-peaks between NH and CH^{Cy} protons are signaled with arrows.

between them and had no coupling to any other proton in the molecule. On one hand, this allows assigning them to the two aromatic protons of **SZMC2$_c$**, which become anisochronous due to the hindered rotation of the bulky urea group, as previously observed for **SZMC1$_c$**. On the other hand, it proves that no bisallylic proton exists in the protonated state of **SZMC2** that could additionally couple to the cyclohexadienyl protons, as proposed in **SZMC2'$_c$**. Consequently, these findings clearly corroborate that the cationic state of **SZMC2** is **SZMC2$_c$** and has the same structure as **SZMC1$_c$**.

Once elucidated the structure of the protonated state **SZMC2**, we also explored the acid-base-mediated chromic and fluorescence switching between the **SZMC2$_{zw}$** and **SZMC2$_a$** states of this compound. For this, we conducted acid (TFA) and base (TBAOH) titration of **SZMC2$_{zw}$** in acetonitrile. As shown in Figure III-17, acid addition over **SZMC2$_{zw}$** led to color and fluorescence disappearance, as reported by Haldar and coworkers[39] and previously observed for **SZMC1**. Moreover, reversibility of this process by the addition of TBAOH was demonstrated, an acid-base switching sequence that could be repeated over at least 5 cycles without apparent degradation.

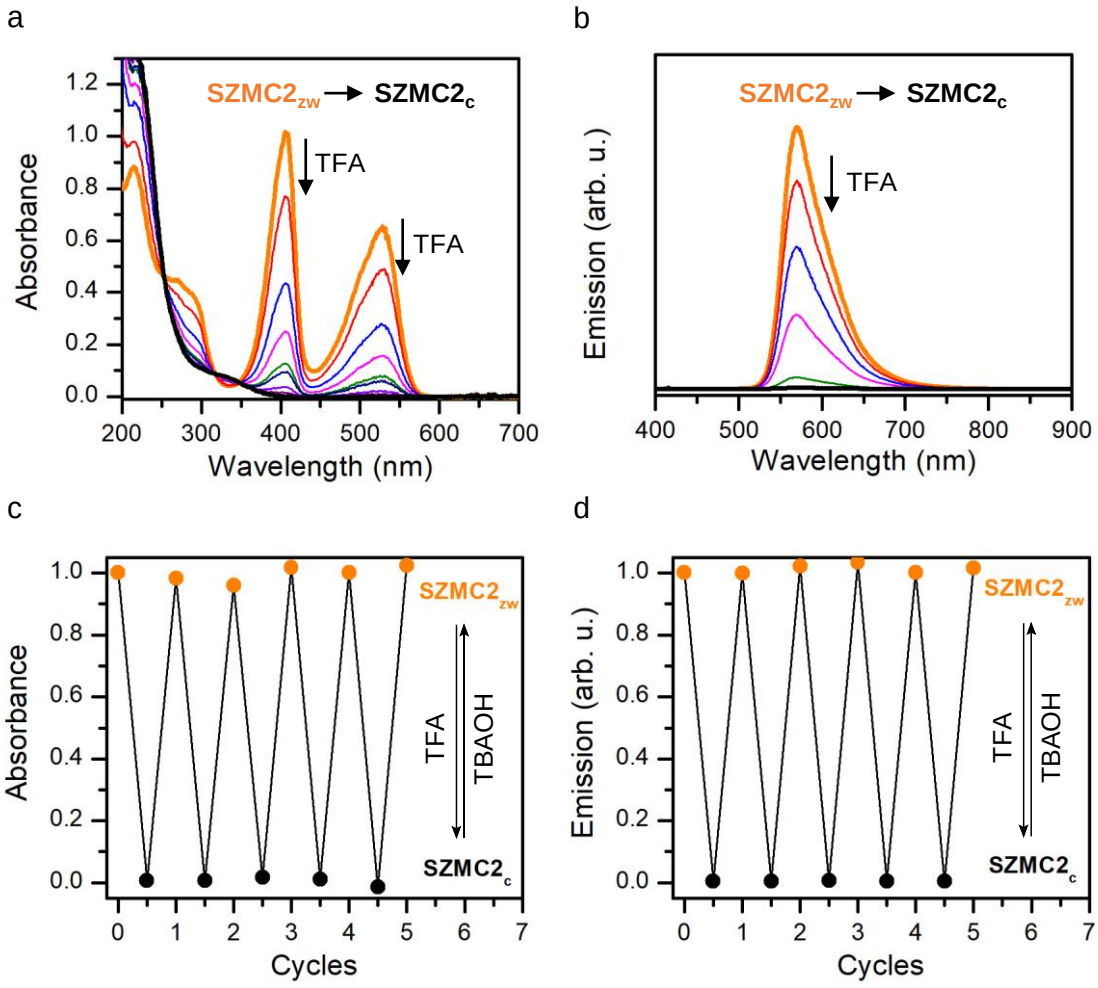

Figure III-17. (a-b) Evolution of the (a) absorbance (c_{SZMC2} = 8.1x10^{-5} M) and (b) emission (c_{SZMC2} = 3.2x10^{-5} M; λ_{exc} = 473 nm) spectra of **SZMC2$_{zw}$** in acetonitrile upon acid titration

with TFA. (c-d) Variation of **SZMC2$_{zw}$** (c) absorbance ($c_{\mathbf{SZMC2}}$ = 5.9x10^{-5} M; λ_{abs} = 527 nm) and (d) emission ($c_{\mathbf{SZMC2}}$ = 2.7x10^{-5} M; λ_{exc} = 473 nm) in acetonitrile upon 5 cycles of acid-base titration with TFA and TBAOH to promote interconversion between the zwitterionic and cationic states of the switch. Absorption and emission values are referred to those measured for the initial **SZMC2$_{zw}$** solution. In all the cases, emission values were obtained by integrating over the fluorescence spectrum of the sample.

III.5.1.c. **SZMC3 cationic state**

Once established that a novel cationic state was possible for the trinitrosubstituted **SZMC1** and **SZMC2** switches, we investigated if this behavior was also shared by other SZMCs bearing different, less thermally-stable spirocyclic fluorescent cores. For this, we focused our attention on **SZMC3**, whose zwitterionic state already exists in equilibrium with a nonnegligible amount of the open neutral form **SZMC3$_n$** that is equivalent to the deprotonated structure of the expected **SZMC3$_c$** state (Scheme III-10).

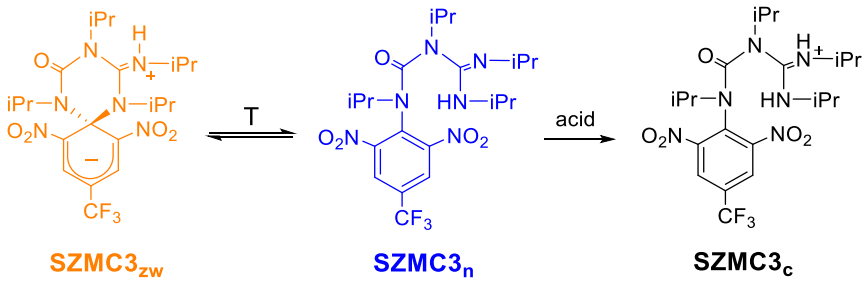

Scheme III-10. Tautomeric equilibrium between **SZMC3$_{zw}$** and **SZMC3$_n$**, which should favor the formation of the protonated **SZMC3$_c$**. structure upon acid addition.

For this reason, we expected **SZMC3** to become colorless and nonfluorescent upon TFA titration in acetonitrile, as we had previously seen for other SZMCs. The results of these experiments are shown in Figure III-18. First, it was observed that both the absorbance and fluorescence of the tautomeric **SZMC3$_{zw}$-SZMC3$_n$** mixture completely faded upon acid addition (Figure III-18a-b). More importantly, we could demonstrate that, after base-mediated recovery of the initial spectra, the acid-base conversion process between the neutral and cationic states of **SZMC3** could be repeated several times without significant absorbance nor emission losses (Figure III-18c-d). Therefore, **SZMC3** also operates as a multistate acid-base fluorescent switch.

After confirming the acid-induced chromic and fluorescence switching of the neutral state of **SZMC3**, we also investigated the protonation process in acetonitrile by ^{1}H-NMR spectroscopy. Interestingly, the complex pattern of signals corresponding to the initial tautomeric mixture of **SZMC3$_{zw}$** and **SZMC3$_n$** converted into a single set of peaks upon addition of sufficient TFA. This corroborates that both isomers convert into a unique cationic product upon protonation (Figure III-19). In a similar fashion to

what was observed for **SZMC1$_c$**, both narrow and broad signals were observed in the ^{1}H-NMR spectrum of **SZMC3$_c$**: (a) a defined singlet for the aromatic protons at δ = 8.68 ppm (2H), two CH^{iPr} multiplets at δ = 4.45 (1H) and 4.02 (1H) ppm, and two CH_3^{iPr} doublets at δ = 1.22 (6H) and 1.15 (6H) ppm; and (b) broad resonances at δ = 7.00 (2H), 3.82 (2H) and around 1.23 (12H) ppm, which were further investigated with a series of temperature-variable ^{1}H-NMR spectra.

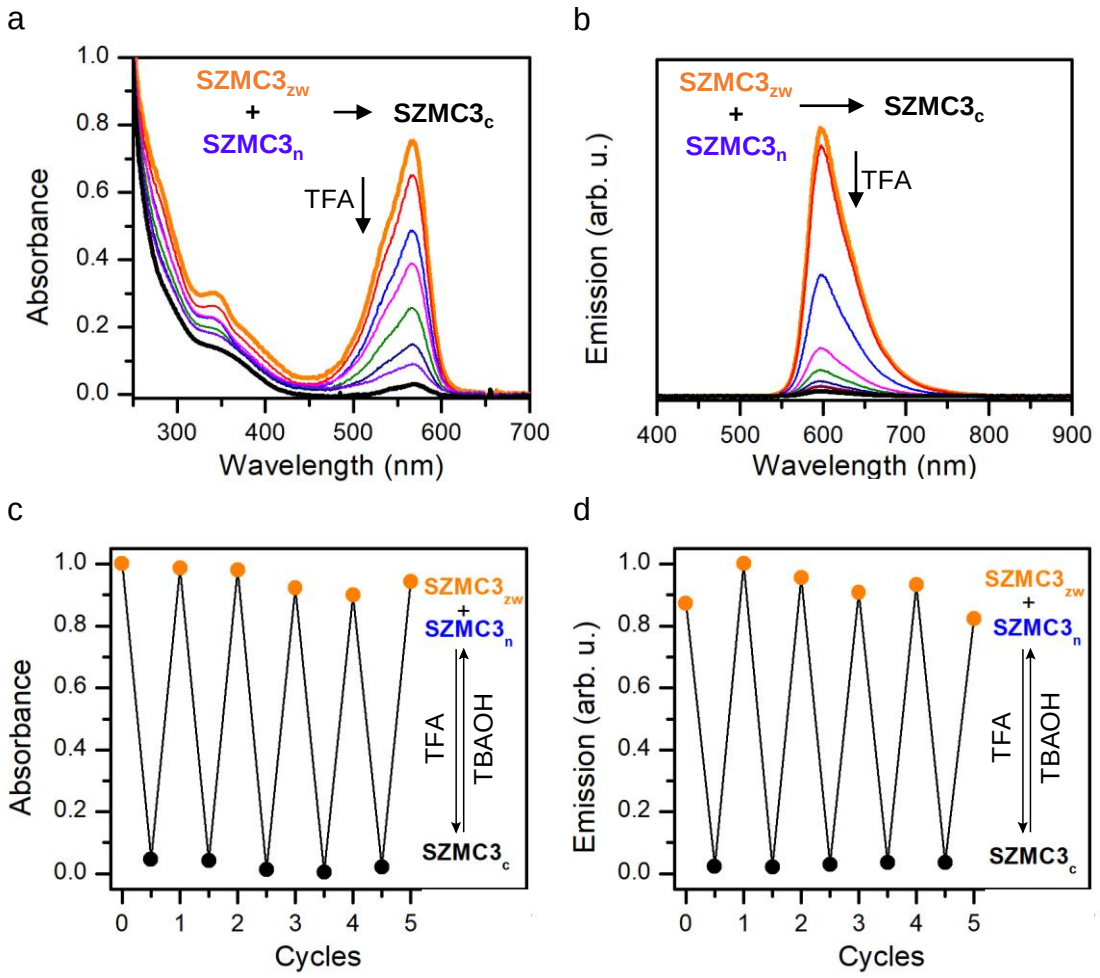

Figure III-18. (a-b) Evolution of the (a) absorbance (c_{SZMC3} = 2.0x10^{-4} M) and (b) emission (c_{SZMC3} = 4.0x10^{-5} M; λ_{exc} = 532 nm) spectra of the tautomeric **SZMC3$_{zw}$** and **SZMC3$_n$** mixture upon acid titration with TFA in acetonitrile. (c-d) Variation of **SZMC3$_{zw}$-SZMC3$_n$** (c) absorbance (c_{SZMC3} = 2.0x10^{-4} M; λ_{abs} = 567 nm) and (d) emission (c_{SZMC3} = 4.0x10^{-5} M; λ_{exc} = 532 nm) in acetonitrile upon 5 cycles of acid-base titration with TFA and TBAOH to promote interconversion between the neutral and cationic states of the switch. Absorption and emission values are referred to those measured for the initial **SZMC3$_{zw}$-SZMC3$_n$** mixture. In all the cases, emission values were obtained by integrating over the fluorescence spectrum of the sample.

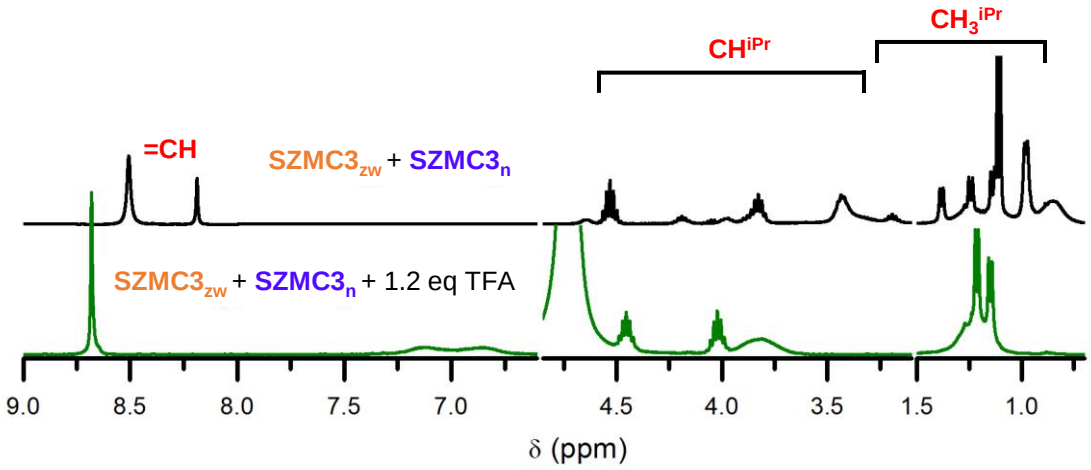

Figure III-19. Variation of the ^{1}H NMR (400 MHz, CD_3CN, 298K) spectrum of the tautomeric mixture **SZMC3$_{zw}$** and **SZMC3$_{n}$** upon titration with TFA.

Upon cooling it was observed that the resonances at δ = 7.00 and 3.82 ppm further split into two separate doublets and multiplets at 238 K, respectively (Figure III-20a). In addition, the 2D ^{1}H-NMR COSY spectrum at 238 K showed the appearance of cross-peaks between the newly split signals (red arrows in Figure III-20b), thus providing evidence that they arise from the nearby NH and CH^{iPr} protons of the guanidinium group of **SZMC3$_{c}$**, as previously observed for **SZMC1$_{c}$**. These results do not only confirm our proposed structure for the cationic state of **SZMC3**, but also prove that this compound also suffers from restricted conformational mobility due to intramolecular H-bonding that causes dynamic effects in its ^{1}H-NMR spectra (see Figure III-14c).

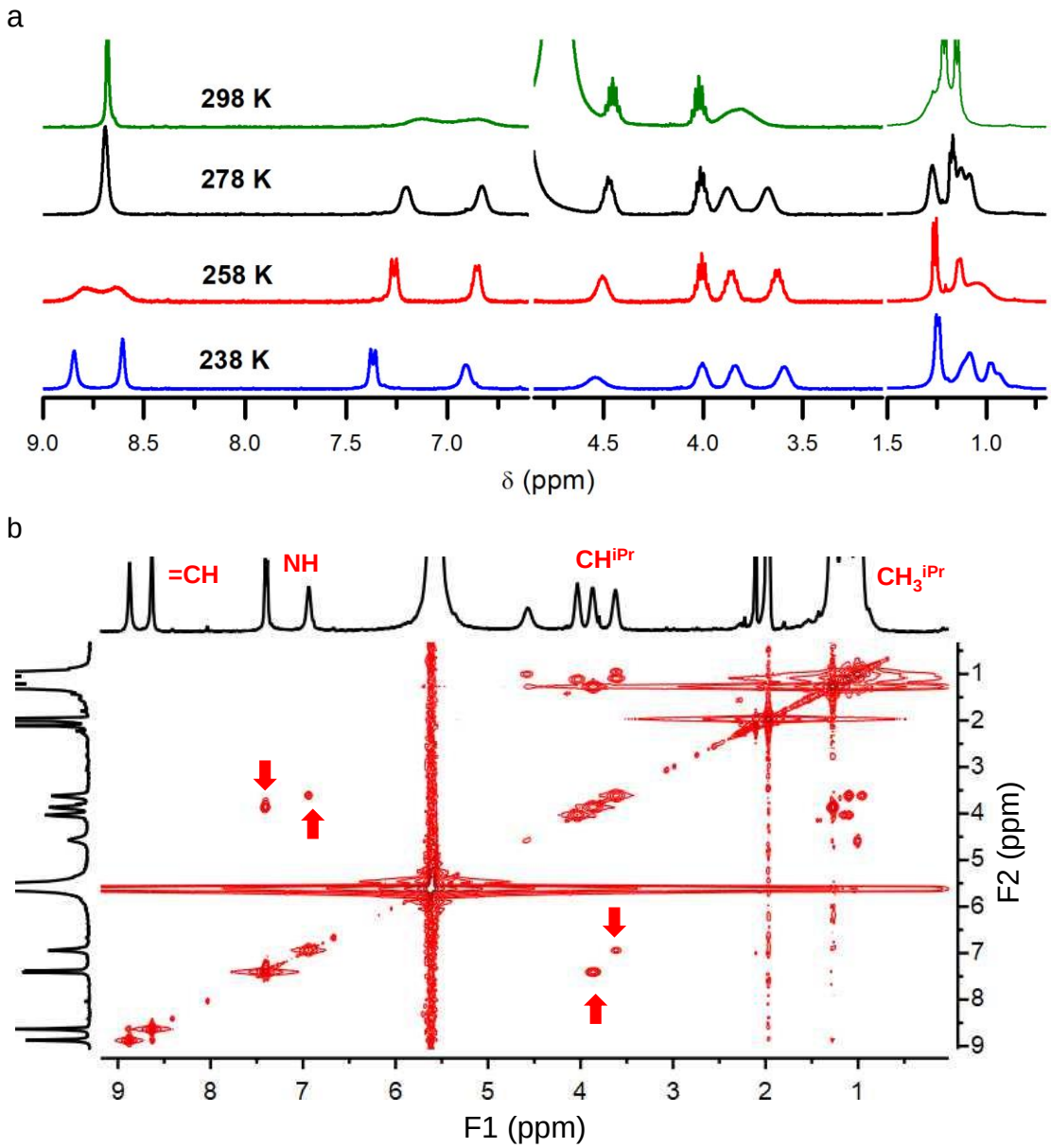

Figure III-20. (b) ^{1}H-NMR spectrum (400 MHz, CD_3CN) of **SZMC3$_c$** at 298**,** 278, 258 and 238 K. (b) 2D ^{1}H-NMR COSY spectrum (400 MHz, CD_3CN) of **SZMC3$_c$** at 238 K. Cross-peaks between NH and CH^{iPr} protons are indicated with arrows.

III.5.1.d. **Wide range pH probe based on SZMC1**

Once demonstrated the capacity of SZMCs to interconvert between three different protonation forms with distinct optical properties, we wanted to explore potential applications for this multistate acid-base switching behavior. As a proof of concept, we envisioned the use of SZMCs as wide range acidity optical probes.[40–42] For this, we decided to employ **SZMC1** as a switchable compound over other SZMCs due to several motives. On one hand, the different protonation states of **SZMC1** are more soluble than those of **SZMC2** and, moreover, **SZMC1** is obtained with the largest synthetic yield. On the other hand, the use of **SZMC3** was ruled out because the

tautomeric equilibrium between its colored and fluorescent zwitterionic state and its colorless and nonfluorescent neutral isomer would lower the amplitude of the variation in optical properties when protonating the system.

For the development of **SZMC1**-based pH probes, the solvent chosen was acetonitrile instead of water for two reasons: (a) **SZMC1** solubility in water is very low, which could trigger intermolecular aggregation processes that might obscure acidity-induced optical changes; and (b) pH sensors in organic solvents are rarer but demanded for many applications.[43–45] It is worth mentioning that, as the autoprotolysis constant of acetonitrile is $pK^{ACN} \geq 33$, the pH scale in this solvent is wider than in water when pH values are referred to pure acetonitrile (i.e., in the ${}^{s}_{s}pH$ scale,[46] which in the case of acetonitrile typically goes from 1 to 33).

A great advantage of SZMCs as acidity probes is that two different optical responses can be evaluated to report on pH, as both absorption and emission change when interconverting between their anionic, neutral and cationic states. In the case of absorption measurements, we set the detection wavelength at λ_{abs} = 423 nm to maximize the signal difference between the colored anionic and zwitterionic states of **SZMC1**, which enabled us to register a two-step pH-dependent absorption increment following an "Off"-"On_1"-"On_2" profile for acetonitrile solutions of this compound when sequentially transforming colorless **SZMC1$_c$** into colored **SZMC1$_{zw}$** and **SZMC1$_a$** (Figure III-21a). Interestingly, these two-consecutive acid-base processes take place at rather different pH windows, which allows measuring absorption changes for a wide pH range (pH ~ 13 - 24). This was confirmed by determining the pK_a values of **SZMC1$_c$** and **SZMC1$_{zw}$** from the pH variation of absorption spectra[40] (pK_{a1} = 15.8 ± 0.1 and pK_{a2} = 21.2 ± 0.1), which prove that **SZMC1** behaves as a diprotic weak acid in acetonitrile with fairly separated ionization processes. As for the pH-dependent emission response, we measured an "Off"-"On"-"Off" pattern since **SZMC1$_{zw}$** is the single emissive state of the system and it only exists in appreciable amounts within the pH ~ 16 – 21 window (Figure III-21a). Importantly, as both optical responses are complementary, univocal values of pH can be assigned to every pair of absorption and emission signals measured for **SZMC1** at pH ~ 13 - 24 (Figure III-21b). This demonstrates the capacity of this compound to behave as a wide range pH optical chemosensor. Actually, this behavior could be potentially expanded to any member of the **SZMC** family and, by tuning the nature of the substituents of the guanidine/guanidinium group, vary the pK_a values of the switch to modify the pH detection window.

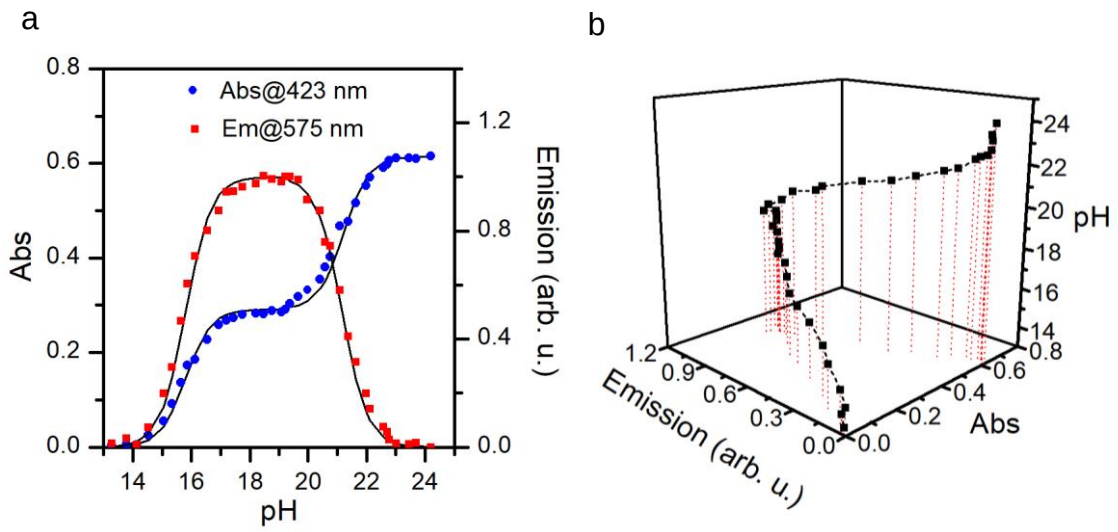

Figure III-21. (a) pH dependence of the absorption at λ_{abs} = 423 nm and of the emission intensity at λ_{fl} = 575 nm for a **SZMC1** solution in acetonitrile ($c_{\mathbf{SZMC1}}$ = 4.4 x 10^{-5} M). Blue and red symbols represent the experimental data obtained by addition of $HClO_4$ and TBAOH over the initial **SZMC1$_{zw}$** solution. Solid lines give the expected values computed using the ionization model for a weak diprotic acid and the pK_a constants, molar absorptivity coefficients and fluorescence quantum yields previously determined for **SZMC1$_a$**, **SZMC1$_{zw}$** and **SZMC1$_c$**. (b) 3D plot showing the univocal correspondence between pH values and pairs of **SZMC1** colorimetric and fluorescent signals at λ_{abs} = 423 and λ_{fl} = 575 nm, respectively.

For a simpler implementation for practical applications, we sought to prove that **SZMC1** could also be employed as a wide range pH sensor in the solid state. To do so, **SZMC1$_{zw}$** was dispersed in a poly(methyl methacrylate) (PMMA) film by evaporating a chloroform solution containing both the polymer and the molecular switch. When this film was exposed to droplets of neutral, 0.1 M TFA and 0.1 M TBAOH acetonitrile solutions, the expected local changes in color and emission were seen as a result of the transformation of the initial colored and emissive **SZMC1$_{zw}$** state into either colorless and nonfluorescent **SZMC1$_c$** (TFA addition) or colored but nonemissive **SZMC1$_a$** (TBAOH addition), respectively. This is illustrated by the photographs in Figure III-22, which successfully demonstrate the possible implementation of **SZMC1**-based pH sensing in solid polymeric materials.

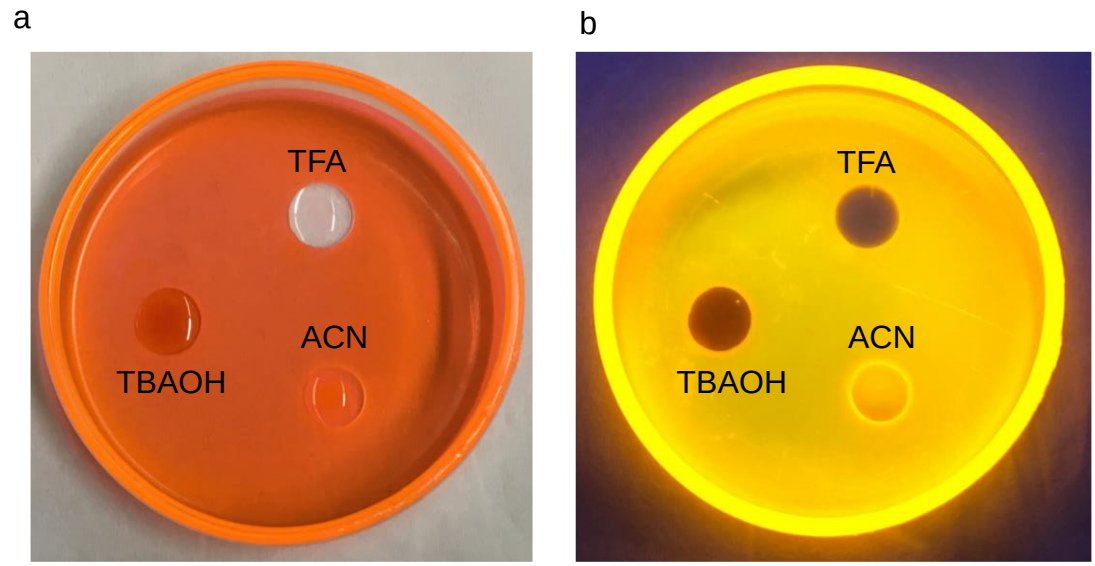

Figure III-22. (a-b) Photographs of a **SZMC1$_{zw}$**-loaded PMMA film after addition of three droplets containing acetonitrile (ACN), 0.1 M TFA in acetonitrile and 0.1 M TBAOH in acetonitrile. Image (b) was taken in the dark and under a 365 nm lamp to detect the fluorescence of the sample.

III.6. Redox switching of spirocyclic zwitterionic Meisenheimer compounds

III.6.1. Redox-induced interconversion between SZMC$_{zw}$ and SZMC$_c$

As just discussed in section III.5, we provided evidence of a new cationic state that could be obtained for SZMC switches upon protonation. Inspired by the fact that our group had previously reported that the acid-base transformation between the zwitterionic **SZMC$_{zw}$** and anionic **SZMC$_a$** states could also be redox-induced,[4,25,26] we tested in this work if the **SZMC$_{zw}$**-**SZMC$_c$** interconversion could be achieved electrochemically as well. As a proof of concept, we focused on **SZMC1** as a benchmark case for these studies due to its simplicity, as its zwitterionic form does not undergo tautomerization to the neutral aromatic state at room temperature. For this system, a series of electrochemical experiments were conducted in collaboration with Dr. Silvia Mena and Marina Benet, two other students of our research group.

First, **SZMC1$_{zw}$** and **SZMC1$_c$** were investigated by cyclic voltammetry (CV) in acetonitrile. As shown in Figure III-23a, the cyclic voltammogram of **SZMC1$_{zw}$** presents two characteristic one-electron waves: (a) a one-electron pseudo-reversible reduction wave at $E_{p,c}$ = -0.85 V (vs SCE), which had already been described to lead to **SZMC1$_a$** by radical anion formation and subsequent capture of a hydrogen atom from the medium;[26,27] and (b) a reversible one-electron wave at E^0 = +1.52 V (vs SCE). In the case of **SZMC1$_c$**, its cyclic voltammogram does not present any

oxidation peak but two reduction waves instead: (a) a one-electron irreversible wave at $E_{p,c}$ = -0.50 V (vs SCE); and (b) a one-electron pseudo-reversible wave at $E_{p,c}$ = -0.85 V (vs SCE), which has the same peak potential and a similar shape to that registered for **SZMC1$_{zw}$** (Figure III-23b). The latter strongly suggests that the irreversible wave at $E_{p,c}$ = -0.50 V (vs SCE) could induce efficient conversion of **SZMC1$_c$** into **SZMC1$_{zw}$** by reduction followed by hydrogen atom elimination, thus accounting for the subsequent appearance of the characteristic **SZMC1$_{zw}$** peak at $E_{p,c}$ =-0.85 V (vs SCE). Moreover, careful observation of the **SZMC1$_{zw}$** cyclic voltammogram reveals the presence of a small reduction wave at $E_{p,c}$ = -0.50 V (vs SCE) which matches that found for **SZMC1$_a$**. This could be explained if the **SZMC1$_{zw}$** oxidation wave at E^0 = +1.52 V (vs SCE) was not fully reversible, but the formation of the corresponding radical cation was coupled with hydrogen abstraction to lead to **SZMC1$_c$** formation. If so, this would mean that reversible **SZMC1$_{zw}$-SZMC1$_c$** interconversion could be promoted electrochemically.

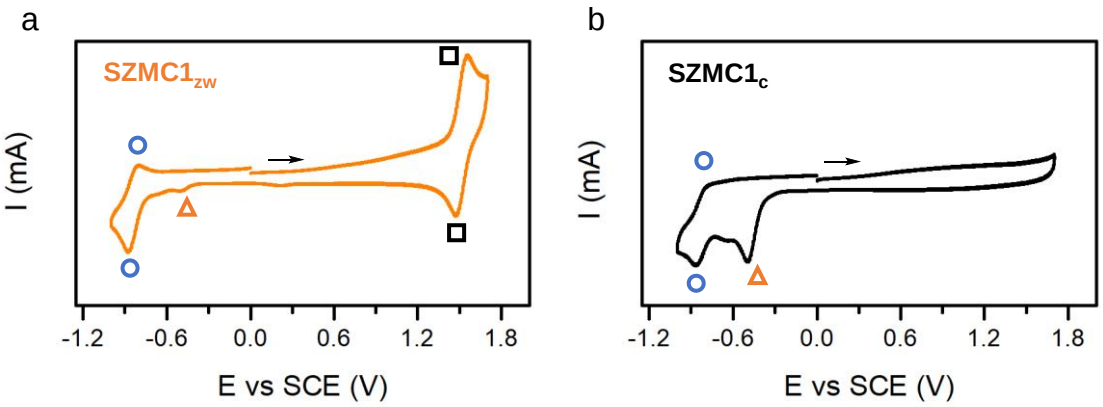

Figure III-23 Cyclic voltammograms of (a) **SZMC1$_{zw}$** and (b) **SZMC1$_c$** in acetonitrile at 298 K (c_{SZMC1} = 5.0 x 10^{-4}, 0.1 M *n*-Bu_4NPF_6, scan rate = 0.5 V s^{-1}). Different symbols are used to assign **SZMC1$_{zw}$** reduction (blue circles) and oxidation (black squares) waves as well as the **SZMC1$_c$** reduction wave (orange triangles). The arrows in the voltammograms indicate the potential scanning direction.

To corroborate this conclusion, the electrochemical transformation between **SZMC1$_{zw}$** and **SZMC1$_c$** was monitored by combined UV-vis spectroelectrochemical and CV measurements. First, an acetonitrile **SZMC1$_{zw}$** sample was first exposed to an oxidative potential (E_{app} = +1.70 V (vs SCE)) to form **SZMC1$_c$**, which resulted in the disappearance of the visible absorption bands at $\lambda_{abs,max}$ = 409 and 525 nm in 40 seconds (Figure III-24a). Therefore, this result is indeed compatible with the formation of colorless **SZMC1$_c$**. Moreover, the CV experiment made at this point showed both the disappearance of the characteristic oxidation wave of **SZMC1$_{zw}$** at E^0 = +1.52 V (vs SCE) and the appearance of the corresponding **SZMC1$_c$** reduction peak at $E_{p,c}$ = -0.50 V (Figure III-24b), thus providing further evidence of the

oxidation-induced transformation from the zwitterionic to the cationic state of **SZMC1**. Next, a reduction potential was applied to the same sample (E_{app} = -0.60 V (vs SCE)), which resulted in the almost complete recovery of the absorption bands in the visible region and the characteristic redox waves of **SZMC1$_{zw}$** (Figure III-24).

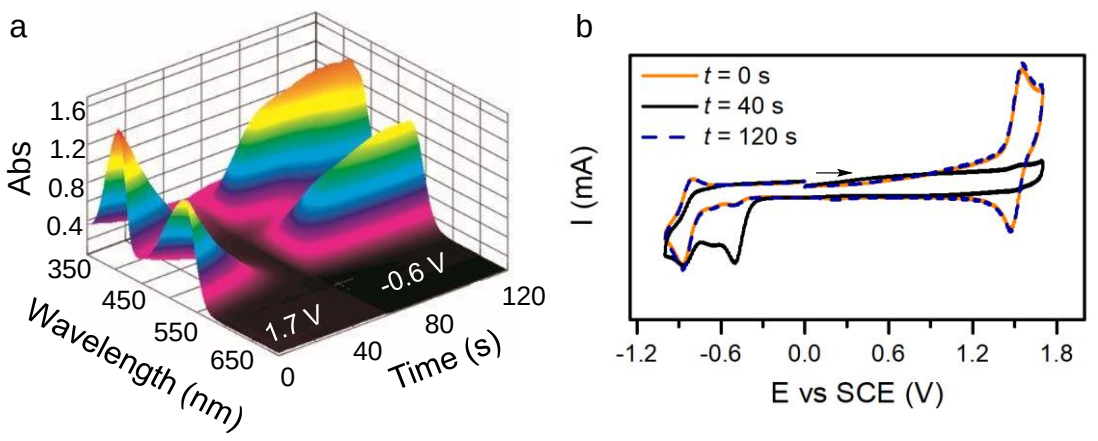

Figure III-24. (a) Variation of the absorption spectrum of **SZMC1$_{zw}$** in acetonitrile (+0.1 M *n*-Bu_4NPF_6) at 298 K during the application of an oxidative potential at E_{app} = +1.70 V (vs SCE) for 40 seconds followed by a reductive potential at E_{app} = -0.60 V (vs SCE) for 80 seconds. (b) Cyclic voltammograms registered at 0, 40 and 120 s for the sample subjected to the spectroelectrochemical experiment shown in (a) (scan rate = 0.5 V s^{-1}). The arrows in the voltammograms indicate the potential scanning direction.

With all these experiments and some others conducted in our group for **SZMC2** and **SZMC3**,[47] we provided unambiguous evidence that the **SZMC$_{zw}$-SZMC$_c$** transformation could be indistinctly done either via acid-base addition or redox processes. Therefore, we proved that the chromic and fluorescent **SZMC$_{zw}$-SZMC$_c$** switching also shows multistimuli-responsive behavior.

III.6.2. SZMC-based electrochromic and electrofluorochromic materials

The capability of SZMCs to switch between three protonation states with distinct colors and emissions by electrochemical stimuli could be exploited to prepare electrochromic and electrofluorochromic devices. Actually, because of the complementary optical properties that **SZMC$_a$**, **SZMC$_{zw}$** and **SZMC$_c$** present, different devices could be fabricated. On one hand, electrochromic materials switching between colored and colorless states could be prepared by taking advantage of the redox-induced **SZMC$_{zw}$-SZMC$_c$** conversion (e.g., for applications in smart windows[48]). On the other hand, electrofluorochromic systems could be realized by making use of either the **SZMC$_{zw}$-SZMC$_c$** or **SZMC$_{zw}$-SZMC$_a$** transformations (e.g. for applications in displays[49]).

To explore this variety of possibilities, we decided to fabricate electrochemically-active **SZMC1**-doped ionogels. To do so, we followed a procedure previously described in the literature[50] and prepared an ionogel by codissolving the ionic liquid 1-butyl-3-methylimidazolium bis(trifluoromethylsulfonyl)imide ([Bmim][TFSI]), the polymer poly(vinylidene fluoride-*co*-hexafluoropropylene) (P(VDF-*co*-HFP)) and the **SZMC1$_{zw}$** switch in acetone. When necessary, a small amount of 1,1'-dimethylferrocene was also added as a redox-reference system. After solvent evaporation onto a mold, a flexible ionogel was obtained (Figure III-25a). To finally prepare the device, a "cut-and-stick" strategy was followed and a thin slice (ca. 1 mm-thick) of the formed ionogel was stuck between two ITO-coated glass plates. Finally, the device was fixed using tape. The result was a slightly conductive material (conductivity = 0.686 mS cm^{-1} at room temperature) that maintained the colorimetric and emissive properties of **SZMC1$_{zw}$** (Figure III-25a-b)

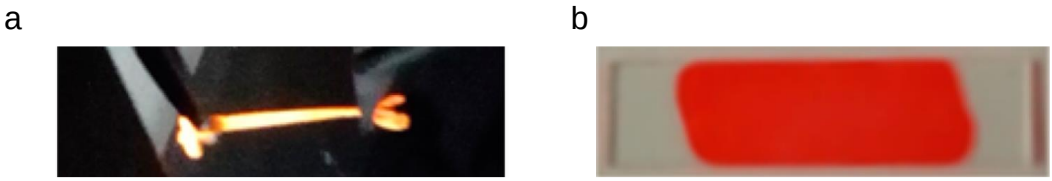

Figure III-25. Photographs of the **SZMC1$_{zw}$**-loaded [BMIM][TFSI]/P(VDF-*co*-HFP) ionogel. In (a) the ionogel was pulled and irradiated in the dark at λ_{exc} = 365 nm to demonstrate its flexibility and fluorescence. In (b) the color of the ionogel after deposition over an ITO-coated glass can be observed.

Because of the low conductivity of the ionogel, higher potentials were required to switch between the different states of **SZMC1**. In spite of this, the electrofluorochromic **SZMC1$_{zw}$**-to-**SZMC1$_{a}$** transformation could be successfully induced by applying an oxidative potential at E_{app} = +2.5 V (vs SCE). This is demonstrated in Figure III-26a, where a colored nonfluorescent ionogel was obtained. Nicely, the initial optical properties could be recovered after exposure to a reductive potential (E_{app} = -4.5 V (vs SCE)). The electrochromic and electrofluorochromic transformation from **SZMC1$_{zw}$** to **SZMC1$_{c}$** could also be carried out by applying a high oxidative potential (E_{app} = +4.0 V (vs SCE)), as illustrated in Figure III-26b. Unfortunately, the loss of color and fluorescence was not complete due to the irregularities in the film thickness and the low conductivity of the material, which did not permit a homogeneous potential application. As already shown for the other redox-induced transformation, recovery of initial **SZMC1$_{zw}$** optical properties was achieved at E_{app} =-3.0 V (vs SCE). Although optimization of the electrochemical-responsive materials and devices fabricated is still required to minimize overpotentials and warrant homogeneous redox-induced responses, the results shown in this work demonstrate the potential of **SZMC**-based ionogels for the

preparation of simple and cost-effective electrochromic and electrofluorochromic systems.

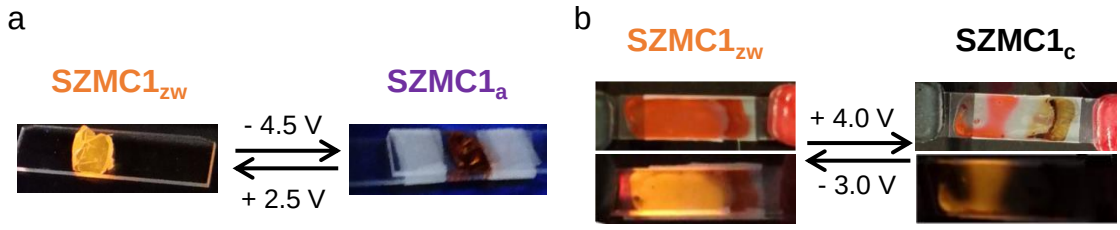

Figure III-26. (a) Redox-induced transformation between **SZMC1$_{zw}$** and **SZMC1$_{a}$** for a **SZMC1**-loaded [BMIM][TFSI]/P(VDF-*co*-HFP) ionogel sandwiched between two ITO-coated glass substrates. Photographs were taken in the dark and under irradiation at λ_{exc} = 365 nm to demonstrate the fluorescence switching. (b) Redox-induced transformation between **SZMC1$_{zw}$** and **SZMC1$_{c}$** in a similar ionogel-based device. The upper photographs were taken under regular illumination to show color switching, while those at the bottom were registered in the dark and under λ_{exc} = 365 nm irradiation to detect fluorescence changes. The brown substance in (b) is due to the formation of ferrocenium ions from the oxidation of 1,1′-dimethylferrocene molecules previously added to the ionogel as a redox reference system.

III.7. Ion switching of spirocyclic zwitterionic Meisenheimer compounds

Besides expanding the multistate behavior of SZMCs, in this thesis we also aimed at exploring new stimuli to which this family of switches could respond. To pursue this objective, we started by focusing our attention in the **SZMC$_{zw}$**-to-**SZMC$_{a}$** transformation that allows PET-based fluorescence switching by guanidinium deprotonation; i.e., by sufficiently enhancing the electron density in the triazine moiety as to activate a PET-based emission quenching process. In light of this, we hypothesized that an anion with a strong interaction with the guanidinium proton could cause a similar effect and, thus, open the door to perform fluorescent ion sensing with SZMCs (Scheme III-11). It is for this reason that two well-known Lewis bases as cyanide (CN^-) and fluoride (F^-) were selected, whose detection is crucial for human health. As it has been reported, fluoride excess can induce fluorosis and osteoscaroma, while its deficiency is a cause of osteoporosis and poor dental health.[51] On the other hand, cyanide is known for its high toxicity towards the environment and humans.[52]

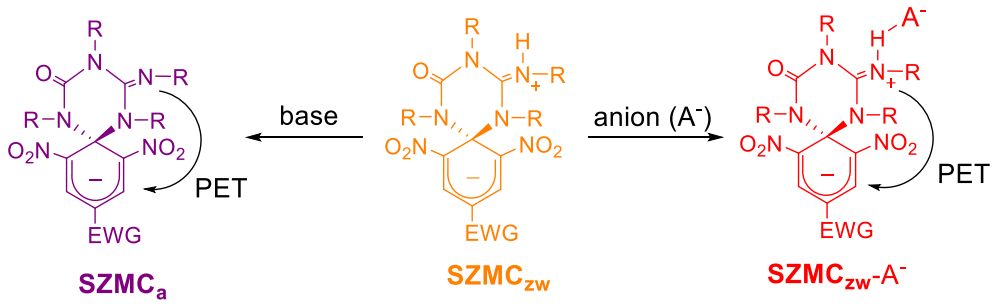

Scheme III-11. Acid-base vs anion-induced interconversion between the fluorescent zwitterionic form and nonfluorescent states of SZMCs.

To validate our concept, titrations of acetonitrile solutions of **SZMC1$_{zw}$** with triethylammonium fluoride (TEAF) and tetraethylammonium cyanide (TEACN) were followed by UV-vis absorption spectroscopy (Figure III-27a-b). In both cases, a red shift of the absorption band at $\lambda_{abs,max}$ = 406 nm was observed, together with the appearance of two isosbestic points at λ = 415 and 510 nm that suggest the unimolecular transformation of **SZMC1$_{zw}$** into a single species. It is worth mentioning that the final absorption spectrum obtained in both cases very much resembles that of **SZMC1$_{a}$**, thus pointing to an acid-base reaction between **SZMC1$_{zw}$** and the selected anions.

In a similar manner, when the emission spectra of acetonitrile solutions of **SZMC1$_{zw}$** were monitored upon F^- and CN^- addition, a 90% decay in fluorescence intensity was detected after titration with an equimolar amount of the anions and it fully vanished when adding a little excess (Figure III-27c-d). More importantly, when concentration-dependent calibration curves were determined, a strong linear dependence was found between the amount of analyte and the loss of fluorescence, thus proving the potential use of **SZMC1** as a F^- and CN^- optical chemosensor (Figure III-27e-f). Interestingly, this could be expanded to other SZMCs, as indeed demonstrated for **SZMC2$_{zw}$** (Figure III-27e-f).

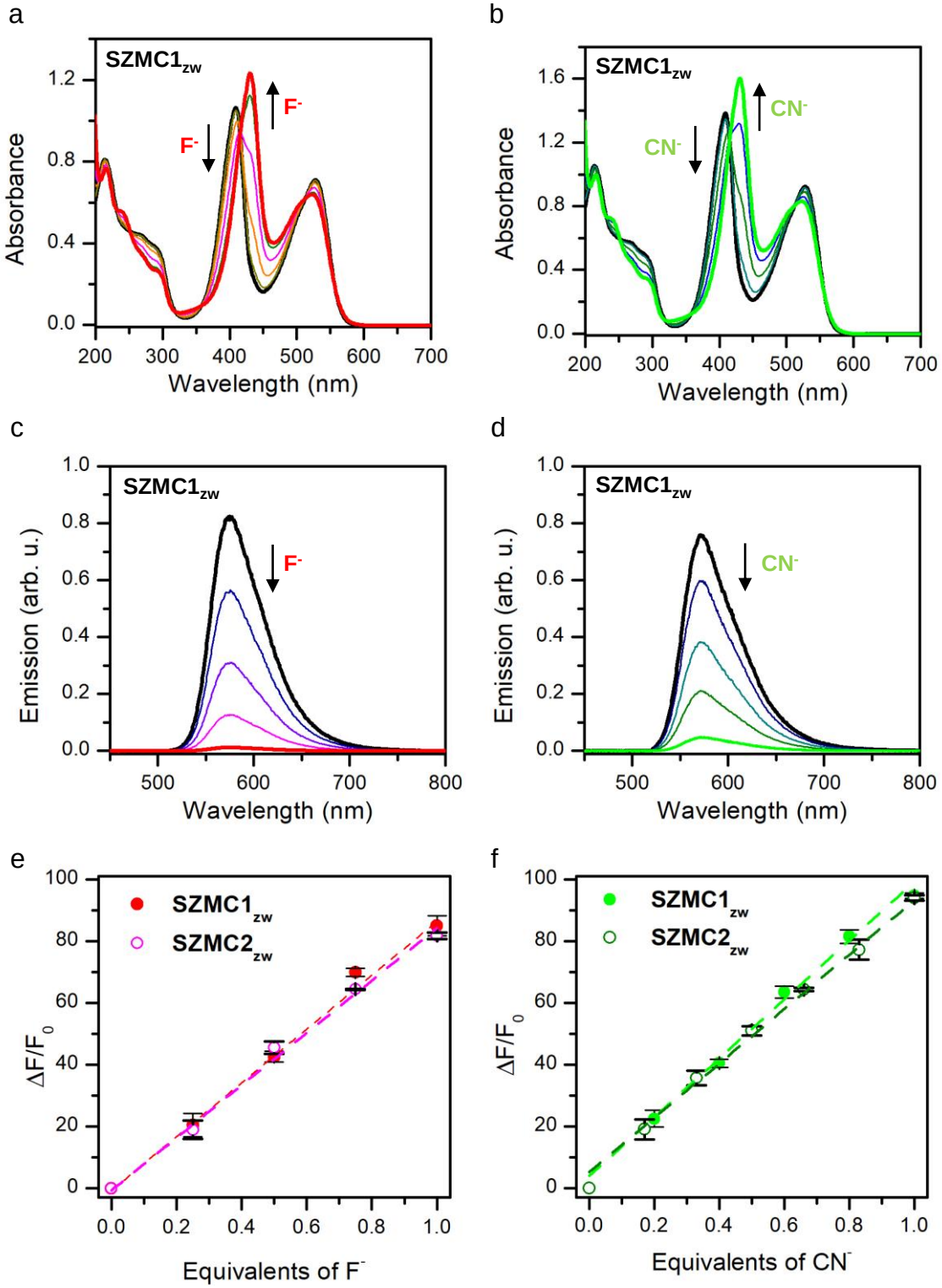

Figure III-27. Spectroscopic analysis of the titration of acetonitrile solutions of **SZMC1$_{zw}$** with F^- (left) and CN^- (right). First, the variation in (a-b) absorption (c_{SZMC} = 5.0x10^{-5} and 7.0x10^{-5} M, respectively) and (c-d) emission (c_{SZMC} = 6.0x10^{-6} and 6.0x10^{-6} M, respectively) spectra upon anion addition are shown. Next, concentration-dependent curves of the fluorescence response for (e) fluoride and (f) cyanide are given for acetonitrile solutions of **SZMC1$_{zw}$** (c_{SZMC1} = 6.0x10^{-6} M) and **SZMC2$_{zw}$** (c_{SZMC2} = 6.0x10^{-6} M). In (e-f) dots correspond to the

percentual average fluorescence loss values ($\Delta F/F_0$) determined from three independent measurements, while the corresponding linear fits are shown as dashed lines.

Once proven the chemosensing behavior of **SZMC1$_{zw}$** and **SZMC2$_{zw}$**, their selectivity towards CN^- and F^- was tested by titration with other relevant anionic analytes such as Cl^-, Br^-, I^-, $H_2PO_4^-$, NO_2^- and NO_3^-. No appreciable changes in absorption were observed for any of these additional anions even when adding up to 1.5 equivalents to acetonitrile solutions of **SZMC1$_{zw}$** and **SZMC2$_{zw}$**. In agreement with these results, the emission from the SZMC solutions also remained unaltered during titration with the only exception of the addition of iodide (Figure III-28). However, this comes as no surprise because iodide is known to have a significant fluorescence quenching effect over many organic dyes.[53] Therefore, colorimetric experiments may be required to eliminate the iodide interference when employing **SZMC1** and **SZMC2** as fluoride and cyanide chemosensors.

a

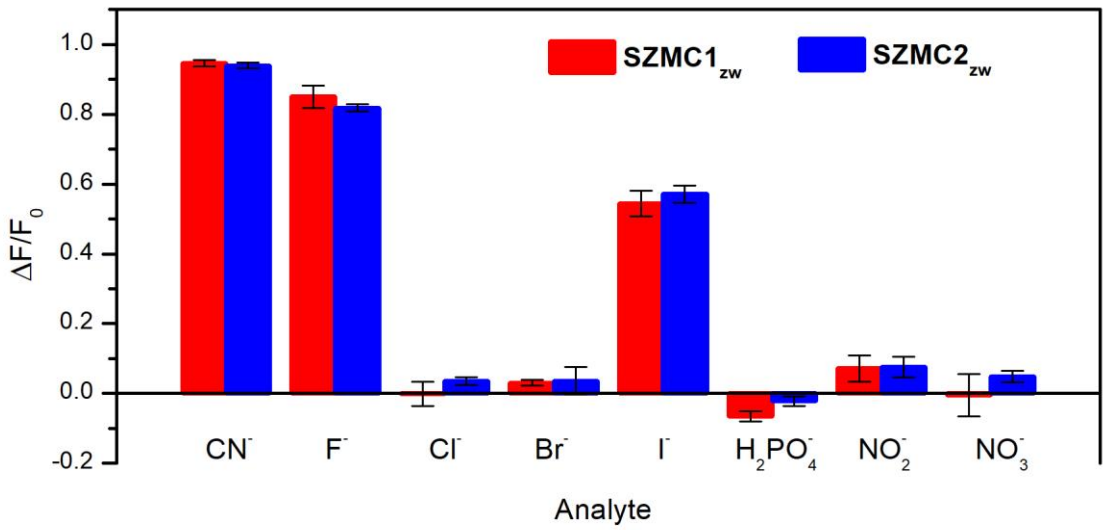

b

Figure III-28. (a) Histogram of the measured fluorescent intensity loss after the addition of 1 equivalent of several anions to acetonitrile solutions of **SZMC1$_{zw}$** (c_{SZMC1} = 6.0x10^{-6} M) and

SZMC2$_{zw}$ (c_{SZMC2} = 6.0x10^{-6} M). Average $\Delta F/F_0$ values are shown that were determined from three independent measurements. (b) Photograph in the dark and under UV irradiation of different vials containing the same **SZMC1$_{zw}$** acetonitrile solution and 1 equivalent of different anions.

To further corroborate these results, the loss of fluorescence caused by F^- or CN^- addition to acetonitrile solutions of **SZMC1$_{zw}$** and **SZMC2$_{zw}$** was tested in the presence of 1 equivalent of each of the other anionic analytes except for iodide. As shown in Figure III-29, **SZMC1$_{zw}$** and **SZMC2$_{zw}$** fluoride titration was unaffected by the presence of these additional anions. However, in the case of CN^- sensing, an interference effect was observed in the presence of $H_2PO_4^-$ and a lower fluorescent change was measured in this case.

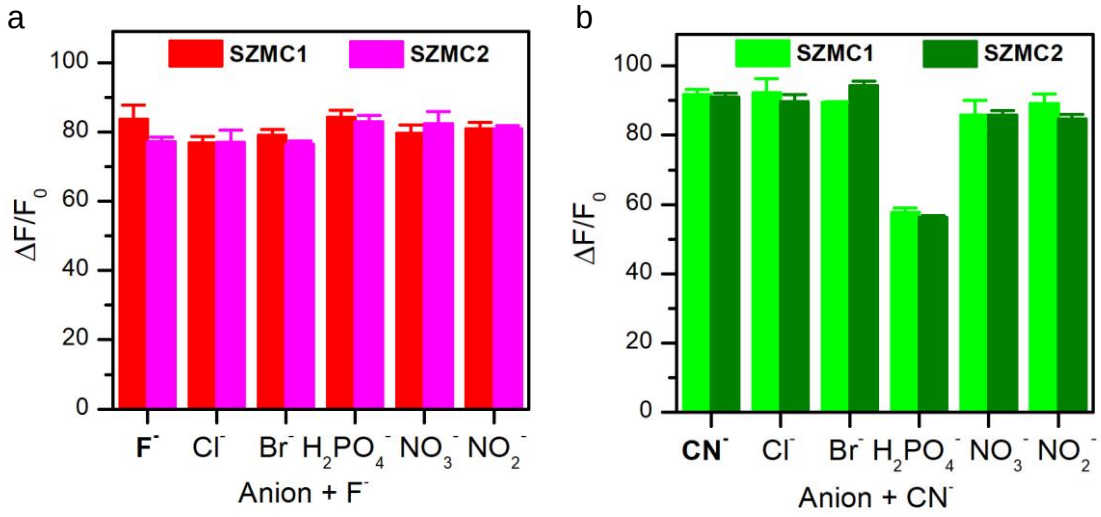

Figure III-29. Histograms showing the loss of fluorescence upon addition of 1 equivalent of (a) fluoride and (b) cyanide to acetonitrile solutions of **SZMC1$_{zw}$** (c_{SZMC1} = 6.0x10^{-6} M) and **SZMC2$_{zw}$** (c_{SZMC2} = 6.0x10^{-6} M) in the presence of 1 equivalent of the other anion. The results shown are the average of 3 replicates.

For better understanding of the underlaying switching mechanism behind fluoride and cyanide chemosensing with SZMCs, we monitored by ^{1}H-NMR spectroscopy the titration of a deuterated acetonitrile solution of **SZMC1$_{zw}$** with fluoride (Figure III-30a). A widening of the signals was seen upon addition of tetrabutyl ammonium fluoride (TBAF) which only became resolved in a new set of signals after 2 equivalents (Figure III-30a). These results are in accordance with the titration of **SZMC1$_{zw}$** with TBAOH that followed the same process but only slightly more than 1 equivalent was required for the signals of the anionic compound to resolve (Figure III-30b).

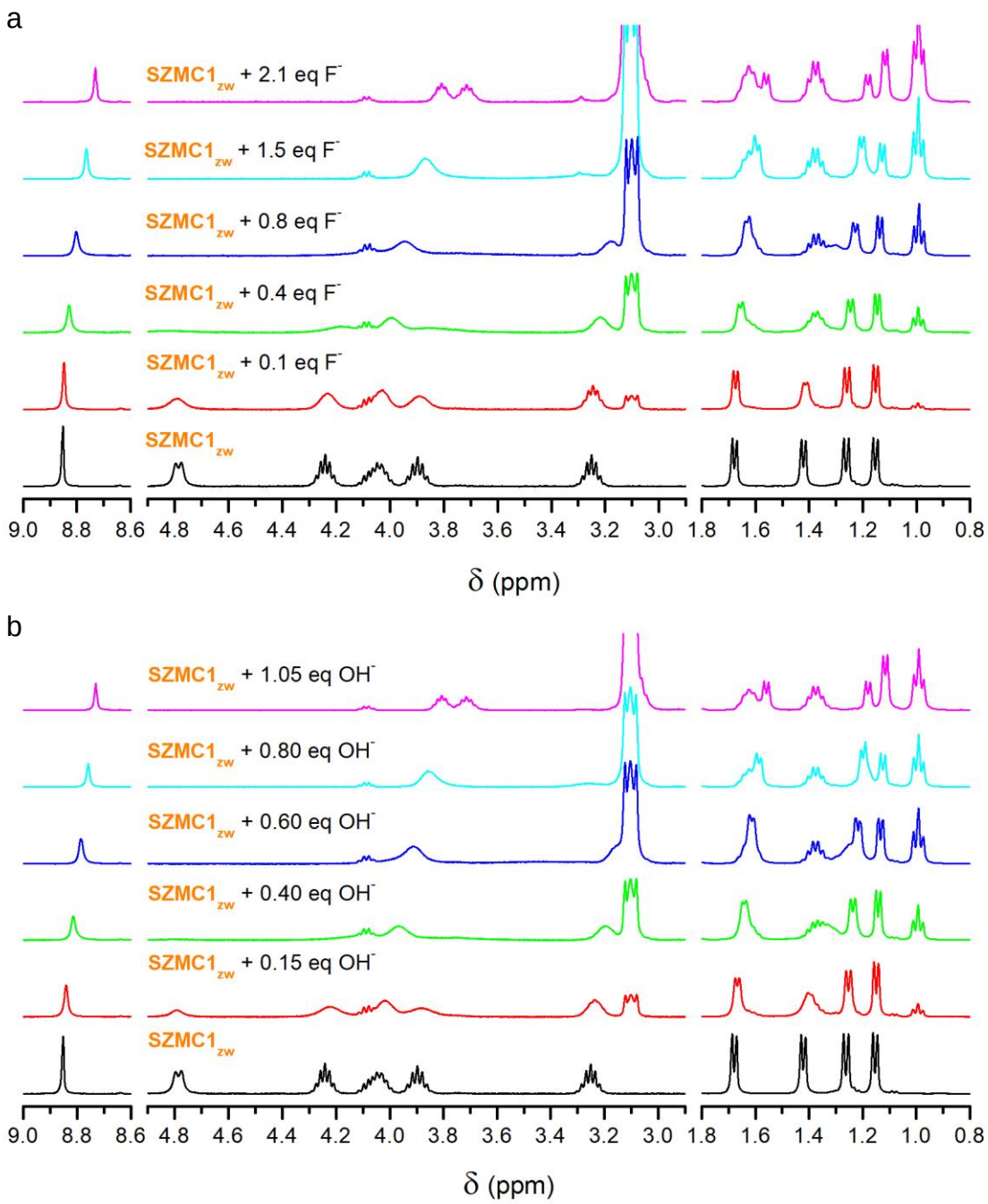

Figure III-30. Variation of the ^{1}H-NMR (400 MHz, CD_3CN) spectrum of **SZMC1$_{zw}$** upon addition of (a) TBAF and (b) TBAOH. The region between 8.6 and 9.0 was amplified 3 times and the one between 4.9 and 2.9 8 times for sake of clarity. Signals at 3.10, 1.62, 1.37 and 0.99 ppm belong to the tetrabutyl ammonium countercation.

Regarding these results, we concluded that the loss of fluorescence was due to an acid-base interaction between **SZMC** and the selected anions CN^- and F^- as they are both known for having K_b values in DMSO orders of magnitude higher than NH_3 and any of the other analytes studied.[54] In this case, we ascribed the interference effect for CN^- to the presence of $H_2PO_4^-$ labile protons that can compete with the **SZMC1$_{zw}$**. We hypothesize that we don't see this effect with F^- because of its hard Lewis base

nature that would preferably interact with the hard acid guanidinium proton. Despite these assumptions we were not able to successfully prove this hypothesis. Regardless of the mechanism, we demonstrated in this section that the switch from **SZMC$_{zw}$** to **SZMC$_{a}$** is not only restricted to OH^- addition but other Lewis bases can be employed. Moreover, we demonstrated that it could be used to selectively quantify analytes of interest as fluoride and cyanide in the presence of other chemical species (Cl^-, Br^-, NO_2^-, NO_3^- or $H_2PO_4^-$).

During my PhD thesis, 2 articles were published employing **SZMC2$_{zw}$** for ion sensing.[55,56] In one of them Haldar and coworkers tested the used of **SZMC2$_{zw}$** for the detection of several transition metal cations and anions in tetrahydrofuran (THF), including fluoride and cyanide.[55] Differently to us they only a decrease of fluorescence was described upon fluoride addition. In a second article by Mohar fluoride detection was achieved with a nonfluorescent gel formed by **SZMC2$_{zw}$** and $FeCl_3$ that became fluorescent upon analyte addition.[56]

III.8. SOLVENT-INDUCED SWITCHING OF SPIROCYCLIC ZWITTERIONIC MEISENHEIMER COMPOUNDS

III.8.1. Solvent effects on the SZMC3 tautomeric equilibrium

In our search for novel stimuli to trigger SZMCs switches, we finally focused our attention on the tautomeric equilibrium between their zwitterionic and aromatic forms, which has been widely discussed in section III.4 of this chapter. There we described the thermal dependence of the **SZMC$_{zw}$-SZMC$_{n}$** interconversion as well as the effect of the steric hindrance imparted by the substituents of the triazine ring on the stability of the spirocyclic structure of the zwitterionc state. It is however another feature of these two isomers that drew our interest in this case: their different charge distributions, which should make **SZMC$_{zw}$** much more polar than **SZMC$_{n}$**. As a consequence, one would expect that control over their tautomeric equilibrium could be exerted by modifying the surrounding solvent. Actually, this behavior has been previously reported for other spirocyclic switches such as spiropyrans, although in that case it is the open form of the system that is zwitterionic and, thus, more polar.[57]

In order to unravel the solvent effects on **SZMC$_{zw}$-SZMC$_{n}$** interconversion, we took **SZMC3** as a reference system and performed a series of ^{1}H-NMR experiments in different solvents for the neutral state of this compound. The results obtained are shown in Figure III-31 and, at a first glance, they evidence that the solvent nature produces dramatic changes in the composition of the tautomeric equilibrium mixture. While almost an unappreciable amount of **SZMC3$_{zw}$** exists in toluene, this compound accounts for nearly 30% of the isomer mixture in acetonitrile or DMSO at room

temperature. These results can be rationalized on the basis of two properties of the solvent: (a) its polarity, and (b) its ability to form H-bonds. As one might expect, the more polar the solvent, the higher the stabilization of the zwitterionic form must be. It is for this reason that higher molar fractions of **SZMC3$_{zw}$** were registered for the solvents with larger dielectric constants (Table III-1). The main exception to this rule are protic solvents, where lower **SZMC3$_{zw}$** relative concentrations were measured. Although the exact mechanism for this behavior is not fully clear to us, we assume that H-bonding between the solvent and the nitrogens of the guanidine moiety in the neutral form prevents cyclization to form the zwitterionic spirocyclic structure and stabilizes **SZMC3$_{n}$** despite the higher polarity of the solvent.

Another feature that we explored via ^{1}H-NMR spectroscopy was **SZMC3$_{zw}$** thermal stability in each of the selected solvents; i.e., the thermal effect on the **SZMC$_{zw}$-SZMC$_{n}$** equilibrium. Interestingly, up to a 33-fold decrease in **SZMC3$_{zw}$** molar fraction was seen in $CHCl_3$ when heating from 273 to 313 K, while the tautomeric equilibrium mixture remained almost unaltered in other solvents like THF or methanol (MeOH). Based on these results, one could argue that temperature must have little effect on the **SZMC3**-solvent H-bonding interactions, while it should critically affect **SZMC3$_{zw}$** stabilization when driven by solvent polarity. It is for this reason that the composition of the **SZMC3$_{zw}$-SZMC3$_{n}$** tautomeric equilibrium is widely affected by temperature in polar solvents with no H-bonding sites as chloroform and dichloromethane, whereas it does not significantly vary in solvents that can form strong H-bonds. Consequently, this uncovers that, if the thermally-induced switching of SZMCs is to be used in a practical application, selection of the surrounding medium will be critical and solvents with high H-bonding capacity should be avoided.

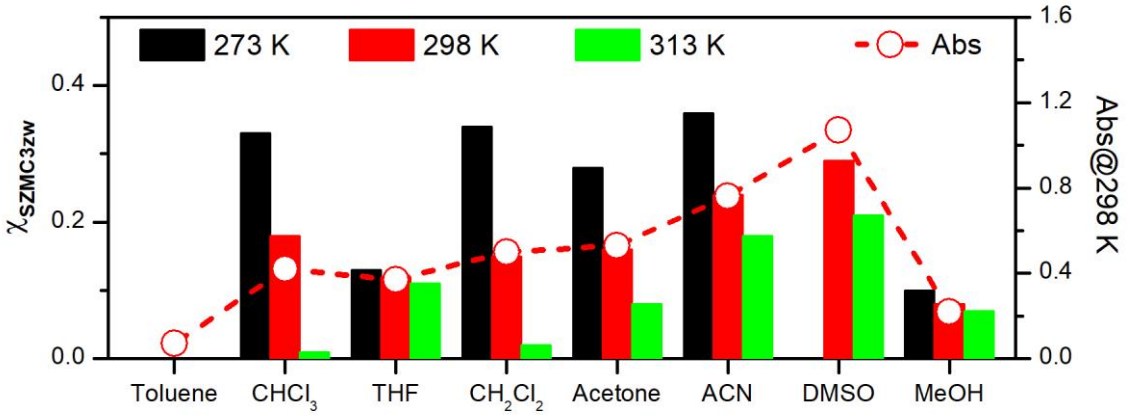

Figure III-31. Molar fractions of **SZMC3$_{zw}$** in the tautomeric equilibrium mixture in different solvents and at 273, 298 and 313 K, which were measured by ^{1}H-NMR spectroscopy. Empty dots show the relative absorbance values at the peak of visible absorption band of **SZMC3$_{zw}$** obtained at 298 K for each solvent.

Table III-1. Temperature dependence of the composition and optical properties of the **SZMC3$_{zw}$-SZMC3$_n$** tautomeric mixture in different solvents at 298 K.

Solvent	ε_D [a]	$\lambda_{abs,max}$	$\chi_{SZMC3zw}$ [b]	$\lambda_{fl,max}$ [c]	Φ_{fl} [c]
Toluene	2.38	560	nd [d]	582	0.71 ± 0.04
$CHCl_3$	4.82	568	0.18	597	0.84 ± 0.03
CH_2Cl_2	10.36	566	0.15	592	0.85 ± 0.01
THF	7.58	561	0.12	584	0.85 ± 0.01
Acetone	20.7	561	0.16	588	0.77 ± 0.02
ACN	37.5	564	0.24	594	0.76 ± 0.01
DMSO	46.7	569	0.29	599	0.65 ± 0.07
MeOH	32.7	563	0.08	599	0.40 ± 0.01
H_2O	80.1	581	nd [e]	619	0.11 ± 0.02

[a] Dielectric constant of the solvent at room temperature. [b] Determined from the integrals of the low-field region signals in the ^{1}H-NMR spectrum of the neutral state of **SZMC3**. [c] Measured at λ_{exc} = 532 nm. [d] Not determined because of the absence of SZMC3$_{zw}$ signals in the ^{1}H-NMR spectrum of the neutral state of **SZMC3** in toluene-d_8. [e] Not determined because of the low solubility of **SZMC3** in **D_2O.** Errors were calculated as the standard deviation of 5 replicates.

As **SZMC3$_{zw}$** and **SZMC3$_n$** present distinct optical properties, significant changes in absorption and emission should result from the solvent-induced effects on their interconversion process. For this reason, the optical properties of **SZMC3** were evaluated in each of the solvents discussed above together with water, which was not included in the previous ^{1}H-NMR experiments because of the low solubility of the switch in aqueous media. Indeed, when we characterized the neutral state of **SZMC3** in different solvents at the same concentration and 298 K, huge changes in intensity were seen for the absorption and fluorescence bands in the visible region that exclusively arise from the colored and fluorescent **SZMC3$_{zw}$** isomer (Figure III-32). In the case of absorbance measurements, the intensity of the visible absorption band

fairly reproduced the trend determined for $\chi_{SZMC3zw}$ by ^{1}H-NMR spectroscopy (Figure III-31). From this, we deduced that only small changes in **SZMC3$_{zw}$** molar absorptivity happen for different solvents. Similarly, minimal solvatochromic effects were observed except for the case of the sample in water, whose $\lambda_{abs,max}$ value ($\lambda_{abs,max}$ = 581 nm) shows a clear spectral red-shift relative to the rest of solutions tested ($\lambda_{abs,max}$ ~ 565 nm; Figure III-32). As for the emission experiments, the overall fluorescence intensity registered was not only affected by **SZMC3$_{zw}$** molar fraction in each solvent, but also by the variation of its fluorescence quantum yield. As shown in Figure III-32, large Φ_{fl} values were determined in aprotic solvents, which are higher than Φ_{fl} = 0.65 in all the cases. By contrast, clearly lower Φ_{fl} values were measured in protic solvents such as water and MeOH, which combined with the poor stability of **SZMC3$_{zw}$** in these media resulted in significantly lower emission intensities. In addition, larger solvatochromic effects were observed for the spectral maxima of the emission spectra of **SZMC3$_{zw}$**, which ranged from $\lambda_{fl,max}$ = 582 nm in toluene to $\lambda_{fl,max}$ = 619 nm in water.

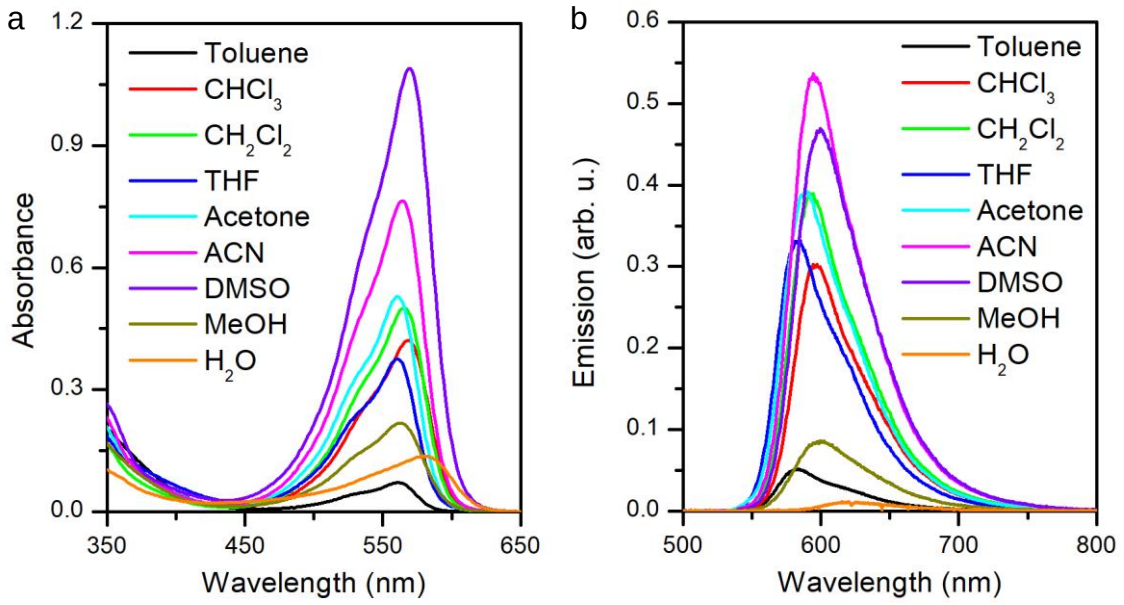

Figure III-32. (a) Absorbance spectra of the **SZMC3$_{zw}$-SZMC3$_a$** equilibrium mixture (c_{SZMC3} = 2.1x10^{-4} M) in selected solvents at 298 K. (b) Emission spectra of the **SZMC3$_{zw}$-SZMC3$_a$** equilibrium mixture (c_{SZMC3} = 4.0x10^{-5} M) in the same solvents at 298 K.

III.8.2. SZMC3-based optical probes for organic solvent detection

Owing to the solvent dependence of **SZMC3$_{zw}$** molar fraction and fluorescence quantum yield in the neutral state of the system, we envisioned the use of this compound as a chromic and fluorescent probe for organic liquid detection. As a proof of concept, we selected acetonitrile as an analyte, as it should lead both to high visible absorbance and fluorescence intensities due to the large $\chi_{SZMC3zw}$ and Φ_{fl}

values that **SZMC3$_{zw}$** has in this solvent. Therefore, if this species was dissolved in a medium where it has low stability and/or fluorescence quantum yield (e.g., toluene and water), the addition of increasing amounts of acetonitrile should result in a clear increase in the registered absorption and emission signals. This is proven by results shown in Figure III-33, which plots the change in fluorescence intensity of **SZMC3$_{zw}$** in toluene-acetonitrile and water-acetonitrile mixtures of variable composition.

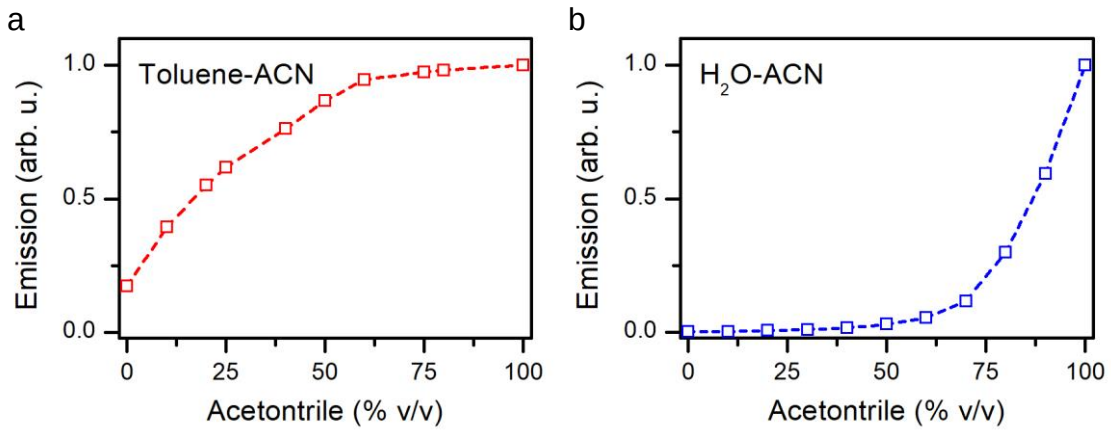

Figure III-33. Relative emission intensities measured for **SZMC3$_{zw}$** upon adding increasing amounts of acetonitrile to (a) toluene and (b) water.

Prompted by these results, we then embedded the neutral state of **SZMC3** in thin films of two different polymers to fabricate solid state sensors of acetonitrile. On one hand, we selected polystyrene (PS), as its polarity resembles that of toluene and, therefore, should lead to low **SZMC3$_{zw}$** absorption and fluorescence in the absence of the analyte. The same applies for the second polymer of choice, polyvinyl alcohol (PVA), whose protic character should result in both low stability and fluorescence quantum yields for **SZMC3$_{zw}$**. In both cases, the films were prepared by drop-casting a solution of the polymer and the molecular switch onto a container and evaporating the solvent. As expected, the resulting films showed dim pink color and red fluorescence (Figure III-34). However, when swollen with acetonitrile, a dramatic increase in coloration was seen for the PS film and a large enhancement in fluorescence emission was observed for the PVA film (Figure III-34). Therefore, these results prove that the solvent-induced switching between the zwitterionic and neutral aromatic isomers of **SZMC3** could be used for the optical detection of organic liquids.

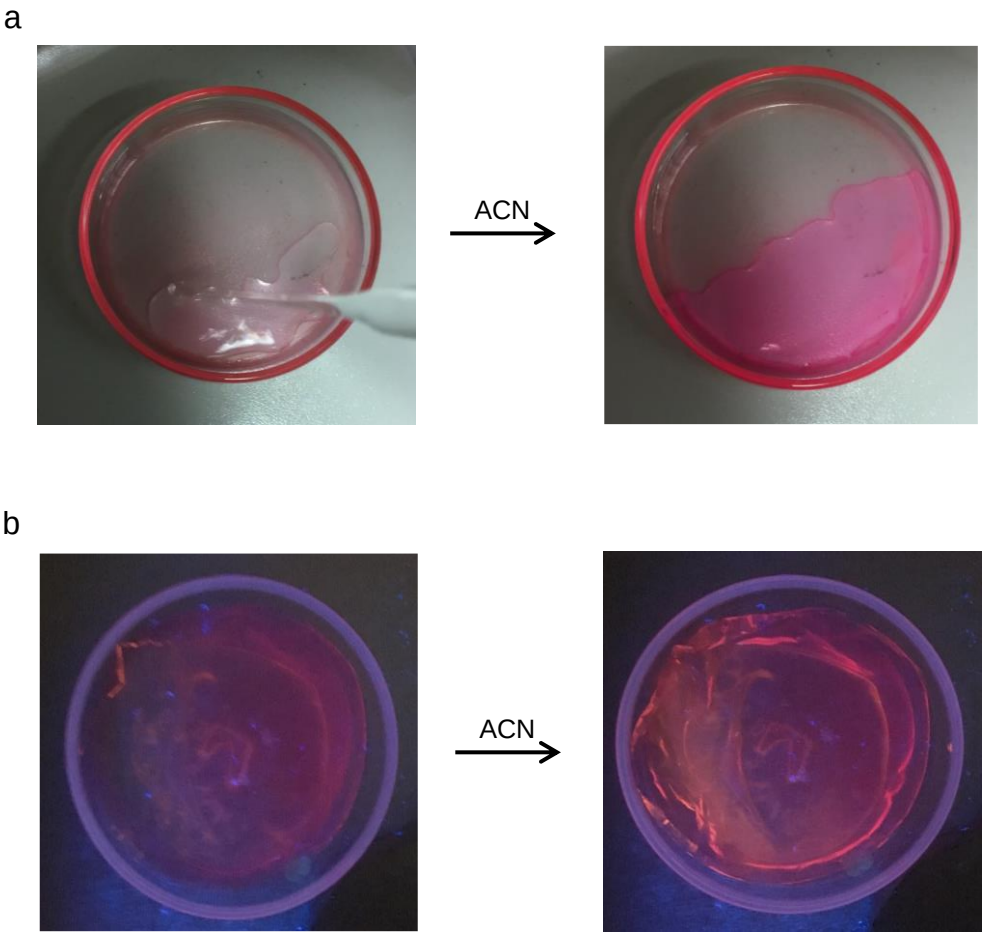

Figure III-34. (a) Photographs under ambient illumination of a **SZMC3**-loaded polystyrene film before and after swelling with acetonitrile. For sake of comparison, only half of the film was exposed to the organic solvent. (b) Photographs in the dark and under UV irradiation of a **SZMC3**-loaded poylviniyl alcohol film before and after acetonitrile swelling.

III.9. SUMMARY AND CONCLUSIONS

In this chapter new responses and stimuli have been described for **SZMC1-4** in combination with its possible applications. The following conclusions are inferred from the results obtained in these studies:

- **SZMC3** *chromic and fluorescent thermal switching* mechanism was observed for **SZMC1**, **SZMC2** and **SZMC4**. **SZMC1** and **SZMC2** ring opening occurred at temperatures higher than 390K and 350K respectively due to stronger electrowithdrawing character of the third nitro group which stabilized the **SZMC$_{zw}$** form. In the case of the **SZMC4**, the equilibrium **SZMC4$_{zw}$:SZMC4$_{n}$** was seen for the whole temperature range studied with a higher proportion of the neutral form than **SZMC3** at the same temperature**.** The thermal stability differences between the pairs **SZMC1$_{zw}$:SZMC2$_{zw}$** and **SZMC3$_{zw}$:SZMC4$_{zw}$** were attributed to the steric hindrance of the pending alkyl chains, observing lower stability for **SZMC2** and

SZMC4 tethering the bulkier cyclohexyl group. These results not only extend the thermal switching to the rest of SZMC studied but also demonstrate that the onset temperature can be tuned by modification of the steric hindrance of the pending groups**.**

- The *protonated* ***SZMC$_c$*** *state* could be reversibly generated for all the SZMC studied in a similar manner than the **SZMC$_{zw}$-SZMC$_a$** transformation. We also provided univocal evidence that the structure of this cationic form is the result of the opening of the spirocyclic structure in contrast to the proposal from Haldar and coworkers[39] that maintains this feature. **SZMC1$_c$** state was used in combination with **SZMC1$_{zw}$** and **SZMC1$_a$** forms to prepare *wide range pH sensors* in acetonitrile and its implementation in solid state by incorporating **SZMC1** in a PMMA film.
- The redox experiments carried out with **SZMC** provided evidence that the transformation between **SZMC$_{zw}$** and **SZMC$_c$** could also achieved *electrochemically*. This results in combination with the already reported redox switching between **SZMC1$_a$** and **SZMC1$_{zw}$**, allowed us to prepare *electrochromic and electrofluorochromic displays* based on ionogels.
- **SZMC1** and **SZMC2** were employed as *chemosensors* for the sensing of cyanide and fluoride in the presence of many common anions. The *addition of anions* resulted in the loss of fluorescence which was attributed to the acid-base interaction of the analytes with the guanidinium proton.
- The effect of the solvent on the **SZMC3$_{zw}$:SZMC3$_n$** was studied for a wide range of solvents. Polar solvents were seen to stabilize the more polar **SZMC3$_{zw}$** in contrast to apolar where almost only **SZMC3$_n$** was present with A significant exception was the higher abundancy of **SZMC3$_n$** in protic solvents which was attributed to hydrogen bonding. Upon temperature modification solvents with no hydrogen bonding sites showed significant changes in the **SZMC3$_{zw}$:SZMC3$_n$** ratio in contrast to solvents with a higher capacity of forming hydrogen bonds which presented lower sensitivity towards temperature modification. Fluorescence quantum yields were seen to decrease significantly in the presence of protic solvents. All these features combined allowed us to prepare sensing devices for organic solvents by embedding **SZMC3** in an apolar PS film and a protic PVA film. In this manner significant changes in color and fluorescence respectively were seen upon acetonitrile addition proving the use of **SZMC3** as a *chemosensor*.

III.10. REFERENCES

1 A. P. de Silva and S. Uchiyama, *Nat. Nanotechnol.*, 2007, **2**, 399–410.

2 T. Sarkar, K. Selvakumar, L. Motiei and D. Margulies, *Nat. Commun.*, 2016, **7**, 11374.

3 T. Majumdar, B. Haldar and A. Mallick, *Sci. Rep.*, 2017, **7**, 3–9.

4 I. Gallardo, G. Guirado, J. Hernando, S. Morais and G. Prats, *Chem. Sci.*, 2016, **7**, 1819–1825.

5 R. Zheng, X. Mei, Z. Lin, Y. Zhao, H. Yao, W. Lv and Q. Ling, *J. Mater. Chem. C*, 2015, **3**, 10242–10248.

6 X. L. Lu and M. Xia, *J. Mater. Chem. C*, 2016, **4**, 9350–9358.

7 P. Chen, Q. Li, S. Grindy and N. Holten-Andersen, *J. Am. Chem. Soc.*, 2015, **137**, 11590–11593.

8 J. Shen, J. Pang, T. Kalwarczyk, R. Hołyst, X. Xin, G. Xu, X. Luan and Y. Yang, *J. Mater. Chem. C*, 2015, **3**, 8104–8113.

9 J. Shen, Z. Wang, D. Sun, C. Xia, S. Yuan, P. Sun and X. Xin, *ACS Appl. Mater. Interfaces*, 2018, **10**, 3955–3963.

10 T. Han, X. Feng, D. Chen and Y. Dong, *J. Mater. Chem. C*, 2015, **3**, 7446–7454.

11 M. Chhatwal, A. Kumar, V. Singh, R. D. Gupta and S. K. Awasthi, *Coord. Chem. Rev.*, 2015, **292**, 30–55.

12 P. S. Hariharan, N. S. Venkataramanan, D. Moon and S. P. Anthony, *J. Phys. Chem. C*, 2015, **119**, 9460–9469.

13 S. J. Yoon, J. W. Chung, J. Gierschner, K. S. Kim, M. G. Choi, D. Kim and S. Y. Park, *J. Am. Chem. Soc.*, 2010, **132**, 13675–13683.

14 W. R. Browne, M. M. Pollard, B. De Lange, A. Meetsma and B. L. Feringa, *J. Am. Chem. Soc.*, 2006, **128**, 12412–12413.

15 H. Gu, L. Bi, Y. Fu, N. Wang, L. Shaoqin and Z. Tang, *Chem. Sci.*, 2013, **4**, 4371–4377.

16 N. L. Bill, J. M. Lim, C. M. Davis, S. Bähring, J. O. Jeppesen, D. Kim and J. L. Sessler, *Chem. Commun.*, 2014, **50**, 6758–6761.

17 C. Zhu, X. Ji, D. You, T. L. Chen, A. U. Mu, K. P. Barker, L. M. Klivansky, Y. Liu and L. Fang, *J. Am. Chem. Soc.*, 2018, **140**, 18173–18182.

18 B. Bin Cui, J. H. Tang, J. Yao and Y. W. Zhong, *Angew. Chem. Int. Ed.*, 2015, **54**, 9192–9197.

19 H. Zou, Y. Hai, H. Ye and L. You, *J. Am. Chem. Soc.*, 2019, **141**, 16344–16353.

20 C. Guerrin, Y. Aidibi, L. Sanguinet, P. Leriche, S. Aloise, M. Orio and S. Delbaere, *J. Am. Chem. Soc.*, 2019, **141**, 19151–19160.

21 G. Szalóki, O. Alévêque, J. L. Pozzo, R. Hadji, E. Levillain and L. Sanguinet, *J. Phys. Chem. B*, 2015, **119**, 307–315.

22 D. S. Kim, V. M. Lynch, J. S. Park and J. L. Sessler, *J. Am. Chem. Soc.*, 2013, **135**, 14889–14894.

23 O. A. Bozdemir, R. Guliyev, O. Buyukcakir, S. Selcuk, S. Kolemen, G. Gulseren, T. Nalbantoglu, H. Boyaci and E. U. Akkaya, *J. Am. Chem. Soc.*, 2010, **132**, 8029–8036.

24 F. Terrier, *Nucleophilic aromatic displacement: The influence of the nitro group*, Wiley-VCH, 1991.

25 G. Prats, Universitat Autònoma de Barcelona, 2012.

26 I. Gallardo and G. Guirado, *Electrochem. commun.*, 2007, **9**, 173–179.

27 R. O. Al-Kaysi, J. L. Bourdelande, I. Gallardo, G. Guirado and J. Hernando, *Chem. Eur. J.*, 2007, **13**, 7066–7074.

28 R. O. Al-Kaysi, I. Gallardo and G. Guirado, *Molecules*, 2008, **13**, 1282–1302.

29 S. H. Park, N. Kwon, J. H. Lee, J. Yoon and I. Shin, *Chem. Soc. Rev.*, 2020, **49**, 143–179.

30 L. Wu, C. Huang, B. P. Emery, A. C. Sedgwick, S. D. Bull, X. P. He, H. Tian, J. Yoon, J. L. Sessler and T. D. James, *Chem. Soc. Rev.*, 2020, **49**, 5110–5139.

31 G. Zhang, D. Zhang, Y. Zhou and D. Zhu, *J. Org. Chem.*, 2006, **71**, 3970–3972.

32 D. H. Qu, Q. C. Wang and H. Tian, *Angew. Chem. Int. Ed.*, 2005, **44**, 5296–5299.

33 T. B. Norsten and N. R. Branda, *J. Am. Chem. Soc.*, 2001, **123**, 1784–1785.

34 H. Tian, B. Chen, H. Y. Tu and K. Müllen, *Adv. Mater.*, 2002, **14**, 918–923.

35 M. Irie, T. Fukaminato, T. Sasaki, N. Tamai and T. Kawai, *Nature*, 2002, **420**, 759–760.

36 R. O. Al-Kaysi, G. Guirado and E. J. Valente, *Eur. J. Org. Chem.*, 2004, 3408–3411.

37 G. Prats, Universitat Autònoma de Barcelona, 2012.

38 N. A. Vázquez-Mera, J. R. Otaegui, R. S. Sánchez, G. Prats, G. Guirado, D. Ruiz-Molina, C. Roscini and J. Hernando, *ACS Appl. Mater. Interfaces*, 2019, **11**, 17751–17758.

39 T. Das, A. Pramanik and D. Haldar, *Sci. Rep.*, 2017, **7**, 1–12.

40 E. Evangelio, J. Hernando, I. Imaz, G. G. Bardají, R. Alibés, F. Busqué and D. Ruiz-Molina, *Chem. Eur. J.*, 2008, **14**, 9754–9763.

41 G. Nishimura, Y. Shiraishi and T. Hirai, *Chem. Commun.*, 2005, **1**, 5313–

5315.

42 T. Zhang, S. Dong, F. Zhao, M. Deng, Y. Fu and C. Lü, *Sensors Actuators, B Chem.*, 2019, **298**, 126869.

43 S. Rondinini, *Anal. Bioanal. Chem.*, 2002, **374**, 813–816.

44 R. J. C. Brown, A. C. Keates and P. J. Brewer, *Sensors*, 2010, **10**, 9982–9993.

45 B. C. Thompson, O. Winther-Jensen, B. Winther-Jensen and D. R. Macfarlane, *Anal. Chem.*, 2013, **85**, 3521–3525.

46 S. Espinosa, E. Bosch and M. Roses, *Anal. Chem.*, 2000, **72**, 5193–5200.

47 M. Benet, Universitat Autònoma de Barcelona, 2018.

48 A. Cannavale, U. Ayr, F. Fiorito and F. Martellotta, *Energies*, 2020, **13**, 1449.

49 P. Audebert and F. Miomandre, *Chem. Sci.*, 2013, **4**, 575–584.

50 H. C. Moon, C. H. Kim, T. P. Lodge and C. D. Frisbie, *ACS Appl. Mater. Interfaces*, 2016, **8**, 6252–6260.

51 K. A. Krishnamachari, *Prog Food Nutr Sci*, 1986, **10**, 279–314.

52 T. I. Mudder, M. M. Botz and A. Akçil, *Bilim. Madencilik Derg.*, 2008, **47**, 27–42.

53 A. Chmyrov, T. Sandén and J. Widengren, *J. Phys. Chem. B*, 2010, **114**, 11282–11291.

54 F. G. Bordwell, *Acc. Chem. Res.*, 1988, **21**, 456–463.

55 T. Das and D. Haldar, *ACS Omega*, 2017, **2**, 6878–6887.

56 M. Mohar, *ChemistrySelect*, 2019, **4**, 5308–5314.

57 L. Kortekaas and W. R. Browne, *Chem. Soc. Rev.*, 2019, **48**, 3406–3424.

Chapter IV

Light-controlled pK_a modulation of phenols using dithienylethene photoswitches

In this chapter we describe the light-induced modulation of the acidity of phenols by conjugation to dithienylethene molecular photoswitches.

IV.1. INTRODUCTION

In the last century a wide range of chemical transformations have been described that grant access to all sort of molecules and materials. Thanks to this knowledge accurate control over what chemical reaction takes place, how it does so, and which products are formed can be accomplished for many reaction mixtures. However, this might be insufficient in cases such as polymer chemistry,[1] pharmacology,[2,3] catalysis,[4–6] or analyte detection,[7,8] in which control over *when* and *where* a certain process occurs is also crucial.[9–11] It is for this reason that the ability to control reactivity on demand using external stimuli has gained a great deal of interest in the recent years. Of special relevance in this field is to employ light as a stimulus,[1,4,9,10] due to the many advantages that were explained in detail in Chapter I.

There are mainly two different strategies to use light as a control agent of chemical reactions. On the one hand, light can be used to trigger a reaction by generating highly reactive and unstable species. This is the case of the excited states involved in most photochemical reactions,[12] the radicals formed via photoredox catalysis.[6] or the high energy intermediates created in many photoclick processes.[13,14] On the other hand, light can be employed to toogle between the two stable or metastable states of a molecular photoswitch exhibiting different reactivity,[9] thus opening the door to start and stop a reaction at will. In this and the two following chapters we will focus on the latter approach, which is applied to modulate a variety of processes with light.

IV.1.1. Light-controlled reactivity with molecular photoswitches

To light-control chemical reactions with molecular switches, a main requirement must be fulfilled: a large modulation in reactivity must be produced when reversibly interconverting between the two states of the system. This is normally achieved by exploiting two of the most obvious changes occurring upon photoconversion: (a) the variation in molecular geometry, and (b) the differences in electronic structure.

On the one hand, molecular photoswitch isomerization is often accompanied by a significant modification of the molecular geometry. Therefore, as the shape of the switch varies, two separate groups that are apart in the initial state of the system can be brought in closer contact, which can be employed to modulate reactivity by: (a) blocking the active site by increasing steric hindrance (Figure IV-1a),[15–17] or (b) approaching two functional groups showing cooperative effects (Figure IV-1b).[18–24] Such spatial changes are specially significant for azobenzenes,[17,19,25] stilbenes[26,27] and other *Z*/E isomerizing molecular switches[28–30] due to the different geometry of the double bond (Figure IV-1). Indeed most of the examples of light-modulated reactivity using geometrical changes employ a Z/E molecular switch.[31]

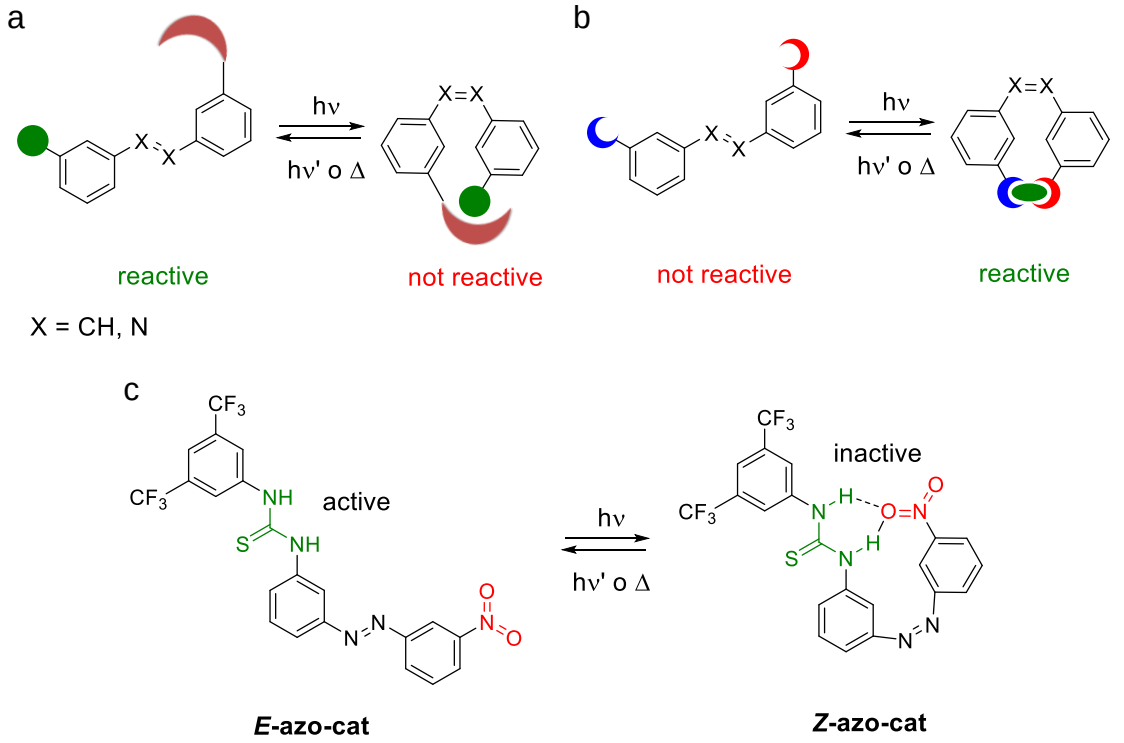

Figure IV-1. (a-b) General cases of light-controlled reactivity with *E*/*Z* molecular photoswitches using geometrical effects. In (a) photoisomerization from the *E*-isomer to the *Z*-isomer deactivates the reactivity by increasing the steric congestion around the active site.[16,17] In (b) the binding pocket required for the reaction is only present in the *Z*-isomer when two separate components become in closer contact and cooperatively interact.[19] (c) Photoisomerization from ***E*-azo-cat** to ***Z*-azo-cat** increases the steric hindrance around the thiourea moiety of the system and reduces its catalytic activity.[17]

An example of light-modulated reactivity employing this strategy is shown in Figure IV-1c, where Wu and coworkers demonstrated the optical control of the activity of the thiourea-based catalyst ***E*-azo-cat** furnishing a nitroazobenzene moiety.[17] Upon photogeneration of ***Z*-azo-cat**, the nitroazoaromatic unit approaches to the thiourea group and decreases its catalytic activity by steric congestion. This effect was applied

to a thiourea-catalyzed ring-opening polymerization process, whose conversion diminished from 94% to 30% upon ***E*-azo-cat**-to-***Z*-azo-cat** photoisomerization.[17]

Besides steric effects, the other common approach to photocontrol reactivity with molecular switches is to take advantage of the variation in electronic structure occurring upon photoisomerization, especially for systems operating under ring-opening and ring-closing isomerization reactions such as spiropyrans. In this case, the changes in conjugation,[32,33] hybridization[34,35] and functional groups[36,37] that occur upon photoisomerization can be exploited to differentiate the reactivity of each isomer (Figure IV-2a). Such strategy is exemplified in Figure IV-2b for the nitrospiropyran derivative **SP2**, where cyanide addition is only possible on **MC2** bearing an iminium moiety.[38] As a result, this system can be employed as a cyanide sensor which is only active after UV irradiation.[38]

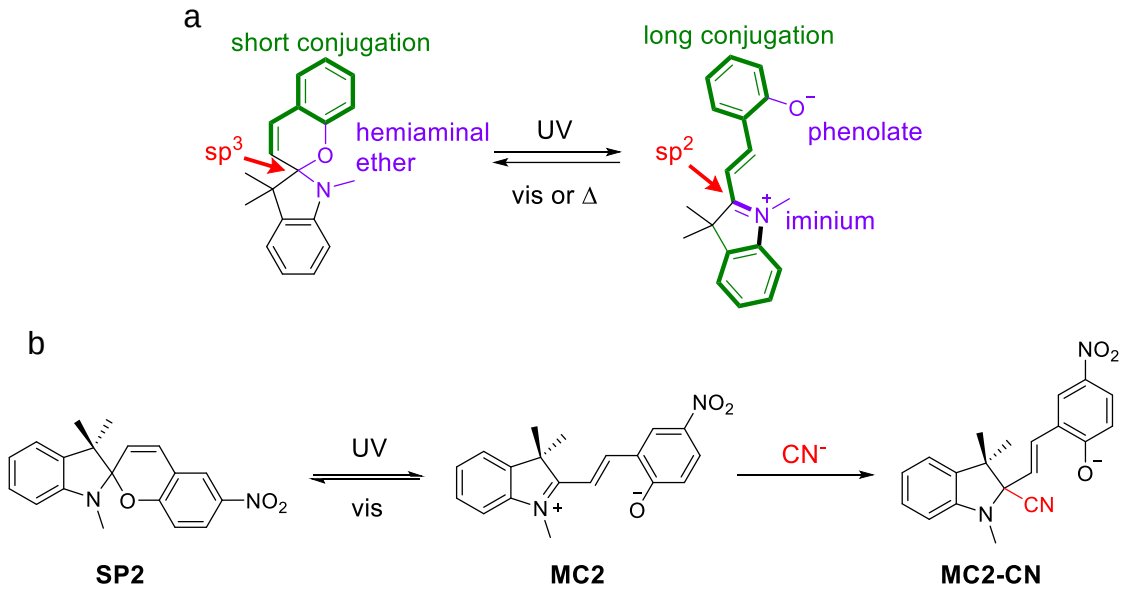

Figure IV-2 (a) Electronical changes that take place upon light-triggered isomerization in spiropyrans: it breaks the hemiaminal moiety to yield iminium and phenolate groups (purple), changes hemiaminal carbon atom from sp^3 to sp^2 hybridization (red) and extends the conjugation along the molecule (green). (b) Cyanide sensor **SP2** which is only active in the photoproduced **MC2** form.[38]

Another important feature about the use of molecular photoswitches to light-control reactivity is the role played by the photoisomerizable species in the target reaction (Figure IV-3). The two examples already described in this section are illustrative of two of the most common situations. On the one hand, the molecular switch can act as a catalyst that is reversibly activated or deactivated under illumination (Figure IV-3a),[17] as it is the case of the azobenzene derivative **azo-cat** in Figure IV-1c. This

is of special interest because high reactivity modulation can then be obtained with small amounts of molecular photoswitches.[5,39,40] Another possibility is to use the photoisomerizable compound directly as a reagent, which selectively (or more likely) reacts in one of its states (Figure IV-3b).[35,41,42] This is the case of the spiropyran **SP2** in Figure IV-2b undergoing cyanide addition only in its photoinduced merocyanine isomer.[41]

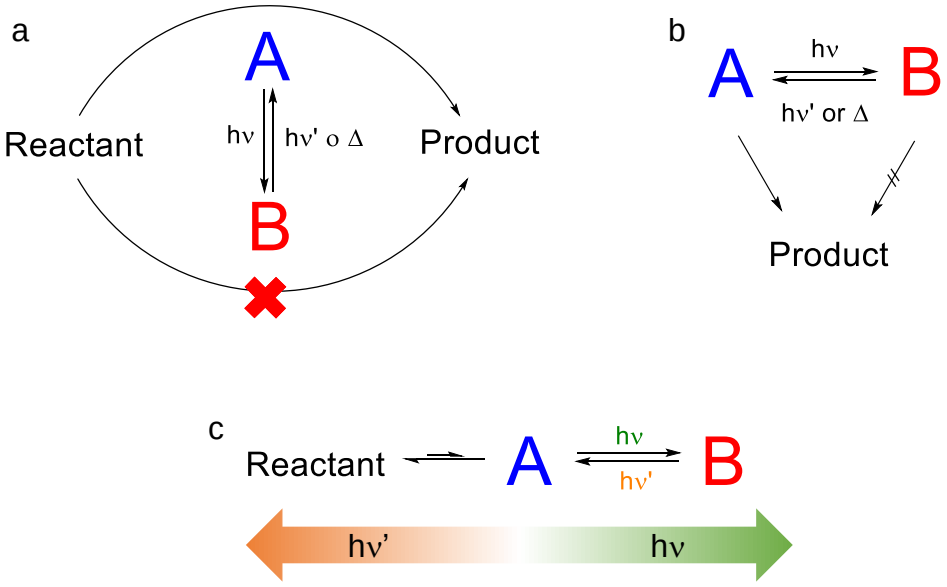

Figure IV-3. Scheme showing the possible roles of molecular switches in light-controlled reactions. (a) Molecular switches can act as modulable catalysts by photoisomerizing between active and inactive states.[17] (b) Molecular switches can be employed as reactants in which one of the states is more reactive than the other.[41] (c) Molecular switches be used to modify thermal equilibrium reactions by inhibiting the back reaction upon photoisomerization of the product and conversion into a different species.[36,43,44]

Alternatively, light-controlled reactivity can also be achieved by illuminating a photoswitchable unit in the product of an equilibrium reaction (Figure IV-3c).[36,43,44] The goal in this case is to remove or separate the functional groups involved in the back reaction of the process of interest upon photoisomerization, and thus modify the thermal equilibrium with light by converting the product into a new nonreacting (o less reacting) species. This situation is illustrated by the stilbene-based system presented in Figure IV-4, which comprises two different disulfide bonds that become labile and can be mutually exchanged in the presence of a base like 1,8-diazabicyclo(5.4.0) undec-7-ene (DBU) and a reducing agent dithiothreitol (DTT).[27] Under these conditions, an equilibrium mixture is therefore formed between compounds **stil1** and **stil2**, which differ in the structure of their intramolecular macrocyclic moiety that contains (**stil2**) or not (**stil1**) the *E*/*Z* photoswitchable stilbene unit. Such macrocyclic structure becomes highly strained for ***E*-stil2** bearing an extended *trans*-stilbene geometry, which explains why the equilibrium mixture in

the *E* state of the system is highly enriched with ***E*-stil1** (> 95%). By contrast, UV-induced photoisomerization into the bent *cis*-stilbene configuration makes ***Z*-stil2** much more stable and shifts the thermal equilibrium toward this compound (40:60 **stil1**:**stil2** concentration ratio).[27]

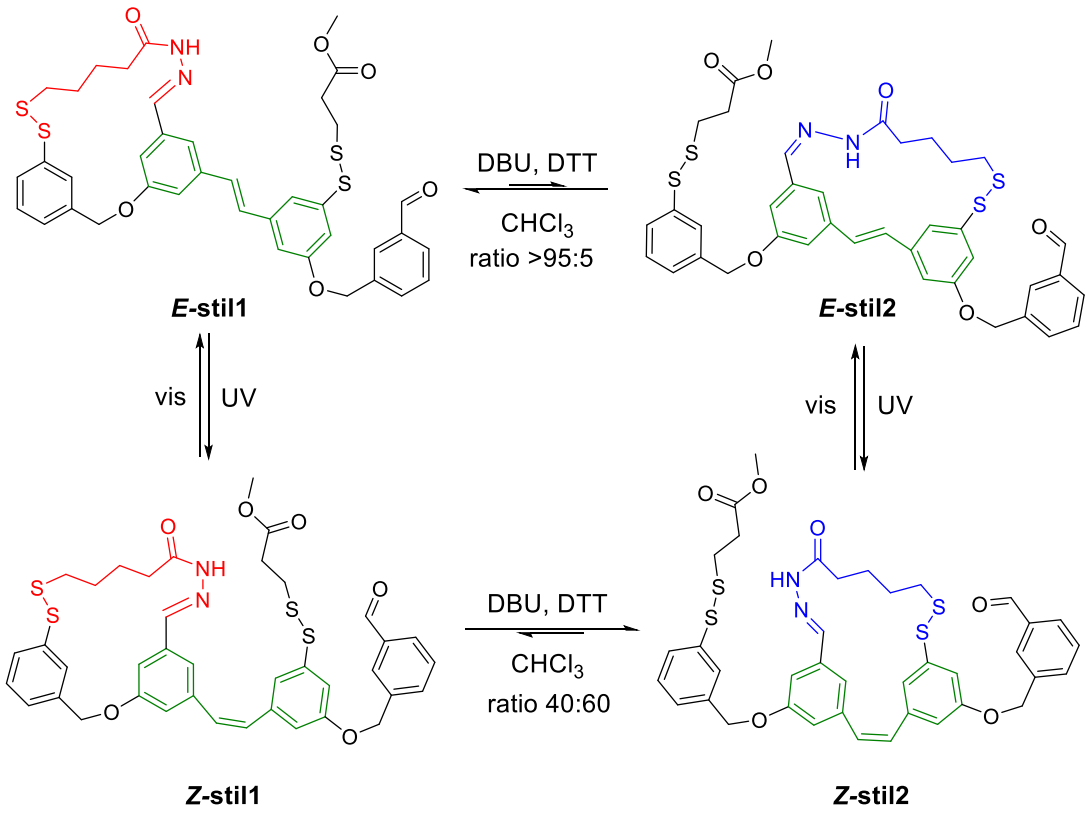

Figure IV-4. Example of thermal equilibrium modulation with light using a photoswitchable stilbene-based molecule.[27]

Despite the multiple possibilities to modulate reactivity with the spiropyran, azobenzene and stilbene photoswitches already shown, in this thesis we focused on a different family of photoisomerizable systems: dithienylethenes, which have also been widely used for light-controlled reactivity.

IV.1.2. Dithienylethenes

Dithienylethenes are molecular photoswitches which, in its more thermodynamically stable open isomer (**DTE$_o$**), are composed by two thiophene moieties connected through a *Z*-ethene bridge (Figure IV-5a).[45] They are the most well-known case of the family of diarylethene (DAE) photoswitches, where the thiophene rings can be replaced by other aryl groups.

Because free rotation takes place between the ethene linker and the thiophene rings, the structure of **DTE$_o$** is not planar. As a result, there is no electronic communication between the two aryl groups and **DTE$_o$** only shows strong absorption in the UV, and

sometimes violet, regions (Figure IV-5b). Upon irradiation with UV light, **DTE$_o$** undergoes a 6π electrocyclization reaction to form the closed isomer **DTE$_c$**, which presents an absorption band in the visible region because of its longer conjugation path (Figure IV-5). **DTE$_c$** is thermally stable in most of the cases and, therefore, it does not back isomerize over time in the dark. Exposure to visible light is instead required to induce the recovery of **DTE$_o$** via a an electrocyclic ring-opening reaction.[46]

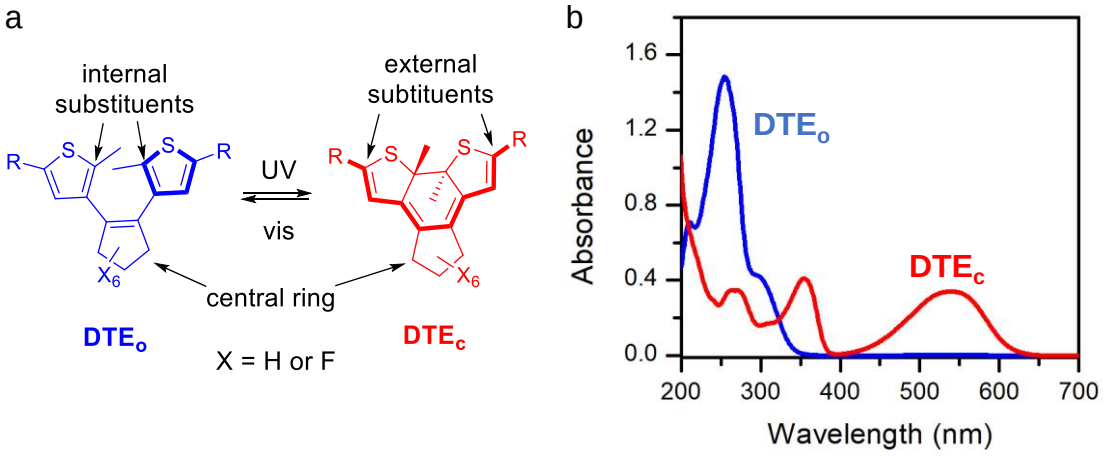

Figure IV-5. (a) General structure of the open (**DTE$_o$**) and closed (**DTE$_c$**) states of DTEs. (b) Characteristic UV-vis absorption spectra of **DTE$_o$** (blue) and **DTE$_c$** (red) (R = COOH and X = F).

Several common structural features are usually found in DTEs, which have an influence on their photochemical behavior (Figure IV-5a).[45,46] First, cyclic *Z*-ethene bridges are normally used (*central ring*), as this inhibits light-induced *cis-trans* photoisomerization in **DTE$_o$** that could compete with the desired ring-closing reaction. Cyclopentene groups are the most common choice for this purpose, which can be perfluorinated to enhance the molecular switch performance.[45,47] Second, *internal* substituents are generally introduced at the 2- and 2'- positions of the thiophene moieties to prevent further oxidation upon ring-closing driven by rearomatization, as observed during the photocyclization of *cis*-stilbenes.[48] In addition, *external* substituents are also typically tethered to the 5- and 5'-positions of the aryl groups, aiming at providing further functionality and/or modify the photochemistry of DTEs.

IV.1.2.a. **Strategies for the synthesis of dithienylethenes**

A great number of DTEs with very different structural motifs have been prepared since their initial discovery in 1987.[49] For this purpose, many synthetic strategies have been developed. In most of them, thiophene derivatives are employed as starting materials, and thus DTE syntheses are dominated by heteroaromatic chemistry, lithiation reactions and Suzuki couplings to either functionalize the heteroaromatic molecules or to tether them into the final structure. It is for this reason

that the formation of the central ring is the main feature that differentiates the most common synthetic methodologies.

A very frequent strategy involves the formation of the central ring through a McMurry reaction from a starting diketone tethering both thiophene rings. Such diketone is often the result of a double Friedel-Crafts acylation reaction with 2,5-substituted thiophene rings, which favors functionalization of the aryl groups at the desired 3-position (Scheme IV-1a). Compound **9** is prepared in this way, which is a common intermediate in many DTE syntheses due to its simple and scalable preparation as well as easy functionalization through lithiation-mediated reactions (Scheme IV-1b).[32]

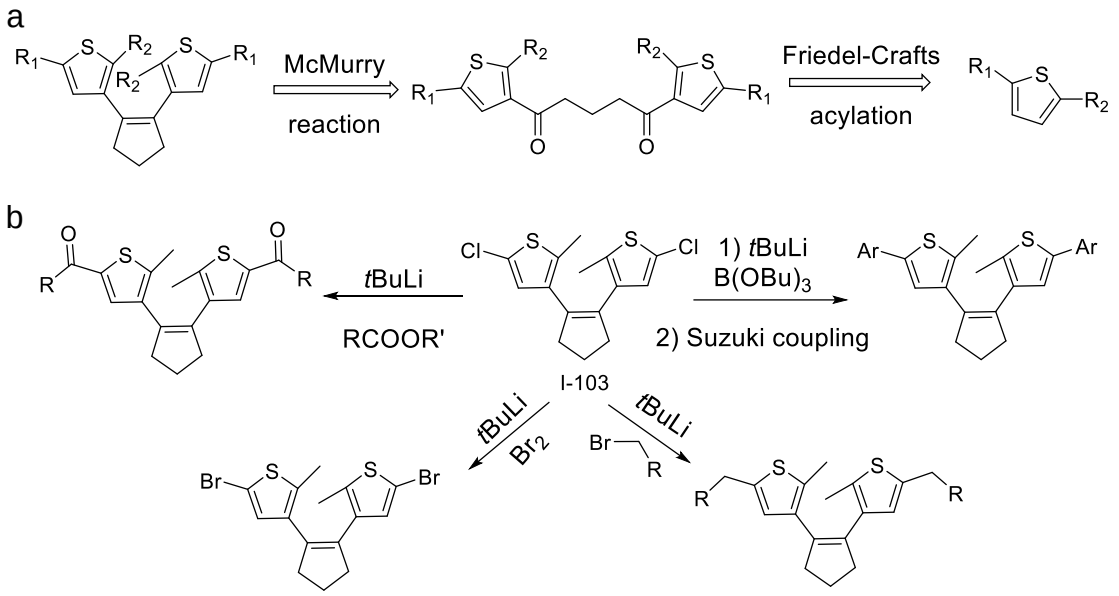

Scheme IV-1. (a) Retrosynthetic analysis for the formation of DTEs via McMurry reaction.[32] (b) Structure of common intermediate **9** obtained in this way, which grants access to a diversity of DTEs via different lithiation-mediated functionalization reactions.

In the case that the central ring cannot be formed by a McMurry reaction, it is generally incorporated through a Suzuki coupling from the corresponding aryl halides and boronic acids (Scheme IV-2). Generally, the boronic acids are formed from an aryl halide through lithiation[50] or via catalyzed direct borylation reactions.[51]

For the synthesis of DTEs bearing a fluorinated central ring, a different strategy is employed. Perfluorocyclopentene is used as a starting material and the thiophene rings are incorporated through direct lithiation reaction from the corresponding thienyl halides (Scheme IV-3).[52]

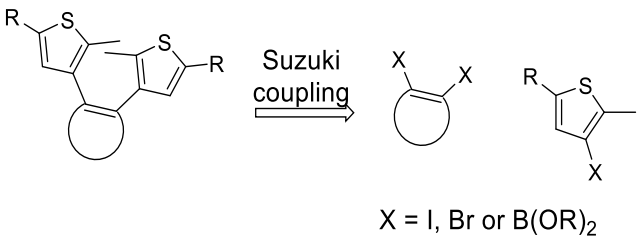

Scheme IV-2. Retrosynthetic analysis for nonfluorinated DTEs via Suzuki coupling.[50]

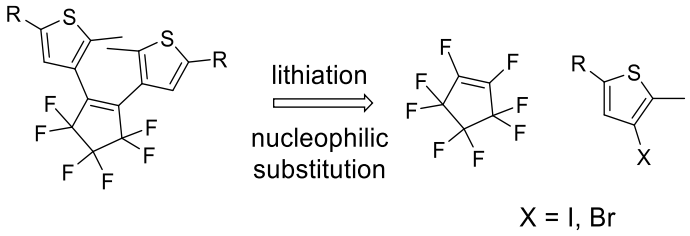

Scheme IV-3. Retrosynthetic analysis of fluorinated DTE.[52]

IV.1.2.b. **Photochemical properties of dithienylethenes**

Several structural, compositional and environmental factors govern the photochemistry of DTEs.[45,47] As mentioned above, the photoinduced ring-closing reaction of DTEs is favored by the presence of cyclic *Z*-ethene and 2-substituted thiophene moieties. However, other additional factors must be considered. One of them has to do with the nonplanar structure of **DTE$_o$**, which can take two main conformations: (a) a *parallel* conformation with both thiophenes arranged in a mirror symmetry, and (b) an *antiparallel* conformation that makes the molecule present a C_2 axis of symmetry (Scheme IV-4).[53] As the Woodward-Hoffman rules predict that the light-induced 6π-electrocyclization reaction of DTEs must be conrotatory (i.e., rings turning in the same direction), this means that only the antiparallel conformation of **DTE$_o$** can be photoconverted into the closed isomer and, indeed, it explains the *trans* relative stereochemistry of the internal substituents of **DTE$_c$** (Scheme IV-4).[53] On the other hand, the parallel conformation of **DTE$_o$** could undergo a thermal disrotatory ring-cyclization reaction (i.e., rings turning in different directions), which it is mostly prevented by the steric hindrance caused by the internal substituents.[53]

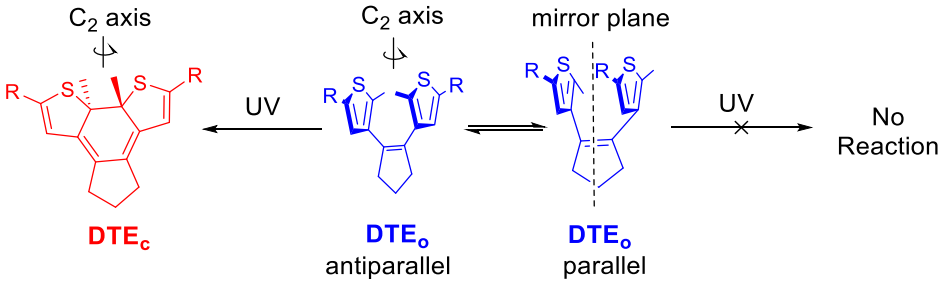

Scheme IV-4. Photochemical behavior of **DTE$_o$** parallel and antiparallel conformations.

Besides stereochemistry, cyclization quantum yields ($\Phi_{o\text{-}c}$) are also affected by the equilibrium between **DTE$_o$** parallel and antiparallel conformations. In general, most **DTE$_o$** isomers exist in a 1:1 ratio between both conformers;[54] therefore, only half of the absorbing **DTE$_o$** molecules can undergo the photochemical reaction and $\Phi_{o\text{-}c}$ values are limited to 0.5. In order to achieve a better efficiency in the cyclization reaction, a higher population of the antiparallel conformer is desired, which can be achieved by stabilizing this conformation by intramolecular interactions[55] or by introducing steric hindrance[56,57] in the internal positions.

Solvent is another feature that must be considered to assess the efficiency of the ring-closing reaction. In many DTEs a huge decrease in $\Phi_{o\text{-}c}$ has been measured upon solvent polarity increase.[58] This effect has been ascribed to intramolecular charge transfer processes that occur in the presence of both electron-rich and electron-poor groups in the molecule, especially when the external positions of the thiophenes are functionalized with electrodonating groups (EDG) and EWGs.[58,59]

In comparison to the ring-closing quantum yields, cycloreversion quantum yields ($\Phi_{c\text{-}o}$) are in general lower for DTEs. The main reason for this behavior is that, unlike the cyclization reaction, this transformation requires to overcome a nonnegligible energy barrier in the excited potential energy surface. As a result, $\Phi_{c\text{-}o}$ values are more affected by temperature than the ring-closing quantum yields.[60] Other differences with respect to the cyclization process is that the cycloreversion efficiency is almost unaffected by the solvent and it does not depend on any conformational equilibrium where **DTE$_c$** is involved. Instead, the aryl group substitution pattern has been proven to have a strong influence on $\Phi_{c\text{-}o}$. For instance, the introduction of EDGs such as methoxy substituents in the internal positions or π-conjugated groups in the external positions further lowers down the cycloreversion quantum yields.[45]

The irradiation of **DTE$_o$** under UV light hardly ever results in the complete transformation to the closed isomer because **DTE$_c$** also absorbs in this spectral region, which can then trigger the back photoisomerization reaction (see Figure IV-5b). It is for this reason that the photostationary state reached during the cyclization process is always a mixture of both isomers.[45] The molar fraction of each isomer in this mixture depends on their extinction coefficients at the irradiation wavelength and the quantum yields of the ring-closing and ring-opening processes. Therefore, high absorbance and $\Phi_{o\text{-}c}$ values for the open isomer at the irradiation wavelength are highly desirable, while low extinction coefficients and low quantum yields are preferred for **DTE$_c$**, especially in the UV and violet region.[45] Actually, the fact that most **DTE$_c$** show very moderate $\Phi_{c\text{-}o}$ values favors in this case the obtaining of **DTE$_c$**-enriched PSS mixtures. By contrast, visible light irradiation of **DTE$_c$** results in quantitative ring-opening, as **DTE$_o$** does not absorb in that region of the spectrum and the closed isomer can be excited selectively (see Figure IV-5b).[45]

DTEs are known to have excellent fatigue resistance and some have even been reported to support more than 10000 ring-opening and ring-closing cycles without a significant performance loss.[46] However, some degradation products can be irreversibly formed during the continuous operation of DTE photoswitches, which are mainly ascribed to the photoreactivity of the closed isomer when irradiated with UV light. In some cases, an oxidation by-product can be formed in the presence of oxygen (Scheme IV-5a).[61] However, for other DTE derivatives, degradation appears after a few cycles even in anoxic conditions due to the formation of the by-product shown in Scheme IV-5b.[61]

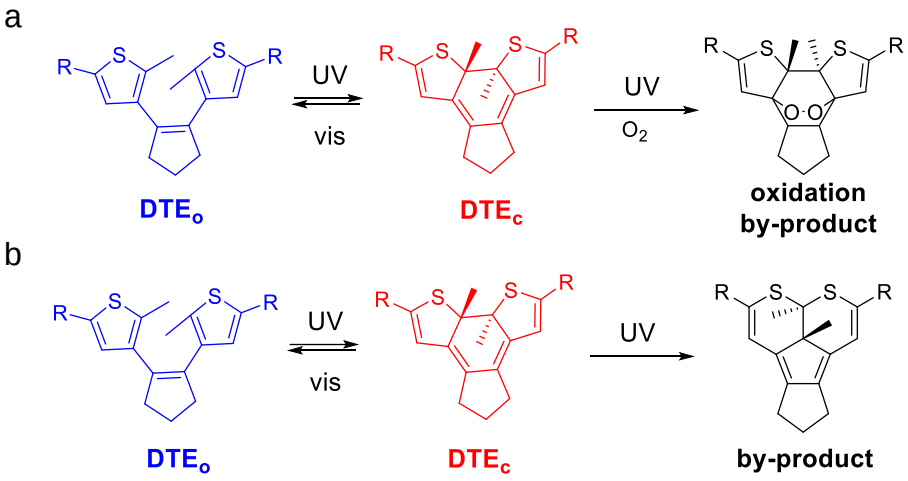

Scheme IV-5. (a) Oxidation by-product and (b) photodegradation by-product described in the literature for DTEs.[61]

IV.1.3. Light-controlled reactivity of dithienylethenes and other diarylethenes

DAEs and DTEs have a wide range of properties that change upon photoisomerization and can be exploited to modulate reactivity. For instance, the flexibility of their open isomer permits the convergence of two different thiophene substituents regardless of their position, which as described above could cooperatively interact to trigger a reaction (Figure IV-6a-b). By contrast, this cannot occur in the closed isomer, either because its defined stereochemistry places the internal substituents in relative *trans* configuration and, therefore, far from each other[22] (Figure IV-6a), or due to its higher rigidity[23,24,62] that does not allow the external substituents to approach (Figure IV-6b). Branda and coworkers used the first of these strategies to light-modulate the activity of a copper catalyst with a DTE ligand bearing two oxazoline moieties in its internal positions (Figure IV-6c).[22] As a consequence, only the **DTE-oxa$_o$** isomer could form a chelate with copper(I) ions and catalyze a cyclopropanation reaction, while the coordination of both ligands to the same metal center was inhibited in **DTE-oxa$_c$**.

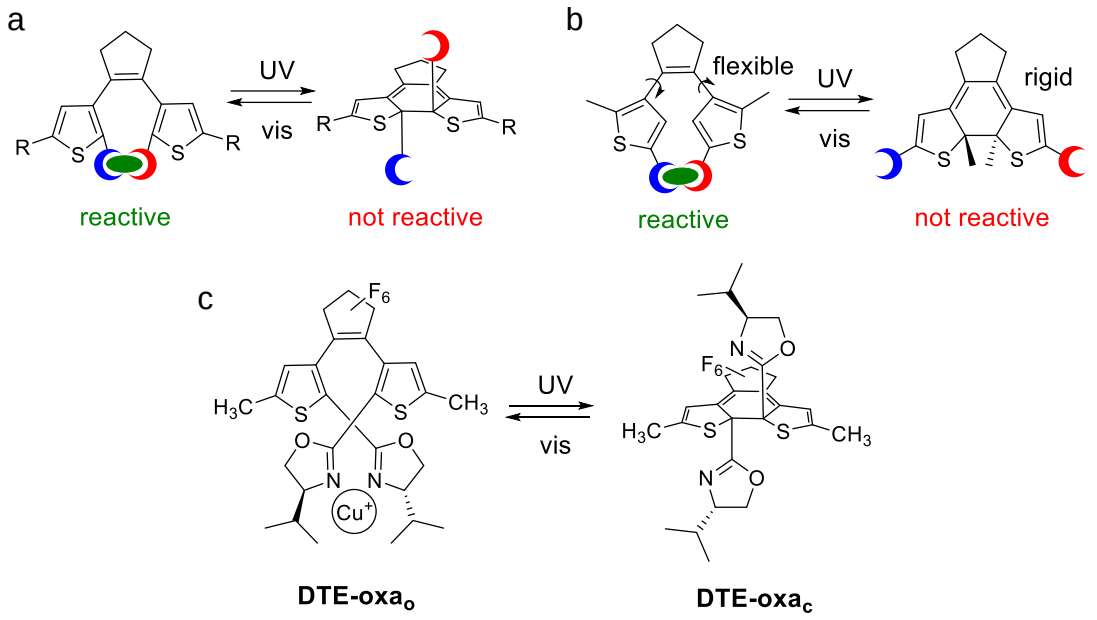

Figure IV-6. (a-b) Light control of chemical reactions using the geometrical changes induced upon DTE photoisomerization, which prevents (a) the internal[22] and (b) external[23,24,62] substituents in the closed isomer to approach each other and cooperatively interact to trigger a reaction. (c) Light-controlled cooper-based catalyst **DTE-oxa** prepared by Branda and coworkers, which is only active on the open state.[22]

Besides geometrical changes, DTEs also suffer a large variation in electronical properties upon isomerization. As shown in Scheme IV-6, carbon atom hybridization,[34,35] double bond location[43,63] or aromaticity[36,64] are some of the features that are modified upon ring-closing and have been exploited for light-controlled reactivity (Scheme IV-6).

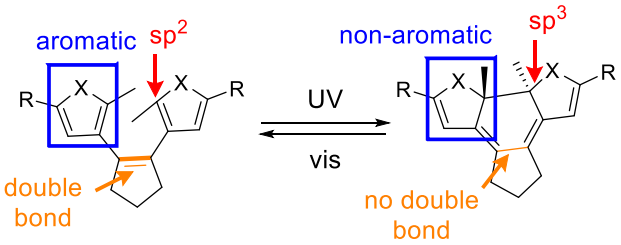

Scheme IV-6. Electronical changes that take place upon light-triggered ring-closing of DTEs: the isolated central double bond is removed and instead a conjugated diene is formed (orange); the hybridization of the carbons at the 2 and 2' positions of the thiophenes changes (red); and the aryl groups aromaticity is lost (blue).

The use of some of these features to modulate chemical reactivity is beautifully illustrated by the example in Scheme IV-7, where Hecht and coworkers employed the changes in aromaticity and carbon atom hybridization to modify the equilibrium between a phenol and an aniline that are interconverted through an imine formation reaction.[36] For this purpose, a **DAE-OH$_{phenol}$** was prepared by replacing a thiophene

group with a phenol moiety. Upon light-induced ring closing, the resulting enol (**DAE-OH$_{enol}$**) losses the aromatic stabilization and, therefore, it tautomerizes to the electrophilic ketone **DAE-OH$_{keto}$** (Scheme IV-7a). This compound can then undergo an equilibrium reaction in the presence of an amine to form **DAE-OH$_{imine}$**, which converts into amine **DAE-NH$_{aniline}$** upon ring opening (Scheme IV-7b). As **DAE-OH$_{keto}$** and **DAE-OH$_{imine}$** have significantly different absorption spectra, they can be selectively transformed into nonreacting **DAE-OH$_{phenol}$** and **DAE-OH$_{imine}$**, which allows pulling the equilibrium mixture towards the starting phenol (by irradiation at 450 nm) or the final aniline (by irradiation at 660 nm) at will.

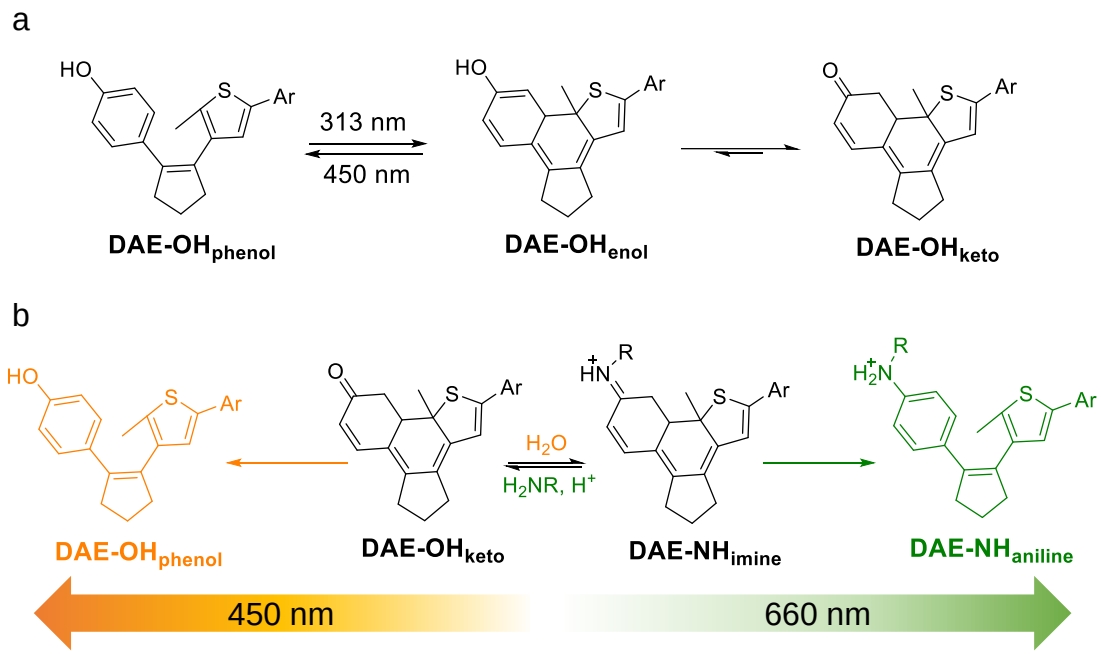

Scheme IV-7. (a) **DAE-OH** photoisomerization and tautomerization which occurs due to the aromaticity loss upon ring closing. (b) The **DAE-NH$_{phenol}$** and **DAE-OH$_{aniline}$** equilibrium mixture produce through an imine formation reaction can be selectively manipulated by illumination at 660 nm and 450 nm.[36]

The conjugation between thiophene substituents in DTEs is another important electronical feature that changes upon photoisomerization. As shown in Scheme IV-8, the two aryl groups are electronically insulated in the open isomer, while there is conjugation between the internal and external substituents of each thiophene - i.e., between A and B, and C and D. Upon isomerization, the conjugation path of the molecule changes and the external substituents (A and D) become electronically communicated while the internal (B and C) are now tethered to sp^3 carbons and become insulated.[45]

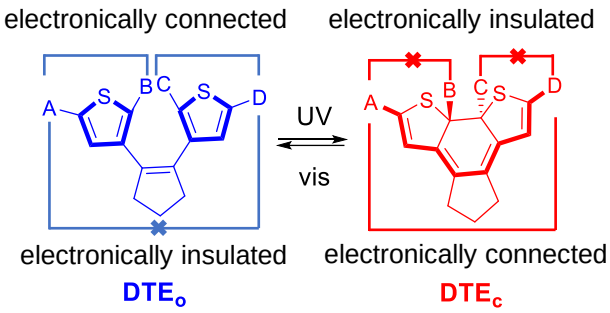

Scheme IV-8. Conjugation changes upon photoisomerization of DTEs.

This behavior has been widely explored to modulate the reactivity of the internal or external substituents by connecting and disconnecting them to EWGs or EDGs upon photoisomerization.[32,42] For instance, in the example shown in Scheme IV-9, the nucleophilic attack of **DTEpy1** to a benzyl bromide was slowed down by an order of magnitude when conjugating the pyridine nucleophile to the electron-withdrawing pyridinium group after photoconversion of **DTEpy1$_o$** to **DTEpy1$_c$**.[42]

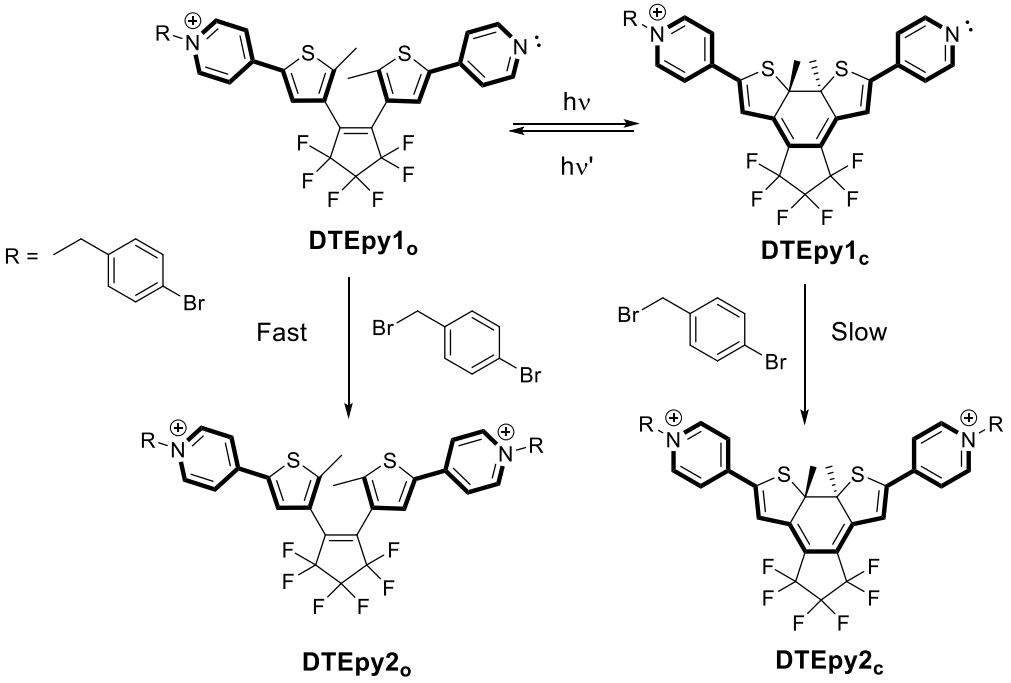

Scheme IV-9. Use of changes in DTE conjugation path to light-control reactivity. The conjugation of the pyridine group with an electron-withdrawing pyridinium moiety upon ring-closing photoisomerization of **DTEpy1** reduces the nucleophilicity of the nitrogen lone pair and, therefore, slows down the reaction.[42]

Because of the wide range of changes that DTEs suffer upon photoisomerization, they can play different roles to control chemical reactivity with light, as previously described for other photoswitches in section IV.1.1. For instance, the system **DTE-oxa** shown in Figure IV-6 is a good example of a light-modulated catalyst, while **DAE-**

OH allows optical modification of an equilibrium process (Scheme IV-8) and **DTEpy1** acts as a photomodulable reactant (Scheme IV-9). For all these reasons, many reactions can be light-controlled using DTEs and, in this thesis, we have focused on three particular cases: (a) the light modulation of the acidity of a phenol moiety, which is covered in this chapter; (b) the development of light-controllable coupling reagents for amide bond formation (see Chapter V); and (c) the optical control of Diels-Alder cycloadditions (see Chapter VI).

IV.1.4. Light modulation of acidity with dithienylethenes and other diarylethenes

To optically modulate acidity is of special interest as remote and noninvasive control of reactivity over time and space is highly attractive for many pH dependent biochemical and chemical processes. For instance, fields like polymer synthesis and processing,[65,66] drug delivery,[67,68] catalysis,[20,69–71] sensing[72] or molecular machines[37] highly benefit from the use of photocontrolled acids. The most common approach to reach this goal is by means of photoacids that release a proton upon irradiation.[73,74] Such method presents the disadvantage that, once triggered, the pH change cannot be reverted back. This issue can be solved if light is used to reversibly switch between two states with different acidity properties – i.e., different pK_a values. It is for this reason that many examples can be found in the literature of light-induced pK_a modulation employing molecular photoswitches such as azobenzenes,[70,75,76] spiropyrans[69,77] or DTEs.[78–81]

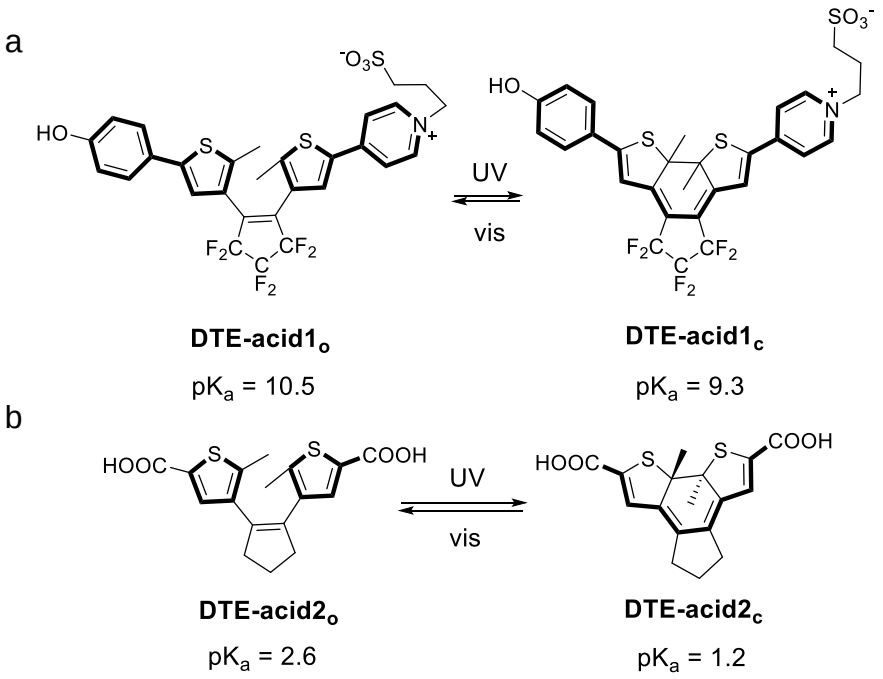

Scheme IV-10. (a-b) Examples of DTEs with light-controlled pK_a due to the different electronical communication between the thiophene substituents upon photoisomerization. (a)

DTE-acid1 was reported by Lehn and coworkers, whose pK_a values were measured in methanol/water 5:2.[78] **DTE-acid1** was described by Coudret and coworkers, who measured pK_a values in acetonitrile.[82] In both cases the conjugation paths of the open an closed isomers are highlighted in bold.

The most common approach to modulate pK_a with DTEs and other DAEs is to capitalize on the different electronic communication between substituents to connect and disconnect an acidic moiety with an EWG upon photoisomerization.[78–82] This is the case of the phenol-DTE[78] and carboxylic acid-DTE[82] conjugates shown in Scheme IV-10, whose closed states have larger acidities because of the stabilizing effect of the electronically conjugated EWG (pyridinium cation, carboxylic acid) on the phenolate and carboxylate moieties formed upon deprotonation, respectively.

In this way only rather moderate pK_a modulations have been achieved, which are typically lower than 1.5 pK_a units.[78,82] Moreover, stability problems have been observed for those DTEs bearing perfluorinated central rings such as **DTE-acid1$_o$**, because fluorine atoms are exchanged through nucleophilic substitution reactions with the base (Scheme IV-11).[78]

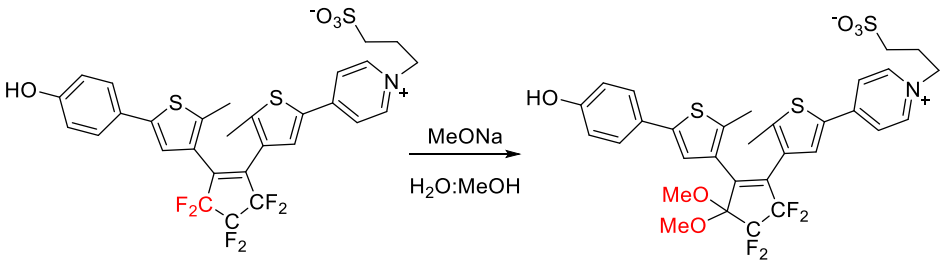

Scheme IV-11. DTE-acid1$_o$ fluorine atoms undergo nucleophilic substitution in the presence of methoxide.[78]

Despite these shortcomings, light-induced pK_a modulation in DTEs has already been proven of use for several applications, even when moderate changes in acidity are optically accomplished.[66,81] This is the case of **DTE-acid3** in Scheme IV-12,[81] where switching the electronic communication between the carboxylic acid moiety and the electron-withdrawing nitrile group resulted in a slight pK_a decrement from 17.6 to 16.4 upon ring closing. In spite of this, when using **DTE-acid3** to trigger the cationic polymerization of vinyl ethers, significant modulation of polymer chain dispersity was achieved under illumination, as it is highly dependent on the strength of the acid initiator employed.

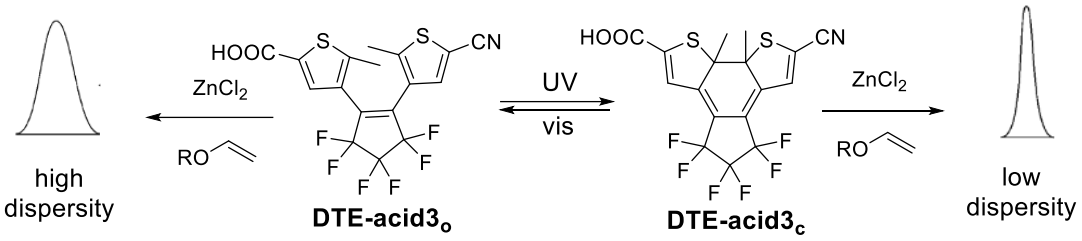

Scheme IV-12. DTE-acid3 with light-variable acidity was employed by Chiu and coworkers to control the chain dispersity in the cationic polymerization of vinyl ethers.[81]

Recently, a different strategy was reported by Hecht and coworkers to achieve larger light-induced pK_a modulation in DAEs. For this purpose, they prepared **DAE-acid** by replacing one of the thiophene groups of DTEs with a 3H-thiazolone moiety showing acid-base properties (Scheme IV-13). In this case, instead of exclusively relying on the difference in electronical communication between substituents, the authors also took advantage of the loss in aromaticity to isolate the acidic moiety and thus avoid stabilization of the conjugate base by charge delocalization. With both effects combined, a modulation of 2.8 pK_a units was achieved, which is so far the highest pK_a modulation obtained with DAEs in the literature.[71]

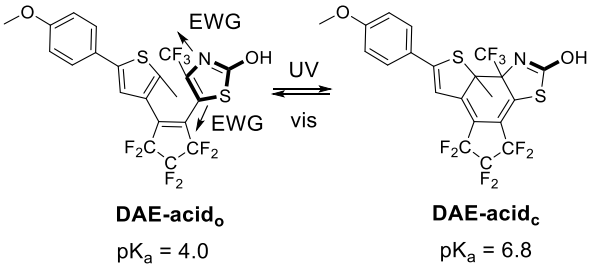

Scheme IV-13. Light-induced pK_a modulation in **DAE-acid** prepared by Hecht and coworkers.[71] Up to 2.8 pK_a units modulation in acetonitrile:water 3:7 was obtained due to the combination of the loss of aromaticity and lack of EWG inductive effects in the closed form.

Despite the landmark set by Hecht's group work, it still falls short when compared to the larger light-induced pK_a modulations obtained with spiropyrans. This is due to the interconversion between two groups with distinctive acidities upon spiropyran photoisomerization: an ammonium moiety in the initial spiropyran state and a phenol group in the photoinduced merocyanine form.[69,77] Indeed, up to an increment of 4.1 units in pK_a was reported by Andréasson and coworkers for **SP-acid**, which is to our knowledge the highest obtained with molecular photoswitches (Scheme IV-14).[77] However, these systems present a severe drawback: their photoisomerization is reverted back in the dark over time as spiropyrans are T-type molecular photoswitches. As a result, intense and constant irradiation is necessary to maintain the pH change.[69] Moreover, thermal back isomerization also hampers the actual pH

modulation obtained despite the high intrinsic pK_a difference between both isomers, as it often leads to lower photoconversions even under strong irradiation.

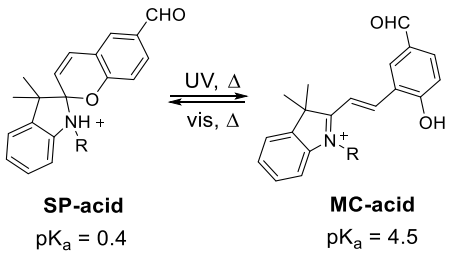

Scheme IV-14. pK_a modulation with spiropyran **SP-acid**. The ring opening process switches the acidic moiety from an ammonium to a phenol group, which allows reaching a difference in 4.1 pK_a units in water.[77]

IV.2. OBJECTIVES

In view of the precedents described above, in this part of thesis we further explored the use of DTE photoswitches to optically control acidity, eventually aiming at:

- Synthesizing and characterizing new DTE derivatives exhibiting *larger light-induced pK_a modulation*.
- Introducing pK_a-modulable functional groups in these compounds that *could find multiple applications in the field of light-controlled reactivity*.

To reach these objectives we applied the following strategy, which is based on three main principles:

(a) To use DTEs to photocontrol the *acidity of phenols*. Phenols were chosen because their aromatic structure can be strongly conjugated to EDGs and EWGs and even altered when incorporated into DTEs, which could dramatically affect their acidity, the basicity and nucleophilicity of their conjugate base, and their capacity to undergo keto-enol tautomerism. As these properties are of relevance in many different chemical processes like polymer synthesis,[66] amide and ester bond formation via coupling reagents,[83] or even CO_2 capture,[84] we envisaged that phenol-DTE conjugates showing ample light-induced pK_a modulation could have an impact in a variety of fields.

(b) To optically *modulate the acidity of phenol-DTE conjugates by switching the electronical communication* between a phenol moiety placed at the external position of one thiophene ring and an EWG introduced at the same position of the other aryl group (**DTE-EWG**, Scheme IV 15). As described above, this makes both substituents to be selectively connected in the closed isomer of the system,

thus stabilizing the phenolate conjugate base formed upon deprotonation and increasing the acidity of **DTE$_c$-EWG**.

(c) To test *the effect of a variety of EWGs* in **DTE-EWG** compounds in order to reach maximal light-induced pKa modulation. In particular, the following electron-withdrawing groups were considered that operate under mesomeric and/or inductive effects (Scheme IV-15): formyl (**DTE-CHO**), trifluoroacetyl (**DTE-COCF$_3$**), pentafluorophenyl (**DTE-C$_6$F$_5$**), pyridinium (**DTE-py-zw**), nitro (**DTE-NO$_2$**), 4-nitrophenyl (**DTE-PhNO$_2$**), 2,4-dinitrophenyl (**DTE-Ph(NO$_2$)$_2$**) and 5-nitropyridinium (**DTE-pyNO$_2$-zw**) groups. A perhydrogenated cyclopentene central ring was used in all the cases to prevent the degradation process observed by Lehn and coworkers for fluorinated phenol-DTE conjugates in basic media (see Scheme IV 11).[78] In spite of this, the introduction of a perfluorinated cyclopentene central ring was considered for one of the EWGs tested (**DTE$_F$-COCF$_3$**) in order to assess the effect of this structural variation on photoinduced acidity modulation.

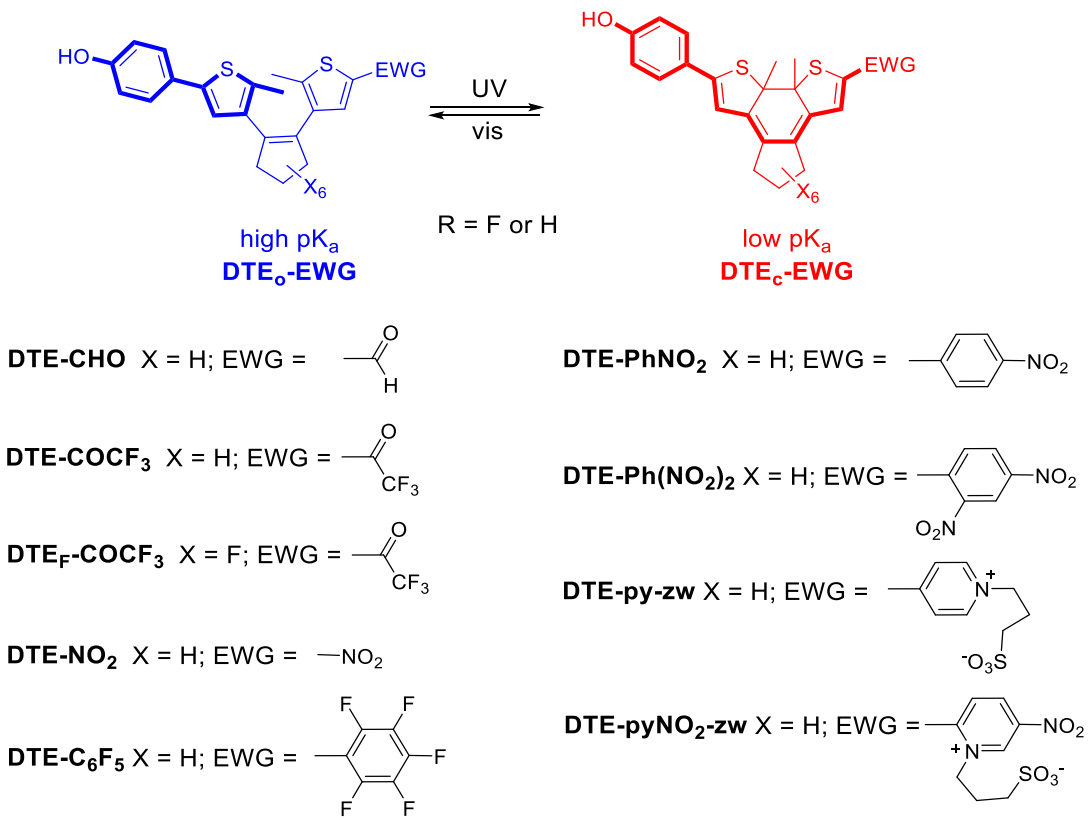

Scheme IV-15. Strategy used in this work to reach high light-induced pK$_a$ modulation in phenols using DTE photoswitches. In bold the electronical communication between substituents in the open and closed states of the system is shown.

Aside from electronic effects, synthetic accessibility was also taken into account when selecting the EWGs to be introduced in target **DTE-EWG** compounds. Actually, most of these molecules could be prepared in a rather simple manner by introducing

the phenol and EWG substituents via lithiation-mediated procedures from common dichlorinated intermediate **9** shown in Scheme IV-1 (**DTE-CHO**, **DTE-COCF$_3$**, **DTE-C$_6$F$_5$**, **DTE-py-zw**, **DTE-PhNO$_2$**, **DTE-Ph(NO$_2$)$_2$** and **DTE-pyNO$_2$-zw**). An exception to that is **DTE-NO$_2$**, as the nitro group cannot be introduced to **9** nor is compatible with most of the common reactions used in DTE synthesis. This made the preparation of this compound especially challenging and prevented the use of the well-established procedures starting from intermediate **9**. As for the **DTE$_F$-COCF$_3$** switch, its synthesis was attempted employing the strategy already described for perfluorinated DTEs (see Scheme IV-3).

IV.3. Synthesis of DTE-EWG compounds from 5,5'-dichlorodithienylethene 9

As just mentioned, all **DTE-EWG** compounds bearing a perhydrogenated central ring except **DTE-NO$_2$** could be prepared from intermediate **9** (Scheme IV-16). For most of these molecules, the synthesis should proceed through intermediate **DTE-Cl**, which could be obtained from **9** via Suzuki coupling with 4-iodophenol after previous lithiation-mediated introduction of a boronic ester to the DTE backbone. From **DTE-Cl** the target EWGs should be introduced by either Suzuki coupling after lithiation-mediated borylation (**DTE-py-zw**, **DTE-PhNO$_2$**, **DTE-Ph(NO$_2$)$_2$** and **DTE-pyNO$_2$-zw**) or via lithiation and reaction with an electrophile (**DTE-COCF$_3$** and **DTE-C$_6$F$_5$**). Because of the use of organolithium compounds for the functionalization with the selected EWG, the phenol moiety of **DTE-Cl** should be previously protected and eventually deprotected. It is for this reason and our previous experience in the preparation of formyl-functionalized DTEs[85] that the synthesis of **DTE-CHO** was devised in a different manner: we would first introduce the formyl moiety that could be easily protected as an acetal with high yields, and later the phenol group would be tethered to the system.

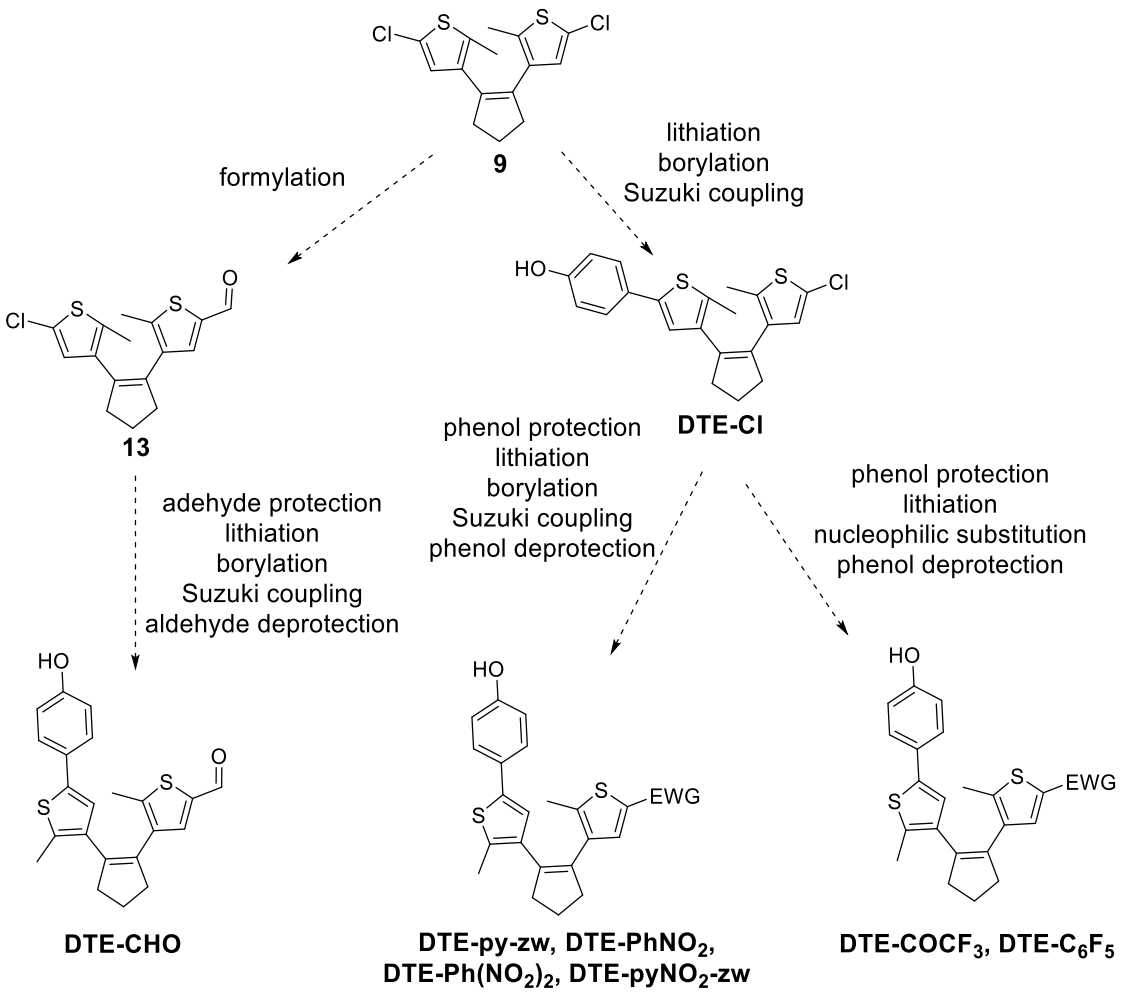

Scheme IV-16. Synthetic strategy followed for the preparation of **DTE-CHO, DTE-COCF$_3$**, **DTE-C$_6$F$_5$**, **DTE-py-zw**, **DTE-PhNO$_2$**, **DTE-Ph(NO$_2$)$_2$** and **DTE-pyNO$_2$-zw.**

IV.3.1. Preparation of intermediate 9

Compound **9** was prepared from commercially available 2-methylthiophene (**10**) through three consecutive chlorination, Friedel-Crafts acylation and McMurry coupling reactions with an overall 26% yield (Scheme IV-17). A procedure previously carried out in our group was followed,[86] although some modifications were introduced.

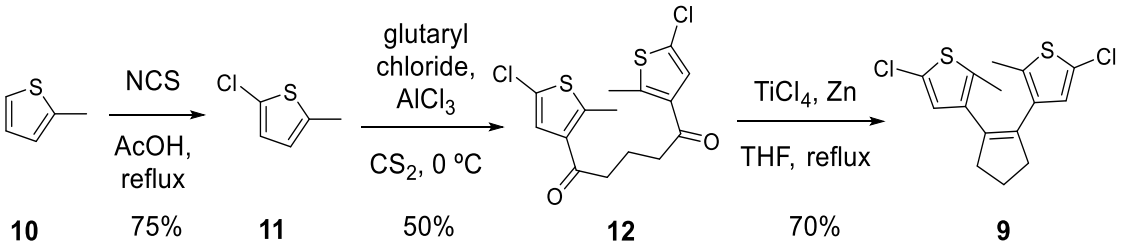

Scheme IV-17. Synthesis of **9**, the key intermediate for the preparation of most **DTE-EWG**.

First, chlorination of the 5-position of **10** to obtain **11** was accomplished with *N*-chlorosuccinimide (NCS) in acetic acid. With respect to the procedure previously described,[86] we did not use benzene but directly employed acetic acid as a solvent. As it is immiscible with acetic acid and water, we could then use low-boiling point hexane to separate the product during the workup of the reaction mixture, which was finally purified by low pressure distillation. In this manner, the yield could be increased from 17% to 75%, as it was easier to remove the solvent of the reaction and less product was lost in the evaporation step at reduced pressure (Scheme IV-17).

Compound **12** was subsequently obtained via a double Friedel-Crafts acylation between **11** and glutaryl chloride employing aluminum chloride as an activating agent and carbon disulfide.[86] The product could be purified by recrystallization in hexane and isolated in 50% yield (Scheme IV-17). However, we proceeded with the next step without purification in most of the cases, as it provided better overall yields for the obtaining of **9**.

Finally, key intermediate **9** was obtained in 70% yield from **12** after a McMurry reaction followed by purification by flash column chromatography (Scheme IV-17). In contrast to the previous reports in our group,[86] in this case we did not use the commercially available $TiCl_3(THF)_3$ complex as a catalyst, but the Ti(III) catalytic species was prepared in situ from $TiCl_4$ and Zn following a procedure described in the literature.[87]

IV.3.2. Synthesis of DTE-CHO

As anticipated in Scheme IV-16, we devised the synthesis of **DTE-CHO** by sequential introduction of the formyl and phenol groups to dichlorinated intermediate **9**. With this aim, compound **13**[88] was first prepared by monolithiation of **9** and subsequent reaction with anhydrous DMF, as described in the literature. After purification by flash column chromatography, **13** was isolated with 90% yield (Scheme IV-18). It is important to note that *tert*-butyllithium had to be used for the lithiation step as no chlorine/lithium exchange was observed with neither *sec*-butyllithium nor *n*-butyllithium.

To avoid side reactions in the next lithiation step required for the introduction of the phenol group, the aldehyde moiety of **13** was protected as the acetal **14**.[89] The protection reaction was done with ethylene glycol in toluene and using *p*-toluenesulfonic acid as a catalyst and a Dean-Stark trap. After purification by flash column chromatography, **14** was obtained in 96% yield (Scheme IV-18).

Finally, **DTE-CHO** was prepared from **14** through a Suzuki coupling following the general procedure described in the literature for the introduction of aryl groups to

intermediate **9**.[87] First, acetal **14** was lithiated with *tert*-butyllithium and the corresponding boronic ester was formed upon subsequent addition of tributyl borate. The crude of this reaction was then directly used for the Suzuki coupling with 4-iodophenol and tetrakis(triphenylphosphine)-palladium (0) as a catalyst, which was freshly prepared from palladium(II) chloride, triphenylphosphine and hydrazine.[90] Interestingly, acetal hydrolysis took place concomitantly and no further deprotection step was needed to obtain **DTE-CHO**, which was isolated in 46% yield for the two steps after purification by flash column chromatography (Scheme IV-18).

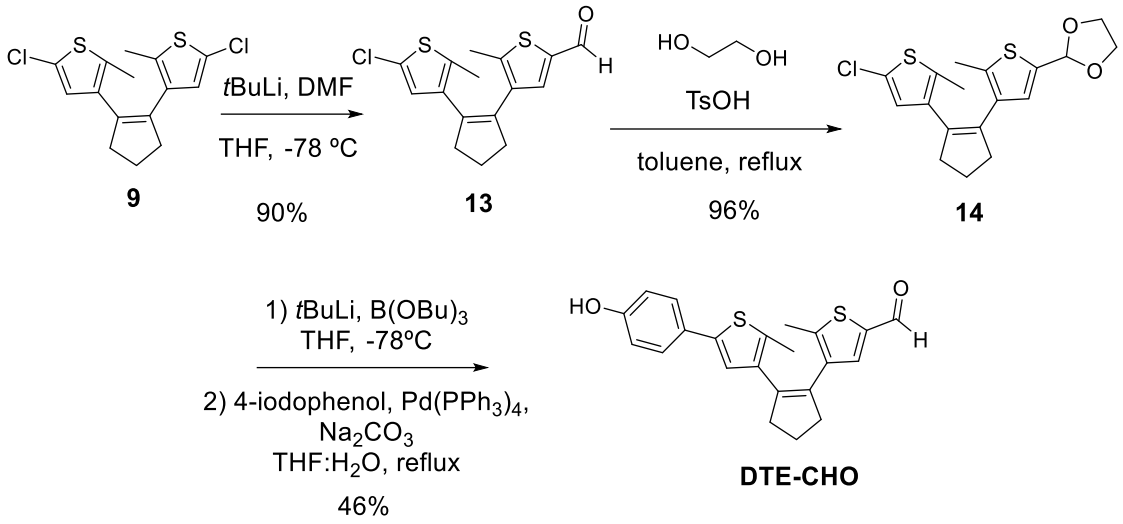

Scheme IV-18. Synthesis of **DTE-CHO** from key intermediate **9**.

Overall, **DTE-CHO** could be prepared in 40% yield from intermediate **9** and it could be successfully identified by its many characteristic spectroscopic features, such as the ^{1}H NMR, ^{13}C NMR and IR signals at 9.71 ppm, 183.3 ppm and 1640 cm^{-1} arising from the formyl group introduced.

IV.3.3. Synthesis and protection of intermediate DTE-Cl

Except for **DTE-CHO**, the rest of the target **DTE-EWG** compounds prepared from **9** were synthesized via formation and protection of **DTE-Cl**. **DTE-Cl**[91] could be prepared from **9** through a Suzuki coupling with 4-ionophenol following the two-step methodology previously described for **DTE-CHO.** After purification by flash column chromatography, this compound was obtained in 61% yield (Scheme IV-19).

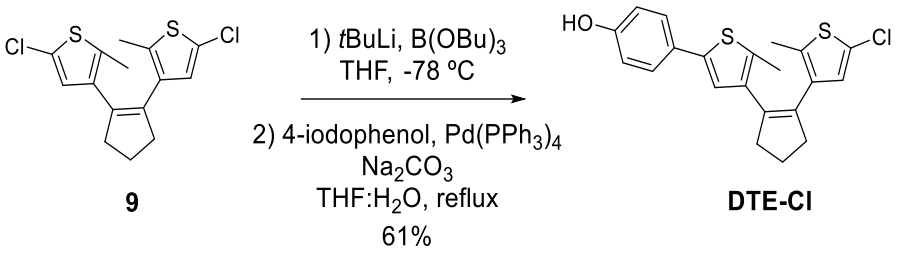

9 **DTE-Cl**

Scheme IV-19. Synthesis of **DTE-Cl** from dichlorinated DTE **9**.

As mentioned in Scheme IV-16, the introduction of the desired EWGs in **DTE-Cl** through lithiation-mediated reactions required previous protection of the phenol moiety, which we carried out by conversion into the corresponding silyl ethers.

Because of its superior overall stability in acid and basic media,[92] preparation of the *tert*-butyldiphenylsilyl (TBDPS) ether of **DTE-Cl** was first attempted by reaction with TBDPSCl in dichloromethane and in the presence of imidazole. This procedure furnished **15** with moderate yields after purification by flash column chromatography (50%, Scheme IV-20).[93]

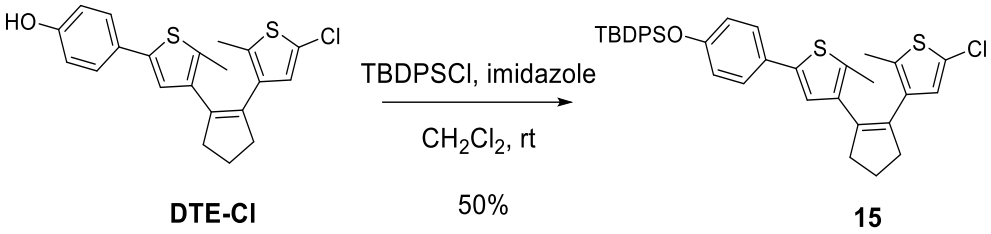

DTE-Cl **15**

Scheme IV-20. Synthesis of protected phenol **15** from **DTE-Cl**.

In view of the moderate yield obtained with TBDPSCl, the phenol protection was tested using *tert*-butyldimethylsilyl chloride (TBSCl). However, silyl ether **16** could only be obtained in a slightly better yield after purification by flash column chromatography (60%, Scheme IV-21).

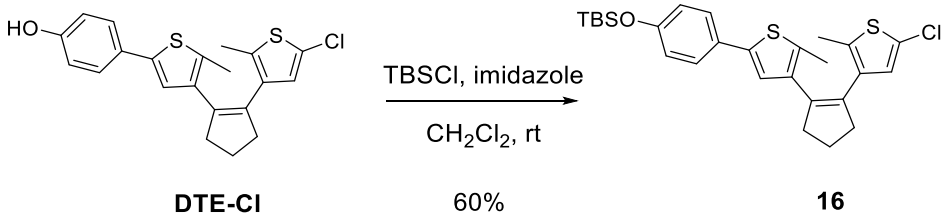

DTE-Cl **16**

Scheme IV-21. Synthesis of protected phenol **16** from **DTE-Cl**.

Because of the similar yields with which **15** and **16** were prepared, both compounds were indistinctively used for the synthesis of **DTE-EWG** products. Thus, protected phenol **15** was utilized to prepare **DTE-COCF$_3$**, **DTE-C$_6$F$_5$** and **DTE-Ph(NO$_2$)$_2$**, while

intermediate **16** was employed for the synthesis of **DTE-py-zw**, **DTE-PhNO$_2$** and **DTE-pyNO$_2$-zw.**

IV.3.4. Synthesis of DTE-COCF$_3$ and DTE-C$_6$F$_5$

DTE-COCF$_3$ and **DTE-C$_6$F$_5$** were obtained in two steps and a similar manner from protected phenol **15**. In the first step, **15** was lithiated using *tert*-butyllithium and then reacted with either ethyltrifloroacetate or hexafluorobenzene to furnish **17** (47% yield) and **18** (74% yield), respectively (Scheme IV-22). These products were then submitted to silyl ether cleavage by incubation with tetrabutylammonium fluoride (TBAF) for 1 hour in chloroform at room temperature. In this manner and after purification by flash column chromatography, deprotected **DTE-COCF$_3$** and **DTE-C$_6$F$_5$** were obtained with 74% and 100% yield, respectively (Scheme IV-22).

Overall, **DTE-COCF$_3$** and **DTE-C$_6$F$_5$** could be prepared from key intermediate **9** in five steps and 10% and 23% yield, respectively. The former product presented the characteristic spectral features arising from the trifluorocarbonyl group introduced, such as the ^{13}C and ^{19}F NMR resonances at 173.1 and -72.39 ppm. As for **DTE-C$_6$F$_5$**, it showed a more complex ^{19}F NMR spectrum that could be unambiguously attributed to its pentafluorophenyl moiety.

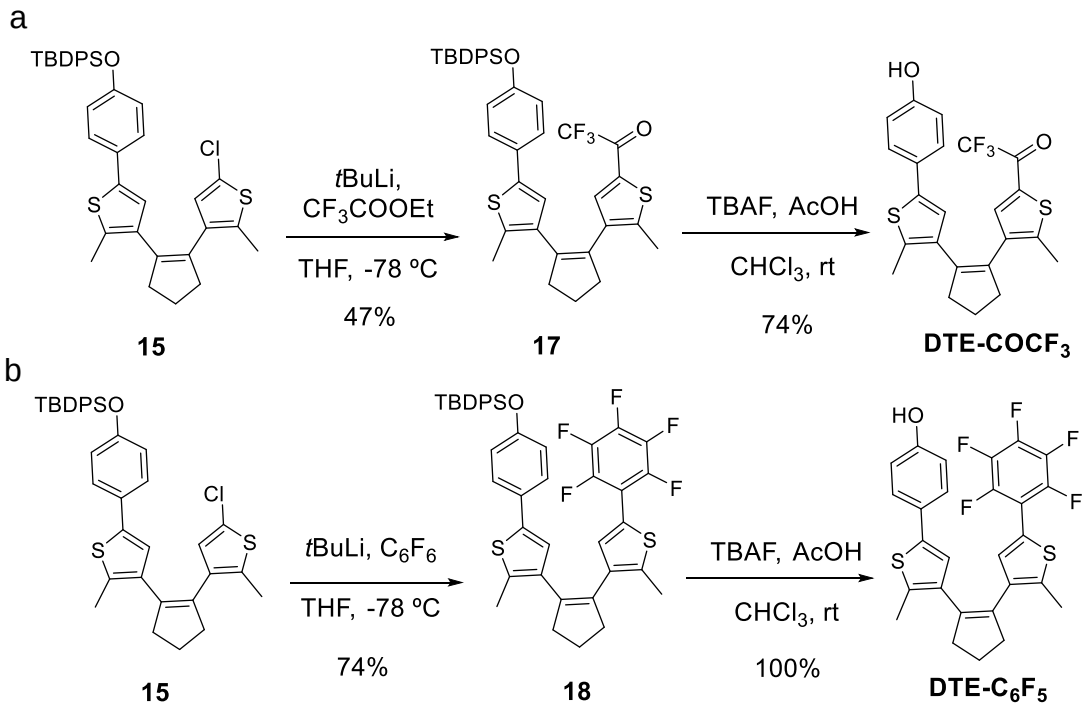

Scheme IV-22. Synthesis of (a) **DTE-COCF$_3$** and (b) **DTE-C$_6$F$_5$** from protected phenol **15**.

IV.3.5. Synthesis of DTE-PhNO$_2$ and DTE-Ph(NO$_2$)$_2$

The target photoswitches **DTE-Ph(NO$_2$)$_2$** and **DTE-PhNO$_2$** were synthesized from the protected intermediates **15** and **16**, where the nitrophenyl groups were incorporated by Suzuki coupling from the corresponding iodoaryl compounds after chlorine/lithium exchange. For this, we employed the same methodology previously used for the introduction of phenol rings in **DTE-CHO** and **DTE-Cl**.[87]

For **DTE-Ph(NO$_2$)$_2$**, the protected intermediate **19** was isolated in this way with 32% yield, which after phenol deprotection with TBAF and purification by flash column chromatography furnished the desired product in 52% yield (Scheme IV-23). Overall, **DTE-Ph(NO$_2$)$_2$** was obtained in six steps and 6% yield from key intermediate **9**, and it could be clearly identified by the characteristic ^{1}H NMR, ^{13}C NMR and IR signals arising from the 2,4-dinitrophenyl group introduced.

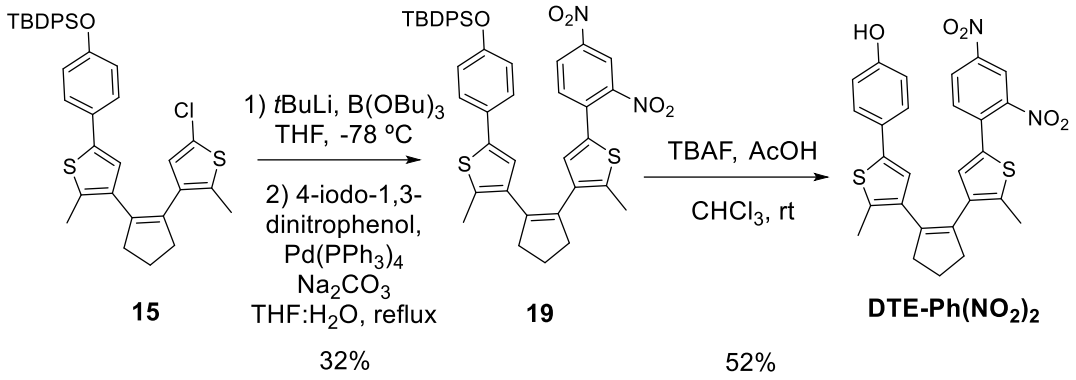

Scheme IV-23. Synthesis of **DTE-Ph(NO$_2$)$_2$** from protected phenol **15**.

In the case of **DTE-PhNO$_2$**, the TBS protecting group was concomitantly removed during the Suzuki coupling because of the basic conditions and, therefore, no additional deprotection step was necessary. **DTE-PhNO$_2$** was then obtained directly from **16** with 46% yield (Scheme IV-24). As a consequence, this compound could be prepared from key intermediate **9** in only 3 steps and 10% overall yield. The presence of the 4-nitrophenyl group in **DTE-PhNO$_2$** could be successfully confirmed by the characteristic signals in ^{1}H NMR at 8.18 and 7.59 ppm.

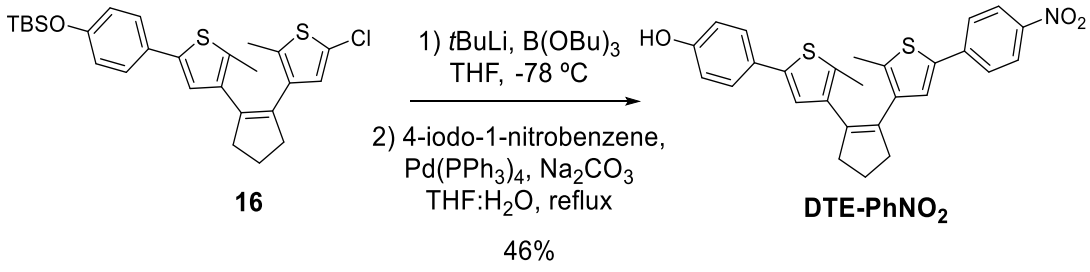

Scheme IV-24. Synthesis of **DTE-PhNO$_2$** from protected phenol **16**.

IV.3.6. Synthesis of DTE-py-zw and DTE-pyNO$_2$-zw

The synthesis of **DTE-py-zw** and **DTE-pyNO$_2$-zw** from protected phenol **16** involved two main steps. First, introduction of the desired pyridine moiety, which we attempted by Suzuki coupling following the same lithiation-mediated process previously used for other DTEs bearing external aryl substituents. Second, pyridine *N*-alkylation to convert it into a strong pyridinium EWG. For this we employed the procedure reported by Lehn's group to prepare **DTE1-acid** (see Scheme IV-11), where a sulfonated propyl group was introduced into the pyridine substituent to make the final molecule zwitterionic and facilitate its manipulation in organic solvents.[78]

For **DTE-py-zw**, pyridine moiety introduction via consecutive lithiation, borylation and Suzuki coupling reactions furnished phenol **20** with 54% yield after purification by flash column chromatography (Scheme IV-25). As previously observed during the synthesis of **DTE-PhNO$_2$**, simultaneous cleavage of the silyl ether group of **16** was again observed in this case. As a result, **DTE-py-zw** could finally prepared from **20** by direct reaction with 1,3-propanesultone in acetonitrile and isolated by filtration after product precipitation in the reaction solvent with 30% yield (Scheme IV-25). Overall, **DTE-py-zw** was obtained in six steps from intermediate **9** in 12% yield, and the introduction of the desired sulfonated pyridinium moiety was confirmed by the new aromatic and alkyl ^{1}H NMR signals at 8.89, 8.19, 4.61 and 2.85 ppm.

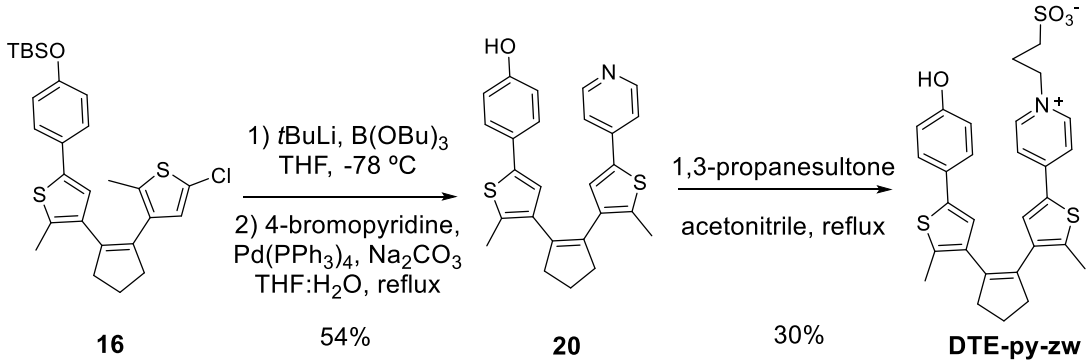

Scheme IV-25. Synthesis of **DTE-py-zw** from protected phenol **16**.

The synthesis of **DTE-pyNO$_2$-zw** was attempted in a similar manner from **16**. First, the nitropyridine moiety was introduced via lithiation-mediated Suzuki coupling in 31% yield, which directly yield deprotected phenol **DTE-pyNO$_2$** by concomitant silyl ether cleavage (Scheme IV-26). Then, the alkylation of pyridine with 1,3-propanesultone was attempted. However, this reaction failed, which we ascribed both to steric hindrance and the lower nucleophilicity of the 5-nitropyridine moiety due to the mesomeric electron-withdrawing effects imparted by the nitro group. Neither did the reaction work with a stronger electrophile as methyl iodide. In view of this, we abandoned the synthesis of **DTE-pyNO$_2$-zw** and took **DTE-pyNO$_2$** for the subsequent optical experiments instead.

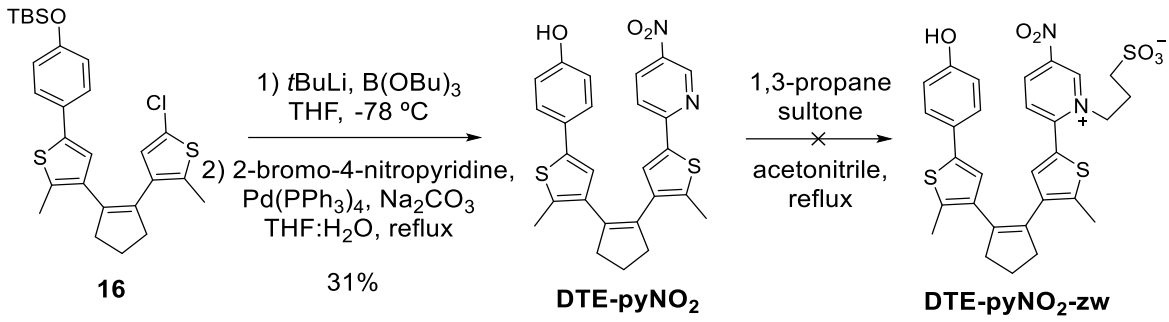

Scheme IV-26. Attempted synthesis of **DTE-pyNO$_2$-zw** from protected phenol **16**.

IV.4. SYNTHESIS OF DTE-NO$_2$

As discussed above, the preparation of DTE photoswitches bearing external nitro substituents such as **DTE-NO$_2$** is rather challenging, because nitro groups cannot be easily introduced to dichlorinated intermediate **9** nor are compatible with the organolithium reagents used in most synthetic procedures toward dithienylethenes. Actually, this may explain why none of this type of compounds have been reported to date. Consequently, a different novel synthetic strategy had to be devised for **DTE-NO$_2$**, where the thiophene external substituents could not be introduced after DTE core formation. Instead, we decided to prepare the functionalized thiophene and cyclopentene rings first separately and then tethered them together through 2 consecutive Suzuki couplings where the nitrosubstituted aryl group could not be exposed to organolithium reagents (Scheme IV-27). To do so, the following steps were proposed:

1) Preparation of 3-iodo-2-methyl-5-nitrothiophene (**23**) that could be used as an aryl halide substrate for a subsequent Suzuki coupling reaction. This actually explains why an iodothiophene ring was synthesized, as Suzuki couplings are known to have better yields with aryl iodides than bromides.[94] Unfortunately, as the regioselectivity of heteroaromatic electrophilic substitutions in thiophenes favors positions 2 and 5 over 3 and 4,[95] selective iodination of the 3-position of the target thiophene ring should not be possible. To circumvent this problem, we thought of conducting a double iodination of commercially available 2-methylthiophene (**10**) to form **21** and, subsequently, to selectively remove the iodine atom at the 5-position to form **22.** After nitration reaction, this should then furnish desired intermediate **23** (Scheme IV-27)**.**

2) Preparation of 1,2-dibromocyclopentene (**25**), which could be synthesized from commercially available ketone **24** through a one pot procedure described in the literature[96] (Scheme IV-27).

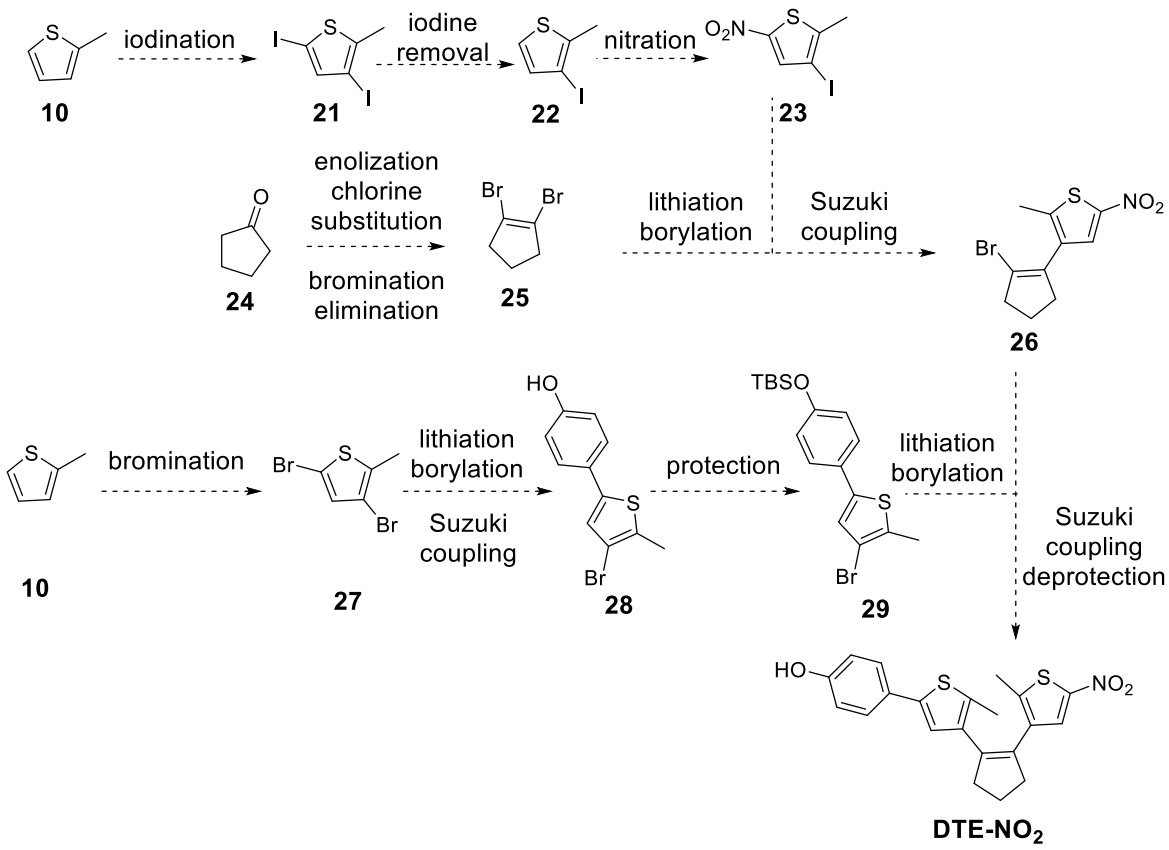

Scheme IV-27. Synthetic strategy devised to prepare **DTE-NO$_2$**.

3) Preparation of phenol-functionalized 3-bromothiophene **29**. For this, we would first dibrominate positions 3 and 5 of **10** to form **27**. Then, the phenol group would be selectively introduced to position 5 of **27** by lithiation-mediated Suzuki coupling as already explained for other DTE-phenol conjugates. Finally, the resulting phenol **28** would be protected as a TBS ether to form **29** and avoid side reactions in later steps (Scheme IV-27).

4) Sequential coupling of fragments **23**, **25** and **29** by consecutive lithiation-mediated Suzuki reactions to yield the desired **DTE-NO$_2$** compound. Because nitro groups are incompatible with organolithium compounds, lithiation and borylation of cyclopentene **25** would be performed to tether this unit with **23** and form compound **26**. For the same reason, protected phenol **29** would be subjected to chlorine/lithium exchange and borylation in order to ensure coupling with **26** and finally provide **DTE-NO$_2$** after deprotection (Scheme IV-27)**.**

Preparation of thiophene **23** the double iodination of 2-methylthiophene with iodine and sodium iodate in methanol following a procedure described in the literature. After purification through filtration, thiophene **21** was achieved in 99% yield (Scheme IV-28).

Next, selective deiodination of the 5-position of **21** was required to form **22**.[97] This was achieved by iodine/lithium exchange with *n*-butilithium, which is known to preferentially take place at position 2.[98] Subsequent quenching with methanol and purification by filtration furnished **22** in 81% yield (Scheme IV-28).

Different conditions were tested for the nitration reaction of **22** to obtain target thiophene **23**. First, it was attempted by adding **22** onto a 1:3 mixture of concentrated nitric and sulfuric acid.[99] Unfortunately, only a mixture of insoluble by-products was obtained through a highly exothermic reaction, which prompted us to believe that thiophene polymerization was occurring.[100] This could not be prevented regardless of the temperature or addition conditions assayed, which we mainly attribute to the fact that small droplets with a high concentration of **22** were formed due to its immiscibility with H_2SO_4. It is for this reason that we replaced H_2SO_4 by trifluoroacetic anhydride[101] and performed the reaction under very controlled conditions. In particular, nitric acid was slowly added onto a solution of **22** in an ice-water bath. In this way the reaction was completed after the addition of 2 equivalents of nitric acid, which allowed us to obtain **23** in 46% yield after purification by flash column chromatography (Scheme IV-28).

Overall, thiophene **23** could be prepared from commercially available **10** in three steps and 37% yield. Successful obtaining of this mononitrated product was confirmed by its characteristic spectral ^{1}H NMR and IR signals at 7.83 ppm.

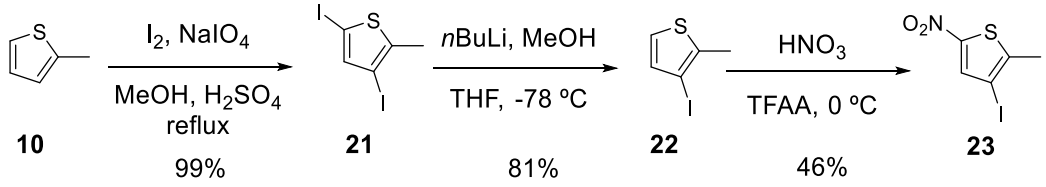

Scheme IV-28. Synthesis of thiophene **23.**

IV.4.1. Preparation of cyclopentene 25

Cyclopentene **25**[96] was prepared through a three-step process from cyclopentanone (**24**) based on a procedure described in the literature. For this **24** was sequentially treated with PCl_5 to induce chlorination and oxygen displacement, bromine to promote the bromination of the substrate, and basic media to favor *anti* elimination of the chlorine atom and formation of the carbon-carbon double bond in the final molecule.[96] In our hands the last step did not work using *tert*-butoxide as a base; accordingly, we used potassium hydroxide instead.[102] In addition, we replaced toluene by dichloromethane as a solvent for the first two steps of the process, which did not detrimentally affect the process. With this changes compound **25** was obtained with 26% yield after purification by flash column chromatography (Scheme IV-29).

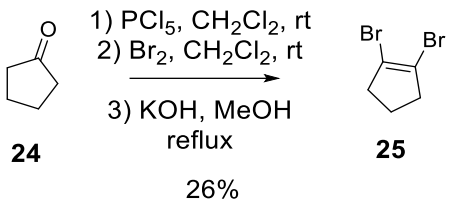

Scheme IV-29. Synthesis of cyclopentene **25.**

IV.4.2. Preparation of thiophene 29

The synthesis of **27**[103] started with the direct dibromination of **10** with bromine in acetic acid as described in the literature. Purification via filtration through a silica plug was sufficient to obtain pure **27** in 95% yield (Scheme IV-30).

Next, Suzuki coupling between **27** and 4-iodophenol was done following a similar procedure to that employed for the synthesis of several **DTE-EWG**, which involved previous lithiation and borylation of the bromothiophene substrate. The only difference was that *n*-butyllithium was used instead of *tert*-buthyllithium, as it was capable of promoting bromine/lithium exchange. In this way and after purification by flash column chromatography, compound **28** was obtained in 67% yield (Scheme IV-30).

Finally, phenol **28** was protected with a TBS ether group to avoid the reaction of the phenolic proton with organolithium reagents in the next steps. The choice of this protecting group was driven by our previous observation that it gets simultaneously cleaved under the Suzuki coupling conditions applied in our experiments, thus preventing the need for an additional deprotection step. Therefore, by applying the same procedure previously described for **16** and after purification by flash column chromatography, compound **29** was obtained in 80% yield (Scheme IV-30).

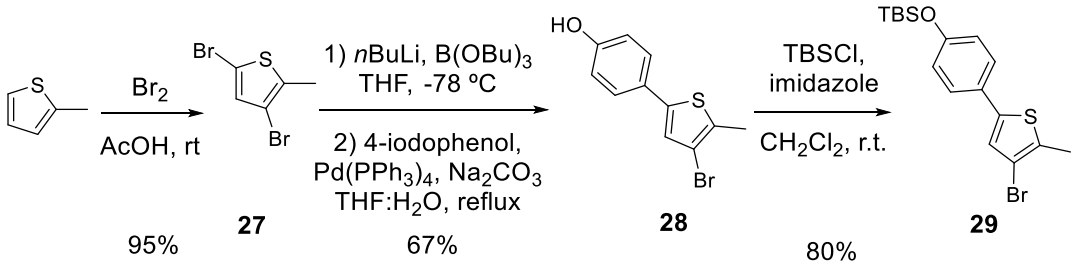

Scheme IV-30. Synthesis of thiophene **29.**

In total, four steps were needed to prepare thiophene **29** from commercially available 2-methylthiophene in 51% overall yield. This compound presented the characteristic ^{1}H and ^{13}C NMR signals of its TBS-protected phenol group.

IV.4.3. Synthesis of DTE-NO_2

The synthesis of **DTE-NO_2** was achieved via consecutive Suzuki coupling between previously prepared fragments **23**, **25** and **29**. The first of these reactions between thiophene **23** and cyclopentene **25** was accomplished after previous lithiation and borylation of **25**, which provided compound **26** in 81% yield after purification by flash column chromatography (Scheme IV-31). In this case, lithium/bromine exchange could be again accomplished with *n*-butyllithium, while borylation and Suzuki coupling reactions were conducted using the same conditions previously described.

In a similar fashion, the boronic ester of bromothiophene **29** was obtained by consecutive treatment with *n*-butyllithium and tributyl borate. Subsequent Suzuki coupling reaction with **26** and simultaneous cleavage of the TBS ether provided the target photoswitch **DTE-NO_2** in 52% yield after purification by flash column chromatography (Scheme IV-31). Successful construction of the DTE core was not only demonstrated by the characteristic ^{1}H and ^{13}C NMR signals of its different constituting units, but also by the color changes observed upon sunlight irradiation (vide infra).

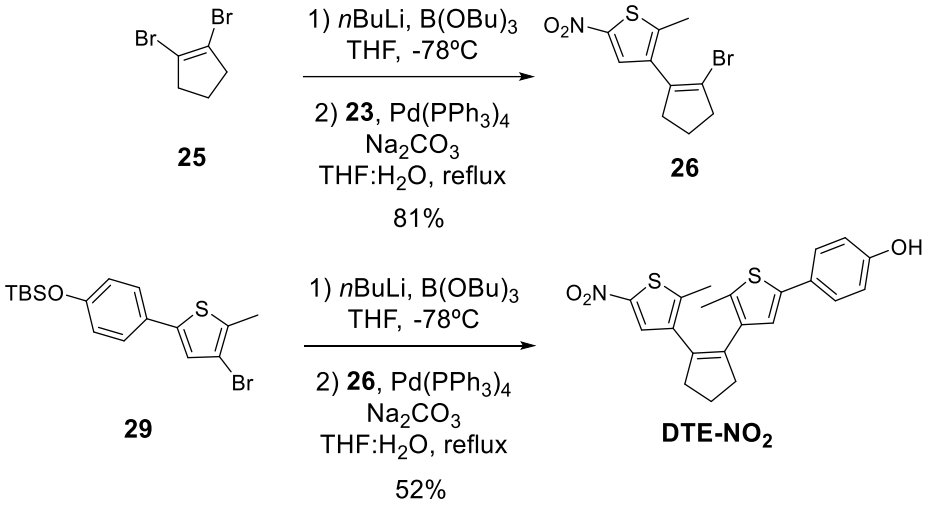

Scheme IV-31 Synthesis of **DTE-NO_2** from previously prepared fragments **23**, **25** and **29**.

IV.5. Synthesis of DTE_F-$COCF_3$

DTE_F-$COCF_3$ was devised to be prepared through a common strategy for the synthesis of perfluorated DTEs,[52] which consists in a sequential nucleophilic substitution over the commercially available perfluorated ring **31** of the organolithiated derivatives of the thiophenes of interest – in our case, protected phenol **29** and thiophene **30** bearing a 5-chlorine substituent for further functionalization (Scheme IV-32). With this aim, thiophene **30** would be first prepared by bromination of the 3-position of previously synthesized 2-chloro-5-

methylthiophene (**11**). Intermediates **32** and **33** would then be formed by consecutive lithiation-mediated nucleophilic substitutions over **31**. Next, the trifluoroacetyl group would be introduced by chlorine/lithium exchange and reaction with ethyl trifluoroacetate, as already done for **DTE-COCF$_3$**. Finally, **DTE$_F$-COCF$_3$** would be obtained after phenol deprotection in acid media.

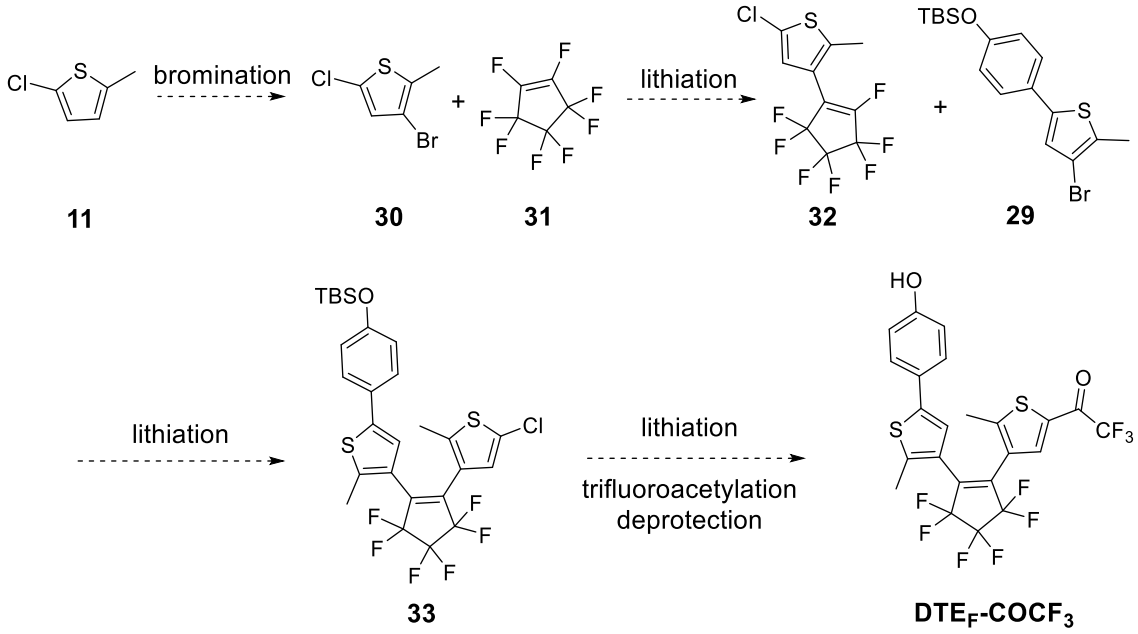

Scheme IV-32. Synthetic strategy proposed for the preparation of **DTE$_F$-COCF$_3$**.

IV.5.1. Preparation of intermediate 32

The synthesis of **32** started with the monobromination of **11** using similar conditions to those previously utilized for the preparation of dibromothiophene **27**. In this manner compound **30**[104] was isolated with 89% yield after purification by filtration through a silica pad (Scheme IV-33).

Then compound **32**[52] was obtained in 42% yield by lithiation of **30** with *n*-butyllithium and subsequent substitution reaction with cyclopentene **31** (Scheme IV-33), following a procedure already reported in the literature.

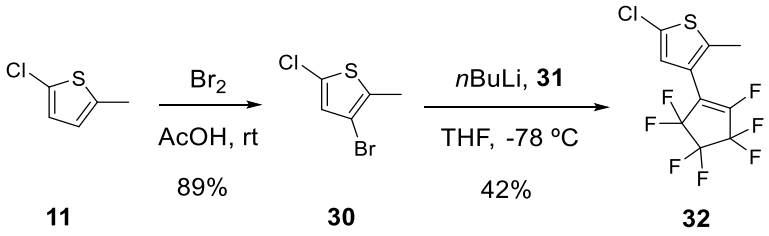

Scheme IV-33. Synthesis of intermediate **32**.

IV.5.2. Synthesis of DTE_F-$COCF_3$

Starting from intermediate **32**, DTE derivative **33** was prepared by means of a second lithiation-mediated substitution reaction on the fluorinated cyclopentene unit. To do so, protected phenol **29** previously derived for the synthesis of **DTE-NO_2** was first treated with *n*-butyllithium and then bromothiophene **32**. After purification by flash column chromatography, DTE **33** was obtained in 29% yield (Scheme IV-34).

Next, the trifluoromethylcarbonyl group was introduced to **33** using the same procedure previously employed for the synthesis of **DTE-$COCF_3$**. This involved the lithiation of **33** with *tert*-butyllithium and then the reaction with ethyl trifluoroacetate. The reaction mixture obtained was treated with acidic aqueous media to ensure silyl ether cleavage. In this way and after purification by flash column chromatography, target compound **DTE_F-$COCF_3$** was isolated with 14% yield (Scheme IV-34). Overall, this photoswitch was synthesized in five steps with a combined 2% starting from **11** and unambiguously identified by its characteristic ^{1}H, ^{13}C and ^{19}F NMR signals.

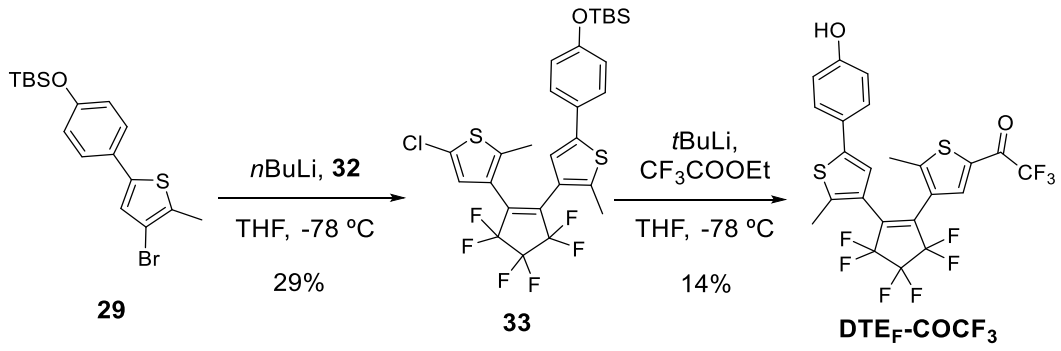

Scheme IV-34. Synthesis of molecular switch **DTE_F-$COCF_3$.**

IV.6. PHOTOCHEMICAL CHARACTERIZATION OF DTE-EWG

Once synthesized, the photochemical properties of all **DTE-EWG** were studied. To do so, acetonitrile was chosen as the solvent of reference due to its large transparency in the UV region (cutoff wavelength = 190 nm) and the good solubility of most of the compounds in this medium.

First, the UV-vis absorption spectra were measured for the open isomers of **DTE-EWG** obtained from the synthesis. All of them showed a strong absorption band in the UV region with spectral maxima between 260 and 300 nm (Figure IV-7, Table IV-1). Additionally, most compounds bearing a second external aryl substituent (**DTE-py-zw**, **DTE-PhNO_2**, **DTE-Ph(NO_2)$_2$** and **DTE-pyNO_2**) exhibited a second, less intense absorption band in the violet region with spectral maxima between 370 and 380 nm (Figure IV-7). These are very common features for DTEs, whose open state

gives rise to colorless (or slightly yellowish) solutions with minimal absorption in the visible region.[45]

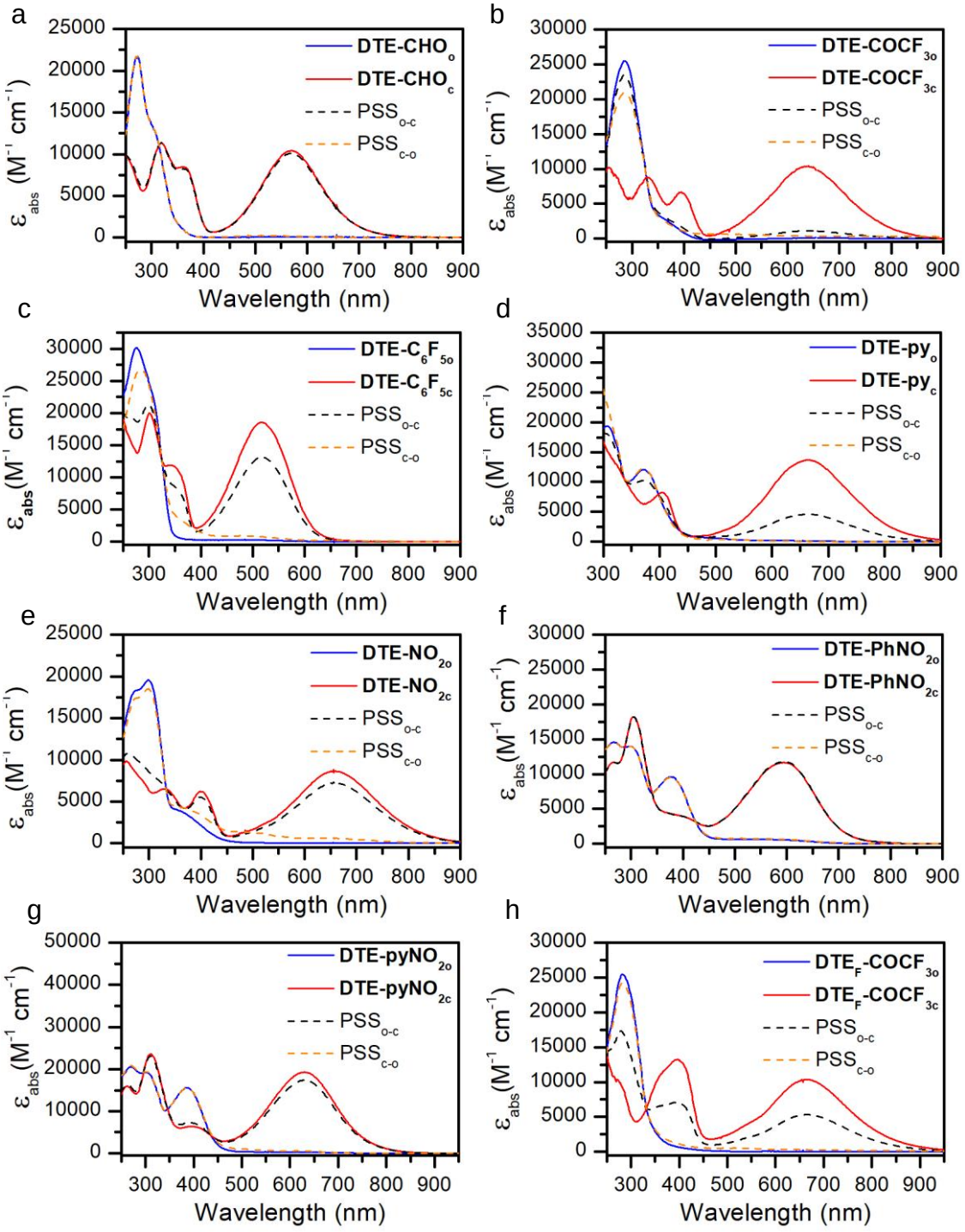

Figure IV-7. Absorption spectra of the open state (blue), closed state (red), PSS_{o-c} (dashed black) and PSS_{c-o} (dashed-orange) of (a) **DTE-CHO**, (b) **DTE-COCF$_3$**, (c) **DTE-C$_6$F$_5$**, (d) **DTE-py-zw**, (e) **DTE-NO$_2$**, (f) **DTE-PhNO$_2$**, (g) **DTE-pyNO$_2$** and (h) **DTE$_F$-COCF$_3$**. The PSS irradiation wavelength are shown in Table IV-1.

By contrast, irradiation with UV light typically provokes strong coloration of DTE solutions, which is ascribed to photoinduced ring cyclization to produce their closed isomer.[45] Actually, this was observed for most **DTE-EWG**, which upon irradiation in the UV-violet region developed a clear absorption band in the visible region – i.e., photoisomerized to the DTE closed state (Figure IV-7). The only exception to that behavior was **DTE-Ph(NO$_2$)$_2$**, which did not photoisomerize regardless of the excitation wavelength used. In contrast to their open states, the closed forms of **DTE-EWG** had their absorption maxima in a wide range of wavelengths between 480 and 660 nm, making the colors of the corresponding solutions vary from red to blue. Significant bathochromic shifts were specifically observed for those compounds bearing strong EWGs and π-conjugated external substituents as well as a perfluorinated cyclopentene central ring (Figure IV-7, Table IV-1), as already reported.[45]

It must be noted that, after prolonged exposure of the initial open forms to UV-violet light, quantitative conversion to the closed states was seldom observed and a photostationary mixture of both isomers was reached. The composition of these PSS$_{o\text{-}c}$ mixtures was determined by ^{1}H NMR and, if necessary, absorption data, from which the absorption spectrum of each **DTE-EWG$_c$** could also be estimated (Figure IV-7, Table IV-1). Large variation of PSS$_{o\text{-}c}$ composition was observed for the photoswitches in these experiments, with the closed isomer content ranging from 11% in **DTE-COCF$_3$** to 99% in **DTE-PhNO$_2$**. Though a detailed rationalization of these results will be given below, it is worth mentioning that these results are influenced by the excitation wavelength used. In our case, we photoexcited **DTE-EWG$_o$** solutions at 312 nm except for the following cases: (a) **DTE-py-zw**, **DTE-PhNO$_2$, DTE-Ph(NO$_2$)$_2$** and **DTE-pyNO$_2$** showing clear absorption bands in the violet region, which were illuminated at 405 nm; (b) **DTE-COCF$_3$** and **DTE$_F$-COCF$_3$**, which were irradiated at 405 nm and 355 nm, respectively, to minimize photodegradation (vide infra).

As for the photoinduced cycloreversion reaction, almost complete recovery of the initial open state was achieved upon visible light irradiation of all **DTE-EWG$_c$** solutions (Figure IV-7, Table IV-1). In this case, the excitation wavelength employed was either 532 nm or 650 nm depending on which was closer to the spectral maximum of the closed isomer. On the other hand, no thermal back-isomerization was observed in the dark, as well-known to occur for most DTE switches.[45]

To better understand the differences observed in PSS$_{o\text{-}c}$ for **DTE-EWG**, their ring closing ($\Phi_{o\text{-}c}$) and ring opening ($\Phi_{c\text{-}o}$) quantum yields were determined in acetonitrile (Table IV-1). A rather uniform behavior was observed for $\Phi_{c\text{-}o}$, which took low values in all the cases ($\Phi_{c\text{-}o} < 0.05$). As mentioned in section IV.1.2, this is expected for DTE switches with external π-conjugated substituents such as phenols, as this lower the

opening quantum yield.[45] For this reason, $\Phi_{c\text{-}o}$ values were especially lower in those cases where the EWG of the compound was also an aryl group, such as **DTE-PhNO$_2$** for which $\Phi_{c\text{-}o}$ = 0.0044 was measured.

Table IV-1. Photochemical properties of **DTE-EWG** in acetonitrile.

DTE-EWG	$\lambda_{abs,max,o}$ (ε_{abs})[a]	$\lambda_{abs,max,c}$ (ε_{abs})[a]	$PSS_{o\text{-}c}$ (λ_{irr})[b]	$PSS_{c\text{-}o}$ (λ_{irr})[c]	$\Phi_{o\text{-}c}$ (λ_{irr})[d]	$\Phi_{c\text{-}o}$ (λ_{irr})[d]
DTE-CHO	272 (21.7)	572 (10.4)	0.97 (312)	1.00 (650)	0.32 ± 0.12 (312)	0.020 ± 0.001 (650)
DTE-COCF$_3$	287 (25.5)	641 (10.4)	0.11 (405)	1.00 (650)	0.054 ± 0.016 (405)	0.047 ± 0.014 (650)
DTE-C$_6$F$_5$	276 (30.1)	518 (18.6)	0.72 (312)	1.00 (532)	0.37 ± 0.13 (312)	0.031 ± 0.005 (532)
DTE-py-zw	282 (17.0)	664 (13.7)	0.33 (405)	1.00 (650)	0.0051 ± 0.0001 (405)	0.038 ± 0.002 (650)
DTE-NO$_2$	298 (19.6)	656 (8.7)	0.83 (312)	1.00 (650)	0.032 ± 0.008 (312)	0.018 ± 0.002 (650)
DTE-PhNO$_2$	266 (14.6)	595 (11.7)	0.99 (405)	1.00 (650)	0.081 ± 0.004 (405)	0.0044 ± 0.0003 (650)
DTE-Ph(NO$_2$)$_2$	295 (19.9)	-	-	-	-	-
DTE-pyNO$_2$	268 (20.5)	630 (19.3)	0.90 (405)	1.00 (650)	0.016 ± 0.001 (405)	0.0050 ± 0.0002 (650)
DTE$_F$-COCF$_3$	279 (13.4)	662 (10.4)	0.50 (405)	1.00 (650)	0.048 ± 0.001 (405)	0.039 ± 0.001 (650)

[a] Absorption maximum in nm. The extinction coefficients in 10^3 M^{-1} cm^{-1} are indicated in parentheses. [b] Molar fraction of the closed isomer after prolonged irradiation. The irradiation wavelength in nm is indicated in parentheses. [c] Molar fraction of the open isomer after irradiation. The irradiation wavelength in nm is indicated in parentheses. [d] Ring opening and closing quantum yields. The irradiation wavelength in nm is indicated in parentheses. The error for Φ is calculated as the standard deviation of 3 replicates.

A higher variation in photoreaction quantum yields was found for the ring closing process (Table IV-1). In general, low values were obtained for the cyclization quantum yields of **DTE-EWG** ($\Phi_{o\text{-}c} < 0.1$), and only **DTE-CHO** and **DTE-C_6F_5** showed moderate $\Phi_{o\text{-}c}$ values between 0.35 and 0.10. To explain these results, two different factors could be considered: (a) **DTE-EWG$_o$** conformational equilibrium, and (b) intramolecular charge transfer (ICT) processes. On the one hand, the low $\Phi_{o\text{-}c}$ values measured for **DTE-PhNO$_2$**, **DTE-pyNO$_2$** and especially **DTE-py-zw** could be attributed to π-π stacking between the phenol and the electron-deficient aryl substituents, which should favor the unreactive parallel conformation of the open isomer over the photoreactive antiparallel conformation. On the other hand, all DTEs bearing strong EWG groups (**DTE-COCF$_3$**, **DTE-py-zw**, **DTE-NO$_2$** and **DTE$_F$-COCF$_3$**) could also suffer from internal charge transfer processes occurring upon photoexcitation due to the different electron densities of some of the constituting units of these compounds: electron-rich phenol and phenol-thiophene groups and electron-poor EWG, thiophene-EWG and perfluorinated cyclopentene groups. To test the latter hypothesis, the ring closing quantum yield of **DTE-COCF$_3$** was also determined in an apolar solvent such as hexane, which should disfavor ICT processes as already reported for other DTEs.[59] A two-fold increase in $\Phi_{o\text{-}c}$ from 0.054 to 0.13 was indeed observed upon solvent change, thus demonstrating the importance of charge transfer processes in the cyclization process of **DTE-EWG**. It must be noted that both effects – i.e., prevalence of the unreactive parallel conformation of the open isomer and ICT – could occur in **DTE-Ph(NO$_2$)$_2$**, which might explain why we could not observe photoisomerization of this compound even when attempted in apolar solvents.

From the photoisomerization quantum yields determined, the $PSS_{o\text{-}c}$ mixtures obtained under illumination of **DTE-EWG$_o$** could be easily rationalized. On the one hand, $PSS_{o\text{-}c}$ mixtures highly enriched with the closed isomer were found for those DTEs with large $\Phi_{o\text{-}c}/\Phi_{c\text{-}o}$ ratios regardless of the actual absolute value of $\Phi_{o\text{-}c}$. For instance, this is the case of **DTE-CHO** ($\Phi_{o\text{-}c}/\Phi_{c\text{-}o} = 16.0$) and **DTE-PhNO$_2$** ($\Phi_{o\text{-}c}/\Phi_{c\text{-}o} = 18.4$ but $\Phi_{o\text{-}c} = 0.081$). On the other hand, the lowest photoconversions were observed for **DTE-EWG** with similar or even smaller $\Phi_{o\text{-}c}$ values than $\Phi_{c\text{-}o}$ (e.g., **DTE-COCF$_3$** with $\Phi_{o\text{-}c}/\Phi_{c\text{-}o} = 1.1$ and **DTE-py-zw** with $\Phi_{o\text{-}c}/\Phi_{c\text{-}o} = 0.4$).

The low cyclization quantum yields measured for most **DTE-EWG** may also have an impact on the fatigue resistance of these compounds, which is often associated with the UV irradiation of the closed isomer. However, as mentioned in section IV.1.2, photodegradation is often prevented in the presence of π-conjugated groups. This may explain why significant photodegradation was seen for **DTE-NO$_2$** and **DTE-COCF$_3$**, as they both have low closing quantum yields and lower π-conjugation. This explains why clear differences are observed for these compounds in Figure IV-7

between the absorption of their open isomer and of the $PSS_{c\text{-}o}$, which worsened after consecutive photoisomerization cycles. By contrast, comparatively similar **DTE-py-zw** with also low $\Phi_{o\text{-}c}$ but longer conjugation did not show as much photodegradation. In addition, as it had been already described,[47] the use of a perfluoro central ring significantly improved as the photostability of **DTE_F-$COCF_3$** relative to **DTE-$COCF_3$.**

IV.7. LIGHT-INDUCED pK_A MODULATION IN DTE-EWG

Once photochemically characterized, the acid-base properties of **DTE-EWG** were studied. For this investigation, we took as a reference compound **DTE-Cl** prepared during the synthesis of several of the target photoswitches, as it presents a weak chlorine EWG and, therefore, should present a much lower pK_a variation upon photoisomerization.

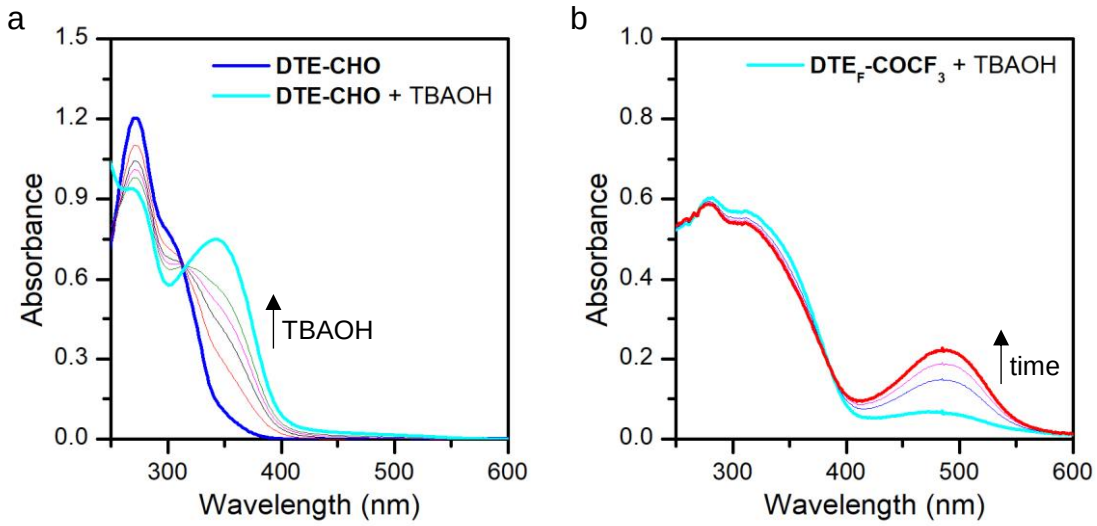

Figure IV-8. (a) Variation of the UV-vis spectrum of **DTE-CHO** (c = $6 \cdot 10^{-5}$ M) upon titration with TBAOH in acetonitrile (from 0 to 10 eq.). (b) Evolution over time of the UV-vis spectrum of **DTE_F-$COCF_3$** (c = $2 \cdot 10^{-5}$ M) after one single TBAOH addition (20 eq.).

In a first step, the pK_a of the phenol moiety in their open isomer was determined. To do so, we used the same procedure already applied in Chapter III to SZMC compounds: we titrated **DTE-EWG$_o$** solutions in acetonitrile with TBAOH to induce phenol deprotonation, a process that was followed by UV-vis spectrophotometry while measuring the pH of the sample after each base addition.[105] As illustrated by the example in Figure IV-8a, phenol deprotonation resulted in a significant red shift of the open isomer maxima to wavelengths between 330 and 360 nm (Table IV-2). Therefore, this spectral changes could be used to determine the concentration ratio between the protonated and deprotonated species in each case and, by correlating this data with pH values, finally determine the pK_a of the compound.[106] It must be

noted that, as also done in Chapter III, pH and pK_a values were measured in acetonitrile and referred to standards also prepared in acetonitrile ($^{ACN}_{ACN}$pH scale), which means that they typically took values from 0 to 33.[106]

Although the abovementioned method could be applied to determine the pK_a of all **DTE-EWG$_o$**, care had to be taken in some particular cases. For **DTE$_F$-COCF$_3$** a secondary reaction was observed in the presence of base over time (Figure IV-8b). Although the nucleophilic substitution of fluorines had been described in the past for the perfluorinated version of **DTE-py-zw** in basic media (see Scheme IV-11),[78] this did not seem to be the case for **DTE$_F$-COCF$_3$** according to the spectral changes registered. Actually, we observed a similar behavior for some nonfluorinated **DTE-EWG$_o$** bearing very strong EWGs at large TBAOH excesses that were not necessary for pK_a determination. Unfortunately, we could not determine which by-product was formed based on ^{1}H NMR measurements. In spite of this, to prevent the effect of the degradation process on the determination of **DTE$_F$-COCF$_3$**, pK_a, measurements were taken in this case by adding different amounts of TBAOH on freshly prepared solutions.

As for the closed isomers of **DTE-EWG**, their pK_a values were determined using the same procedure already described, because titration with TBAOH also led to a pronounced bathochromic shift of the visible absorption band. Such red shift widely varied depending on the EWG nature, and it ranged from about 50 nm in the case of **DTE-C$_6$F$_5$** to more than 300 nm for **DTE-py-zw** (Figure IV-9 and Table IV-2). It is worth mentioning that these experiments could be conducted on the $PSS_{o\text{-}c}$ mixtures instead of the purified **DTE-EWG$_c$** compounds, because the closed isomers had significantly lower pK_a and, thus, they could be selectively deprotonated in the presence of the open state. In addition, as phenol deprotonation was achieved at significantly lower TBAOH concentrations in this case, no apparent degradation effects were observed. However, when **DTE-EWG$_c$** were exposed to larger pH values as their open isomer counterparts, lower stability was observed (Figure IV-9).

Table IV-2 shows the pK_a values determined for the open and closed states of all **DTE-EWG**. For all the open states of the compounds bearing a perhydrogenated central cyclopentene ring, very similar pK_a values were found that range from 24.2 to 25.0 and resemble that reported for phenol in acetonitrile ($pK_{a,ACN}$ = 26.6[106]). Therefore, this demonstrates the little electronic communication existing between the external phenol and EWG substituents in **DTE-EWG$_o$**. On the other hand, a significantly lower pK_a value was found for the open isomer of **DTE$_F$-COCF$_3$** ($pK_{a,ACN,o}$ = 21.7), thus indicating that the perfluorinated cyclopentene group does have an inductive electrowithdrawing effect on the external substituents of DTEs regardless of the isomerization state.

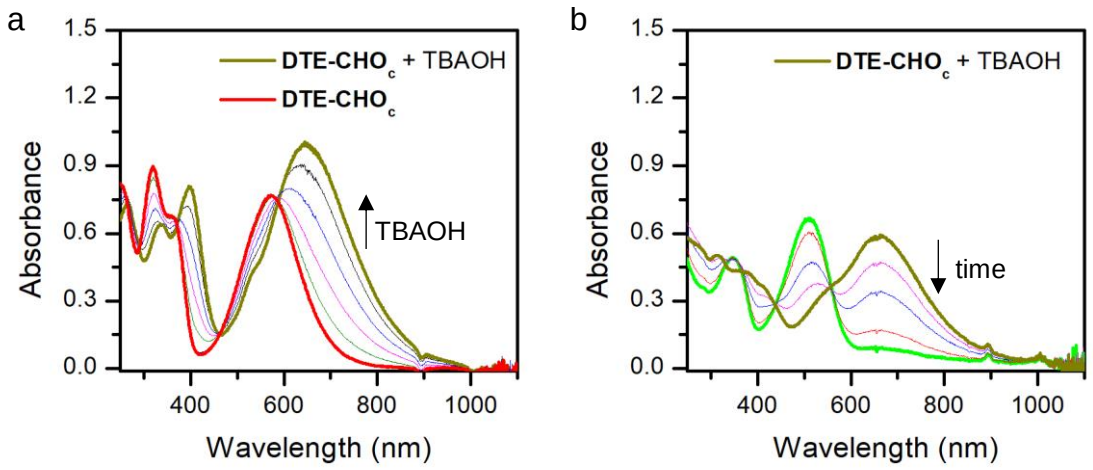

Figure IV-9. (a) Variation of the UV-vis spectrum of **DTE-CHO$_c$** (c = 8·10^{-5} M) upon titration with TBAOH in acetonitrile (from 0 to 1.5 eq.). (b) Variation of the UV-vis absorption of **DTE-CHO$_c$** (c = 4·10^{-5} M) in acetonitrile upon degradation over time after addition of 25 eq. of base.

Table IV-2. Characterization of **DTE-EWG** acidity properties in acetonitrile.

DTE-EWG	$\lambda_{abs,max,o}$ [a]	$\lambda_{abs,max,c}$ [a]	$pK_{a,ACN,o}$ [b]	$pK_{a,ACN,c}$ [b]	$\Delta pK_{a,ACN}$	$\delta_{H4,o}$ [c]
DTE-Cl	342	515	25.0 ± 0.4	23.9 ± 0.2	1.1	6.64
DTE-CHO	331	648	24.2 ± 0.2	21.3 ± 0.2	2.9	7.51
DTE-COCF$_3$	345	896	24.4 ± 0.1	19.4 ± 0.1	5.0	7.67
DTE-C$_6$F$_5$	344	564	24.5 ± 0.1	21.2 ± 0.1	3.3	7.20
DTE-py-zw	340	980	24.5 ± 0.3	20.8 ± 0.4	3.7	8.13[d]
DTE-NO$_2$	336	748	25.0 ± 0.7	19.8 ± 0.3	5.2	7.72
DTE-PhNO$_2$	353	677	24.7 ± 0.1	22.6 ± 0.2	2.1	7.18
DTE-pyNO$_2$	351	764	24.6 ± 0.1	22.6 ± 0.3	2.0	7.48
DTE$_F$-COCF$_3$	311	829	21.4 ± 0.5	19.2 ± 0.1	2.2	7.90

[a] Maximum absorption wavelength in nm of the conjugate base of the open and closed isomers. [b] pK_a values determined for the open and closed isomers. [c] Chemical shifts obtained

from ^{1}HNMR (CD_3CN) of the proton in the thiophene ring tethering the EWG in the open form expressed in ppm. [d] Measured in DMSO-d_6 because of low solubility in acetonitrile. The error for pK_a values is calculated as the standard deviation of 3 replicates.

As expected, more variation was observed for the pK_a values of the closed isomers of **DTE-EWG** ($pK_{a,ACN}$ = 19.2 – 22.6), which in all the cases became more acidic than the corresponding open states (Table IV-2). Actually, this was also observed for reference **DTE-Cl**, which suggests that the higher conjugation pathway of the closed form may also influence pK_a aside from the EWG nature. However, the pK_a variation measured upon photoisomerization in this case was the lowest ($\Delta pK_{a,ACN}$ = 1.1), which proves the benefit of introducing strong electron-withdrawing substituents in **DTE-EWG**.

According to the ΔpK_a values measured for these compounds, four different cases could be discriminated. First, the closed isomer of **DTE$_F$-COCF$_3$** turned to be the most acidic compound; however, its pK_a modulation ($\Delta pK_{a,ACN}$ = 2.5) was found to be lower than for most **DTE-EWG**, including its perhydrogenated counterpart **DTE-COCF$_3$**. This must be due to the effect caused by the perfluorinated central ring, which increases the acidity of both the open and closed states. This result, in combination with the lower stability of **DTE$_F$-COCF$_{3o}$** in basic media, indicate that nonfluorinated cyclopentene groups should be preferred for the design of DTEs exhibiting light-induced pK_a modulation. Second, lower acidity and ΔpK_a values were measured for **DTE-PhNO$_2$** and **DTE-pyNO$_2$** ($\Delta pK_{a,ACN}$ ~ 2.0), which present the weaker EWGs of **DTE-EWG**. Actually, when other electron-poorer aryl substituents were introduced in **DTE-C$_6$F$_5$** and **DTE-py-zw**, larger changes in acidity were measured ($\Delta pK_{a,ACN}$ ~ 3.5). However, the highest ΔpK_a values were registered for other strong EWGs that were directly connected to the thiophene moiety without any aryl spacer. Thus, though a moderate ΔpK_a value was measured for **DTE-CHO** ($\Delta pK_{a,ACN}$ = 2.9), very large pK_a modulation was obtained for **DTE-COCF$_3$** and **DTE-NO$_2$** bearing stronger EWGs ($\Delta pK_{a,ACN}$ ~ 5.0). These are therefore the best candidates to control phenol acidity in **DTE-EWG** conjugates.

To further analyze the EWG effect on the pK_a variation of **DTE-EWG** upon photoisomerization, we investigated the correlation with ^{1}H NMR data. First, we hypothesized that the chemical shift of the proton of the thiophene tethering the EWG in **DTE-EWG$_o$** ($\delta_{H4,o}$) could report on the electron-withdrawing strength of such group and, consequently, show a linear dependency with the pK_a value measured for **DTE-EWG$_c$** after ring closing (Table IV-2). As shown in Figure IV-10a, a moderate correlation was found between both properties, especially after taken out the data for **DTE-py-zw** whose ^{1}H NMR could not be measured in CD_3CN. Therefore, this means that ^{1}H NMR data could be used to estimate the light-induced variation of acidity for DTE-phenol conjugates.

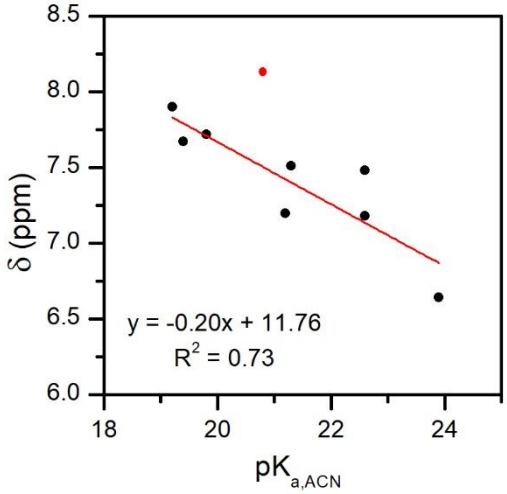

Figure IV-10. Plot of $pK_{a,ACN,c}$ vs the ^1H NMR chemical shift of the thiophene proton tethering the EWG (δ_{H4}) in CD_3CN for each DTE studied. The red dot represents the value for **DTE-py-zw**, whose chemical shift could only be obtained in DMSO-d_6.

It must be noted that little change was observed in the phenolic protons chemical shifts in the closed state compared to the thiophene ones. This would suggest that little communication occurs in the neutral state due to the free rotation of the phenol moiety and thus the pKa modulation would come from the stabilization of the negative charge through conjugation.

As already mentioned, herein we measured the pK_a constants of **DTE-EWG** in acetonitrile. This hampers the comparison of our results with most of the other pK_a modulating systems based on molecular photoswitches reported in the literature, which except for **DTE-acid3** ($pK_{a,ACN,o}$ = 17.6, $pK_{a,ACN,c}$ = 16.4, $\Delta pK_{a,ACN}$ = 1.2)[81] were measured in a variety of media and often referred to the pH scale in water. To solve this issue, we conducted the conversion of the pK_a values obtained from the acetonitrile to the water scales. To do so, a calibration curve was obtained for a set of 14 different phenol molecules whose $pK_{a,H2O}$ and $pK_{a,ACN}$ constants have been reported,[106] for which a clear linear dependence was obtained. Interpolation of the $pK_{a,ACN}$ values measured for **DTE-EWG** in this work led to the $pK_{a,H2O}$ constants shown in Table IV-3. Importantly, for **DTE-NO_2** and **DTE-$COCF_3$** exhibiting the largest acidity modulation in acetonitrile, $\Delta pK_{a,H2O}$ values as high as 3.0 and 2.9 were estimated, respectively, which are slightly better than that obtained by Hecht and co-workers for **DAE-acid** ($\Delta pK_{a,H2O}$ = 2.8; see Scheme IV-13).[71] Therefore, this demonstrates the potential of the strategy explored in this chapter to reach high acidity modulation using DTE photoswitches.

Table IV-3. Estimated pK_a constants of **DTE-EWG** in water.

DTE	$pK_{a,H_2O,o}$[a]	$pK_{a,H_2O,c}$[a]	$\Delta pK_{a,H_2O}$[a]
DTE-Cl	9.1	8.4	0.6
DTE-CHO	8.6	6.9	1.7
DTE-$COCF_3$	8.7	5.8	2.9
DTE-C_6F_5	8.8	6.8	1.9
DTE-py-zw	8.8	6.6	2.1
DTE-NO_2	9.1	6.0	3.0
DTE-$PhNO_2$	8.9	7.7	1.2
DTE-$pyNO_2$	8.8	7.7	1.2
DTE_F-$COCF_3$	7.1	5.7	1.5
DTE-acid1[78]	10.5	9.3	1.2
DTE-acid2[82]	2.6	1.2	1.4
DAE-acid[71]	4.0	6.8	2.8

[a] pK_a in water estimated for the open and closed states of **DTE-EWG** from the formula $pK_{a,H2O} = 0.58\ pK_{a,ACN} - 5.45$ obtained from several phenol pK_a values in ACN and H_2O.[106]

IV.8. SUMMARY AND CONCLUSIONS

In this chapter we described the preparation and study of a series of phenol-functionalized **DTE-EWG** compounds with the aim of photomodulating their pK_a upon photoisomerization. The main results obtained were the following:

- The synthesis of all the proposed **DTE-EWG** was successfully achieved employing 3 different strategies with the only exception of the final alkylation step

of **DTE-pyNO$_2$** to form the target zwitterion **DTE-pyNO$_2$-zw. DTE-CHO**, **DTE-COCF$_3$**, **DTE-C$_6$F$_5$**, **DTE-PhNO$_2$**, **DTE-Ph(NO$_2$)$_2$**, **DTE-py-zw** and **DTE-pyNO$_2$** were prepared from the common intermediate **9** through a divergent synthesis. **DTE-NO$_2$** and **DTE$_F$-COCF$_3$** were prepared via a convergent synthesis strategy by tethering the three DTE rings together via double Suzuki coupling or double nucleophilic substitution reactions with organolithium compounds, respectively. To our knowledge **DTE-NO$_2$** is the first example of a DTE photoswitch directly functionalized with a nitro external substituent.

- All **DTE-EWG** operate as molecular photoswitches interconverting between open and closed states, except for **DTE-Ph(NO$_2$)$_2$**. However, the photoconversion to the closed isomer was in general not quantitative for most of these compounds and PSS$_{o\text{-}c}$ mixtures with a wide variation of compositions were achieved. These results were attributed two to main factors affecting the ring-closing photoreaction quantum yield:
  (a) π-π stacking between the phenol and aryl EWG groups, which favor the photoinactive parallel conformation of **DTE-EWG$_o$**;
  (b) the electronic asymmetry of **DTE-EWG** bearing both strong EWG and EDG groups, which promotes charge transfer processes that compete with the photoisomerization reaction.

- Light-induced pK_a modulation of the phenol moiety was observed for all photoisomerizable **DTE-EWG**, whose closed state was found to be more acidic than the open form in all the cases. The largest acidity variation upon photoisomerization was determined for **DTE-COCF$_3$** and **DTE-NO$_2$**, which exhibited ΔpK_a values around 5.0 and 3.0 in acetonitrile and water, respectively, which are slightly larger than the best results reported to date with DAEs. This is due to a variety of factors:
  (a) as proven for reference **DTE-Cl**, a small increase in acidity intrinsically occurs in **DTE-EWG** upon cyclization due to the longer conjugation path of the closed formed;
  (b) the presence of an external EWG substituent in one thiophene ring does not affect the acidity of the phenol moiety in the other thiophene unit of the open isomer, as they are not electronically connected; by contrast, they do become conjugated in the closed state, which further decreases the pK_a constant of this form.
  (c) larger pK_a decrements upon ring-closing occur for stronger external EWG substituents, especially if they are directly connected to the thiophene ring without any aryl spacer;

(d) the use of perhydrogenated central cyclopentene rings maximizes acidity modulation by removing the inductive electro-withdrawing effects affecting the open isomer acidity when a perfluorinated cyclopentene unit is employed.

In view of the results obtained, **DTE-COCF$_3$** and **DTE-NO$_2$** are very promising photoswitches to be applied to optically control reactivity in pH-dependent processes. Actually, we inspired in these compounds to develop photoactivable coupling reagents for amide bond formation, a study that is described in next Chapter V.

IV.9. REFERENCES

1 S. Aubert, M. Bezagu, A. C. Spivey and S. Arseniyadis, *Nat. Rev. Chem.*, 2019, **3**, 706–722.

2 K. Hüll, J. Morstein and D. Trauner, *Chem. Rev.*, 2018, **118**, 10710–10747.

3 M. J. Fuchter, *J. Med. Chem.*, 2020, **63**, 11436–11447.

4 D. Majee and S. Presolski, *ACS Catal.*, 2021, **11**, 2244–2252.

5 S. P. Ihrig, F. Eisenreich and S. Hecht, *Chem. Commun.*, 2019, **55**, 4290–4298.

6 N. A. Romero and D. A. Nicewicz, *Chem. Rev.*, 2016, **116**, 10075–10166.

7 K. Fries, S. Samanta, S. Orski and J. Locklin, *Chem. Commun.*, 2008, 6288–6290.

8 V. Lemieux and N. R. Branda, *Org. Lett.*, 2005, **7**, 2969–2972.

9 M. Kathan and S. Hecht, *Chem. Soc. Rev.*, 2017, **46**, 5536–5550.

10 L. Wang and Q. Li, *Chem. Soc. Rev.*, 2018, **47**, 1044–1097.

11 W. Ho, *J. Chem. Phys.*, 2002, **117**, 11033–11061.

12 N. Kaur, *Synth. Commun.*, 2018, **48**, 1259–1284.

13 G. S. Kumar and Q. Lin, *Chem. Rev.*, 2021, **121**, 6991–7031.

14 J. T. Offenloch, M. Gernhardt, J. P. Blinco, H. Frisch, H. Mutlu and C. Barner-Kowollik, *Chem. Eur. J.*, 2019, **25**, 3700–3709.

15 R. S. Stoll and S. Hecht, *Org. Lett.*, 2009, **11**, 4790–4793.

16 R. S. Stoll, M. V. Peters, A. Kuhn, S. Heiles, R. Goddard, M. Bühl, C. M. Thiele and S. Hecht, *J. Am. Chem. Soc.*, 2009, **131**, 357–367.

17 Z. Dai, Y. Cui, C. Chen and J. Wu, *Chem. Commun.*, 2016, **52**, 8826–8829.

18 R. Cacciapaglia, S. Di Stefano and L. Mandolini, *J. Am. Chem. Soc.*, 2003, **125**, 2224–2227.

19 T. Imahori, R. Yamaguchi and S. Kurihara, *Chem. Eur. J.*, 2012, **18**, 10802–10807.

20 M. Samanta, V. S. R. Krishna and S. Bandyopadhyay, *Chem. Commun.*, 2014, **50**, 10577–10579.

21 T. Imahori and S. Kurihara, *Chem. Lett.*, 2014, **43**, 1524–1531.

22 D. Sud, T. B. Norsten and N. R. Branda, *Angew. Chem. Int. Ed.*, 2005, **44**, 2019–2021.

23 M. Takeshita, K. Uchida and M. Irie, *Chem. Commun.*, 1996, 1807–1808.

24 M. Takeshita and M. Irie, *Tetrahedron Lett.*, 1998, **39**, 613–616.

25 M. Li, P. Zhang and C. Chen, *Macromolecules*, 2019, **52**, 5646–5651.

26 H. Sugimoto, T. Kimura and S. Inoue, *J. Am. Chem. Soc.*, 1999, **121**, 2325–2326.

27 M. J. Barrell, A. G. Campaña, M. Von Delius, E. M. Geertsema and D. A. Leigh, *Angew. Chem. Int. Ed.*, 2011, **50**, 285–290.

28 B. Koeppe, S. Rühl and F. Römpp, *ChemPhotoChem*, 2019, **3**, 71–74.

29 I. Aprahamian, *Chem. Commun.*, 2017, **53**, 6674–6684.

30 M. Vlatkovic, L. Bernardi, E. Otten and B. L. Feringa, *Chem. Commun.*, 2014, **50**, 7773–7775.

31 R. Dorel and B. L. Feringa, *Chem. Commun.*, 2019, **55**, 6477–6486.

32 D. Wilson and N. R. Branda, *Angew. Chem. Int. Ed.*, 2012, **51**, 5431–5434.

33 M. Kathan, P. Kovaříček, C. Jurissek, A. Senf, A. Dallmann, A. F. Thünemann and S. Hecht, *Angew. Chem. Int. Ed.*, 2016, **55**, 13882–13886.

34 H. Nakagawa, T. Nakashima and T. Kawai, *Eur. J. Org. Chem.*, 2012, 4493–4500.

35 R. Mizutsu, R. Asato, C. J. Martin, M. Yamada, Y. Nishikawa, S. Katao, M. Yamada, T. Nakashima and T. Kawai, *J. Am. Chem. Soc.*, 2019, **141**, 20043–20047.

36 M. Kathan, F. Eisenreich, C. Jurissek, A. Dallmann, J. Gurke and S. Hecht, *Nat. Chem.*, 2018, **10**, 1031–1036.

37 S. Silvi, A. Arduini, A. Pochini, A. Secchi, M. Tomasulo, F. M. Raymo, M. Baroncini and A. Credi, *J. Am. Chem. Soc.*, 2007, **129**, 13378–13379.

38 Y. Shiraishi, S. Sumiya and T. Hirai, *Chem. Commun.*, 2011, **47**, 4953–4955.

39 V. Blanco, D. A. Leigh and V. Marcos, *Chem. Soc. Rev.*, 2015, **44**, 5341–5370.

40 B. M. Neilson and C. W. Bielawski, *J. Am. Chem. Soc.*, 2012, **134**, 12693–12699.

41 H. Nakagawa, S. Kawai, T. Nakashima and T. Kawai, *Org. Lett.*, 2009, **11**, 1475–1478.

42 H. D. Samachetty, V. Lemieux and N. R. Branda, *Tetrahedron*, 2008, **64**, 8292–8300.

43 V. Lemieux, S. Gauthier and N. R. Branda, *Angew. Chem. Int. Ed.*, 2006, **45**, 6820–6824.

44 Z. Erno, A. M. Asadirad, V. Lemieux and N. R. Branda, *Org. Biomol. Chem.*, 2012, **10**, 2787–2792.

45 M. Irie, T. Fukaminato, K. Matsuda and S. Kobatake, *Chem. Rev.*, 2014, **114**, 12174–12277.

46 M. Irie, *Chem. Rev.*, 2000, **100**, 1685–1716.

47 P. R. Hania, A. Pugzlys, L. N. Lucas, J. J. D. De Jong, B. L. Feringa, J. H. Van Esch, H. T. Jonkman and K. Duppen, *J. Phys. Chem. A*, 2005, **109**, 9437–9442.

48 D. H. Waldeck, *Chem. Rev.*, 1991, **91**, 415–436.

49 M. Irie and M. Mohri, *J. Org. Chem.*, 1988, **53**, 803–808.

50 J. Von Irmer, F. Frieß, D. Herold, J. Kind, C. M. Thiele and M. Gallei, *J. Mater. Chem. C*, 2019, **7**, 14088–14097.

51 D. G. Patel, T. B. Mitchell, S. D. Myers, D. A. Carter and F. A. Novak, *J. Org. Chem.*, 2020, **85**, 2646–2653.

52 G. Sevez and J. L. Pozzo, *Dyes Pigm.*, 2011, **89**, 246–253.

53 S. Nakamura and M. Irie, *J. Org. Chem.*, 1988, **53**, 6136–6138.

54 M. Irie, K. Sakemura, M. Okinaka and K. Uchida, *J. Org. Chem.*, 1995, **60**, 8305–8309.

55 S. Fukumoto, T. Nakashima and T. Kawai, *Angew. Chem. Int. Ed.*, 2011, **50**, 1565–1568.

56 K. Uchida, E. Tsuchida, Y. Aoi, S. Nakamura and M. Irie, *Chem. Lett.*, 1999, **28**, 63–64.

57 T. Yamaguchi and M. Irie, *J. Photochem. Photobiol. A Chem.*, 2006, **178**, 162–169.

58 M. Irie and K. Sayo, *J. Phys. Chem.*, 1992, **96**, 7671–7674.

59 S. Kobatake, Y. Terakawa and H. Imagawa, *Tetrahedron*, 2009, **65**, 6104–6108.

60 M. Cipolloni, F. Ortica, L. Bougdid, C. Moustrou, U. Mazzucato and G. Favaro, *J. Phys. Chem. A*, 2008, **112**, 4765–4771.

61 M. Irie, T. Lifka, K. Uchida, S. Kobatake and Y. Shindo, *Chem. Commun.*, 1999, 747–748.

62 A. Mulder, A. Juković, F. W. B. Van Leeuwen, H. Kooijman, A. L. Spek, J. Huskens and D. N. Reinhoudt, *Chem. Eur. J.*, 2004, **10**, 1114–1123.

63 A. M. Asadirad, S. Boutault, Z. Erno and N. R. Branda, *J. Am. Chem. Soc.*,

2014, **136**, 3024–3027.

64 T. Nakashima, M. Goto, S. Kawai and T. Kawai, *J. Am. Chem. Soc.*, 2008, **130**, 14570–14575.

65 G. Kocak, C. Tuncer and V. Bütün, *Polym. Chem.*, 2017, **8**, 144–176.

66 F. Eisenreich, M. Kathan, A. Dallmann, S. P. Ihrig, T. Schwaar, B. M. Schmidt and S. Hecht, *Nat. Catal.*, 2018, **1**, 516–522.

67 K. Neumann, A. Lilienkampf and M. Bradley, *Polym. Int.*, 2017, **66**, 1756–1764.

68 Y. Zhu and F. Chen, *Chem. an Asian J.*, 2015, **10**, 284–305.

69 R. M. D. Nunes, M. Pineiro and L. G. Arnaut, *J. Am. Chem. Soc.*, 2009, **131**, 9456–9462.

70 M. V Peters, R. S. Stoll, A. Kühn and S. Hecht, *Angew. Chem.*, 2008, **47**, 5968–5972.

71 B. M. Schmidt, D. Jacquemin, S. Hecht and J. Gurke, *Angew. Chem.*, 2018, **57**, 4797–4801.

72 R. Wang, N. Wang, S. Pu, X. Zhang and G. Liu, *Dyes Pigm.*, 2017, **146**, 445–454.

73 S. Kohse, A. Neubauer, A. Pazidis, S. Lochbrunner and U. Kragl, *J. Am. Chem. Soc.*, 2013, **135**, 9407–9411.

74 S. Abbruzzetti, M. Carcelli, D. Rogolino and C. Viappiani, *Photochem. Photobiol. Sci.*, 2003, **2**, 796–800.

75 C. E. Weston, R. D. Richardson and M. J. Fuchter, *Chem. Commun.*, 2016, **52**, 4521–4524.

76 S. Samanta, A. Babalhavaeji, M. Dong and G. A. Woolley, *Angew. Chem. Int. Ed.*, 2013, **52**, 14127–14130.

77 M. Hammarson, J. R. Nilsson, S. Li and J. Andréasson, *J. Phys. Chem. B*, 2013, **117**, 13561–13571.

78 S. H. Kawai, S. L. Gilat and J. M. Lehn, *Eur. J. Org. Chem.*, 1999, 2359–2366.

79 G. Guirado, C. Coudret, M. Hliwa and J. P. Launay, *J. Phys. Chem. B*, 2005, **109**, 17445–17459.

80 Y. Odo, K. Matsuda and M. Irie, *Chem. Eur. J.*, 2006, **12**, 4283–4288.

81 D. Liu, A. D. Sponza, D. Yang and M. Chiu, *Angew. Chem.*, 2019, **58**, 16210–16216.

82 J. Massaad, J. Micheau, C. Coudret, R. Sanchez and G. Guirado, *Chem. Eur. J.*, 2012, **18**, 6568–6575.

83 X. Wu, C. C. Ling and D. R. Bundle, *Org. Lett.*, 2004, **6**, 4407–4410.

84 C. Wang, H. Luo, H. Li, X. Zhu, B. Yu and S. Dai, *Chem. Eur. J.*, 2012, **18**,

2153–2160.

85 M. Villabona, Universitat Autònoma de Barcelona, 2016.

86 R. S. Sánchez, R. Gras-Charles, J. L. Bourdelande, G. Guirado and J. Hernando, *J. Phys. Chem. C*, 2012, **116**, 7164–7172.

87 L. N. Lucas, J. J. D. De Jong, J. H. Van Esch, R. M. Kellogg and B. L. Feringa, *Eur. J. Org. Chem.*, 2003, 155–166.

88 Q. Zou, J. Jin, B. Xu, L. Ding and H. Tian, *Tetrahedron*, 2011, **67**, 915–921.

89 J. Zhang, J. Jin, L. Zou and H. Tian, *Chem. Commun.*, 2013, **49**, 9926–9928.

90 D. R. Coulson, L. C. Satek and S. O. Grim, *Inorganic Syntheses*, McGraw-Hill, 1972, vol. XIII.

91 W. Tan, X. Li, J. Zhang and H. Tian, *Dyes Pigm.*, 2011, **89**, 260–265.

92 T. W. Greene and P. G. M. Wuts, *Protective Groups In Organic Synthesis*, John Wiley & Sons, New York, 3rd edn., 1991.

93 P. Wei, F. Xue, Y. Shi, R. Strand, H. Chen and T. Yi, *Chem. Commun.*, 2018, **54**, 13115–13118.

94 N. Miyaura and A. Suzuki, *Chem. Rev.*, 1995, **95**, 2457–2483.

95 F. De Proft, *Structure, Bonding and Reactivity of Heterocyclic Compounds*, Springer, 2014.

96 T. C. Pijper, T. Kudernac, W. R. Browne and B. L. Feringa, *J. Phys. Chem. C*, 2013, **117**, 17623–17632.

97 M. Kogami and N. Watanabe, *Synth. Commun.*, 2013, **43**, 681–688.

98 H. Chen, N. Cheng, W. Ma, M. Li, S. Hu, L. Gu, S. Meng and X. Guo, *ACS Nano*, 2016, **10**, 436–445.

99 J. A. Mikroyannidis, A. N. Kabanakis, P. Suresh and G. D. Sharma, *J. Phys. Chem. C*, 2011, **115**, 7056–7066.

100 R. Yang, S. Wang, K. Zhao, Y. Li, C. Li, Y. Xia and Y. Liu, *Polym. Sci. - Ser. B*, 2017, **59**, 16–27.

101 K. Smith, T. Gibbins, R. W. Millar and R. P. Claridge, *J. Chem. Soc. Perkin Trans. 1*, 2000, 2753–2758.

102 Z. Huang, Y. Yang, Q. Xiao, Y. Zhang and J. Wang, *Eur. J. Org. Chem.*, 2012, 6586–6593.

103 V. I. Nikolayenko, D. C. Castell, D. P. van Heerden and L. J. Barbour, *Angew. Chem. Int. Ed.*, 2018, **57**, 12086–12091.

104 S. Hermes, G. Dassa, G. Toso, A. Bianco, C. Bertarelli and G. Zerbi, *Tetrahedron Lett.*, 2009, **50**, 1614–1617.

105 S. Espinosa, E. Bosch and M. Roses, *Anal. Chem.*, 2000, **72**, 5193–5200.

106 S. Espinosa, E. Bosch and M. Rosés, *J. Chromatogr. A*, 2002, **964**, 55–66.

Chapter V

Dual-color control of amide bond formation with dithienylethene photoswitches

In this chapter we describe the development of photoresponsive activated esters based on dithienylethene switches for the optical control of amide bond formation with two colors of light.

V.1. INTRODUCTION

V.1.1. Photoligation reactions

Photoligation reactions are high yield chemical processes in which a covalent bond is formed between two molecules upon light irradiation. These photoreactions are of special interest due to the noninvasive time and spatial control that they provide to chemical assembly and functionalization, which makes them very powerful tools to be applied in fields like polymer synthesis and processing,[1–3] 3D printing,[4–6] bioconjugation and biomolecule manipulation[7,8] and nanochemistry.[9,10]

Many types of reactions are employed for photoligation.[11–13] Commonly, they rely on the photoinduced generation of a highly reactive intermediate that undergoes a fast thermal ligation reaction such as, for instance, Diels-Alder cycloadditions,[1,2] imine formation,[6,14] disulfide bond formation[4,6,9] and 1,3-dipolar cycloadditions.[15–18] However, there are other examples where light is used to create excited states that directly react via dimerization processes like [2+2] and [4+4] cycloadditions (Scheme V-1).[15,19,20]

Most of these photoligation reactions present two main disadvantages. First, they mainly rely on illumination with UV light, which features low penetration depth in solid and liquid materials and can damage other chemical species present such as solvents, biological tissues, or polymeric chains due to its high energy photons.[15] As a result, the applications of these systems are often limited because of the occurrence of unwanted side reactions and decompositions. It is for this reason that photoligation reactions in the visible region are highly desired.[15]

Second, photoligation reactions can only be controlled with one wavelength of light in most cases, which irreversibly photogenerates the reactive species. This reduces the spatial and time resolution of the photoligation process because of the nonnegligible lifetime of the reactive molecules that can diffuse out of the illuminated area. But even in the case where diffusion could be avoided, like for instance with

very short-lived photogenerated species, the spatial precision of photoligation is limited to the sub-micrometer range because of the diffraction limit of far-field optics.[21,22] To overcome these limitations, the development of two-color controlled photoreactive systems has been proposed.

a Diels-Alder cycloadditions

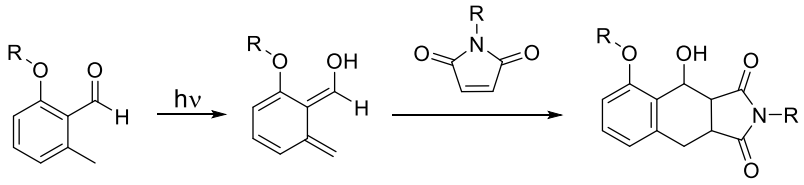

b Substitution reactions

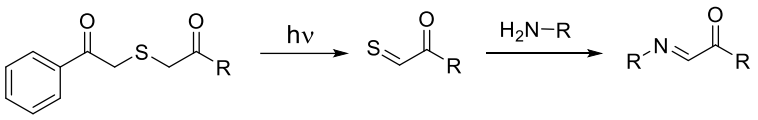

c Redox reactions

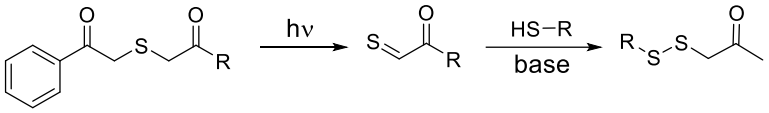

d 1,3-dipolar cycloadditions

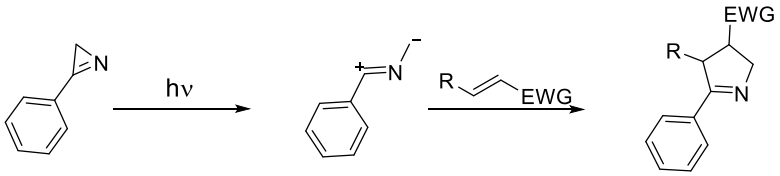

e [4+4] cycloadditions

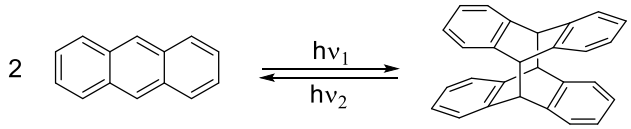

f [2+2] cycloadditions

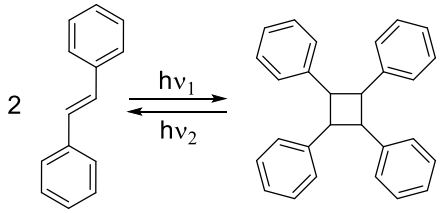

Scheme V-1. Examples of some of the most representative photoligation reactions: (a) Diels-Alder cycloadditions of dienophiles with photogenerated *orto*-quinodimethanes (*o*-QDM) as dienes;[1,2] (b) imine formation with a thioaldehyde generated upon irradiation;[6] (c) disulfide bond formation between a thiol and a photogenerated thioaldehyde;[4,6,9] (d) 1,3-dipolar

cycloadditions between a light-generated 1,3-dipole and an electron-poor alkene;[15–18] (e) [4+4][15,19] and (f) [2+2][15,20] cycloadditions.

V.1.2. Dual-color control of photoligation reactions

The use of two orthogonal photoexcitation wavelengths allows enhancing the spatial, time and even chemical precision of photoligation processes. Different strategies can be applied to achieve this goal. On the one hand, reactions can be employed that require photoactivation with two different colors of light; e.g., by photogenerating a reactive species via two consecutive one-photon absorptions of the starting material at different wavelengths. As a result, greater resolutions would be achieved if ligation only occurs in the overlapping region of the two irradiation sources (Figure V-1a).[5,23,24] This is the case of the system shown in Figure V-1b, which uses ***o*-MBA-S$_2$** as a photoreagent.[23] ***o*-MBA-S$_2$** bears a thioacetal protecting group that can be removed by irradiation at λ_{exc1} = 450 nm in the presence of a photosensitizer. The resulting aldehyde ***o*-MBA-OMe** is unaltered by irradiation with blue light, but at λ_{exc2} = 350 nm it undergoes an isomerization to the highly reactive diene ***o*-QD-OMe** that rapidly reacts with a maleimide through a Diels-Alder cycloaddition. Because the presence of an aldehyde is required for diene formation, ***o*-MBS-S$_2$** is unreactive under illumination with UV light. In this manner, the photoligation reaction to yield **adduct1** only occurs upon concomitant irradiation at 350 nm and 450 nm.[23]

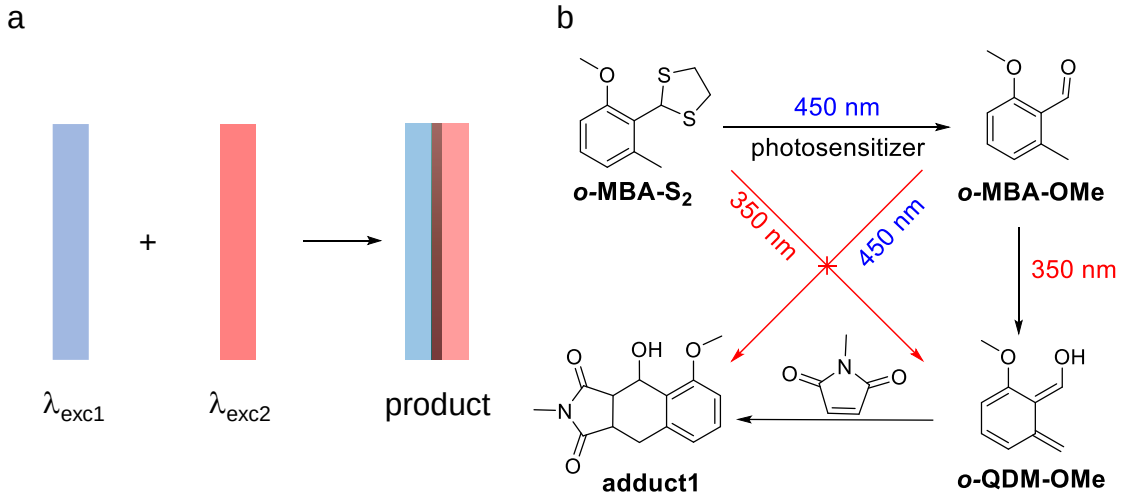

Figure V-1. (a) Two-color strategy for enhancing the resolution of photoligation reactions by selectively inducing a light-induced process in the overlap region of two different excitation wavelengths.[23,24] (b) Photoligation system requiring ***o*-MBA-S$_2$** irradiation at both 450 nm and 350 nm to undergo a Diels-Alder photoligation reaction to form **adduct1** in the presence of a photosensitizer and maleimide.[23]

Alternatively, light-triggered reactions that can be depleted upon irradiation with a second wavelength can also show improved resolution by inhibiting the ligation process in the overlap region of the activating (λ_{exc}) and deactivating (λ_{depl}) beams

(Figure V-2a).[5,20,22,25,26] This strategy is inspired in the stimulated emission depletion (STED) technique developed by Nobel laureate in Chemistry Stefan W. Hell to achieve super-resolution fluorescence microscopy.[27] One way to perform such type of two-color controlled photoligation reactions is the use of photoreversible [2+2] or [4+4] cycloadditions, as they can also be reverted back upon light irradiation.[15,20] For instance, **PEG-stil** has been used as a photogelator which dimerizes by irradiation at λ_{exc} = 400 nm. Upon UV exposure, the photoligation reaction is reversed and, thus, self-healing of a **PEG-stil**-based hydrogel can be achieved when both wavelengths are applied in the same spot to dissociate and form new cycloadduct cross-linking points in the material (Figure V-2b and c).[20]

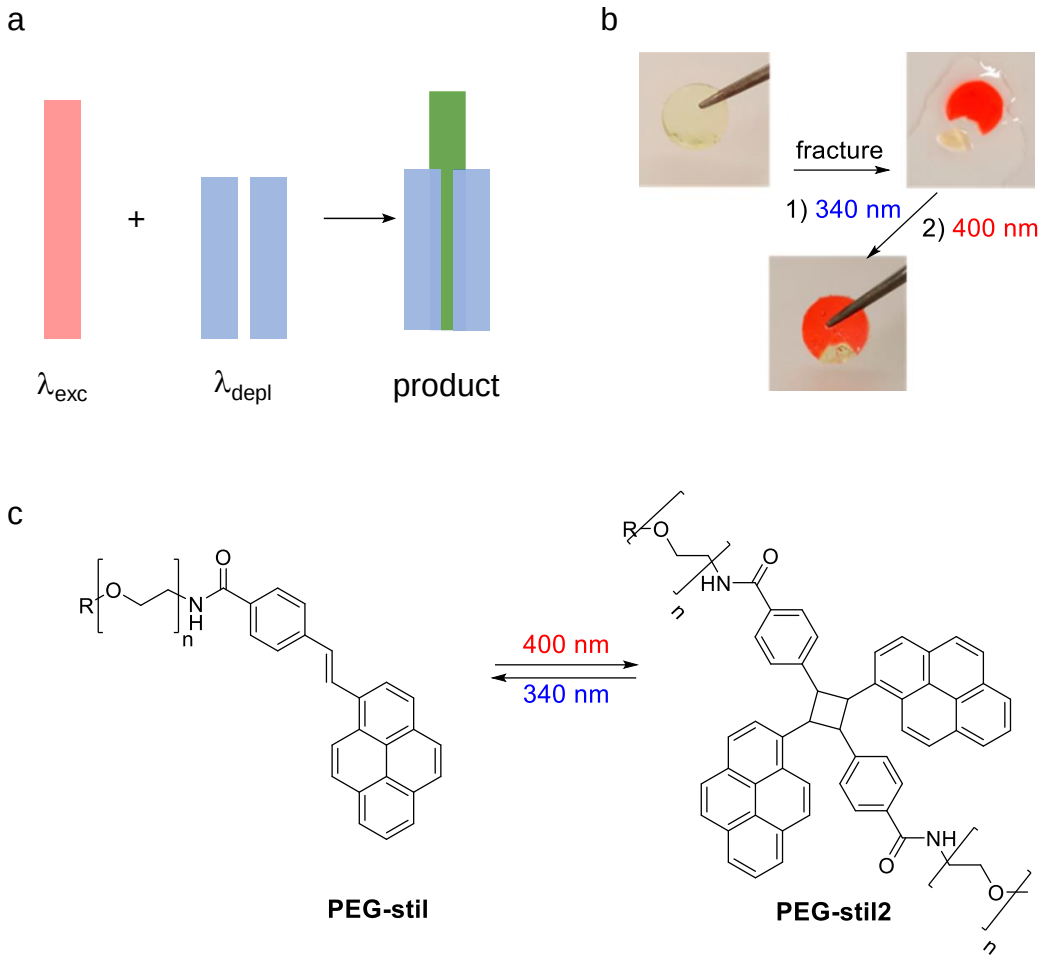

Figure V-2. (a) STED-based strategy for enhancing resolution in two-color controlled photoligation processes, which consists in inhibiting a photochemical reaction with a second irradiation wavelength.[5,20,25,26] (b-c) Pictures showing the light-induced self-healing of a **PEG-stil**-based hydrogel, which relies on the reversible photodimerization reaction of **PEG-stil** to yield **PEG-stil2**.[20]

However, photoreversible cycloadditions often suffer from an important drawback when applied to the two-color control of photoligation reactions: as the absorption spectra of the monomer and cycloadduct frequently overlap, partial photostationary

equilibrium mixtures are formed upon irradiation. Consequently, the efficiency of the depletion reaction is far from complete and very much dependent on the extinction coefficients and reaction quantum yields of the species and processes involved. This is a critical limitation to reach optimal resolution under two-wavelength irradiation, as total inhibition of the ligation reaction by λ_{depl} is required.

To overcome this drawback, an alternative to the [2+2] and [4+4] cycloadditions are molecular photoswitches toggling between reactive and unreactive states upon illumination with two colors of light. Although they often also give rise to photostationary mixtures between the two isomers under irradiation, complete conversion can be achieved if coupled with an irreversible ligation reaction that is only possible for one of the two photoswitch states.[5,25,26] Therefore, as the ligation process occurs, that particular state of the photoswitch is consumed, thus further driving the photoisomerization reaction towards the reactive isomer of the system.[5,25,26]

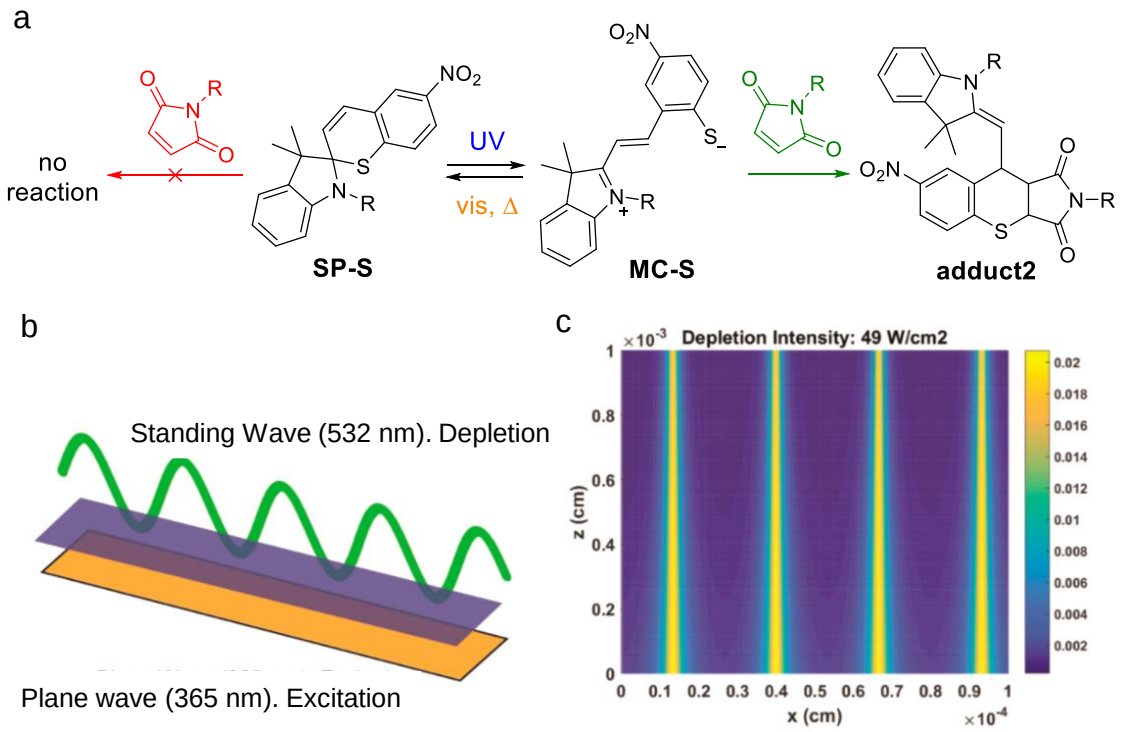

Figure V-3 (a) Photoligation system based on molecular photoswitch **SP-S/MC-S**, which can only undergo the addition reaction to yield **adduct2** in the **MC-S** state. As a result, it is triggered by UV light and depleted with visible irradiation.[26] (b) Setup used by the authors[28] for simulating 1D interference lithography in a spirothiopyran−*N*-ethyl maleimide system. (c) Thiol-Michael addition product concentration in the resist (XZ view) obtained for depletion intensity 49 W/cm^2.[28]

To illustrate this behavior, a dual-wavelength controlled photoligation reaction with molecular photoswitches is shown in Figure V-3.[26,28] It is based on spirothiopyran **SP-S**, which can be converted to merocyanine **MC-S** bearing a reactive thiophenolate

moiety upon UV irradiation.[26] Such transformation can be reverted back with visible light and, therefore, the amount of **MC-S** in the photostationary state is dependent on both UV and visible light intensities. In this way, two-color control can be achieved for the selective addition reaction of **MC-S** with a maleimide electrophile to form **adduct2.** On the one hand, UV light is required for the reaction to happen; on the other hand, sufficient visible irradiation can dramatically diminish the amount of **MC-S** and eventually prevent the ligation process in the overlapping region between the UV and visible beams (Figure V-3).[28]

This latter strategy has been employed in this and the following chapter to develop dual-color controlled photoligation reactions with dithienylethenes.

V.1.3. Light-modulation of bond formation reactions with dithienylethenes and other diarylethenes

So far only a few examples of photoligation reactions using DTEs or other DAEs have been reported in the literature. Usually, they rely on cycloaddition reactions like Diels-Alder reactions to optically modulate the formation of covalent bonds,[29–31] which will be covered in more detail in Chapter VI. Instead, in this section the interest is focused on other types of photoligation processes such as imine formation[32,33] and nucleophilic substitutions,[34] which have also been used for the optical control of bond formation reactions with DTEs. Actually, examples of these systems have already been shown in Chapter IV (see Scheme IV.7 for an imine formation reaction[32] and Scheme IV.9 for a nucleophilic substitution process[34] photoregulated with DTE switches).

Another exquisite example of this behavior is shown in Figure V-4, where Hecht and co-workers prepared a DTE photoswitch bearing two formyl substituents at the external thiophene positions that could be anchored to amine-functionalized surfaces through imine bond formation (Figure V-4).[33] Upon ring closing of the partially anchored **DTE-imine** compound, the second formyl group becomes more reactive because of the conjugation to the electron-withdrawing imine moiety and, thus, the reaction with another amine group to yield **DTE-imine2** is accelerated (Figure V-4a and b).[33] Nicely, the authors exploited this feature to photomodulate the self-healing process of a siloxane polymer with amino-terminated side chains. As clearly seen in Figure V-4c, UV irradiated regions enriched with the more reactive cross-linking **DTE-imine$_c$** agent healed faster than the nonirradiated areas.

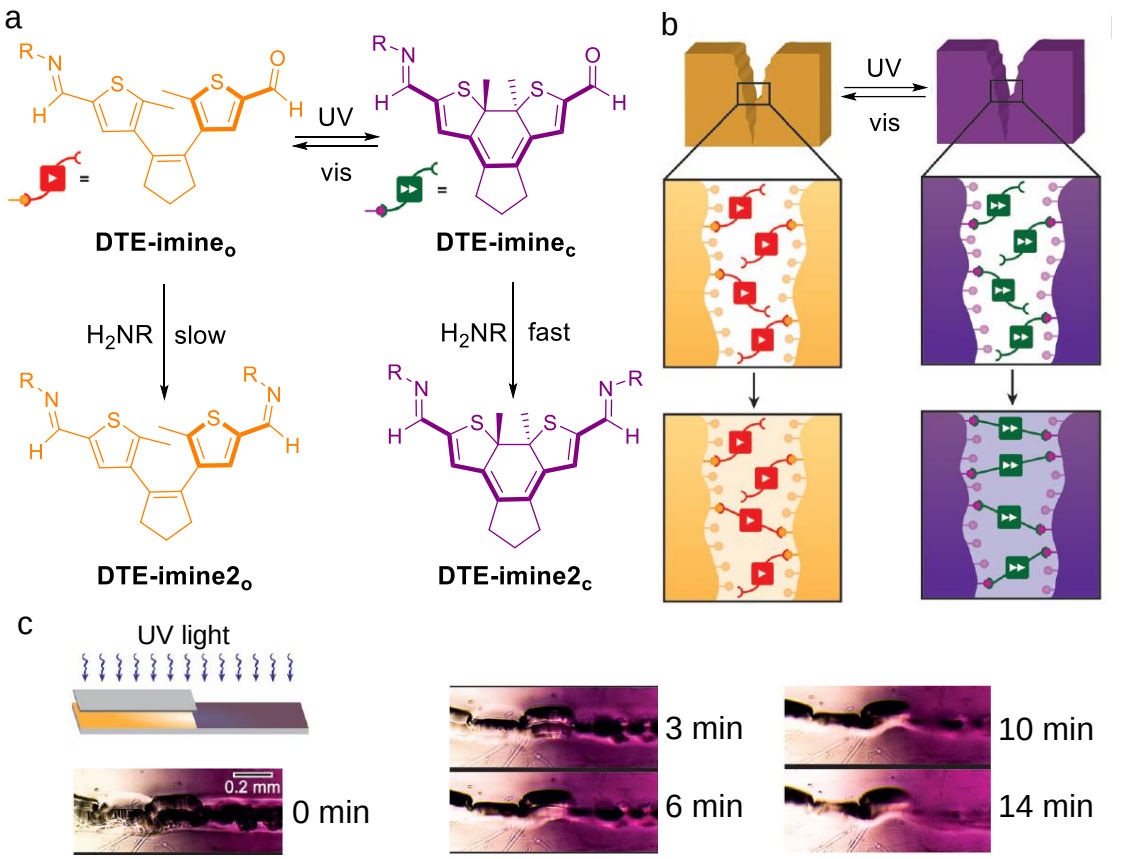

Figure V-4. (a) Two-light controlled **DTE-imine** system, which undergoes a faster second imine formation reaction upon ring closing.[33] (b) Schematic representation of light-healing materials based on **DTE-imine**.[33] (c) Photographs of a self-healing process under UV illumination (purple, right) and in the dark (yellow, left) of an amino-functionalized siloxane polymer containing **DTE-imine**.[33]

Differently to all these examples, herein we aimed to control another type of reaction with DTEs and two-color illumination: amide bond formation, which is one of the most important ligation processes in both materials science[35–38] and biology.[39,40]

V.1.4. Amide bond formation strategies

Amide bonds are not only the backbones of proteins, but they are also present in commodity plastics like nylons and in up to 25% of the known drugs.[41,42] In fact, the formation of amides is the most common reaction in pharmaceutical chemistry, accounting for 16% of the total number of transformations in this sector.[42] Because of its many advantages as high stability, polarity, or conformational diversity,[43] amide bond formation has also been extensively used for chemical ligation such as in the functionalization of biological compounds,[39,40] surfaces,[35,36] polymers,[37,38] and nanoparticles.[44]

Despite its importance, one of the main drawbacks of amide formation is that harsh conditions are required to directly produce an amide from an amine and a carboxylic

acid.[41,45] It is for this reason that several strategies have been developed to perform amidation at milder conditions. Among the most common are the use of acyl halides or acid anhydrides,[46] of coupling agents (i.e., carbodiimides, phosphonium salts) to activate carboxylic acids,[43,46] and of catalysts[42,45,47] (Scheme V-2).

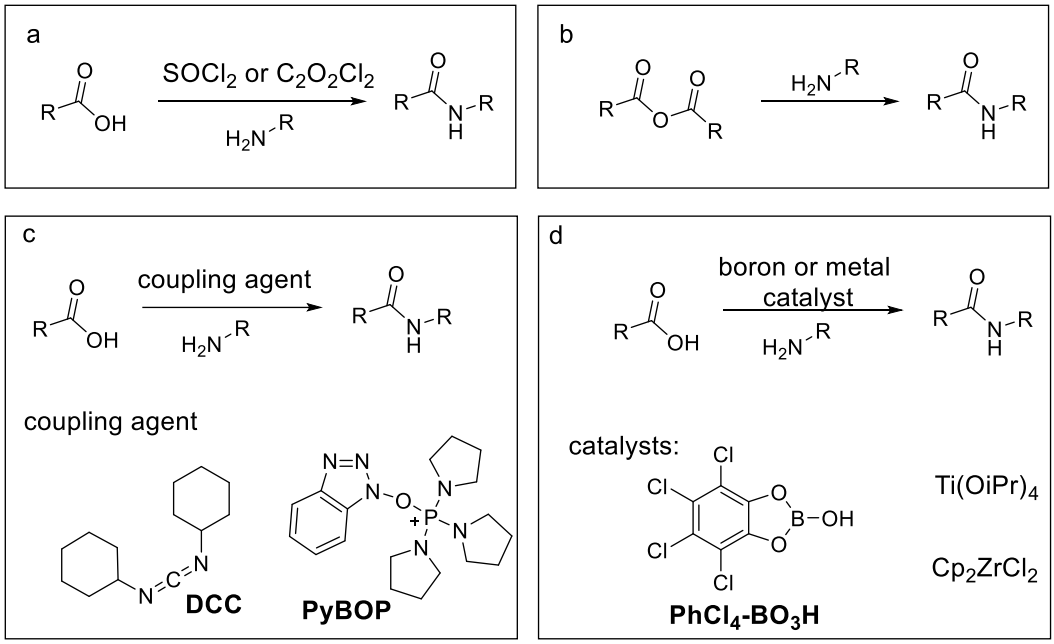

Scheme V-2. (a) Amide formation through acyl halides.[46] (b) Amide formation through acid anhydrides.[46] (c) Coupling agent mediated amidation. Examples of some of the most used coupling agents are shown: *N*,*N'*-dicyclohexylcarbodiimide (DCC) and benzotriazol-1-yloxytripyrrolidinophosphonium hexafluorophosphate (PyBOP).[43] (d) Catalyzed formation of amides. Examples of some of the catalysts used are shown.[42,47]

Some recent examples can also be found in the literature where light is employed to trigger amide formation. In most cases they are based on photoredox reactions in which light is used to activate the reactants upon electron transfer in the presence of an optically active species. The strategies employed are diverse and mainly rely on organic photosensitizers,[48,49] photoactive inorganic catalysts[50] or even charge-transfer complexes[51] to form amides starting from different substrates such as thiocarboxylic acids,[48,52] aldehydes,[50,53] or carboxylic acids (Scheme V-3).[49,51]

However, all those photoinduced methods lack precise temporal and spatial control of amidation, as only a single excitation wavelength is employed. It is for this reason that herein we aimed to develop a two-color photodriven system to accomplish amide bond formation with ultimate spatiotemporal precision. To do so we did not consider the use of photoredox chemistry, but focused our attention in one of the most common strategies applied to achieve amidation under regular thermal conditions: the use of active esters,[54,55] which have been extensively employed for the functionalization of amino-terminated molecules and materials such as peptides,[56] polymers[38,57] and surfaces,[58,59] among others.

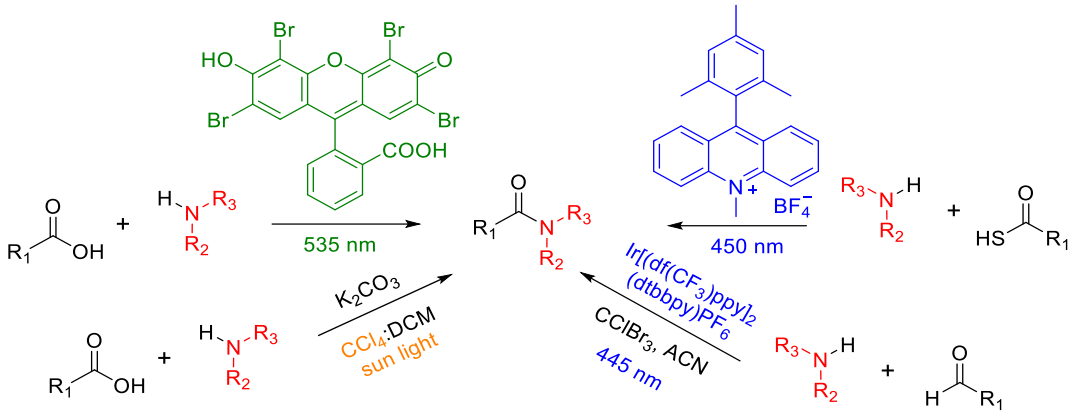

Scheme V-3. Examples of photoinduced amide formation.[48–51] The photoactive species is colored in each case.

Active esters are compounds that are highly reactive with nucleophiles and, therefore, are very active acylating agents.[54,55] Consequently, they can be used to form amide bonds in the presence of an amine at mild conditions and without the addition of other chemical species.[54,55] For this they must contain a good alkoxy leaving group (LG) – i.e., of low basicity – that is stabilized by mesomeric and/or inductive effects. This is typically accomplished by introducing strong EWGs, as illustrated by the examples in Scheme V-4. Interestingly, some of these LGs are electron-poor phenolates (e.g., 4-nitrophenolate), which we demonstrated in Chapter IV that can be selectively generated by the photoisomerization of DTE-phenol conjugates.

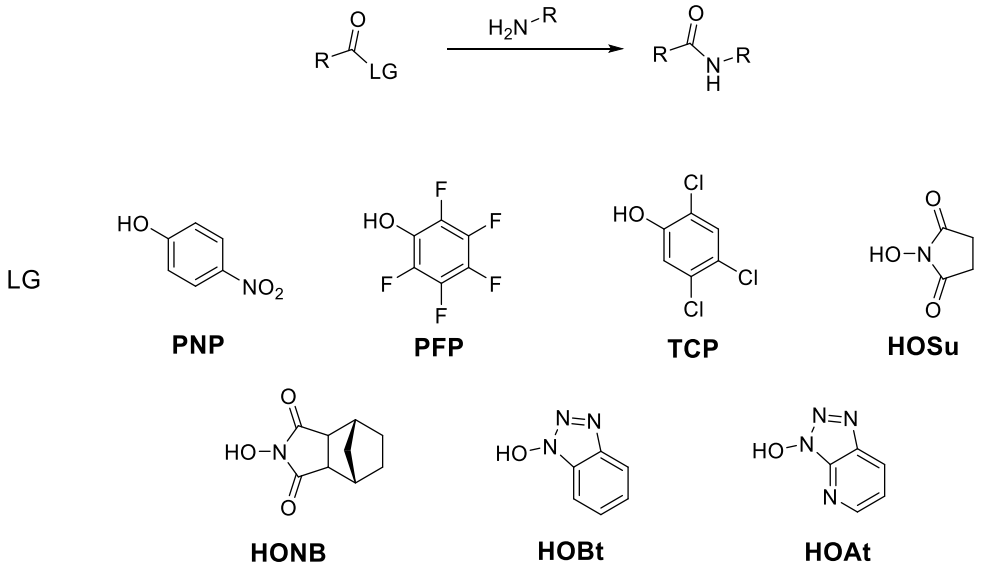

Scheme V-4. Examples of some of the most common leaving groups in active esters.[54,55]

V.2. OBJECTIVES

In view of the advantages of active esters to conduct amidation reactions in combination with the capacity of DTEs to enable two-color photocontrol of reactivity, the following objectives were proposed in this chapter:

- To synthesize model photoresponsive active esters based on dithienylethene switches to reach *dual-wavelength control over amide formation*.
- To demonstrate the applicability of this strategy for *the introduction of functional molecular units via photocontrolled amide ligation*.

In order to pursue these goals, the following design principles were applied:

(a) The use of *electron-poor phenolates as the leaving group of the active esters*. According to literature,[54,55] these must be low-basicity phenolates – i.e., the conjugate base of high-acidity phenols.

(b) To *control the electronic character of the phenolate LG by means of the photoisomerization of a conjugated DTE unit*. In this way, it could be transformed from an electron-rich to an electron-poor phenolate – i.e., from a bad to a good LG – by interconversion between the ring-open and ring-closed states of the photoswitch with UV and visible radiation, respectively. As a result, the reactivity with amines to generate the corresponding amides could be photomodulated with two different colors of light.

(c) To apply the strategy used in Chapter IV to light-control the acidity of phenols in order to reach photomodulation of the electronic character of the phenolate leaving group – i.e., *to prepare DTE-phenolate ester conjugates where the electronic communication of the phenolate group with a strong EWG is controlled upon photoisomerization*. According to the results obtained in Chapter IV, the largest photoinduced electronic effect should be expected when the EWG is a nitro or a trifluoromethylketone group. Because of the concerns raised by the stability of the $COCF_3$ group in front of nucleophile addition, our system of choice was phenolate esters conjugated to a photoisomerizable nitrodithienylethene derivative (**DTE-NO_2-Ac**, Scheme V-5). For such type of compounds, no electronic communication must take place between the nitro and phenolate groups in the open isomer, which should make the latter a bad LG for the amidation reaction. By contrast, both groups become conjugated in the closed state, thus converting the phenolate moiety into a good LG and accelerating the amidation reaction.

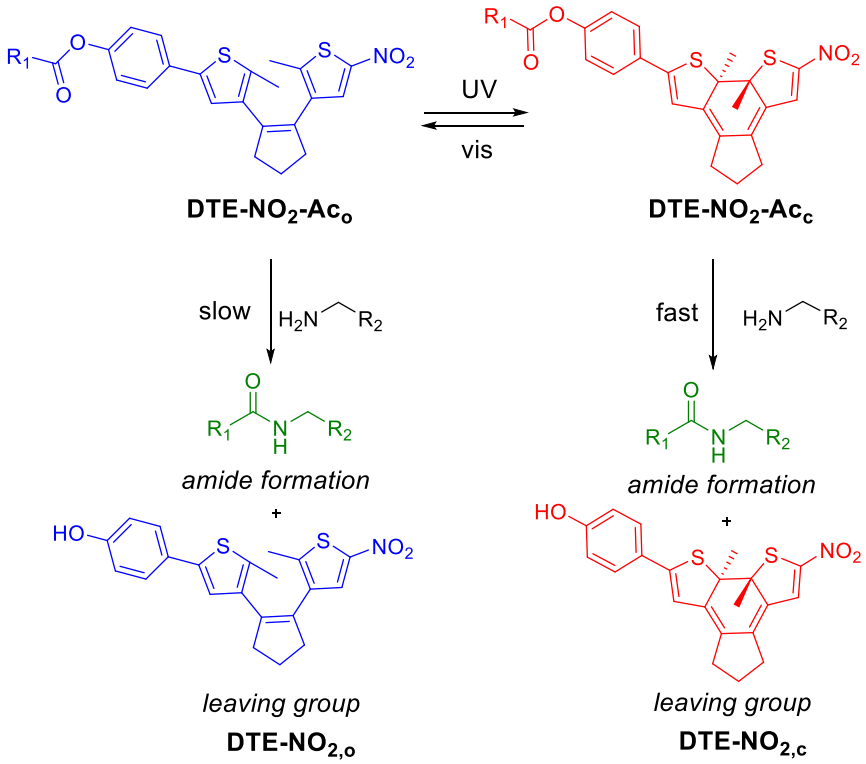

Scheme V-5. DTE-NO₂-Ac active ester system for the two-color control of amide bond formation.

V.3. TWO-COLOR CONTROLLED AMIDATION WITH A MODEL DTE-PHENOLATE ESTER CONJUGATE

To test the viability of our strategy toward dual-wavelength control of amidation processes, we first focused our attention on a model phenolate ester conjugated to a nitrodithienylethene derivative. For this purpose, phenol acetate **DTE-NO₂-Ac** was synthesized, characterized and tested in reactions with amines (Scheme V-6).

V.3.1. SYNTHESIS OF DTE-NO₂-AC

DTE-NO₂-Ac was synthesized in an 89% yield by direct reaction of the previously prepared **DTE-NO₂** (see Section IV.3) and acetyl chloride in the presence of triethyl amine in THF (Scheme V-6). The acetylation of **DTE-NO₂** was confirmed by the characteristic signals in ^{1}H NMR at 2.31 ppm and ^{13}C NMR at 169.6 ppm corresponding to the acetyl protons and the carbonylic carbon atom, respectively.

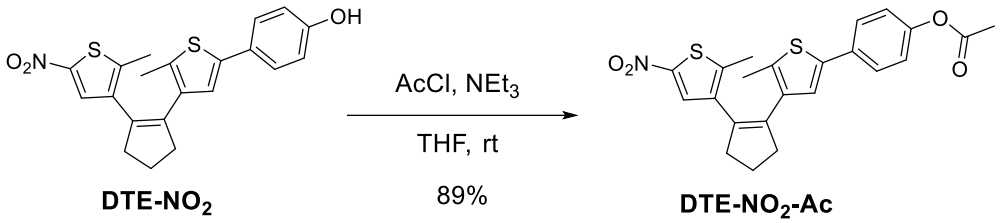

DTE-NO$_2$ **DTE-NO$_2$-Ac**

Scheme V-6. Synthesis of **DTE-NO$_2$-Ac** from **DTE-NO$_2$**.

V.3.2. OPTICAL CHARACTERIZATION DTE-NO$_2$-AC

As already discussed in Chapter IV, solvent polarity is very important in determining the optical properties of DTEs, especially when both electron-rich and electron-poor aryl groups are present in these compounds. Indeed, it was demonstrated in section IV.6 that the ring-closing efficiency of **DTE-EWG** was significantly lower in polar solvents due to ICT. Therefore, a similar effect is expected for **DTE-NO$_2$-Ac**. However, solvent polarity also plays a role in nucleophile substitution reactions like amide bond formation, which are typically favored in polar solvents. Therefore, a compromise must be reached to select the proper solvent that ensures both an adequate photochemical behavior of **DTE-NO$_2$-Ac** and a high amide formation kinetics for its closed isomer. For this reason, the optical properties of **DTE-NO$_2$-Ac** were studied in 4 different solvents of increasing polarity: toluene, THF, acetonitrile and DMSO.

In all the solvents, the open state of the system (**DTE-NO$_2$-Ac$_o$**) showed a similar absorption spectrum with a maximum around 300 nm (Figure V-6, Table V-1). Upon irradiation at 355 nm, an absorption band in the visible region appeared that is characteristic of the closed isomer, whose spectral maximum bathochromically shifted upon increasing solvent polarity (Figure V-6, Table V-1).

Upon prolonged irradiation with UV light, a PSS$_{o\text{-}c}$ was reached whose content in the closed isomer **DTE-NO$_2$-Ac$_c$** decreased with the polarity of the solvent (Figure V-6, Table V-1). Thus, irradiation at 355 nm resulted in an almost complete photoisomerization to **DTE-NO$_2$-Ac$_c$** in toluene and THF, whereas 82% and 72% conversions were obtained for acetonitrile and DMSO, respectively. It must be noted that this is a rather similar behavior to that found for **DTE-NO$_2$** (83% conversion in acetonitrile, see Table IV-1), which indicates a minor effect of phenol acetylation on the optical properties of the photoswitch. Finally, exposure to visible light at 650 nm resulted in the complete recovery of **DTE-NO$_2$-Ac$_o$** in all the solvents (Figure V-6, Table V-1).

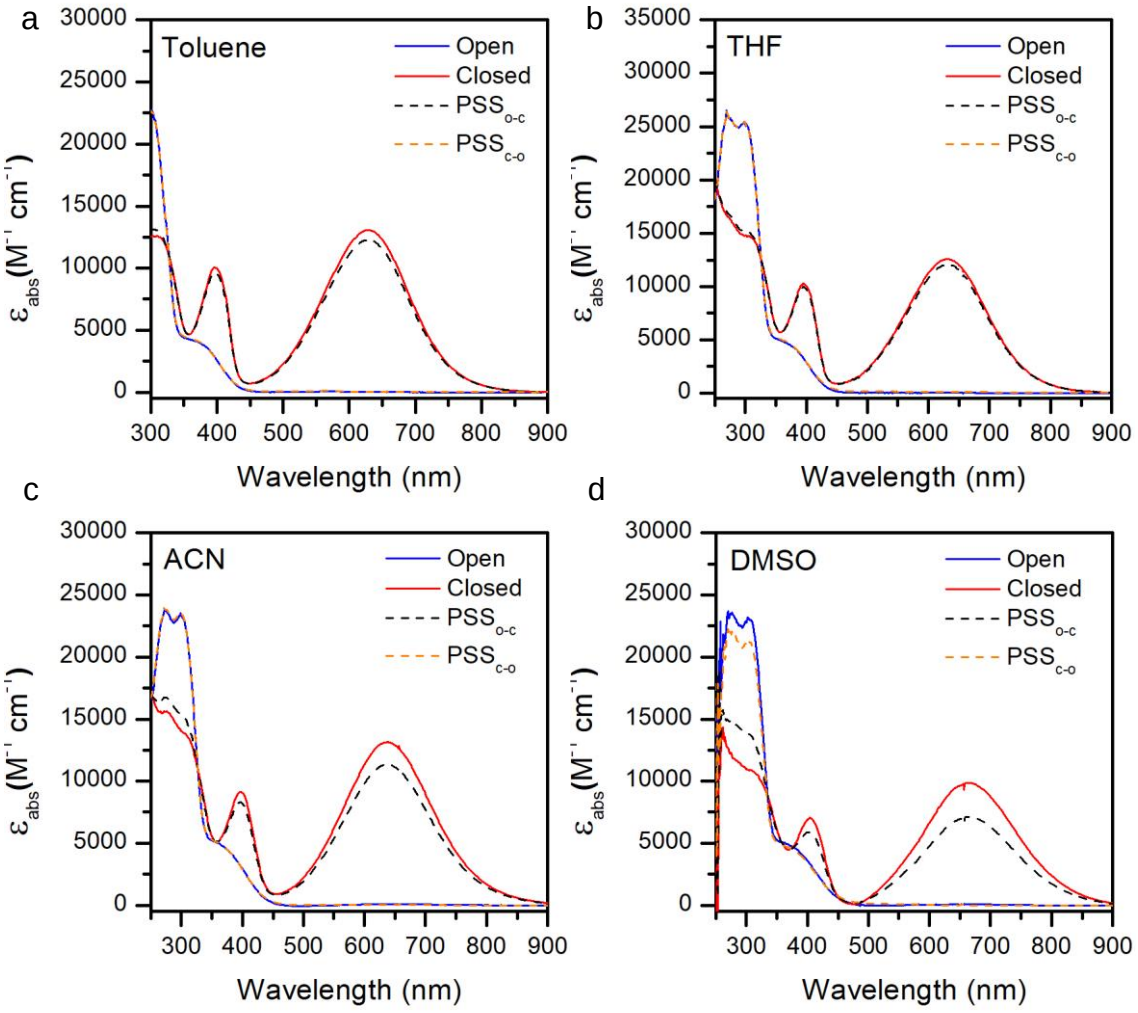

Figure V-5. DTE-NO_2-Ac extinction coefficients in (a) toluene, (b) THF, (c) acetonitrile and (d) DMSO for the open isomer **DTE-NO_2-Ac_o** (blue), the closed isomer **DTE-NO_2-Ac_c** (closed), the PSS reached under photoexcitation at 355 nm (dashed black), and the PSS obtained upon subsequent irradiation at 650 nm (dashed orange).

Photoisomerization quantum yields were determined in each solvent in order to rationalize the results obtained for the ring-closing reaction conversions. Two different tendencies were observed (Table V-1). On the one hand, a uniform behavior was found for $\Phi_{c\text{-}o}$ in all the solvents , obtaining very low values within the 0.005 - 0.009 range that are even smaller than that determined for **DTE-NO_2** in acetonitrile ($\Phi_{c\text{-}o}$ = 0.018, see Table IV-1). On the other hand, a huge solvent variation in $\Phi_{c\text{-}o}$ was measured, with a more than 10-fold decrease from toluene to acetonitrile and DMSO. Therefore, the significantly larger $\Phi_{o\text{-}c}/\Phi_{c\text{-}o}$ ratio values registered in toluene ($\Phi_{o\text{-}c}/\Phi_{c\text{-}o}$ = 45) and THF ($\Phi_{o\text{-}c}/\Phi_{c\text{-}o}$ = 20) relative to acetonitrile ($\Phi_{o\text{-}c}/\Phi_{c\text{-}o}$ = 4.4) and DMSO ($\Phi_{o\text{-}c}/\Phi_{c\text{-}o}$ = 5.0) should account for the higher ring-closing efficiencies found in the less polar solvents. Importantly, this was proven to have a clear effect on the

fatigue resistance of the system. Thus, when performing 5 photoisomerization cycles of **DTE-NO_2-Ac** by sequential irradiation at 355 and 650 nm, clear photodegradation was only observed in DMSO and, in a lesser extent, in acetonitrile (Figure V-6). Most probably, this comes as a result of the lower efficiency of the ring-closing reaction in polar solvents, which implies that longer UV irradiation times are required to reach the $PSS_{o\text{-}c}$ – i.e., the photosensitive **DTE-NO_2-Ac_c** state is subjected to longer exposure times to harmful UV light.

Table V-1 Optical properties of **DTE-NO_2-Ac**.

Solvent	$\lambda_{abs,max,o}$ (ε)[a]	$\lambda_{abs,max,c}$ (ε)[a]	$PSS_{o\text{-}c}$[b]	$PSS_{c\text{-}o}$[c]	$\Phi_{o\text{-}c}$[d]	$\Phi_{c\text{-}o}$[e]
Toluene	297 (23.5)	628 (13.1)	0.94	1.00	0.35 ± 0.03	0.0077 ± 0.0001
THF	298 (25.4)	632 (12.6)	0.96	1.00	0.18 ± 0.01	0.0089 ± 0.0002
ACN	299 (23.5)	638 (13.2)	0.82	1.00	0.025 ± 0.004	0.0057 ± 0.0007
DMSO	303 (23.2)	657 (9.3)	0.72	1.00	0.027 ± 0.002	0.0054 ± 0.0002

[a] Maximum absorption in nm. The extinction coefficients in 10^3 M^{-1} cm^{-1} are indicated in parenthesis. [b] Molar fraction of the closed isomer after prolonged irradiation at 355 nm. The values were determined by combined ^{1}H NMR and UV-vis absorption measurements. [c] Molar fraction of the open isomer after irradiation at 650 nm. [d] Ring-closing quantum yields upon irradiation at 355 nm. [e] Ring-opening quantum yields upon irradiation at 650 nm. The error for Φ is calculated as the standard deviation of 3 replicates.

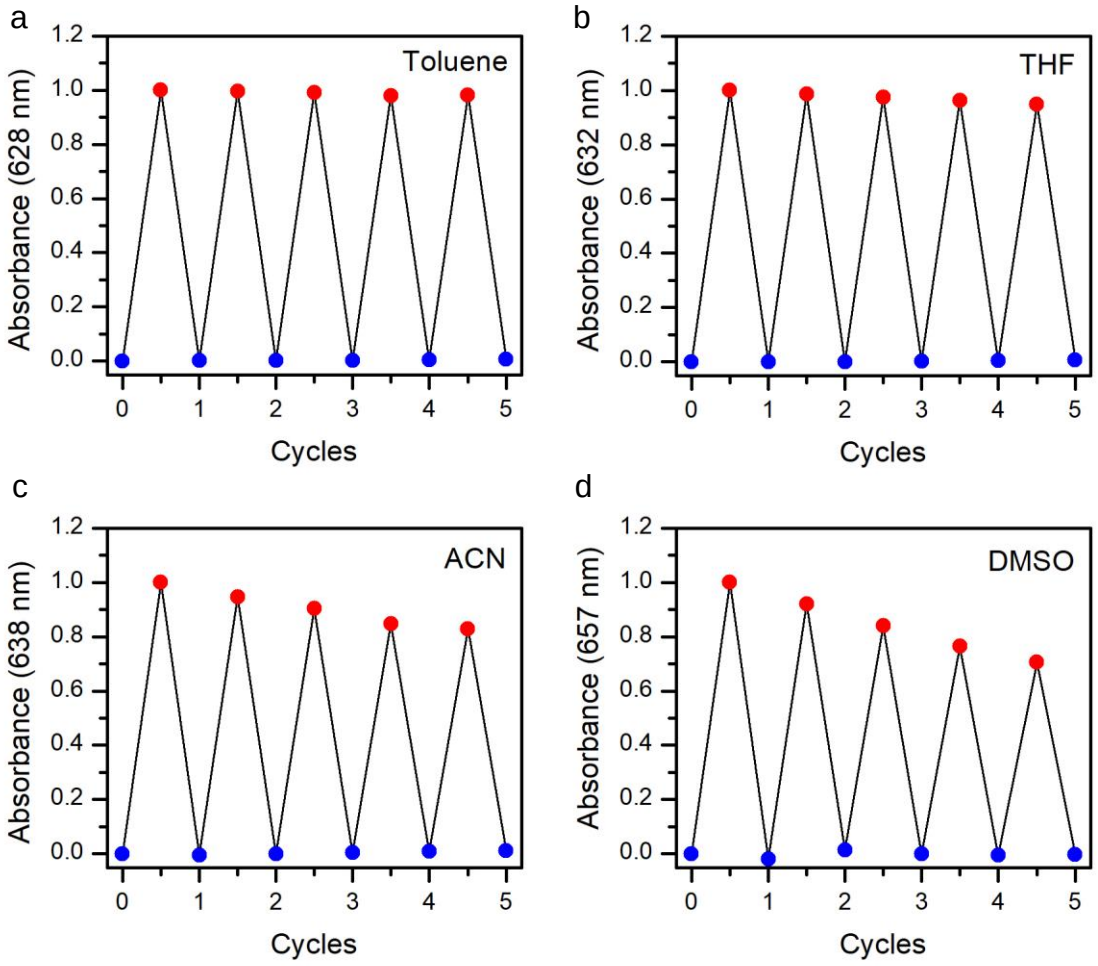

Figure V-6. Variation of the absorption maximum of the closed isomer of **DTE-NO_2-Ac** when it was subjected to 5 cycles of consecutive irradiation at 355 nm and 650 nm in (a) toluene, (b) THF, (c) acetonitrile and (d) DMSO.

V.3.3. DUAL-WAVELENGTH CONTROL OF AMIDATION WITH DTE-NO_2-AC

To study light-controlled amide formation with **DTE-NO_2-Ac**, we first monitored by ^{1}H NMR the kinetics of the reaction of both isomers of this compound with model alkylamine **34** to form amide **35** at room temperature and ambient conditions (Scheme V-7). Because of the poor photostability found for **DTE-NO_2-Ac** in DMSO, the kinetic measurements were only carried out in toluene, THF and acetronitrile. An excess of amine **34** (20 equivalents) was used in these experiments to warrant that the formation of **35** followed a pseudo-first order kinetics (Table V-2, Figure V-7a-c). For sake of comparison, the same studies were conducted for a common active ester, the commercially available **NO_2-Ph-Ac** bearing a 4-nitrophenolate LG (Scheme V-7). However, it must be noted that, because of the higher reaction rate, amide formation had to be followed by UV-vis absorption spectroscopy for **NO_2-Ph-**

Ac in acetonitrile and THF (Table V-2, Figure V-7d), while ^{1}H NMR could be used for toluene.

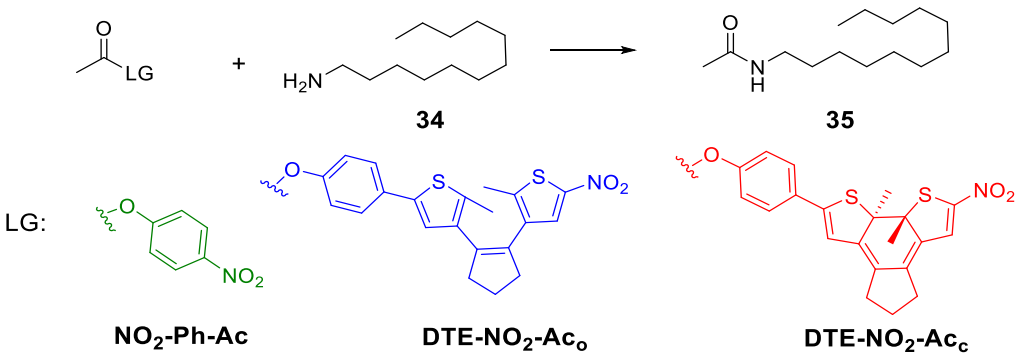

Scheme V-7. Amide formation reaction of **DTE-NO_2-Ac** and reference **NO_2-Ph-Ac** with **34.**

As shown in Table V-2 and Figure V-7, the amidation reaction was observed to be significantly faster for **NO_2-Ph-Ac** than for any of the isomers of **DTE-NO_2-Ac** regardless of the solvent used. Two main factors could account for this result. First, stronger conjugation between the nitro and phenolate groups should be expected for **NO_2-Ph-Ac** than for **DTE-NO_2-Ac$_c$** because of the shorter separation distance. As a consequence, this should favor the amine addition (Figure V-7e) by increasing the electrophilicity of the carbonyl group. Second, lower steric hindrance must be found around the carbonylic group in **NO_2-Ph-Ac**, which should further facilitate the addition step of the process .

In spite of this, the amidation reaction of **34** with the closed isomer **DTE-NO_2-Ac$_c$** was also found to be fairly rapid in THF and acetonitrile, where the starting ester was consumed in about 3 h at room temperature (Table V-2 and Figure V-7). More interestingly, a clear decrease in reactivity was observed for the open state **DTE-NO_2-Ac$_o$**, as expected according to our molecular design (Table V-2 and Figure V-7). Therefore, this result confirms that switching the communication between the phenolate LG and the nitro EWG modulates the rate constant of amide bond formation. However, the amplitude of this modulation was found to vary depending on the solvent and an increase was seen in polar media. Thus, the rate constant ratio between the closed and open isomers ($k_{DTE\text{-}NO2\text{-}Acc}/k_{DTE\text{-}NO2\text{-}Aco}$) raised from 2.3 in toluene to 24 in acetonitrile (Table V-2). A possible explanation for such variation is that the rate determining step of the amidation process might change with solvent due to the different stabilization of the reaction intermediates (Figure V-7e). On the one hand, the first addition step that forms a highly polar intermediate should be especially disfavored in apolar solvents and thus, have a greater influence in the reaction rate. Because this step should be little affected by the electronic nature of the leaving group, small reactivity modulation should be expected in these media. Actually, this would also explain why the rate constants for **DTE-NO_2-Ac** and

reference active ester **NO_2-Ph-Ac** become the most similar in toluene: $k_{NO2\text{-}Ph\text{-}Ac}/k_{DTE\text{-}NO2\text{-}Acc}$ = 9.7 and 100 in toluene and acetonitrile, respectively. On the other hand, as the polar intermediate formed after amine addition becomes more stabilized in polar solvents, the effect of the elimination step on the reaction rate should be more relevant, thus leading to a larger variation in amidation kinetics for the two isomers of **DTE-NO_2-Ac**.

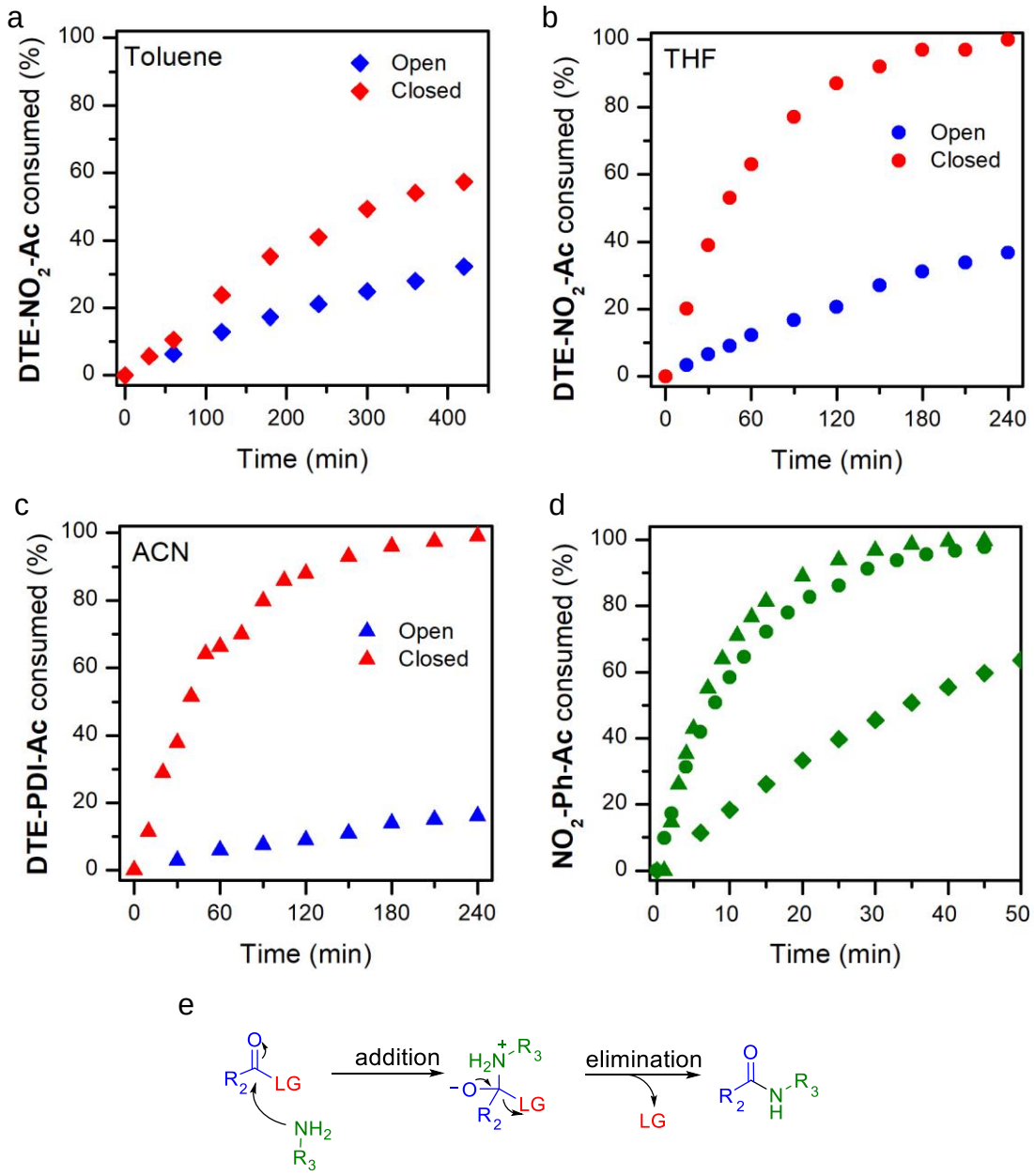

Figure V-7. (a-c) Consumption rate of **DTE-NO_2-Ac$_o$** (blue) and **DTE-NO_2-Ac$_c$** (red) for the amidation reaction with amine **34** ($c_{DTE\text{-}NO2\text{-}Ac}$ = 5 mM, c_{34} = 100 mM) in (a) toluene, (b) THF and (c) acetonitrile. Data obtained by integration of the ^{1}H NMR signals of **DTE-NO_2-Ac** and amide **35**. (d) Consumption rate of **NO_2-Ph-Ac** for the amidation reaction with amine **34** in toluene (diamonds), THF (circles) and acetonitrile (triangles). For toluene, data was obtained by integration of the ^{1}H NMR signals of **NO_2-Ph-Ac** and amide **35** ($c_{NO2\text{-}Ph\text{-}Ac}$ = 5 mM, c_{34} =

100 mM). For THF and acetonitrile, the reaction was monitored by UV-vis absorption measurements ($c_{\mathbf{NO2\text{-}Ph\text{-}Ac}}$ = 0.02 mM, $c_{\mathbf{34}}$ = 6.2 mM). (e) Amide formation mechanism.

Table V-2. Rate constants of the amide formation reaction of **DTE-NO$_2$-Ac** and **NO$_2$-Ph-Ac** with amine **34**.

Solvent	$k_{DTE\text{-}NO2\text{-}Aco}$ (M^{-1} s^{-1})[a]	$k_{DTE\text{-}NO2\text{-}Acc}$ (M^{-1} s^{-1})[b]	$\frac{k_{DTE\text{-}NO2\text{-}Acc}}{k_{DTE\text{-}NO2\text{-}Aco}}$	$k_{NO2\text{-}Ph\text{-}Ac}$ (M^{-1} s^{-1})	$\frac{k_{DTE\text{-}NO2\text{-}Acc}}{k_{NO2\text{-}Ph\text{-}Ac}}$
Toluene	1.6×10^{-4}	3.7×10^{-4}	2.3	3.5×10^{-3} [a]	9.7
THF	3.3×10^{-4}	2.8×10^{-3}	8.4	0.20[b]	73
ACN	1.2×10^{-4}	2.9×10^{-3}	24	0.29[b]	100

[a] *k* values determined by ^{1}H NMR with a 20-fold excess of amine **34**. [b] *k* values determined by UV-vis absorption spectroscopy with a 300-fold excess of amine **34**.

Based on the satisfactory reactivity modulation and closed isomer rate constant found for amide bond formation with **DTE-NO$_2$-Ac** in acetonitrile, we next aimed to demonstrate *in situ* photocontrol of this process with two colors of light. To do so the amidation reaction of **DTE-NO$_2$-Ac** with model amine **34** in acetonitrile and room temperature was followed by ^{1}H NMR while applying a sequence of different illumination conditions (Figure V-8): (a) no irradiation, where very low reactivity was observed for nonactive ester **DTE-NO$_2$-Ac$_o$**; (b) UV illumination (LED λ_{max} = 365 nm, 0.017 mW cm^{-2}), which led to photoconversion to active **DTE-NO$_2$-Ac$_c$** and, consequently, fast amidation reaction; (c) red light irradiation (LED λ_{max} = 625 nm; 1300 mW cm^{-2}), which returned **DTE-NO$_2$-Ac** back to the poorly reactive open isomer; and (d) combined UV (LED λ_{max} = 365 nm, 0.017 mW cm^{-2}) and red irradiation (LED λ_{max} = 625 nm; 1300 mW cm^{-2}), which also displaced the photostationary equilibrium toward **DTE-NO$_2$-Ac$_o$** and, therefore, dramatically slowed down amide bond formation. Importantly, when the red illumination source was switched off while preserving UV irradiation, **DTE-NO$_2$-Ac$_c$** was again formed and the amidation reaction was reactivated. Hence, these results demonstrate that our model DTE-phenolate ester conjugate allows two-color control of amidation, which prompted us to apply this ligation strategy for the preparation of functional molecules.

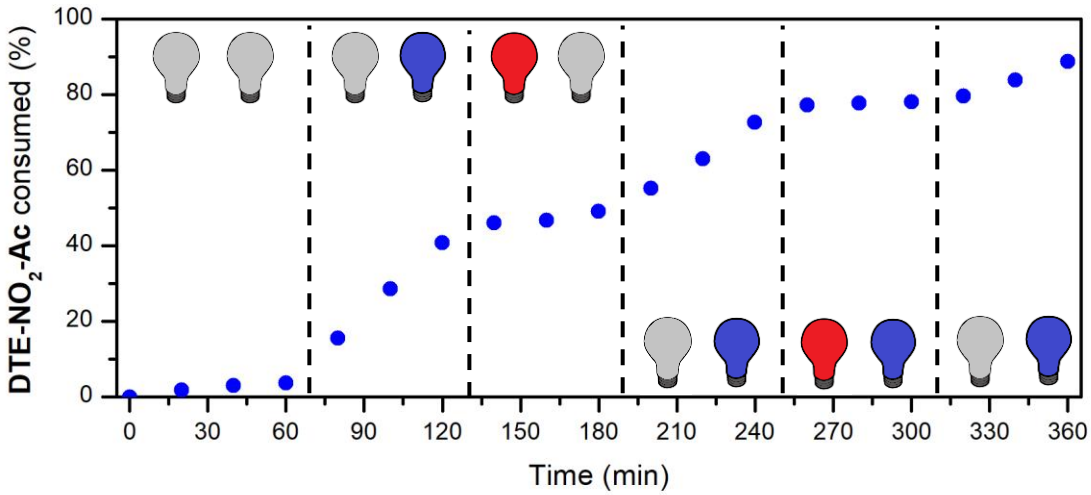

Figure V-8. Time evolution of the amidation reaction between **DTE-NO$_2$-Ac** and **34** in acetonitrile and room temperature at different irradiation conditions ($c_{\text{DTE-NO2-Ac}}$ = 5 mM, c_{34} = 100 mM): 60 min in the dark; 60 min with UV light (LED λ_{max} = 365 nm, 0.017 mW cm^{-2}); 60 min with red light (LED λ_{max} = 625 nm; 1300 mW cm^{-2}); 60 min with UV light; 60 min with both UV and red light; and 60 min with UV light.

V.4. TWO-COLOR CONTROLLED AMIDATION WITH A FUNCTIONAL DTE-PHENOLATE ESTER CONJUGATE

V.4.1. Synthesis of DTE-PDI

To prove the potential of our methodology to photomodulate amide bond formation, we envisioned the preparation of a photoisomerizable DTE-based active ester bearing a fluorescent moiety that could be transferred to any amino-terminated system of interest under dual-wavelength control. For this purpose a perylendiimide (PDI) fluorophore was selected because of its excellent photophysical and photochemical properties.[60] The target dyad **DTE-PDI** would be obtained through the direct coupling of **DTE-NO$_2$**, whose synthesis was described in Chapter IV, with PDI fluorophore **38** (Scheme V-8). Compound **38** would be synthesized from intermediate **37** upon partial saponification and subsequent introduction of a carboxylic acid-terminated alkyl chain introduced by condensation. Compound **37** would be previously prepared from commercially available perylene-3,4,9,10-tetracarboxylic dianhydride (**36**) through consecutive chlorination, imide formation and nucleophilic aromatic substitution reactions previously carried out in our group.[61]

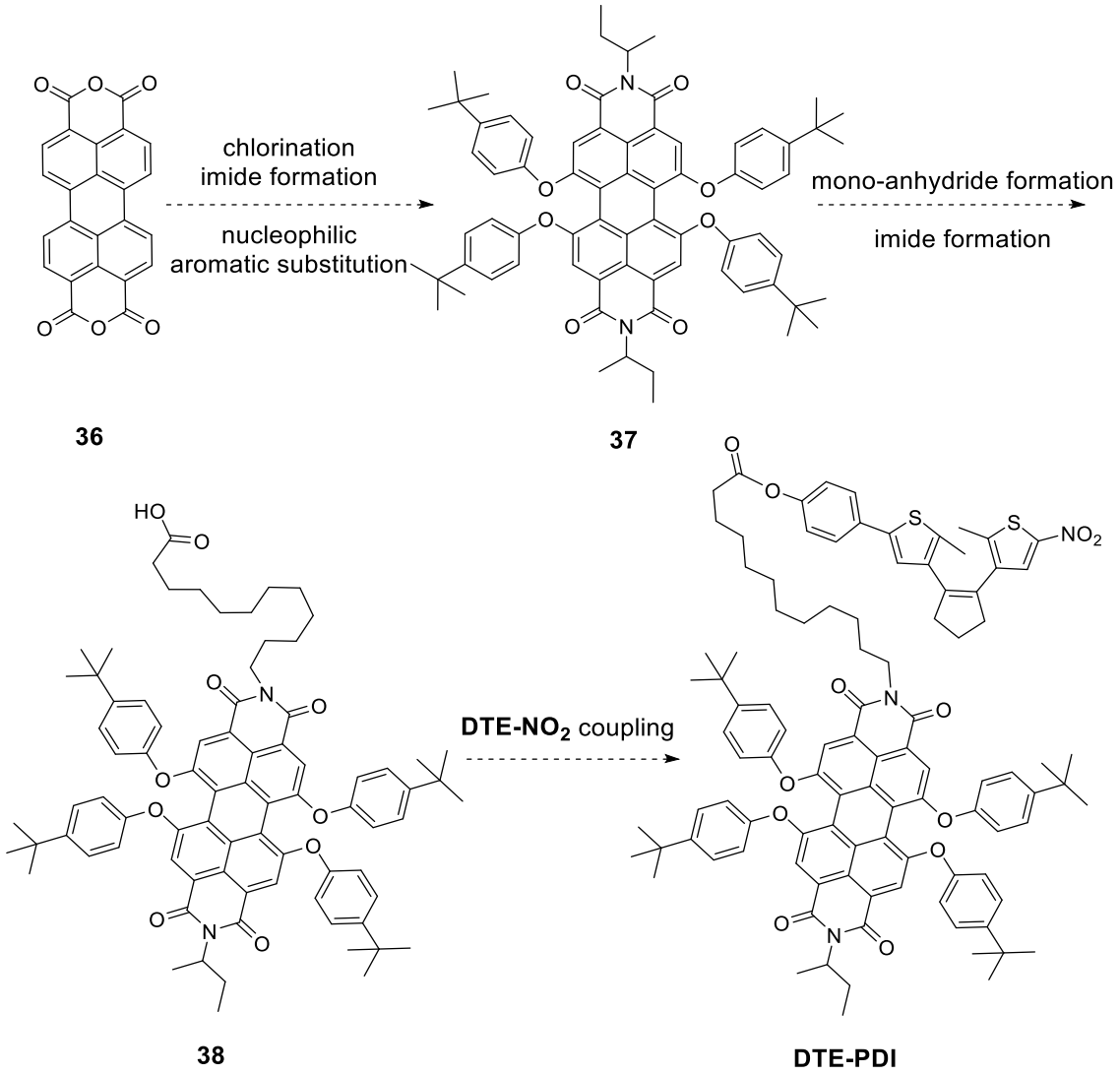

Scheme V-8. Synthetic strategy for the preparation of **DTE-PDI**.

Together with **DTE-PDI**, a 4-nitrophenolate ester bearing the fluorescent PDI dye (**NO_2-Ph-PDI**) would also be synthesized through the direct coupling of **38** and 4-nitrophenol (**39**) (Scheme V-9). This compound had to be used as a reference active ester for the light-controlled reactivity experiments to be performed with **DTE-PDI**.

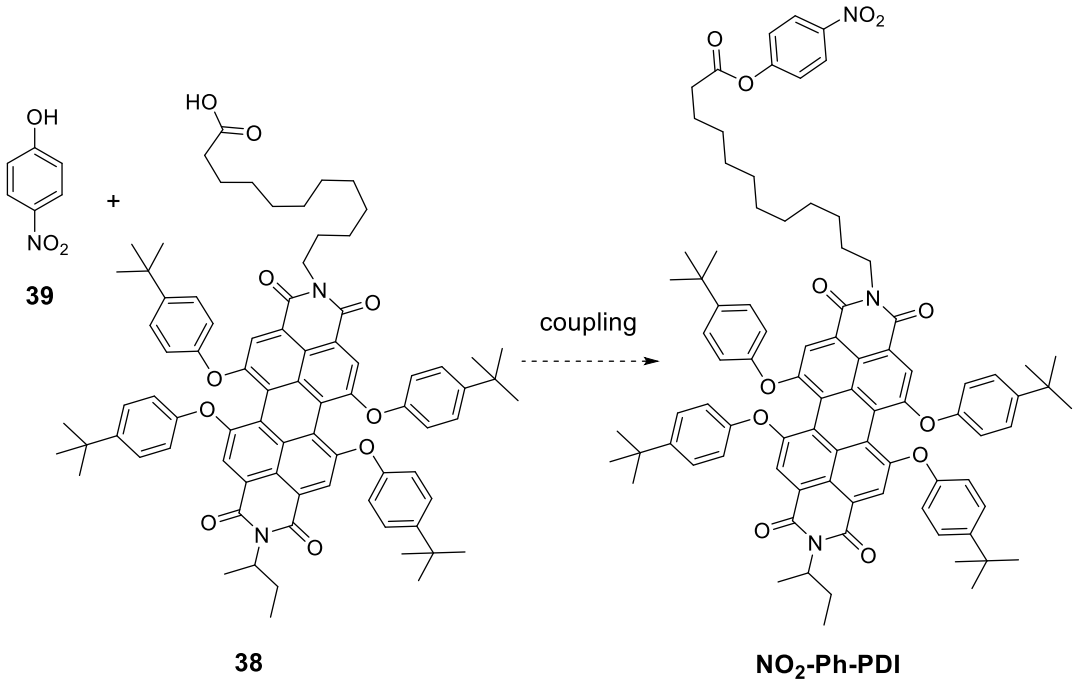

Scheme V-9. Synthetic strategy for the preparation of **NO_2-Ph-PDI.**

V.4.1.a. **Synthesis of fluorophore 38**

For the preparation of fluorophore **38** we used the well-known strategies developed for the functionalization of the *N*-imide and bay positions of PDIs,[60] which have already been applied in our group.[61] Starting from the parent dianhydride **36**, we first conducted the quadruple chlorination of its bay positions using chlorosulphonic acid and in the presence of iodine at 70ºC.[61] Importantly, the reaction time was optimized to 15 hours to ensure the major formation of **40** instead of the penta- and trichlorinated byproducts. Overall, **40** was obtained in 95% yield after drying the solid formed in the reaction mixture in a vacuum oven at 130 ºC for 2 hours as an irresoluble mixture tetra- and penta-chlorinated products in a 4:1 ratio (Scheme V-10).

Symmetric diimide **41** was then prepared in 75% yield from dianhydride **40** through condensation with *sec*-butylamine (Scheme V-10).[61] Molten imidazole was used as a solvent because of the low solubility of the starting material in most media. To facilitate the precipitation of the desired product, we slightly varied the previously reported procedure:[61] the reaction mixture was first dissolved in the minimum amount of ethanol before adding a 2 M HCl solution in water until no more solid was formed. The precipitate was isolated via filtration and dried in a vacuum oven for 3 hours at 130ºC.

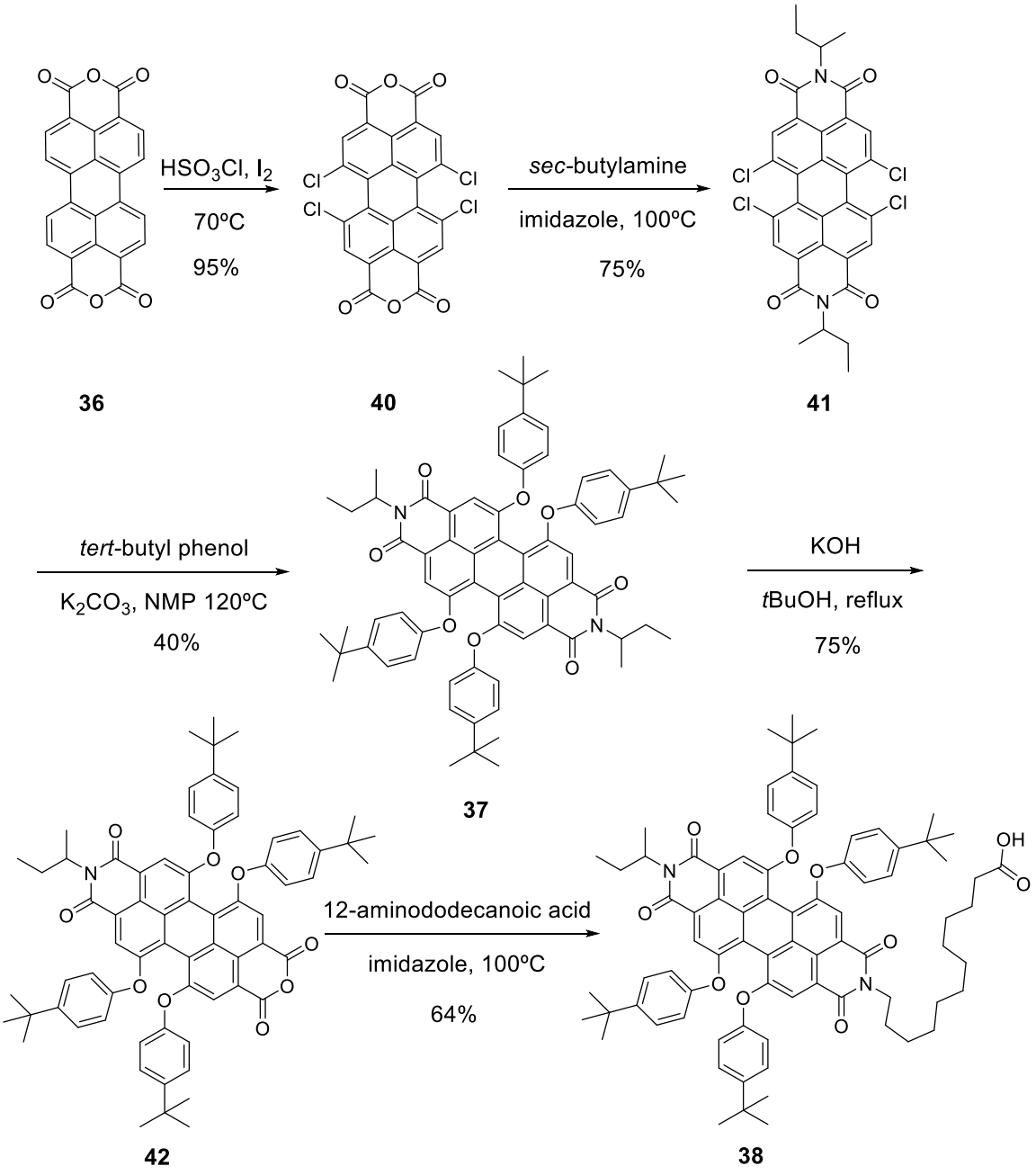

Scheme V-10. Synthesis of PDI fluorophre **38.**

Next, compound **37** was formed after nucleophilic aromatic substitution of tetrachlorinated **41** with *tert*-butylphenol in the presence of a base and using high boiling point *N*-methyl-2-pyrrolidone (NMP) as a solvent (Scheme V-10).[61] Some variations had to be introduced to the reported procedure to better remove the excess of *tert*-butylphenol and NMP. In this way, diimide **37** was obtained in 40% yield. Partial saponification of this compound was subsequently conducted to obtain monoimide **42** as described in the literature.[61] To carefully control the reaction time was crucial to ensure that the desired monohydrolized compound was the major

product formed, which allowed us obtaining **42** in 75% yield after purification by flash column chromatography (Scheme V-10).

Finally, target PDI derivative **38** was prepared in 64% yield through condensation of monoanhydride **42** and 12-aminododecanoic acid (Scheme V-10). For simplicity, the same conditions applied for the condensation of dianhydride 40 and *sec*-butylamine were followed. Overall, compound **38** was prepared in five steps with 14% yield for commercially available dianhydride **36**. Its successful formation was confirmed by several spectroscopic features, such as the characteristic ^{1}H NMR signals at 4.09 ppm and 2.32 ppm corresponding to the α-imide and α-carboxylic acid protons of the alkyl chain introduced.

V.4.1.b. Synthesis of DTE-PDI and NO2-Ph-PDI

The formation of the active ester **DTE-PDI** was finally achieved through a Steglich esterification[62] between phenol **DTE-NO$_2$** and carboxylic acid **38**, where DCC is used as a coupling agent and 4-(dimethylamino)pyridine (DMAP) as an additive. The desired product was isolated in 74% yield after purification by flash column chromatography (Scheme V-11). The incorporation of **DTE-NO$_2$** to **38** was confirmed by the appearance of the characteristic DTE ^{1}H NMR signals as well as the resonance at 2.53 ppm arising from the α-ester protons.

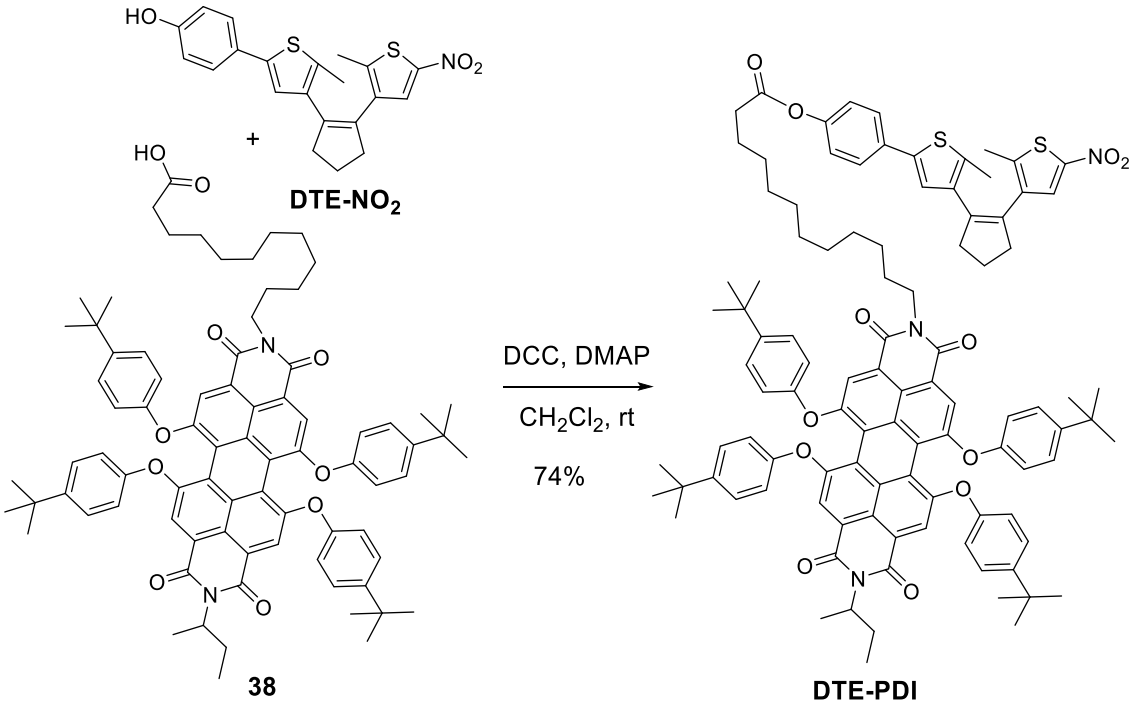

Scheme V-11. Synthesis of functional photoisomerizable active ester **DTE-PDI**.

Reference active ester **NO$_2$-Ph-PDI** was synthesized following the same procedure as **DTE-PDI** from PDI **38** and 4-nitrophenol (**39**) in 60% yield (Scheme V-12).[62] The formation of **NO$_2$-Ph-PDI** was confirmed by the characteristic ^{1}H NMR triplet at 2.57

ppm corresponding to the α-ester protons and the two doublets at 8.26 and 7.26 ppm arising from the 4-nitrophenol moiety introduced.

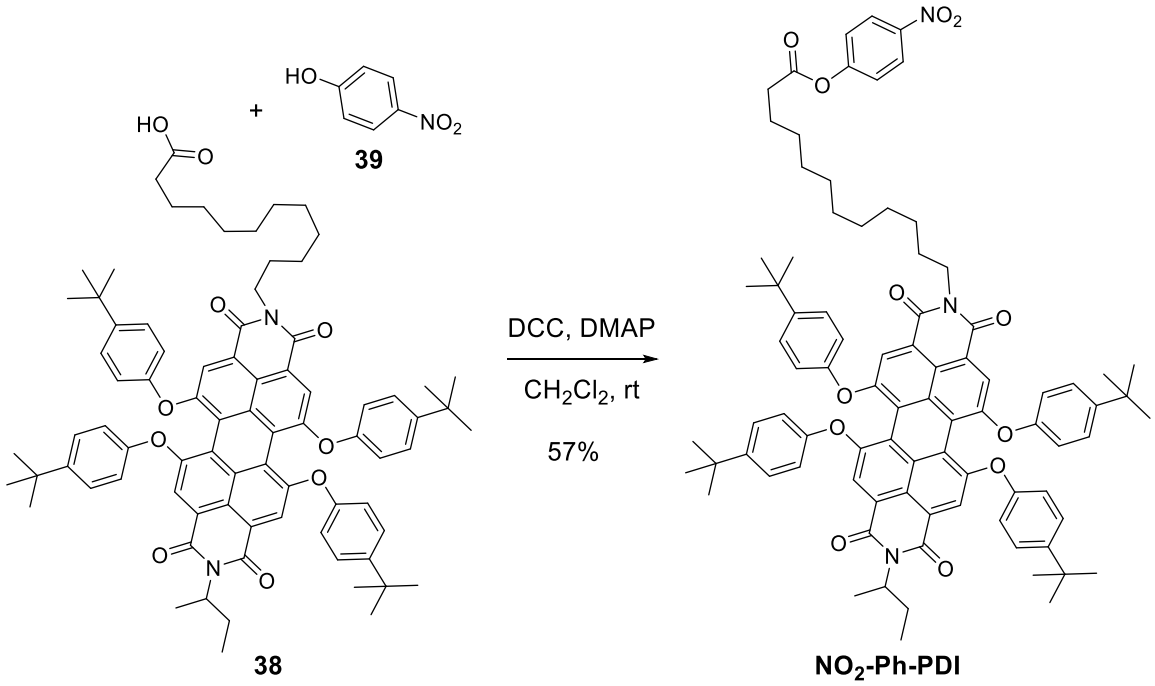

Scheme V-12. Synthesis of reference active ester **NO_2-Ph-PDI**.

V.4.2. Optical characterization of DTE-PDI

After its preparation, the photochemical characterization of **DTE-PDI** was carried out. Initially, acetonitrile was intended to be used as a solvent due to the higher reactivity modulation obtained with **DTE-NO_2-Ac** in this medium when attempting the two-color control of amidation. Unfortunately, both **DTE-PDI** isomers were found to be poorly soluble in acetonitrile. For this reason, THF was employed as a solvent, which also yielded significant reactivity photomodulation for **DTE-NO_2-Ac** with better photoisomerization behavior.

The UV-vis absorption spectrum of the open isomer **DTE-PDI$_o$** presented several signals that can be assigned to its two different photoactive building blocks: (a) two bands with maxima at 445 and 570 nm that can be attributed to the PDI moiety by comparison to fluorophore **37**; and (b) a peak at 284 nm corresponding to the ring-open DTE unit, as similarly observed for **DTE-NO_2-Ac$_o$** (Figure V-9a, Table V-3). Upon irradiation at 355 nm new absorption bands appeared in the visible region that are similar to those of **DTE-NO_2-Ac$_c$** (λ_{max} ~ 400 and 600 nm), thus proving the cyclization of the DTE moiety to produce the closed isomer **DTE-PDI$_c$** (Figure V-9a). The $PSS_{o\text{-}c}$ reached was determined by ^{1}H NMR to be formed by an 89% of **DTE-PDI$_c$** (Figure V-9a, Table V-3), which is slightly lower than the value found for **DTE-**

NO$_2$-Ac (96%). As for the cycloreversion reaction, it was performed under illumination at 650 nm and quantitative conversion back to **DTE-PDI$_o$** was achieved.

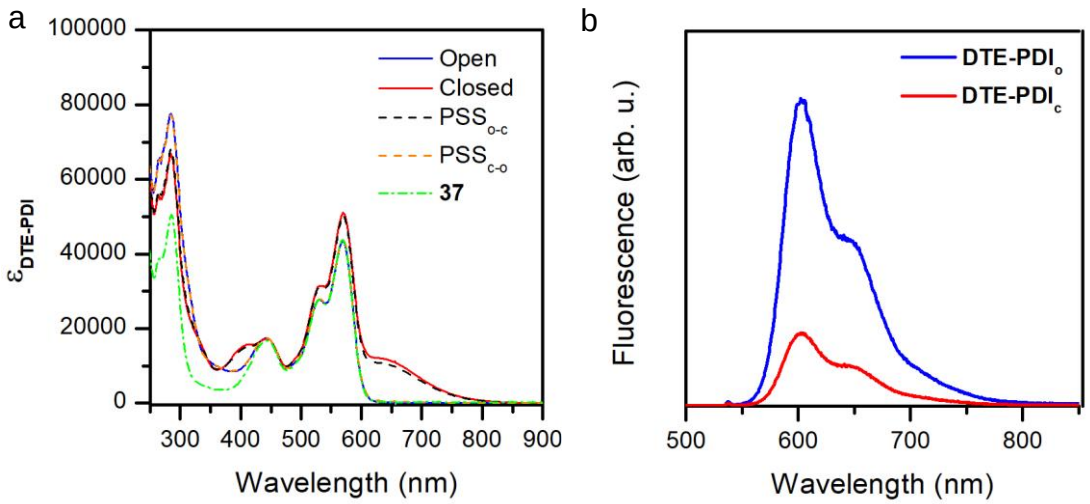

Figure V-9. (a) Extinction coefficients in THF of **DTE-PDI$_o$** (blue), **DTE-PDI$_c$** (red) and the PSSs obtained at 355 nm (dashed black) and 650 nm (dashed orange). For sake of comparison, the absorption spectrum of PDI fluorophore **37** in THF is also shown. (b) Fluorescence spectra of each isomer of **DTE-PDI$_o$** and **DTE-PDI$_c$** in THF.

Table V-3. Optical properties of **DTE-PDI** in THF.

Isomer	$\lambda_{abs,max}$[a]	$\varepsilon_{abs,max}$[b]	PSS$_{o-c}$[c]	PSS$_{c-o}$[c]	Φ_i	Φ_f[f]
DTE-PDI$_o$	284, 570	77.5, 43.6	0.11	1.00	0.041 ± 0.004[d]	0.80 ± 0.02
DTE-PDI$_c$	570, 632[g]	51.2, 12.0[g]	0.89	0.00	0.013 ± 0.002[e]	0.19 ± 0.01

[a] Absorption maxima in nm of the PDI and DTE units in the compound. [b] Extinction coefficients at the absorption maxima in 10^3 M^{-1} cm^{-1}. [c] Molar fraction of each isomer under continuous irradiation at 355 nm and 650 nm measured by ^{1}H NMR. [d] Ring-closing quantum yield measured upon irradiation at 355 nm. [e] Ring-opening quantum yield measured under 650 nm irradiation. [f] Fluorescence quantum yield (λ_{exc} = 532 nm). [g] DTE-PDIc 632 nm was a shoulder due to the overlap with the PDI S_0-S_1 band. The error for Φ is calculated as the standard deviation of 3 replicates.

Photoisomerization quantum yields were also measured for **DTE-PDI** in THF (Table V-3). While a similar Φ_{c-o} value to **DTE-NO$_2$-Ac$_c$** was measured for **DTE-PDI**, about a 4-fold decay in Φ_{o-c} was observed. However, it must be noted that most of this effect was due to the large contribution of the PDI unit to the absorption at the photoexcitation wavelength: $\varepsilon_{355\ nm}$ = 3700 and 5000 M^{-1} cm^{-1} for **DTE-PDI** and **DTE-**

NO_2-Ac_c in THF, respectively. This means that the intrinsic DTE absorption was overestimated when calculating $\Phi_{o\text{-}c}$, thus leading to an excessively low ring-closing quantum yield for **DTE-PDI**. As a consequence, such decrement in $\Phi_{o\text{-}c}$ had a minor effect on the efficiency of the cyclization reaction and, therefore, on the composition of the corresponding $PSS_{o\text{-}c}$. Hence, we concluded that the introduction of the PDI fluorophore in **DTE-PDI** did not significantly affected the photoswitching properties of the nearby DTE phenolate ester.

The fluorescence behavior of **DTE-PDI** was also evaluated for the two isomers of the system. The open state **DTE-PDI_o** preserved the bright red luminescence from its PDI unit (Figure V-9b, Table V-3), though a slight decrease in fluorescence quantum yield was observed (Φ_f = 0.80 and 1.00[61] for **DTE-PDI** in THF and reference fluorophore **37** in ACN). By contrast, a dramatic loss of emission was observed upon photocyclization and the Φ_f value determined for the $PSS_{o\text{-}c}$ lowered to 0.26 (Figure V-9b, Table V-3). In fact, if the contribution of the residual open isomer molecules to the fluorescence signal of the photostationary mixture was subtracted, a much smaller Φ_f value of 0.19 could be estimated for the ring-closed state **DTE-PDI_c**. Such quenching of the fluorescence emission can be explained by intramolecular resonance energy transfer from the PDI unit to the DTE_c group of the compound, which is caused by the overlap of the emission and absorption spectra of these components. Actually, a similar effect has been reported for other PDI-DTE dyads.[61]

V.4.3. Two-color control of amide bond formation with DTE-PDI

Once the optical properties of **DTE-PDI** were stablished, we investigated the kinetics of the reaction of **DTE-PDI_o** and **DTE-PDI_c** with model amine **34** in THF and room temperature. In a similar manner to **DTE-NO_2-Ac**, the amidation process was followed by ^{1}H NMR and we used nonphotoisomerizable **NO_2-Ph-PDI** as a reference active ester (Figure V-10).

Table V-4 summarizes the rate constant values obtained from our kinetic experiments, from which several conclusions can be inferred. First, a 10-fold decrease in reactivity was observed for reference active ester **NO_2-Ph-PDI** relative to PDI-free **NO_2-Ph-Ac** (see Table V-4). This feature could be attributed to the higher steric hindrance imparted by the perylenediimide group introduced in **NO_2-Ph-PDI**, which must hinder the initial amine addition step of the process. Therefore, steric effects seem to play a relevant effect on the kinetics of the amidation reaction, as already suggested on the basis of the rate constant differences previously observed between **DTE-NO_2-Ac** and **NO_2-Ph-Ac** (see Table V-4). Actually, this should also account for the larger *k* value determined for **NO_2-Ph-PDI** relative to both isomers of **DTE-PDI**, as the presence of the additional DTE unit must further increase the steric congestion around the carbonyl electrophile. More importantly, large reactivity

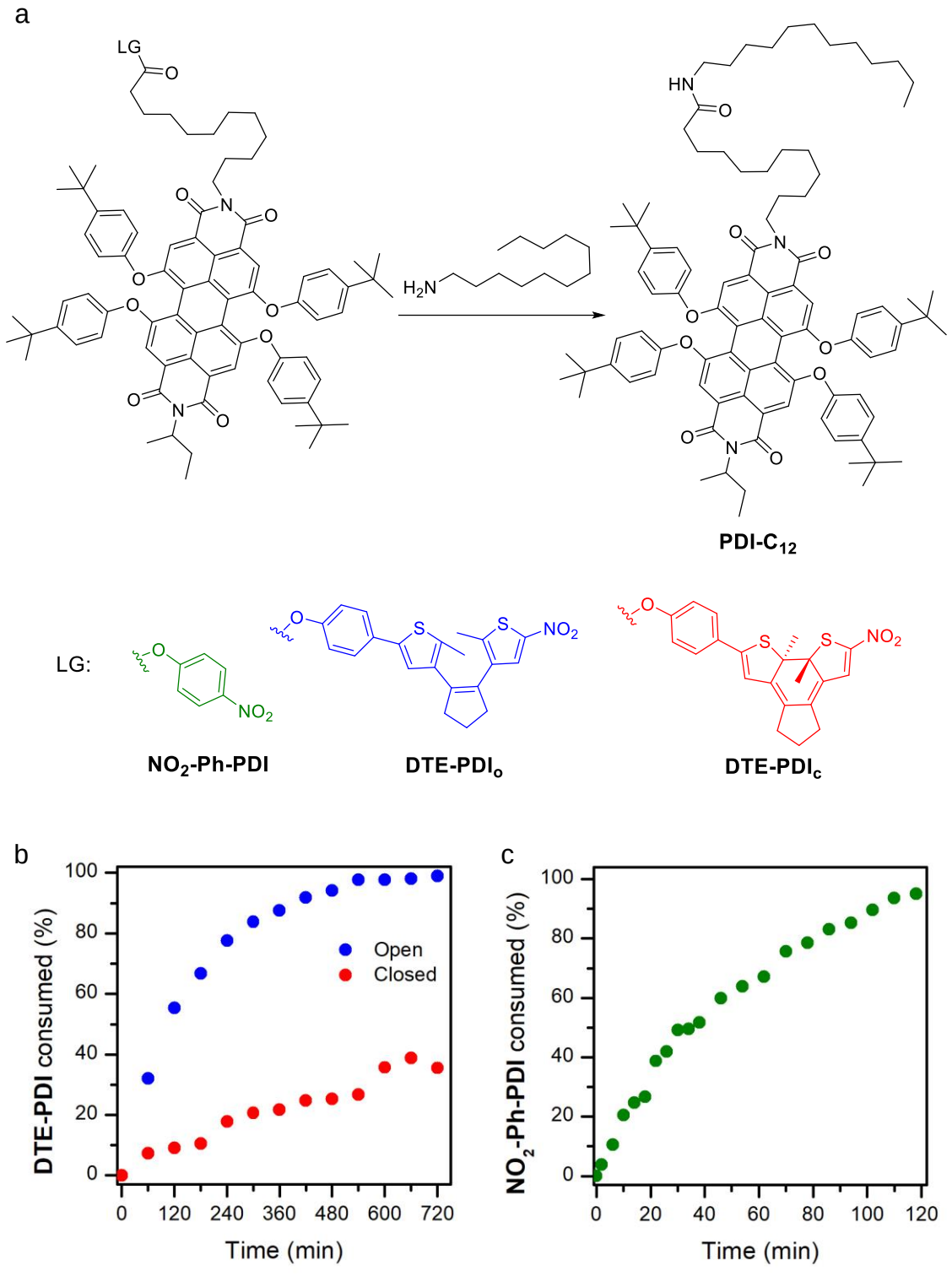

Figure V-10. (a) Amidation reaction between model amine **34** and PDI-containing phenolate esters **DTE-PDI$_o$**, **DTE-PDI$_c$** and **NO$_2$-Ph-PDI**. (b) Evolution of the amidation reaction of **34** with **DTE-PDI$_o$** and **DTE-PDI$_c$** ($c_{DTE\text{-}PDI}$ = 5 mM, c_{34} = 100 mM) in THF and room temperature. Data obtained by integration of the ^{1}H NMR signals of **DTE-PDI** and amide **PDI-C$_{12}$**. (c) Evolution of the amidation reaction between **34** and **NO$_2$-Ph-PDI** ($c_{NO2\text{-}Ph\text{-}PDI}$ = 0.7 mM, c_{34} =

17 mM) in THF and room temperature. Data obtained by integration of the ^{1}H NMR signals of **NO_2-Ph-PDI** and amide **PDI-C_{12}**.

modulation was determined for the two isomers of **DTE-PDI**: a 14-fold increase in the amidation rate was observed upon ring closing, which is even larger than the value found for **DTE-NO_2-Ac** (see Table V-4). Therefore, the introduction of a functional unit such as the PDI fluorophore to the photoisomerizable DTE-based active ester did not detrimentally affect its capacity to promote light-controlled amide bond formation. Consequently, this would open the door to apply the dual-wavelength photoligation strategy developed in this chapter to the functionalization of amine-terminated compounds and materials with high spatiotemporal resolution.

Table V-4. Rate constants of the amide formation reaction of **34** with **DTE-PDI** and **NO_2-Ph-PDI** in THF.

Isomer	k (M^{-1} s^{-1})[a]	$k/k_{DTE\text{-}PDIo}$	$k/k_{DTE\text{-}PDIc}$
DTE-PDI_o	7.4 x10^{-5} [b]	1	0.07
DTE-PDI_c	1.0 x10^{-3} [b]	14	1
NO2-Ph-PDI	2.0x10^{-2} ± 3x10^{-4}[c]	264	19

[a] *k* values determined at room temperature. [b] Values obtained by ^{1}H NMR ($c_{DTE\text{-}PDI}$ = 5 mM, c_{34} = 100 mM). [c] Values obtained by ^{1}H NMR ($c_{NO2\text{-}Ph\text{-}PDI}$ = 0.7 mM, c_{34} = 17 mM,).

V.5. SUMMARY AND CONCLUSIONS

In this chapter we reported the development of a novel strategy for the two-color control of amidation reactions using DTE-based photoisomerizable phenolate esters. The main results and conclusions obtained are summarized as follows:

- Model photoisomerizable phenolate ester **DTE-NO_2-Ac** was successfully synthesized from the previously prepared nitrodithienylethene derivative **DTE-NO_2** (see Chapter IV). **DTE-NO_2-Ac** preserves the characteristic photoswitching behavior of dithienylethenes, though its cyclization efficiency decreases in polar media due to competitive intramolecular charge transfer that negatively affects its fatigue resistance.

- The introduction of a DTE unit in phenolate ester **DTE-NO_2-Ac** decreases the rate of the amidation process with a model primary amine relative to a similar DTE-free active ester. Steric effects must primarily account for this effect. In spite of this, the amide bond formation reaction proceeds at a fairly rapid rate with the closed isomer **DTE-NO_2-Ac_c**, especially in polar media.

- Variation of the rate constant of the amidation reaction was found between the open and closed isomers of **DTE-NO_2-Ac**. Because electronic communication between the phenolate and nitro DTE substituents is selectively established upon ring-closing, the closed isomer **DTE-NO_2-Ac_c** presents a better leaving group and, as a result, undergoes faster amide bond formation. However, reactivity modulation is solvent dependent and the largest amplitude was found in acetonitrile, where a 24-fold increase in reaction rate was observed upon cyclization. This can be ascribed to the fact that the quality of the leaving group particularly affects the elimination step of the amidation process, which becomes more determinant for the reaction rate in polar solvents.

- Successful two-color control of the amidation reaction can be accomplished with **DTE-NO_2-Ac** in acetonitrile: it is selectively activated with UV irradiation and deactivated under simultaneous red light illumination. This therefore validates our molecular design to accomplish dual-wavelength photoregulation of amide bond formation with DTE switches.

- Our two-color controlled photoligation methodology can be expanded to other DTE-based photoisomerizable phenolate esters bearing functional units, such as the perylenediimide fluorophore in **DTE-PDI**. **DTE-PDI** shows a large modulation in amidation reactivity upon photoisomerization, which could be exploited for the light-controlled functionalization of amine-terminated substances.

V.6. REFERENCES

1 K. Hiltebrandt, K. Elies, D. R. D'Hooge, J. P. Blinco and C. Barner-Kowollik, *J. Am. Chem. Soc.*, 2016, **138**, 7048–7054.

2 N. Zydziak, W. Konrad, F. Feist, S. Afonin, S. Weidner and C. Barner-Kowollik, *Nat. Commun.*, 2016, **7**, 1–10.

3 L. Delafresnaye, K. Jung, C. Boyer and C. Barner-Kowollik, *Polym. Chem.*, 2020, **11**, 6453–6462.

4 M. M. Zieger, P. Mueller, A. S. Quick, M. Wegener and C. Barner-Kowollik, *Angew. Chem. Int. Ed.*, 2017, **56**, 5625–5629.

5 M. Regehly, Y. Garmshausen, M. Reuter, N. F. König, E. Israel, D. P. Kelly, C. Y. Chou, K. Koch, B. Asfari and S. Hecht, *Nature*, 2020, **588**, 620–624.

6 T. K. Claus, B. Richter, V. Hahn, A. Welle, S. Kayser, M. Wegener, M. Bastmeyer, G. Delaittre and C. Barner-Kowollik, *Angew. Chem. Int. Ed.*, 2016, **55**, 3817–3822.

7 B. Koo, H. Yoo, H. J. Choi, M. Kim, C. Kim and K. T. Kim, *Molecules*, 2021, **26**, 556.

8 A. Losi, K. H. Gardner and A. Möglich, *Chem. Rev.*, 2018, **118**, 10659–10709.

9 W. Wang, A. Kapur, X. Ji, M. Safi, G. Palui, V. Palomo, P. E. Dawson and H. Mattoussi, *J. Am. Chem. Soc.*, 2015, **137**, 5438–5451.

10 D. Mendez-Gonzalez, P. P. Silva-Ibáñez, F. Valiente-Dies, O. G. Calderón, J. L. Mendez-Gonzalez, M. Laurenti, A. Egatz-Gómez, E. Díaz, J. Rubio-Retama and S. Melle, *J. Colloid Interface Sci.*, 2021, **596**, 64–74.

11 G. S. Kumar and Q. Lin, *Chem. Rev.*, 2021, **121**, 6991–7031.

12 H. Frisch, D. E. Marschner, A. S. Goldmann and C. Barner-Kowollik, *Angew. Chem. Int. Ed.*, 2018, **57**, 2036–2045.

13 S. Aubert, M. Bezagu, A. C. Spivey and S. Arseniyadis, *Nat. Rev. Chem.*, 2019, **3**, 706–722.

14 T. Pauloehrl, G. Delaittre, M. Bruns, M. Meißler, H. G. Börner, M. Bastmeyer and C. Barner-Kowollik, *Angew. Chem. Int. Ed.*, 2012, **51**, 9181–9184.

15 J. T. Offenloch, M. Gernhardt, J. P. Blinco, H. Frisch, H. Mutlu and C. Barner-Kowollik, *Chem. Eur. J.*, 2019, **25**, 3700–3709.

16 L. Zhang, X. Zhang, Z. Yao, S. Jiang, J. Deng, B. Li and Z. Yu, *J. Am. Chem. Soc.*, 2018, **140**, 7390–7394.

17 O. Altintas, M. Glassner, C. Rodriguez-Emmenegger, A. Welle, V. Trouillet and C. Barner-Kowollik, *Angew. Chem. Int. Ed.*, 2015, **54**, 5777–5783.

18 J. O. Mueller, F. G. Schmidt, J. P. Blinco and C. Barner-Kowollik, *Angew. Chem. Int. Ed.*, 2015, **54**, 10284–10288.

19 T. K. Claus, S. Telitel, A. Welle, M. Bastmeyer, A. P. Vogt, G. Delaittre and C. Barner-Kowollik, *Chem. Commun.*, 2017, **53**, 1599–1602.

20 V. X. Truong, F. Li, F. Ercole and J. S. Forsythe, *ACS Macro Lett.*, 2018, **7**, 464–469.

21 J. Fischer and M. Wegener, *Laser Photonics Rev.*, 2013, **7**, 22–44.

22 P. Mueller, M. M. Zieger, B. Richter, A. S. Quick, J. Fischer, J. B. Mueller, L. Zhou, G. U. Nienhaus, M. Bastmeyer, C. Barner-Kowollik and M. Wegener, *ACS Nano*, 2017, **11**, 6396–6403.

23 J. Alves, T. Krappitz, F. Feist, J. P. Blinco and C. Barner-Kowollik, *Chem. Eur. J.*, 2020, **26**, 16985–16989.

24 N. Corrigan, M. Ciftci, K. Jung and C. Boyer, *Angew. Chem. Int. Ed.*, 2021, **60**, 1748–1781.

25 J. Alves, S. Wiedbrauk, D. Gräfe, S. L. Walden, J. P. Blinco and C. Barner-Kowollik, *Chem. Eur. J.*, 2020, **26**, 809–813.

26 Z. Liu, T. Liu, Q. Lin, C. Bao and L. Zhu, *Angew. Chem. Int. Ed.*, 2015, **54**, 174–178.

27 S. W. Hell, *Science*, 2007, **316**, 1153–1158.

28 H. Vijayamohanan, E. F. Palermo and C. K. Ullal, *Chem. Mater.*, 2017, **29**, 4754–4760.

29 R. Göstl and S. Hecht, *Angew. Chem. Int. Ed.*, 2014, **53**, 8784–8787.

30 V. Lemieux, S. Gauthier and N. R. Branda, *Angew. Chem. Int. Ed.*, 2006, **45**, 6820–6824.

31 A. Fuhrmann, R. Göstl, R. Wendt, J. Kötteritzsch, M. D. Hager, U. S. Schubert, K. Brademann-Jock, A. F. Thünemann, U. Nöchel, M. Behl and S. Hecht, *Nat. Commun.*, 2016, **7**, 13626.

32 M. Kathan, F. Eisenreich, C. Jurissek, A. Dallmann, J. Gurke and S. Hecht, *Nat. Chem.*, 2018, **10**, 1031–1036.

33 M. Kathan, P. Kovaříček, C. Jurissek, A. Senf, A. Dallmann, A. F. Thünemann and S. Hecht, *Angew. Chem. Int. Ed.*, 2016, **55**, 13882–13886.

34 H. D. Samachetty, V. Lemieux and N. R. Branda, *Tetrahedron*, 2008, **64**, 8292–8300.

35 R. M. Arnold, D. L. Patton, V. V. Popik and J. Locklin, *Acc. Chem. Res.*, 2014, **47**, 2999–3008.

36 J. J. Gooding and S. Ciampi, *Chem. Soc. Rev.*, 2011, **40**, 2704–2718.

37 A. Das and P. Theato, *Chem. Rev.*, 2016, **116**, 1434–1495.

38 E. Blasco, M. B. Sims, A. S. Goldmann, B. S. Sumerlin and C. Barner-Kowollik, *Macromolecules*, 2017, **50**, 5215–5252.

39 O. Koniev and A. Wagner, *Chem. Soc. Rev.*, 2015, **44**, 5495–5551.

40 J. M. Humphrey and A. R. Chamberlin, *Chem. Rev.*, 1997, **97**, 2243–2266.

41 E. Valeur and M. Bradley, *Chem. Soc. Rev.*, 2009, **38**, 606–631.

42 H. Lundberg, F. Tinnis, N. Selander and H. Adolfsson, *Chem. Soc. Rev.*, 2014, **43**, 2714–2742.

43 V. R. Pattabiraman and J. W. Bode, *Nature*, 2011, **480**, 471–479.

44 J. Conde, J. T. Dias, V. Grazú, M. Moros, P. V. Baptista and J. M. de la Fuente, *Front. Chem.*, 2014, **2**, 1–27.

45 R. M. De Figueiredo, J. S. Suppo and J. M. Campagne, *Chem. Rev.*, 2016, **116**, 12029–12122.

46 J. R. Dunetz, J. Magano and G. A. Weisenburger, *Org. Process Res. Dev.*, 2016, **20**, 140–177.

47 M. T. Sabatini, L. T. Boulton, H. F. Sneddon and T. D. Sheppard, *Nat. Catal.*, 2019, **2**, 10–17.

48 W. Song, K. Dong and M. Li, *Org. Lett.*, 2020, **22**, 371–375.

49 V. Srivastava, P. K. Singh and P. P. Singh, *Tetrahedron Lett.*, 2019, **60**, 40–43.

50 G. Pandey, S. Koley, R. Talukdar and P. K. Sahani, *Org. Lett.*, 2018, **20**, 5861–5865.

51 I. Cohen, A. K. Mishra, G. Parvari, R. Edrei, M. Dantus, Y. Eichen and A. M. Szpilman, *Chem. Commun.*, 2017, **53**, 10128–10131.

52 Z. Z. Gao, Y. Y. Xu, Z. K. Wang, H. Wang, D. W. Zhang and Z. T. Li, *ACS Appl. Polym. Mater.*, 2020, **2**, 4885–4892.

53 G. N. Papadopoulos and C. G. Kokotos, *J. Org. Chem.*, 2016, **81**, 7023–7028.

54 C. A. G. N. Montalbetti and V. Falque, *Tetrahedron*, 2005, **61**, 10827–10852.

55 A. El-Faham and F. Albericio, *Chem. Rev.*, 2011, **111**, 6557–6602.

56 M. Meldal and K. Book, *Tetrahedron Lett.*, 1990, **31**, 6987–6990.

57 R. M. Arnold, C. D. McNitt, V. V. Popik and J. Locklin, *Chem. Commun.*, 2014, **50**, 5307–5309.

58 S. V. Orski, K. H. Fries, G. R. Sheppard and J. Locklin, *Langmuir*, 2010, **26**, 2136–2143.

59 R. M. Arnold, G. R. Sheppard and J. Locklin, *Macromolecules*, 2012, **45**, 5444–5450.

60 F. Würthner, *Chem. Commun.*, 2004, **4**, 1564–1579.

61 R. S. Sánchez, R. Gras-Charles, J. L. Bourdelande, G. Guirado and J. Hernando, *J. Phys. Chem. C*, 2012, **116**, 7164–7172.

62 Y. Monguchi, K. Kunishima, T. Hattori, T. Takahashi, Y. Shishido, Y. Sawama and H. Sajiki, *ACS Catal.*, 2016, **6**, 3994–3997.

Chapter VI

Two-color control of Diels Alder cycloadditions with dithienylethene photoswitches

In this chapter we explore novel strategies to accomplish two-color photocontrol of Diels-Alder cycloadditions using dithienylethene photoswitches.[b]

[b] Some of the results described in this chapter have been published in: “Dual-Wavelength Gated *oxo*-Diels–Alder Photoligation”, M. Villabona, S. Wiedbrauk, F. Feist, G. Guirado, J. Hernando, C. Barner-Kowollik, *Org. Lett.*, 2021, **23**, 2405-2410.

VI.1. INTRODUCTION

In Chapter V the importance of two-color controlled photoligation reactions to achieve higher spatiotemporal resolution for chemical functionalization was discussed. Among all possible photoligation reactions, Chapter V centered on substitution reactions and, especially, in amide bond formation processes. In this chapter attention is instead focused on the dual-wavelength control of Diels-Alder cycloadditions using DTEs.

VI.1.1. Photocontrol of cycloaddition reactions with dithienylethenes and other diarylethenes

Because of the electronic changes caused by their ring-closing isomerization, DAEs are good candidates to light-control cycloaddition reactions. In particular, the π-bond reorganization produced upon photoisomerization modifies the diene-dienophile character of the different molecular fragments of DAEs, which can be utilized to photomodulate Diels-Alder reactions (DA) in two different manners (Scheme VI-1).[1] On the one hand, the heteroaromatic rings in **DAE$_o$** are *dienes* that are removed upon ring closing and become conjugated olefins that may show *dienophile* character. On the other hand, the ethylene bridge between the two heteroaromatic rings in **DAE$_o$** that could behave as a *dienophile* is replaced by a cyclohexa*diene* moiety in **DAE$_c$** (Scheme VI-1).[1] Actually, both the electronic changes in the external and central rings of DAEs have been exploited for the development of distinct strategies to control DA reactions with light.

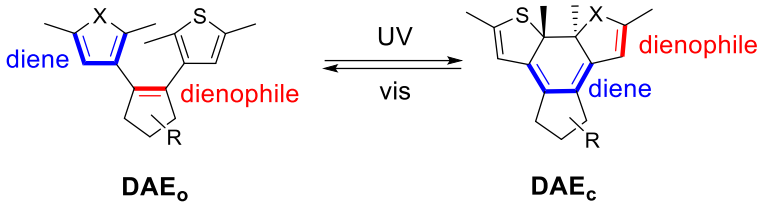

Scheme VI-1. Electronic changes upon DAE isomerization that modify the diene-dienophile character of the different building blocks of the molecular switch.

One of these strategies was first reported by Hecht and coworkers, who capitalized on the diene-to-dienophile switch in the external heteroaromatic rings of DAEs upon ring closing.[2,3] To do so, one of the thiophenes of DTEs was replaced by a furan group, which is a better diene for DA cycloadditions (Scheme VI-2).[2] In this manner, the DA reaction between **DAE-fur** and a maleimide dienophile was only possible in the open state (**DAE-fur$_o$**), as **DAE-fur$_c$** lacks the diene moiety required for the process. Moreover, the resulting adduct **DAE-fur-mal** maintained the photoswitching properties of DAEs and could photoisomerize between open and closed forms. Interestingly, this removed the double bond required for the retro-DA reaction in the closed state **DAE-fur-mal$_c$**, which allowed blocking the cycloaddition product upon UV-induced ring closing. Because of the excellent two-color photocontrolled reactivity of this system, it could be used as a self-healing agent of maleimide-pending polymers.[3] More recently, the same strategy was applied by Otsuka and coworkers to regulate the mechanochemical scission of polymer chains with light.[4]

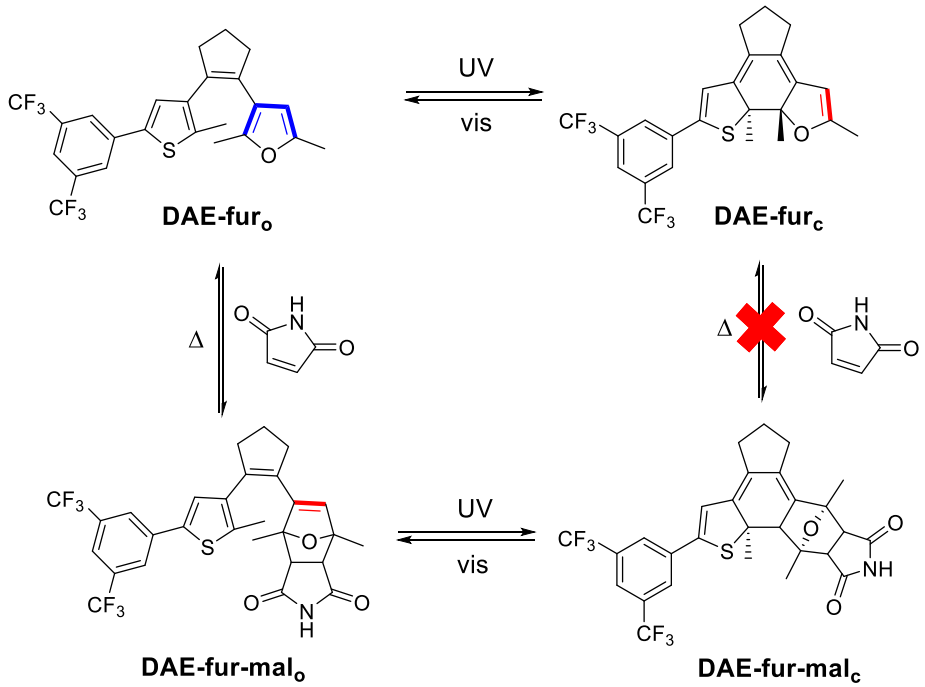

Scheme VI-2. Light-gated Diels-Alder cycloaddition with **DAE-fur**. Because of the removal of the furan diene in **DAE-fur$_c$** (in blue) and of double bond of the adduct in **DAE-fur-mal$_c$**

(in red), neither the cycloaddition nor the cycloreversion reactions are possible in the closed state.[2]

Another strategy to photocontrol DA reactions with DAEs was developed by Branda and coworkers, who profited from the π-bond reorganization in the central ring of the photoswitch that takes place under photoisomerization.[5–7] For this, the authors prepared a DTE analogue (***p*DTE-fur**) where the central cyclopentene ring was replaced by a furan diene (Scheme VI-3).[7] As a result, ***p*DTE-fur** could not photoisomerize, but it transformed into photoswitchable **DTE-fur$_o$** upon DA cycloaddition with maleimide by creating an ethylene bridge between the two thiophene groups. Importantly, UV-induced photoisomerization of **DTE-fur$_o$** to **DTE-fur$_c$** removed the central ring olefin, which therefore prevented the retro-DA process and enabled light control of the DA adduct dissociation (Scheme VI-3).[7] This feature was later applied for the preparation of light-controlled polymer adhesives.[8]

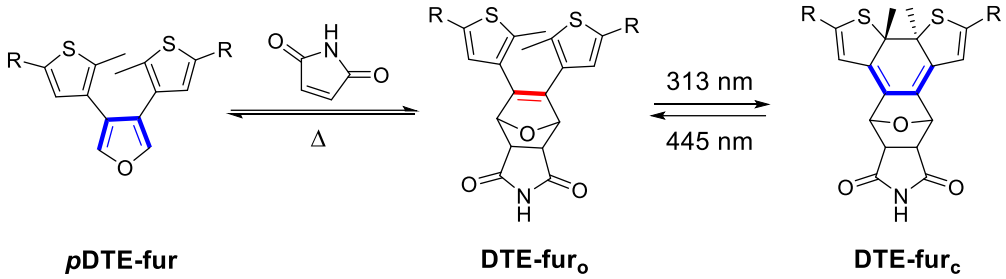

Scheme VI-3. Light-gated retro-DA reaction for **DTE-fur$_o$**, which is formed by cycloaddition between nonphotoisomerizable ***p*DTE-fur** and maleimide.[7]

Despite the different principles exploited, all the examples shown above for the light control of DA (and retro-DA) reactions have in common a very important feature: the DAE switch (or switch precursor) is always used as a diene, which is reacted with a nonphotoactive dienophile. Actually, to our knowledge, no examples had been reported by the beginning of this thesis where DAEs were used as dienophiles for DA reactions. For this reason we explored herein the possibility of (a) employing DTEs as dienophiles in photocontrolled DA cycloadditions, and (b) using them in combination with photogenerated dienes to reach further light control. To do so, we started a collaboration with Prof. Christopher Barner-Kowollik at the Queensland University of Technology (Australia), who is a worldwide expert in the use of photogenerated dienes based on *o*-quinodimethanes (*o*-QDM) for several applications.[9–13] In fact, some of the work described in this chapter was performed during a three-month research stay in his group.

VI.1.2. Photocontrol of cycloadditions based on *o*-quinodimethanes

o-QDMs are well-known dienes for DA reactions which are highly reactive with dienophiles due the rearomatization process that occurs upon cycloaddition.[14] It is because of their high reactivity that *o*-QDMs are unstable and must be generated in situ by different methods; e.g., the thermolysis of benzo-fused cyclobutanes or heterocyclic compounds, 1,4 elimination from *ortho*-disubstituted arenes, or from *o*-xylylene–metal complexes (Scheme VI-4).[14]

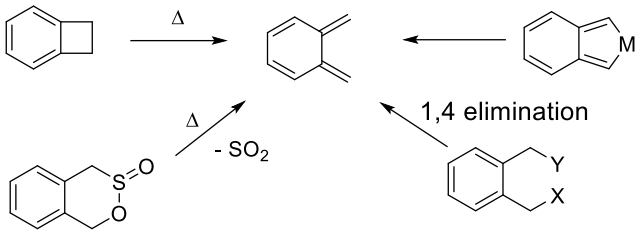

Scheme VI-4. *o*-QDM structure and examples of usual reagents employed for its in situ formation.[14]

An alternative for the preparation of *o*-QDMs are *o*-methylbenzaldehydes (*o*-MBA), which enolize upon irradiation through a 1,5-hydrogen transfer that leads to the formation of *o*-quinodimethanes (Scheme VI-5a). Typically, illumination with UV light is required to induce this process, which leads to two different *o*-QDM isomers: (a) the *Z*-isomer, which rapidly tautomerizes back to the *o*-MBA form; and (b) the *E*-isomer, which is more stable kinetically as it places the OH proton and the methylidine group further away and, therefore, shows slower tautomerization to the initial *o*-MBA through back-hydrogen transfer. This explains why *E*-*o*-QDM is considered to be the only reactive isomer of the system, while *Z*-*o*-QDM just undergoes rearomatization to the starting *o*-MBA tautomer.[15]

After photogeneration, *E*-*o*-QDMs fast react in the presence of dienophiles to form DA adducts[15] or they can slowly dimerize under sufficient light irradiation (Scheme VI-5a).[16] The latter process is complex and involves [4+4] and [2+4] cycloadditions to give rise to at least the three different dimerization products that have been identified (Scheme VI-5a).[16] However, these bimolecular reactions have to compete with back-tautomerization to the *o*-MBA form, which is often the most common evolution pathway for *o*-QDMs and, as a result, lowers the efficiency of the desired processes. For this reason several strategies have been developed to improve the lifetimes of the reactive *E*-*o*-QDMs by diminishing the tautomerization rate to the initial aldehyde tautomer.[12] On the one hand, *o*-MBAs are often functionalized with an ether group at position 2 to stabilize the *E*-*o*-QDM form through hydrogen bonding (Scheme VI-5b).[12] On the other hand, the use of aprotic and nonhydrogen-bonding solvents which do not facilitate the back-hydrogen transfer process to regenerate the starting *o*-MBA is recommended.[17]

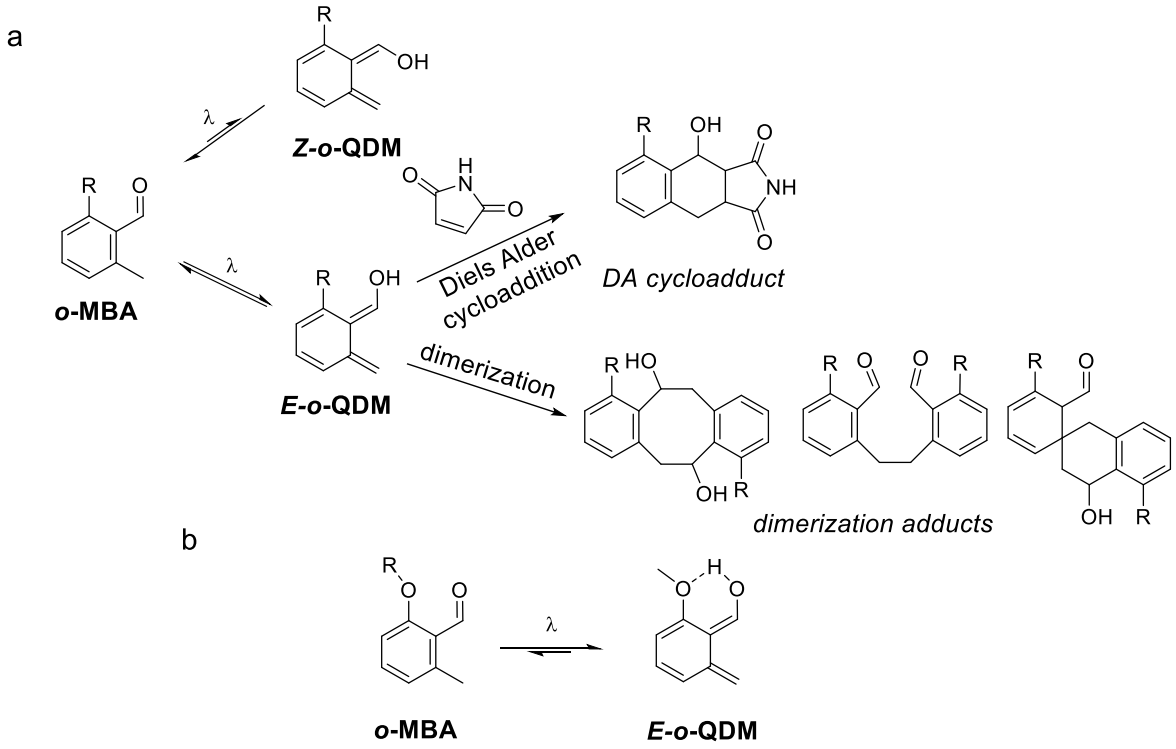

Scheme VI-5. (a) *o*-MBA photoisomerization to *o*-QDM and reactivity of the *E*-isomer formed. (b) Hydrogen-bonding stabilization of *E*-*o*-QDM.

Because of their capacity to photogenerate transient and highly reactive *o*-QDMs in a simple and controlled way, *o*-MBAs have been extensively used as light-activable reagents in polymer chemistry[9,10] and materials science.[12,13] For instance, ***o*-MBA-OMe** has been employed in photoligation reactions with self-reporting fluorescence after photoinduced DA reaction with electron poor alkynes (e.g., **alk**).[18] Upon light-triggered cycloaddition between ***o*-MBA-OMe** and **alk**, the intermediate **adduct3** is formed which can undergo an elimination reaction driven by rearomatization that produces the fluorescent naphthalene derivative **Napth** (Scheme VI-6). In this manner, the efficiency of the photoligation reaction can be monitored through fluorescence measurements.[18]

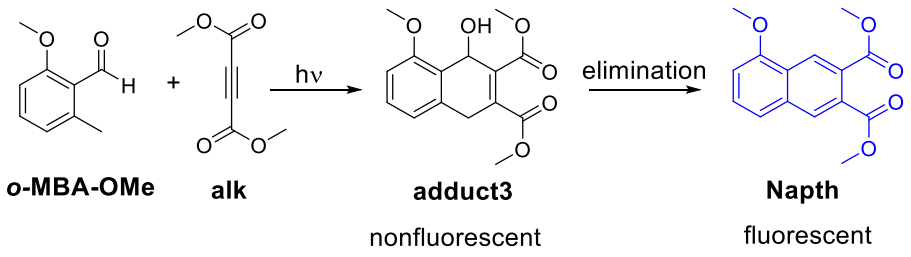

Scheme VI-6. Photoligation reaction between ***o*-MBA-OMe** and **alk** to obtain the fluorescent **Napth** after consecutive photoenolization, DA and elimination reactions.[18]

Although *o*-MBAs are typically employed to trigger photoligation processes with a single excitation wavelength, their application to the two-color control of chemical reactivity has already been reported (Figure VI-1).[19] To do so, a STED-inspired strategy was used where (a) two-photon absorption at 700 nm photogenerated the reactive ***E*-*o*-QDM-Si** species from ***o*-MBA-Si**, and (b) one-photon excitation at 440 nm photoisomerized ***E*-*o*-QDM-Si** to the nonreactive ***Z*-*o*-QDM-Si** form. As a consequence, the photoinduced DA reaction of ***o*-MBA-Si** with maleimide **Mal2** could be triggered with NIR radiation and inhibited with blue light (Figure VI-1a-b). By introducing suitable functionalities in ***o*-MBA-Si** and **Mal2** that allowed chemisorption to glass substrates and radical polymerization initiation, respectively, Barner-Kowollik and coworkers demonstrated that this two-color controlled photoligation system could be used to perform STED-like sub-diffraction lithography (Figure VI-1b-c).[19]

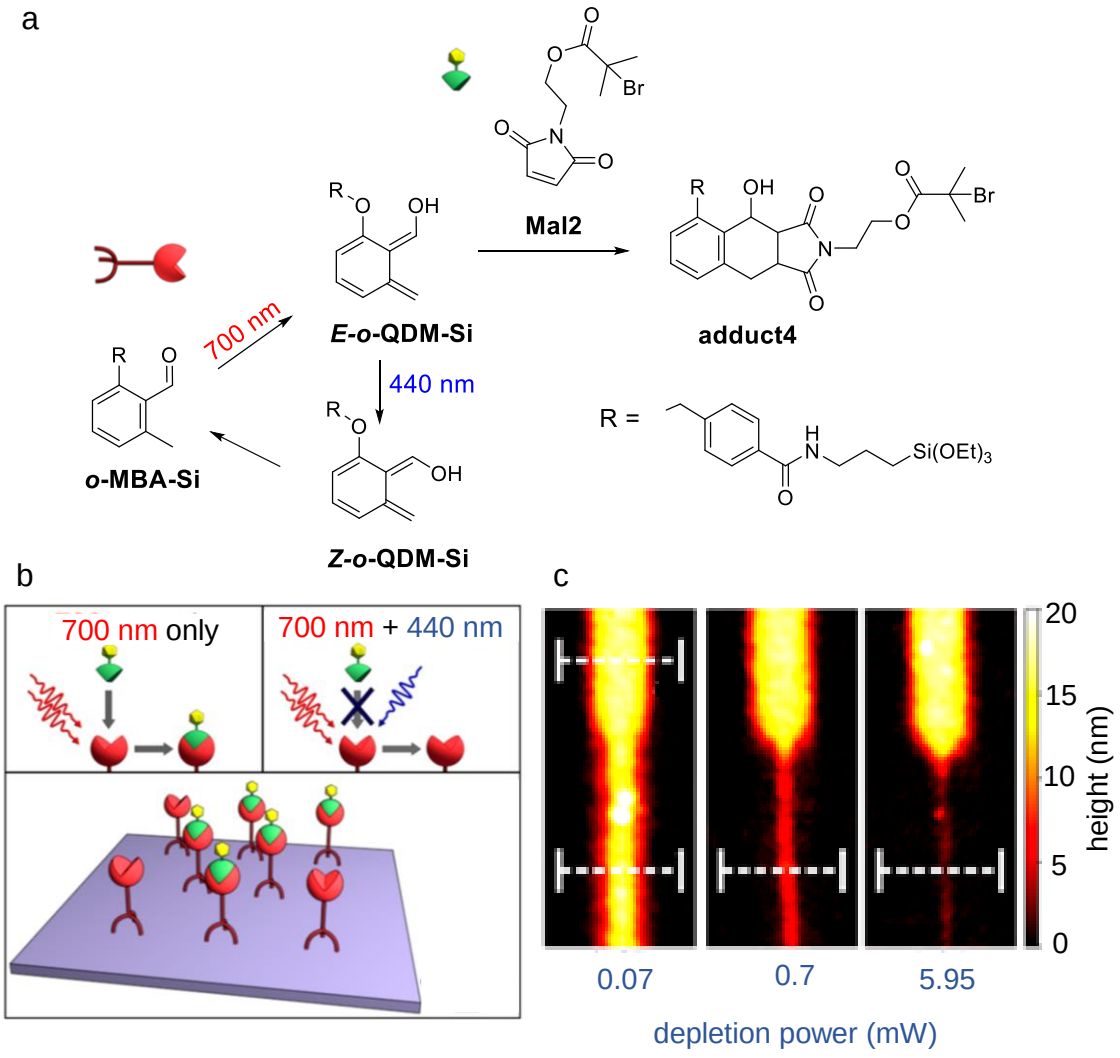

Figure VI-1. (a) Dual-wavelength controlled DA reaction of ***o*-MBA-Si** and maleimide **Mal2**. (b) Schematic representation of the photocontrolled DA reaction between **Mal** and a glass surface functionalized with ***o*-MBA-Si**. (c) AFM images of a photopatterned surface with ***o***-

MBA2 and **MaI2** employing a 700 nm activating laser beam (power = 0.8 mW) in the central section and a 440 nm depletion laser beam on the external regions with increasing power.[19]

Recently, Barner-Kollowik and coworkers also described a new family of *o*-MBAs as photoresponsive precursors of *o*-QDMs that bear a thiol group instead of an ether substituent (e.g., ***o*-MBA-S** in Figure VI-2a).[20] Such change provides a two-fold advantage to the system: (a) a significant improvement of photoreactivity in polar solvents, and (b) a higher and red-shifted absorption (Figure VI-2b). As result, the thioderivatives of *o*-MBAs allow conducting photoligation reactions with lower excitation intensities and, more importantly, under irradiation with visible light.[20]

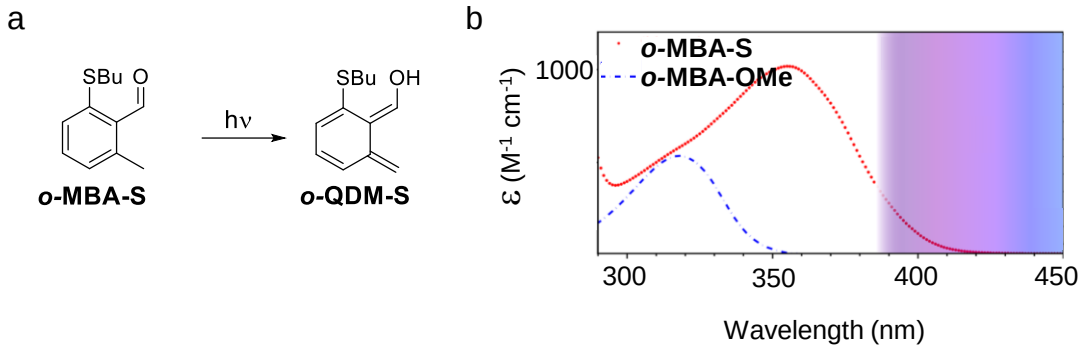

Figure VI-2. (a) ***o*-MBA-S** isomerization process. (b) Absorption comparison between ***o*-MBA-S** and ***o*-MBA-OMe**.

VI.2. OBJECTIVES

In light of the precedents on the separate use of dithienylethene switches and *o*-methylbenzaldehydes to phototrigger DA reactions, in this chapter we aimed to combine these two types of photoreactive systems to develop new strategies for the two-color control of photoligation chemistry. To do so, the following objectives were proposed:

- To prepare *model DTE-based dienophiles* whose reactivity with photogenerated *o*-QDM dienes via DA cycloaddition could be modulated upon photoisomerization.
- To demonstrate the *two-color control of DA cycloadditions* between the model DTE-based dienophiles prepared and photogenerated *o*-QDM dienes. In this way, finer control of DA photoligation could be accomplished relative to current methods relying on a single photoactive component, either the diene or the dienophile.
- To apply our dual-wavelength gated reactive systems to the *light-controlled preparation of cross-linked solid matrices*.

Clearly, the key step to reach these objectives is to design DTE-based dienophiles that could undergo DA cycloaddition reactions with *o*-QDM dienes selectively in one of its two isomeric states. For this two different strategies were explored:

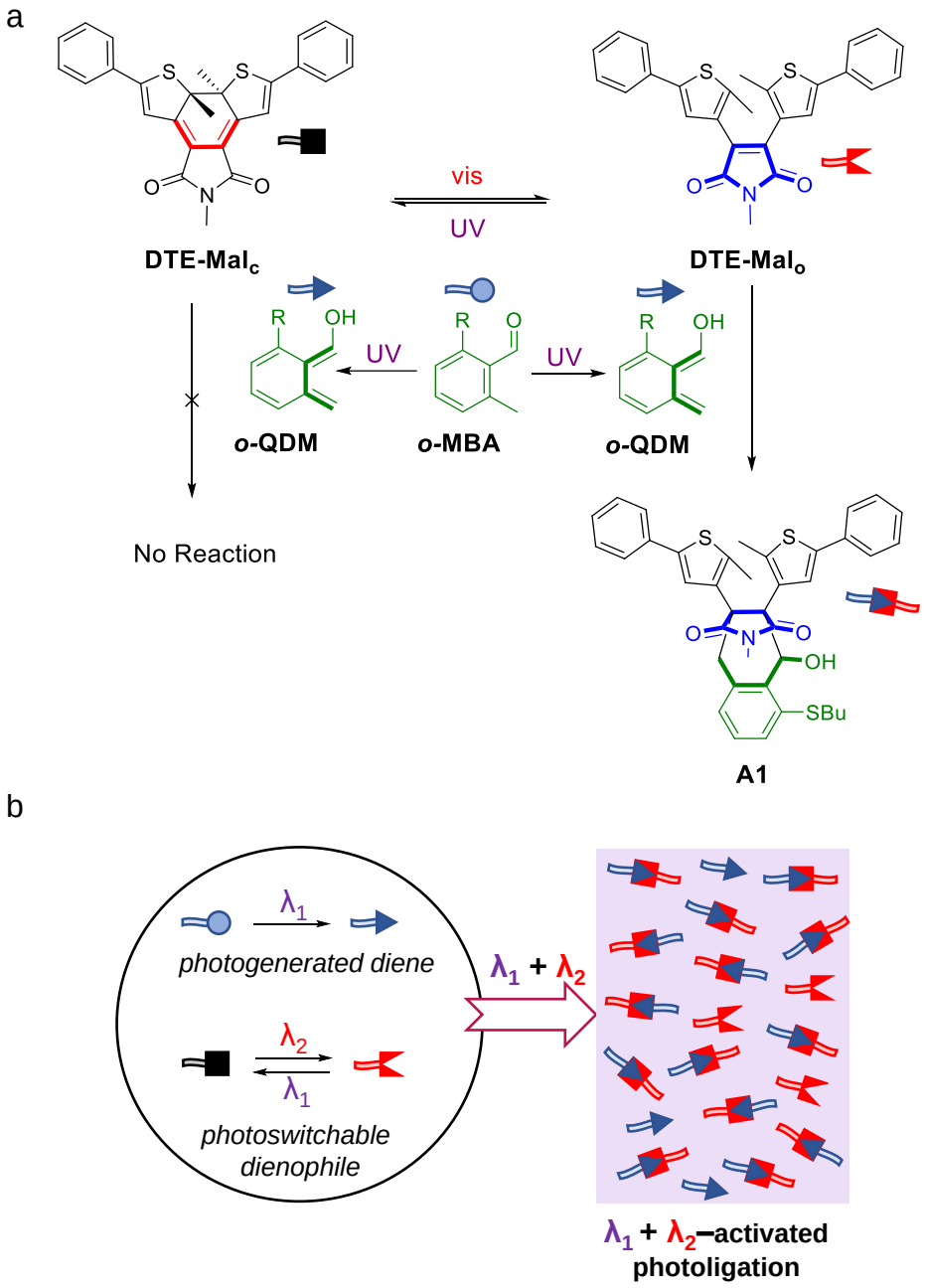

Scheme VI-7. (a) Strategy designed to reach two-color control of DA cycloaddition with photoisomerizable dienophile **DTE-Mal** and photogenerated *o*-QDM dienes. (b) For this strategy, DA photoligation would take place upon concomitant irradiation with UV and visible light.

(a) To *introduce a maleimide dienophile in the central ring of DTEs*, such as in **DTE-Mal** (Scheme VI-7a). In this case, DA cycloaddition with UV-photogenerated *o*-QDM dienes would only be expected for the open isomer **DTE-Mal$_o$**, as the

dienophile species would be removed upon ring closing. Consequently, *DA photoligation in this case would require simultaneous photoexcitation with both UV radiation* - to photogenerate the reactive diene from an *o*-MBA precursor - *and visible light* - to favor photoisomerization toward dienophile **DTE-Mal$_o$** (Scheme VI-7b). By contrast, single irradiation with UV or visible light should not trigger the cycloaddition process because the nonreactive **DTE-Mal$_c$** isomer would be produced or the *o*-QDM ene would not be generated, respectively.

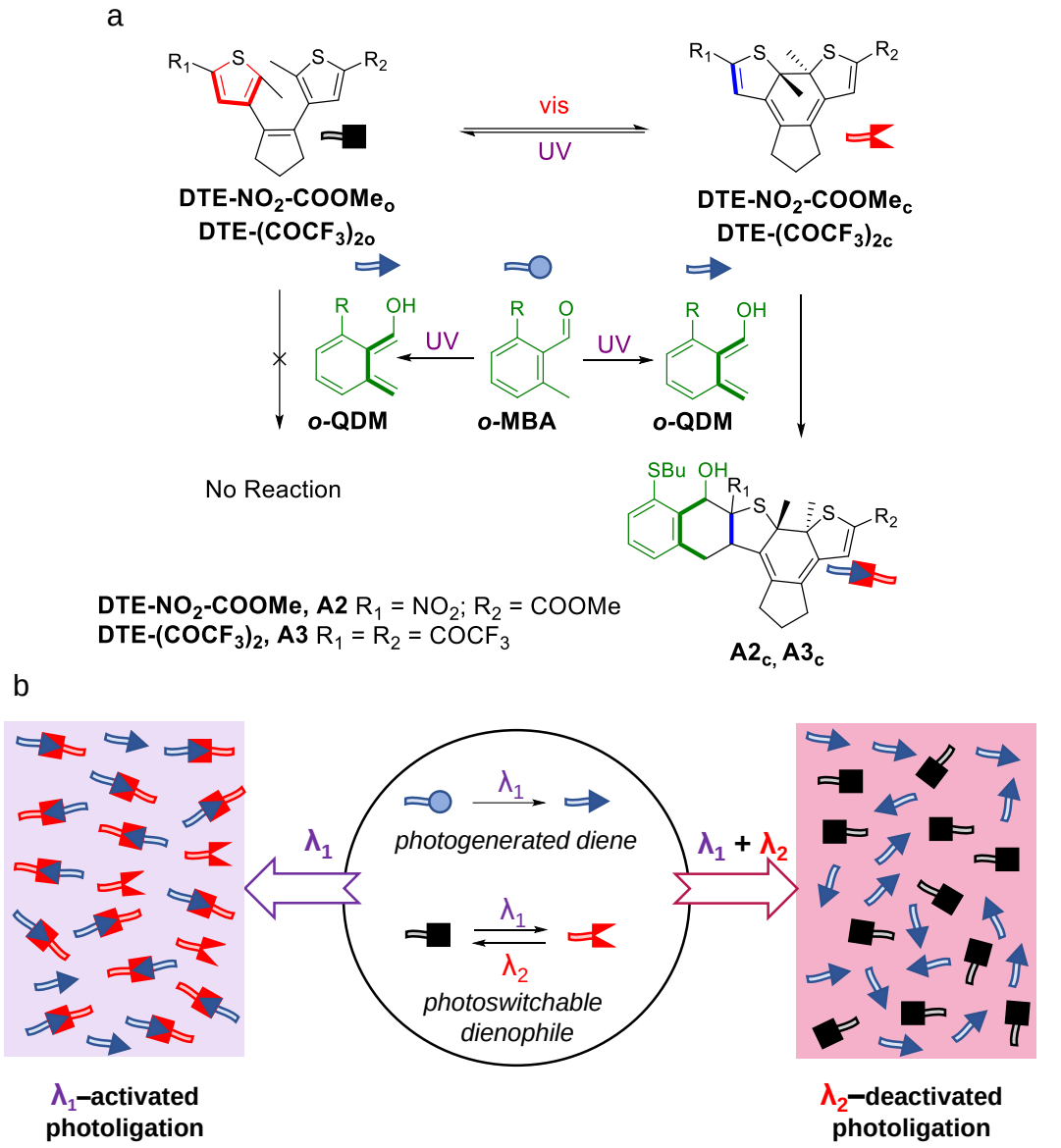

Scheme VI-8. (a) Strategy devised to reach two-color control of DA cycloaddition with photoisomerizable dienophiles **DTE-(COCF$_3$)$_2$** or **DTE-NO$_2$-COOMe** and light-generated *o*-QDM dienes. (b) For this strategy, DA photoligation would take place upon UV irradiation and inhibited with visible light.

(b) To *introduce EWGs in the external positions of the thiophenes of DTEs*, such as the trifluoromethyl ketones in **DTE-(COCF$_3$)$_2$** or the nitro substituent in **DTE-NO$_2$-COOMe** (Scheme VI-8a). As a result, a reactive dienophile would be selectively

created in the closed state of the photoswitch that could undergo DA cycloadditions with photogenerated *o*-QDM dienes. Accordingly, *DA photoligation would occur under UV irradiation* – by producing both the reactive dienophile and diene species – *while it could be inhibited with visible light* by favoring photoisomerization to the nonreactive open DTE isomer (Scheme VI-8a). Therefore, a STED-based strategy would be followed in this case to reach dual-wavelength control of DA cycloaddition processes.

VI.3. SYNTHESIS OF DTE-BASED DIENOPHILES AND *O*-MBA DIENE PRECURSOR

VI.3.1. Synthesis of DTE-based dienophile DTE-Mal

To explore the first of our strategies toward two-color controlled DA cycloadditions, model photoswitch **DTE-Mal** was prepared bearing a central maleimide ring. Two phenyl groups were introduced as external substituents on the thiophenes of this compound to decrease the ring-opening quantum yield,[21] which should allow achieving higher conversions for the cyclization reaction under UV irradiation. **DTE-Mal** would be synthesized by a double Suzuki coupling between intermediates **45** and **44**. Compound **44** would be obtained from commercially available 3,4-dibromomailimide (**43**) by direct *N*-methylation, a process that was conducted to avoid undesired side reactions with the imide NH proton in later stages of the synthesis. As for compound **45**, it would be prepared from dibromothiophene derivative **27** (see section IV.3) through regioselective Suzuki coupling to incorporate the desired phenyl moieties (Scheme VI-9).

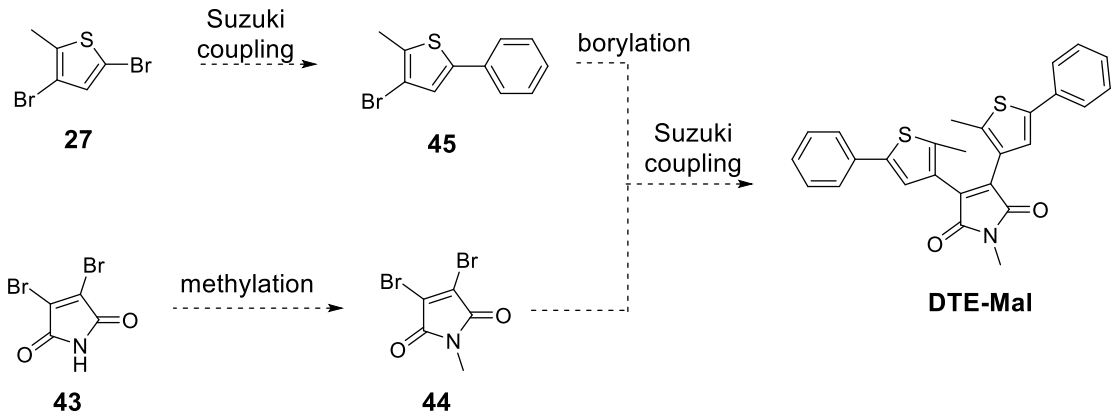

Scheme VI-9. Synthetic strategy for the preparation of **DTE-Mal**.

The preparation of maleimide **44** from **43** was achieved as described in the literature,[22] using methyl iodide as methylation agent. After purification through flash column chromatography, compound **43** was obtained in 60% yield (Scheme VI-10).

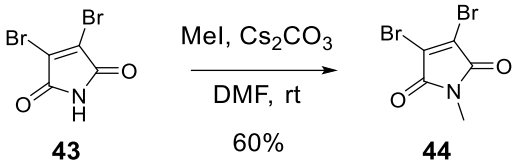

43 **44**

Scheme VI-10. Synthesis of *N*-methylated maleimide **44.**

Thiophene derivative **45**[23] was prepared from **27** following the procedure previously employed for other Suzuki couplings in this thesis (see section IV.3), where $Pd(PPh_3)_4$ was used as a catalyst. In this case, we employed the commercially available phenyl boronic acid (**46**) as a starting material, which eventually furnished compound **45** in 93% yield (Scheme VI-11).

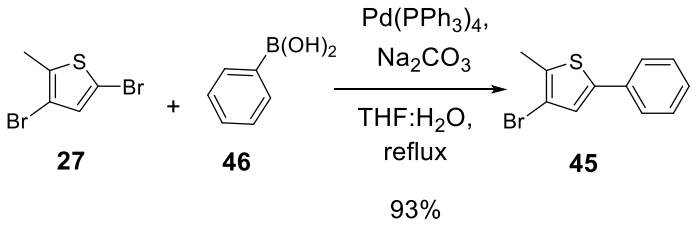

27 **46** **45**

93%

Scheme VI-11. Synthesis of arylated thiophene derivative **45.**

Because of the instability of maleimide **44** to the common Suzuki reaction conditions used in this thesis, we had to slightly modify the procedure to tether together fragments **44** and **45** via consecutive lithiation, borylation and Suzuki coupling. First, the boronic acid of **45** was isolated after preparation through the previously employed method of bromine/lithium exchange and subsequent reaction with tributyl borate. Upon precipitation in acid media, boronic acid **47**[24] was isolated in 72% yield (Scheme VI-11). Next, a double Suzuki coupling between maleimide **44** and boronic acid **47** was conducted. To avoid maleimide hydrolysis, cesium fluoride was used as a base and anhydrous THF as a solvent[24] in this case. Heating under reflux overnight was required for the starting materials to be consumed, which produced **DTE-Mal** in 60% yield after purification by flash column chromatography (Scheme VI-12). The synthesis of the target product was confirmed by the characteristic ^{13}C NMR signal of the carbonyl groups at 171.6 ppm and the ^{1}H NMR resonances of the methyl substituents of the maleimide (3.07 ppm) and thiophene (2.05 ppm) fragments.

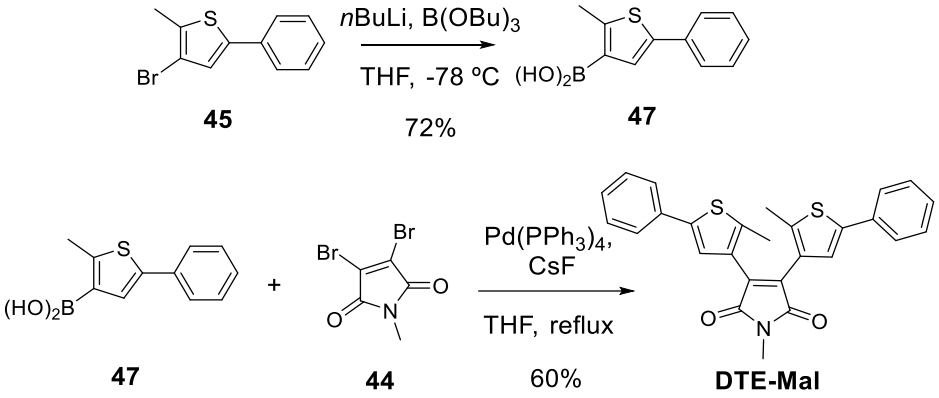

Scheme VI-12. Synthesis of **DTE-MaI** by coupling thiophene **45** and maleimide **44**.

VI.3.2. Synthesis of DTE-based dienophile DTE-NO_2-COOMe

The second of our strategies toward photoisomerizable dienophiles consisted in introducing EWGs on the thiophenes of DTEs to generate electron-deficient olefins upon ring closing that could selectively react with *o*-QDM enes. Based on our previous experience in Chapter IV, we decided these EWGs to be nitro and trifluoroacetyl groups. Accordingly, we first considered the synthesis of **DTE-NO_2-COOMe**, where one nitro group would be tethered to the external position of one of the thiophene rings. As symmetric dinitrosubstituted DTEs are not accessible with the synthetic strategy developed in Chapter IV, an ester EWG would be introduced on the other thiophene because of the following reasons: (a) it is compatible with the synthetic conditions devised, (b) it should further decrease the electron-density on the potential dienophile created after cyclization, (c) it must prevent ICT processes upon irradiation that could detrimentally affect the ring-closing efficiency of the system and (d) it can be easily functionalized

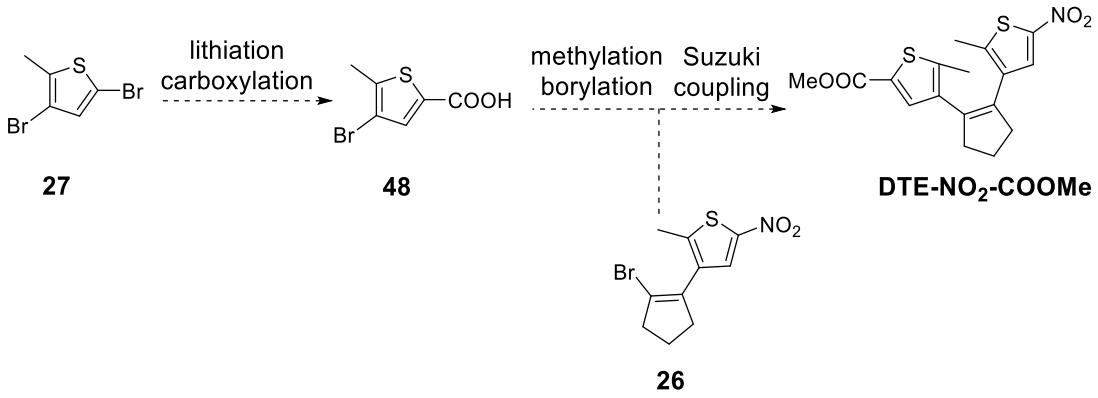

Scheme VI-13. Synthetic strategy for the preparation of **DTE-NO_2-COOMe.**

Target **DTE-NO_2-COOMe** would be obtained by Suzuki coupling between the previously prepared nitrothiophene **26** (see section IV.3) and compound **48** after methylation of its carboxylic acid to avoid side reactions. In turn, compound **48** would

be synthesized from **27** (see section IV.3) after lithiation and direct reaction with CO_2 (Scheme VI-13).

Compound **48**[25] was prepared as described in the literature via lithiation and carboxilation with CO_2. After purification by precipitation in acid media, **48** was obtained in 89% yield (Scheme VI-14).[26] Then, the carboxylic acid m

oiety of **48** was protected as a methyl ester to form compound **49** in 94% yield via nucleophilic substitution with methyl iodide (Scheme VI-14).[27]

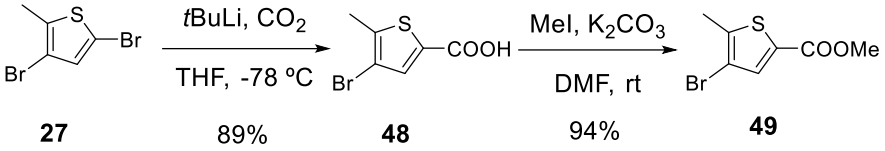

Scheme VI-14. Synthesis of methyl ester **49**.

The synthesis of **DTE-NO_2-COOMe** was then done through a two-step process from **49** and **26**. The first step consisted in the borylation of compound **49**, which could not be performed via the previous formation of the organolithiated derivative of **48** because of the presence of the ester moiety. For this reason, an alternative procedure was undertaken and the borylation process was performed through a palladium-catalyzed coupling with bis(pinacolato)diboron (Scheme VI-15).[28] The resulting boronic ester was used in the next step after filtration through celite pad and solvent removal without further purification. As this compound was observed to be unstable under the typical Suzuki coupling conditions employed in this thesis (see section IV.3) and mostly lead to protodeboronation byproducts, a different procedure for the reaction with nitrothiophene **26** was developed. In particular, anhydrous THF was used as a solvent instead of an aqueous phase and Cs_2CO_3 was selected as a based to improve its solubility in organic media. In this manner, **DTE-NO_2-COOMe** was obtained in 38% yield (Scheme VI-15), as spectroscopically confirmed by the ^{1}H NMR downfield signals at 7.62 and 7.48 ppm assigned to the two thiophene protons and the ^{13}C NMR resonance at 162.5 ppm characteristic of the carbonyl group.

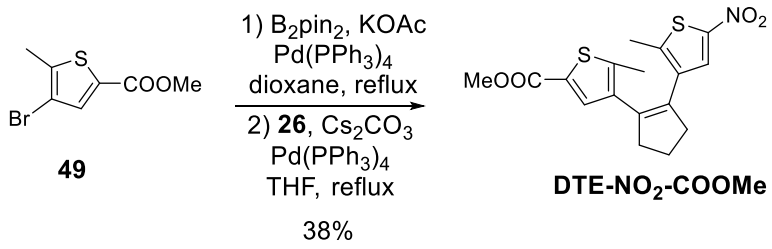

Scheme VI-15. Synthesis of **DTE-NO_2-COOMe** by coupling ester **48** and nitrothiophene **26**.

VI.3.3. Synthesis of DTE-based dienophile DTE-$(COCF_3)_2$

Aside from nitroderivative **DTE-NO_2-COOMe**, **DTE-$(COCF_3)_2$** bearing two trifluoroacetyl substituents on its thiophene rings was also prepared to explore the second of our strategies toward DTE-based dienophiles. A relevant advantage of this compound is that it can be easily prepared from the common dichlorinated DTE **9** extensively used in Chapter IV (see section IV.3). In particular, lithiation of **9** and subsequent reaction with ethyl trifluoroacetate furnished **DTE-$(COCF_3)_2$** in 53% yield after purification by flash column chromatography (Scheme VI-16). The synthesis of this product was corroborated by the downfield shift of the thiophene ^{1}H NMR signal to 7.57 ppm and the appearance of a ^{19}F NMR resonance at -72.20 ppm that is characteristic of the trifluoroacetyl groups introduced.

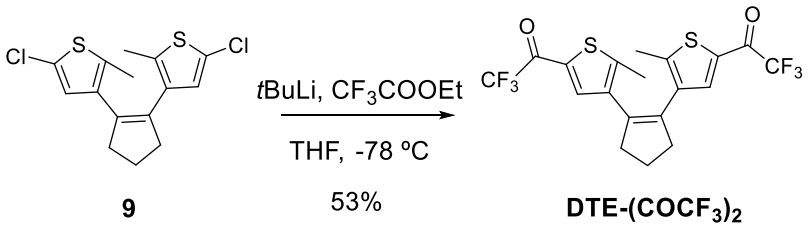

9 **DTE-$(COCF_3)_2$**

Scheme VI-16. Synthetic strategy for the preparation of **DTE-$(COCF_3)_2$**.

VI.3.4. Synthesis of diene precursor *o*-MBA-S

For the reactivity photomodulation studies with model DTE-based dienophiles **DTE-Mal**, **DTE-NO_2-COOMe** and **DTE-$(COCF_3)_2$**, a simple *o*-MBA diene precursor was synthesized. For this purpose, ***o*-MBA-S**[18] bearing a thioether group was selected, as it has already been shown to present superior photochemical properties over nonsulfurated *o*-MBAs (see section VI.1.2). Following a procedure described in the literature by Barner-Kowollik and coworkers,[20] ***o*-MBA-S** was synthesized by nucleophilic aromatic substitution on commercially available 6-methyl-2-fluorobenzaldehyde (**50**) and obtained in 98% yield (Scheme VI-17).

50 98% ***o*-MBA-S**

Scheme VI-17. Synthesis of ***o*-MBA-S.**

VI.4. PHOTOCHEMICAL CHARACTERIZATION OF THE DTE-BASED DIENOPHILES

Once synthesized, the photochemical properties of **DTE-Mal**, **DTE-NO$_2$-COOMe** and **DTE-(COCF$_3$)$_2$** were studied. Because of its large transparency in the UV region (cutoff wavelength = 190 nm), acetonitrile was used as a solvent in these experiments.

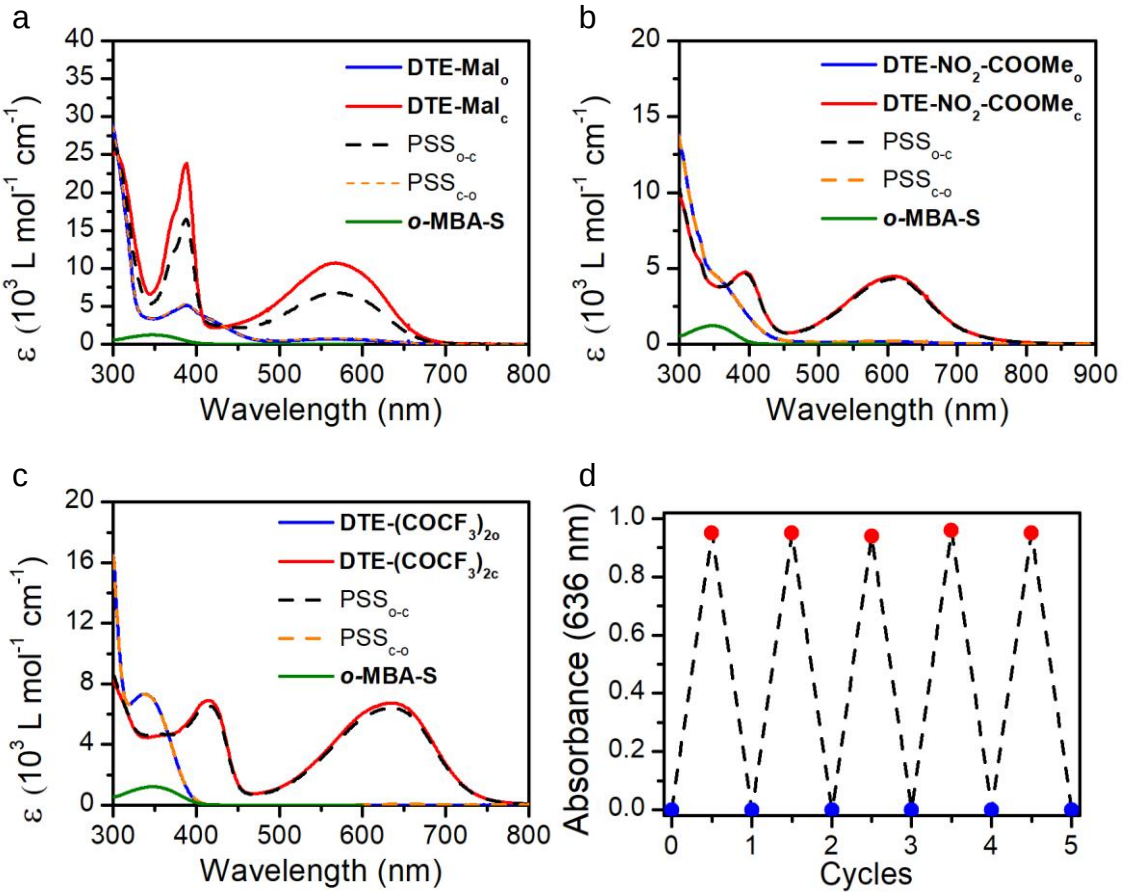

Figure VI-3. (a-c) Absorption spectra of the open state (blue), closed state (red), PSS$_{o-c}$ (dashed-black) and PSS$_{c-o}$ (dashed-orange) of (a) **DTE-Mal**, (b) **DTE-NO$_2$-COOMe**, and (c) **DTE-(COCF$_3$)$_2$** in acetonitrile. For sake of comparison, the absorption spectrum of ***o*-MBA-S** (green) in acetonitrile is also shown. (d) Variation of the absorbance at 635 nm of **DTE-(COCF$_3$)$_2$** in acetonitrile after 5 consecutive cycles of ring closing at 355 nm and ring opening at 650 nm.

Figure VI-3a-c depicts the absorption spectra of the open isomer of the three DTE derivatives in acetonitrile. Together with a strong band at $\lambda_{abs,\,max}$ < 300 nm (Table VI-1), all of them showed significant absorption above 350 nm that extended into the visible region, probably due to the presence of strong EWGs – i.e., maleimide, nitro, ester or trifluoroacetyl groups – and, in the case of **DTE-Mal**, aryl substituents in the external thiophene positions. This would therefore open the door to attempt the

photocyclization of these systems with visible light (e.g., at 405 nm). However, it must be noted that, when applying these compounds to the two-color control of DA cycloaddition, the same photoexcitation source should be used to induce DTE ring closing and *o*-QDM photogeneration from ***o*-MBA-S**. As ***o*-MBA-S** does not absorb above 400 nm and presents $\lambda_{abs,\ max}$ ~ 350 nm (Figure VI-3a), we then decided to investigate DTE photocyclization at 365 nm.

Upon irradiation at 365 nm, an absorption band in the visible region characteristic of the closed isomer of DTEs appeared for all the three molecular photoswitches investigated (Figure VI-3a-c). Ring-closing photoisomerization was confirmed by ^{1}H NMR, which demonstrated that **DTE-NO$_2$-COOMe** and **DTE-(COCF$_3$)$_2$** underwent almost complete conversion to the closed state (>95%) while **DTE-Mal** presented a moderate $PSS_{o\text{-}c}$ containing 61% of **DTE-Mal$_c$** (Figure VI-3a-c, Table VI-1). As expected, irradiation with visible light at 650 nm quantitatively reverted the photocyclization process in all the cases and yielded back the initial open isomers (Figure VI-3a-c, Table VI-1). Interestingly, high fatigue resistance was observed for all three compounds upon repetitive photoisomerization, as it is exemplified in Figure VI-3d for an acetronitrile solution of **DTE-(COCF$_3$)$_2$** subjected to 5 consecutive cycles of irradiation under UV and visible light.

Table VI-1. Photochemical properties of the DTE-based dienophiles synthesized in acetonitrile.

DTE	$\lambda_{abs,max,o}$ (ε)[a]	$\lambda_{abs,max,c}$ (ε)[a]	$PSS_{o\text{-}c}$[b]	$PSS_{c\text{-}o}$[c]	$\Phi_{o\text{-}c}$[d]	$\Phi_{c\text{-}o}$[d]
DTE-Mal	282 (32.8)	567 (10.7)	0.61	1.00	0.48	0.13
DTE-(COCF$_3$)$_2$[e]	284 (21.4)	636 (6.7)	0.95	1.00	0.37	0.031
DTE-NO$_2$-COOMe	254 (22.2)	611 (4.5)	0.96	1.00	0.13	0.0041

[a] Absorption maximum in nm. The extinction coefficients in 10^3 M^{-1} cm^{-1} are indicated in parentheses. [b] Molar fraction of the closed isomer after prolonged irradiation at 365 nm and determined by ^{1}H NMR. [c] Molar fraction of the open isomer after irradiation. [d] Ring-closing (λ_{exc} = 355 nm) and ring-closing (λ_{exc} = 650 nm) quantum yields. Photochemical properties were also determined for **DTE-(COCF$_3$)$_2$** in toluene ($\lambda_{abs,max,o}$ = 284 nm; $\varepsilon_{abs,max,o}$ = 21400 M^{-1} cm^{-1}; $\lambda_{abs,max,c}$ = 636 nm; $\varepsilon_{abs,max,c}$ = 6700 M^{-1} cm^{-1}; $PSS_{o\text{-}c}$ = 0.95; $PSS_{c\text{-}o}$ = 1.00; $\Phi_{o\text{-}c}$ = 0.37; $\Phi_{c\text{-}o}$ = 0.031).

As for the photoisomerization quantum yields, all three DTE photoswitches presented moderate-to-high $\Phi_{o\text{-}c}$ values ($0.5 > \Phi_{o\text{-}c} > 0.1$) in acetonitrile, which are in contrast to those measured for **DTE-EWG** in Chapter IV and **DTE-NO$_2$-Ac** and **DTE-PDI** in Chapter V. Such higher values could be attributed to the absence of a strong charge density gradient in **DTE-Mal**, **DTE-NO$_2$-COOMe** and **DTE-(COCF$_3$)$_2$**, and thus the lack of ICT processes that could compete with photoisomerization. On the other hand, large variations were seen in $\Phi_{c\text{-}o}$, ranging from 0.13 for **DTE-Mal** to 0.0041 for **DTE-NO$_2$-COOMe**. Because of such differences, the composition of their $PSS_{o\text{-}c}$ could be rationalized on the basis of the $\Phi_{o\text{-}c}/\Phi_{c\text{-}o}$ ratio. On the one hand, high $\Phi_{o\text{-}c}/\Phi_{c\text{-}o}$ values were measured for **DTE-NO$_2$-COOMe** ($\Phi_{o\text{-}c}/\Phi_{c\text{-}o}$ = 32) and **DTE-(COCF$_3$)$_2$** ($\Phi_{o\text{-}c}/\Phi_{c\text{-}o}$ = 12), which indicate that the photocyclization reaction is clearly favored over the ring-opening process and, therefore, explain the large open-to-closed conversions observed under UV irradiation. On the other hand, the lower $\Phi_{o\text{-}c}/\Phi_{c\text{-}o}$ value determined for **DTE-Mal** ($\Phi_{o\text{-}c}/\Phi_{c\text{-}o} \sim 3$) accounts for the moderate content of closed isomer reached in the PSS mixture of the ring-closing photoreaction.

VI.5. PHOTOINDUCED DA REACTION BETWEEN DTE-BASED DIENOPHILES AND DIENE PRECURSOR *O*-MBA-S

To validate our strategies toward DA cycloaddition photomodulation with DTE-based dienophiles and photogenerated *o*-QDM dienes, we first investigated the photoreactivity between ***o*-MBA-S** and the isomer of **DTE-Mal**, **DTE-NO$_2$-COOMe** and **DTE-(COCF$_3$)$_2$** with potential dienophile character: the open isomer **DTE-Mal$_o$** and the closed isomers **DTE-NO$_2$-COOMe$_c$** and **DTE-(COCF$_3$)$_{2c}$**. As discussed in detail below, this required sequential or simultaneous photoexcitation with UV and visible light, for which we used two different LED sources: LED 365 (λ_{max} = 365 nm) and LED 625 (λ_{max} = 625 nm), whose exact emission spectra are shown in section VIII.1. In all the cases, these irradiation experiments were conducted at room temperature, under air and using an excess of ***o*-MBA-S** to favor complete conversion to the cycloaddition products.

While only the closed state of the three DTEs synthesized could absorb at 625 nm, illumination at 365 nm could photoexcite different species in our reaction mixtures: the two DTE isomers and ***o*-MBA-S**. Hence, similar molar absorptivities at 365 nm would ideally be desired for all these compounds to avoid light screening from one of the mixture components over the others. Unfortunately, ***o*-MBA-S** has significantly lower absorptivities than both DTE isomers in the whole UV-vis spectrum (see Figure VI-3a-c). In spite of this, it must be noted that: (a) the spectral maximum of ***o*-MBA-S** is close to 365 nm; (b) all the DTE open states show lower absorptions at $\lambda > 350$ nm than at shorter wavelengths; and (c) **DTE-(COCF$_3$)$_2$** and **DTE-NO$_2$-COOMe**

present isosbestic points around 365 nm when photoisomerizing while **DTE-Mal$_c$** has an absorption minimum around 350 nm, which means that the overall absorption of the DTE states should not significantly vary upon ring closing and opening. These are therefore the reasons why UV irradiation in our photoreactivity experiments was conducted with LED 365.

VI.5.1. Photoinduced DA reaction between DTE-Mal$_o$ and *o*-MBA-S

To assay the photoreaction between **DTE-Mal$_o$** and ***o*-MBA-S**, experiments were performed not only in acetonitrile but also in toluene, a solvent that is known to increase the reactivity of ***o*-MBA-S** under UV irradiation.[20] In addition, concomitant photoexcitation at 365 nm and 650 nm had to be conducted to (a) photoproduce ***E*-o-QMD-S** under UV irradiation, and (b) ensure that the PSS mixture created for **DTE-Mal** was highly enriched with the potentially reactive open isomer by strongly illuminating with red light (Scheme VI-18). However, DA adduct formation could not be observed by ^{1}H NMR or LC-MS in any of the attempts performed with different solvents, concentration ratios, excitation powers and irradiation times, even when all ***o*-MBA-S** had disappeared. Actually, in the resulting irradiated mixtures, we could only distinguish several dimerization and oxidation byproducts ascribed to ***o*-MBA-S**.

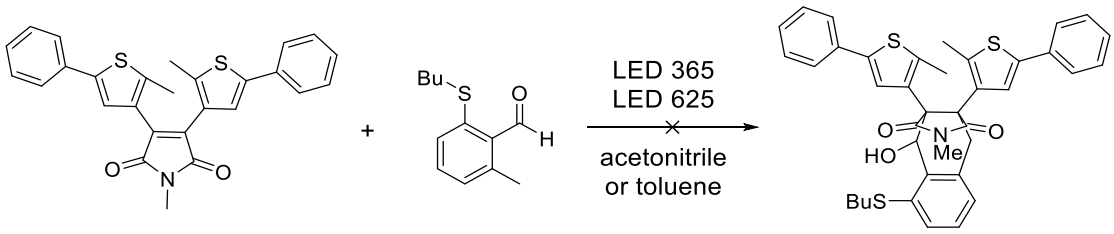

DTE-Mal$_o$ ***o*-MBA-S** **A1$_o$**

Scheme VI-18. DA reaction attempted between **DTE-Mal$_o$** and ***o*-MBA-S.**

We attributed these results to the low reactivity of the maleimide dienophile in **DTE-Mal$_o$** due to steric congestion, which made ***o*-QDM-S** eventually dimerize after sufficient irradiation. For this reason, no more photoreactivity experiments were carried out with **DTE-Mal.**

VI.5.2. Photoinduced DA reaction between DTE-NO$_2$-COOMe$_c$ and *o*-MBA-S

For the photoreaction between **DTE-NO$_2$-COOMe$_c$** and ***o*-MBA-S**, the closed state of the DTE switch was initially prepared by irradiation at 365 nm. As this leads to nearly quantitative photocyclization (see Table VI-1), the reaction with ***o*-MBA-S** was

attempted directly with the $PSS_{o\text{-}c}$ mixture obtained. In this case, illumination with 365 nm was only required, as it produces both the reactive **DTE-NO_2-$COOMe_c$** and ***E*-o-QMD-S** species. However, **DTE-NO_2-$COOMe_c$** did not react with ***o*-MBA-S** neither in toluene nor in acetonitrile regardless of the experimental conditions applied (Scheme VI-19). This time, besides the formation of the dimeric and oxidized byproducts of ***o*-MBA-S,** degradation of the DTE also occurred and, after long irradiation times (> 15h), barely no **DTE-NO_2-COOMe** was present in the reaction mixture.

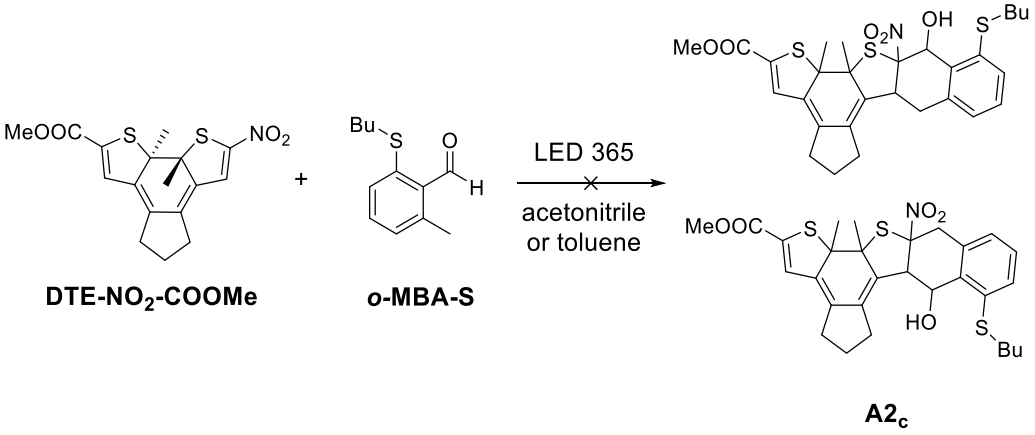

DTE-NO_2-COOMe ***o*-MBA-S** **$A2_c$**

Scheme VI-19. DA reaction attempted between **DTE-NO_2-$COOMe_c$** and ***o*-MBA-S**. The two possible regioisomers for this reaction are shown.

We ascribed these results to the poor dienophile character of the nitrosubstituted carbon-carbon double bond of **DTE-NO_2-$COOMe_c$**. In view of this and the promising results that were being simultaneously obtained for **DTE-$(COCF_3)_2$**, no more experiments were carried out with **DTE-NO_2-COOMe**.

VI.5.3. Photoinduced DA reaction between DTE-$(COCF_3)_{2c}$ and *o*-MBA-S

As in the previous case, the potentially reactive closed isomer **DTE-$(COCF_3)_{2c}$** had to be previously prepared before testing its photoreactivity with ***o*-MBA-S**. To do so, irradiation of **DTE-$(COCF_3)_{2o}$** at 365 nm in the solvent of choice (toluene or acetonitrile) was initially conducted until reaching the $PSS_{o\text{-}c}$, which was essentially composed of the desired DTE state. Then, an excess of ***o*-MBA-S** was added and further irradiation with LED 365 was applied to photogenerate ***o*-QDM-S** and thus induce DA cycloaddition (Figure VI-4). By taking advantage of the presence of fluorine atoms in **DTE-$(COCF_3)_2$**, the evolution of the reaction between **DTE-$(COCF_3)_{2c}$** and ***o*-MBA-S** was initially followed by ^{19}F NMR. This provided us with a more selective manner to monitor adduct formation, as we were only sensitive to the products derived from **DTE-$(COCF_3)_2$** (Figure VI-5a).

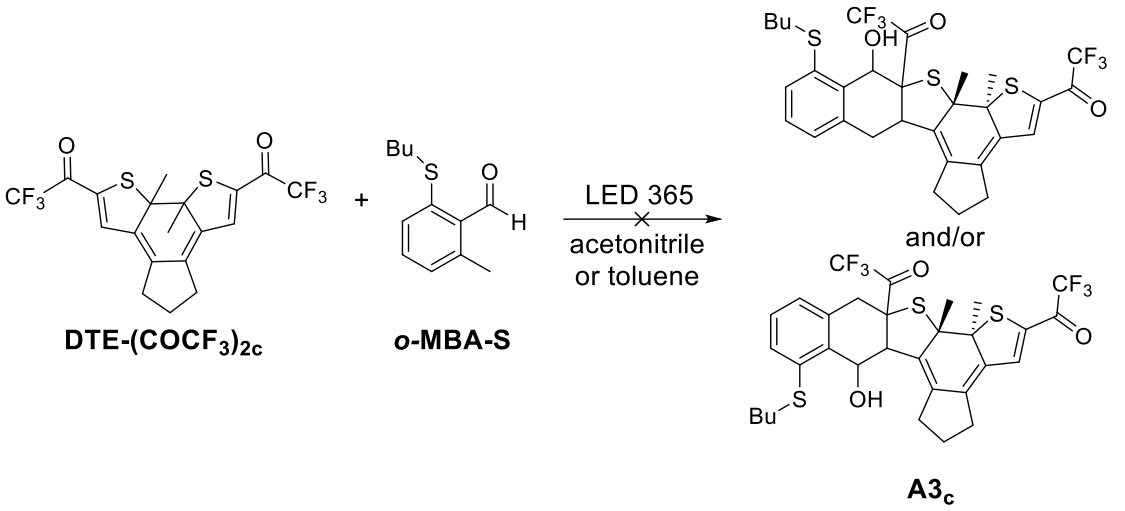

DTE-$(COCF_3)_{2c}$ ***o*-MBA-S** **$A3_c$**

Figure VI-4. DA reaction attempted between **DTE-$(COCF_3)_{2c}$** and ***o*-MBA-S**.

Figure VI-5a shows the typical evolution of the ^{19}F NMR spectra of a **DTE-$(COCF_3)_{2c}$** - ***o*-MBA-S** mixture in acetonitrile under irradiation at 365 nm, which presents similar features to those found when using toluene as a solvent. Clearly, the formation of new fluorine-containing products different to **DTE-$(COCF_3)_{2c}$** and **DTE-$(COCF_3)_{2o}$** was observed upon irradiation at 365 nm. Actually, the ^{19}F NMR signal of the initial DTE switch fully vanished after illumination for 90 min, when a rather complicated spectrum was measured containing up to 6 new ^{19}F NMR signals between -75 and -80 ppm. Therefore, this suggested complete transformation of the initial **DTE-$(COCF_3)_{2c}$** reagent into a set of new compounds, which we expected to be the corresponding DA cycloadducts produced by reaction with ***o*-QDM-S**.

This hypothesis seemed to be corroborated by three additional experiments. First, we observed by ^{19}F NMR that irradiation of ***o*-MBA-S**-free solutions of **DTE-$(COCF_3)_{2c}$** under the same conditions did not induce any photodegradation of the photoswitch (Figure VI-5b). Therefore, the new ^{19}F NMR signals found for the irradiated mixtures should arise from the photoreaction between **DTE-$(COCF_3)_{2c}$** and ***o*-MBA-S**. Second, while the irradiated **DTE-$(COCF_3)_{2c}$-*o*-MBA-S** mixture essentially preserved the blue coloration of the closed DTE isomer, subsequent photoexcitation at 625 nm turned the sample colorless, a behavior that is reminiscent of DTE ring-opening photoisomerization (Figure VI-5a). Consequently, this indicates that the products formed maintained the DTE backbone, as expected for the corresponding DA cycloadducts. Finally, when analyzing by LC-MS the final reaction mixture obtained after irradiation with red light, a single relevant peak was detected in the chromatogram corresponding to a product with the mass expected for the DA cycloaddition product between **DTE-$(COCF_3)_{2c}$** and ***o*-MBA-S** (Figure VI-6).

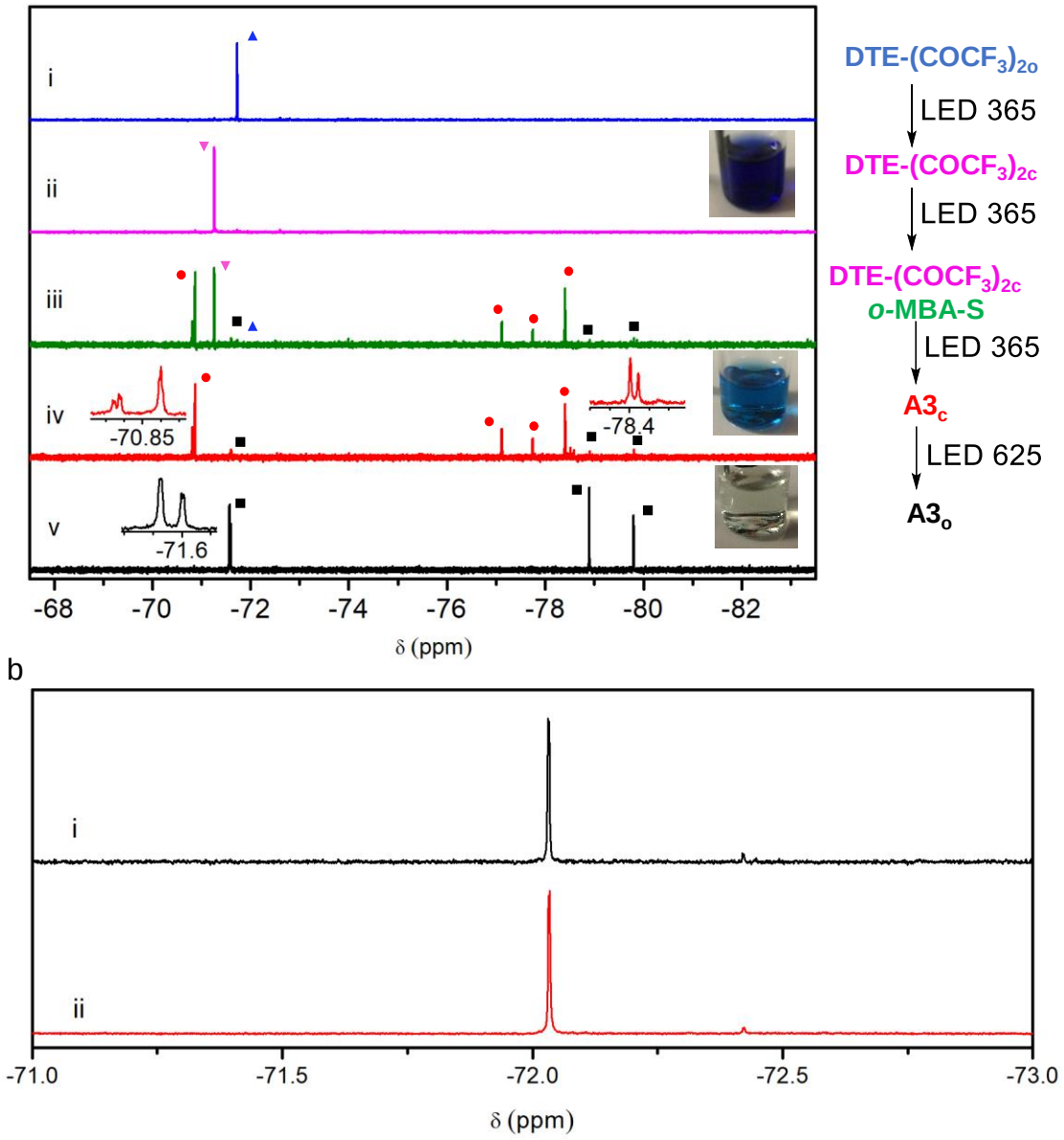

Figure VI-5. (a) ^{19}F NMR spectra (565 MHz, CD_3CN) of (i) **DTE-$(COCF_3)_{2o}$**; (ii) **DTE-$(COCF_3)_{2c}$**; (iii) a mixture of **DTE-$(COCF_3)_{2c}$** and ***o*-MBA-S** (1:30 molar ratio) after UV illumination (LED 365, 0.017 mW cm^{-2}) for 45 min in CD_3CN; (iv) the same mixture of **DTE-$(COCF_3)_{2c}$** and ***o*-MBA-S** after UV illumination (LED 365, 0.017 mW cm^{-2}) for 90 min in CD_3CN, which resulted in nearly quantitative transformation into adduct products bearing a ring-closed DTE unit; (v) the final mixture from (iv) upon irradiation with visible light (LED 625 nm, 35 mW cm^{-2}) for 2 min in CD_3CN, which led to quantitative isomerization of the adduct product to the corresponding open DTE state. For clarity, the ^{19}F NMR resonances in each spectrum arising from **DTE-$(COCF_3)_{2o}$** (blue ▲), **DTE-$(COCF_3)_{2c}$** (pink ▼), closed-state adducts (red ●), and open-state adducts (black ■) are indicated with different symbols. The changes in color of the reaction mixture before illumination (ii, **DTE-$(COCF_3)_{2c}$**) and after UV (iv, closed-state adducts) and subsequent visible (v, open-state adducts) irradiation are shown as insets in (a). (b) ^{19}F NMR spectra of (565 MHz, toluene-d_8): (i) **DTE-$(COCF_3)_{2c}$**; (ii) **DTE-$(COCF_3)_{2c}$** after UV irradiation (LED 365 nm, 0.017 mW cm^{-2}) for 360 min. The low intensity peak at δ = -72.42 ppm corresponds to the residual amount of the open isomer left

when initially preparing **DTE-$(COCF_3)_{2c}$** by photoisomerization of **DTE-$(COCF_3)_{2c}$** (96:4 closed:open ratio for the PSS generated in toluene-d_8 by irradiation with a LED 365 nm).

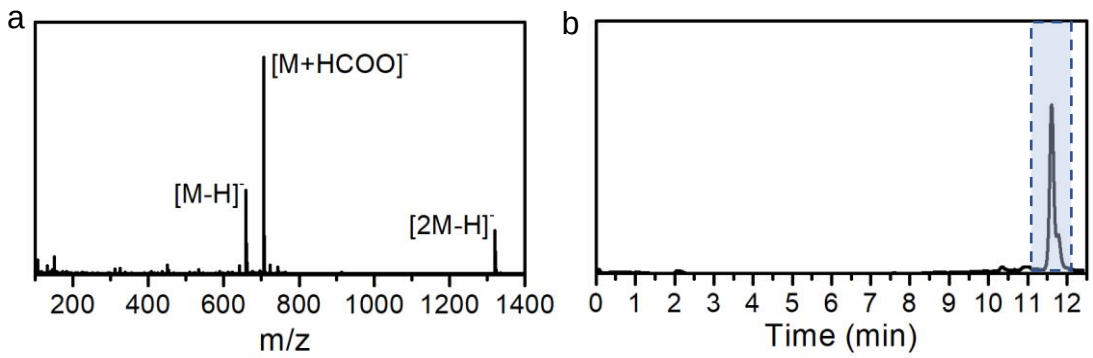

Figure VI-6 (a) LC trace (254 nm detector wavelength) measured for the open-state adducts isolated from the reaction mixture obtained by UV irradiation of a 30:1 mixture of *o*-MBA-S and DTE-$(COCF_3)_{2c}$ in CD_3CN for 90 min (LED 365, 0.017 mW cm^{-2}) followed by 2 min illumination with red light (LED 625, 35 mW cm^{-2}). (b) ESI-MS of the main peak eluted at t = 11.6. HRMS (ESI): m/z calcd. for $C_{31}H_{29}F_6O_3S_3^-$: 659.1188 $[M-H]^-$; found: 659.1191.

To unambiguously elucidate their structure, we further characterized the products formed by photoreaction between **DTE-$(COCF_3)_{2c}$** and ***o*-MBA-S**. With this aim, we focused on the reaction mixture obtained after irradiation at 625 nm – i.e., the open isomer of those products –, as they showed a reduced number of ^{19}F NMR signals (see Figure VI-5a). In particular, only two sets of resonances were observed in the ^{19}F NMR spectrum of that sample at -71.57 and -78.90 ppm and -71.60 ppm and -79.80 ppm (in CD_3CN), which we tentatively ascribed to two different isomers of the cycloaddition process on the basis of the single mass value obtained by LC-MS: the head-to-head and head-to-tail regioisomers of **$A3_o$** in Figure VI-7a showing two different trifluoroacetyl groups each. Unfortunately, such isomeric mixture was irresoluble by HPLC or flash column chromatography and, in fact, we observed that the relative concentration ratio between the two components of the mixture changed dramatically in time or upon manipulation. Therefore, this result suggested that spontaneous interconversion was taking place between the different cycloaddition isomers generated, a behavior that cannot be explained according to the structures of the **$A3_o$** DA adducts shown in Figure VI-7a.

In addition, when thoroughly analyzing the ^1H NMR and ^{13}C NMR spectra of the mixture of cycloaddition isomers, several spectral features were found that did not agree either with the structures proposed for the expected DA reaction between **DTE-$(COCF_3)_{2c}$** and ***o*-MBA-S** (Figure VI-7b-c). In particular, the sets of ^1H NMR signals at 6.58 and 6.70-6.90 ppm could not be attributed to any of the aliphatic CH protons of the tetrahydronaphthalene moiety of **$A3_o$** allegedly generated by DA cycloaddition on the basis of (a) their high chemical shift, (b) the lack of mutual coupling, and (c)

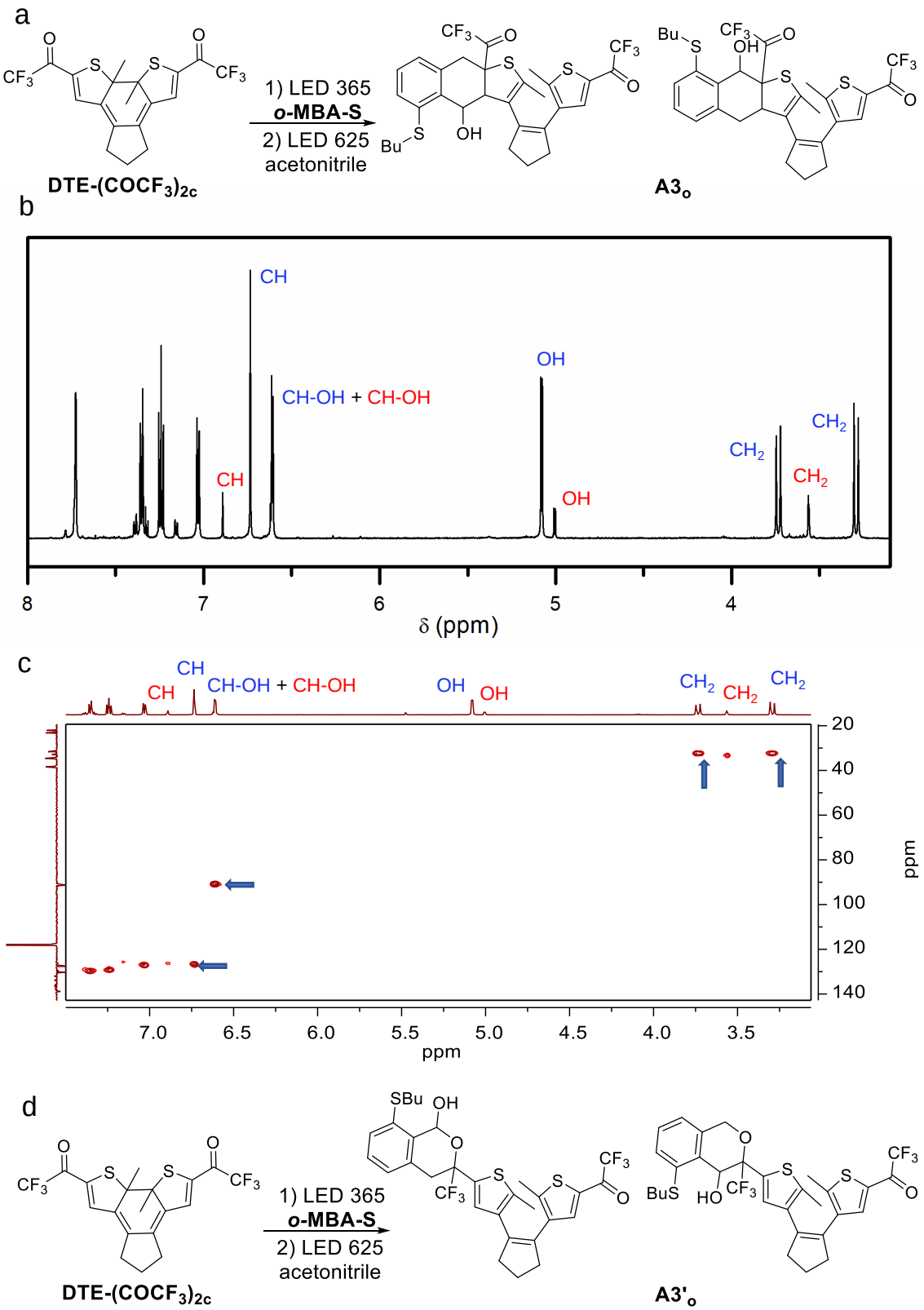

Figure VI-7. (a) **A3$_o$** regioisomers structure as a result of the DA reaction between **DTE-(COCF$_3$)$_{2c}$** and **o-MBA-S**. (b) ^{1}H NMR and (c) ^{1}H-^{13}C HSQC NMR of open-state adducts photoproduced (600 MHz, CD_3CN). The ^{1}H NMR signals labeled in the spectra are those arising from the new cyclic structure created by cycloaddition, which were assigned on the basis of ^{1}H NMR, ^{1}H-^{1}H COSY and ^{1}H-^{13}C HSQC NMR data. They are indicated in blue for

the major isomer and in red for the minor isomer. (b) **A3'$_o$** regioisomers structure as a result of the *oxo*-DA reaction between **DTE-(COCF$_3$)$_{2c}$** and **o-MBA-S**.

the ^{13}C NMR high chemical shift of the adjacent carbon atoms revealed by HSQC (91.7 and 127.6 ppm). In view of these results, the structures proposed for the cycloaddition products in Figure VI-7a had to be ruled out and new ones had to be proposed.

An alternative reaction that could take place between **DTE-(COCF$_3$)$_{2c}$** and ***o*-MBA-S** under UV irradiation is an *oxo*-Diels-Alder cycloaddition (*o*-DA), a hetero-Diels-Alder type of reaction between dienes and carbonyl groups.[29] When driven under normal electron demand, catalyst-free *oxo*-Diels−Alder cycloadditions are highly favored for electron-rich dienes and electron-poor carbonyl dienophiles,[30] which is the case of the ***o*-QDM-S** ene photogenerated from ***o*-MBA-S** and the trifluoromethyl ketone group in **DTE-(COCF$_3$)$_{2c}$**. We thus proposed that we had generated the product of the *o*-DA reaction between these compounds (**A3'$_c$** and **A3'$_o$**), which could led to a mixture of two different regioisomers bearing 1,3,8-trisubstituted and 1,2,8-trisubstituted isochroman moieties resulting from the cycloaddition process (Figure VI-7d).

Interestingly, such hypothesis was validated by all the experimental evidences collected. First, the mass of the *o*-DA cycloadducts shown in Figure VI-7d agreed with the value obtained by LC-MS analysis of the reaction mixture. Second, the presence of two rather different types of trifluoromethyl groups in these cycloadducts could account for the ^{19}F NMR signals measured (see Figure VI-5a). On the one hand, the intact trifluoroacetyl substituent in **A3'$_o$** should be responsible for the ^{19}F NMR resonances at -71.57 and -71.60 ppm in CD_3CN, which show very similar chemical shifts to those measured for the same group in **DTE-(COCF$_3$)$_{2c}$** (-71.26 ppm in CD_3CN) and **DTE-(COCF$_3$)$_{2o}$** (-71.73 ppm in CD_3CN). On the other hand, the considerably highfield-shifted signals at -78.90 and -79.80 ppm in CD_3CN are compatible with the CF_3 substituent of the isochroman moiety of **A3'$_o$** formed through cycloaddition.[31] Third, the structure of the **A3'$_o$** regioisomer with the 1,3,8-trisubstituted isochroman group was fully consistent with the ^{1}H NMR and ^{13}C NMR data, as: (a) it presents an additional thiophene olefin relative to the DA cycloadducts that could account for the ^{1}H NMR and ^{13}C NMR signals at 6.70-6.90 and 127.2-127.6 ppm, respectively (see Figure VI-7c); (b) it contains an hemiacetal moiety that could be assigned to the ^{1}H NMR and ^{13}C NMR signals at 6.58 and 91.7 ppm, respectively (see Figure VI-7c); and (c) this assignment is consistent with the lack of mutual coupling between the ^{1}H NMR resonances at 6.59 and 6.70-6.90 ppm. It is important to notice that such assignment could not be made for the other regioisomer of the *o*-DA reaction shown in Figure VI-7d, which bears a 1,2,8-trisubstituted isochroman moiety that presents no hemiacetal group. This would mean that the *o*-

DA cycloaddition between **DTE-(COCF$_3$)$_{2c}$** and ***o*-QDM-S** would be regiospecific, which is actually a typical feature of this type of reactions.[29]

In view of this, the generation of other types of isomers should account for the different sets of NMR signals found for the *o*-DA cycloaddition products. As shown in Figure VI-8, this requires considering the stereochemistry of the process. First of all, it must be taken into account that **DTE-(COCF$_3$)$_{2c}$** exists as a mixture of two enantiomers with relative *anti* configuration of their methyl groups because the photoinduced 6π electrocyclization reaction of **DTE-(COCF$_3$)$_{2o}$** takes place in a conrotatory fashion.[21] As a result, *o*-DA cycloaddition between **DTE-(COCF$_3$)$_{2c}$** and ***o*-QDM-S** should produce a mixture of four diastereomeric pairs of closed-state enantiomers for **A3'$_c$**, which would simplify to a mixture of two diastereomeric pairs of enantiomers for **A3'$_o$** upon ring-opening with visible light. As these diastereomeric pairs must be resolvable by NMR, this would explain the 7 and 4 ^{19}F NMR signals observed for **A3'$_c$** and **A3'$_o$**, taking into account that the ^{19}F NMR signals of the trifluoroacetyl group of two pairs of enantiomers of **A3'$_c$** overlap at -70.87 ppm in CD_3CN and they could not be resolved.

Another of the experimental observations that could be fully explained for the *o*-DA reaction between **DTE-(COCF$_3$)$_{2c}$** and ***o*-QDM-S** is the spontaneous interconversion found for the cycloaddition products. This feature can be attributed to the epimerization of the hemiacetal moiety of **A3'$_o$**, which induces the mutual interconversion between two pairs of diastereomers (Figure VI-9a). As a result, they would not be separable and their concentration ratio could vary in time until an equilibrium mixture is formed and be sensitive to the surrounding medium (e.g., treatment with acidic media such as silica, Figure VI-9b). It must be noted that no NMR signals for the intermediate aldehyde species of the tautomerization process were observed in our case, which indicates that the tautomerization equilibria were completely displaced towards the hemiacetal forms. Actually, this behavior had been previously reported for the cycloadducts formed from other trifluoromethyl ketones and *o*-QDMs.[32]

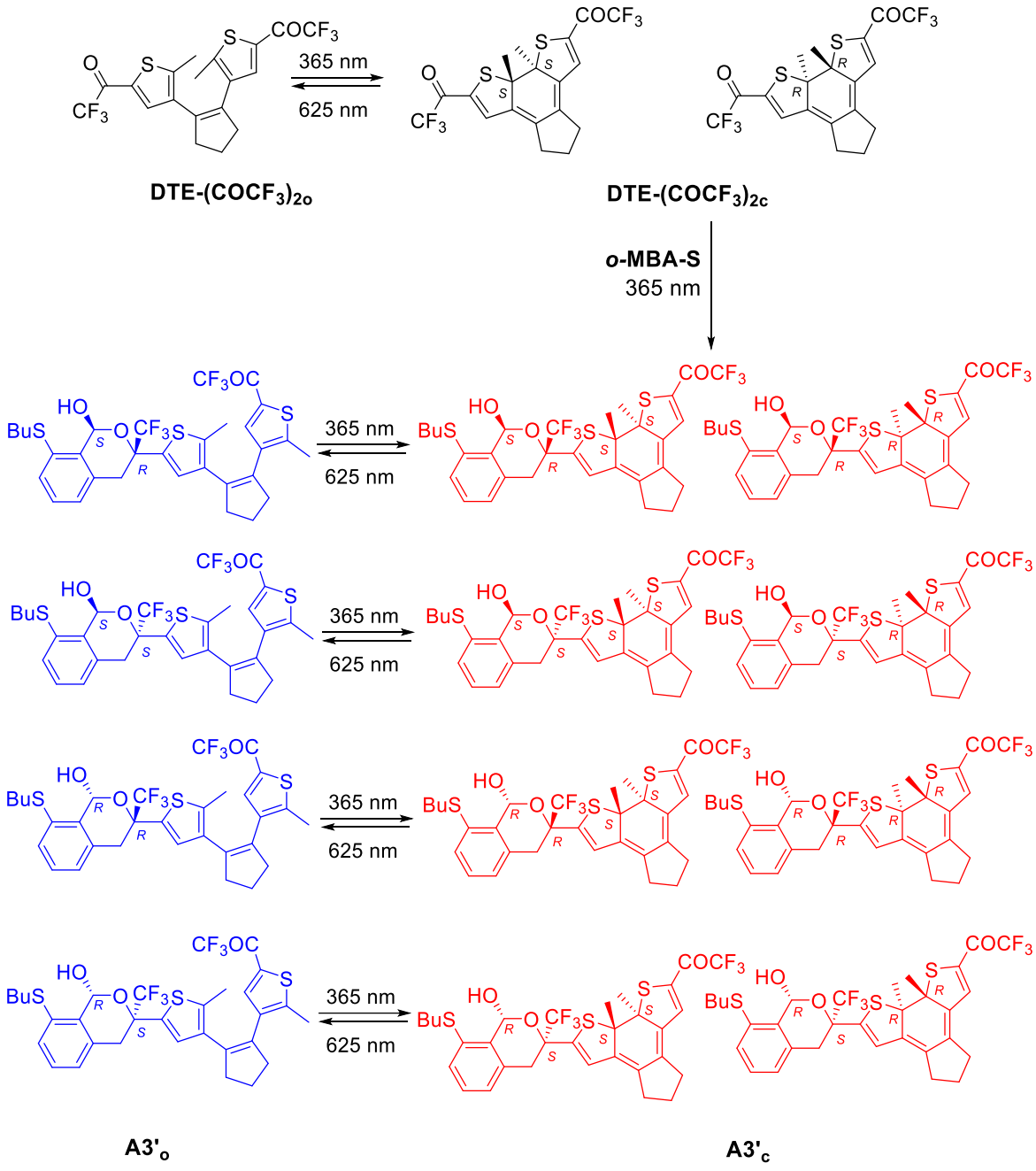

Figure VI-8. Structures of all the possible adducts that could be formed by UV-induced *oxo*-Diels-Alder reaction between **DTE-(COCF$_3$)$_{2c}$** and ***o*-MBA-S** (**A3'$_c$**) as well as of the corresponding open isomers obtained by photoisomerization of these products with visible light (**A3'$_o$**).

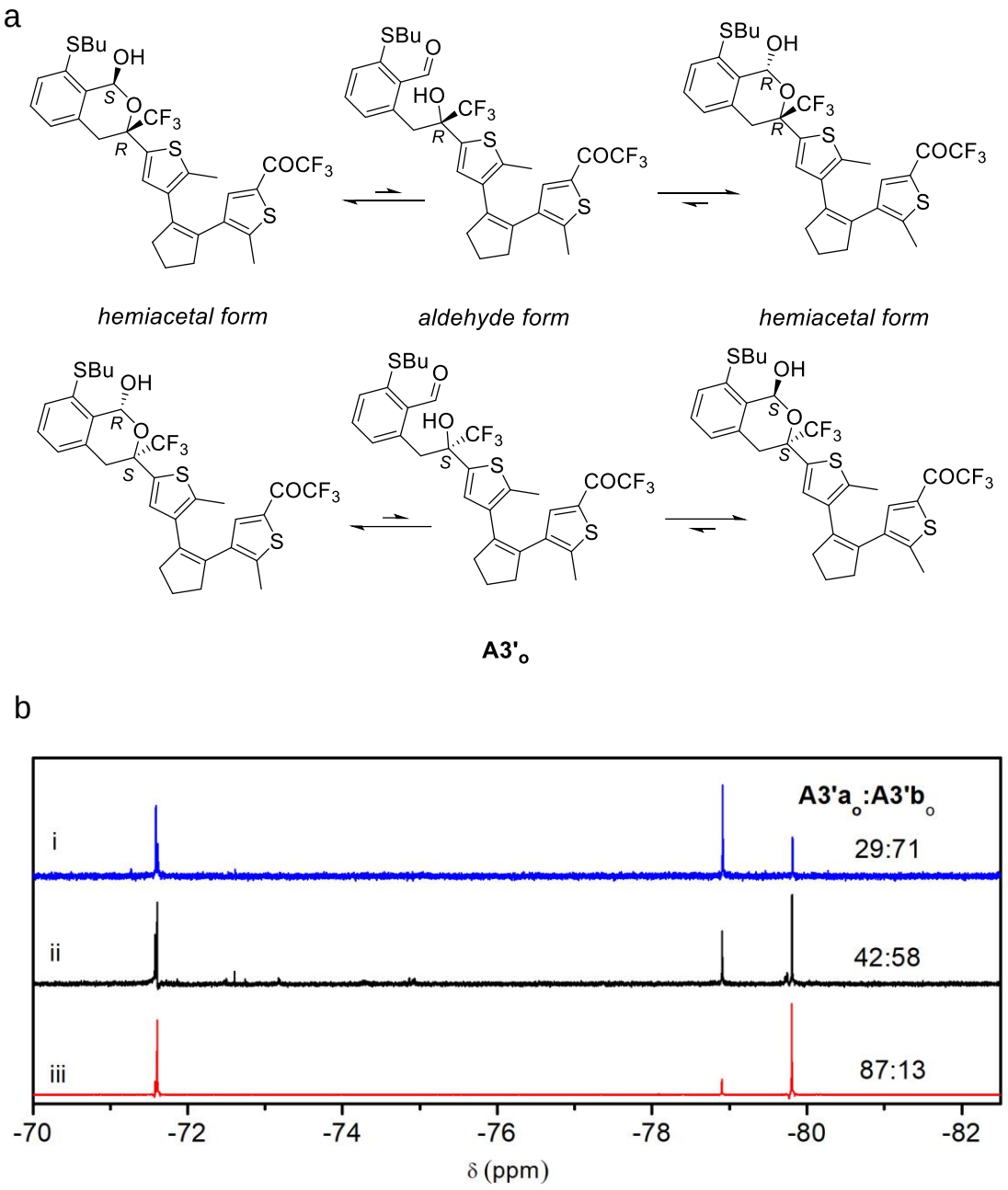

Figure VI-9. (a) Epimerization of **A3'$_o$** by hemiacetal-aldehyde tautomerism. (b) ^{19}F NMR spectra (565 MHz, CD_3CN) of **A3'$_o$**: (i) right after photochemical preparation; (ii) 30 min later after photochemical preparation; (iii) after filtration through silica.

A final aspect that could be justified on the basis of the structures proposed for **A3'$_c$** and **A3'$_o$** is their mutual interconversion upon irradiation and the concomitant changes of color observed. As cycloadduct **A3'** preserves the DTE core, it was observed to undergo the same photoisomerization behavior as **DTE-(COCF$_3$)$_2$**. Thus, **A3'$_c$** could be regenerated from **A3'$_o$** upon irradiation at 365 nm with a total 94% conversion, while subsequent illumination at 650 nm led to the complete recovery of **A3'$_o$** (Figure VI-10).

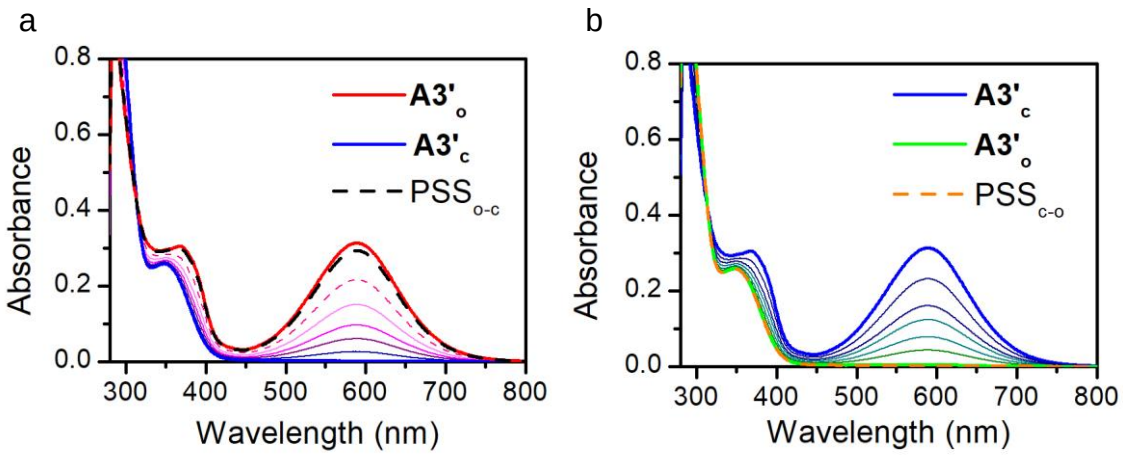

Figure VI-10. (a) Variation of the absorption spectrum of **A3'$_c$** in toluene (c = 4.0·10^{-5} M) when irradiated at λ_{exc} = 650 nm until a photostationary state is obtained ($PSS_{c\text{-}o}$). For sake of comparison, the spectrum of **A3'$_o$** is also shown. (b) Variation of the absorption spectrum of **A3'$_o$** in toluene (c = 4.0·10^{-5} M) when irradiated at λ_{exc} = 365 nm until a photostationary state is obtained ($PSS_{o\text{-}c}$). For sake of comparison, the spectrum of **A3'$_c$** is also shown.

VI.6. Dual-wavelength control of the *oxo*-Diels-Alder reaction between DTE-$(COCF_3)_2$ and *o*-MBA-S

In the previous section we unambiguously proved that **DTE-$(COCF_3)_{2c}$** and ***o*-MBA-S** efficiently react through an *o*-DA cycloaddition under UV irradiation. For this process to be of use for the two-color control of photoligation, a change in reactivity should be observed for the open isomer **DTE-$(COCF_3)_{2o}$** – i.e., the *o*-DA reaction should be inhibited (or highly disfavored) for the open state of the system. Although this may seem unlikely because trifluoromethyl ketone dienophiles are also present in **DTE-$(COCF_3)_{2o}$**, the electronic changes that occur under DTE photoisomerization and how they affect the electron density on the trifluoroacetyl groups cannot be overlooked. In particular, these EWGs are electrically connected in **DTE-$(COCF_3)_{2c}$**, which makes them electron-poorer and, therefore, more prone to undergo *o*-DA reactions. Such effect must be lost in **DTE-$(COCF_3)_{2o}$** upon ring opening, which led us to envisage that a decay in cycloaddition reactivity should indeed be observed.

A first evidence to support this conjecture derived from the data already obtained for **DTE-$(COCF_3)_{2c}$** and ***o*-MBA-S** mixtures. Thus, although large excesses of ***o*-MBA-S** were used in the photoreactivity experiments with **DTE-$(COCF_3)_{2c}$**, selective UV-induced formation of the monocycloaddition adduct **A3'$_c$** was found. In fact, only when exposing the reaction mixture to very long irradiation times (> 10 h), the formation of the dicycloaddition product **dA3'c** was detected by LC-MS, together with some DTE photodegradation compounds. These results demonstrate the importance of the conjugation between the trifluoroacetyl EWGs in **DTE-$(COCF_3)_{2c}$** to promote

the *o*-DA reaction with ***o*-QDM-S**: once one of these groups transformed into an hemiacetal moiety showing no mesomeric electron-withdrawing effect after the first cycloaddition process, the dienophile character of the intact trifluoromethyl ketone decreased and thus the second cycloaddition reaction slowed down significantly (Figure VI-11).

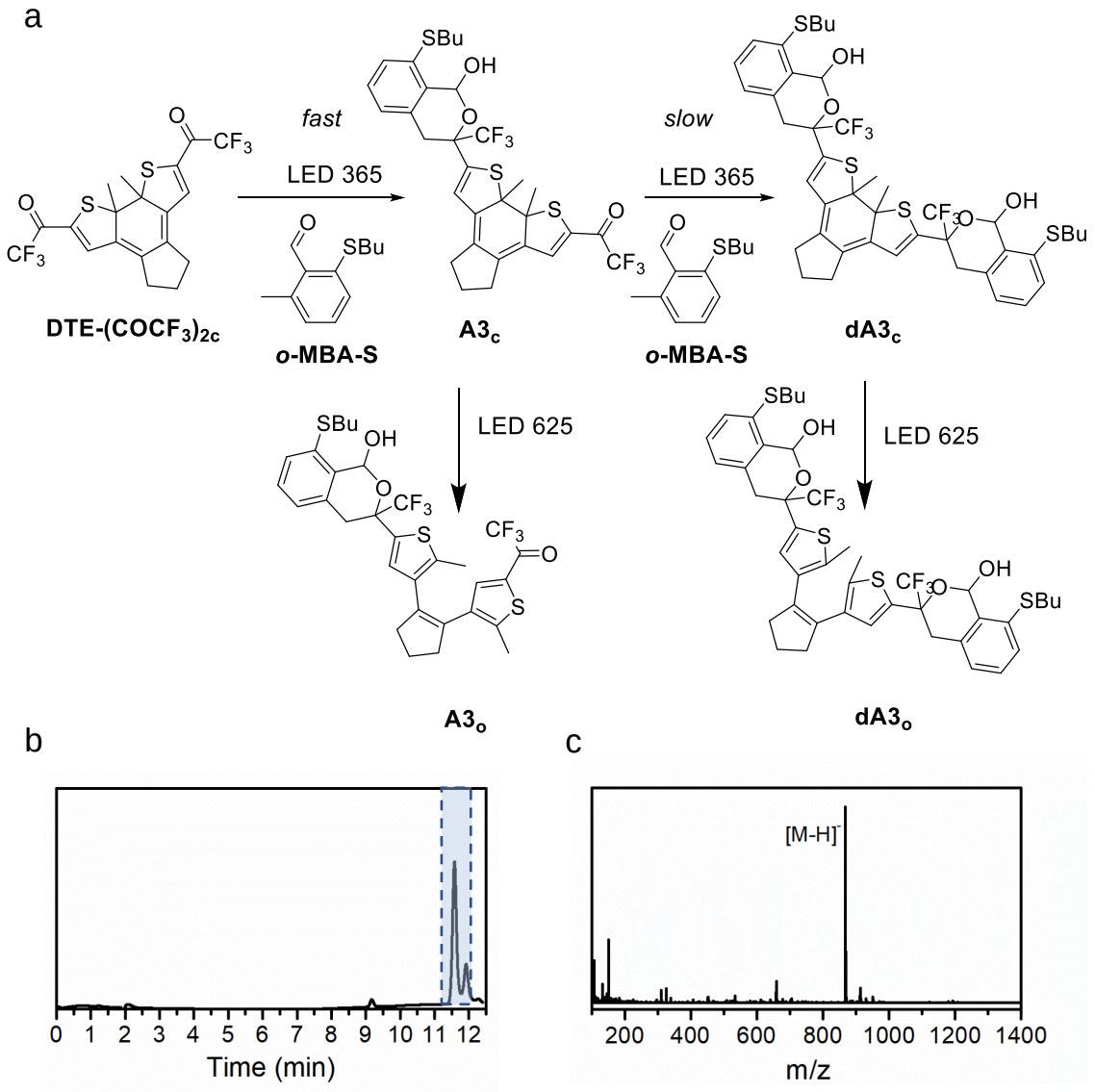

Figure VI-11. (a) Formation of adduct **dA3'$_c$** by double *o*-DA cycloaddition on both trifluoroacetyl groups of **DTE-(COCF$_3$)$_{2c}$**, which could be next photoisomerized to the open state **dA3'$_o$**. (b) LC trace (254 nm detector wavelength) measured for the **dA3'$_o$** product isolated by preparative TLC (hexanes:EtOAc 9:1) from a reaction mixture of **DTE-(COCF$_3$)$_{2o}$** (c = 0.16 mM) and ***o*-MBA-S** (c = 5 mM) subjected to UV illumination (LED 365 nm, 0.017 mW cm^{-2}) for 12 hours in toluene followed by 10 min of visible light irradiation (LED 625 nm, 10 mW cm^{-2}). The two peaks eluted at t = 11.6 and 11.9 min showed the same molecular mass in ESI-MS and were assigned to two different sets of stereoisomers of the dicycloaddition product **dA3'$_o$**. (c) Mass spectrum (ESI-MS) of the peak eluted at t = 11.6 min in the LC chromatogram shown in (b), which was assigned to adduct **dA3'$_o$** (m/z calcd for $C_{43}H_{45}F_6O_4S_4^-$: 867.2104 [M-H]$^-$; found: 867.2109).

To further confirm this conclusion, compound **thio-COCF$_3$** was prepared as a nonphotoisomerizable analogue of **DTE-(COCF$_3$)$_{2o}$**, since it also presents an electronically-insulated trifluoromethyl ketone dienophile tethered to a thiophene ring (Figure VI-12a). Next, the *o*-DA photoreaction of **thio-COCF$_3$** and **DTE-(COCF$_3$)$_{2c}$** with ***o*-MBA-S** was conducted under equivalent conditions and monitored by ^{19}F NMR. As clearly show in Figure VI-12b, while complete conversion to the monocycloaddition product was observed for **DTE-(COCF$_3$)$_{2c}$** after UV illumination for 90 minutes, no adduct formation was measured for **thio-COCF$_3$** during this period (Figure VI-12b). In fact, the formation of appreciable amounts of the adduct product for **thio-COCF$_3$** could only be verified after much longer reaction times (> 24 hours) and higher reagent concentrations. In light of this result, we predicted a much lower dienophile reactivity for **DTE-(COCF$_3$)$_{2o}$** relative to **DTE-(COCF$_3$)$_{2c}$**, which would open the door to effectively controlling the *o*-DA photoreaction with ***o*-MBA-S** using two colors of light.

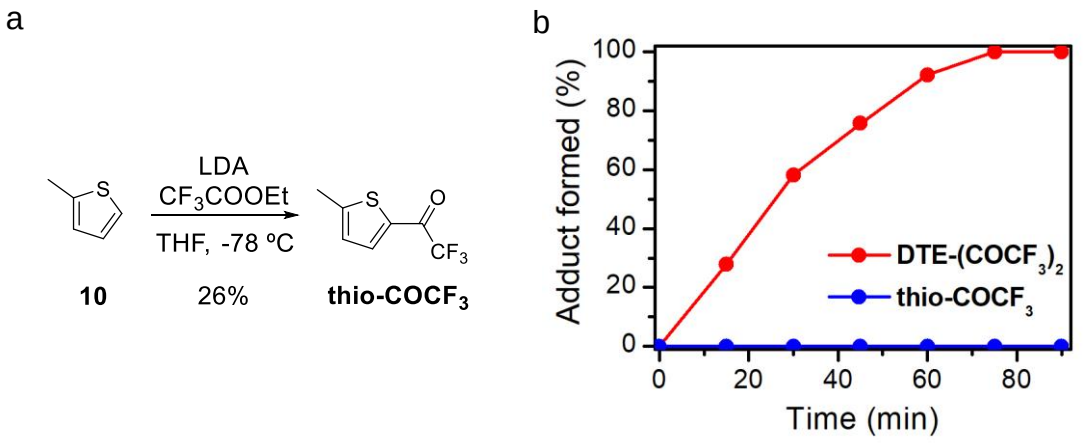

Figure VI-12. (a) Synthesis of **thio-COCF$_3$** via lithium diisopropylamide-mediated (LDA) lithiation of **10** followed by reaction with ethyl trifluoroacetate. (b) Formation rate of the adduct produced by *o*-DA cycloaddition of the diene photogenerated from ***o*-MBA-S** under UV illumination (LED 365, 0.017 mW cm^{-2}) and two different trifluoromethyl ketones in toluene: **DTE-(COCF$_3$)$_{2c}$** and **thio-COCF$_3$**.

To demonstrate this concept, we finally monitored by ^{19}F NMR the evolution of the *o*-DA cycloaddition between **DTE-(COCF$_3$)$_{2o}$** and ***o*-MBA-S** under different irradiation conditions (Figure VI-13a): UV illumination to trigger the process by generating the reactive **DTE-(COCF$_3$)$_{2c}$** dienophile and ***o*-QDM-S** diene, and red light illumination to inhibit the cycloaddition reaction by producing back the less active **DTE-(COCF$_3$)$_{2o}$** dienophile. Careful selection of the experimental conditions was required to achieve maximum modulation of photoreactivity between the open and closed states of **DTE-(COCF$_3$)$_2$**, some of which had already been applied in previous measurements. On the one hand, the photogeneration of ***o*-QDM-S** should not be the rate determining

step of the *o*-DA reaction, as it only depends on the UV irradiation intensity and would make the cycloaddition rate be insensitive to red light illumination. For this reason, we used a low concentration of **DTE-(COCF$_3$)$_2$** – though sufficient enough for reliable ^{19}F NMR detection – and a larger excess of ***o*-MBA-S** (30:1 molar ratio). In this way, we also increased the amount of light absorbed by ***o*-MBA-S**, as **DTE-(COCF$_3$)$_2$** extinction coefficients are up to 10-fold higher at the UV irradiation wavelength. On the other hand, the solvent chosen was toluene, where ***o*-QDM-S** is known to have higher reaction rates.[33] Finally, the UV irradiation intensity was adjusted to be high enough as to allow the reaction to occur in a reasonable time scale for the most favorable case – i.e., in the absence of visible light –, but not too intense as to make ***o*-QDM-S** dimerization processes become relevant.

Following these conditions, the *o*-DA photoreaction between **DTE-(COCF$_3$)$_{2o}$** and ***o*-MBA-S** was first tested in the absence of visible light. After 120 min, complete conversion into the monocycloaddition product was seen, which is only a slightly slower than what had been observed for **DTE-(COCF$_3$)$_{2o}$**. under equivalent conditions (Figure VI-13a). Hence, efficient UV-induced photoligation occurred even when starting from the DTE open state, as it rapidly isomerized to the active closed isomer and reacted with the o-MBA-S molecules that were being concomitantly produced. In contrast, a dramatic reduction in photoreactivity was observed when the reaction mixture was simultaneously irradiated with red light of increasing intensity (Figure VI-13a). This could be attributed to the photoinduced ring opening of the active **DTE-(COCF$_3$)$_{2c}$** molecules produced to yield back **DTE-(COCF$_3$)$_{2o}$**, as neither **DTE-(COCF$_3$)$_{2o}$** nor **o-MBA-S** absorb at 625 nm. Indeed, upon largely increasing the intensity of the red light irradiation source, the *o*-DA reaction was nearly inhibited and only 3% conversion was observed after 120 min.

In conclusion, these results unambiguously demonstrate the light-induced modulation of **DTE-(COCF$_3$)$_2$** reactivity with *o*-QMDs and, consequently, the viability of our dual-wavelength gated photoligation strategy - i.e., whereas UV irradiation triggers the *o*-DA reaction by concurrently generating the reactive **DTE-(COCF$_3$)$_{2c}$** and ***o*-QDM-S**, illumination with visible light halts the process by photoisomerizing **DTE-(COCF$_3$)$_{2c}$** back to inactive **DTE-(COCF$_3$)$_{2o}$**.

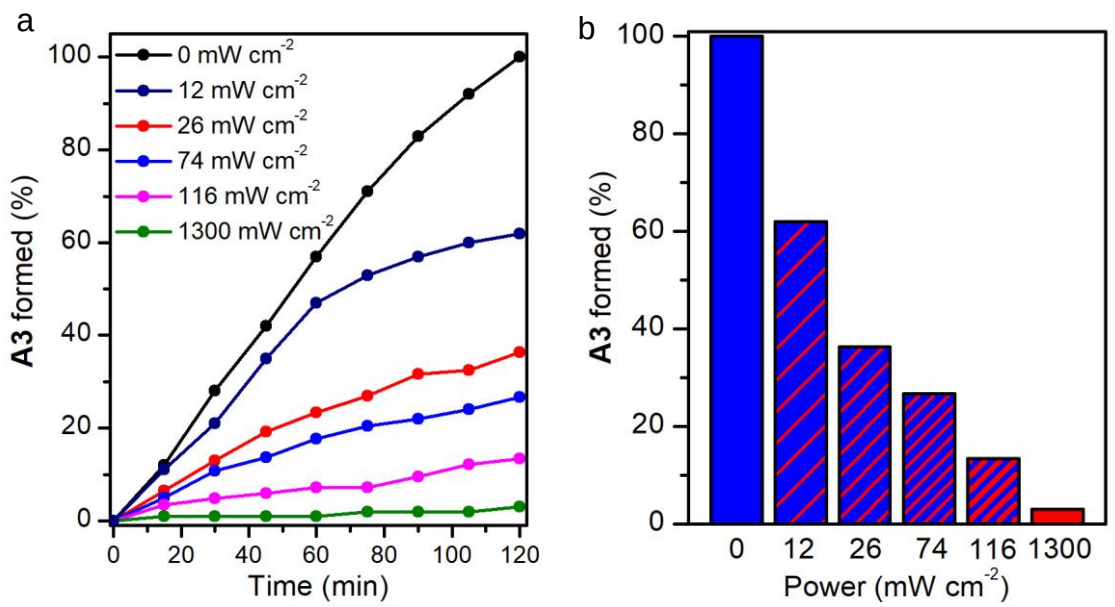

Figure VI-13. (a) Two-color modulation of the formation rate of the *oxo*-DA cycloadduct formed by the reaction between **DTE-(COCF$_3$)$_2$** and **o-MBA-S** in toluene upon simultaneous irradiation with constant UV intensity (LED λ_{max} = 365 nm, 0.017 mW cm^{-2}) and variable visible light power density (LED λ_{max} = 625 nm; 0 to 1300 mW cm^{-2}). (b) DTE-(COCF3)2 conversion upon constant UV irradiation for 120 min (LED λ_{max} = 365 nm, 0.017 mW cm^{-2}) and variable visible light power density (LED λ_{max} = 625 nm; 0 to 1300 mW cm^{-2}).

VI.7. TWO-COLOR PHOTOCONTROLLED POLYMERIZATION WITH DTE-BASED DIENOPHILES AND *O*-MBA DIENE PRECURSORS

To demonstrate the potential of the *o*-DA photoligation strategy developed in this chapter, its application to induce polymer network formation with dual-wavelength control was devised. For this, the synthesis of two new functional molecules was proposed: (a) **DTE-Dimer**, a dimer of the DTE-based trifluoromethyl ketone dienophile investigated in the previous section that preserves the photoswitchable behavior of model compound **DTE-(COCF$_3$)$_2$** (Figure VI-14a); and (b) ***o*-MBA-T**, a trimer of the ***o*-MBA-S** diene precursor (Figure VI-14a). Long and flexible alkyl spacers were introduced between the photoreactive units in both compounds to favor their *o*-DA photoligation reaction and, as a result, the formation of extended cross-linked polymer networks under UV illumination – i.e., when photoisomerization to the active dienophile **DTE-Dimer$_c$** and photogeneration of *o*-QMD dienes in ***o*-MBA-T** concomitantly occurs (Figure VI-14b). By contrast, simultaneous irradiation with visible light should deactivate the photoswitchable dienophile groups by back-isomerization into **DTE-Dimer$_o$** and, as a consequence, preclude polymerization (Figure VI-14b).

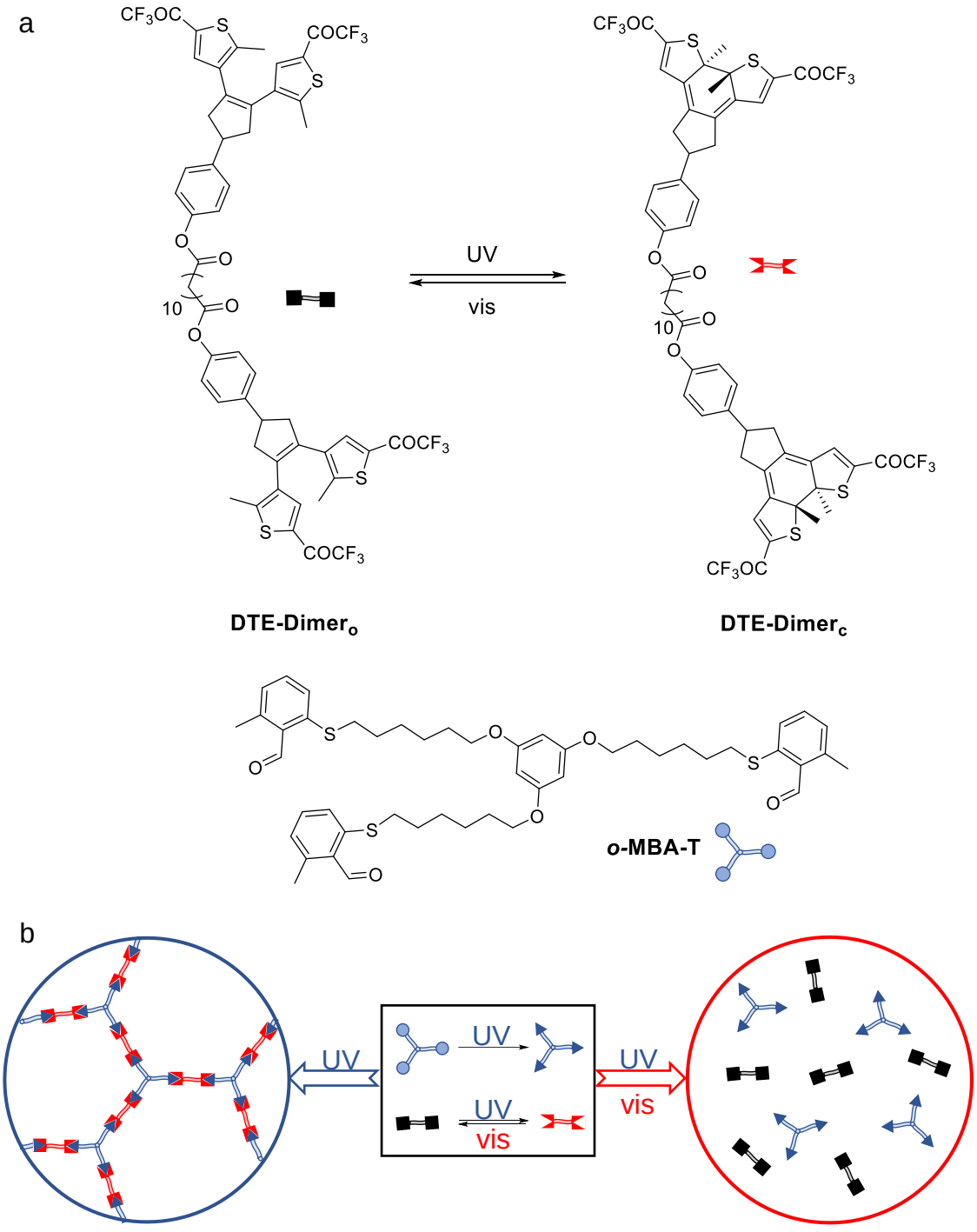

Figure VI-14. (a) Structures of the photoisomerizable **DTE-Dimer** and ***o*-MBA-T**. (b) Cross-linked polymer network formation from **DTE-Dimer** and ***o*-MBA-T**, which should be activated under irradiation with UV light and halted by simultaneous illumination with visible radiation.

VI.7.1. Synthesis and photochemical characterization of the DTE-based dienophile DTE-Dimer

DTE-Dimer would be synthesized starting from intermediate **11** (see section IV.3) following a similar strategy to that reported by Johnson and coworkers for the preparation of the dimer of another DTE photoswitch[34] (Scheme VI-20). The first step would consist in a Friedel-Crafts acylation reaction to introduce an acetyl group at position 3 of previously prepared chlorothiophene **11** (see Section IV.3) to obtain ketone **51** (Scheme VI-20). The acetyl group in **51** would be used to perform first an aldol condensation with *p*-anisaldehyde and next a Michael addition with a second molecule of **51** to produce **52** (Scheme VI-20). Later, the DTE central ring of compound **53** would be formed through a McMurry reaction, and then the two trifluoroacetyl groups would be introduced via lithiation to obtain **54** after deprotection of the phenol moiety (Scheme VI-20). Finally, **DTE-dimer** would be prepared through a double acylation reaction between dodecanoyl dichloride and **54** (Scheme VI-20).

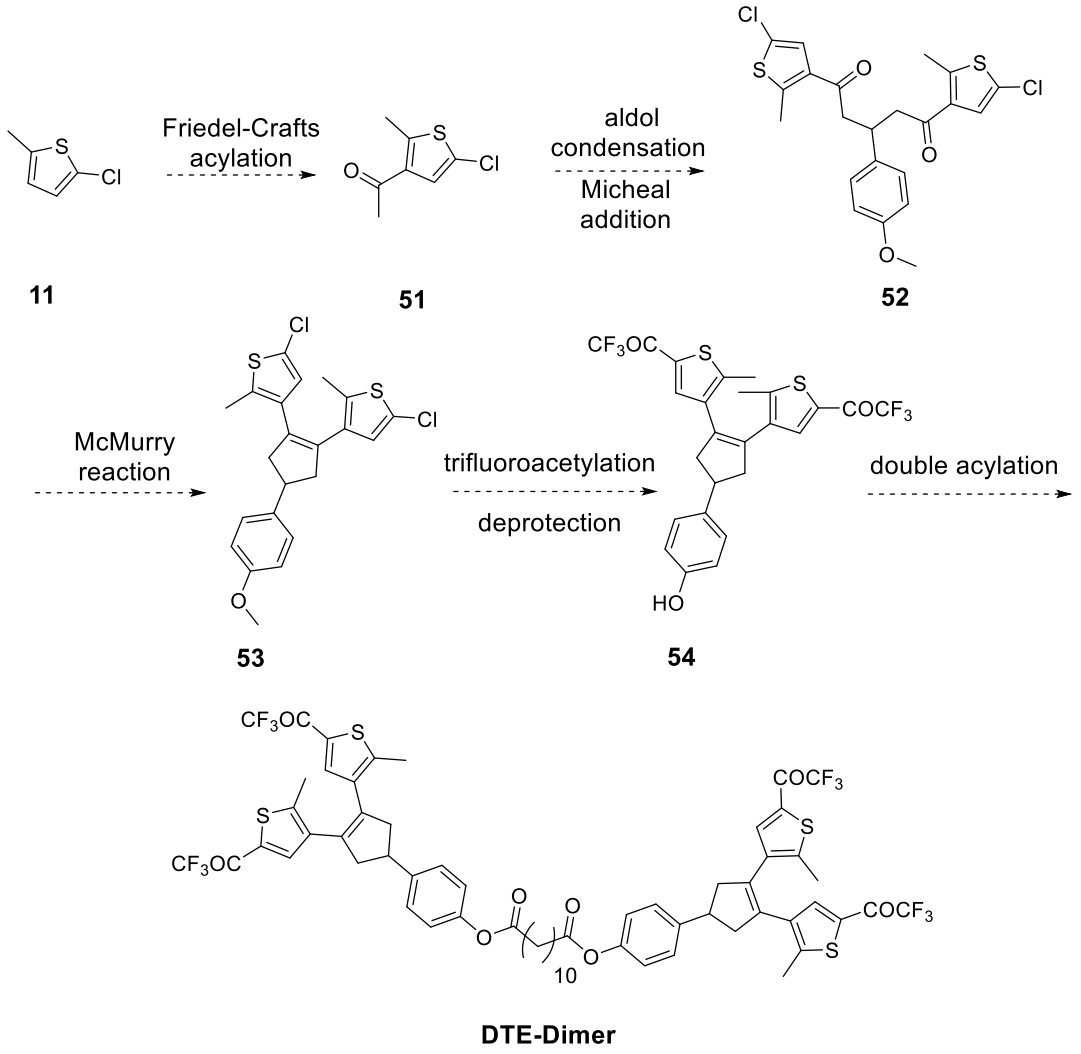

Scheme VI-20. Synthetic strategy devised for the preparation of **DTE-Dimer.**

The first four steps of the synthesis of **DTE-Dimer** were done following the methodology described in the literature by Johnson and coworkers (Scheme VI-21).[34] First, a Friedel-Crafts acylation between **11** and acetyl chloride in the presence of aluminum trichloride furnished **51**[34] in 89% yield. Next, an aldol condensation between *p*-anisaldehyde and **51** in basic ethanol medium was conducted to obtain **55**[34] in 96% yield. Interestingly, a precipitate was formed during this reaction which could be isolated through filtration and identified as the pure product **55**, thus greatly simplifying the purification process relative to the reported procedure.[34] Then, a Michael addition between the LDA-generated enolate of **51** with olefin **55** was carried out to incorporate a second thiophene ring to the system and form the symmetric compound **52**[34] in 97% yield. Finally, the synthesis of the DTE core was completed through a McMurry reaction with $TiCl_4$ and Zn to yield **53**[34] in 72% (Scheme VI-21).

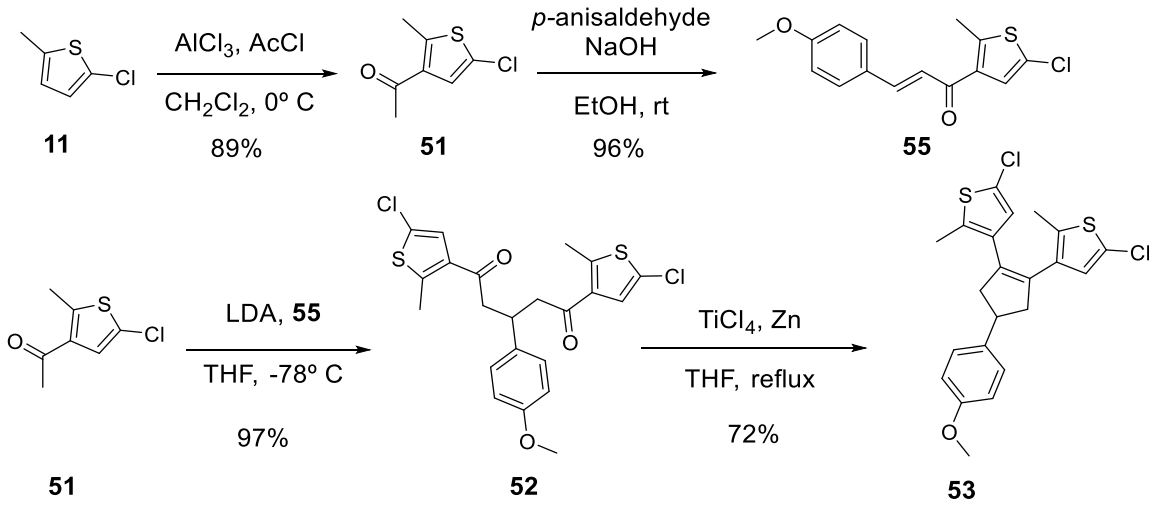

Scheme VI-21 Synthesis of intermediate DTE **53** from 2-chloro-5-methylthiophene (**11**).

Once prepared the dichlorinated DTE derivative **53,** the two trifluoroacetyl groups were introduced using the same methodology previously used for the preparation of **DTE(COCF$_3$)$_2$** – i.e., through a double lithiation of **53** with *tert*-butyllithium and subsequent reaction with ethyl trifluoroacetate, which produced **56** in 65% yield (Scheme VI-22). Then, the protecting methyl ether group of **56** had to be removed to recover the phenol moiety, for which we used boron tribromide. Although this reaction had been described for many DTEs, no product was obtained following the described conditions.[34] In fact, a competing reaction occurred which led to degradation of the DTE system, and for this reason, the temperature and time conditions were optimized. After reaction during 4 hours in an ice-bath, target phenol **54** could be obtained in 61% yield (Scheme VI-22). Finally, the last step of the synthesis consisted in a double acylation reaction employing dodecanodioyl dichloride and **54**. Upon stirring at room temperature in the presence of triethylamine, **DTE-dimer** was

obtained in 54% yield (13% overall in 7 steps from thiophene **10**, Scheme VI-22).[35] The obtention of **DTE-dimer** was confirmed by different spectroscopic features, such as the characteristic ^{1}H NMR and ^{13}C NMR signals corresponding to both the DTE and long alkyl tether fragments.

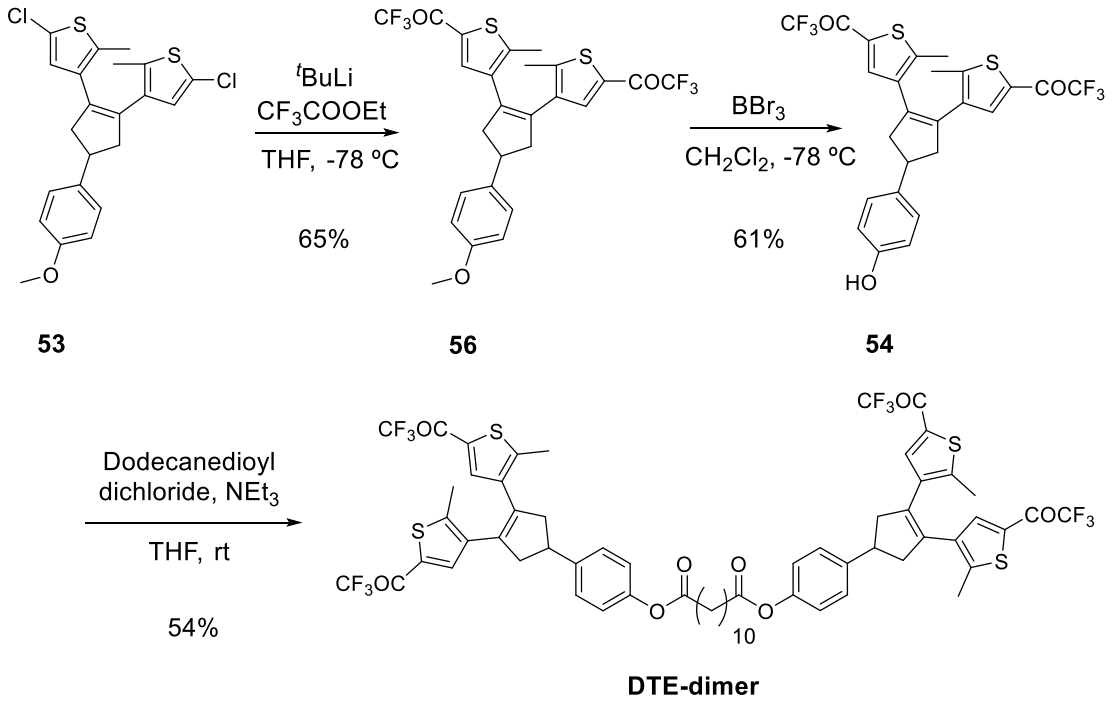

Scheme VI-22. Synthesis of **DTE-dimer** from intermediate DTE **53**.

Next, the photochemical properties of **DTE-Dimer** were studied in acetonitrile. In a similar manner to monomer **DTE-(COCF$_3$)$_2$**, the open isomer **DTE-Dimer$_o$** showed an intense absorption band in the UV region ($\lambda_{abs,max,o}$ = 281 nm, $\varepsilon_{abs,max,c}$ = 65.3 10^3 M^{-1} cm^{-1}) and an additional absorption shoulder that extended up to ~ 400 nm (Figure VI-15). Morever, upon irradiation at 365 nm, it developed a new absorption band corresponding to the photoisomerization to **DTE-Dimer$_c$** ($\lambda_{abs,max,c}$ = 630 nm, $\varepsilon_{abs,max,c}$ = 20.5 10^3 M^{-1} cm^{-1}) (Figure VI-15). This process was found to be slightly less efficient than for **DTE-(COCF$_3$)$_2$**, with 88% conversion of the individual DTE units in the $PSS_{o\text{-}c}$ mixture and $\Phi_{o\text{-}c}$ = 0.14. On the other hand, photoexcitation of $PSS_{o\text{-}c}$ with visible light resulted in quantitative back-photoisomerization to **DTE-Dimer$_o$**, though with lower quantum yield ($\Phi_{c\text{-}o}$ = 0.007) than for **DTE-(COCF$_3$)$_2$** (Figure VI-15).

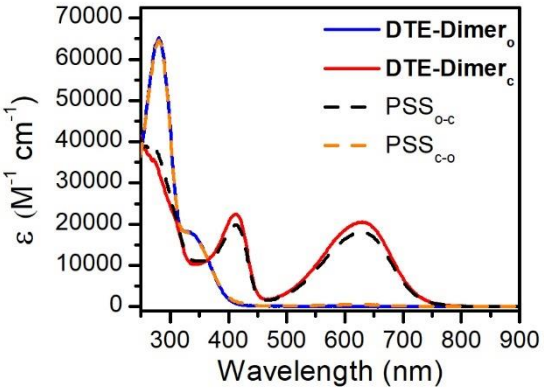

Figure VI-15. Extinction coefficients for **DTE-Dimer$_o$** (blue), **DTE-Dimer$_c$** (red), the $PSS_{o\text{-}c}$ generated by irradiation at 365 nm (dashed black) and the $PSS_{c\text{-}o}$ created upon illumination at 650 nm (dashed orange).

VI.7.2. Synthesis of the diene precursor *o*-MBA-T

The *o*-MBA trimer ***o*-MBA-T** would be prepared starting from commercially available phloroglucinol (**57**), which would constitute the branched core of the compound (Scheme VI-23). First, the bridging alkyl chains would be introduced through a nucleophilic substitution to form **58** bearing terminal bromide substituents (Scheme VI-23). They would then be converted into thiol moieties through a two-step process involving a nucleophilic substitution with thioacetate to obtain **59** after subsequent hydrolysis in basic media (Scheme VI-23). The last step of the process would consist in a triple aromatic nucleophilic substitution of thiol **59** with commercially available 6-methyl-2-fluorobenzaldehyde (**50**) to obtain ***o*-MBA-T** (Scheme VI-23).

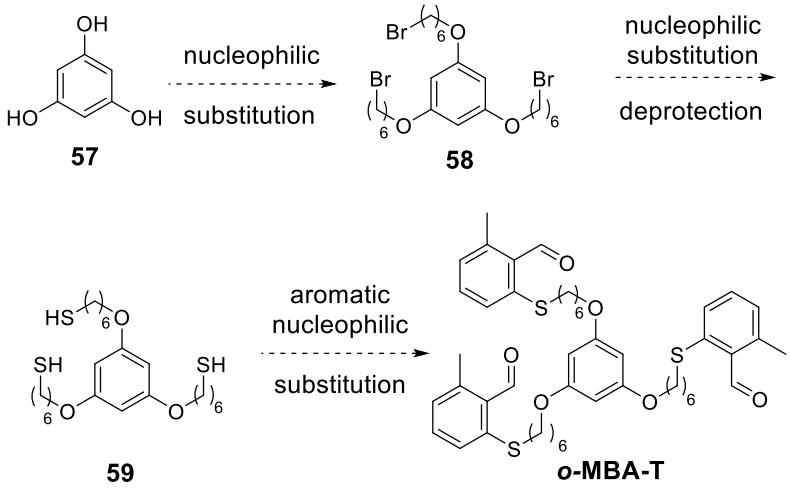

Scheme VI-23. Synthetic strategy designed for the preparation of ***o*-MBA-T.**

The first three steps of this synthetic route were carried out following a procedure described in the literature for a similar compound.[36] The first step consisted in a

nucleophilic substitution between aromatic triol **57** and a large excess of 1,6-dibromohexane in DMF. Such conditions were required to reduce the formation of oligomers upon double substitution on the alkyl chains, which afforded compound **58** was obtained in 40% yield (Scheme VI-24). Next, a nucleophilic substitution reaction between tribromide **58** and potassium thioacetate was conducted in DMF to obtain **60** in 98% yield (Scheme VI-24). Finally, the acetyl groups of **60** were removed by hydrolysis in basic media to yield trithiol **59**. Importantly, compound **59** was found difficult to purify, as it rapidly oxidized to form disulphide bonds. For this reason, only moderate yields were obtained (38%) and, after purification, trithiol **59** had to be rapidly used in the next step, as it could only be stored for a few days in the freezer (Scheme VI-24).

From trithiol **59**, target ***o*-MBA-T** could be obtained following the procedure employed for the preparation of ***o*-MBA-S**, which consists in a nucleophilic aromatic substitution between the thiol of choice and 6-methyl-2-fluorobenzaldehyde (**50**) in the presence of a base.[20] This last step was accomplished with 58% yield to obtain ***o*-MBA-T** in 9% overall yield from 57 after 4 steps. The successful introduction of the *o*-MBA moieties was confirmed by the characteristic aldehyde signals in ^{1}H NMR (10.67 ppm) and ^{13}C NMR (192.7 ppm), which together with some other spectroscopic features unambiguously corroborated the preparation of trimer ***o*-MBA-T**.

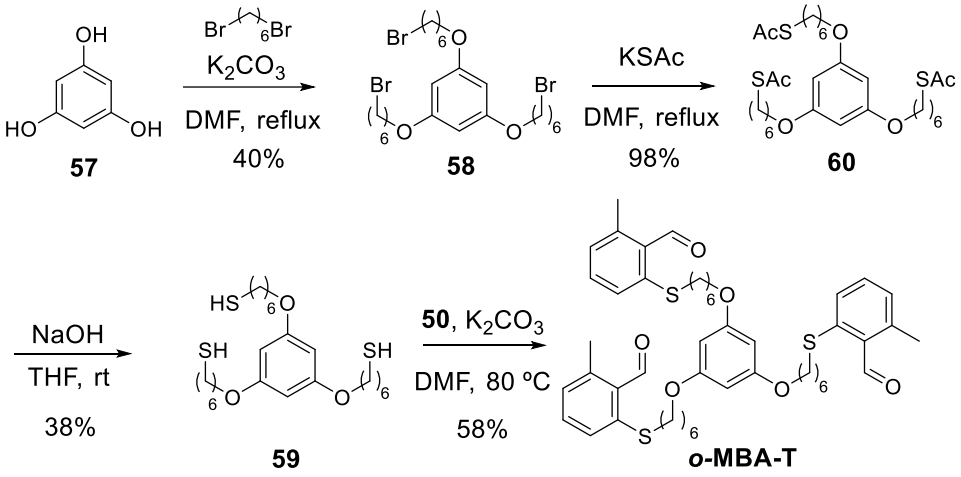

Scheme VI-24. Synthesis of trimer ***o*-MBA-T** from phloroglucinol (**57**).

VI.7.3. Dual-color photocontrolled polymerization with DTE-Dimer and *o*-MBA-T

Once **DTE-Dimer** and ***o*-MBA-T** were synthesized and characterized, their photoinduced polymerization via *o*-DA cycloaddition was assayed in toluene. As discussed above, this should require UV illumination to form the closed isomer **DTE-Dimer$_c$** with active dienophiles and the *o*-QDMs dienes in trimer ***o*-MBA-T**, whereas red light irradiation should inhibit the cross-link process by recovering the inactive

DTE-based dienophiles in **DTE-Dimer$_o$**. For this reason, we first followed by ^{19}F NMR the photoreaction of an equimolar mixture of **DTE-Dimer** and ***o*-MBA-T** exclusively under UV irradiation (c = 0.16 mM, LED 365, 0.017 mW cm^{-2}). To simplify the ^{19}F NMR spectra registered, the analyzed samples were subjected to short irradiation with red light to convert the closed state of the cycloadducts formed to their corresponding open isomers.

As can be seen in Figure VI-16, several new broad ^{19}F NMR signals appeared upon irradiation of the **DTE-Dimer** - ***o*-MBA-T** mixture at 365 nm and room temperature under air. Most notably, new peaks at -71.81, -72.30, -78.80 and -80.49 ppm were found, which are indicative of the formation of *o*-DA adducts according to our previous photoreactivity experiments with **DTE-(COCF$_3$)$_2$** and ***o*-MBA-S** (see Section VI.5.3). However, longer reaction times were required in this case to observe full disappearance of the^{19}F NMR signals from starting **DTE-Dimer** (~ 20 h), probably because less equivalents of ***o*-MBA-T** were employed. As a consequence, the rates of photogeneration of the reactive *o*-QDM enes should be slower due to the competitive UV absorption by **DTE-Dimer**.

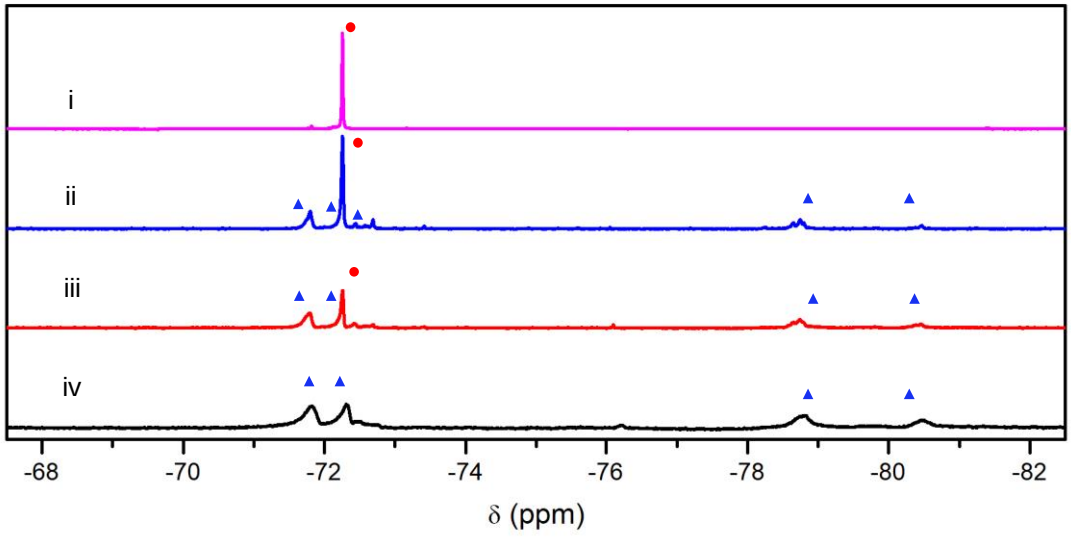

Figure VI-16. ^{19}F NMR spectra (250 MHz, toluene-d_8) of: (i) **DTE-Dimer$_o$**; (ii) a mixture of **DTE-Dimer** and ***o*-MBA-T** in deuterated toluene after UV illumination for 2 hours (LED 365, 0.017 mW cm^{-2}) and posterior red light irradiation for 1 min (LED 625 nm, 5.0 mW cm^{-2}); (iii) a mixture of **DTE-Dimer** and ***o*-MBA-T** in deuterated toluene after UV illumination for 6 hours (LED 365, 0.017 mW cm^{-2}) and subsequent red light irradiation for 1 mi (LED 625, 5.0 mW cm^{-2}); (iv) a mixture of **DTE-Dimer** and ***o*-MBA-T** in deuterated toluene after UV illumination for 20 hours (LED 365, 0.017 mW cm^{-2}) followed by red light irradiation for 1 min (LED 625, 5.0 mW cm^{-2}). For clarity, the ^{19}F NMR resonances in each spectrum arising from the open state of **DTE-Dimer** (red ●) and of the *o*-DA adducts (blue ▲) are indicated with different symbols.

Prompted by these results obtained at a small scale, the bulk copolymerization of **DTE-Dimer** and ***o*-MBA-T** was explored under UV irradiation. First, the *o*-DA-based cross-link process was attempted by mixing **DTE-Dimer** and ***o*-MBA-T** in toluene at a 3:2 molar ratio in various concentrations ranging from 0.25% to 2.5% wt. (LED 365 nm, 5 mW cm^{-2}). These experiments allowed us to determine that the minimum concentration needed to obtain a precipitated solid under our reaction conditions was 2% wt. Nevertheless, as a result of the large concentration demanded ($c_{\mathbf{DTE\text{-}dimer}}$ = 6.9 mM, $c_{\mathbf{o\text{-}MBA\text{-}T}}$ = 4.6 mM), very long irradiation times (>20 hours) were required that also led to an increasing amount of (photo)degradation products.

The UV-triggered generation to the *o*-QDM enes in ***o*-MBA-T** was seen as the limiting factor to minimize the photoreaction times due to lower extinction coefficient of ***o*-MBA-T** compared to **DTE-Dimer**. For this reason, we explored a different strategy to produce solid cross-linked networks upon UV irradiation of **DTE-Dimer** - ***o*-MBA-T** mixtures in shorter times: to start the process with a defect of **DTE-Dimer** (1:0.25 equivalent ratio), and sequentially adding more of this reagent until reaching a 1:0.75 equivalent ratio by the end of the reaction. In this manner, 10.5 hours of UV irradiation were needed to observe the appearance of the blue solid shown by the inverted tube in Figure VI-17. When analysing the reaction mixture by ^{19}F NMR at this point, we observed that most of the DTE moieties of **DTE-Dimer** in solution had underwent *o*-DA cycloaddition. Unfortunately, we also saw the presence of about 6% of photodegradation products in solution.

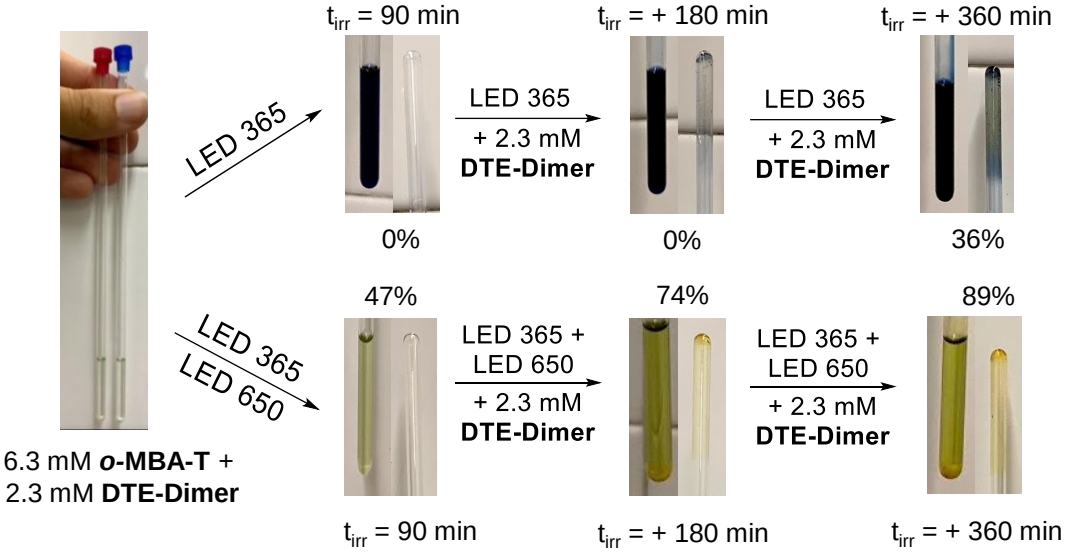

Figure VI-17. Pictures of NMR tubes containing ***o*-MBA-T** and **DTE-Dimer** in toluene-d_8 upon irradiation with LED 365 (5 mW cm^{-2}) and LED 625 nm (1300 mW cm^{-2}) for different times (t_{irr}). The starting concentrations were $c_{\mathbf{o\text{-}MBA\text{-}T}}$ = 6.3 mM and $c_{\mathbf{DTE\text{-}Dimer}}$ = 2.3 mM, and further additions of **DTE-dimer** were carried out as indicated. The percentages in each photograph indicate the amount of unreacted DTE moieties present in solution as determined by ^{19}F NMR.

Once optimized the conditions for the photopolymerization process under UV irradiation, concurrent photoexcitation with red light was applied to demonstrate that the cross-link reaction could be inhibited under two-color illumination. Unfortunately, the formation of a yellowish solid was observed in this case, despite little conversion of the initial reagents to the corresponding *o*-DA cycloadducts was observed by ^{19}F NMR (Figure VI-17). Such findings suggested that the solid formed was not due to *o*-DA-based cross-linking, but to a competitive secondary reaction.

To shed light on this issue, several additional experiments were conducted. First, analogous photoreaction experiments were conducted under inert atmosphere, but the same results were obtained. Second, MS analysis of the solids produced under UV irradiation and upon combined UV and visible illumination was attempted, but no clear conclusions could be inferred. Finally, separate irradiation experiments of **DTE-Dimer** and ***o*-MBA-T** under the reaction conditions and only visible light were performed. For **DTE-Dimer** the formation of significant amounts of yellowish byproducts was observed under UV irradiation, probably because of photodegradation, but no precipitate was found. By contrast, 365 nm irradiation of ***o*-MBA-T** in the absence of **DTE-Dimer** did result in the appearance of a precipitate, which was attributed to the dimerization of the photogenerated *o*-QDMs due to the long irradiation times and high irradiation intensities required. No reaction was seen upon irradiation with 625 nm. As a result, cross-linking of ***o*-MBA-T** should take place, eventually producing an insoluble network that precipitates in our reaction mixture.

Based on these results, we hypothesized that the preparation of solid materials based on our system would require the use of lower concentrations of the photoactive species as: (a) it would increase the light penetration in the sample; (b) lower irradiation times would be required and thus decrease the amount of photodegradation by-products; and (c) lower intensities could be employed which should diminish the dimerization processes which have a quadratic relation with the light intensity. This could be achieved by functionalizing a polymer with ***o*-MBA-S** moieties and employ **DTE-Dimer** as a crosslinking agent.

VI.8. SUMMARY AND CONCLUSIONS

In this chapter we explored a novel strategy to achieve two-color control of Diels-Alder cycloadditions by combining DTE-based photoisomerizable dienophiles with photogenerated *o*-quinodimethane dienes. The main results and conclusions obtained were the following:

- Three different model DTE photoswitches were successfully synthesized to test two complementary strategies to derive photoswitchable dienophiles:

(a) **DTE-Mal** bearing a maleimide dienophile as a central ring in its open state, which should be removed upon photocyclization with UV light.
(b) **DTE-NO_2-COOMe** and **DTE-$(COCF_3)_2$**, whose ring-closing isomerization with visible light should selectively create electron-poor olefins in their thiophene rings with potential dienophile activity.

- **DTE-Mal**, **DTE-NO_2-COOMe** and **DTE-$(COCF_3)_2$** operate as molecular switches interconverting between open and closed states under irradiation with UV and visible light. Because they lack the electron density gradient found in other DTEs prepared along this thesis, they showed very good photochemical properties, with **DTE-$(COCF_3)_2$** and **DTE-NO_2-COOMe** exhibiting nearly quantitatively photoisomerization between their two isomers.

- Preliminary photoreactivity studies revealed the failure of the strategies devised for the two-color control of Diels-Alder cycloadditions :
  (a) The open isomer of **DTE-Mal** failed to react with *o*-QDM dienes, probably due to steric congestion around its maleimide moiety.
  (b) The low reactivity of the electron-poor olefin created in **DTE-NO_2-COOMe** and **DTE-$(COCF_3)_2$** upon photocyclization prevented Diels-Alder cycloaddition with *o*-QDM dienes.

- A UV-induced *oxo*-Diels-Alder reaction was instead observed to occur between the trifluoromethyl ketone moieties in **DTE-$(COCF_3)_2$** and *o*-QDM dienes. Because this reaction is driven by the electron deficiency in the carbonyl dienophile, it was found to be especially favored for the closed isomer of **DTE-$(COCF_3)_{2c}$** because of the electronic communication selectively established in this state between the two trifluoroacetyl groups. Actually, the removal of such effect produced a dramatic decrement in the reaction rate of the *oxo*-Diels-Alder cycloaddition.

- Two-color control of the *oxo*-Diels-Alder reaction between **DTE-$(COCF_3)_2$** and *o*-QDM diene precursors could be demonstrated. While irradiation with UV light efficiently induced the photoligation process by generating the reactive dienophile and diene species, simultaneous illumination with red light effectively halted the reaction by deactivating the DTE-based dienophile upon photoisomerization.

- Attempts to apply this *oxo*-Diels-Alder reactive system to the two-color control of polymerization processes were unsuccessful. Although a dimer of the DTE-based photoisomerizable dienophile and a trimer of the *o*-QDM diene precursor were prepared and shown to undergo dual-wavelength gated *oxo*-Diels-Alder cycloaddition at low concentrations, this behavior could not be transferred to photocontrol the formation of bulk cross-linked polymer matrices. We ascribed this result to the photodegradation and photodimerization of the *o*-QDM diene precursor, which are favored by the high concentrations and long irradiation times

required for the *oxo*-Diels-Alder-based photopolymerization process. Further studies are therefore needed to demonstrate the potential applicability of the two-color controlled photoligation system developed in this chapter.

VI.9. REFERENCES

1 M. Kathan and S. Hecht, *Chem. Soc. Rev.*, 2017, **46**, 5536–5550.

2 R. Göstl and S. Hecht, *Angew. Chem. Int. Ed.*, 2014, **53**, 8784–8787.

3 A. Fuhrmann, R. Göstl, R. Wendt, J. Kötteritzsch, M. D. Hager, U. S. Schubert, K. Brademann-Jock, A. F. Thünemann, U. Nöchel, M. Behl and S. Hecht, *Nat. Commun.*, 2016, **7**, 13626.

4 J. Kida, K. Imato, R. Goseki, D. Aoki, M. Morimoto and H. Otsuka, *Nat. Commun.*, 2018, **9**, 1–6.

5 V. Lemieux and N. R. Branda, *Org. Lett.*, 2005, **7**, 2969–2972.

6 V. Lemieux, S. Gauthier and N. R. Branda, *Angew. Chem. Int. Ed.*, 2006, **45**, 6820–6824.

7 Z. Erno, A. M. Asadirad, V. Lemieux and N. R. Branda, *Org. Biomol. Chem.*, 2012, **10**, 2787–2792.

8 A. M. Asadirad, S. Boutault, Z. Erno and N. R. Branda, *J. Am. Chem. Soc.*, 2014, **136**, 3024–3027.

9 N. Zydziak, W. Konrad, F. Feist, S. Afonin, S. Weidner and C. Barner-Kowollik, *Nat. Commun.*, 2016, **7**, 1–10.

10 O. Altintas, J. Willenbacher, K. N. R. Wuest, K. K. Oehlenschlaeger, P. Krolla-Sidenstein, H. Gliemann and C. Barner-Kowollik, *Macromolecules*, 2013, **46**, 8092–8101.

11 T. K. Claus, B. Richter, V. Hahn, A. Welle, S. Kayser, M. Wegener, M. Bastmeyer, G. Delaittre and C. Barner-Kowollik, *Angew. Chem. Int. Ed.*, 2016, **55**, 3817–3822.

12 T. Pauloehrl, G. Delaittre, V. Winkler, A. Welle, M. Bruns, H. G. Börner, A. M. Greiner, M. Bastmeyer and C. Barner-Kowollik, *Angew. Chem. Int. Ed.*,

2012, **51**, 1071–1074.

13 L. Chen, M. Xu, J. Hu and Q. Yan, *Macromolecules*, 2017, **50**, 4276–4280.

14 B. Yang and S. Gao, *Chem. Soc. Rev.*, 2018, **47**, 7926–7953.

15 J. L. Segura and N. Martín, *Chem. Rev.*, 1999, **99**, 3199–3246.

16 T. Krappitz, F. Feist, I. Lamparth, N. Moszner, H. John, J. P. Blinco, T. R. Dargaville and C. Barner-Kowollik, *Mater. Horizons*, 2019, **6**, 81–89.

17 A. S. Quick, H. Rothfuss, A. Welle, B. Richter, J. Fischer, M. Wegener and C. Barner-Kowollik, *Adv. Funct. Mater.*, 2014, **24**, 3571–3580.

18 F. Feist, L. L. Rodrigues, S. L. Walden, T. W. Krappitz, T. R. Dargaville, T. Weil, A. S. Goldmann, J. P. Blinco and C. Barner-Kowollik, *J. Am. Chem. Soc.*, 2020, **142**, 7744–7748.

19 P. Mueller, M. M. Zieger, B. Richter, A. S. Quick, J. Fischer, J. B. Mueller, L. Zhou, G. U. Nienhaus, M. Bastmeyer, C. Barner-Kowollik and M. Wegener, *ACS Nano*, 2017, **11**, 6396–6403.

20 F. Feist, J. P. Menzel, T. Weil, J. P. Blinco and C. Barner-Kowollik, *J. Am. Chem. Soc.*, 2018, **140**, 11848–11854.

21 M. Irie, T. Fukaminato, K. Matsuda and S. Kobatake, *Chem. Rev.*, 2014, **114**, 12174–12277.

22 E. Surmiak, A. Twarda-Clapa, K. M. Zak, B. Musielak, M. D. Tomala, K. Kubica, P. Grudnik, M. Madej, M. Jablonski, J. Potempa, J. Kalinowska-Tluscik, A. Dömling, G. Dubin and T. A. Holak, *ACS Chem. Biol.*, 2016, **11**, 3310–3318.

23 L. N. Lucas, J. J. D. De Jong, J. H. Van Esch, R. M. Kellogg and B. L. Feringa, *Eur. J. Org. Chem.*, 2003, 155–166.

24 S. M. Büllmann and A. Jäschke, *Chem. Commun.*, 2020, **56**, 7124–7127.

25 J. D. Einkauf, R. E. Ortega, L. Mathivathanan and D. T. De Lill, *New J. Chem.*, 2017, **41**, 10929–10934.

26 M. J. Rudolph, C. R. Illig, N. L. Subasinghe, K. J. Wilson, J. B. Hoffman, T.

Randle, D. Green, C. J. Molloy, R. M. Soll, F. Lewandowski, M. Zhang, R. Bone, J. C. Spurlino, I. C. Deckman, C. Manthey, C. Sharp, D. Maguire, B. L. Grasberger, R. L. DesJarlais and Z. Zhou, *Bioorg. Med. Chem. Lett.*, 2002, **12**, 491–495.

27 P. J. Milner, Y. Yang and S. L. Buchwald, *Organometallics*, 2015, **34**, 4775–4780.

28 S. Hiroto, K. Suzuki, H. Kamiya and H. Shinokubo, *Chem. Commun.*, 2011, **47**, 7149–7151.

29 K. A. Jorgensen, *Angew. Chem. Int. Ed.*, 2000, **39**, 3558–3588.

30 M. F. Hentemann, J. G. Allen and S. J. Danishefsky, *Angew. Chem. Int. Ed.*, 2000, **39**, 1937–1940.

31 D. Janssen-Müller, S. Singha, T. Olyschläger, C. G. Daniliuc and F. Glorius, *Org. Lett.*, 2016, **18**, 4444–4447.

32 K. Takaki, T. Fujii, H. Yonemitsu, M. Fujiwara, K. Komeyama and H. Yoshida, *Tetrahedron Lett.*, 2012, **53**, 3974–3976.

33 W. Wang, A. Kapur, X. Ji, M. Safi, G. Palui, V. Palomo, P. E. Dawson and H. Mattoussi, *J. Am. Chem. Soc.*, 2015, **137**, 5438–5451.

34 Y. Gu, E. A. Alt, H. Wang, X. Li, P. Adam and J. A. Johnson, *Nature*, 2018, **560**, 65–69.

35 J. S. Zakhari, I. Kinoyama, M. S. Hixon, A. Di Mola, D. Globisch and K. D. Janda, *Bioorg. Med. Chem.*, 2011, **19**, 6203–6209.

36 B. M. Kiran and N. Jayaraman, *Macromolecules*, 2009, **42**, 7353–7359.

Chapter VII

Summary and conclusions

This thesis focused on the development of photofunctional materials and processes based on molecular switches. More precisely, it was centered on two main topics: (a) the use of spirocyclic zwitterionic Meisenheimer complexes for the preparation of multistimuli-responsive and multistate chromic and fluorescent materials; and (b) the application of dithienylethene switches to the modulation of chemical reactivity with light. In this chapter, the main results and conclusions obtained from the work conducted are summarized.

VII.1. Stimuli-responsive chromic and fluorescent materials based on spirocyclic zwitterionic Meisenheimer complexes

From a fundamental point of view, new switching states and stimuli were established for the family of spirocyclic zwitterionic Meisenheimer complexes. On the one hand, the multistate character of SZMCs was broadened by identifying a novel cationic state with distinctive optical properties, which could be achieved electrochemically or via acid addition. On the other hand, we extensively investigated the thermo(fluoro)chromic behavior of SZMCs as well as demonstrated that they can respond to certain ions and solvents. This multistimuli-responsive and multistate character was then exploited for the preparation of a variety of photofunctional materials based on SZMCs: wide-range pH detectors, electro(fluoro)chromic displays, and thermal, ionic and solvent sensors (Figure VII-1).

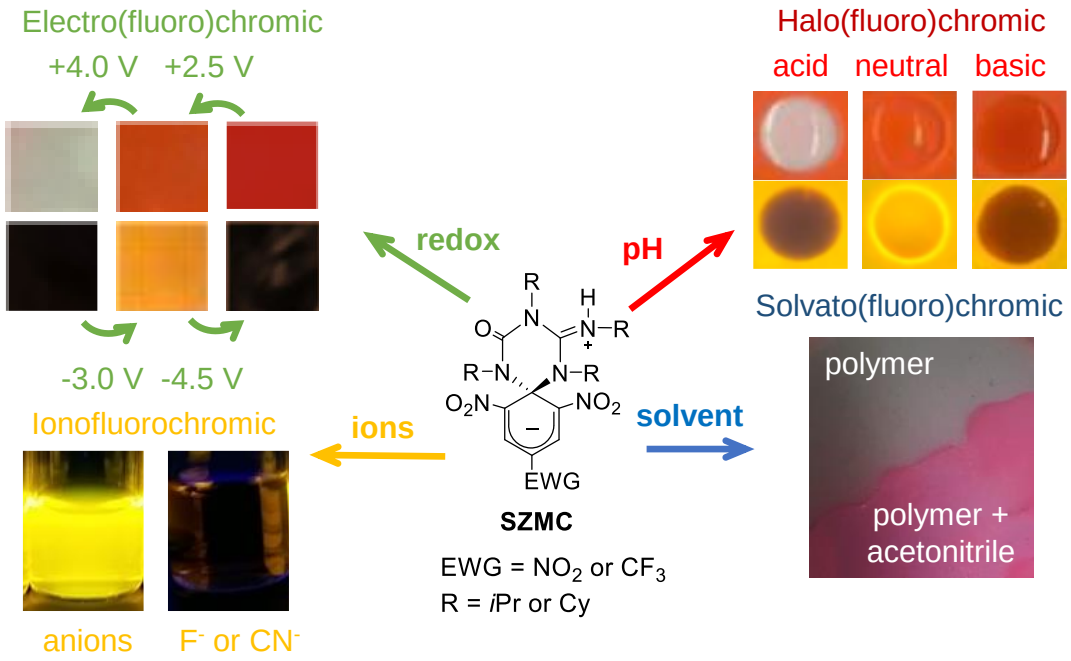

Figure VII-1. Main switching mechanisms and responses studied in this thesis for SZMCs.

VII.2. LIGHT-CONTROLLED CHEMICAL REACTIVITY BASED ON DITHIENYLETHENE PHOTOSWITCHES

Up to three different types of reactions were attempted to be controlled with light using dithienylethene photoswitches in this thesis: (a) the acidity of phenols, (b) amide bond formation reactions, and (c) Diels-Alder cycloadditions.

- To explore the photocontrol of the acidity of phenols, a series of **DTE-EWG** compounds were synthesized and characterized composed of a photoisomerizable DTE core bearing phenol and electron-withdrawing substituents on the external positions of the thiophene rings (Figure VII 2). This allowed us uncovering the main factors leading to large pK_a modulation of the phenol moiety upon DTE photoisomerization between its open and closed states. The best results were achieved for **DTE-EWG** functionalized with nitro and trifluoroacetyl substituents, which were found to show ample phenol acidity variation when irradiated with light: $\Delta pK_a \sim 5.0$ in acetonitrile, which we estimated to correspond to $\Delta pK_a \approx 3.0$ in water, thus matching the largest values reported to date with other diarylethene systems.

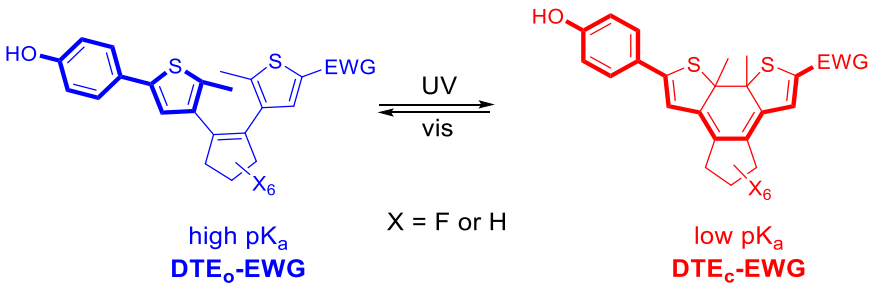

Figure VII-2. Schematic representation of our strategy to achieve photomodulation of phenol acity using **DTE-EWG** compounds.

- Based on the results obtained for **DTE-EWG**, a novel strategy was devised and demonstrated to photocontrol amide bond formation using two colors of light: the preparation of esters of **DTE-EWG** phenols, whose quality as leaving groups in amidation reactions changes upon photoisomerization due to the variation in phenolate basicity. This approach was validated with phenolate esters bearing a nitro EWG, whose amidation reaction with primary amines was successfully photocontrolled by: (a) irradiation at 365 nm, which transformed the system to its active closed form; and (b) illumination 625 nm, which converted the switch back to the inactive open form (Figure VII-3). In this manner, we did not only demonstrate the dual-color control of photoligation via amide bond formation, but

also expanded this approach to DTE-based esters bearing functional units such as fluorescent groups.

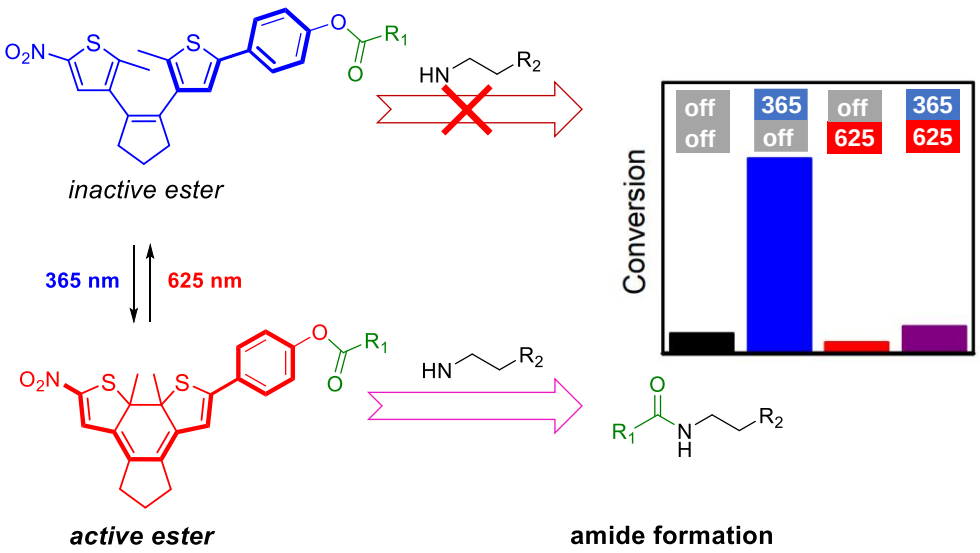

Figure VII-3. Dual-color photomodulation of amide formation by employing DTE-based photoisomerizable phenolate esters.

- Two complementary strategies were assayed for the dual-color control of Diels-Alder cycloadditions between UV-generated *o*-quinodimethane dienes and DTE-based photoisomerizable dienophiles. Although none of them was found to work because of steric and electronic effects, the photomodulation of a similar type of photoligation reaction could be demonstrated: the *oxo*-Diels-Alder cycloaddition between *o*-QDM enes and trifluoromethyl ketone dienophiles appended to DTE switches. The dual-color control over this system was successfully demonstrated by: (a) activation of the diene and dienophile upon irradiation at 365 nm, and (b) deactivation of the DTE-based dienophile upon irradiation at 625 nm (Figure VII-4). Unfortunately, the attempts to apply this strategy to photocontrol polymer network formation were unsuccessful due to competitive photoreactions affecting the *o*-QDM dienes.

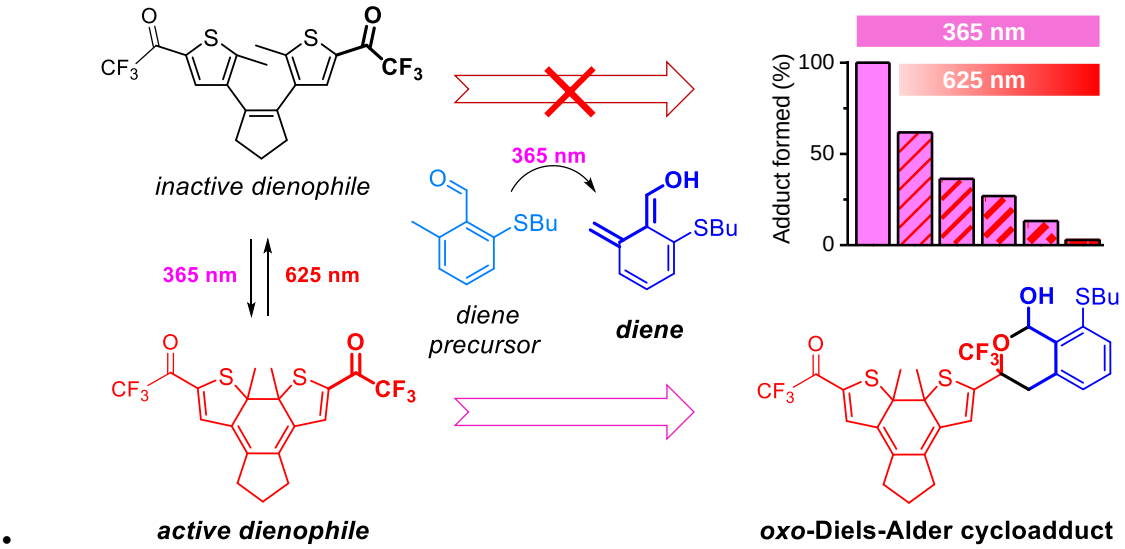

Figure VII-4. Two-color gated *oxo*-Diels-Alder reaction between DTE-tethered trifluoromethyl ketone dienophiles and *o*-QDM precursors.

Chapter VIII

Experimental section

VIII.1. MATERIALS AND INSTRUMENTATION

NMR spectra were recorded on Bruker DPX250 (250 MHz for ^{1}H), DPX360 (360MHz for ^{1}H), AvanceIII 400NB (400 MHz for ^{1}H) and Bruker System 600 Ascend LH (600 MHz for ^{1}H). The δ-scale was normalized relative to the residual solvent signal for ^{1}H NMR and ^{13}C NMR ($CDCl_3$ (7.26 ppm for ^{1}H; 77.2 ppm for ^{13}C), CD_3CN (1.94 ppm for ^{1}H; 118.3 and 1.3 ppm for ^{13}C), DMF-d^7 (8.03, 2.92 and 2.75 ppm for ^{1}H; 163.2, 34.9 and 29.8 ppm for ^{13}C), acetone-d^6 (2.05 ppm for 1H; 206.2 and 29.8 ppm for ^{13}C), DMSO-d^6 (2.50 ppm for ^{1}H; 39.5 ppm for ^{13}C), CD_2Cl_2 (5.32 ppm for ^{1}H; 54.0 ppm for ^{13}C), THF-d^8 (3.58 and 1.73 ppm for ^{1}H; 67.6 and 25.4 ppm for ^{13}C), CD_3OD (3.31 ppm for ^{1}H; 49.0 ppm for ^{13}C) and C_7D_8 (7.09, 7.01, 6.97 and 2.08 ppm for ^{1}H; 137.5, 128.9, 128.0, 125.1 and 20.4 ppm for ^{13}C)) and relative to $CFCl_3$ for ^{19}F NMR (0.00 ppm in all the solvents). NMR signals for selected molecules were assigned with the help of COSY, HSQC, HMBC and DEPT135.

The abbreviations used to describe signal multiplicities are: s (singlet), d (doublet), t (triplet), q (quadruplet), p (pentuplet), h (hexaplet), sept (septuplet), dd (double doublet), dt (double triplet), dq (double quadruplet), tt (triple triplet) and m (multiplet).

IR-ATR spectra were recorded in a Bruker Tensor 27 Golden Gate spectrometer with a diamond tip.

UV/vis spectra were recorded on a Shimadzu UV-2700 spectrophotometer equipped with a CPS-100 electronic temperature-controlled cell positioner or on an Agilent HP 8453 spectrophotometer. Samples were measured in Hellma Analytics quartz high precision cells with a path length of 10 mm at ambient temperature. Photoswitch isomerization was investigated using a VL-6.M UV lamp (λ_{exc}= 312 nm, 6 W), a Nd:YAG pulsed laser as an excitation source (Brilliant, Quantel, λ_{exc}= 355 or 532 nm) and diode cw lasers at λ_{exc} = 405 (SciTech) and λ_{exc} = 650 nm, (SciTech) as irradiation sources. Photoisomerization quantum yields were determined using a procedure previously reported.[1] 1,2-bis(5-chloro-2-methyl-3-thienyl)perfluorocyclopentene ($\Phi_{o\text{-}c}$= 0.47 and $\Phi_{c\text{-}}$

$_{o}$ = 0.13 in hexane)[2] and 1,2-bis(5-phenyl-2-methyl-3-thienyl)perfluorocyclopentene ($\Phi_{o\text{-}c}$ = 0.59 and $\Phi_{c\text{-}o}$ = 0.013 in hexane) were used as references.[3]

Figure VIII-1 shows the emission spectra of the LED used in this work: (a) LED 365 (3 W LED λ_{max} = 365 nm) and (b) LED 625 (100 W LED λ_{max} = 625 nm).

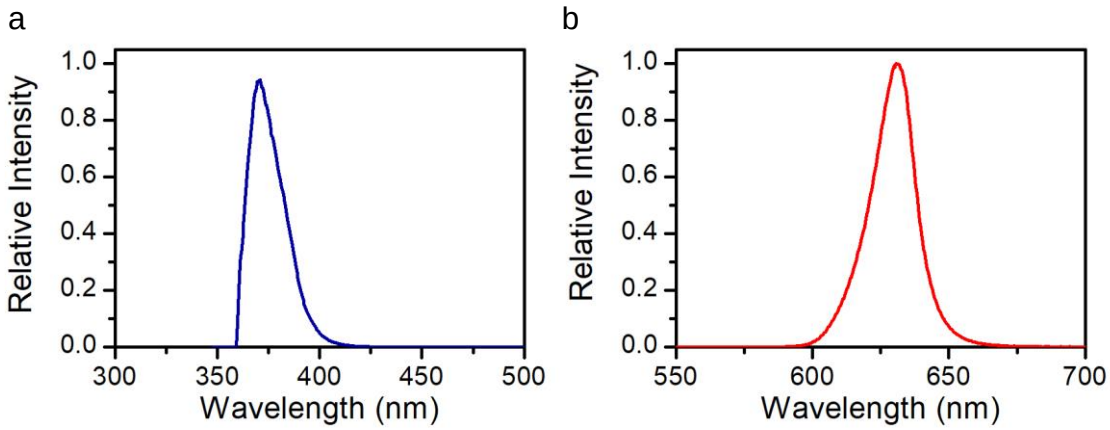

Figure VIII-1. Emission spectra of (a) LED 365 and (b) LED 625.

Fluorescence spectra were recorded by means of a custom-made spectrofluorometer using cw lasers (BeamQ, λ_{exc} = 473 nm; Z-laser, λ_{exc} = 532 nm) as excitation sources. Emitted photons were detected using an Andor ICCD camera coupled to a spectrograph. All the emission spectra registered were corrected by the wavelength dependence of the spectral response of the detection system. In all the cases spectroscopic quality solvents and 1 cm quartz cuvettes were used. Temperature was controlled using a refrigerated circulator bath (Huber MPC-K6) connected to the sample holder. Fluorescence quantum yields were determined using the standard method[4] for highly diluted solutions of the compounds of interest to prevent self-absorption processes (absorption <0.05 at the excitation wavelength) and relative to N,N′-bis(1-hexylheptyl)perylene-3,4,9,10-tetracarboxybismide in acetonitrile (Φ_{fl} = 1)[5] or N,N'-bis(butyl)-1,6,7,12-tetra-(4-tert-butylphenoxy)perylene-3,4:9,10-tetracarboxylicdiimide in CH_2Cl_2 (Φ_{fl} = 1).[6] The same excitation wavelength was used for both the sample of interest and the standard in all these measurements.

LC-MS measurements were performed on an UltiMate 3000 UHPLC System (Dionex) consisting of a pump (LPG 3400SZ, autosampler WPS 3000TSL) and a temperature-controlled column department (TCC 3000). Separation was performed on a C_{18} HPLC-column (Phenomenex Luna 5µm, 100 Å, 250 × 2.0 mm) operating at 40 °C. A gradient of CD_3CN:H2O 80:20 – 100:0 v/v at a flow rate of 0.40 mL·min^{-1} during 10 min was used as the eluting solvent. The flow was split in a 9:1 ratio, where 90% of the eluent were directed through the UV-detector (VWD 3400, Dionex, detector wavelengths 215, 254, 280, 360 nm) and 10% were infused into the electrospray source. Spectra were recorded on a LTQ Orbitrap Elite mass

spectrometer (ThermoFisher Scientific) equipped with an HESI II probe. The instrument was calibrated in the m/z range 74-1822 using premixed calibration solutions (Thermo Scientific). A constant spray voltage of 3.5 kV, a dimensionless sheath gas and a dimensionless auxiliary gas flow rate of 5 and 2 were applied, respectively. The capillary temperature and was set to 300 °C, the Slens RF level was set to 68, and the aux gas heater temperature was set to 125 °C.

Cyclic voltammograms were registered using a VSP100 BIOLOGIC potentiostat and a conical electrochemical cell equipped with an argon bubbling source for degassing, a glassy carbon working electrode (WE, d = 0.45 mm), a glassy carbon auxiliary electrode (CE, d = 3 mm) and a saturated calomel reference electrode (SCE, RE). All the potentials are reported versus a SCE isolated from the working electrode by a salt bridge. All measurements were performed in acetonitrile solution containing 0.1 M of n-Bu_4NPF_6 as a supporting electrolyte. Electrolysis experiments at controlled potentials were undertaken with a EG&G Princeton Applied Research (PAR) 273A potentiostat and an electrochemical cell equipped with an argon bubbling source, a carbon graphite rod, an auxiliary platinum electrode and a SCE reference electrode. All experiments were performed in acetonitrile solutions containing n-Bu_4NPF_6 (0.1 M) as a supporting electrolyte.

Spectroelectrochemical experiments were performed in a 1 mm thin layer quartz glass cell using platinum gauze and platinum wire as working and counter electrodes, respectively, whereas a saturated calomel electrode (SCE) was used as a reference electrode. A PC-controlled VSP-Potentiostat synchronized with an MMS-UV−vis high speed diode array spectrometer with a bandwidth of 330−1100 nm and a deuterium/ tungsten light source (HM) and optical fiber (SMA, J&M) was employed to register the spectroelectrochemical measurements. Each spectrum was recorded after 0.05 s. BioKine32 software was used for data acquisition and treatment.

pH measurements upon acid−base addition on acetonitrile solutions of 1 were performed at room temperature with a Crison 5028 pH electrode in a Crison BASIC 20+ potentiometer. pH values are given relative to the acetonitrile solvent ($^{s}_{s}$pH scale).[7] To calibrate the electrode system we used reference buffers in acetonitrile (pyridine-pyridinium bromide, phenol-sodium phenolate and 4-nitrophenol-sodium 4-nitrophenolate), whose $^{s}_{s}$pH can be derived from the Henderson−Hasselbach equation using the pKa values in acetonitrile reported forthese systems.[7] The equation $pK_{a,H2O} = 0.58\ pK_{a,ACN} - 5.45$ was obtained from the correlation between the pK_a values of several phenols in water and acetonitrile (Figure VIII-2).[7]

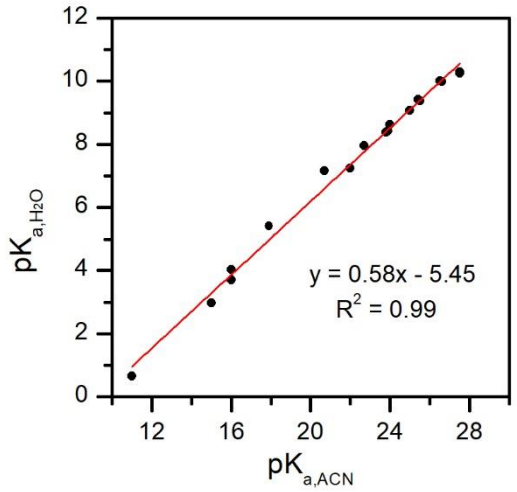

Figure VIII-2. Correlation between $pK_{a,ACN}$ and $pK_{a,H2O}$ for several substituted phenols.[7]

VIII.2. SYNTHESIS OF SZMC

VIII.2.1. Synthesis of SZMC1

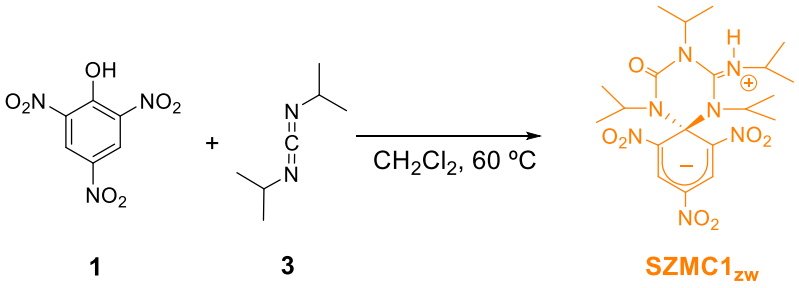

1 **3** **SZMC1$_{zw}$**

A solution of 0.140 g of **1** (0.62 mmol) in CH_2Cl_2 (10 mL) was slowly added to a solution of 0.79 g of **3** (6.2 mmol) in 5 mL of CH_2Cl_2. The reaction mixture was stirred at room temperature under argon atmosphere for 4 h. The organic solvent was removed under reduced pressure and the resulting solid redissolved in hot methanol (15 mL). Water (10 mL) was then added to this solution and stored at 0 ºC for 72 h. A gelatinous mass was separated and purified by flash column chromatography (silica gel, hexane/ethyl acetate, 3:2), which yielded 0.105 g of the target product **SZMC1$_{zw}$** (0.22 mmol, 35% yield).

^{1}H NMR (360 MHz, $CDCl_3$): δ (ppm) 8.80 (s, 2H) 4.21 (m, 1H), 3.87 (sept, *J* = 7.2, 1H), 4.74 (sept, *J* = 6.6 Hz, 1H), 4.30 (d, *J* = 6.9 Hz, 1H), 3.24 (sept, *J* = 6.9 Hz, 1H), 1.66 (d, *J* = 6.6 Hz, 6H), 1.38 (d, *J* = 6.3 Hz, 6H), 1.22 (d, *J* = 7.2 Hz, 6H), 1.11 (d, *J* = 6.9 Hz, 6H).

^{13}C NMR (75 MHz, $CDCl_3$) : δ (ppm) 154.7, 145.0, 130.8, 125.5, 120.1, 82.3, 58.4, 53.1, 51.1, 51.0, 24.1, 23.1, 22.0, 19.0.

IR (KBr, cm^{-1}): 3449, 2978, 1709, 1586, 1523, 1488, 1316,1280, 1205, 1194, 1051.

HRMS (ESI-QTOF): m/z calcd for $C_{20}H_{32}N_7O_7^+$: 482.2358 $[M-H]^+$; found: 482.2353.

VIII.2.2. Synthesis of SZMC2

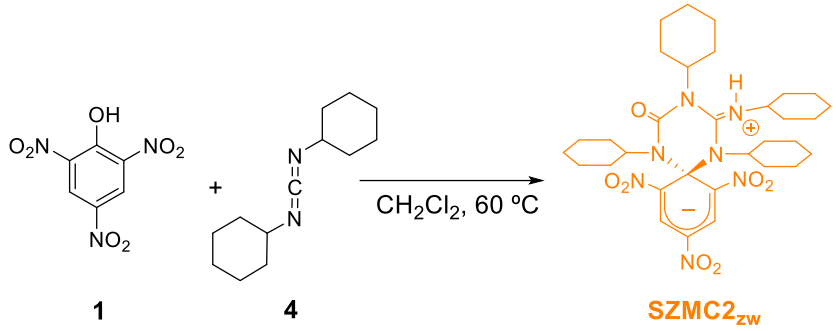

A solution containing 1.2 g of **4** (5.8 mmol) in 5 mL of CH_2Cl_2 was slowly added to a dichloromethane solution (10 mL) containing 0.13 g of **1** (0.58 mmol). This mixture was stirred at room temperature and under Ar atmosphere for 4 h. Afterwards, the solvent was evaporated in vacuo and the resulting solid was redissolved in 15 mL of hot methanol. Water (10 mL) was then added to this solution and it was stored at 0º for 12 h. After this treatment, the sample separated into a liquid and a jelly-like phases, which were separated by filtration. The crude was then purified through flash column chromatography (silica gel, hexane/ethyl acetate, 3:2) to isolate 0.082 g of **SZMC2$_{zw}$** (0.13 mmol, 22% yield).

.

^{1}H NMR (360 MHz, $CDCl_3$): δ (ppm) 9.03 (s, 2H), 4.53 (d, *J* = 9.0 Hz, 1H), 3.65 (tt, *J* = 11.7, 3.2 Hz, 1H), 3.48 (m, 1H), 3.29 (m, 1H), 2.64 (tt, *J* = 11.9, 3.6 Hz, 1H), 2.49 (q, *J* = 11.9 Hz, 2H), 2.34–1.50 (m, 20H), 1.43–0.92 (m, 18H).

IR (KBr, cm^{-1}): 3417, 2938, 2854, 1706, 1586, 1512, 1488, 1430, 1247

HRMS (ESI-QTOF): m/z calcd for $C_{32}H_{48}N_7O_7^+$: 642.3610 $[M-H]^+$; found: 642.3601.

VIII.2.3. Synthesis of SZMC3

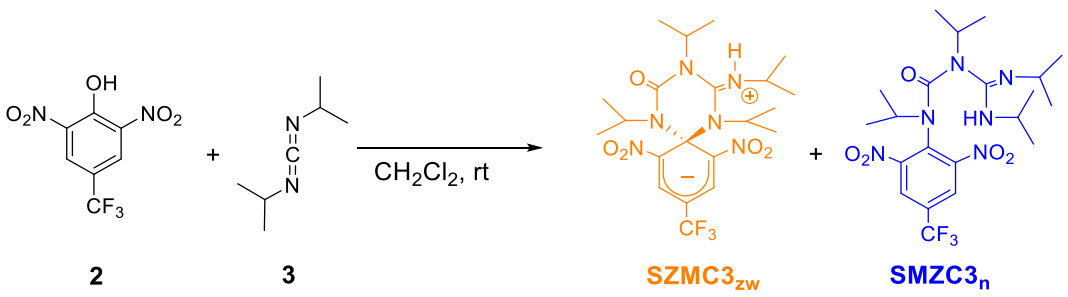

A solution containing 12 g of **3** (95.0 mmol) in 20 mL of CH_2Cl_2 was slowly added to a dichloromethane solution (35 mL) containing 2.5 g of **2** (9.9 mmol). This mixture was stirred at room temperature and under Ar atmosphere for 4 h. Afterwards, the solvent was evaporated in vacuo and the resulting solid was redissolved in 120 mL of hot methanol. Water (80 mL) was then added to this solution and it was stored at 0º for 72 h. After this treatment, the sample separated into a liquid and a jelly-like phases, which were separated by filtration. The crude was then purified through flash column chromatography (silica gel, hexane/ethyl acetate, 3:2) to isolate 1.30 g of an irresoluble mixture of **SZMC3$_n$** and **SZMC3$_{zw}$** (2.6 mmol, 26% yield).

^{1}H NMR (400 MHz, CD_3CN): δ (ppm) 8.51 (s, 2H, **SZMC3$_{zw}$**), 8.19 (s, 2H, **SZMC3$_n$**), 4.64 (m, 1H, **SZMC3$_n$**), 4.53 (sept, *J* = 6.7 Hz, 1H, **SZMC3$_{zw}$**), 4.19 (sept, *J* = 6.6 Hz, 1H, **SZMC3$_n$**), 3.97 (m, 1H, **SZMC3$_n$**), 3.93-3.78 (m, 1H, **SZMC3$_n$**, 1H, **SZMC3$_{zw}$**), 3.55-3.25 (m, 3H, **SZMC3$_{zw}$**), 3.19 (sept, *J* = 6.7 Hz, 1H, **SZMC3$_n$**), 1.64 (d, *J* = 7.1 Hz, 6H, **SZMC3$_n$**), 1.38 (d, *J* = 7.1 Hz, 6H, **SZMC3$_n$**), 1.24 (d, *J* = 7.1 Hz, 6H, **SZMC3$_n$**), 1.14 (d, *J* = 7.1 Hz, 6H, **SZMC3$_n$**), 1.11 (d, *J* = 7.1 Hz, 6H, **SZMC3$_{zw}$**), 0.98 (d, *J* = 7.1 Hz, 6H, **SZMC3$_{zw}$**), 0.93-0.74 (m, 12H, **SZMC3$_{zw}$**);

^{13}C NMR (100.6 MHz, CD_3CN) : δ (ppm) 157.1, 154.1, 150.6, 149.0, 142.1, 134.2, 132.5, 129.9 (q, *J* = 35.9 Hz), 127.6 (q *J* = 3.0 Hz), 124.7, 124.4 (q, *J* = 265.6 Hz), 121.9 (q, *J* = 273.6 Hz), 97.2 (q, *J* = 34.5 Hz), 82.8, 57.7, 55.1, 54.2, 51.8, 51.7, 51.4, 46.9, 43.3, 24.3, 23.7, 22.1, 21.1, 20.9, 20.2, 19.6, 18.6.

IR (KBr, cm^{-1}): 3417, 2938, 2854, 1706, 1586, 1512, 1488, 1430, 1247.

HRMS (ESI-QTOF): m/z calcd for $C_{21}H_{32}F_3N_6O_5^+$: 505.2386 $[M-H]^+$; found: 505.2385.

VIII.2.4. Synthesis of SZMC4

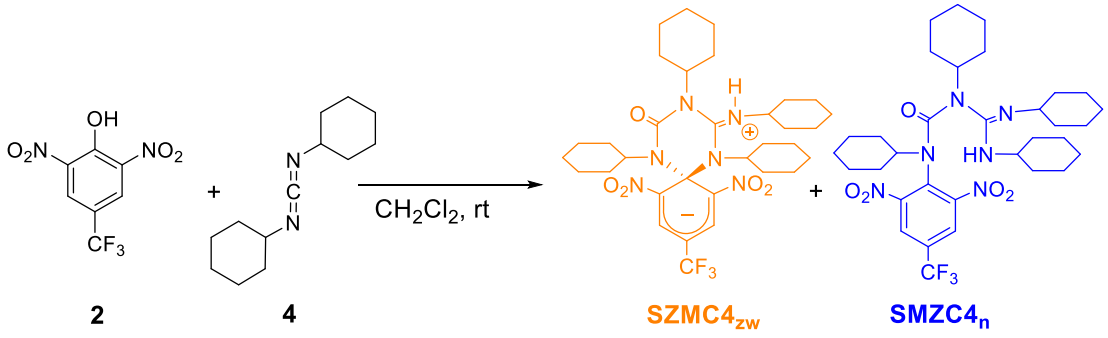

A solution of 2.5 g of **2** (9.9 mmol) in CH_2Cl_2 (35 mL) was slowly added to a solution of 18.6 g of **4** (95.0 mmol) in 20 mL of CH_2Cl_2. The reaction mixture was stirred at room temperature under argon atmosphere for 4 h. The organic solvent was removed under reduced pressure and the resulting solid redissolved in hot methanol (120 mL). Water (80 mL) was then added to this solution and stored at 0 ºC for 72 h. A

gelatinous mass was separated and purified by flash column chromatography (silica gel, hexane/ethyl acetate, 3:2), which yielded 0.80 g of the target product **SZMC4** as an irresoluble mixture of isomers **SZMC4$_{zw}$** and **SZMC4$_{n}$** (1.2 mmol, 11% yield).

^{1}H NMR (400 MHz, CD_3CN): δ (ppm) 8.48 (s, 2H, **SZMC4$_{zw}$**), 8.20 (s, 2H, **SZMC4$_{n}$**), 4.17 (m, 1H, **SZMC4$_{zw}$**), 4.12 (m, 1H, **SZMC4$_{n}$**), 3.45 (m, 1H, **SZMC4$_{zw}$**), 3.40 (m, 1H, **SZMC4$_{n}$**), 3.08 (m, 2H, **SZMC4$_{zw}$**, 2H, **SZMC4$_{n}$**), 1.70-1.35 (m, 20H, **SZMC4$_{zw}$**, 20H, **SZMC4$_{n}$**), 1.34-1.13 (m, 18H, **SZMC4$_{zw}$**, 18H, **SZMC4$_{n}$**).

^{13}C NMR (100.6 MHz, CD_3CN) : δ (ppm) 164.3, 157.9, 135.3, 130.8 (q, J = 37.6 Hz), 128.6, 123.0 (q, J = 267.1 Hz), 79.1, 64.7, 60.7, 56.2, 34.8, 32.8, 31.4, 29.3, 29.0, 25.5, 25.4, 25.3, 24.7.

IR (KBr, cm^{-1}): 2928, 2854, 1629, 1552, 1450, 1342, 1313, 1176, 1138, 897, 753, 718.

HRMS (ESI-QTOF): m/z calcd for $C_{33}H_{48}F_3N_6O_5^+$: 665.3638 $[M-H]^+$; found: 665.3632.

VIII.2.5. Fabrication of Electrofluorochromic Ion Gels.

Electrofluorochromic ion gels were prepared following the procedure described in ref 53 by codissolving 150 mg of 1-butyl-3-methylimidazolium bis(trifluoromethylsulfonyl)imide, 36 mg of poly(vinylidene fluoride-co-hexafluoropropylene), 9 mg of 1b and, when necessary, 5 mg of 1,1′-dimethylferrocene in 3 mL of acetone. The mixture was fully dissolved after heating at 50 °C for a few minutes. The solution was cast onto a glass slide and, after solvent evaporation, a flexible ion gel was obtained. The “cut-and-stick” strategy[8] was then followed to measure the electrochromic and electrofluorochromic behavior of the ion gels prepared, for which they were cut and the thin films obtained were sandwiched between two ITO-coated glass substrates that were fixed using double-sided tape

VIII.2.6. Preparation of Polymer Thin Films.

- **Halochromic PMMA film**

Halochromic polymer films were prepared by dissolving 143 mg of PMMA (Mw = 120 000) in 5 mL of chloroform. Afterward, 2 mg of **SZMC1** were added to the mixture and the solution was poured into a Petri dish (6 cm in diameter). The solution was left to evaporate over 2 h at room temperature to obtain an orange, fluorescent film (∼1 mm in thickness).

- **Acetonitrile sensitive PS film**

Acetonitrile sensitive films were prepared by dissolving 150 mg of PS (Mw = 350 000) in 5 mL of chloroform upon sonication. Afterwards, 2 mg of **SZMC3** were added to the mixture and the solution was poured into a Petri dish (6 cm in diameter). The solution was left to evaporate over 2 h at room temperature to obtain a homogeneous, almost colorless PS film (~1 mm in thickness). Another set of acetonitrile-sensitive films were prepared by dissolving

- **Acetonitrile sensitive PVA film**

93 mg of PVA (Mw = 125000) in 5 mL of hot water. To this mixture, 200 µL of a 0.25 mM solution of **SZMC3** in acetonitrile were added. The solution was then poured into a glass Petri plate (6 cm in diameter) and water was left to evaporate overnight at room temperature to obtain a homogeneous, slightly purple PVA film (~1 mm in thickness).

VIII.3. SYNTHESIS OF DTE-EWG FOR PHENOL ACIDITY MODULATION

VIII.3.1. Synthesis of intermediate 9

- **Synthesis of 2-chloro-5-methylthiophene, 11**

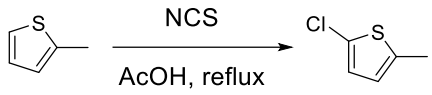

10 **11**

In a 250 mL round bottom flask, 23.1 g of *N*-chlorosuccinimide (173 mmol) and 15.5 mL of **10** (160 mmol) were heated under reflux for two hours in 100 mL of glacial acetic acid. After cooling, 100 mL of hexane and 200 mL of water were added, and the organic layer was separated. Then it was washed twice with 100 mL of a 2 M NaOH solution, dried with anhydrous Na_2SO_4, filtered and the solvent was removed under vacuum to obtain an orange oil. The product was purified as a colorless liquid by low pressure distillation (50-52 ºC at 32 mbar) yielding 15.85 g of **11** (120 mmol; 75% yield).

^{1}H NMR (250 MHz, $CDCl_3$): δ (ppm) 6.69 (d, J = 3.5 Hz, 1H), 6.52 (dq, J_1 = 3.5 Hz, J_2 = 1.3 Hz, 1H), 2.41 (d, J = 1.3 Hz, 3H).

^{13}C NMR (63 MHz, $CDCl_3$): δ (ppm) 138.3, 126.3, 125.6, 124.2, 15.2.

- **Synthesis of 1,5-bis(5-chloro-2-methylthien-3-yl)pentadione, 12**

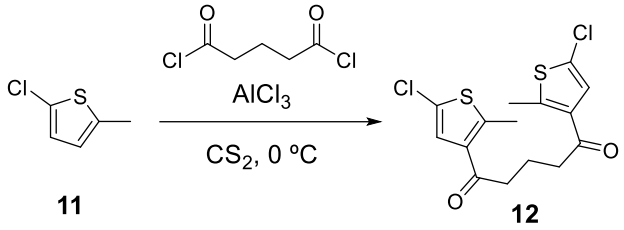

Under strong stirring, 0.934 g of $AlCl_3$ (6.86 mmol) were added on portions onto an ice-cooled solution of 0.40 mL of **11** (3.65 mmol) and 0.22 mL of glutaryl chloride (1.69 mmol) in 50 mL of anhydrous CS_2. Once the addition was finished, the crude was stirred for two hours at room temperature. Then the reaction was quenched with 30 mL of water and ice. Afterwards, 50 mL of water were additionally added, and the mixture was extracted four times with 50 mL of Et_2O. The organic layers were dried with anhydrous Na_2SO_4 and the solvent removed under vacuum, obtaining 0.688 g of a dark tar, which was purified by recrystallization in hexane to yield 0.306 g of **12** as a white solid (0.85 mmol; 50% yield). However, purification was not necessary to proceed with the next reactions.

^{1}H NMR (250 MHz, $CDCl_3$): δ (ppm) 7.18 (s, 2H), 2.86 (t, *J* = 6.9 Hz, 4H), 2.66 (s, 6H), 2.05 (p, *J* = 6.9 Hz, 2H).

^{13}C NMR (90 MHz, CDCl3): δ (ppm) 194.9, 147.7, 134.8, 126.8, 125.3, 40.5, 18.1, 16.1.

- **Synthesis of 1,2-bis(5-chloro-2-methylthien-3-yl)cyclopentene, 9.**

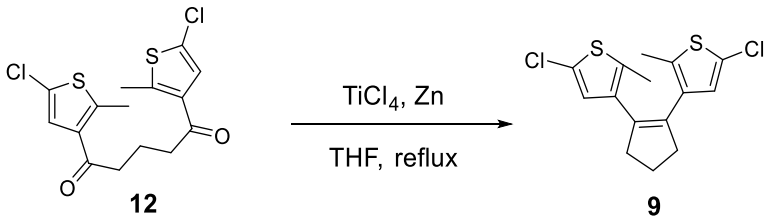

In a 250 mL three-necked flask, 2.30 g of Zn (59.4 mmol) were suspended in 50 mL of anhydrous THF under inert atmosphere. 20.1 mL of 1 M $TiCl_4$ in CH_2Cl_2 (20.1 mmol) were added dropwise and just after the addition, the mixture was heated under reflux for 45 min until it turned dark blue. Then the crude was cooled down to 0 ºC, when a solution of 4.40 g of **12** (12.2 mmol) in 50 mL of anhydrous THF was cautiously added and the mixture was stirred under reflux for 3 additional hours. Once cooled down, 50 mL of a 2 M Na_2CO_3 aqueous solution were added and the mixture was stirred until the blue color of the Ti(III) complex disappeared. Then the reaction mixture was filtered through celite and extracted with 100 mL Et_2O. The organic phase was separated, and the aqueous phase washed with additional 50 mL of Et_2O. The combined organic phases were dried with anhydrous Na_2SO_4, filtered

and the solvent removed under vacuum. Compound **9** was purified through flash column chromatography (silica gel, hexane) to yield 2.81 g of a crystalline white solid (8.53 mmol; 70% yield).

^{1}H NMR (250 MHz, $CDCl_3$): δ (ppm) 6.57 (s, 2H), 2.72 (t, *J* = 7.5 Hz, 4H), 2.02 (p, *J* =7.5 Hz, 2H), 1.89 (s, 6H).

^{13}C NMR (90 MHz, $CDCl_3$): δ (ppm) 134.8, 134.4, 133.3, 126.6, 125.1, 38.3, 22.8, 14.1.

VIII.3.2. Synthesis of molecular switch DTE-CHO

- **Synthesis of 1-(5-chloro-2-methylthien-3-yl)-2-(5-formyl-2-methylthien-3-yl)cyclopentene, 13**

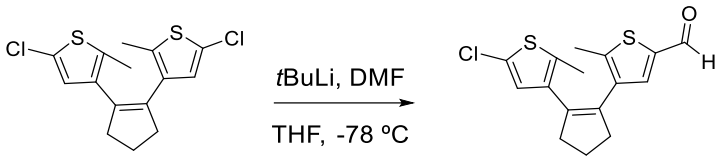

9 **13**

In a 100 mL Schlenk tube, a solution of 1.19 g of **9** (3.60 mmol) and 40 mL of anhydrous THF was cooled to -78ºC under inert atmosphere. Under vigorous stirring, 3 mL of a 1.7 M *tert*-butyllithium solution in pentane (5.10 mmol) were added dropwise during a minute.

The solution was stirred for 30 min at -78ºC and then 0.42 mL of anhydrous DMF were added at once (5.42 mmol). The reaction was stirred until it reached room temperature, and then it was poured onto a 2 M aqueous solution of Na_2CO_3. The mixture was extracted with 2x50 mL of Et_2O. Then the organic layers were combined, dried with Na_2SO_4, and filtered. After removing the solvent under vacuum, the dark oil obtained was purified through flash column chromatography (silica gel, hexane/EtOAc 9:1) to isolate 1.06 g of an orange oil **13** (3.27 mmol; 90% yield).

^{1}H NMR (360 MHz, $CDCl_3$): δ (ppm) 9.73 (s, 1H), 7.43 (s, 1H), 6.57 (s, 1H), 2.80-2.70 (m, 4H), 2.10-2.02 (m, 5H), 1.83 (s, 3H).

^{13}C NMR (100 MHz, $CDCl_3$): δ (ppm) 181.5, 145.5, 138.9, 136.8, 136.4, 134.6, 133.5, 132.8, 132,3, 125.5, 124.6, 37.4, 37.3, 21.8, 14.4, 13.1.

- **Synthesis of 1-(5-chloro-2-methylthien-3-yl)-2-(5-(1, 3-dioxolane)-2-methylthien-3-yl)cyclopentene, 14**

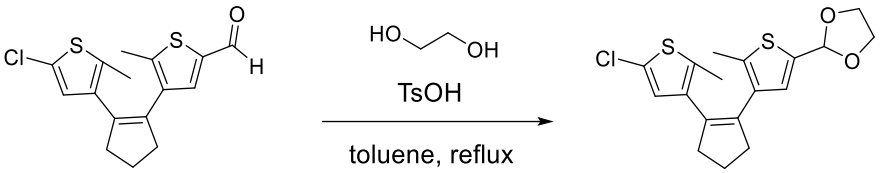

13 **14**

In a two necked bottom flask equipped with a Dean-Stark apparatus, a solution of 1.035 g of **13** (3.21 mmol), 1 mL of ethylene glycol (17.9 mmol) and 57.0 mg of *p*-toluene sulfonic acid (0.33 mmol) in 50 mL of toluene was heated under reflux overnight. Afterwards the reaction was poured into 50 mL of a 2 M NaOH aqueous solution, and the mixture was extracted twice with 50 mL of methylene chloride. Once the organic phase was dried with anhydrous Na_2SO_4, filtered and the solvent removed under vacuum, compound **14** was purified through flash column chromatography (silica gel, EtOAc/hexane, 1:1) obtaining 1.128 g of a slightly red oil (3.07 mmol; 96% yield).

^{1}H NMR (250 MHz, $CDCl_3$): δ (ppm) 6.82 (s, 1H), 6.58 (s, 1H), 5.97 (s, 1H), 4.18-3.90 (m, 4H), 2.81-2.65 (m, 4H), 2.01 (p, *J* = 7.5 Hz, 2H), 1.96 (s, 3H), 1.82 (s, 3H).

^{13}C NMR (101 MHz, $CDCl_3$): δ (ppm) 137.2, 136.0, 135.2, 134.9, 133.7, 133.2, 127.4, 126.8, 125.0, 100.4, 65.1, 38.4, 38.4, 22.9, 14.4, 14.1.

- **Synthesis of $Pd(PPh_3)_4$**

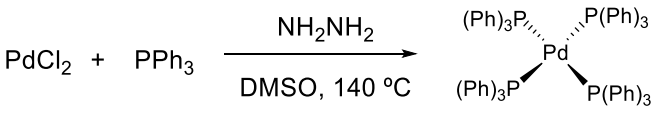

$Pd(PPh_3)_4$

A suspension of 0.331 g of $PdCl_2$ (1.86 mmol) and 2.613 g of PPh_3 (9.97 mmol) in 20 mL of DMSO was degassed and heated to 140 ºC under vigorous stirring. When the mixture reached this temperature, the suspended solid dissolved forming an orange solution and 3.6 mL of hydrazine monohydrate (57.8 mmol) were added at once. The solution was then cooled down to room temperature and the bright yellow precipitate formed was filtered and washed (2x ethanol, 2x diethyl ether) to yield 2.030 mg of $Pd(PPh_3)_4$ as a bright yellow solid (1.76 mmol; 94% yield).

IR (ATR, cm^{-1}): 3053, 2999, 1956, 1884, 1813, 1583, 1475, 1431, 1315, 1304, 1273, 1178, 1153, 1082, 1026, 997, 910, 847, 741, 690.

- **Synthesis of 1-(2-methyl-5-(4-hydroxyl)phenyl)thien-3-yl)-2-(5-formyl-2-methylthien-3-yl)cyclopentene, DTE-CHO**

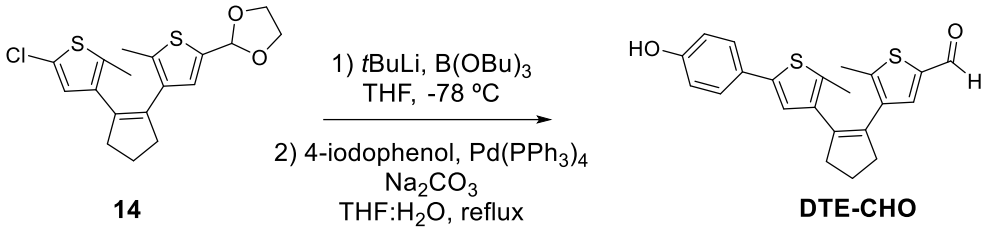

14 **DTE-CHO**

A solution of 1.460 g of **14** (3.98 mmol) in 30 mL of anhydrous THF was cooled down to -78ºC before adding dropwise 3.00 mL of a 1.7 M solution of *tert*-butyllithium in pentane (5.10 mmol). After stirring for 30 min at -78 ºC, the mixture was quenched with 1.40 mL of tributyl borate (5.19 mmol) and stirred for 30 min more until it reached room temperature.

Then the crude was added onto a degassed two-phase mixture of 1.001 g of 4-iodophenol (5.79 mmol) and 80 mg of $Pd(PPh_3)_4$ (0.070 mmol) in 25 mL of THF and 25 mL of a 2 M Na_2CO_3 aqueous solution. The crude was then heated under reflux for 2 hours. Once the crude was cooled down to room temperature, 50 mL of Et_2O were added and the organic mixture was separated. The remaining aqueous phase was extracted once with further 50 mL of Et_2O, and the combined organic layers were dried with anhydrous Na_2SO_4. After filtration and solvent removal under vacuum, a brownish oil was obtained. The product was then purified through flash column chromatography (silica gel, EtOAc/hexane 1:3) to yield 0.695 g of compound **DTE-CHO** (1.83 mmol, 46% yield).

^{1}H NMR (400 MHz, $CDCl_3$): δ (ppm) 9.71 (s, 1H), 7.51 (s, 1H), 7.34 (d, *J* = 8.6 Hz, 2H), 6.88 – 6.81 (m, 3H), 2.88 – 2.76 (m, 4H), 2.15 – 2.03 (m, 5H), 1.93 (s, 3H).

^{13}C NMR (101 MHz, $CDCl_3$): δ (ppm) 183.3, 155.6, 147.6, 140.5, 139.4, 139.0, 138.2, 136.9, 135.9, 133.3, 132.9, 127.0, 126.9, 122.4, 115.9, 38.6, 38.3, 23.0, 15.6, 14.3.

IR (ATR, cm^{-1}): 3307, 2915, 2842, 2051, 1640, 1610, 1513, 1434, 1369, 1252, 1166, 1142, 1103, 1026, 948, 919, 824, 752, 721, 650.

HRMS (ESI): m/z calcd for $C_{22}H_{21}O_2S_2^+$: 381.0977 $[M-H]^+$; found: 381.0978

VIII.3.3. Synthesis and protection of molecular switch DTE-Cl

- **1-(2-methyl-5-(4-hydroxyl)phenyl)thien-3-yl)-2-(5-chloro-2-methylthien-3-yl)cyclopentene, DTE-Cl**

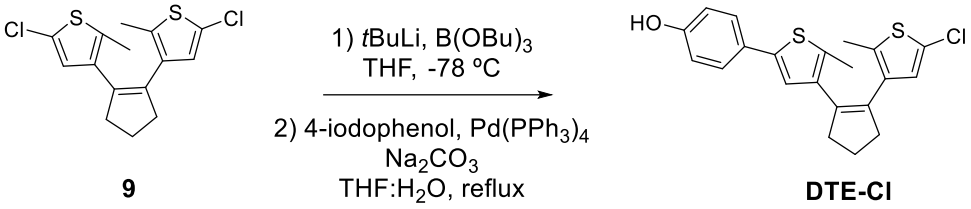

9 **DTE-Cl**

A solution of 1.824 g of **9** (5.54 mmol) in 30 mL of anhydrous THF was cooled down to -78º C. Then 3.8 mL of 1.7 M a solution of *tert*-butyllithium in pentane (6.4 mmol) were added cautiously. After stirring for 30 min at -78º C, the mixture was quenched with 1.8 mL of tributyl borate (6.7 mmol) and then it was stirred for 30 min more until it reached room temperature.

Later the reaction mixture was added onto a degassed solution of 1.221 g of 4-iodophenol (7.06 mmol) and 248.0 mg of $Pd(PPh_3)_4$ (0.22 mmol) in 30 mL of THF and 30 mL of a 2 M Na_2CO_3 aqueous solution. The two-phase system was heated under reflux for 2 hours. Afterwards, the crude was cooled down to room temperature and 50 mL of Et_2O were added. After separating the organic layer, the aqueous phase was extracted with additional 50 mL of Et_2O. The combined organic layers were dried with anhydrous Na_2SO_4 and, after filtration and removal of the solvent under vacuum, a red oil was obtained. The product was then purified through flash column chromatography (silica gel, EtOAc/hexane 1:9) to yield 1.309 g of compound **DTE-Cl** (3.38 mmol; 61% yield).

^{1}H NMR (250 MHz, $CDCl_3$): δ (ppm) 7.02 (d, *J* = 8.5 Hz, 2H), 6.71 (d, *J* = 8.6 Hz, 2H), 6.46 (s, 1H), 6.13 (s, 1H), 4.72 (s, 1H), 2.64 (t, *J* = 7.4 Hz, 2H), 2.56 (t, *J* = 7.4 Hz, 2H), 2.41 (s, 3H), 1.95 (p, *J* = 7.9 Hz, 2H), 1.82 (s, 3H).

^{13}C NMR (101 MHz, $CDCl_3$): δ (ppm) 154.8, 139.6, 136.2, 135.4, 135.2, 133.6, 133.5, 133.3, 127.6, 126.9, 126.8, 124.9, 122.8, 115.7, 38.4, 38.3, 22.9, 14.3, 14.2.

- **1-(2-methyl-5-(4-*tert*-butyldiphenylsilyl)oxy)phenyl)thien-3-yl)-2-(5-chloro-2-methylthien-3-yl)cyclopentene, 15**

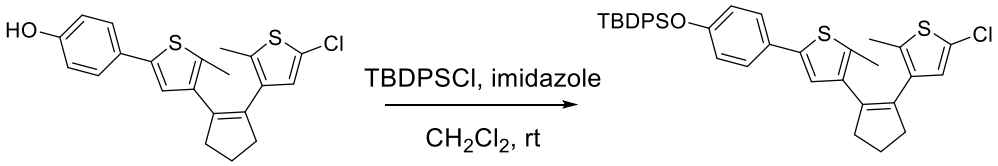

DTE-Cl **15**

0.580 g of **DTE-Cl** (1.50 mmol), 0.5 mL of TBDPSCl (1.92 mmol) and 0.140 g of imidazole (2.00 mmol) were stirred in 20 mL of anhydrous CH_2Cl_2 at room

temperature overnight. Once the reaction had finished, the crude was washed with 20 mL of water. The organic phase was dried over Na_2SO_4, filtered and the solvent removed under vacuum. Compound **15** was then purified via flash column chromatography (silica gel, hexane/EtOAc 19:1) to obtain 0.471 g (0.75 mmol, 50% yield).

^{1}H NMR (250 MHz, $CDCl_3$): δ (ppm) 7.72 (dd, *J* = 7.8, 1.6 Hz, 4H), 7.48 – 7.30 (m, 6H), 7.22 (d, *J* = 8.7 Hz, 2H), 6.80 (s, 1H), 6.73 (d, *J* = 8.7 Hz, 2H), 6.59 (s, 1H), 2.82 – 2.65 (m, 4H), 2.02 (p, *J* = 7.3 Hz, 2H), 1.93 (s, 3H), 1.86 (s, 3H), 1.10 (s, 9H).

^{13}C NMR (91 MHz, $CDCl_3$): δ (ppm) 155.0, 139.9, 136.3, 135.6, 135.5, 135.3, 133.6, 133.5, 133.3, 132.9, 130.1, 128.0, 127.7, 127.0, 126.4, 125.0, 122.8, 120.1, 38.6, 38.5, 26.6, 23.0, 19.6, 14.4, 14.4.

IR (ATR, cm^{-1}): 2929, 2857, 1606, 1512, 1473, 1430, 1392, 1363, 1257, 1174, 1108, 1071, 1008, 972, 915, 826, 740, 701, 635, 613.

HRMS (ESI): m/z calcd for $C_{37}H_{36}ClOS_2Si^-$: 623.1671 $[M]^-$; found: 623.1702.

- **Synthesis of 1-(2-methyl-5-(4-*tert*-butyldimethylsilyl) oxy)phenyl)thien-3-yl)-2-(5-chloro-2-methylthien-3-yl) cyclopentene, 16**

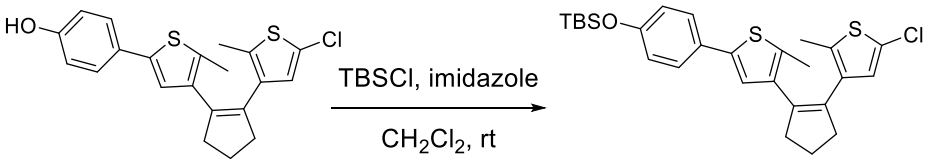

DTE-Cl **16**

1.510 g of **DTE-Cl** (3.90 mmol), 0.649 g of TBSCl (4.31 mmol) and 0.343 g of imidazole (5.00 mmol) were stirred in 40 mL of anhydrous CH_2Cl_2 at room temperature overnight. Then the crude was washed with 40 mL of water. The organic phase was dried over Na_2SO_4, filtered and the solvent removed under vacuum. Compound **16** was then purified via flash column chromatography (silica gel, hexane) to obtain 1.177 g (2.34 mmol, 60% yield).

^{1}H NMR (400 MHz, $CDCl_3$): δ (ppm) 7.36 (d, *J* = 8.7 Hz, 2H), 6.87 (s, 1H), 6.81 (d, *J* = 8.7 Hz, 2H), 6.62 (s, 1H), 2.80 (t, *J* = 7.5 Hz, 2H), 2.74 (t, *J* = 7.5 Hz, 2H), 2.04 (p, *J* = 7.5 Hz, 2H), 1.98 (s, 3H), 1.89 (s, 3H), 0.99 (s, 9H), 0.21 (s, 6H).

^{13}C NMR (101 MHz, $CDCl_3$): δ (ppm) 155.2, 140.0, 136.3, 135.6, 135.4, 133.7, 133.6, 133.4, 128.0, 127.0, 126.6, 125.1, 122.9, 120.5, 38.6, 38.5, 25.8, 23.1, 18.4, 14.5, 14.4, -4.2.

IR (ATR, cm^{-1}): 2930, 2858, 1606, 1512, 1473, 1441, 1363, 1255, 1217, 1168, 1104, 1007, 972, 910, 828, 807, 782, 755, 669.

HRMS (ESI): m/z calcd for $C_{27}H_{34}ClOS_2Si^+$: 501.1503 $[M-H]^+$; found: 501.1494.

VIII.3.4. Synthesis of molecular switch DTE-$COCF_3$

- **Synthesis of 1-(2-methyl-5-(4-*tert*-butyldiphenylsilyl) oxy)phenyl)thien-3-yl)-2-(2-methyl-5-trifluoroacetylthien-3-yl)cyclopentene, 17**

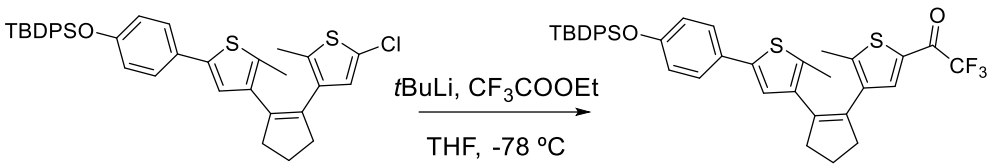

15 **17**

In a 100 mL Schlenk tube, a solution of 0.157 g of **15** (0.25 mmol) and 20 mL of anhydrous THF was cooled down to -78ºC under inert atmosphere. 1 mL of a 1.7 M *tert*-butyllithium solution in pentane (1.7 mmol) was added dropwise during a minute under vigorous stirring. The solution was stirred for 30 min and then 0.35 mL of anhydrous ethyl trifluoroacetate were added at once (2.94 mmol). The solution was stirred until it reached room temperature, and then it was poured onto 50 mL of a 2 M aqueous solution of Na_2CO_3 and the mixture was extracted with 2x50 mL of Et_2O. The organic layers were combined and dried with Na_2SO_4 and filtered. After removing the solvent under vacuum, the crude was purified through flash column chromatography (silica gel, hexanes/EtOAc, 9:1) obtaining 80.2 mg of pure **17** (0.12 mmol, 47% yield).

^{1}H NMR (360 MHz, $CDCl_3$): δ (ppm) 7.72 (d, *J* = 6.7 Hz, 4H), 7.66 (s, 1H), 7.47 – 7.33 (m, 6H), 7.20 (d, *J* = 8.5 Hz, 2H), 6.76 (s, 1H), 6.73 (d, *J* = 8.5 Hz, 2H), 2.80 (t, *J* = 7.4 Hz, 4H), 2.16 – 2.01 (m, 5H), 1.91 (s, 3H), 1.10 (s, 9H).

^{13}C NMR (91 MHz, $CDCl_3$): δ (ppm) 173.1 (q, *J* = 44.1 Hz), 155.2, 150.3, 140.8, 139.0, 138.2 (q, *J* = 2.9 Hz), 137.6, 135.8, 135.6, 133.5, 132.9, 132.5, 132.0, 130.1, 128.0, 127.4, 126.5, 122.4, 120.1, 116.6 (q, *J* = 290.6 Hz), 38.7, 38.4, 26.6, 23.0, 19.6, 15.6, 14.4.

^{19}F NMR (235 MHz, $CDCl_3$): δ (ppm) -72.39.

IR (ATR, cm^{-1}): 2932, 2857, 2324, 2051, 1982, 1683, 1605, 1510, 1471, 1428, 1391, 1332, 1256, 1195, 1140, 1108, 1012, 911, 869, 825, 738, 699, 634, 611.

HRMS (ESI): m/z calcd for $C_{39}H_{37}F_3NaO_2S_2Si^+$: 709.1849 $[M-Na]^+$; found: 709.1815.

- **Synthesis of 1-(2-methyl-5-(4-hydroxyl)phenyl)thien-3-yl)-2-(2-methyl-5-trifluoroacetylthien-3-yl)cyclopentene, DTE-COCF$_3$**

17 **DTE-COCF$_3$**

67 mg of **17** (0.10 mmol) were stirred for 1 hour in 5 mL of chloroform containing 46 mg of TBAF (0.17 mmol) and 14 µL of acetic acid. The solution was washed with water (2x5 mL), dried with Na_2SO_4, filtered and the solvent was removed under vacuum. The product was finally purified via flash column chromatography (silica gel, hexane/EtOAc, 17:3) to obtain 33.1 mg of a yellow solid identified as **DTE-COCF$_3$** (0.074 mmol, 74% yield).

^{1}H NMR (250 MHz, $CDCl_3$): δ (ppm) 7.67 (s, 1H), 7.35 (d, *J* = 8.7 Hz, 2H), 6.87 – 6.75 (m, 3H), 4.86 (s, 1H), 2.83 (t, *J* = 6.7 Hz, 4H), 2.22 – 1.99 (m, 5H), 1.95 (s, 3H).

^{13}C NMR (91 MHz, $CDCl_3$): δ (ppm) 173.1 (q, *J* = 36.2 Hz), 155.2, 150.4, 140.6, 139.1, 138.3 (q, *J* = 2.9 Hz), 137.7, 135.8, 133.6, 132.6, 132.0, 127.4, 127.0, 122.5, 116.6 (q, *J* = 290.8 Hz), 115.8, 38.6, 38.4, 23.1, 15.6, 14.4.

^{19}F NMR (235 MHz, $CDCl_3$): δ (ppm) -72.38.

IR (ATR, cm^{-1}): 3368, 2920, 2051, 1679, 1611, 1514, 1432, 1371, 1195, 1141, 1045, 948, 926, 869, 824, 754, 718, 678, 660.

HRMS (ESI): m/z calcd for $C_{23}H_{18}F_3O_2S_2^-$: 447.0706 [M]$^-$; found: 447.0692

VIII.3.5. Synthesis of molecular switch DTE-C$_6$F$_5$

- **1-(2-methyl-5-(4-*tert*-butyldiphenylsilyl)oxy)phenyl)thien-3-yl)-2-(5-(2,3,4,5,6-pentafluorophenyl)-2-methylthien-3-yl)cyclopentene, 18**

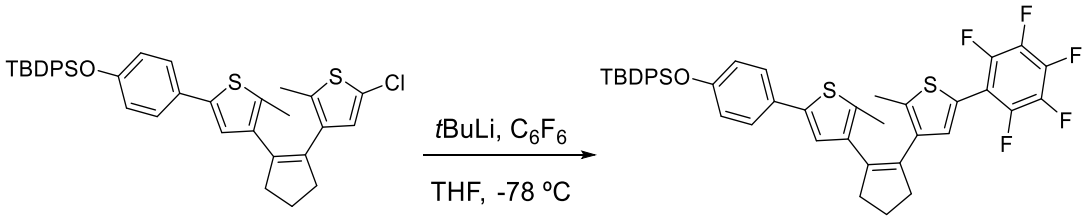

15 **18**

In a 100 mL Schlenk tube, a solution of 0.134 g of **15** (0.22 mmol) and 10 mL of anhydrous THF was cooled down to -78 ºC under inert atmosphere. Under vigorous stirring, 0.5 mL of a 1.7 M *tert*-butyllithium solution in pentane (0.85 mmol) was added. The solution was stirred for 30 min and then 0.2 mL of perfluorobenzene were

added at once (1.7 mmol). The solution was stirred until it reached room temperature, and then it was poured onto 20 mL of a 2 M aqueous solution of Na_2CO_3. The mixture was then extracted with 2x50 mL of Et_2O. The organic layers were combined and dried with Na_2SO_4. After filtration and removal of the solvent, the crude was purified through flash column chromatography (silica gel, hexane) to obtain 121 mg of **18** as a white powder (0.16 mmol, 74% yield).

^{1}H NMR (360 MHz, $CDCl_3$) δ (ppm) 7.73 (d, *J* = 7.3 Hz, 4H), 7.49 – 7.33 (m, 6H), 7.26 – 7.16 (m, 3H), 6.82 (s, 1H), 6.73 (d, *J* = 8.4 Hz, 2H), 2.88 – 2.76 (m, 4H), 2.14 – 1.97 (m, 5H), 1.93 (s, 3H), 1.11 (s, 9H).

^{13}C NMR (91 MHz, $CDCl_3$): δ (ppm) 155.1, 144.0 (d, *J* = 250.8 Hz), 140.0, 139.5 (d, *J* = 255.5 Hz), 138.2 (dd, J_1 = 251.9, J_2 = 14.9 Hz), 138.1, 136.5, 136.3, 135.8, 135.6, 133.7, 133.5, 132.9, 131.6, 130.1, 128.0, 127.9, 127.7, 126.4, 122.8, 120.0, 110.3 (t, *J* = 14.5 Hz), 38.6, 38.5, 26.6, 23.1, 19.6, 14.4, 14.3.

^{19}F NMR (235 MHz, $CDCl_3$): δ (ppm) -140.76 (dd, J_1 = 22.2 Hz, J_2 = 7.0 Hz), -157.47 (t, *J* = 21.1 Hz), -162.92 (dt, J_1 = 22.3, J_2 = 7.1 Hz).

IR (ATR, cm^{-1}): 2931, 2857, 2051, 1723, 1605, 1511, 1495, 1471, 1428, 1391, 1256, 1171, 1107, 1036, 986, 909, 825, 735, 699, 634, 612.

HRMS (ESI): m/z calcd for $C_{43}H_{36}F_5OS_2Si^-$: 755.1902 [M]$^-$; found: 755.1882.

- **Synthesis of 1-(2-methyl-5-(4-hydroxyl)phenyl)thien-3-yl)-2-(5-(2,3,4,5,6-pentafluorophenyl)-2-methylthien-3-yl)cyclopentene, DTE-C_6F_5**

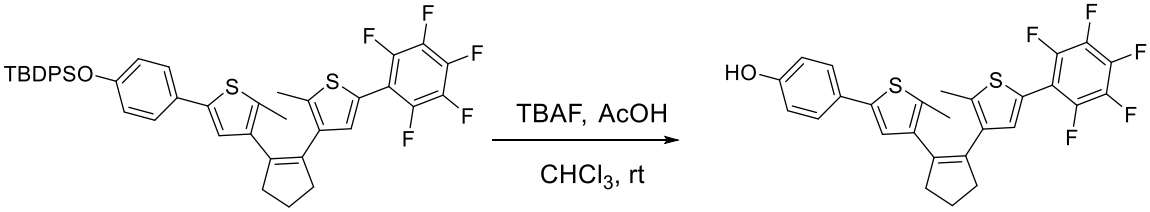

18 **DTE-C_6F_5**

22 mg of **18** (0.03 mmol) were stirred for 1 hour in 5 mL of chloroform containing 15 mg of TBAF (0.06 mmol) and 14 µL of acetic acid. The solution was washed with water (2x5 mL), dried with Na_2SO_4, filtered and the solvent was removed under vacuum. The product was finally purified via flash column chromatography (silica gel, hexanes/EtOAc, 9:1) to obtain 15 mg of a slightly purple solid identified as **DTE-C_6F_5** (0.03 mmol, 100% yield).

^{1}H NMR (400 MHz, $CDCl_3$): δ (ppm) 7.36 (d, *J* = 8.8 Hz, 2H), 7.20 (s, 1H), 6.86 (s, 1H), 6.80 (d, *J* = 8.8 Hz, 2H), 2.84 (t, *J* = 7.5 Hz, 4H), 2.14 – 2.04 (m, 5H), 1.97 (s, 3H).

^{13}C NMR (101 MHz, $CDCl_3$): δ (ppm) 154.8, 139.7, 138.0, 136.4, 136.2, 135.7, 133.7, 133.5, 131.5, 127.6, 126.8, 126.8, 122.8, 115.6, 38.5, 38.4, 23.0, 14.2, 14.1.

^{19}F NMR (235 MHz, $CDCl_3$): δ (ppm) -140.81 (dd, J_1 = 22.2, J_2 = 6.8 Hz), -157.41 (t, J = 21.1 Hz), -162.92 (td, J_1 = 22.0, J_2 = 7.0 Hz).

IR (ATR, cm^{-1}): 3339, 2920, 2849, 2325, 2051, 1706, 1611, 1516, 1494, 1437, 1371, 1242, 1171, 1104, 1036, 986, 825, 767, 740, 631.

HRMS (ESI): m/z calcd for $C_{27}H_{18}F_5OS_2^-$: 517.0725 $[M]^-$; found: 517.0704

VIII.3.6. Synthesis of molecular switch DTE-Ph(NO_2)$_2$

- **1-(2-methyl-5-(4-*tert*-butyldiphenylsilyloxy)phenyl)thien-3-yl)-2-(5-(2,5-dinitrophenyl-2-methylthien-3-yl)cyclopentene, 19**

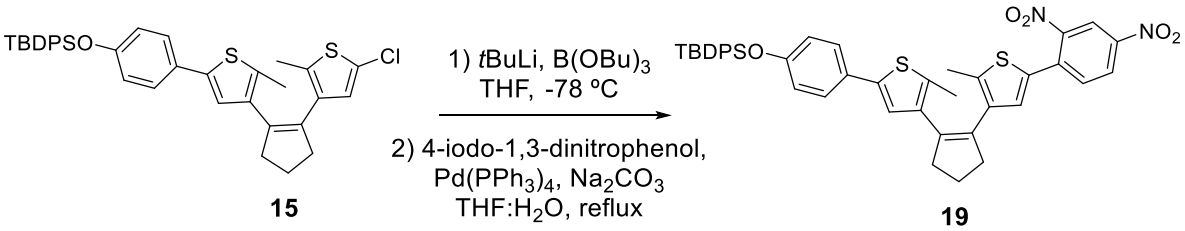

A solution of 0.150 g of **15** (0.24 mmol) in 30 mL of anhydrous THF was cooled down to -78 ºC before adding dropwise 0.5 mL of a 1.7 M solution of *tert*-butyllithium in pentane (0.85 mmol). After stirring for 30 min at -78 ºC, the mixture was quenched with 0.4 mL of tributyl borate (1.5 mmol) and stirred for 30 min more until it reached room temperature.

Later the solution was added onto a degassed solution of 0.264 g of 4-iodo-1,3-dinitrophenol (0.90 mmol) and 96 mg of $Pd(PPh_3)_4$ (0.09 mmol) in 25 mL of THF, 25 mL of a 2 M Na_2CO_3 aqueous solution and 10 drops of ethylene glycol. The two-phase system was then heated under reflux for 2 hours. Then once cooled down the reaction mixture, 25 mL of water and 25 mL of Et_2O were added and the organic layer was separated by extraction. The organic phase was washed with a 0.2 M $NaHCO_3$ aqueous solution, and after drying with anhydrous Na_2SO_4, filtration and removal of the solvent under vacuum, a red oil was obtained. The curde was then purified through flash column chromatography (silica gel, hexanes/EtOAc, 49:1) to yield 58 mg of compound **19** (0.076 mmol, 32% yield).

^{1}H NMR (250 MHz, $CDCl_3$): δ (ppm) 8.50 (d, J = 2.3 Hz, 1H), 8.31 (dd, J_1 = 8.6, J_2 = 2.3 Hz, 1H), 7.72 (dd, J_1 = 7.8, J_2 = 1.6 Hz, 4H), 7.62 (d, J = 8.6 Hz, 1H), 7.48 – 7.32 (m, 6H), 7.23 (d, J = 8.6 Hz, 2H), 6.90 (s, 1H), 6.80 (s, 1H), 6.72 (d, J = 8.6 Hz, 2H), 2.78 (t, J = 7.4 Hz, 4H), 2.14 – 1.99 (m, 5H), 1.94 (s, 3H), 1.09 (s, 9H).

^{13}C NMR (63 MHz, $CDCl_3$): δ (ppm) 155.1, 146.2, 140.2, 140.0, 138.0, 136.5, 136.1, 135.6, 134.5, 133.6, 133.4, 132.9, 132.4, 130.4, 130.3, 130.1, 128.8, 128.0, 127.6, 126.4, 126.2, 122.8, 120.1, 119.7, 38.6, 38.4, 26.6, 23.1, 19.6, 14.6, 14.4.

IR (ATR, cm^{-1}): 2931, 2856, 2324, 2050, 1600, 1510, 1471, 1428, 1342, 1256, 1171, 1148, 1106, 1071, 1012, 909, 827, 736, 700, 634, 612.

HRMS (ESI): m/z calcd for $C_{43}H_{39}N_2O_5S_2Si^-$: 755.2075 $[M]^-$; found: 755.2066

- **Synthesis of 1-(2-methyl-5-(4-hydroxyl)phenyl)thien-3-yl)-2-(5-(2,5-dinitrophenyl-2-methylthien-3-yl)cyclopentene, DTE-Ph$(NO_2)_2$**

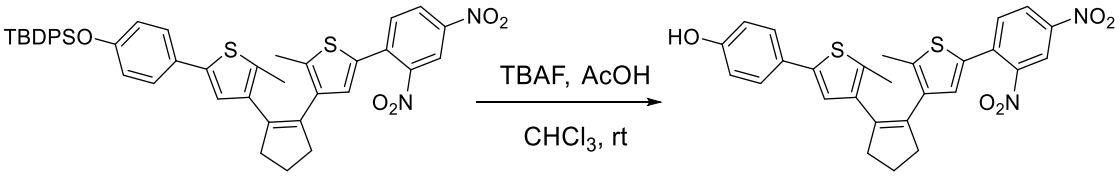

19 **DTE-Ph$(NO_2)_2$**

54 mg of **19** (0.07 mmol) were stirred for 1 hour in 5 mL of chloroform containing 56 mg of TBAF (0.21 mmol) and 14 µL of acetic acid. The solution was washed with water (2x5 mL). Then it was dried with Na_2SO_4, filtered and the solvent was removed under vacuum. The crude was finally purified via flash column chromatography (silica gel, hexanes/EtOAc, 4:1) to obtain 19.1 mg of a brownish solid identified as **DTE-Ph$(NO_2)_2$** (0.04 mmol, 52% yield).

^{1}H NMR (360 MHz, $CDCl_3$): δ (ppm) 8.51 (d, *J* = 1.5 Hz, 1H), 8.33 (dd, *J* = 8.5, 1.3 Hz, 1H), 7.65 (d, *J* = 8.6 Hz, 1H), 7.38 (d, *J* = 8.4 Hz, 2H), 6.93 (s, 1H), 6.85 (s, 1H), 6.81 (d, *J* = 8.3 Hz, 2H), 2.88 – 2.73 (m, 4H), 2.14 – 2.02 (m, 5H), 1.99 (s, 3H).

^{13}C NMR (91 MHz, $CDCl_3$): δ (ppm) 155.0, 148.4, 146.1, 140.1, 140.0, 137.9, 136.5, 136.1, 134.5, 133.7, 133.4, 132.4, 130.4, 130.2, 127.6, 126.9, 126.2, 122.8, 119.7, 115.8, 38.5, 38.4, 23.1, 14.6, 14.4.

IR (ATR, cm^{-1}): 3357, 2921, 2850, 2324, 2051, 1981, 1708, 1597, 1515, 1435, 1340, 1261, 1171, 1149, 1104, 1073, 1027, 955, 907, 826, 734, 663.

HRMS (ESI): m/z calcd for $C_{27}H_{21}N_2O_5S_2^-$: 517.0897 $[M]^-$; found: 517.0871

VIII.3.7. Synthesis of molecular switch 1-(2-methyl-5-(4-hydroxyl)phenyl)thien-3-yl)-2-(5-(4-nitrophenyl)-2-methylthien-3-yl)cyclopentene, DTE-PhNO$_2$

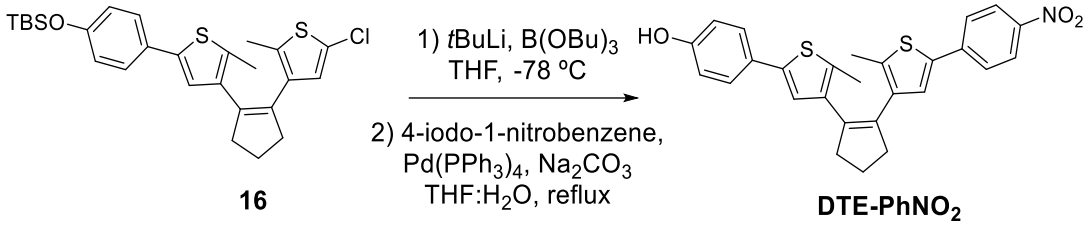

16 **DTE-PhNO$_2$**

A solution of 0.100 g of **16** (0.20 mmol) in 10 mL of anhydrous THF was cooled down to -78 ºC before adding dropwise 0.5 mL of a 1.7 M solution of *tert*-butyllithium in pentane (0.85 mmol). After stirring for 30 min at -78 ºC, the mixture was quenched with 0.5 mL of tributyl borate (1.85 mmol) and stirred for additional 30 min until it reached room temperature.

Then the solution was added onto a degassed mixture of 80 mg of 4-iodo-1-nitrobenzene (0.32 mmol) and 40 mg of $Pd(PPh_3)_4$ (0.03 mmol) in 10 mL of THF, 15 mL of a 2 M Na_2CO_3 aqueous solution. The two-phase system was then heated under reflux for 2 hours. Once cooled down the reaction mixture, 25 mL of water and 25 mL of Et_2O were added and the organic layer was separated by extraction. The organic phase was washed with a 0.2 M $NaHCO_3$ aqueous solution, and after drying with anhydrous Na_2SO_4, filtration and further removal of the solvent under vacuum, a brownish oil was obtained. The crude was then purified through flash column chromatography (silica gel, hexane/EtOAc, 9:1) to yield 43.6 mg of compound **DTE-PhNO$_2$** (0.092 mmol, 46% yield).

^{1}H NMR (400 MHz, $CDCl_3$): δ (ppm) 8.18 (d, *J* = 8.8 Hz, 2H), 7.59 (d, *J* = 8.8 Hz, 2H), 7.37 (d, *J* = 8.6 Hz, 2H), 7.18 (s, 1H), 6.89 (s, 1H), 6.81 (d, *J* = 8.6 Hz, 2H), 2.85 (t, *J* = 7.4 Hz, 4H), 2.10 (p, *J* = 7.5 Hz, 2H), 2.06 (s, 3H), 1.98 (s, 3H).

^{13}C NMR (63 MHz, $CDCl_3$): δ (ppm) 155.1, 146.3, 140.9, 140.0, 138.2, 137.8, 137.0, 136.4, 135.9, 133.9, 133.6, 127.6, 127.1, 127.0, 125.4, 124.5, 122.9, 115.8, 38.6, 38.5, 23.2, 14.8, 14.5.

IR (ATR, cm^{-1}): 3329, 2919, 2850, 2051, 1700, 1593, 1510, 1435, 1335, 1261, 1170, 1109, 950, 825, 750, 691, 668.

HRMS (ESI): m/z calcd for $C_{27}H_{22}NO_3S_2^{\cdot-}$: 472.1047 [M]$^{\cdot-}$; found: 472.1051

VIII.3.8. Synthesis of molecular switch DTE-py-zw

- **Synthesis of 1-(2-methyl-5-(4-hydroxyl)phenyl)thien-3-yl)-2-(5-pyridyl-2-methylthien-3-yl)cyclopentene, 20**

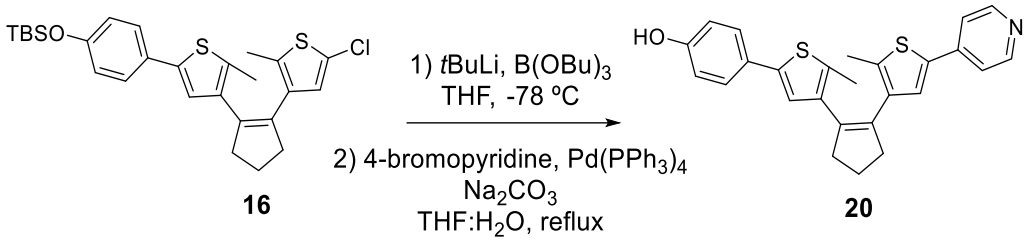

A solution of 0.228 g of **16** (0.46 mmol) in 30 mL of anhydrous THF was cooled down to -78 ºC before adding dropwise 0.65 mL of a 1.7 M solution of *tert*-butyllithium in pentane (0.94 mmol). After stirring for 30 min at -78 ºC, the mixture was quenched with 0.25 mL of tributyl borate (0.93 mmol) and stirred for 30 min more until it reached room temperature.

Later the solution was added onto a degassed mixture of 0.107 g of 4-bromo-pyridinium hydrochloride (0.55 mmol) and 38.2 mg of $Pd(PPh_3)_4$ (0.03 mmol) in 25 mL of THF and 25 mL of a 2 M Na_2CO_3 aqueous solution. The two-phase system was then heated under reflux for 2 hours. Afterwards, and once cooled down the reaction mixture, 50 mL of water and 50 mL of Et_2O were added and the organic layer was separated by extraction. The organic phase was washed with 0.2 M $NaHCO_3$ aqueous solution, and after drying with anhydrous Na_2SO_4, filtration and further removal of the solvent under vacuum, a brownish oil was obtained. The crude was then purified through flash column chromatography (silica gel, EtOAc/hexane 1:3) to yield 0.106 g of compound **20** (0.25 mmol, 54% yield).

^{1}H NMR (400 MHz, $CDCl_3$): δ (ppm) 8.50 (d, *J* = 5.9 Hz, 2H), 7.37 (d, *J* = 6.2 Hz, 2H), 7.32 (d, *J* = 8.6 Hz, 2H), 7.22 (s, 1H), 6.84 – 6.79 (m, 3H), 2.88 – 2.80 (m, 4H), 2.13 – 2.06 (m, 5H), 2.04 (s, 3H).

^{13}C NMR (101 MHz, $CDCl_3$): δ (ppm) 156.1, 149.8, 142.2, 140.1, 137.9, 137.6, 136.4, 136.1, 136.0, 134.0, 133.4, 127.1, 127.0, 126.9, 122.9, 119.7, 116.0, 38.4, 38.4, 23.2, 14.8, 14.5.

IR (ATR, cm^{-1}): 3061, 2916, 2845, 1774, 1598, 1514, 1437, 1371, 1273, 1249, 1217, 1169, 1104, 1065, 1006, 947, 908, 816, 756, 730, 665, 636.

HRMS (ESI): m/z calcd for $C_{26}H_{24}NOS_2^+$: 430.1294 $[M-H]^+$; found: 430.1294

- **1-(2-methyl-5-(4-hydroxyl)phenyl)thien-3-yl)-2-(5-(4-(3-sulfopropyl)-4-pyridyl)-2-methyl-3-thien-3-yl)cyclopentene, DTE-py-zw**

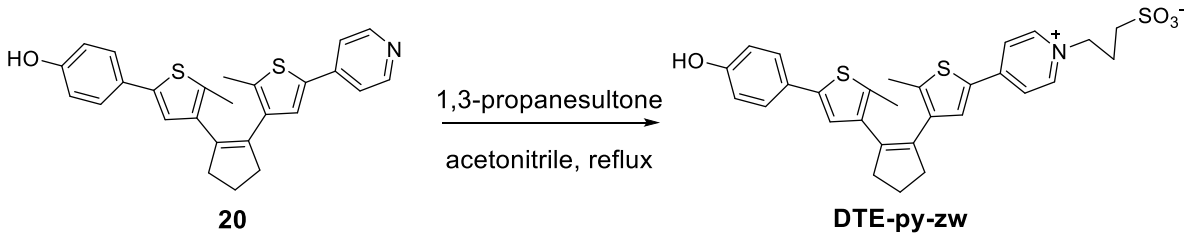

20 **DTE-py-zw**

86 mg of **20** (0.20 mmol) were heated under reflux in acetonitrile overnight with 20 µL of 1,3-propanesultone (0.23 mmol). The resulting precipitate was isolated through filtration and washed with acetone twice obtaining 33.6 mg of a light brown powder identified as **DTE-py-zw** (0.06 mmol, 30% yield).

^{1}H NMR (400 MHz, DMSO): δ (ppm) 9.58 (s, 1H), 8.89 (d, *J* = 6.7 Hz, 2H), 8.19 (d, *J* = 6.8 Hz, 2H), 8.13 (s, 1H), 7.32 (d, *J* = 8.5 Hz, 2H), 7.03 (s, 1H), 6.75 (d, *J* = 8.5 Hz, 2H), 4.61 (t, *J* = 6.7 Hz, 2H), 2.85 (t, *J* = 7.3 Hz, 4H), 2.44 (t, *J* = 6.9 Hz, 2H), 2.21 (p, *J* = 6.8 Hz, 2H), 2.07 (p, *J* = 7.5 Hz, 2H), 2.00 (s, 3H) 1.89 (s, 3H).

^{13}C NMR (101 MHz, DMSO): δ (ppm) 157.0, 147.6, 144.7, 143.4, 139.8, 139.0, 136.0, 135.9, 133.3, 132.8, 132.7, 131.8, 126.3, 124.7, 122.2, 121.5, 115.7, 58.3, 47.0, 38.1, 38.1, 27.1, 22.3, 14.6, 14.0.

IR (ATR, cm^{-1}): 3047, 2946, 2850, 2112, 1634, 1610, 1548, 1510, 1472, 1436, 1360, 1313, 1282, 1236, 1209, 1164, 1105, 1035, 873, 829, 814, 782, 749, 734, 663, 607.

HRMS (ESI): m/z calcd for $C_{29}H_{30}NO_4S_3^+$: 552.1331 $[M-H]^+$; found: 552.1317.

VIII.3.9. Synthesis of molecular switch DTE-pyNO$_2$-zw

- **Synthesis of 1-(2-methyl-5-(4-hydroxyl)phenyl)thien-3-yl}-2-(5-(4-nitro-2-pyridyl)-2-methyl-3-thienyl) cyclopentene, DTE-pyNO$_2$**

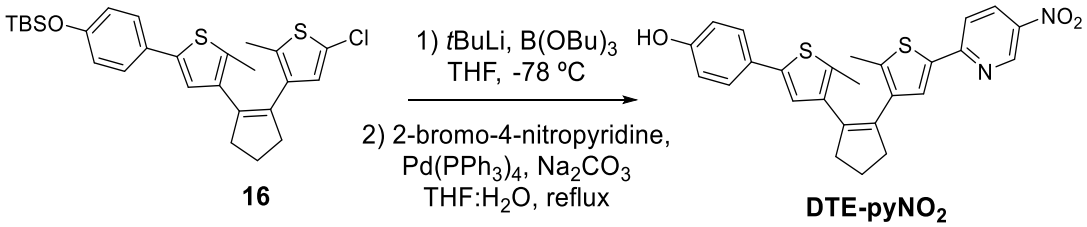

16 **DTE-pyNO$_2$**

A solution of 0.228 g of **16** (0.46 mmol) in 30 mL of anhydrous THF was cooled down to -78 ºC before adding dropwise 0.65 mL of a 1.7 M solution of *tert*-butyllithium in pentane (0.94 mmol). After stirring for 30 min at -78 ºC, the mixture was quenched with 0.25 mL of tributyl borate (0.93 mmol) and stirred for 30 min more until it reached room temperature.

Later the solution was added onto a degassed mixture of 0.118 g of 5-bromo-2-nitropyridine (0.58 mmol) and 37 mg of $Pd(PPh_3)_4$ (0.03 mmol) in 25 mL of THF, 25 mL of a 2 M Na_2CO_3 aqueous solution. The two-phase system was then heated under reflux for 2 hours. Once the reaction mixture had cooled down, 25 mL of water and 25 mL of Et_2O were added and the organic layer was separated by extraction. The organic phase was washed with 0.2 M $NaHCO_3$ aqueous solution, and after drying with anhydrous Na_2SO_4, filtration and further removal of the solvent under vacuum, a red oil was obtained. The crude was then purified through flash column chromatography (silica gel, hexanes/EtOAc, 9:1) to yield 66.3 mg of compound **DTE-pyNO₂** (0.14 mmol, 31% yield).

^{1}H NMR (400 MHz, $CDCl_3$): δ (ppm) 9.31 (dd, J_1 = 2.6 Hz, J_2 = 0.6 Hz, 1H), 8.37 (dd, J_1 = 8.8 Hz, J_2 = 2.7 Hz, 1H), 7.58 (dd, J_1 = 8.9 Hz, J_2 = 0.6 Hz, 1H), 7.46 (s, 1H), 7.37 (d, J = 8.7 Hz, 2H), 6.89 (s, 1H), 6.80 (d, J = 8.7 Hz, 2H), 2.85 (t, J = 7.4 Hz, 4H), 2.14 – 2.03 (m, 5H), 1.98 (s, 3H).

^{13}C NMR (101 MHz, $CDCl_3$): δ (ppm) 157.6, 155.1, 145.7, 142.4, 142.0, 140.1, 138.2, 138.0, 136.4, 136.1, 133.8, 133.7, 131.9, 129.6, 127.7, 127.0, 122.9, 117.8, 115.9, 38.7, 38.5, 23.2, 15.2, 14.5.

IR (ATR, cm^{-1}): 2918, 2847, 1702, 1590, 1572, 1510, 1475, 1434, 1391, 1338, 1263, 1170, 1112, 1013, 965, 947, 852, 825, 754, 719, 667, 628.

HRMS (ESI): m/z calcd for $C_{26}H_{23}N_2O_3S_2^+$: 475.1145 $[M-H]^+$; found: 475.1167

VIII.3.10. Synthesis of molecular switch, DTE-NO₂

- **Synthesis of 3,5-diiodo-2-methylthiophene, 21**

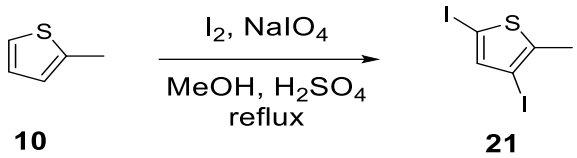

10 **21**

0.595 g of sodium periodate (2.78 mmol) were dissolved in 10 mL of methanol and 2.80 mL of a 2.4 M H_2SO_4 aqueous solution. Over this mixture a solution of 1.325 g of iodine (5.22 mmol) and 0.5 mL of **10** (5.17 mmol) in 10 mL of methanol was added. The resulting mixture was heated under reflux overnight. After the reaction mixture was cooled down to room temperature, it was mixed with 50 mL of a 2 M aqueous solution of sodium sulphite, and the product was extracted with diethyl ether. The resulting organic layer was washed with distilled water (3 x 20 mL), dried over Na_2SO_4, filtered and then the solvent was evaporated under reduced pressure obtaining 1.804 g of **21** (5.16 mmol, 99% yield). This product was purified by a

filtration through a short silica pad, and it was employed in the next step without further treatment.

^{1}H NMR (360 MHz, $CDCl_3$) δ (ppm) 7.08 (s, 1H), 2.42 (s, 3H).

^{13}C NMR (101 MHz, $CDCl_3$): δ (ppm) 145.1, 143.2, 80.4, 70.8, 18.1.

- **Synthesis of 3-iodo-2-methylthiophene, 22**

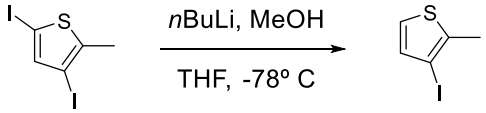

21 **22**

In a 50 mL round bottom flask, 1.804 g of **21** (5.23 mmol) were dissolved in 20 mL of anhydrous THF under inert atmosphere. The solution was cooled down to -78 ºC when 2.4 mL of a 2.5 M solution of *n*-butyllithium was added slowly (6.00 mmol). After 15 min stirring at this temperature, 0.5 mL of methanol were added (12.3 mmol) and the mixture was let to reach room temperature. Extractions were then performed with 50 mL of water and 50 mL diethyl ether and the aqueous phase was washed once with 50 mL of diethyl ether. The combined organic phases were dried over anhydrous Na_2SO_4, filtered and the solvent was removed under vacuum. Finally, the brown liquid was diluted in hexanes and filtered through a silica gel plug to obtain 0.945 g of a colorless liquid identified as **22** after solvent removal under vacuum (4.22 mmol, 81% yield).

^{1}H NMR (360 MHz, $CDCl_3$): δ (ppm) 7.09 (d, *J* = 5.3 Hz, 1H), 6.97 (d, *J* = 5.2 Hz, 1H), 2.44 (s, 3H).

- **3-iodo-2-methyl-5-nitrothiophene, 23**

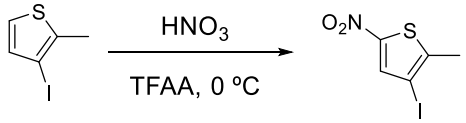

22 **23**

3.312 g of **22** (14.7 mmol) in 50 mL of trifluoroacetic anhydride were cooled down with an ice-bath. Over a period of 20 min, 2 mL of concentrated nitric acid were added dropwise at 0ºC. Once added, the mixture was stirred at room temperature for 2 hours. The solvent was removed under vacuum and after evaporation 30 mL of water and 30 mL of diethyl ether were added. The organic phase was extracted and washed once with 20 mL of water. The organic phase was dried with Na_2SO_4, filtered and the solvent removed under vacuum. The product was then purified via flash column chromatography (silica gel, hexane/EtOAc, 49:1) to yield 1.813 g of **23** as a reddish liquid (6.74 mmol, 46% yield).

^{1}H NMR (360 MHz, $CDCl_3$): δ (ppm) 7.83 (s, 1H), 2.46 (s, 3H).

^{13}C NMR (91 MHz, $CDCl_3$): δ (ppm) 150.1, 147.6, 136.1, 80.4, 19.3.

IR (ATR, cm^{-1}): 3086, 2411, 2307, 1717, 1513, 1492, 1422, 1383, 1341, 1317, 1171, 1152, 1096, 991, 857, 818, 777, 729, 707, 639.

HRMS (ESI): m/z calcd for $C_5H_3INO_2S^-$: 267.8935 $[M]^-$; found: 267.8922

- **Synthesis of 1,2-dibromocyclopentene**

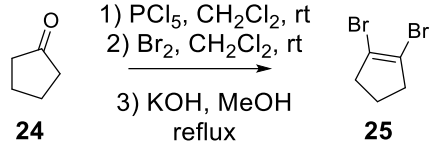

24 **25**

5.0 mL of **24** (56.5 mmol) were added onto a suspension of 15.14 g of PCl_5 (72.7 mmol) in 100 mL of dichloromethane. This mixture was stirred vigorously at room temperature until all phosphorous pentachloride dissolved. Then 2.9 mL of bromine were added dropwise. The mixture was stirred for 1 hour and then all volatiles were removed under vacuum. The pale-yellow liquid was dissolved in 50 mL of diethyl ether and washed with a 2 M NaOH aqueous solution (3x50mL). The organic layer was then dried with Na_2SO_4, filtered and the solvent removed under vacuum.

The oil obtained was then dissolved in 100 mL of MeOH and 10.2 g of KOH (178 mmol) were introduced. The mixture was then heated under reflux overnight. After cooling down the mixture, it was filtered to eliminate the excess of KOH and then the solvent removed under vacuum. 50 mL of chloroform were added and washed 3 times with brine. Once dried the organic layer with Na_2SO_4, filtered and the solvent removed, the resulting dark liquid was purified by flash column chromatography in hexanes to obtain 3.372 g of **25** (14.9 mmol, 26% yield).

^{1}H NMR (360 MHz, $CDCl_3$): δ (ppm) 2.63 (t, *J* = 7.2 Hz, 4H), 2.06 (p, *J* = 7.2 Hz, 2H).

^{13}C NMR (101 MHz, $CDCl_3$): δ (ppm) 121.8, 39.0, 22.4.

- **Synthesis of 3,5-dibromo-2-methylthiophene, 27**

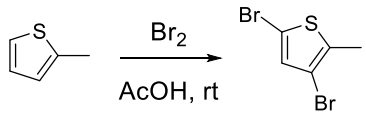

10 **27**

Onto a solution of 5 mL of **10** (53.5 mmol) in 100 mL of acetic acid placed in a 250 mL round bottom flask, 6.2 mL of bromine (121 mmol) were added over 10 min at room temperature. The reaction was stirred for 30 min when 200 mL of water and 100 mL of hexane were added. The organic layer was separated by extractions and the aqueous phase was then washed twice with 50 mL of hexane. Afterwards the combined organic phases were washed with 50 mL of a 1 M NaOH solution until the resulting aqueous phase had basic pH. Then the organic phase was dried with

anhydrous Na_2SO_4, filtered and the solvent was removed under vacuum. Finally, the yellowish liquid obtained was filtered through a silica plug and rinsed with hexane. Removal of the solvent yield 12.2 g of **27** as a colorless liquid (50.4 mmol, 95% yield).

^{1}H NMR (360 MHz, $CDCl_3$): δ (ppm) 6.86 (s, 1H), 2.33 (s, 3H).

^{13}C NMR (101 MHz, $CDCl_3$): δ (ppm) 136.0, 131.9, 108.7, 108.5, 14.8.

Synthesis of 3-bromo-5-(4-hydroxylphenyl)-2-methylthiophene, 28

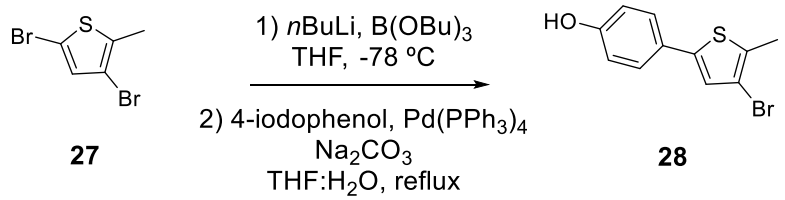

27 **28**

A solution of 2.003 g of **27** (7.84 mmol) in 20 mL of anhydrous THF was cooled down to -78 ºC before adding dropwise 4 mL of a 2.5 M solution of *n*-butyllithium in pentane (10 mmol). After stirring for 30 min at -78ºC, the mixture was quenched with 3 mL of tributyl borate (11.1 mmol) and stirred for 30 min more until it reached room temperature.

Then the resulting solution was added onto a degassed two-phase mixture of 1.585 g of 4-iodophenol (7.20 mmol) and 295 mg of $Pd(PPh_3)_4$ (0.022 mmol) in 25 mL of THF and 40 mL of a 2 M Na_2CO_3 aqueous solution. The two-phase system was then heated under reflux for 2 hours. When the mixture reached room temperature, 25 mL of water and 25 mL of Et_2O were added and the organic layer was separated by extraction. The organic phase was then washed with 0.2 M $NaHCO_3$ aqueous solution. After drying with anhydrous Na_2SO_4, filtration and further removal of the solvent under vacuum, a red oil was obtained. The crude was then purified through flash column chromatography (silica gel, EtOAc/hexane, 1:9) to yield 1.311 g of **28** (4.83 mmol, 67% yield).

^{1}H NMR (250 MHz, $CDCl_3$): δ (ppm) 7.38 (d, *J* = 8.7 Hz, 2H), 6.98 (s, 1H), 6.83 (d, *J* = 8.7 Hz, 2H), 2.40 (s, 3H).

^{13}C NMR (91 MHz, $CDCl_3$): δ (ppm) 155.5, 141.1, 132.8, 127.0, 126.8, 124.7, 116.0, 109.7, 14.9.

IR (ATR, cm^{-1}): 3313, 2921, 2053, 1886, 1610, 1545, 1512, 1442, 1381, 1290, 1254, 1178, 1108, 1016, 949, 813, 791, 757, 705, 670.

HRMS (ESI): m/z calcd for $C_{11}H_8BrOS^-$: 266.9485 $[M]^-$; found: 266.9492

- **Synthesis of 3-bromo-5-(4-(*tert*butyldimethylsyliloxy)phenyl)-2-methylthiophene, 29**

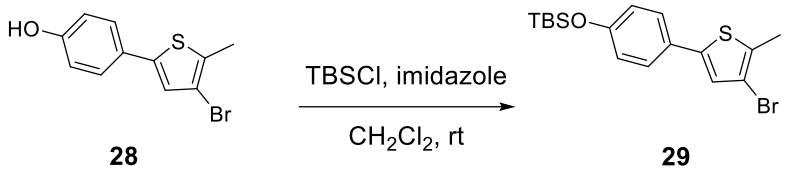

28 **29**

0.152 g of **28** (0.57 mmol), 0.090 g of TBSCl (0.60 mmol) and 0.040 g of imidazole (0.062 mmol) were stirred in 5 mL of anhydrous CH_2Cl_2 at room temperature overnight. Then the resulting organic solution was washed with 20 mL of water. The organic phase was dried over Na_2SO_4, filtered and the solvent removed under vacuum. Compound **29** was then purified via flash column chromatography (silica gel, hexane) to obtain 173 mg (0.45 mmol, 80% yield).

^{1}H NMR (250 MHz, $CDCl_3$): δ (ppm) 7.37 (d, *J* = 8.7 Hz, 2H), 6.99 (s, 1H), 6.84 (d, *J* = 8.7 Hz, 2H), 2.40 (s, 3H), 1.00 (s, 9H), 0.22 (s, 6H).

^{13}C NMR (63 MHz, $CDCl_3$): δ (ppm) 155.8, 141.3, 132.7, 127.1, 126.7, 124.7, 120.6, 109.7, 25.8, 18.4, 14.9, -4.2.

IR (ATR, cm^{-1}): 2929, 2857, 1604, 1509, 1473, 1362, 1255, 1172, 1103, 1007, 905, 838, 821, 806, 781, 730, 674, 649.

HRMS (ESI): m/z calcd for $C_{17}H_{23}BrOSSi$: 382.0417 [M]; found: 382.0419

- **Synthesis of 2-bromo-1-(2-methyl-5-nitro-thien-3-yl)cyclopentene, 26**

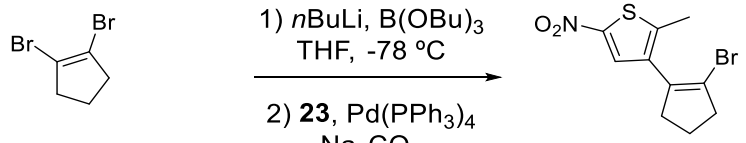

25 **26**

A solution of 1.428 g of **25** (5.58 mmol) in 20 mL of anhydrous THF was cooled down to -78 ºC before adding dropwise 3 mL of a 2.5 M solution of *n*-butyllithium in pentane (7.50 mmol). After stirring for 30 min at -78ºC, 2.2 mL of tributyl borate (8.15 mmol) were added and the mixture was stirred for 30 min more until it reached room temperature. Then the reaction mixture was quenched with 25 mL of a 2 M Na_2CO_3 aqueous solution.

Later the resulting solution was added onto a degassed mixture of 1.131 g of **23** (4.2 mmol) and 237 mg of $Pd(PPh_3)_4$ (0.21 mmol) in 25 mL of THF. The two-phase system was then heated under reflux for 2 hours. Once the reaction mixture had cooled down, 50 mL of water and 50 mL of Et_2O were added and the organic phase was

separated by extractions. The organic phase was then washed with a 0.2 M $NaHCO_3$ aqueous solution, and after drying with anhydrous Na_2SO_4, filtration and solvent removal under vacuum, a dark oil was obtained. The crude was then purified through flash column chromatography (silica gel, hexane/EtOAc, 49:1) to obtain 0.957 g of **26** as a brownish liquid (3.42 mmol, 81% yield).

^{1}H NMR (250 MHz, $CDCl_3$): δ (ppm) 7.76 (s, 1H), 2.82 (tt, J_1 = 7.6 Hz, J_2 = 2.5 Hz, 2H), 2.61 (tt, J_1 = 7.5 Hz, J_2 = 2.5 Hz, 2H), 2.45 (s, 3H), 2.09 (p, J = 7.5 Hz, 2H).

^{13}C NMR (63 MHz, $CDCl_3$): δ (ppm) 147.9, 145.0, 134.5, 134.3, 129.5, 122.0, 41.0, 36.8, 22.5, 15.7.

IR (ATR, cm^{-1}): 2921, 2848, 1649, 1499, 1420, 1375, 1322, 1234, 1201, 1153, 1093, 1029, 896, 869, 815, 768, 736, 710, 656, 633.

HRMS (APCI): m/z calcd for $C_{10}H_9BrNO_2S^-$: 285.9543 $[M]^-$; found: 285.9553

- **Synthesis of 1-(2-methyl-5-(4-hydroxyl)phenyl)thien-3-yl)-2-(2-methyl-5-nitrothien-3-yl)cyclopentene, DTE-NO_2.**

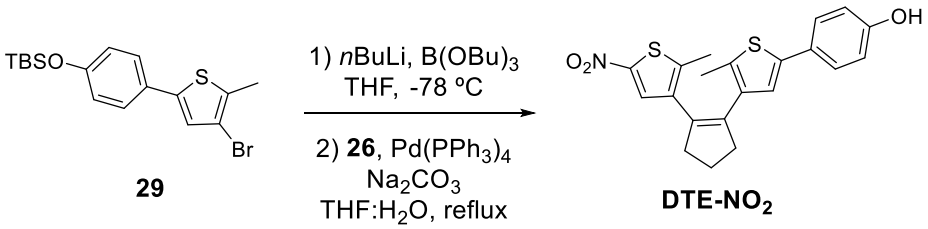

A solution of 0.61 g of **29** (1.59 mmol) in 20 mL of anhydrous THF was cooled down to -78 ºC before adding dropwise 0.75 mL of a 2.5 M solution of *n*-butyllithium in pentane (1.88 mmol). After stirring for 30 min at -78 ºC, 0.50 mL of tributyl borate (1.69 mmol) were added and the mixture stirred for 30 min more until it reached room temperature. Then, the reaction mixture was quenched with 25 mL of 2 M Na_2CO_3 aqueous solution.

Later the resulting mixture was added onto a degassed mixture of 480 mg of **26** (1.66 mmol) and 58 mg of $Pd(PPh_3)_4$ (0.05 mmol) in 25 mL of THF. The two-phase system was then heated under reflux for 2 hours. Afterwards, once cooled down the crude, 25 mL of water and 25 mL of Et_2O were added and the organic layer was separated after extractions. The organic phase was then washed with a 0.2 M $NaHCO_3$ aqueous solution, and after drying with anhydrous Na_2SO_4, filtration and further removal of the solvent under vacuum, a dark oil was obtained. The crude was then purified through flash column chromatography (silica gel, hexane/EtOAc, 9:1) to obtain 331 mg of **DTE-NO_2** as a brownish oil (0.80 mmol, 52% yield).

^{1}H NMR (400 MHz, $CDCl_3$): δ (ppm) 7.70 (s, 1H), 7.35 (d, J = 8.6 Hz, 2H), 6.88 – 6.76 (m, 3H), 2.89 – 2.73 (m, 4H), 2.09 (p, J = 7.7 Hz, 2H), 1.99 (s, 3H), 1.98 (s, 3H).

^{13}C NMR (101 MHz, $CDCl_3$): δ (ppm) 155.2, 147.8, 144.4, 140.6, 138.0, 136.6, 135.7, 133.6, 132.3, 129.9, 127.4, 127.0, 122.5, 115.9, 38.7, 38.5, 23.0, 15.3, 14.5.

IR (ATR, cm^{-1}): 3356, 2920, 2848, 2051, 1707, 1611, 1496, 1432, 1374, 1319, 1264, 1168, 1094, 1027, 949, 869, 823, 757, 736, 656.

HRMS (ESI): m/z calcd for $C_{21}H_{18}NNaO_3S_2^+$: 420.0698 $[M-Na]^+$; found: 420.0705.

VIII.3.11. Synthesis of molecular switch DTE_F-$COCF_3$

- **Synthesis of 3-bromo-5-chloro-2-methylthiophene, 30**

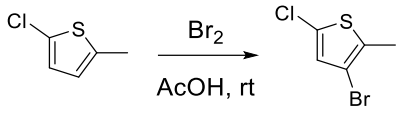

11 **30**

Onto a solution of 4.252 g of **11** (32.2 mmol) in 100 mL of acetic acid placed in a 250 mL round bottom flask, 1.6 mL of bromine (31.2 mmol) were added during 10 min at room temperature. The reaction was stirred for 30 min at room temperature after which 200 mL of water and 100 mL of hexane were added. After extractions and separation of the organic the aqueous phase was then washed twice with 50 mL of hexane. Afterwards, the combination of organic phases was washed with 50 mL of a 1 M NaOH solution until the resulting aqueous phase had basic pH. Then, the organic phase was dried with anhydrous Na_2SO_4, filtered and the solvent was removed under vacuum. Finally, the yellowish liquid obtained was filtered through a silica plug and rinsed with hexane. Removal of the solvent yielded 6.027 g of **30** as a colorless liquid (28.4 mmol, 89% yield).

^{1}H NMR (360 MHz, $CDCl_3$): δ (ppm) 6.73 (s, 1H), 2.32 (s, 3H).

^{13}C NMR (75.4 MHz, $CDCl_3$): δ (ppm) 133.0, 128.3, 126.7, 107.4, 14.5.

- **Synthesis of 1-(5-chloro-2-methylthien-3-yl)-2,3,3,4,4,5,5-heptafluorocyclopentene, 32**

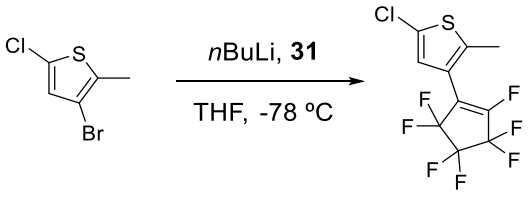

30 **32**

In a 100 mL Schlenk tube, a solution of 0.788 g of **30** (3.73 mmol) in 40 mL of anhydrous THF was cooled down to -78 ºC under inert atmosphere. Under vigorous stirring, 1.6 mL of a 2.5 M *n*-butyllithium solution in pentane (4.00 mmol) were added dropwise during a minute. The solution was stirred during 30 min after the addition

and then 0.96 mL of perfluorocyclopentene were added at once (7.15 mmol). The solution was let to reach room temperature, and afterwards it was poured onto 50 mL of a 2 M aqueous solution of Na_2CO_3. The reaction was extracted with Et_2O (2x50 mL). The organic layers were combined, dried with Na_2SO_4 and filtered. After removing the solvent, the pale-yellow oil was purified through flash column chromatography (silica gel, hexane) to isolate 0.506 g of a slightly yellow oil **32** (1.56 mmol; 42% yield).

^{1}H NMR (360 MHz, $CDCl_3$): δ (ppm) 6.91 (s, 1H), 2.39 (s, 3H).

^{13}C NMR (75.5 MHz, $CDCl_3$): δ (ppm) 153.5 (m), 149.5 (m), 142.5 (s), 128.5, 125.7, 119.2, 118.4 (m), 114.3 (m), 110.8 (m), 107.1 (m), 14.6.

^{19}F NMR (235 MHz, $CDCl_3$): δ (ppm) -109.03 (d, *J* = 12.0 Hz), -118.62 (d, *J* = 15.7 Hz), -126.95 (m), -130.43.

Synthesis of 1-(5-chloro-2-methylthien-3-yl)-2-(5-(4-*tert*butyldimethylsilyloxy)phenyl)-2-methylthien-3-yl)-3,3,4,4,5,5-hexafluorocyclopentene, 33

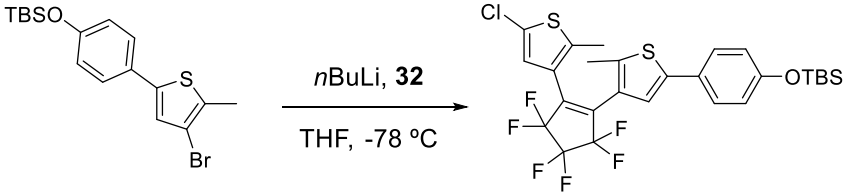

29 **33**

In a 100 mL Schlenk tube, a solution of 231 mg of **29** (0.60 mmol) and 10 mL of anhydrous THF was cooled down to -78 ºC under inert atmosphere. Under vigorous stirring, 0.25 mL of a 2.5 M *n*-butyllithium solution in pentane (0.75 mmol) were added dropwise during a minute. The solution was stirred for 30 min after the addition, and 147 mg of **32** (0.45 mmol) were then added at once. The solution was stirred until it reached room temperature, and then it was poured onto 20 mL of a 2 M aqueous solution of Na_2CO_3. Then, the mixture was extracted with Et_2O (2x50 mL). The organic layers were combined and dried with Na_2SO_4 and filtered. After removing the solvent, the pale-yellow oil was purified through a flash column chromatography (silica gel, hexane) to isolate 73 mg of **33** (0.13 mmol; 29% yield).

^{1}H NMR (400 MHz, $CDCl_3$): δ (ppm) 7.40 (d, *J* = 8.8 Hz, 2H), 7.11 (s, 1H), 6.92 (s, 1H), 6.85 (d, *J* = 8.8 Hz, 2H), 1.95 (s, 3H), 1.88 (s, 3H), 0.99 (s, 9H), 0.22 (s, 6H).

^{13}C NMR (101 MHz, $CDCl_3$): δ (ppm) 156.0, 142.6, 140.6, 140.5, 127.8, 127.0, 126.8, 125.8, 125.5, 124.6, 121.2, 120.8, 77.2, 25.8, 18.4, 14.6, 14.5.

^{19}F NMR (235 MHz, $CDCl_3$): δ (ppm) -110.60 (d, *J* = 5.1 Hz), -132.34 (p, *J* = 5.3 Hz).

IR (ATR, cm^{-1}): 2931, 2860, 2051, 1607, 1552, 1512, 1473, 1435, 1362, 1331, 1308, 1264, 1192, 1176, 1105, 1058, 1021, 1001, 979, 953, 911, 823, 806, 778, 735, 720, 678, 666, 620.

HRMS (APCI): m/z calcd for $C_{27}H_{26}ClF_6OS_2Si^{\cdot}$: 607.0793 $[M]^{\cdot}$; found: 607.0765

- **Synthesis of 1-(5-chloro-2-methylthien-3-yl)-2-(5-(4-hydroxyl)phenyl)-2-methylthien-3-yl)-3,3,4,4,5,5-hexafluorocyclopentene, DTE_F-$COCF_3$**

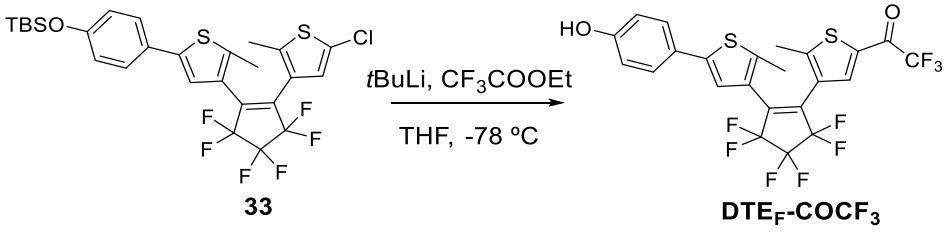

In a 100 mL Schlenk tube, a solution of 94 mg of **33** (0.15 mmol) in 10 mL of anhydrous THF was cooled to -78 ºC under inert atmosphere. Under vigorous stirring, 0.25 mL of a 1.7 M *tert*-butyllithium solution in pentane (0.43 mmol) were added dropwise during a minute. The solution was stirred for 30 min after the addition, when 0.3 mL of anhydrous ethyl trifluoroacetate were added at once (2.5 mmol). The solution was let to reach room temperature, and it was poured onto 20 mL of a 2 M aqueous solution of Na_2CO_3. Then, the mixture was extracted with Et_2O (2x50 mL). The organic layers were washed with 20 mL 1 M HCl aqueous solution, combined and dried with Na_2SO_4. After filtration and solvent removal under vacuum, it was purified through flash column chromatography (silica gel, hexanes/EtOAc, 4:1), obtaining 12.0 mg of pure **DTE_F-$COCF_3$** (0.022 mmol, 14% yield).

^{1}H NMR (360 MHz, $CDCl_3$): δ (ppm) 7.90 (s, 1H), 7.40 (d, *J* = 8.5 Hz, 2H), 7.09 (s, 1H), 6.86 (d, *J* = 8.5 Hz, 2H), 2.13 (s, 3H), 1.95 (s, 3H).

^{13}C NMR (91 MHz, $CDCl_3$): δ (ppm) 173.1 (d, *J* = 37.1 Hz) , 155.9, 154.9, 143.2, 140.5, 136.6, 134.0, 127.7, 127.4, 126.1, 125.0, 120.9, 116.3 (q, *J* = 290.2 Hz), 116.1, 15.6, 14.6.

^{19}F NMR (235 MHz, $CDCl_3$): δ (ppm) -72.81, -110.44, -111.00, -132.30.

IR (ATR, cm^{-1}): 2927, 2051, 1692, 1612, 1542, 1515, 1439, 1339, 1269, 1192, 1139, 1112, 1051, 986, 928, 901, 867, 823, 751, 732, 666, 631.

HRMS (ESI): m/z calcd for $C_{23}H_{12}F_9O_2S_2^{\cdot}$: 555.0140 $[M]^{\cdot}$; found: 555.0146.

VIII.4. SYNTHESIS OF PHOTOISOMERIZABLE ACTIVE ESTERS FOR LIGHT-CONTROLLED AMIDATION

VIII.4.1. Synthesis of 1-(2-methyl-5-(4-acetoxy)phenyl)thien-3-yl)-2-(2-methyl-5-nitrothien-3-yl)cyclopentene, DTE-NO_2-Ac

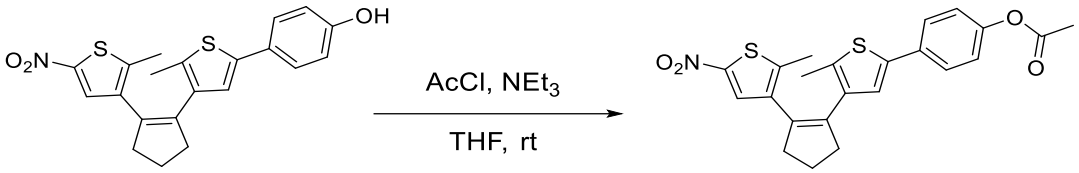

DTE-NO_2 **DTE-NO_2-Ac**

101 mg of **DTE-NO_2** (0.25 mmol) were added onto a solution containing 0.1 mL of triethylamine (0.71 mmol) and 0.1 mL of acetyl chloride (1.40 mmol) in 5 mL of THF. The mixture was stirred for 3 hours, after which 10 mL of water and 10 mL of Et_2O were poured. The organic phase was washed with water once and then dried over Na_2SO_4, filtered and the solvent was removed under vacuum. The crude was purified via flash column chromatography (silica gel, hexanes/EtOAc, 9:1) to obtain 99 mg of **DTE-NO_2-Ac** (0.23 mmol, 89% yield).

^{1}H NMR (400 MHz, $CDCl_3$): δ (ppm) 7.69 (s, 1H), 7.47 (d, *J* = 8.6 Hz, 2H), 7.07 (d, *J* = 8.7 Hz, 2H), 6.90 (s, 1H), 2.84 (t, *J* = 7.4 Hz, 2H), 2.78 (t, *J* = 7.5 Hz, 2H), 2.31 (s, 3H), 2.10 (p, *J* = 7.5 Hz, 2H), 2.00 (s, 3H), 1.98 (s, 3H).

^{13}C NMR (101 MHz, $CDCl_3$): δ (ppm) 169.6, 150.0, 147.8, 144.3, 139.8, 137.7, 136.5, 135.9, 134.8, 132.5, 132.1, 129.8, 126.5, 123.7, 122.1, 38.7, 38.5, 23.0, 21.2, 15.3, 14.6.

IR (ATR, cm^{-1}): 2916, 2844, 2051, 1750, 1499, 1422, 1367, 1321, 1191, 1165, 1093, 1015, 949, 909, 835, 817, 800, 753, 736, 664.

HRMS (ESI): m/z calcd for $C_{23}H_{21}NNaO_4S_2^+$: 462.0804 $[M-Na]^+$; found: 462.0803.

VIII.4.2. Synthesis of DTE-PDI

- **Synthesis of 1,6,7,12-tetrachloroperylene-3,4:9,10-tetracarboxylic dianhydride, 40**

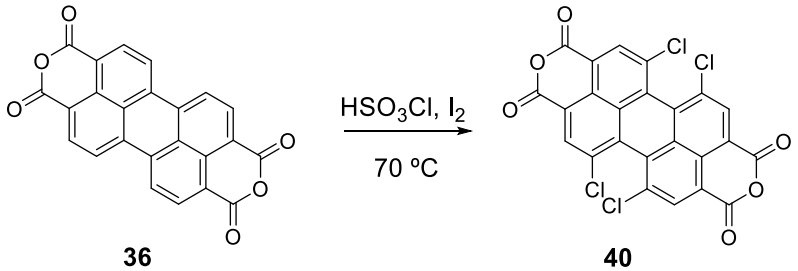

36 **40**

2.5 g of **36** (6.4 mmol), 0.45 g (1.7 mmol) of iodine and 15 mL of chlorosulfonic acid (231 mmol) were stirred in a 100 mL round bottom flask under argon atmosphere. The mixture was heated at 70 ºC for 15 hours. After the reaction time, the crude was cooled down to room temperature and the reaction mixture was added over 100 g of ice and 100 mL of water. The solid obtained was filtered under vacuum and dried at 130ºC under vacuum for 2 hours obtaining 3.2 g of compound **40** (6.1 mmol, yield: 96%).

^{1}H NMR (360 MHz, $CDCl_3$): δ (ppm) 8.75 (s).

- **Synthesis of *N,N´*-bis(*sec*-butyl)-1,6,7,12-tetrachloroperylene-3,4:9,10-tetracarboxylic diimide, 41**

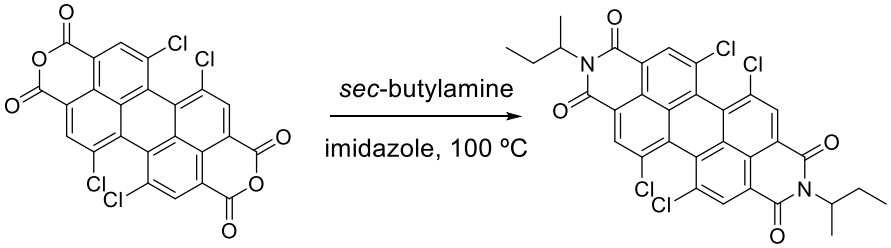

40 **41**

2.00 g (3.7 mmol) of dianhydride **40**, 1.57 g of commercial *sec*-butylamine (15.5 mmol) and 8.0 g of imidazole were introduced in a 100 mL round bottom flask under argon atmosphere. The mixture was heated at 100 ºC under stirring for 3 hours. After the reaction time the mixture was cooled down to room temperature and ethanol was added until all the solid had dissolved. Then 300 mL of a 2 M HCl aqueous solution were added and the mixture was stirred for 1 hour. The resulting suspension was then filtered under vacuum. The orange solid obtained was dried in a vacuum oven at 130ºC for 3 hours obtaining 1.82 g of compound **41** (2.85 mmol, 75% yield).

^{1}H NMR (360 MHz, $CDCl_3$): δ (ppm) 8.66 (s, 4H), 5.20 (m, 2H), 2.28-2.14 (m, 2H), 2.03-1.91 (m, 2H), 1.59 (d, *J* = 6.4 Hz, 6H), 0.90 (t, *J* = 7.6 Hz, 6H).

- **Synthesis of N,N'-bis(*sec*-butyl)-1,6,7,12-tetra-(4-*tert*-butylphenoxy)perylene-3,4:9,10-tetracarboxylic diimide,38.**

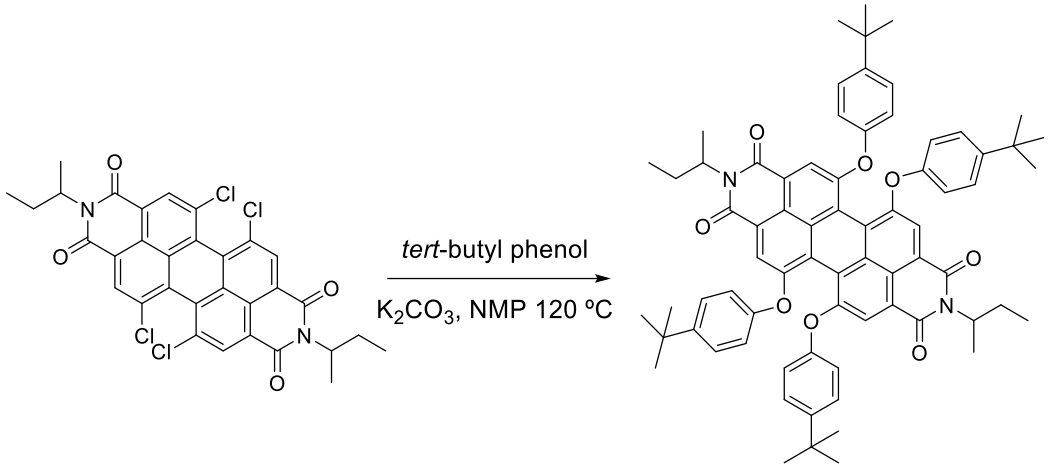

41 **37**

1.82 g of diimide **41** (2.8 mmol), 3.9 g (26.0 mmol) of commercial *tert*-butylphenol, 4.43 g of K_2CO_3 (32.1 mmol) and 125 mL of NMP were introduced in a 250 mL round bottom flask equipped with magnetic stirring. The mixture was warmed up to 120 ºC for 16 hours. After the reaction time the mixture was cooled down to room temperature, acidified with 100 mL of aqueous HCl 2 M and 200 mL of a 1:1 solution of EtOAc:hexane was added. The phases were separated, and the organic layer was washed once with 100 mL of water. Then the solvent was removed under vacuum and the solid formed dissolved in the minimum amount of MeOH, after which the solution was added onto 100 mL of a 2 M NaOH aqueous solution. The solid formed was filtered washed with 2 M HCl aqueous solution and dried under vacuum at 130 ºC overnight to obtain 1.423 g of **37** (1.30 mmol, 40% yield).

^{1}H NMR (360 MHz, $CDCl_3$): δ (ppm) 8.20 (s, 4H), 7.23 (d, *J* = 8.4 Hz, 8H), 6.83 (d, *J* = 8.4 Hz, 8H), 5.12 (m, 2H), 2.22-2.07 (m, 2H), 1.93-1.80 (m, 2H), 1.50 (d, *J* = 7.5 Hz, 6H), 1.29 (s, 36H), 0.87 (t, *J* = 7.3 Hz, 6H).

^{13}C NMR (90 MHz, $CDCl_3$): δ (ppm) 164.0, 155.9, 152.9, 147.2, 132.8, 126.6, 122.8, 120.4, 119.8, 119.6, 119.3, 51.4, 34.4, 31.5, 26.5, 18.1, 11.5.

- **Synthesis of *N*-(*sec*-butyl)-1,6,7,12-tetra(4-*tert*-butylphenoxy)perylene-3,4:9,10-tetracarboxylic-3,4-anhydride-9,10-imide, 42**

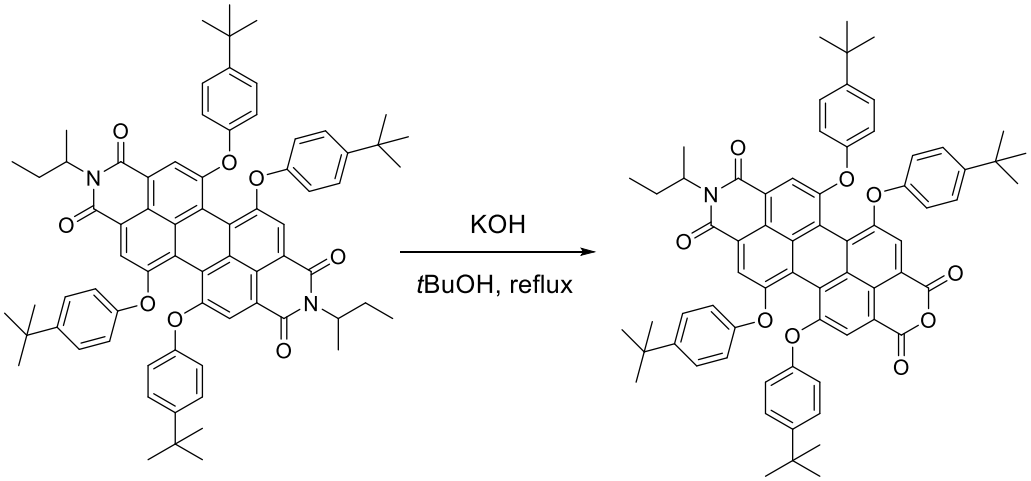

37 **42**

0.240 mg of **37** (0.22 mmol), 0.047 g of KOH (0.84 mmol) and 12 mL of *tert*-butanol were introduced in a 100 mL round bottom flask equipped with magnetic stirring. The mixture was heated under reflux until **38** disappearance after 45 min followed by TLC. After the reaction time, the mixture was cooled down to room temperature and acidified by adding 30 mL of a 2 M HCl aqueous solution. The precipitate formed was filtered under vacuum and the solid was dried at 120 ºC during 3 hours under vacuum. This crude was purified by flash column chromatography (silica gel, $CHCl_3$/hexane, 1:1). 0.183 g of the desired product **42** were obtained (0.18 mmol, yield: 75%).

^{1}H NMR (360 MHz, $CDCl_3$): δ (ppm) 8.24 (m, 4H), 7.27 (m, 8H), 6.8 (m, 8H), 5.14 (m, 1H), 2.17 (m, 1H), 1.89 (m, 1H), 1.53 (d, *J* = 7.5 Hz, 3H), 1.31 (s, 18H), 1.27 (s, 18H), 0.89 (t, J = 7.4 Hz, 3H).

^{13}C NMR (90 MHz, $CDCl_3$): δ (ppm) 163.8, 160.21, 156.7, 155.8, 152.8, 152.6, 147.7, 147.5, 145.3, 139.6, 133.1, 133.0, 126.6, 124.6, 123.7, 122.3, 121.7, 121.5, 119.5, 117.9, 51.5, 34.4, 31.5, 26.5, 18.1, 11.5.

- **Synthesis of *N*-(*sec*-butyl)-*N*-(11-carboxyundecyl)-1,6,7,12-tetra(4-*tert*-butylphenoxy)perylene-3,4:9,10-tetracarboxylic-3,4-anhydride-9,10-imide, 38**

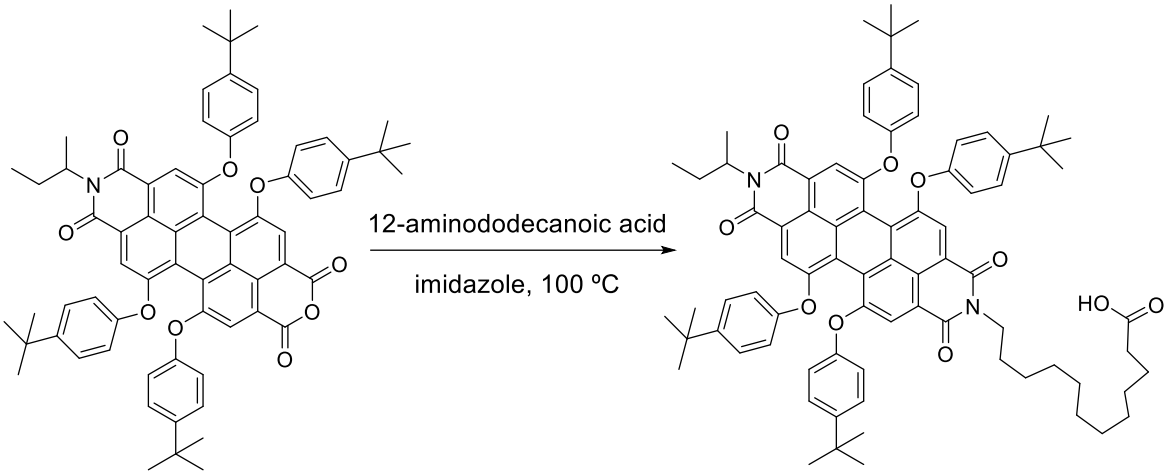

42 **38**

0.183 g of anhydride **42** (0.18 mmol), 0.081 g of 12-aminododecanoic acid (0.38 mmol) and 2.0 g of imidazole were heated at 100 ºC for 3 hours in a 50 mL round bottom flask under argon atmosphere. Afterwards the reaction mixture was cooled down to room temperature and it was dissolved in the minimum amount of ethanol required. Then, 100 mL of an aqueous 2 M HCl solution were added, and the mixture was stirred for 30 min. The precipitate was filtered under vacuum and dried in a vacuum oven at 130 ºC for 3 hours. The crude was purified via flash column chromatography (silica gel, $CHCl_3$) to obtain 0.140 g of **38** (0.11 mmol, 64% yield).

^{1}H NMR (400 MHz, $CDCl_3$): δ (ppm) 8.22 (s, 2H), 8.20 (s, 2H), 7.23 (d, *J* = 8.5 Hz, 8H), 6.82 (d, *J* = 6.9 Hz, 8H), 5.12 (h, *J* = 6.4 Hz, 1H), 4.09 (t, *J* = 7.6 Hz, 2H), 2.32 (t, *J* = 7.5 Hz, 2H), 2.14 (m, 1H), 1.86 (m, 1H), 1.73 – 1.53 (m, 4H), 1.50 (d, *J* = 6.8 Hz, 3H), 1.38 – 1.19 (m, 50H), 0.86 (t, *J* = 7.4 Hz, 3H).

^{13}C NMR (101 MHz, $CDCl_3$): δ (ppm) 164.1, 163.6, 156.2, 156.0, 153.0, 153.0, 152.9, 147.4, 133.1, 132.9, 126.9, 126.8, 123.0, 122.5, 120.7, 120.4, 120.0, 119.9, 119.7, 119.6, 119.5, 119.4, 119.4, 51.5, 40.8, 34.5, 33.8, 31.6, 29.8, 29.8, 29.6, 29.5, 29.4.

IR (ATR, cm^{-1}): 2928, 2325, 2050, 1696, 1658, 1586, 1503, 1461, 1410, 1339, 1281, 1210, 1172, 1110, 1014, 877, 832, 803, 750, 702, 668.

HRMS (ESI): m/z calcd for $C_{80}H_{87}N_2O_{10}^-$: 1235.6366 $[M]^-$; found: 1235.6369.

- **Synthesis of *N*-(*sec*-butyl)-*N*-(12-(4-(5-methyl-4-(2-(2-methyl-5-nitrothiophen-3-yl)cyclopent-1-en-1-yl)thiophen-2-yl)phenoxy)-12-oxododecyl)-1,6,7,12-tetra(4-*tert*-butylphenoxy)perylene-3,4:9,10-tetracarboxylic-3,4-anhydride-9,10-imide, DTE-PDI**

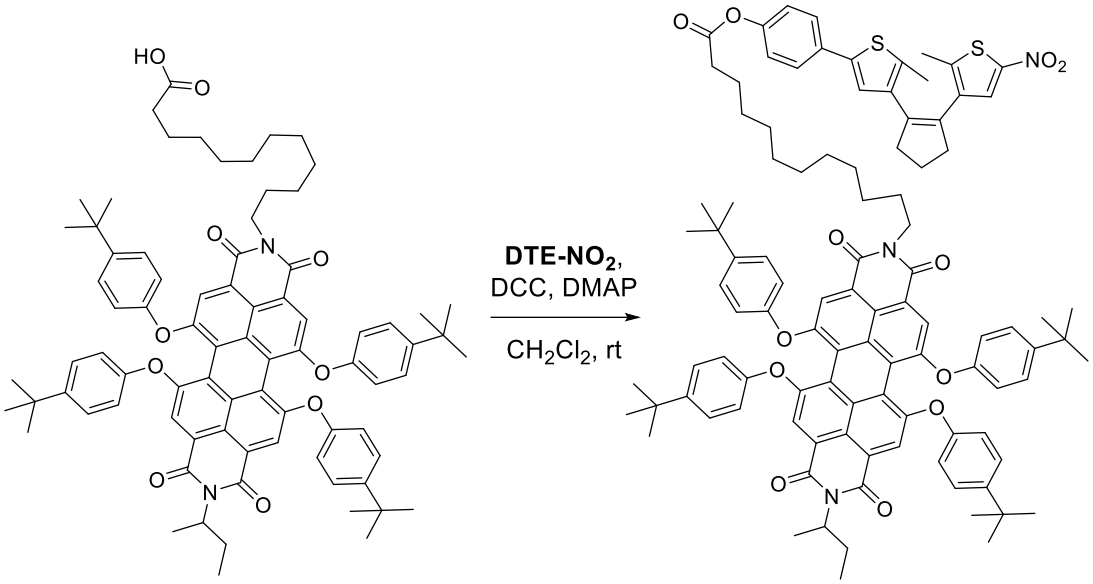

38 **DTE-PDI**

0.233 g of perylenediimide **38** (0.19 mmol), 0.101 g of **DTE-NO₂** (0.25 mmol), 0.152 g of DCC (3.9 mmol) and 0.005 g of DMAP (0.04 mmol) were stirred overnight in 10 mL of anhydrous CH_2Cl_2. Afterwards the solvent was removed under vacuum, and the crude was purified via flash column chromatography (silica gel, hexanes/EtOAc 4:1) to obtain 0.231 g of **DTE-PDI** (0.14 mmol, 74% yield).

^{1}H NMR (360 MHz, $CDCl_3$): δ (ppm) 8.22 (s, 2H), 8.20 (s, 2H), 7.69 (s, 1H), 7.45 (d, *J* = 8.7 Hz, 2H), 7.23 (d, *J* = 8.4 Hz, 8H), 7.04 (d, *J* = 8.8 Hz, 2H), 6.90 (s, 1H), 6.83 (d, *J* = 8.6 Hz, 8H), 5.12 (h, *J* = 6.3 Hz, 1H), 4.10 (t, *J* = 7.6 Hz, 2H), 2.89 – 2.74 (m, 4H), 2.53 (t, *J* = 7.5 Hz, 2H), 2.11 (m, 1H), 1.99 (s, 3H), 1.97 (s, 3H), 1.86 (m, 1H), 1.78 – 1.61 (m, 4H), 1.50 (d, *J* = 6.9 Hz, 3H), 1.43 – 1.18 (m, 50H), 0.86 (t, *J* = 7.3 Hz, 3H).

^{13}C NMR (91 MHz, $CDCl_3$): δ (ppm) 172.4, 164.1, 163.6, 156.1, 156.0, 153.0, 153.0, 150.1, 147.8, 147.4, 144.3, 139.9, 137.7, 136.5, 135.9, 134.7, 133.1, 132.9, 132.5, 132.0, 129.8, 126.8, 126.8, 126.5, 123.6, 123.0, 122.5, 122.2, 120.7, 120.4, 120.0, 119.9, 119.7, 119.6, 119.5, 119.4, 119.4, 51.5, 40.8, 38.7, 38.5, 34.5, 31.8, 31.6, 29.8, 29.8, 29.6, 29.6, 29.5, 29.4, 29.4, 29.2, 28.2, 27.3, 26.6, 25.1, 23.0, 18.3, 15.3, 14.6, 11.6.

IR (ATR, cm^{-1}): 2927, 2857, 2361, 2325, 2051, 1981, 1754, 1694, 1656, 1586, 1503, 1461, 1410, 1335, 1284, 1209, 1168, 1109, 1014, 879, 832, 803, 750, 703, 668.

HRMS (ESI): m/z calcd for $C_{101}H_{106}N_3O_{12}S_2^+$: 1616.7212 $[M-H]^+$; found: 1616.7214.

VIII.4.3. Synthesis of *N-(sec*-butyl)-*N*-(12-(4-nitrophenoxy)-12-oxododecyl)-1,6,7,12-tetra(4-*tert*-butylphenoxy)perylene-3,4:9,10-tetracarboxylic-3,4-anhydride-9,10-imide, NO_2-PDI.

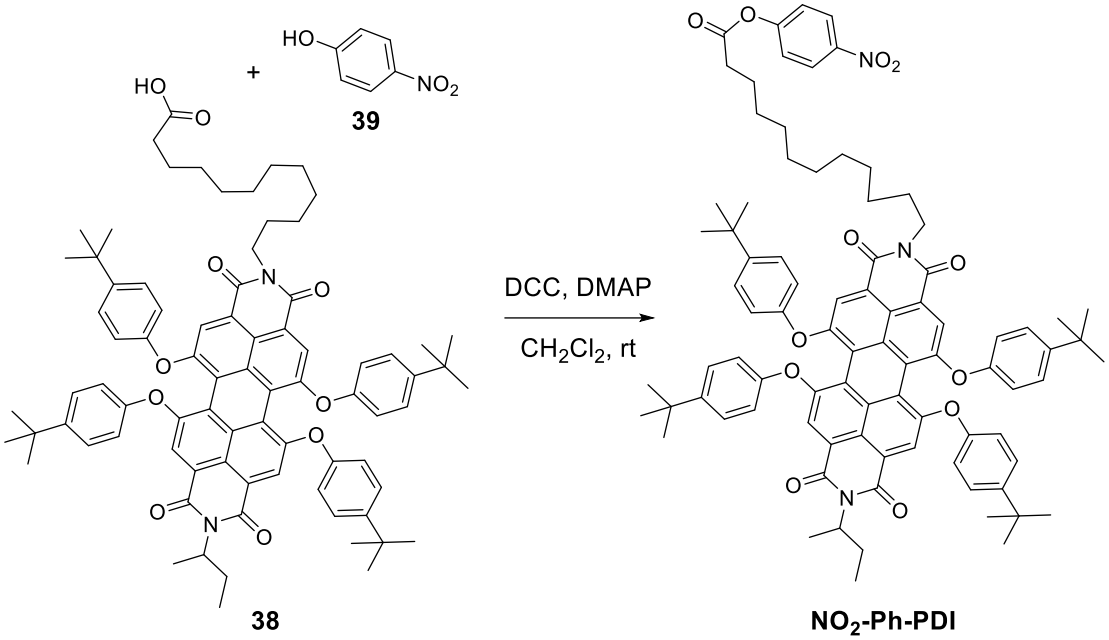

39 mg of perylenediimide **38** (0.03 mmol), 15 mg of **39** (0.11 mmol), 17 mg of DCC (0.82 mmol) and 5 mg of DMAP (0.04 mmol) were stirred overnight in 10 mL of anhydrous CH_2Cl_2. After this time the solvent was removed under vacuum and the crude purified via flash column chromatography (silica gel, hexanes/EtOAc, 9:1) to obtain 25 mg of **NO_2-Ph-PDI** (0.02 mmol, 57% yield).

^{1}H NMR (400 MHz, $CDCl_3$): δ (ppm) 8.26 (d, *J* = 9.1 Hz, 2H), 8.22 (s, 2H), 8.20 (s, 2H), 7.26 (d, *J* = 9.2 Hz, 2H), 7.24 – 7.20 (m, 8H), 6.85 – 6.80 (m, 8H), 5.12 (m, 1H), 4.09 (t, *J* = 7.6 Hz, 2H), 2.57 (t, *J* = 7.5 Hz, 2H), 2.14 (m, 1H), 1.86 (m, 1H), 1.78 – 1.62 (m, 4H), 1.50 (d, *J* = 6.9 Hz, 3H), 1.44 – 1.14 (m, 50H), 0.86 (t, *J* = 7.4 Hz, 3H).

^{13}C NMR (101 MHz, $CDCl_3$): δ (ppm) 171.4, 164.1, 163.6, 156.2, 156.0, 155.7, 153.1, 153.0, 147.4, 145.4, 133.1, 132.9, 126.8, 126.8, 125.3, 123.1, 122.6, 122.5, 120.8, 120.4, 120.1, 119.9, 119.7, 119.6, 119.5, 119.5, 51.5, 40.8, 34.5, 34.5, 31.6, 29.8, 29.6, 29.6, 29.5, 29.4, 29.3, 29.2, 28.2, 27.2, 26.7, 24.9, 18.3, 11.6.

IR (ATR, cm^{-1}): 2930, 2857, 2051, 1765, 1695, 1656, 1587, 1524, 1503, 1461, 1433, 1410, 1341, 1283, 1209, 1173, 1109, 1014, 878, 832, 804, 749, 702, 667.

HRMS (ESI): m/z calcd for $C_{86}H_{92}N_3O_{12}^+$: 1358.6676 $[M-H]^+$; found: 1358.6661

VIII.5. SYNTHESIS OF DTE-BASED DIENOPHILES AND O-MBA DIENES FOR THE TWO-COLOR CONTROL OF DIELS-ALDER CYCLOADDITIONS.

VIII.5.1. Synthesis of molecular switch DTE-Mal.

- **Synthesis of *N*-methyl-3,4-dibromomaleimide, 44**

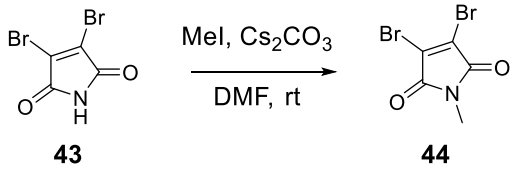

43 **44**

0.521 g of **43** (2.0 mmol) and 0.821 g of Cs_2CO_3 (2.5 mmol) were dissolved in 20 mL of DMF under argon atmosphere. 0.50 mL methyl iodide (8.0 mmol) were added to the reaction mixture and it was stirred overnight. Upon reaction completion the solvent was removed under vacuum, and the reaction mixture was dissolved in 20 mL Et_2O. The organic layer was washed twice with water (2x20 mL), dried over anhydrous Na_2SO_4, filtered and the solvent removed under vacuum. The crude was purified via flash column chromatography (silica gel, hexanes/EtOAc, 9:1) and 0.331 g of **44** were obtained as a slightly yellow solid (1.2 mmol, 60% yield).

^{1}H NMR (360 MHz, $CDCl_3$): δ (ppm) 3.15 (s, 3H).

^{13}C NMR (75 MHz, $CDCl_3$): δ (ppm) 164.1, 129.5, 25.6.

- **Synthesis of 3-bromo-2-methyl-5-phenylthiophene, 45**

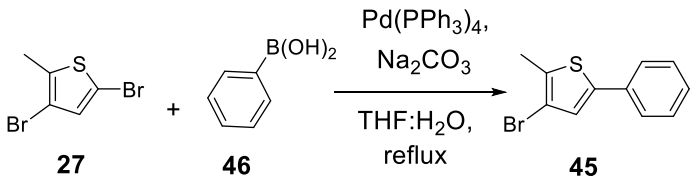

27 **46** **45**

A degassed solution of 0.683 g of **27** (2.7 mmol), 0.325 g of **46** (2.7 mmol) and 92 mg of $Pd(PPh_3)_4$ (0.07 mmol) in 25 mL of THF, 25 mL of a 2 M Na_2CO_3 aqueous solution and 10 drops of ethylene glycol was heated under reflux for 2 hours. Afterwards, the reaction was cooled down to room temperature and 25 mL of water and 25 mL of Et_2O were added. The organic phase was separated, dried with anhydrous Na_2SO_4, filtered, and the solvent removed under vacuum to obtain a brownish oil. The crude was then purified through flash column chromatography (silica gel, hexane) to yield 0.628 g of compound **45** (2.5 mmol, 93% yield).

^{1}H NMR (360 MHz, $CDCl_3$): δ (ppm) 7.51 (d, J = 7.0 Hz, 2H), 7.37 (t, J = 7.5 Hz, 2H), 7.28 (t, J = 7.3 Hz, 1H), 7.11 (s, 1H), 2.42 (s, 3H).

^{13}C NMR (101 MHz, $CDCl_3$): δ (ppm) 141.1, 133.6, 133.4, 128.9, 127.7, 125.5, 125.2, 109.9, 14.8.

- **Synthesis of 2-methyl-5-phenylthien-3-ylboronic acid, 47**

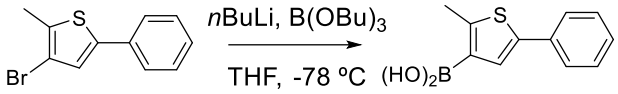

45 **47**

1.103 g of **45** (4.4 mmol) were dissolved in 20 mL of THF and cooled down to -78 ºC. Then 1.8 mL of a 2.7 M solution of *n*-butyllithium in toluene (4.9 mmol) were added and the reaction mixture was stirred at low temperature for 15 min. Then 1.3 mL of tributyl borate were added (4.8 mmol) and the reaction mixture was stirred for additional 30 min without cooling. Once it had reached room temperature, 60 mL of a 2 M HCl aqueous solution were added, and the two-phase solution was stirred overnight. The organic phase was separated and extracted 1 M NaOH (4x20 mL). The aqueous phase was acidified to pH 1 and the white solid formed was filtrated. After washings with distilled water (2x10 mL) 0.684 g of a white powder were isolated identified as **47** (3.1 mmol, 72% yield).

^{1}H NMR (250 MHz, DMSO): δ (ppm) 7.95 (s, 2H), 7.61 (s, 1H), 7.53 (dd, J_1 = 8.3 Hz, J_2 = 1.3 Hz, 2H), 7.38 (dd, J_1 = 8.3 Hz, J_2 = 7.4 Hz, 2H), 7.24 (tt, J_1 = 7.4 Hz, J_2 = 1.1 Hz, 1H), 2.60 (s, 3H).

- **Synthesis of molecular switch *N*-methyl-3,4-bis(2-methyl-5-phenyl-thien-3-yl)maleimide, DTE-Mal**

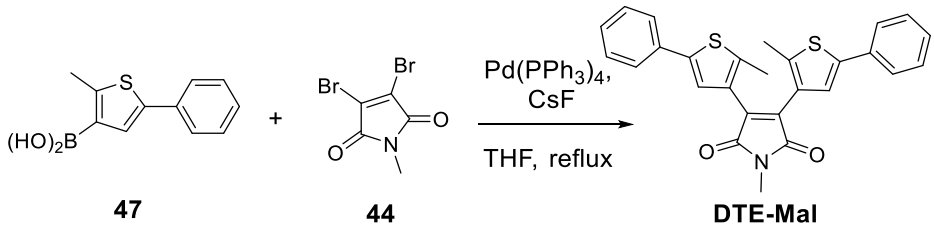

47 **44** **DTE-Mal**

1.532 g of CsF (10.1 mmol), 0.679 g of **47** (3.11 mmol) and 0.381 g of **44** (1.42 mmol) were mixed in 20 mL or anhydrous THF under inert atmosphere. The mixture was degassed and 86 mg of $Pd(PPh_3)_4$ (0.075 mmol) were added. The reaction mixture was heated under reflux overnight. Then, 20 mL saturated aqueous solution of $NaHCO_3$ and 20 mL of Et_2O were added and the organic layer was separated by extraction, dried with anhydrous Na_2SO_4, filtered and the organic solvent removed under vacuum. The crude was purified via flash column chromatography (silica gel, hexane/EtOAc, 9:1) to obtain 0.390 g of **DTE-Mal** as a brownish powder (0.86 mmol, 60% yield).

^{1}H NMR (360 MHz, CD_3CN): δ (ppm) 7.57 (d, *J* = 7.1 Hz, 4H), 7.39 (t, *J* = 7.5 Hz, 4H), 7.30 (t, *J* = 7.3 Hz, 2H), 3.07 (s, 3H), 2.05 (s, 6H).

^{13}C NMR (91 MHz, CD_3CN): δ (ppm) 171.6, 141.7, 141.7, 134.7, 134.4, 130.0, 129.2, 128.7, 126.2, 125.5, 24.5, 14.9.

IR (ATR, cm^{-1}): 2914, 2325, 2051, 1981, 1765, 1696, 1598, 1553, 1433, 1385, 1252, 1181, 1074, 1029, 986, 950, 911, 846, 757, 738, 688, 653, 620.

HRMS (ESI): m/z calcd for $C_{27}H_{21}NO_2S_2$: 455.1014 $[M-H]^-$; found: 455.1007

VIII.5.2. Synthesis of molecular switch DTE-NO_2-COOMe.

- **Synthesis of 3-bromo-2-methylthien-5-yl formic acid, 45**

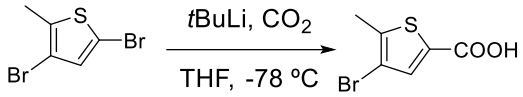

27 **48**

1.018 g of **27** (3.96 mmol) were dissolved in 20 mL of anhydrous THF under argon atmosphere. The solution was cooled down to -78 ºC and 3 mL of a 1.6 M solution of *n*-butyllithium in hexanes (4.8 mmol) were added. After stirring for 15 min, CO_2 was bubbled into the solution until no more precipitate was formed. Then the reaction mixture was stirred until it reached room temperature. At this point 20 mL of 1 M NaOH aqueous solution and 20 mL of Et_2O were added. The aqueous phase was separated by extraction and next acidified to acidic pH until no more precipitate was formed. Compound **48** was isolated as pure after filtration under vacuum obtaining 0.781 g of a white powder (3.53 mmol, 89% yield).

^{1}H NMR (360 MHz, $CDCl_3$): δ (ppm) 7.69 (s, 1H), 2.47 (s, 3H).

- **Synthesis of 3-bromo-2-methylthien-5-yl methyl formate, 49**

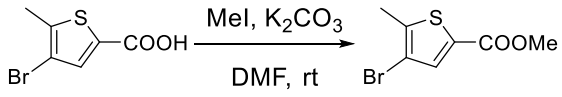

48 **49**

0.581 g of **48** (2.63 mmol), 0.5 mL of methyl iodide (8.03 mmol) and 0.525 g of K_2CO_3 (3.80 mmol) were stirred overnight in DMF at room temperature. Then, the solvent was removed under vacuum and the reaction mixture was disolved in 20 mL of diethyl ether. The organic phase was washed twice with 20 mL of a 1 M NaOH solution, dried with Na_2SO_4, filtered and the solvent was removed under vacuum. The crude was purified via flash column chromatography (silica gel, hexanes:EtOAc 1:9) to obtain 0.582 g of **49** as a white solid (2.48 mmol, 94% yield).

^{1}H NMR (250 MHz, $CDCl_3$): δ (ppm) 7.59 (s, 1H), 3.86 (s, 3H), 2.43 (s, 3H).

^{13}C NMR (125 MHz, $CDCl_3$): δ (ppm) 161.8, 142.4, 135.9, 130.2, 110.4, 52.4, 15.5.

- **Synthesis of molecular switch 1-(2-methyl-5-(methoxycarbonyl)-thien-3-yl)-2-(2-methyl-5-nitro-thien-3-yl)cyclopentene DTE-NO_2-COOMe**

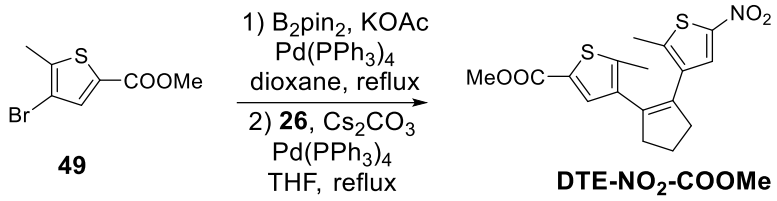

0.363 g of **49** (1.54 mmol) was dissolved in 10 mL of anhydrous dioxane with 0.458 g of bis(pinacolato)diboron (1.80 mmol) and 0.584 g of KOAc (5.95 mmol). Then the mixture was degassed with argon and 55 mg of $Pd(PPh_3)_4$ (0.048 mmol) were added. The reaction mixture was heated under reflux overnight and after cooling down, it was filtered through a plug of celite, and the solvent was removed under vacuum.

The resulting solid was dissolved in 20 mL of anhydrous THF and 1.513 g of Cs_2CO_3 (4.64 mmol) and 0.165 g of **26** (0.57 mmol) were added. The mixture was degassed before 0.101 g $Pd(PPh_3)_4$ (0.09 mmol) were added. The reaction mixture was heated under reflux overnight and, after cooling down, 20 mL of Et_2O were added and it was washed with 20 mL of a saturated $NaHCO_3$ aqueous solution. The organic layer was dried with Na_2SO_4, filtered and the solvent removed under vacuum. The crude was purified by flash column chromatography (silica gel, hexane:EtOAc, 9:1) to obtain 78 mg of **DTE-NO_2-COOMe** (0.22 mmol, 38% yield).

^{1}H NMR (400 MHz, $CDCl_3$): δ (ppm) 7.62 (s, 1H), 7.48 (s, 1H), 3.84 (s, 3H), 2.79 (m, 4H), 2.09 (p, *J* = 7.5 Hz, 2H), 2.00 (s, 3H), 1.96 (s, 3H).

^{13}C NMR (101 MHz, $CDCl_3$): δ (ppm) 162.5, 148.0, 144.0, 142.8, 136.8, 136.1, 136.1, 134.2, 133.6, 129.9, 129.5, 52.2, 38.8, 38.6, 22.9, 15.3, 15.0.

IR (ATR, cm^{-1}): 2949, 2051, 1703, 1499, 1432, 1374, 1323, 1289, 1244, 1151, 1080, 927, 869, 816, 751, 736, 650.

HRMS (ESI): m/z calcd for $C_{17}H_{18}NO_4S_2^+$: 364.0672 $[M-H]^+$; found: 364.0675

VIII.5.3. Synthesis of the molecular switch 1,2-bis(2-methyl-5-trifluoroacetylthien-3-yl)cyclopentene, DTE-$(COCF_3)_2$

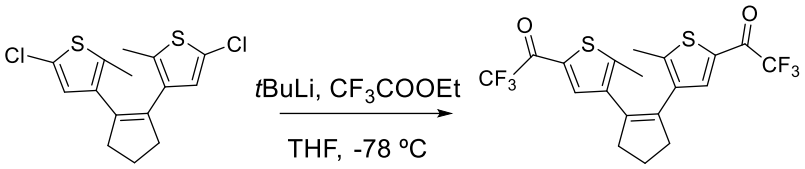

9 **DTE-$(COCF_3)_2$**

0.32 g of **9** (0.98 mmol) were dissolved in 20 mL of dry THF under argon atmosphere. The solution was cooled down to -78 ºC and 1.3 mL of a 1.7 M solution of *tert*-butyllithium in hexanes (2.2 mmol) were added. After stirring for 15 min, 0.3 mL of ethyl trifluoroacetate (2.5 mmol) were added to the reaction mixture. Then, the solution was allowed to reach room temperature and stirred for additional 30 min. Once the reaction had finished, 50 mL of water and 50 mL of diethyl ether were added. The organic layer was separated by extractions, dried with Na_2SO_4, filtered and the solvent removed under vacuum. The crude was then purified through flash column chromatography (silica, gel, hexane/EtOAc, 9:1) to obtain 4.5 g of **DTE-$(COCF_3)_2$** (0.51 mmol, 53% yield).

^{1}H NMR (400 MHz, $CDCl_3$): δ (ppm) 7.57 (s, 2H), 2.84 (t, *J* = 7.5 Hz, 4H), 2.20 – 2.09 (m, 8H).

^{13}C NMR (101 MHz, $CDCl_3$): δ (ppm) 173.0 (q, *J* = 36.6 Hz), 149.9, 138.0, 137.6 (q, *J* = 3.2 Hz), 135.6, 132.6, 116.5 (q, *J* = 290.6 Hz), 38.3, 23.0, 15.4 ppm.

^{19}F NMR (376 MHz, $CDCl_3$): δ (ppm) -72.20 ppm (s).

IR (ATR, cm^{-1}): 2956, 2848, 2325, 2051, 1681, 1529, 1424, 1373, 1333, 1234, 1194, 1136, 1028, 925, 868, 754, 738, 719, 676, 636.

HRMS (ESI): m/z calcd for $C_{19}H_{13}F_6O_2S_2^-$: 451.0267 [M-H]$^-$; found: 451.0261.

VIII.5.4. Synthesis of 2-(butylthio)-6-methyl-benzaldehyde, *o*-MBA-S

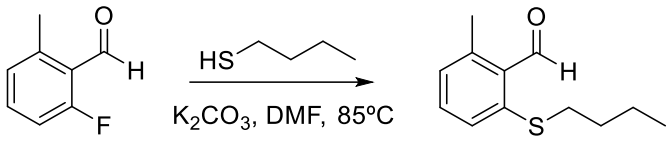

50 ***o*-MBA-S**

A dry 100 mL round bottom flask was charged with 1.01 g of K_2CO_3 (7.5 mmol), 0.50 mL of **50** (4.2 mmol) and 0.6 mL of 1-butanethiol (5.6 mmol) and the mixture was dissolved in 30 mL of dry DMF under an argon atmosphere. The reaction mixture was heated to 85 °C overnight. Next, the reaction mixture was cooled down to room temperature, dissolved in 75 mL of ethyl acetate and the organic phase was washed

with 50 mL of water. Then the organic layer was dried with Na_2SO_4, filtered and the solvent removed under vacuum. The crude was purified through flash column chromatography (silica gel, hexanes/EtOAc, 49:2) to obtain 0.86 g of ***o*-MBA-S** (4.1 mmol, 98% yield).

^{1}H NMR (360 MHz, $CDCl_3$): δ (ppm) 10.68 (s, 1H), 7.35 (t, *J* = 7.7 Hz, 1H), 7.29 (d, *J* = 7.9 Hz, 1H), 7.04 (d, *J* = 7.3 Hz, 1H), 2.91 (t, *J* = 7.4 Hz, 2H), 2.60 (s, 3H), 1.66 (p, *J* = 7.3 Hz, 2H), 1.47 (h, *J* = 7.3 Hz, 2H), 0.93 (t, *J* = 7.3 Hz, 3H).

^{13}C NMR (151 MHz, $CDCl_3$): δ (ppm) 192.7, 143.0, 142.1, 132.9, 132.7, 129.0, 126.9, 33.9, 30.8, 22.2, 20.8, 13.8 ppm.

VIII.5.5. Synthesis of *o*-DA adduct A3'$_o$

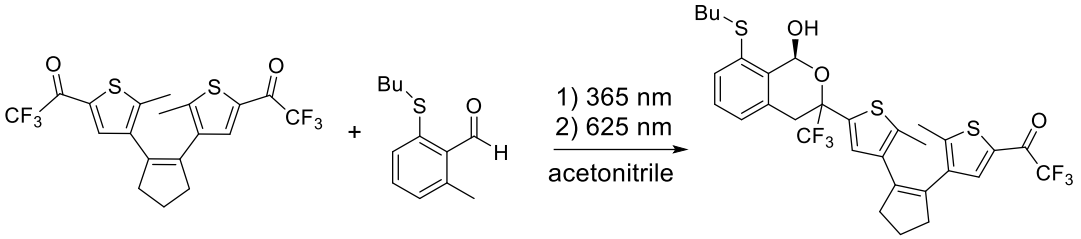

DTE-$(COCF_3)_2$ ***o*-MBA-S** **A3$_o$**

A 20 mL vial containing 10.2 mg of ***o*-MBA-S** (0.049 mmol) and 19.9 mg of **DTE-$(COCF_3)_2$** (0.043 mmol) in 15 mL of degassed acetonitrile was irradiated overnight using LED 365 (23 mW cm^{-2}). After reaction completion, the crude was irradiated for 15 min with LED 625 (100 mW cm^{-2}). The solvent was removed and the product purified by preparative TLC (hexanes:EtOAc 9:1) obtaining **A3'$_o$** as a mixture of two diastereomeric pairs of enantiomers **A3'a$_o$** and **A3'b$_o$** in a 87:13 ratio.

^{1}H NMR (600 MHz, CD_3CN): δ (ppm) 7.72 – 7.68 (m, 1H, **A3'a$_o$**, 1H, **A3'b$_o$**), 7.36 (d, *J* = 8.1 Hz, 1H, **A3'b$_o$**), 7.33 (d, *J* = 8.0 Hz, 1H, **A3'a$_o$**), 7.30 (t, *J* = 7.8 Hz, 1H, **A3'b$_o$**), 7.21 (t, *J* = 7.7 Hz, 1H, **A3'a$_o$**), 7.13 (d, *J* = 7.4 Hz, 1H, **A3'b$_o$**), 7.00 (d, *J* = 7.5 Hz, 1H, **A3'a$_o$**), 6.87 (s, 1H, **A3'b$_o$**), 6.70 (s, 1H, **A3'a$_o$**) 6.59 (d, *J* = 4.8 Hz, 1H, **A3'b$_o$**), 6.58 (d, *J* = 4.8 Hz, 1H, **A3'a$_o$**), 5.02 (d, *J* = 4.9 Hz, 1H, **A3'a$_o$**), 4.96 (d, *J* = 4.9 Hz, 1H, **A3'b$_o$**), 3.71 (d, *J* = 14.6 Hz, 1H, **A3'a$_o$**), 3.54 (s, 2H, **A3'b$_o$**), 3.27 (d, *J* = 14.5 Hz, 1H, **A3'a$_o$**), 2.97 – 2.79 (m, 2H, **A3'a$_o$**, 2H, **A3'b$_o$**), 2.78 – 2.65 (m, 2H, **A3'a$_o$**, 2H, **A3'b$_o$**), 2.11 – 2.06 (m, 5H, **A3'b$_o$**), 2.02 (p, *J* = 7.6 Hz, 2H, **A3'a$_o$**), 2.01 (s, 3H, **A3'b$_o$**) 1.80 (s, 3H, **A3'a$_o$**), 1.68 (s, 3H, **A3'a$_o$**), 1.54 (m, 2H, **A3'b$_o$**), 1.49 (q, *J* = 7.1 Hz, 1H, **A3'a$_o$**), 1.43 – 1.33 (m, 2H, **A3'a$_o$**, 2H, **A3'b$_o$**), 0.89 (t, *J* = 7.4 Hz, 3H, **A3'b$_o$**), 0.86 (t, *J* = 7.3 Hz, 3H, **A3'a$_o$**).

^{13}C NMR (151 MHz, CD_3CN): δ (ppm) 175.8 (q, *J* = 54.9 Hz, **A3'b$_o$**), 173.5 (q, *J* = 36.1 Hz, **A3'a$_o$**), 151.6 (**A3'a$_o$**), 141.4 (**A3'b$_o$**), 140.1 (**A3'b$_o$**), 140.0 (**A3'a$_o$**), 139.2 (q, *J* = 2.7 Hz, **A3'a$_o$**), 138.9 (**A3'a$_o$**), 138.3 (**A3'b$_o$**), 137.9 (**A3'a$_o$**), 137.0 (**A3'b$_o$**),

136.8 (**A3'a$_o$**), 136.6 (**A3'a$_o$**), 136.4 (**A3'b$_o$**), 136.3 (**A3'a$_o$**), 135.9 (**A3'b$_o$**), 134.3 (**A3'a$_o$**), 134.3 (**A3'b$_o$**), 134.0 (**A3'b$_o$**), 134.0 (**A3'a$_o$**), 133.8 (**A3'b$_o$**), 132.7 (**A3'a$_o$**), 132.7 (**A3'b$_o$**), 132.4 (**A3'a$_o$**), 130.9 (**A3'b$_o$**), 130.7 (**A3'a$_o$**), 130.3 (**A3'b$_o$**), 130.2 (**A3'a$_o$**), 129.9 (**A3'b$_o$**), 128.0 (**A3'a$_o$**), 127.6 (**A3'a$_o$**), 127.3 (**A3'b$_o$**), 126.7 (**A3'b$_o$**), 125.7 (q, *J* = 276.5 Hz, **A3'b$_o$**), 125.4 (q, *J* = 283.3 Hz, **A3'a$_o$**), 117.5 (q, *J* = 289.8 Hz, **A3'a$_o$**), 92.2 (**A3'b$_o$**), 91.7 (**A3'a$_o$**), 79.4 (q, *J* = 30.2 Hz, **A3'a$_o$**), 77.6 (q, *J* = 29.1 Hz, **A3'b$_o$**), 38.9 (**A3'a$_o$**), 38.8 (**A3'a$_o$**), 38.8 (**A3'b$_o$**), 38.5 (**A3'b$_o$**), 35.0 (**A3'a$_o$**), 34.7 (**A3'b$_o$**), 34.3 (**A3'b$_o$**), 33.3 (**A3'a$_o$**), 32.0 (**A3'a$_o$**), 32.0 (**A3'b$_o$**), 27.6 (**A3'b$_o$**), 23.8 (**A3'b$_o$**), 23.6 (**A3'a$_o$**), 22.5 (**A3'a$_o$**), 15.4 (**A3'b$_o$**), 15.3 (**A3'a$_o$**), 14.2 (**A3'b$_o$**), 14.1 (**A3'a$_o$**), 14.0 (**A3'a$_o$**), 13.9 ppm (**A3'b$_o$**).

^{19}F NMR (565 MHz, CD_3CN): δ (ppm) -71.57 (d, *J* = 1.6 Hz, 3F, **A3'b$_o$**), -71.60 (d, *J* = 1.6 Hz, 3F, **A3'a$_o$**), -78.90 (s, 3F, **A3'b$_o$**), -79.80 ppm (s, 3F, **A3'a$_o$**);

IR (ATR, cm^{-1}): 2929, 1735, 1681, 1649, 1583, 1560, 1534, 1437, 1334, 1289, 1267, 1227, 1142, 1024, 984, 869, 843, 755, 718, 681, 662, 628;

HRMS (ESI): m/z calcd for $C_{31}H_{29}F_6O_3S_3^-$: 659.1183 $[M-H]^-$; found: 659.1188.

VIII.5.6. Synthesis of 2,2,2-trifluoro-1-(5-methylthiophen-2-yl)ethan-1-one, thio-$COCF_3$

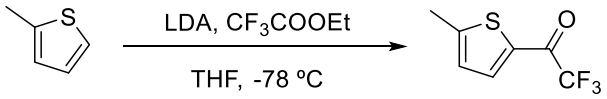

10 **thio-$COCF_3$**

Under inert atmosphere 0.5 mL of **10** (5.0 mmol) were dissolved in 20 mL of anhydrous THF. The solution was cooled down to -78 ºC and 3 mL of 2 M LDA (6.0 mmol) were added. The reaction was stirred for 15 min before adding 0.8 mL of ethyl trifluoroacetate (6.7 mmol). After stirring at room temperature for 30 min the reaction was quenched with 15 mL of brine and the organic phase was separated. The aqueous phase was extracted once with 20 mL of diethyl ether and the combined organic phases were dried over $MgSO_4$ and the solvent removed under vacuum. 0.257 mg of compound **thio-$COCF_3$** (1.4 mmol, 26% yield) were obtained by flash column chromatography (silica gel, cyclohexane to cyclohexane:EtOAc 19:1).

^{1}H NMR (600 MHz, $CDCl_3$): δ (ppm) 7.79 (m, 1H), 6.92 (dq, J_1 = 4.0, J_2 = 1.0 Hz, 1H), 2.61 ppm (s, 3H).

^{13}C NMR (75 MHz, $CDCl_3$): δ (ppm) 172.9 (q, *J* = 36.1 Hz), 155.1, 137.3, 134.1, 128.1, 116.5 (q, *J* = 289.0 Hz), 16.1.

^{19}F NMR (565 MHz, $CDCl_3$): δ (ppm) -72.06.

VIII.5.7. Synthesis of DTE-based dienophile DTE-Dimer

- **Synthesis of 1-(5-chloro-2-methylthiophen-3-yl)ethan-1-one, 51**

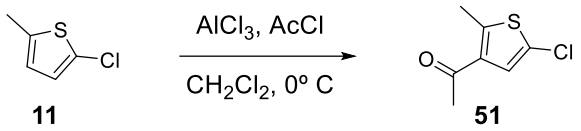

11 **51**

15.68 g of $AlCl_3$ (117 mmol) were placed in a 250 mL round bottom flask under argon atmosphere. 7.0 mL acetyl chloride (98 mmol) and 100 mL of dry dichloromethane were then added, and the mixture was cooled down to 0 ºC. In a separate flask, 12.98 g of **11** (98 mmol) were dissolved in 20 mL of dichloromethane and then slowly added to the first flask at 0 ºC. The reaction mixture was allowed to stir at this temperature for 2 hours, after which 40 g of ice were added to quench the reaction. The organic layer was separated and washed with 100 mL of water and 100 mL brine. Then, the organic layer was separated, dried over Na_2SO_4, filtered, and concentrated under vacuum. The crude was purified via flash column chromatography (silica gel, hexane/EtOAc, 19:1) to obtain 15.27 g of **51** (87 mmol, 89% yield) and recovering 1.090 g of **11** (96% yield after starting material recovery).

^{1}H NMR (250 MHz, $CDCl_3$): δ (ppm) 7.14 (s, 1H), 2.64 (s, 3H), 2.43 (s, 3H)

^{13}C NMR (126 MHz, $CDCl_3$): δ (ppm) 193.1, 147.6, 135.3, 127.4, 125.1, 29.8, 16.0.

- **Synthesis of 1-(5-chloro-2-methylthiophen-3-yl)-3-(4-methoxyphenyl)prop-2-en-1-one, 55**

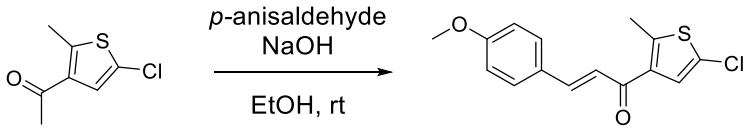

51 **55**

6.33 g of **51** (36 mmol) and 4.80 g of *p*-anisaldehyde (35 mmol) were dissolved in 80 mL ethanol. 5.62 g of NaOH were dissolved in 15 mL of water and added to the reaction mixture. The solution was stirred for 15 min. Then, it was cooled down to 0 ºC and it was filtered. The solid was washed with cold EtOH (2x10 mL) and cold diethyl ether (1x10 mL) to obtain 10.06 g of **55** as a pale-yellow solid (34 mmol, 96% yield).

^{1}H NMR (250 MHz, $CDCl_3$): δ (ppm) 7.68 (d, *J* = 15.6 Hz, 1H), 7.56 (d, *J* = 8.8 Hz, 2H), 7.22 (s, 1H), 7.07 (d, *J* = 15.6 Hz, 1H), 6.93 (d, *J* = 8.8 Hz, 2H), 3.85 (s, 3H), 2.69 (s, 3H).

^{13}C NMR (126 MHz, $CDCl_3$): δ (ppm) 185.7, 161.7, 146.9, 144.4, 136.43, 130.2, 127.4, 126.8, 125.4, 122.0, 114.4, 55.4, 15.8.

- **Synthesis of 1,5-bis(5-chloro-2-methylthiophen-3-yl)-3-(4-methoxyphenyl)pentane-1,5-dione, 52**

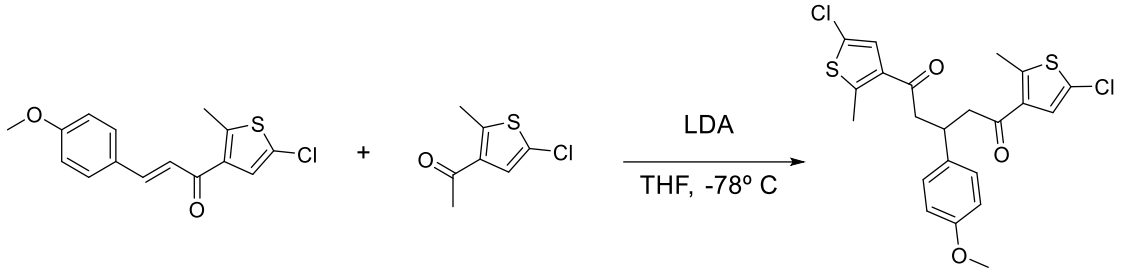

55 **51** **52**

To 5.20 g of **51** (28.7 mmol) were dissolved in 60 mL of anhydrous THF under argon and cooled down to -78 ºC. Then 17.0 mL of a 2.0 M solution of LDA solution in THF/heptane/ethylbenzene (34 mmol) were added to the reaction mixture and it was stirred at -78 ºC for 5 minutes. Afterwards, 8.10 g of **55** (29.0 mmol) dissolved in 20 mL of THF were added and the reaction mixture was allowed to stir at room temperature for 40 minutes. The reaction was quenched with 50 mL of water. Then, diethyl ether was added (50 mL) and the aqueous phase was extracted (3x50 mL). The organic layers were combined, dried over Na_2SO_4, filtered, and concentrated under vacuum. The crude was purified via flash column chromatography (silica gel, hexane/EtOAc, 9:1) to obtain 12.55 g of **52** (26.8 mmol, 97% yield)

^{1}H NMR (250 MHz, $CDCl_3$): δ (ppm) 7.18 (s, 2H), 7.14 (d, *J* = 8.7 Hz, 2H), 6.81 (d, *J* = 8.7 Hz, 2H), 3.85 (p, *J* = 7.1 Hz, 1H), 3.77 (s, 3H), 3.19 (dd, J_1 = 16.5 Hz, J_2 = 7.0 Hz, 2H), 3.04 (dd, J_1 = 16.4 Hz, J_2 = 7.1 Hz, 2H), 2.57 (s, 6H).

^{13}C NMR (126 MHz, $CDCl_3$): δ (ppm) 193.8, 158.3, 147.9, 135.6, 134.9, 128.3, 126.8, 125.3, 114.0, 55.3, 48.2, 36.0, 16.0.

- **Synthesis of 3,3'-(4-(4-methoxyphenyl)cyclopent-1-ene-1,2-diyl)bis(5-chloro-2-methylthiophene), 53**

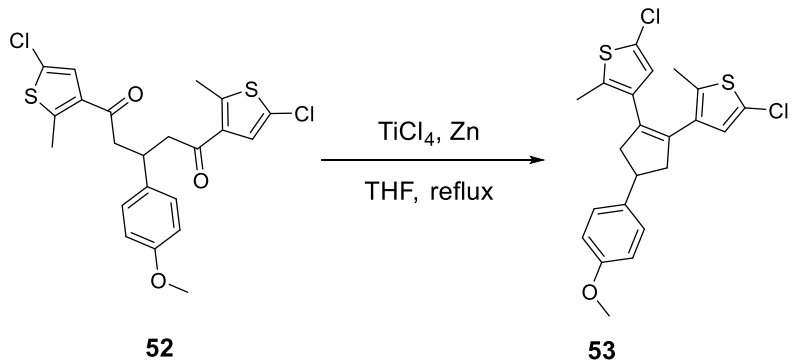

52 **53**

5.54 g of Zn powder (84 mmol) were added to 60 mL of THF under argon atmosphere and cooled down to 0 ºC. Then, 42 mL of a 1 M $TiCl_4$ solution in dichloromethane

(42 mmol) were slowly added. The mixture was stirred for 10 min at room temperature after which 9.80 g of **52** (21 mmol) in 20 mL of THF were added and the mixture was heated under reflux for 2 hours. After cooling down to room temperature, 50 mL of water were added and the mixture was stirred for 10 min. Then, it was filtered through Celite. The resulting filtrate was diluted with 100 mL of diethyl ether and extracted. The organic layer was dried over Na_2SO_4. After filtration and removal of the solvent, the crude was purified using flash column chromatography (silica gel, hexane/ethyl acetate, 95:5) to obtain 6.53 g of **53** (15 mmol, 72% yield).

^{1}H NMR (250 MHz, $CDCl_3$): δ (ppm) 7.23 (d, *J* = 8.6 Hz, 2H), 6.87 (d, *J* = 8.7 Hz, 2H), 6.60 (s, 2H), 3.81 (s, 3H), 3.61 (p, *J* = 7.7 Hz, 1H), 3.14 (dd, J_1 = 14.2 Hz, J_2 = 8.5 Hz, 2H), 2.84 (dd, J_1 = 14.1 Hz, J_2 = 7.1 Hz, 2H), 1.93 (s, 6H).

^{13}C NMR (126 MHz, $CDCl_3$): δ (ppm) 158.0, 138.3, 134.5, 133.6, 133.4, 127.7, 126.6, 125.4, 113.9, 55.3, 46.4, 41.8, 14.3.

- **Synthesis of 3,3'-(4-(4-methoxyphenyl)cyclopent-1-ene-1,2-diyl)bis(5-trifluoroacetyl-2-methylthiophene), 56**

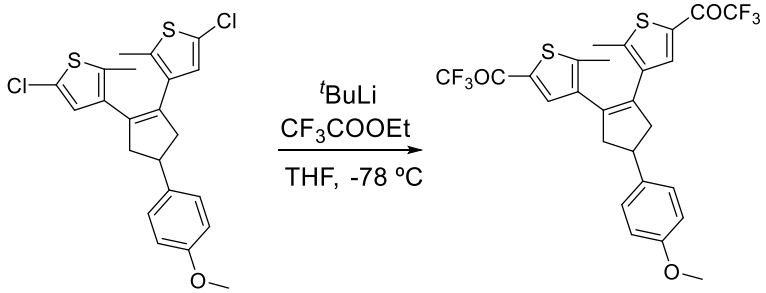

53 **56**

Under inert atmosphere, 1.081 g of **53** (2.48 mmol) were dissolved in 100 mL of anhydrous THF. Once the solution was cooled down to -78 ºC, 3.7 mL of a 1.7 solution of *tert*-butyllithium in hexanes (6.29 mmol) were added to the mixture. After stirring for 30 min, 0.80 mL of ethyl trifluoroacetate (2.71 mmol) were added and then the temperature was allowed to rise. Once the solution reached room temperature, the reaction was quenched with 100 mL of water and it was extracted with diethyl ether (2x50 mL). The organic layers were combined, dried with anhydrous Na_2SO_4, filtered, and the solvent removed under vacuum. Compound **56** was purified through flash column chromatography (silica gel, hexane/EtOAc, 9:1) obtaining 0.902 g of a brownish oil (1.62 mmol, 65% yield).

^{1}H NMR (400 MHz, $CDCl_3$): δ (ppm) 7.60 (m, 2H), 7.27 (d, *J* = 8.7 Hz, 2H), 6.91 (d, *J* = 8.7 Hz, 2H), 3.82 (s, 3H), 3.76 (p, *J* = 7.9 Hz, 1H), 3.25 (dd, J_1 = 14.1 Hz, J_2 = 8.8 Hz, 2H), 2.99 (dd, J_1 = 14.2 Hz, J_2 = 7.8 Hz, 2H), 2.17 ppm (s, 6H)**.**

^{13}C NMR (101 MHz, $CDCl_3$): δ (ppm) 173.0 (q, *J* = 36.6 Hz), 158.4, 150.1, 137.6, 137.4 (q, *J* = 3.2 Hz), 137.2, 134.5, 132.7, 127.8, 116.5 (q, *J* = 290.6 Hz), 114.2, 55.4, 46.3, 42.3, 15.5**.**

^{19}F NMR (376 MHz, $CDCl_3$): δ (ppm) -72.15**.**

IR (ATR, cm^{-1}): 2926, 2838, 2287, 1737, 1681, 1612, 1512, 1424, 1373, 1333, 1303, 1244, 1195, 1136, 1036, 924, 868, 829, 754, 738, 719, 680, 657, 637**.**

HRMS (ESI): m/z calcd for $C_{26}H_{19}F_6O_3S_2^-$: 557.0685 $[M-H]^-$; found: 557.0668.

- **Synthesis of 3,3'-(4-(4-hidroxyphenyl)cyclopent-1-ene-1,2-diyl)bis(5-trifluoroacetyl-2-methylthiophene), 54**

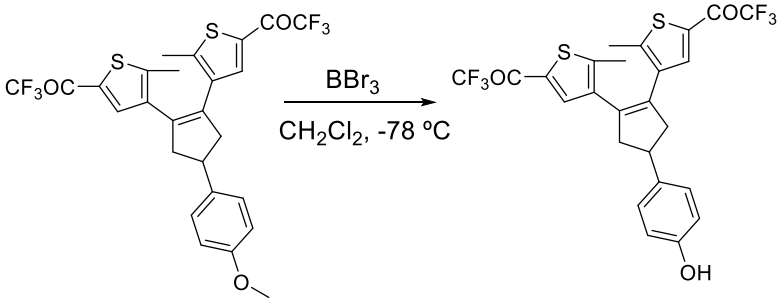

56 **54**

2.0 g of **56** (3.6 mmol) dissolved in 100 mL of anhydrous CH_2Cl_2 were cooled down to -78 ºC under inert atmosphere. Then 15 mL of a 1 M BBr_3 solution in CH_2Cl_2 (15 mmol) were added and the mixture was stirred for 4 hours in an ice bath. The reaction was quenched with 100 g of ice and extracted with CH_2Cl_2 (3x50 mL). The combined organic phases were, dried over anhydrous Na_2SO_4 filtered, and the solvent removed under vacuum. 1.2 g of **54** were obtained as a brown solid (2.2 mmol, 61% yield) after flash column chromatography (silica gel, hexane/EtOAc, 4:1).

^{1}H NMR (400 MHz, $CDCl_3$): δ (ppm) 7.60 (s, 2H), 7.22 (d, *J* = 8.5 Hz, 2H), 6.84 (d, *J* = 8.5 Hz, 2H), 3.74 (p, *J* = 8.4 Hz, 1H), 3.23 (dd, J_1 = 14.4 Hz, J_2 = 8.7 Hz, 2H), 2.98 (dd, J_1 = 14.4, J_2 = 7.8 Hz, 2H), 2.17 (s, 6H)**.**

^{13}C NMR (101 MHz, $CDCl_3$): δ (ppm) 173.0 (q, *J* = 36.7 Hz), 154.4, 150.2, 137.6, 137.4 (q, *J* = 2.9 Hz), 137.3, 134.5, 132.7, 128.0, 116.5 (q, *J* = 290.5 Hz), 115.6, 46.2, 42.3, 15.5**.**

^{19}F NMR (235 MHz, $CDCl_3$): δ (ppm) -72.61**.**

IR (ATR, cm^{-1}): 2923, 2852, 1681, 1614, 1514, 1424, 1389, 1333, 1234, 1196, 1140, 924, 869, 832, 753, 719, 679**.**

HRMS (ESI): m/z calcd for $C_{25}H_{17}F_6O_3S_2^-$: 543.0529 $[M-H]^-$; found: 543.0528.

- **Synthesis of DTE-dimer**

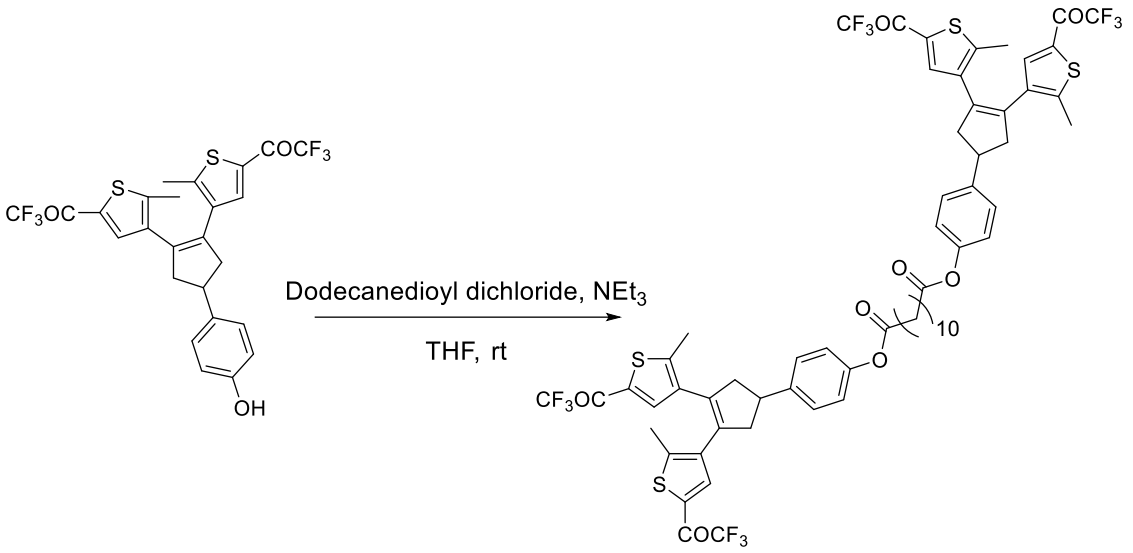

54 **DTE-dimer**

In a 100 mL round bottom flask, 0.864 g of **54** (1.59 mmol) and 0.170 g of dodecanedioyl dichloride (0.64 mmol) were dissolved in 20 mL of anhydrous THF. Then, 0.40 mL of anhydrous triethylamine (2.86 mmol) were added, and the solution was stirred overnight under inert atmosphere. The work up was done by adding 50 mL of diethyl ether and 50 mL of water, and after separation of the organic layer with extractions, it was dried over anhydrous Na_2SO_4, filtered and the solvent removed under vacuum. Finally, **DTE-dimer** was purified by flash column chromatography (silica gel, chloroform) to obtain 0.443 g (0.35 mmol, 54% yield).

^{1}H NMR (400 MHz, $CDCl_3$): δ (ppm) 7.60 (s, 4H), 7.35 (d, *J* = 8.5 Hz, 4H), 7.07 (d, *J* = 8.5 Hz, 4H), 3.80 (p, *J* = 8.1 Hz, 2H), 3.27 (dd, J_1 = 14.5 Hz, J_2 = 8.7 Hz, 4H), 3.02 (dd, J_1 = 14.7 Hz, J_2 = 7.6 Hz, 4H), 2.57 (t, *J* = 7.5 Hz, 4H), 2.17 (s, 12H), 1.77 (p, *J* = 7.5 Hz, 4H), 1.48 – 1.31 (m, 12H)**.**

^{13}C NMR (101 MHz, $CDCl_3$): δ (ppm) 172.9 (q, *J* = 36.8 Hz), 172.6, 150.1, 149.4, 142.6, 137.4, 137.3, 134.4, 132.8, 127.8, 121.9, 116.5 (q, *J* = 290.5 Hz), 46.1, 42.4, 34.5, 29.5, 29.3, 29.2, 25.1, 15.5**.**

^{19}F NMR (235 MHz, $CDCl_3$): δ (ppm) -72.61**.**

IR (ATR, cm^{-1}): 2926, 2854, 2287, 2051, 1752, 1682, 1509, 1424, 1334, 1195, 1135, 924, 869, 753, 719, 680.

HRMS (ESI): m/z calcd for $C_{62}H_{54}F_{12}NaO_8S_4^+$: 1305.2402 $[M\text{-}Na]^+$; found: 1305.2389.

VIII.5.8. Synthesis of diene precursor *o*-MBA-T.

- **Synthesis of 1,3,5-tris((6-bromohexyl)oxy)benzene, 58.**

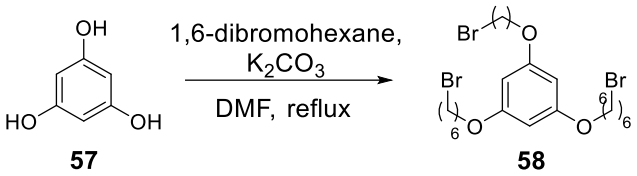

57 **58**

1.0 g of compound **57** (8.0 mmol), 7.0 mL of 1,6-dibromohexane (45.0 mmol) and 6.0 g K_2CO_3 were stirred for 36 h in 100 mL of anhydrous DMF. The solvent was then removed under vacuum and the crude redissolved in 100 mL of EtOAc and 100 mL of water. The organic phase was separated and washed with 50 mL of brine. The organic layer was dried over Na_2SO_4, filtered and the solvent removed under vacuum. 2.0 g of **58** (3.25 mmol, 40% yield) were obtained after purification by flash column chromatography (silica gel, hexane/EtOAc; 9:1).

^{1}H NMR (250 MHz, $CDCl_3$): δ (ppm) 6.05 (s, 3H), 3.91 (t, *J* = 6.4 Hz, 6H), 3.42 (t, *J* = 6.8 Hz, 6H), 1.89 (p, *J* = 7.0 Hz, 6H), 1.77 (p, *J* = 6.8 Hz, 6H), 1.49 (m, 12H).

^{13}C NMR (91 MHz, $CDCl_3$): δ (ppm) 161.0, 93.9, 67.9, 34.0, 32.8, 29.2, 28.1, 25.5.

IR (ATR, cm^{-1}): 2935, 2858, 1592, 1460, 1385, 1220, 1154, 1059, 817, 753, 681, 644.

HRMS (ESI): m/z calcd for $C_{24}H_{39}Br_3NaO_3^+$: 635.0342 [M-Na]$^+$; found: 635.0341.

- **Synthesis of 1,3,5-tris((6-thioacetylhexyl)oxy)benzene, 60**

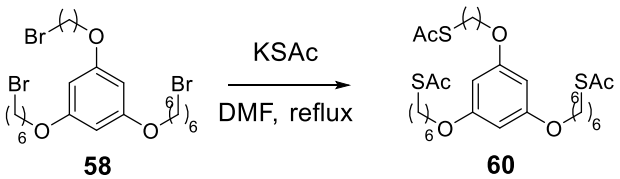

58 **60**

4.0 g of **58** (6.6 mmol) and 4.0 g of potassium acetate (5.3 mmol) were stirred overnight in 50 mL of anhydrous DMF at room temperature. Once the reaction was completed, the solvent was removed under vacuum and the resulting solid dissolved in 50 mL of water and 50 mL of diethyl ether. The organic phase was separated and washed with additional 50 mL of water. After drying the organic layer with Na_2SO_4, filtering and removing the solvent, 3.9 g of **60** (6.5 mmol, 98% yield) were isolated after flash column chromatography (silica gel, hexane/EtOAc; 9:1).

^{1}H NMR (250 MHz, $CDCl_3$): δ (ppm) 6.03 (s, 3H), 3.89 (t, *J* = 6.4 Hz, 6H), 2.87 (t, *J* = 7.2 Hz, 6H), 2.31 (s, 9H), 1.73 (p, *J* = 6.8 Hz, 6H), 1.58 (p, *J* = 6.9 Hz, 6H), 1.52-1.40 (m, 12H).

^{13}C NMR (91 MHz, $CDCl_3$): δ (ppm) 196.2, 161.0, 93.9, 67.9, 30.8, 29.6, 29.2, 29.2, 28.7, 25.8.

IR (ATR, cm^{-1}): 2932, 2857, 1737, 1687, 1592, 1460, 1386, 1353, 1240, 1153, 1058, 950, 817, 733, 679, 623.

HRMS (ESI): m/z calcd for $C_{30}H_{48}NaO_6S_3^+$: 623.2505 $[M\text{-}Na]^+$; found: 623.2493.

- **Synthesis of 1,3,5-tris((6-mercaptohexyl)oxy)benzene, 59**

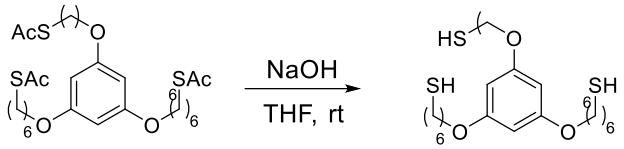

60 **59**

10 mL of a 2 M NaOH aqueous solution were added onto a degassed solution of 1.6 g of **60** (2.8 mmol) in 10 mL of THF. The two-phase system was stirred overnight under inert atmosphere. The reaction was quenched with 4 mL of concentrated HCl and then 20 mL of Et_2O were added. The organic phase was washed with a 1 M HCl aqueous solution (2x20 mL) and dried over anhydrous Na_2SO_4. After filtration and removal of the solvent under vacuum, **59** was purified via flash column chromatography (silica gel, hexanes/EtOAc; 19:1) to obtain 0.50 g (1.0 mmol; 38% yield).

^{1}H NMR (250 MHz, $CDCl_3$): δ (ppm) 6.05 (s, 3H), 3.90 (t, *J* = 6.4 Hz, 6H), 2.53 (q, *J* = 7.4 Hz, 6H), 1.75 (m, 6H), 1.63 (m, 6H), 1.51-1.39 (m, 12H), 1.34 (t, *J* = 7.7 Hz, 3H).

^{13}C NMR (63 MHz, $CDCl_3$): δ (ppm) 161.0, 93.9, 67.9, 34.0, 29.2, 28.2, 25.7, 24.7.

IR (ATR, cm^{-1}): 2929, 2855, 1591, 1460, 1385, 1247, 1151, 1058, 817, 754, 680.

HRMS (ESI): m/z calcd for $C_{24}H_{42}NaO_3S_3^+$: 497.2188 $[M\text{-}Na]^+$; found: 497.2186.

- **Synthesis of *o*-MBA-T**

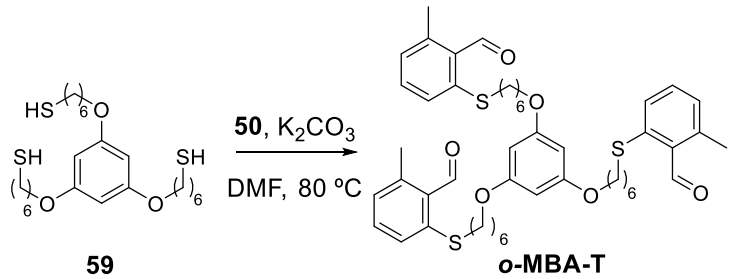

59 ***o*-MBA-T**

0.50 g of **59** (1.0 mmol) and 0.4 mL of **50** (3.3 mmol) were dissolved in a suspension containing 20 mL of dry DMF and 0.60 g of K_2CO_3 (4.2 mmol). The mixture was stirred at 80ºC overnight and then 50 mL of water were added. The mixture was

extracted with 50 mL of EtOAc. The combined organic phases were then dried over anhydrous Na_2SO_4. After filtration and after solvent removal under vacuum, the crude was purified through flash column chromatography (silica gel, hexanes:EtOAc; 4:1) to obtain 0.49 g of ***o*-MBA-T** (0.6 mmol; 60% yield)

^{1}H NMR (250 MHz, $CDCl_3$): δ (ppm) 10.67 (s, 3H), 7.33 (m, 6H), 7.04 (d, *J* = 6.9 Hz, 3H), 6.04 (s, 3H), 3.89 (t, *J* = 6.4 Hz, 6H), 2.91 (t, *J* = 7.3 Hz, 6H), 2.60 (s, 9H), 1.73 (m, 12H), 1.54-1.42 (m, 12H).

^{13}C NMR (63 MHz, $CDCl_3$): δ (ppm) 192.7, 161.0, 142.8, 142.2, 133.0, 132.6, 129.0, 126.7, 93.9, 67.9, 34.0, 29.2, 28.8, 28.7, 25.8, 20.8.

IR (ATR, cm^{-1}): 2923, 2853, 1689, 1674, 1579, 1455, 1380, 1260, 1150, 1059, 908, 881, 817, 758, 733, 671.

HRMS (ESI): m/z calcd for $C_{48}H_{60}NaO_6S_3^+$: 851.3444 $[M-Na]^+$; found: 851.3419.

VIII.6. REFERENCES

1 A. J. Lees, *Anal. Chem.*, 1996, **68**, 226–229.

2 K. Higashiguchi, K. Matsuda, Y. Asano, A. Murakami, S. Nakamura and M. Irie, *European J. Org. Chem.*, 2004, 91–97.

3 M. Irie, T. Lifka, S. Kobatake and N. Kato, *J. Am. Chem. Soc.*, 2000, **122**, 4871–4876.

4 J. R. Lakowicz, *Principles of fluorescence spectroscopy*, 2006.

5 T. Kircher and H. G. Löhmannsröben, *Phys. Chem. Chem. Phys.*, 1999, **1**, 3987–3992.

6 R. S. Sánchez, R. Gras-Charles, J. L. Bourdelande, G. Guirado and J. Hernando, *J. Phys. Chem. C*, 2012, **116**, 7164–7172.

7 S. Espinosa, E. Bosch and M. Roses, *Anal. Chem.*, 2000, **72**, 5193–5200.

8 H. C. Moon, C. Kim, T. P. Lodge and C. D. Frisbie, , DOI:10.1021/acsami.6b01307.

Chapter IX

Annex

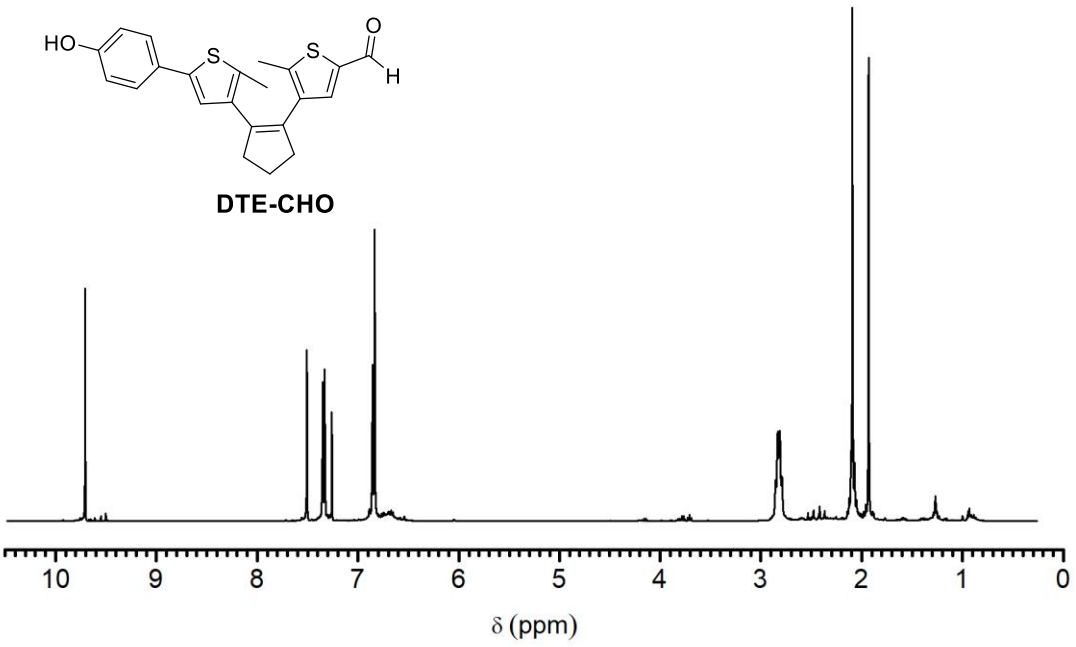

^{1}H NMR (400 MHz, $CDCl_3$)

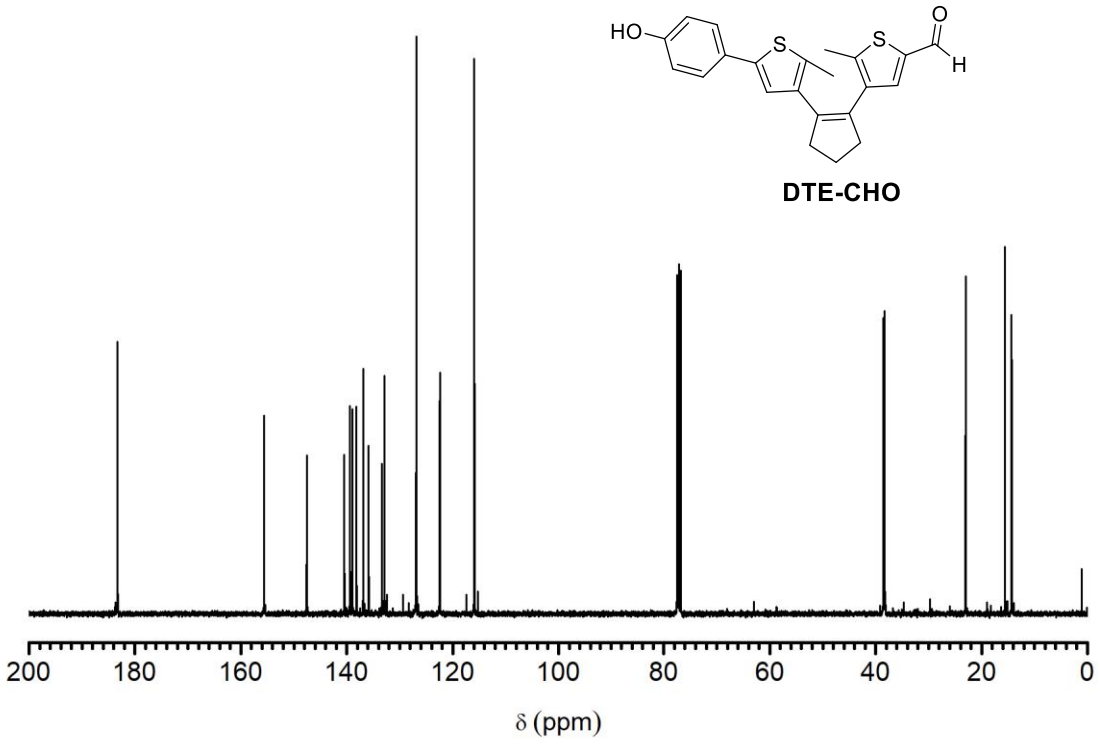

^{13}C NMR (101 MHz, $CDCl_3$)

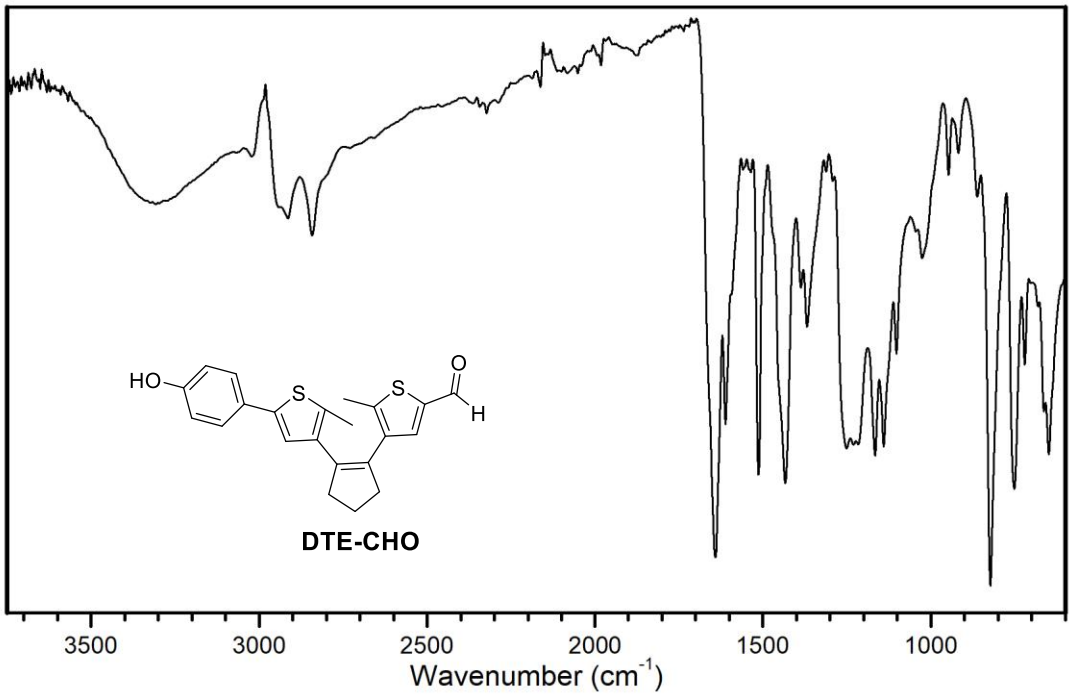

IR (ATR, cm^{-1})

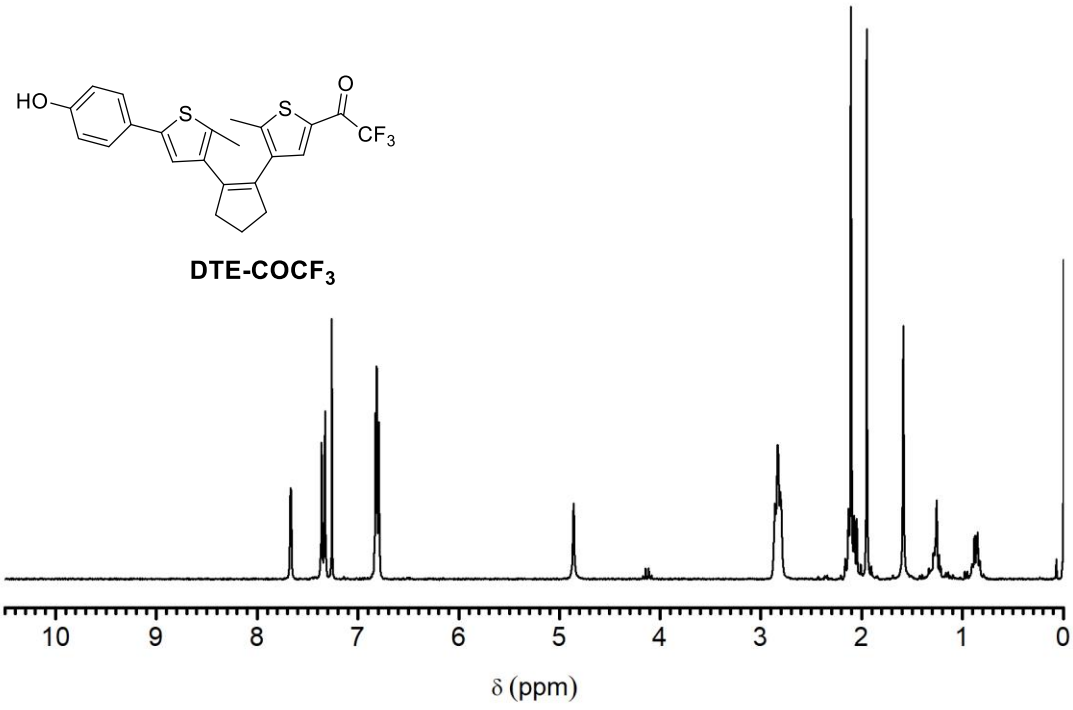

^{1}H NMR (250 MHz, $CDCl_3$)

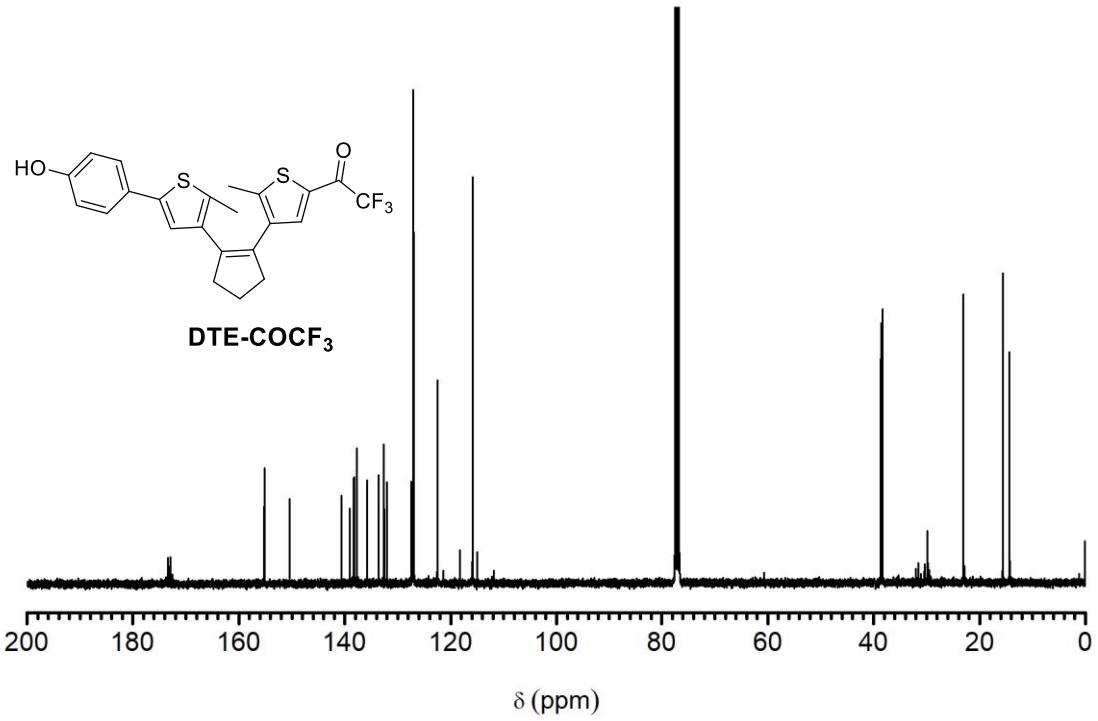

^{13}C NMR (91 MHz, $CDCl_3$)

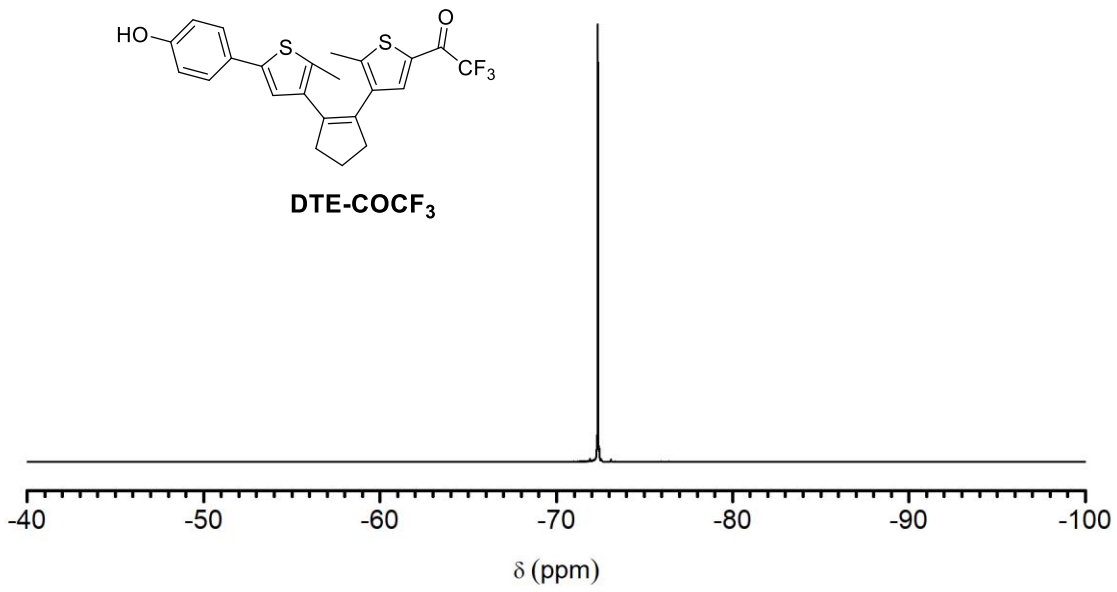

^{19}F NMR (235 MHz, $CDCl_3$)

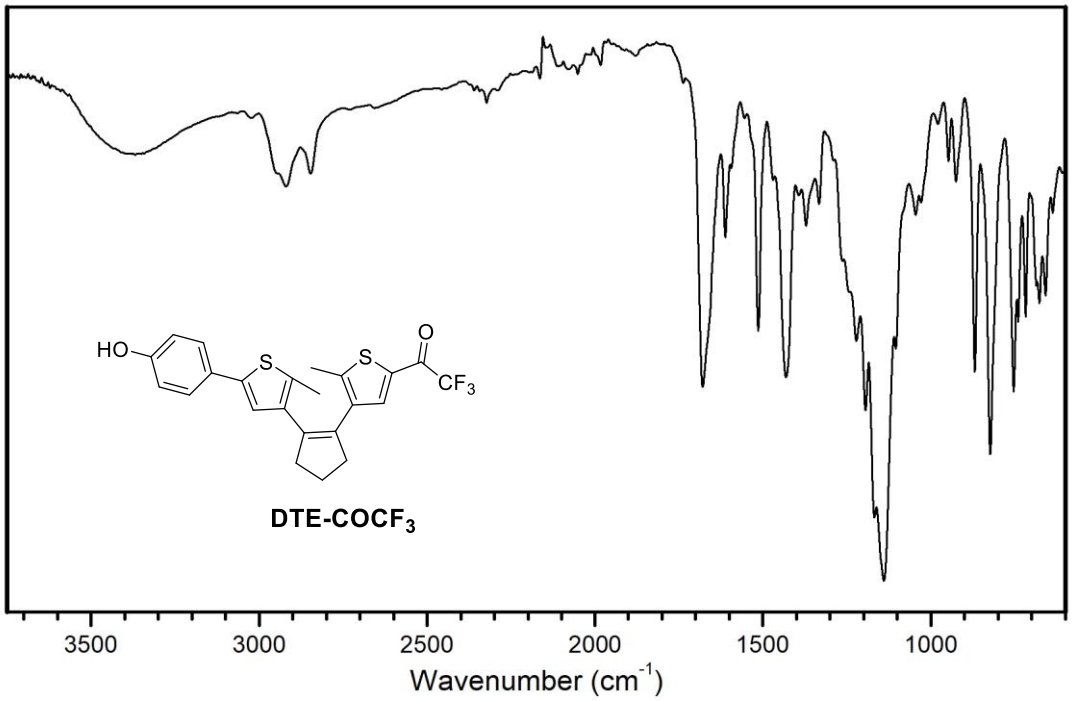

IR (ATR, cm^{-1})

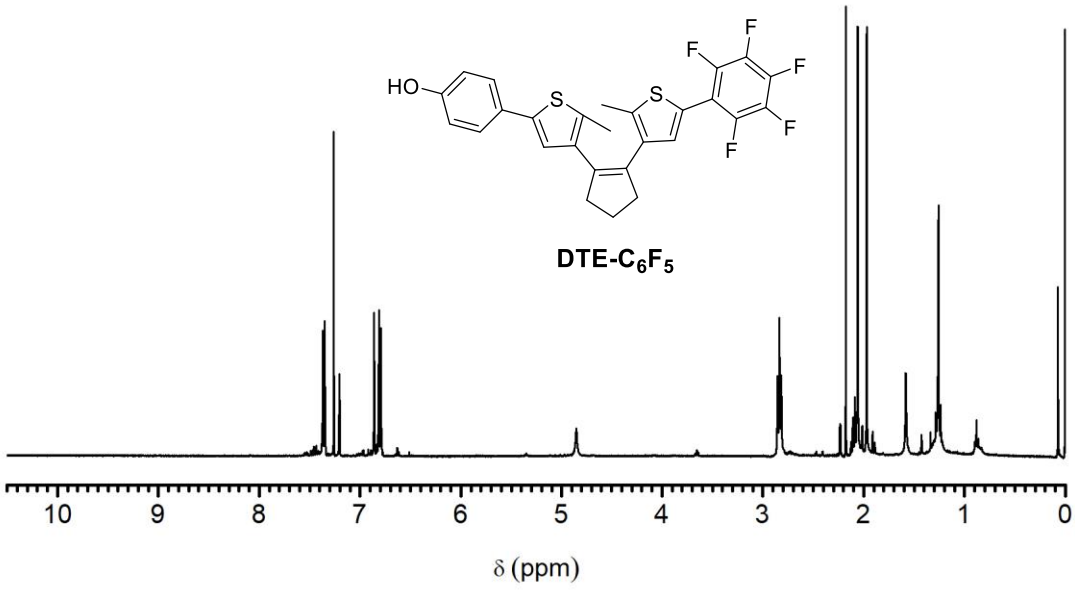

^{1}H NMR (400 MHz, $CDCl_3$)

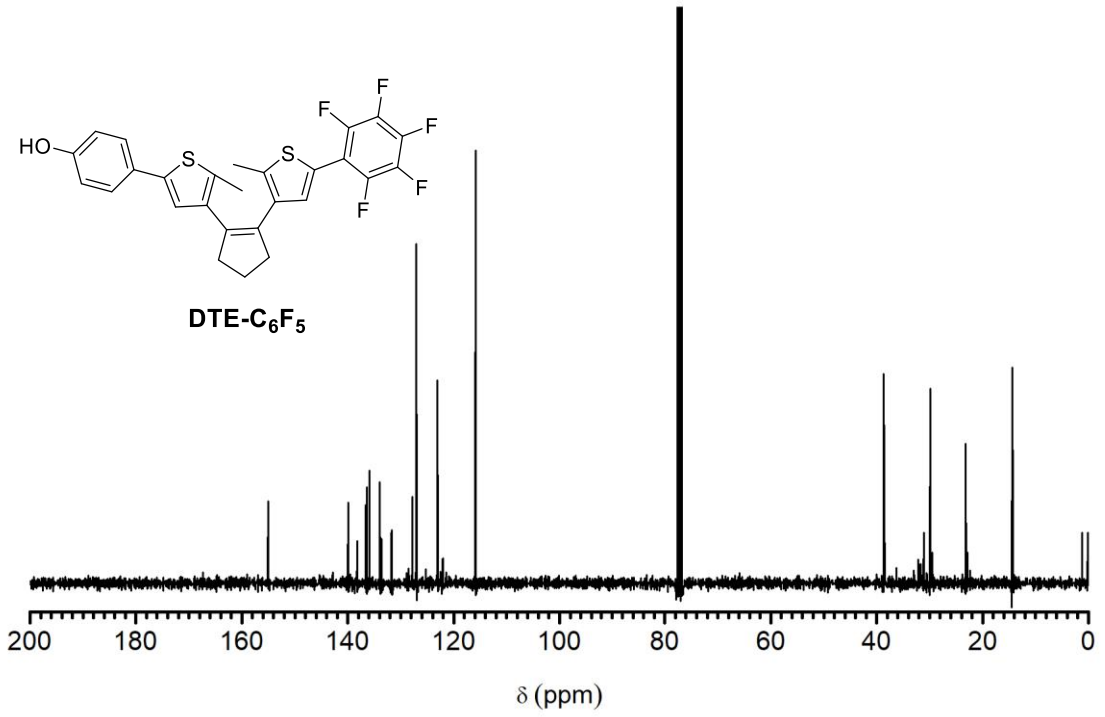

^{13}C NMR (101 MHz, $CDCl_3$)

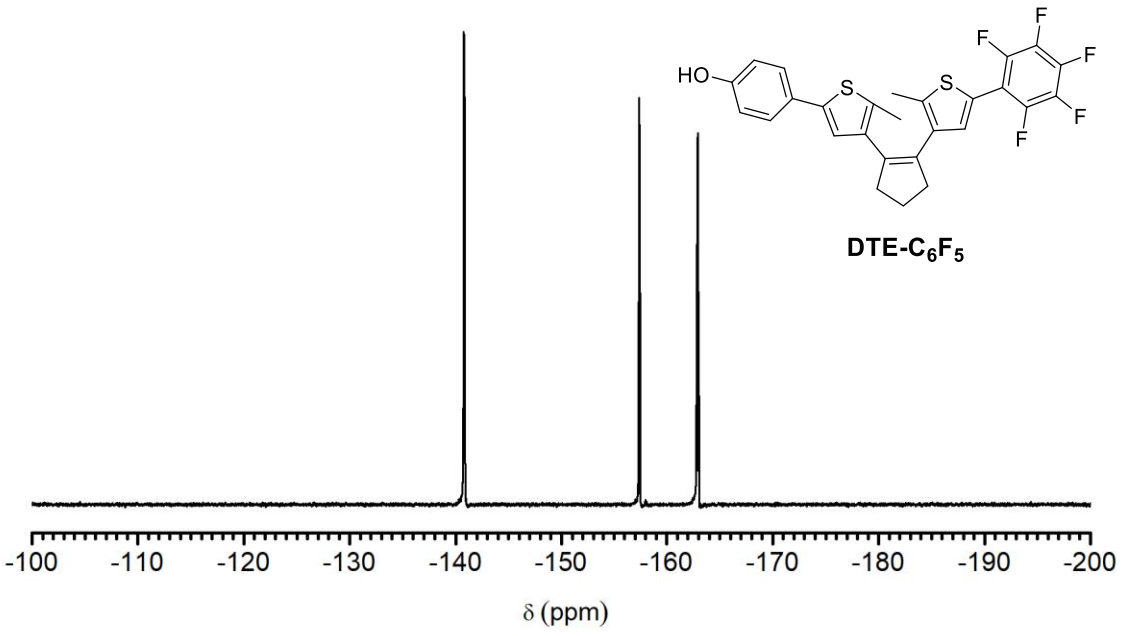

^{19}F NMR (235 MHz, $CDCl_3$)

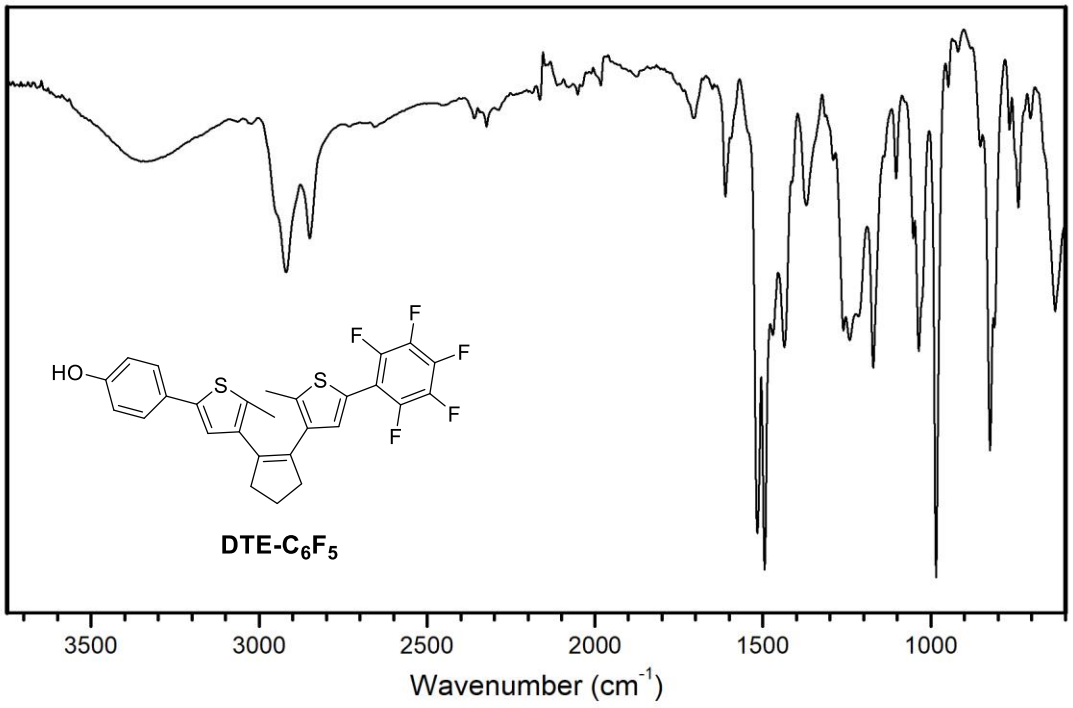

IR (ATR, cm^{-1})

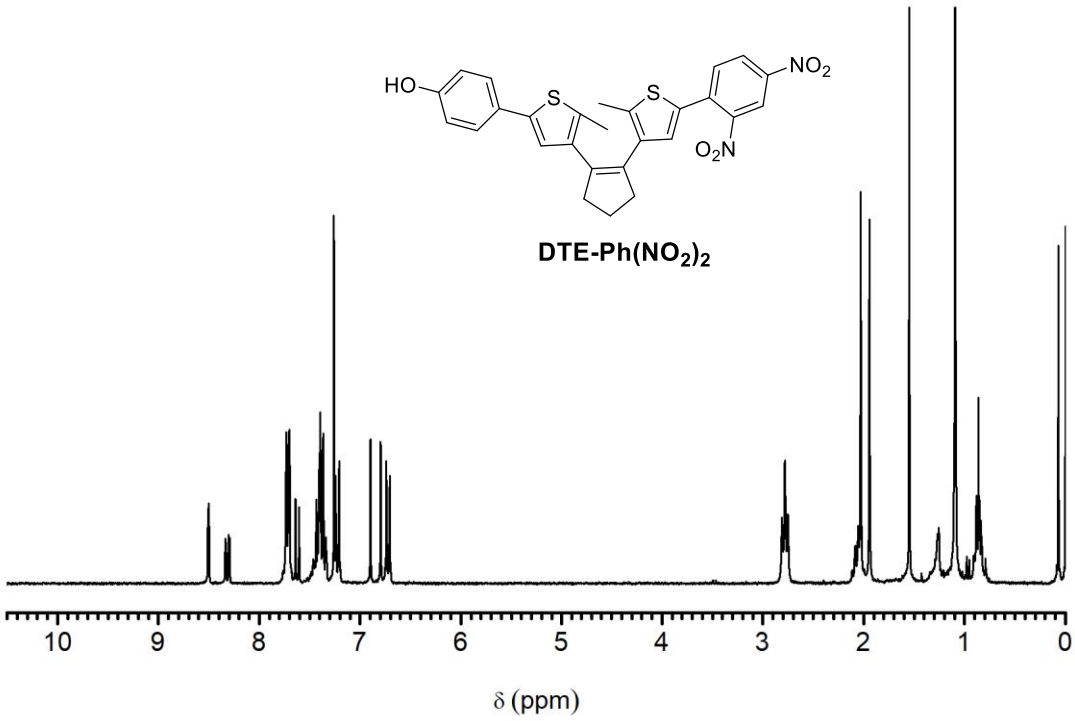

^{1}H NMR (360 MHz, $CDCl_3$)

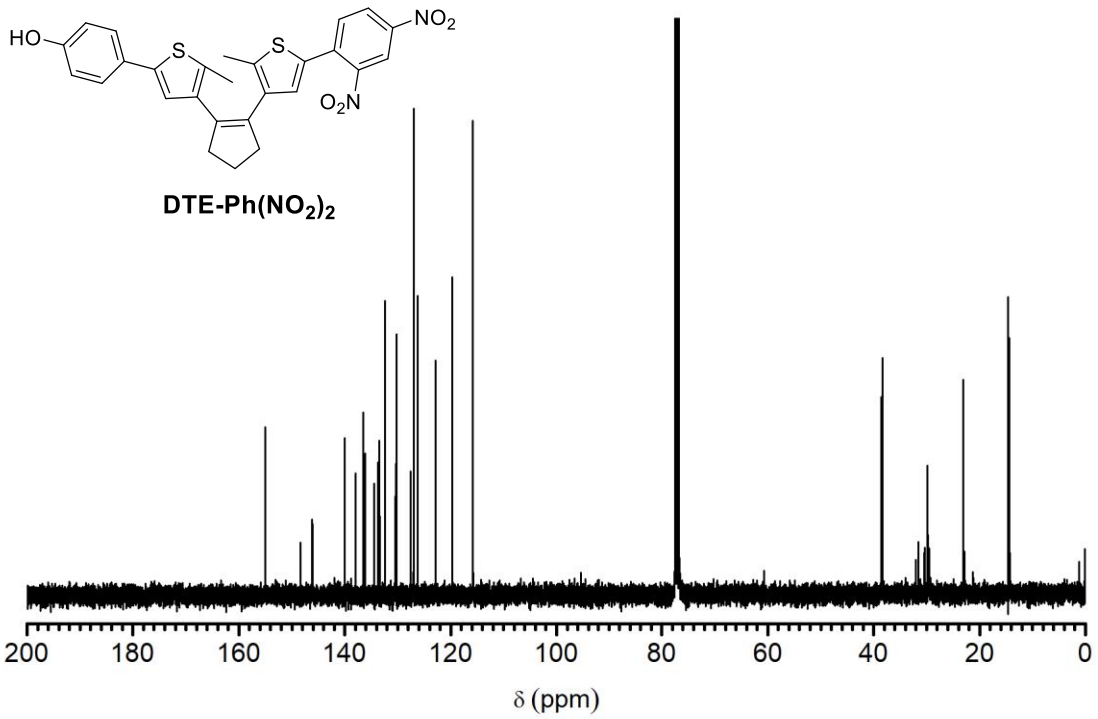

^{13}C NMR (91 MHz, $CDCl_3$)

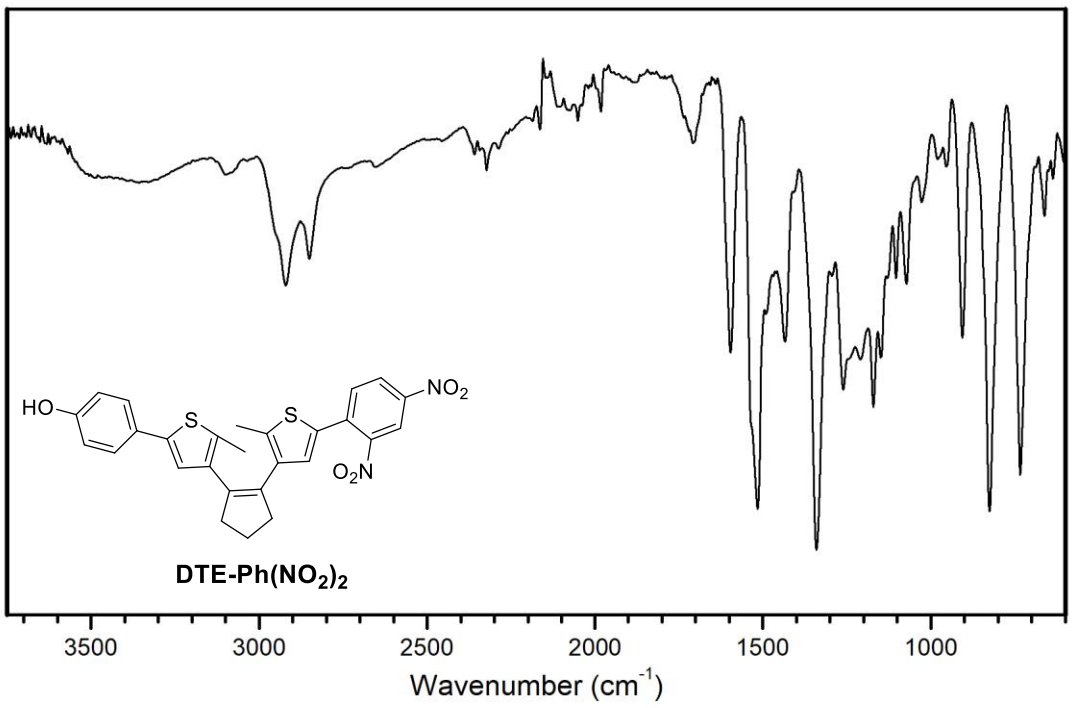

IR (ATR, cm^{-1})

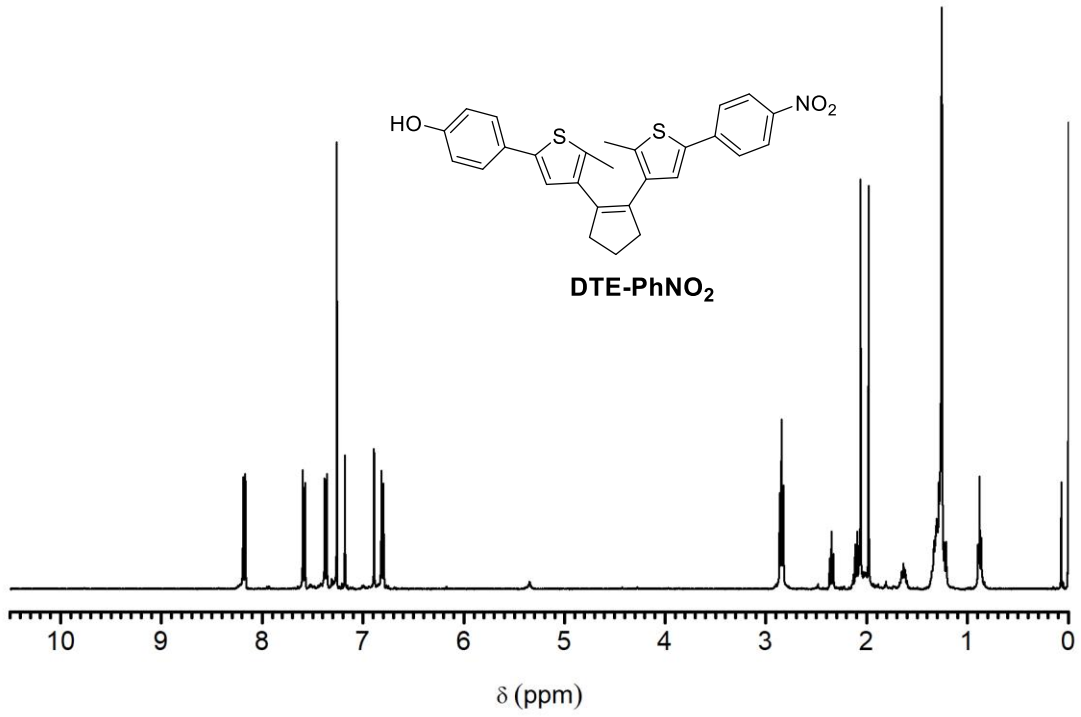

^{1}H NMR (400 MHz, $CDCl_3$)

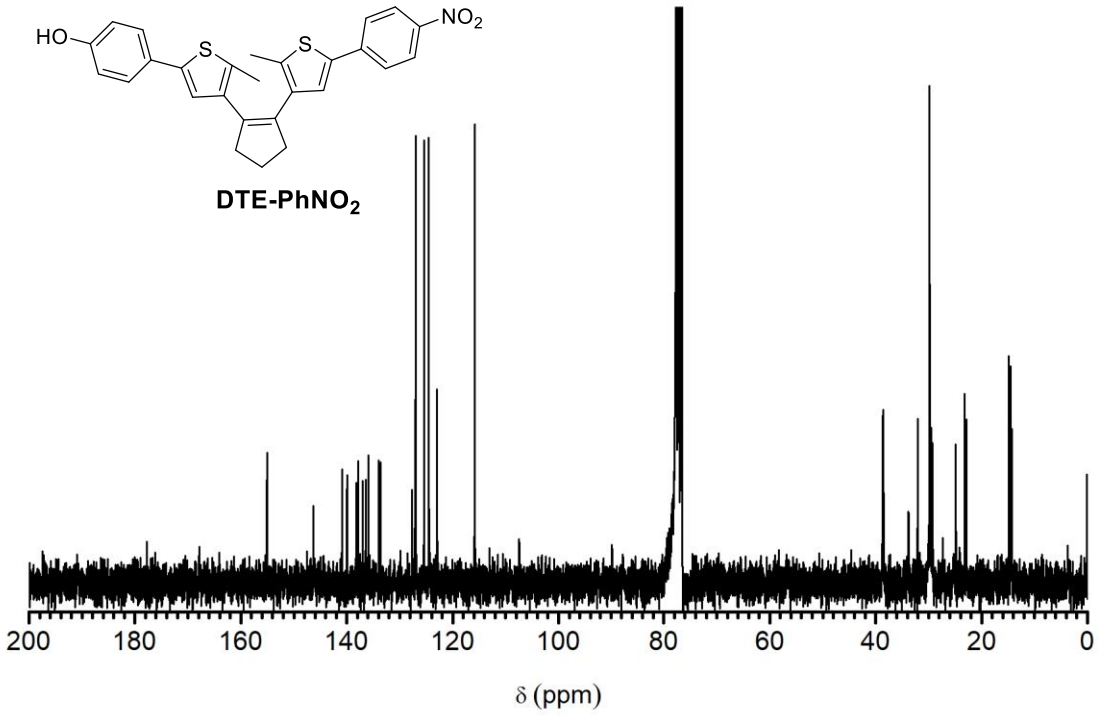

^{13}C NMR (63 MHz, $CDCl_3$)

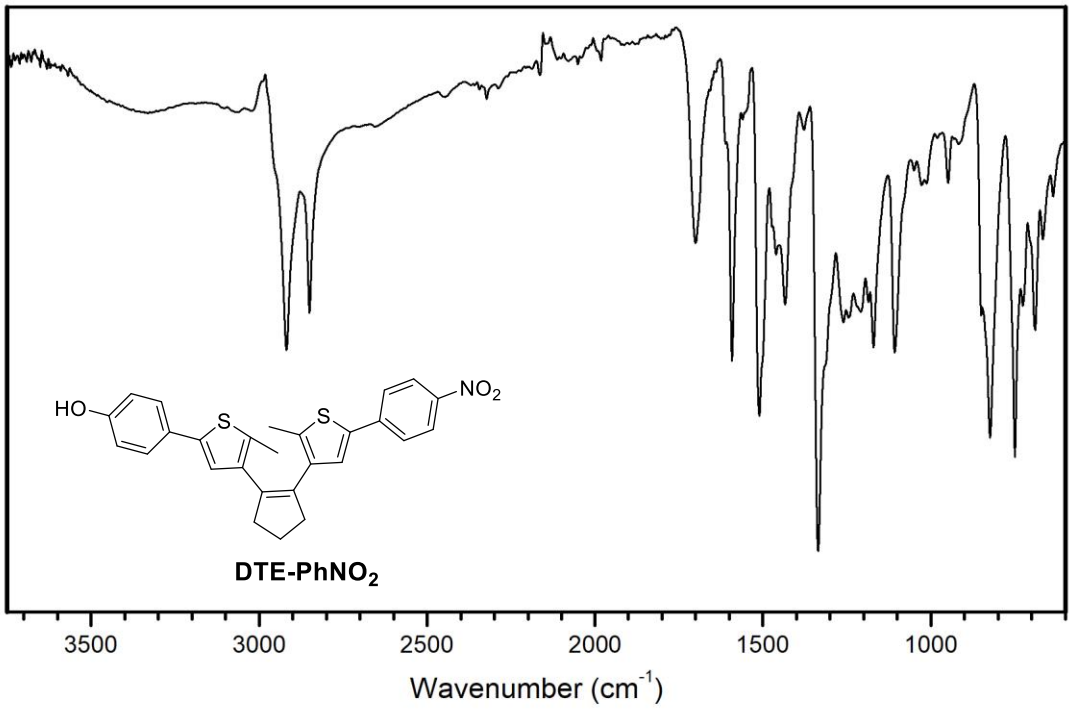

IR (ATR, cm^{-1})

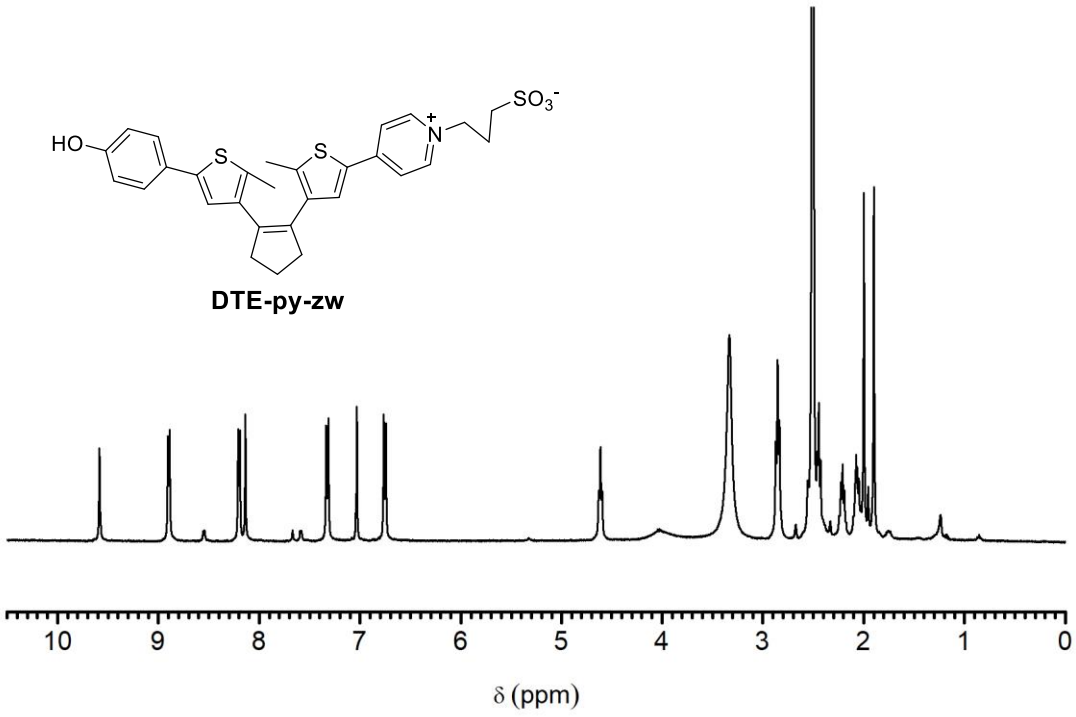

^{1}H NMR (400 MHz, DMSO)

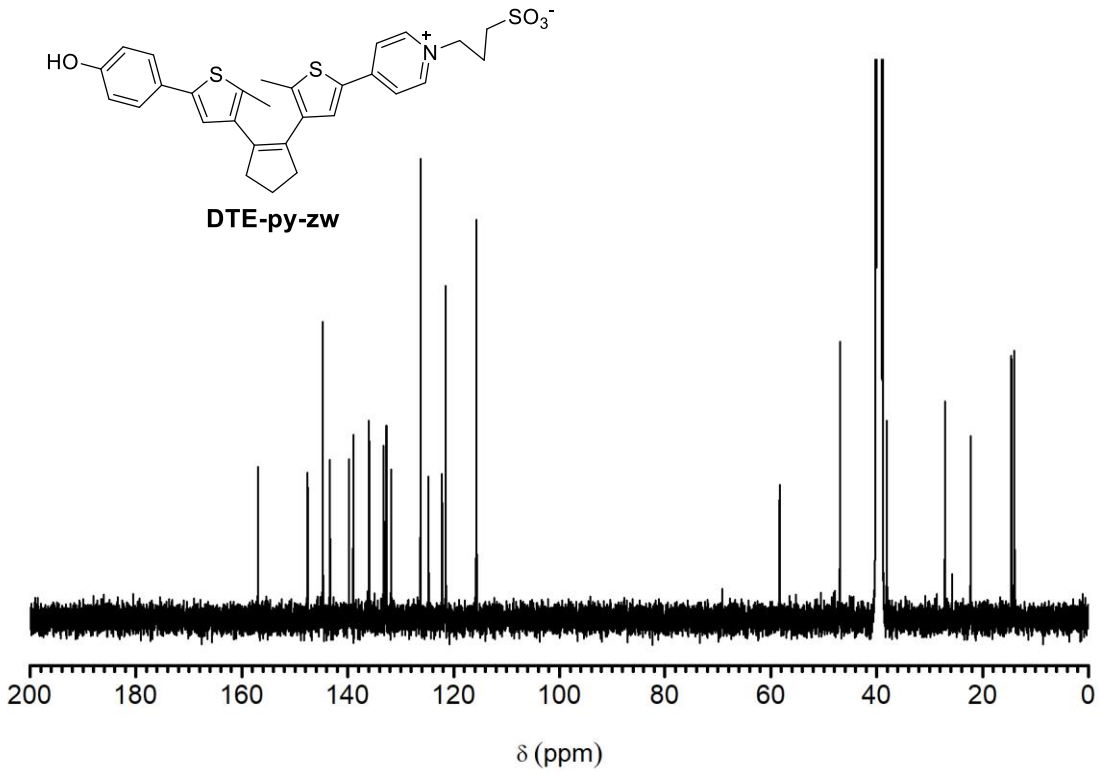

^{13}C NMR (101 MHz, DMSO)

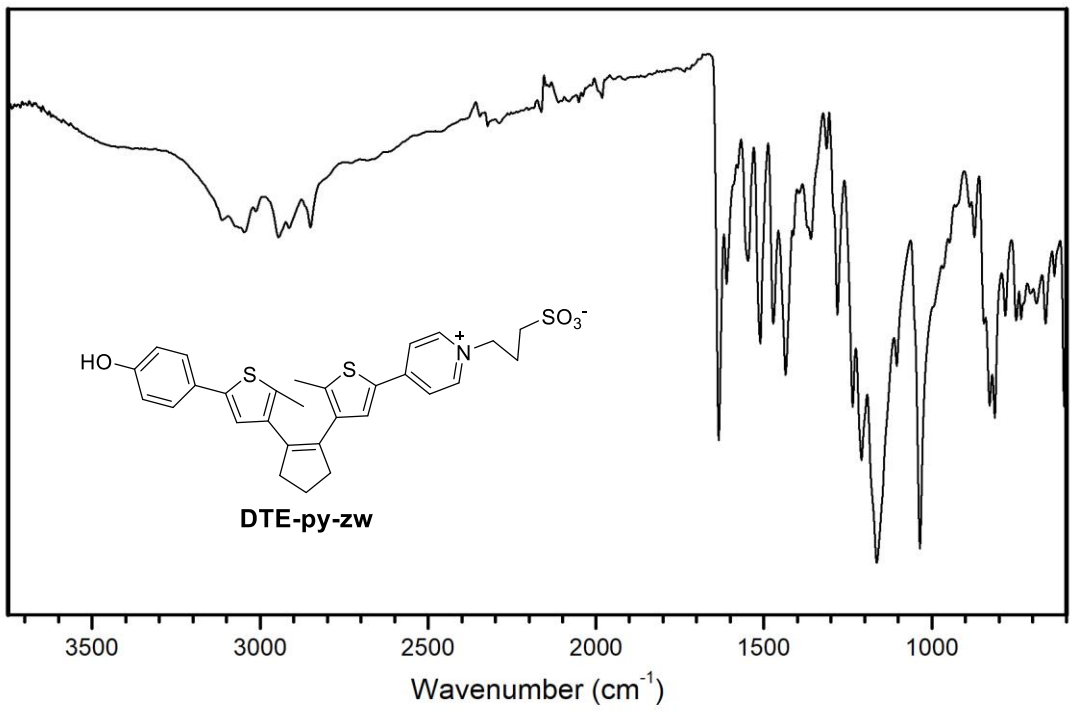

IR (ATR, cm^{-1})

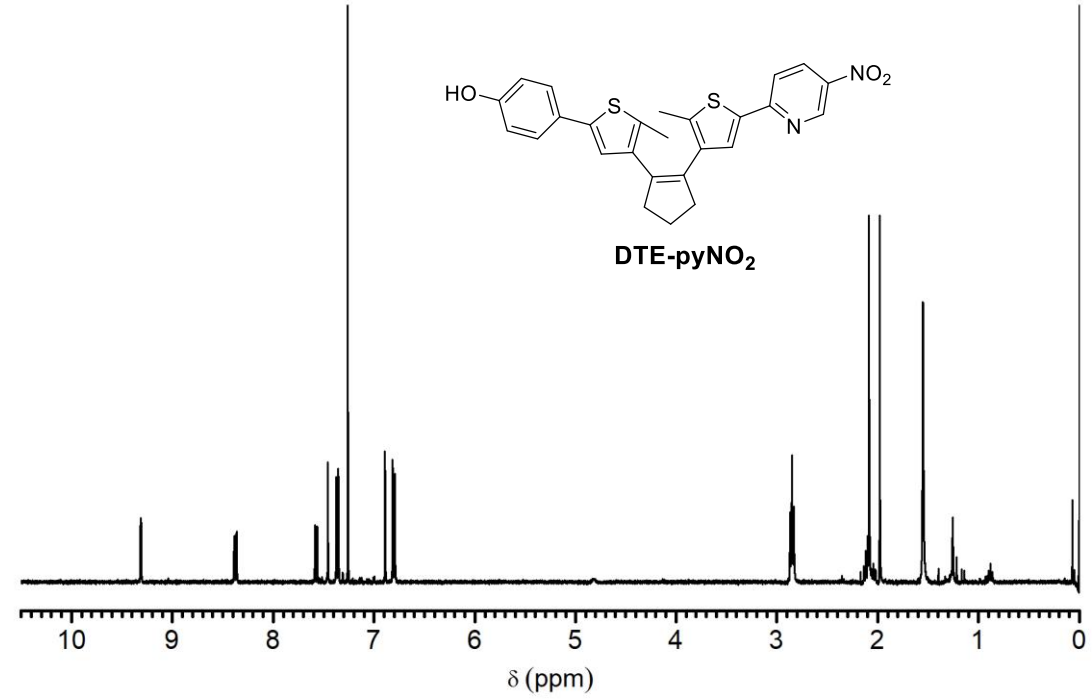

^{1}H NMR (400 MHz, $CDCl_3$)

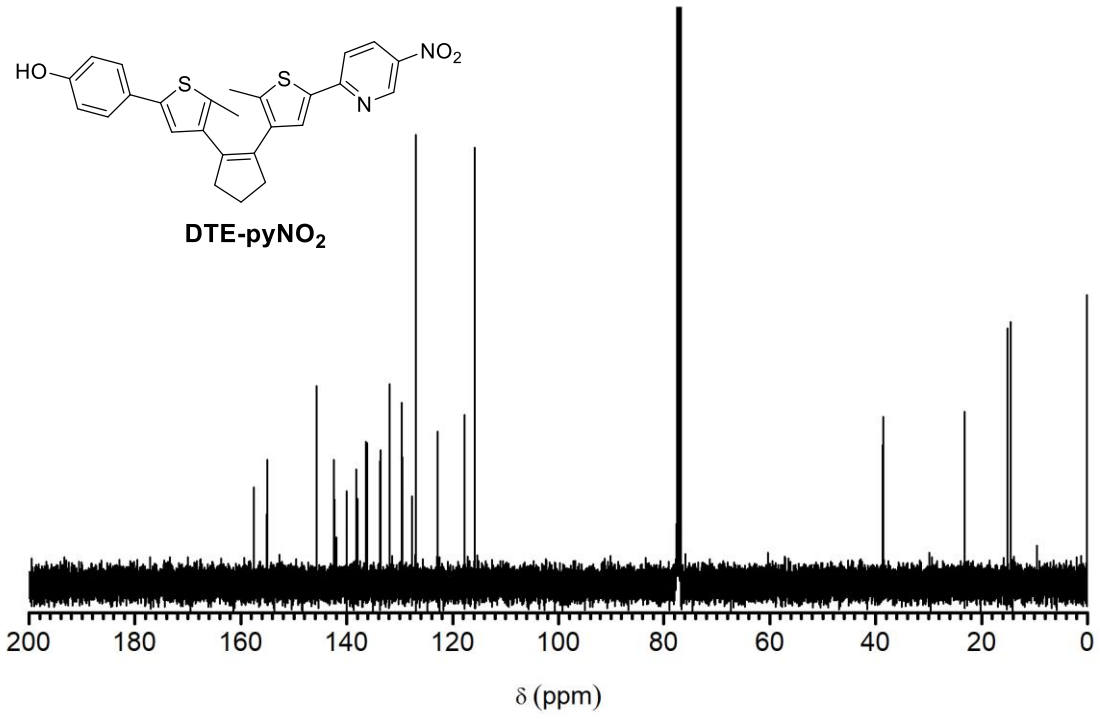

^{13}C NMR (101 MHz, $CDCl_3$)

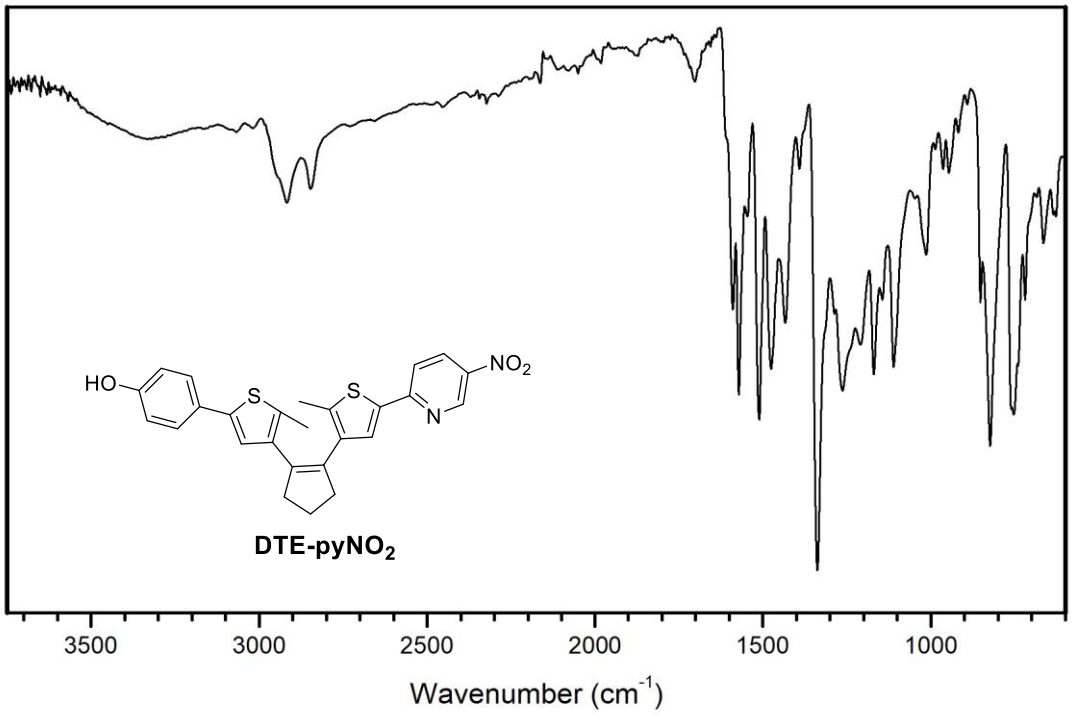
HO
S
S
N
NO2
DTE-pyNO2
3500
3000
2500
2000
1500
1000
Wavenumber (cm-1)

IR (ATR, cm^{-1})

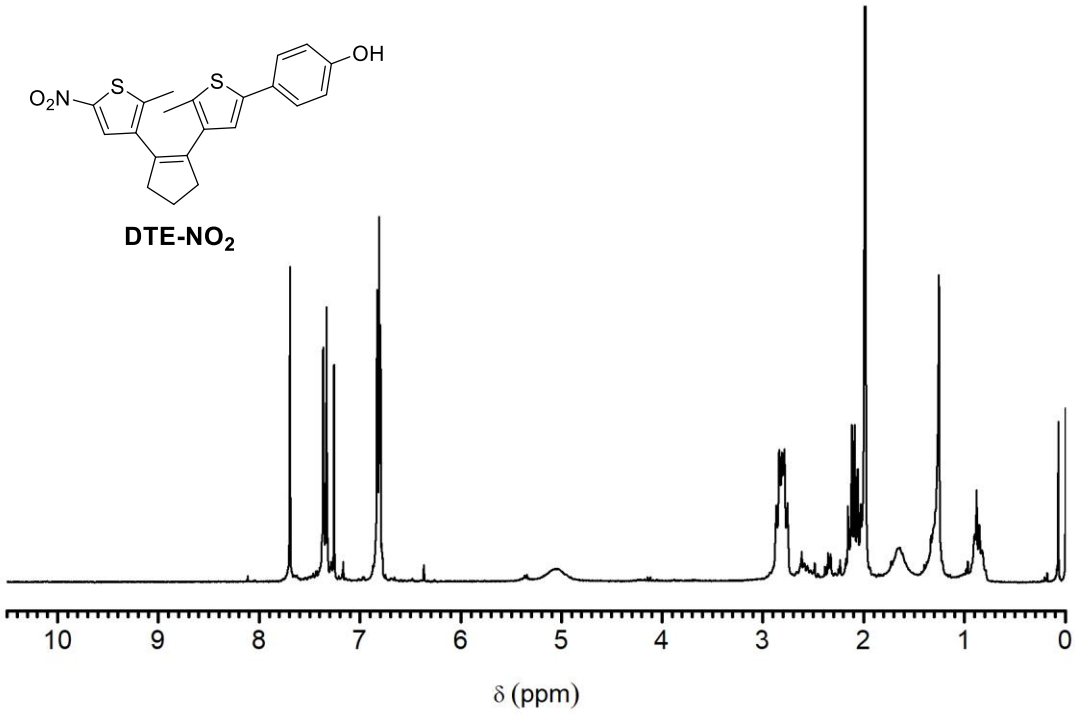
O2N
S
S
OH
DTE-NO2
10
9
8
7
6
5
4
3
2
1
0
δ (ppm)

^{1}H NMR (400 MHz, $CDCl_3$)

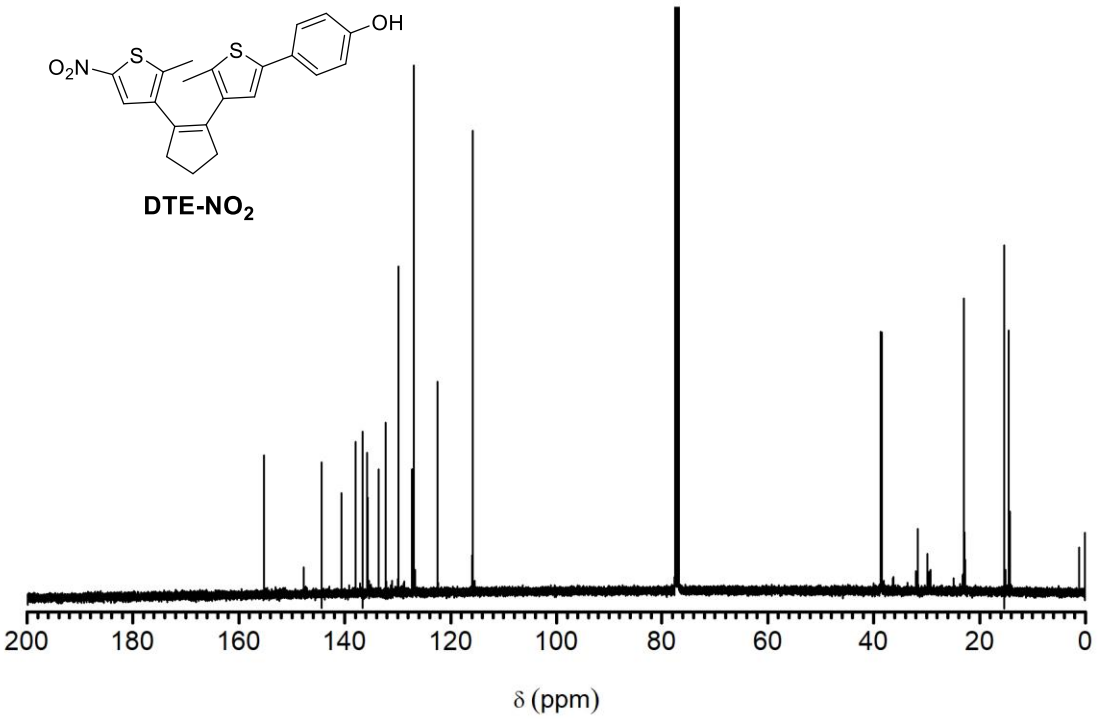

^{13}C NMR (101 MHz, $CDCl_3$)

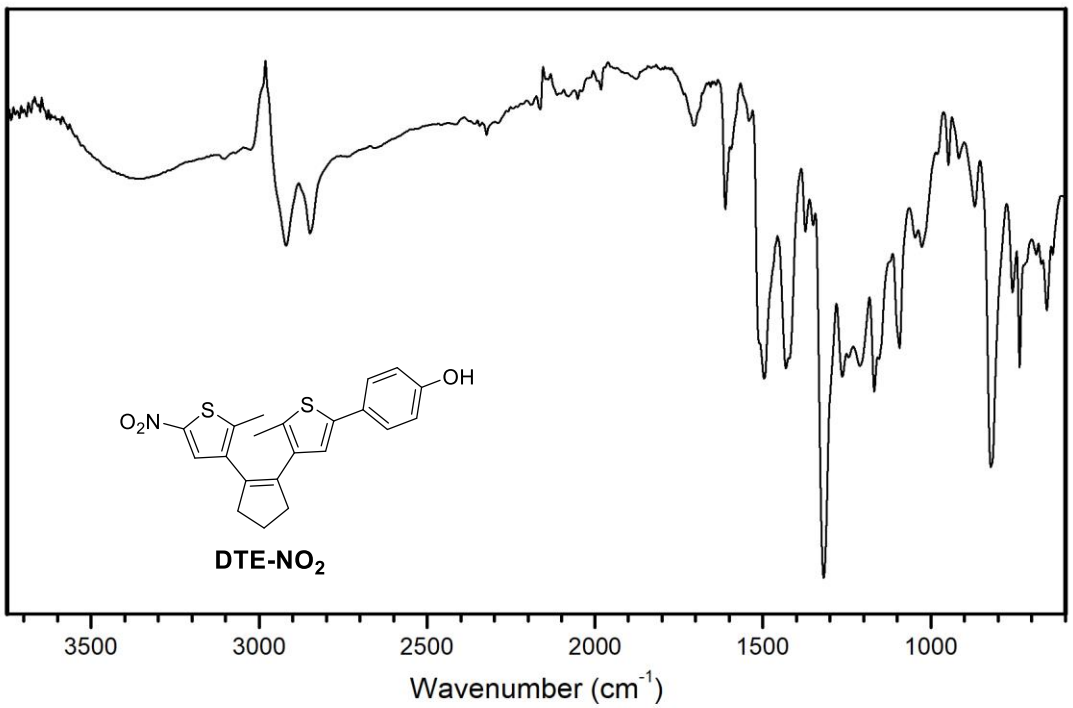

IR (ATR, cm^{-1})

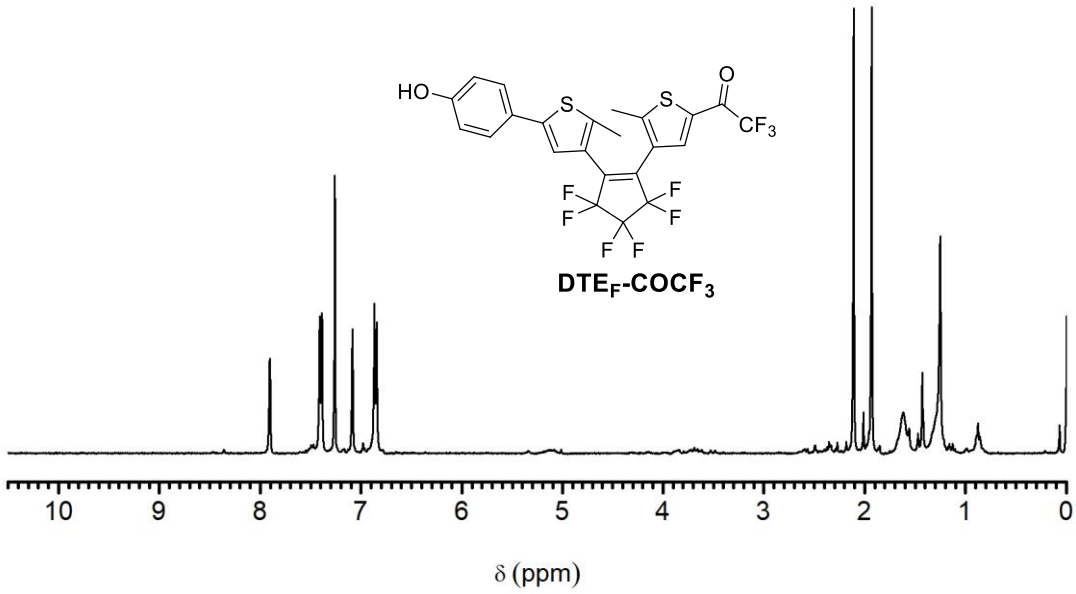

^{1}H NMR (360 MHz, $CDCl_3$)

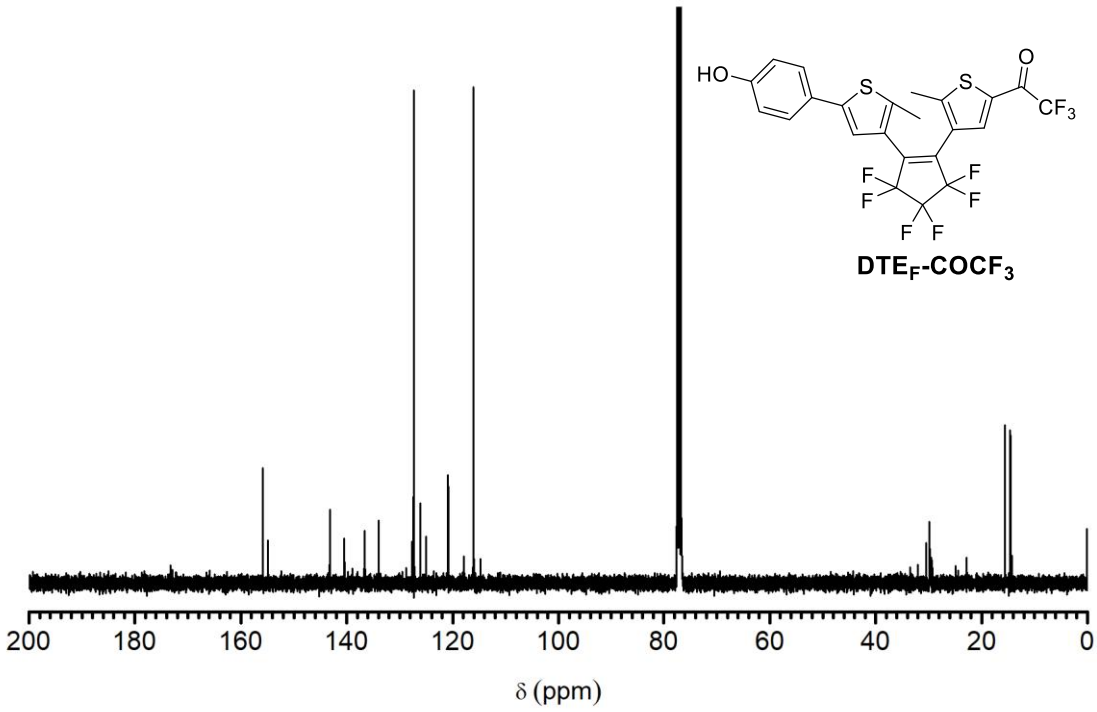

^{13}C NMR (91 MHz, $CDCl_3$)

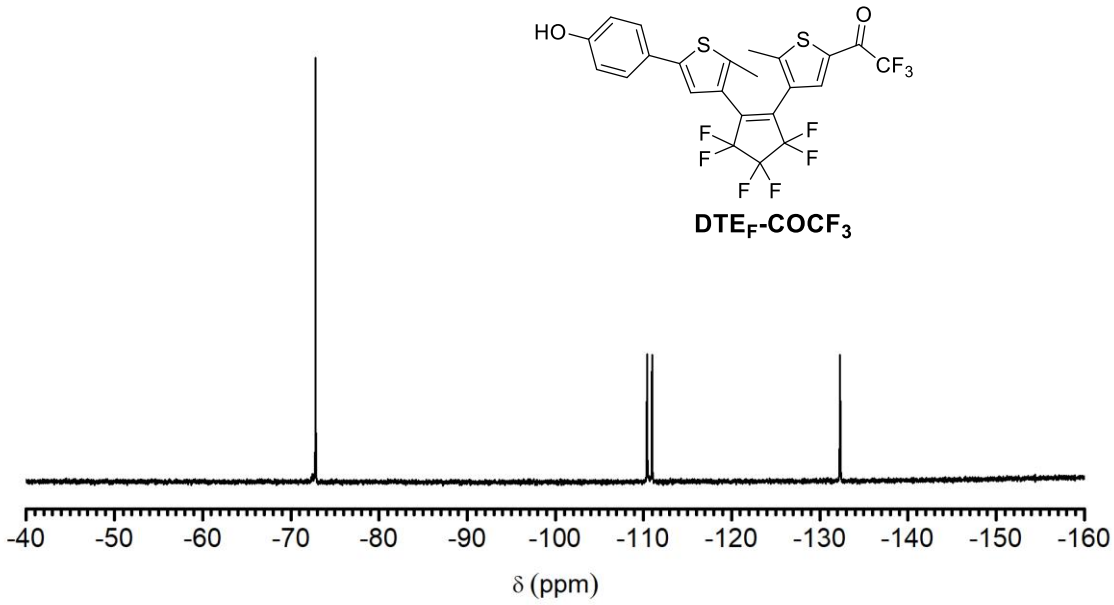

^{19}F NMR (235 MHz, $CDCl_3$)

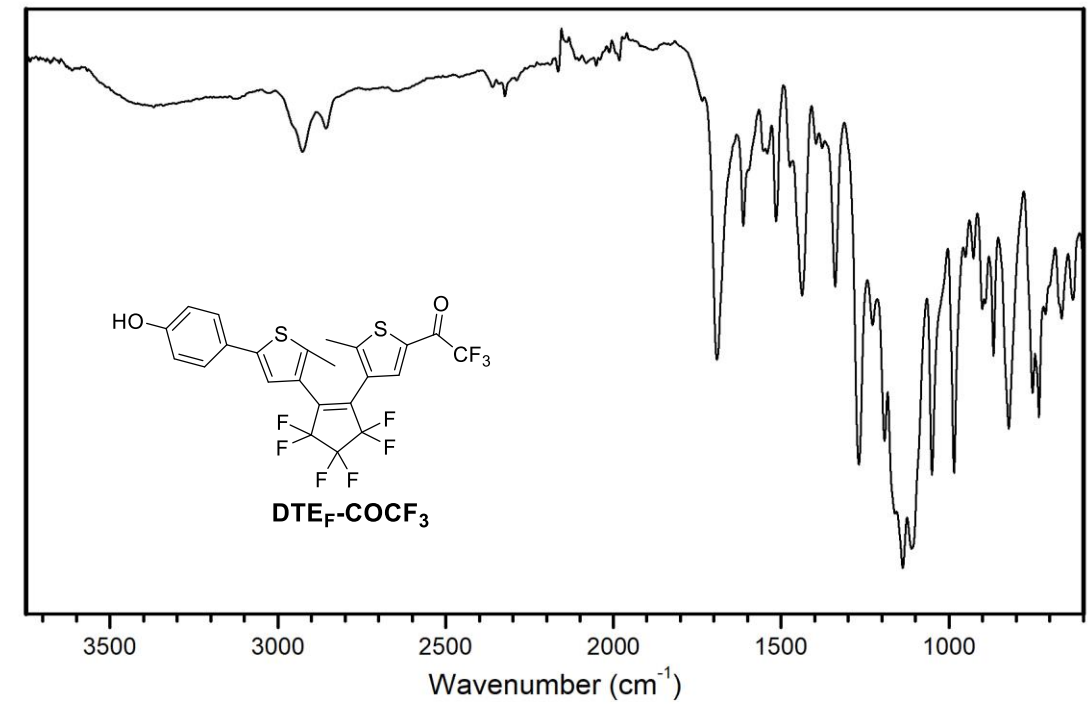

IR (ATR, cm^{-1})

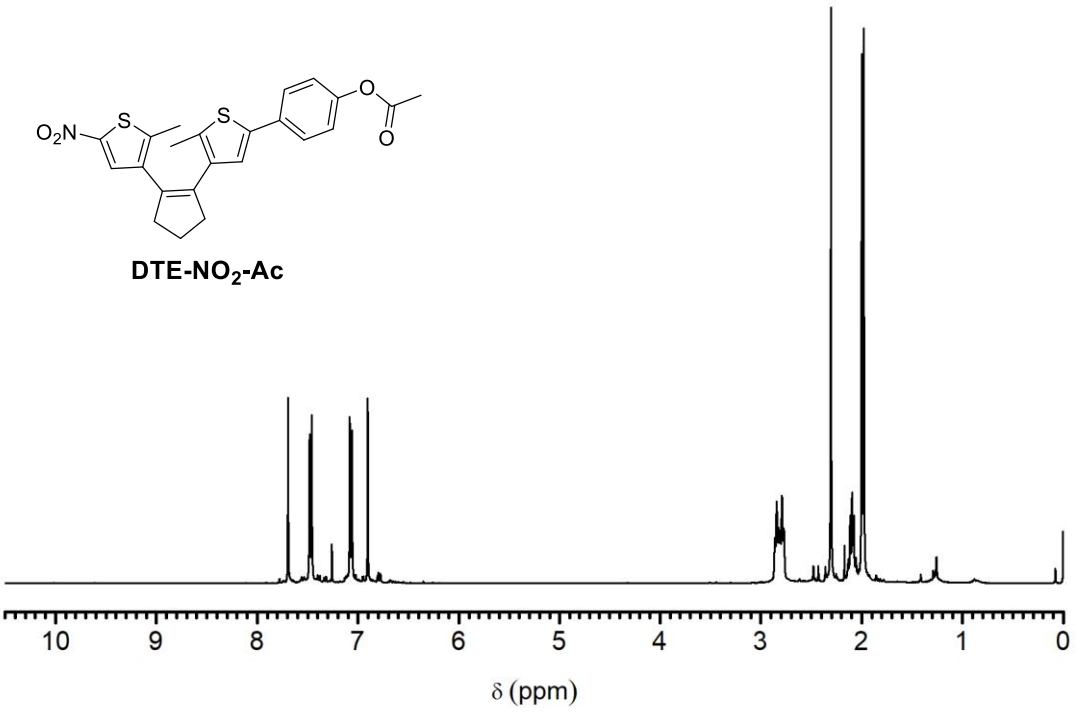

DTE-NO_2-Ac

^{1}H NMR (400 MHz, $CDCl_3$)

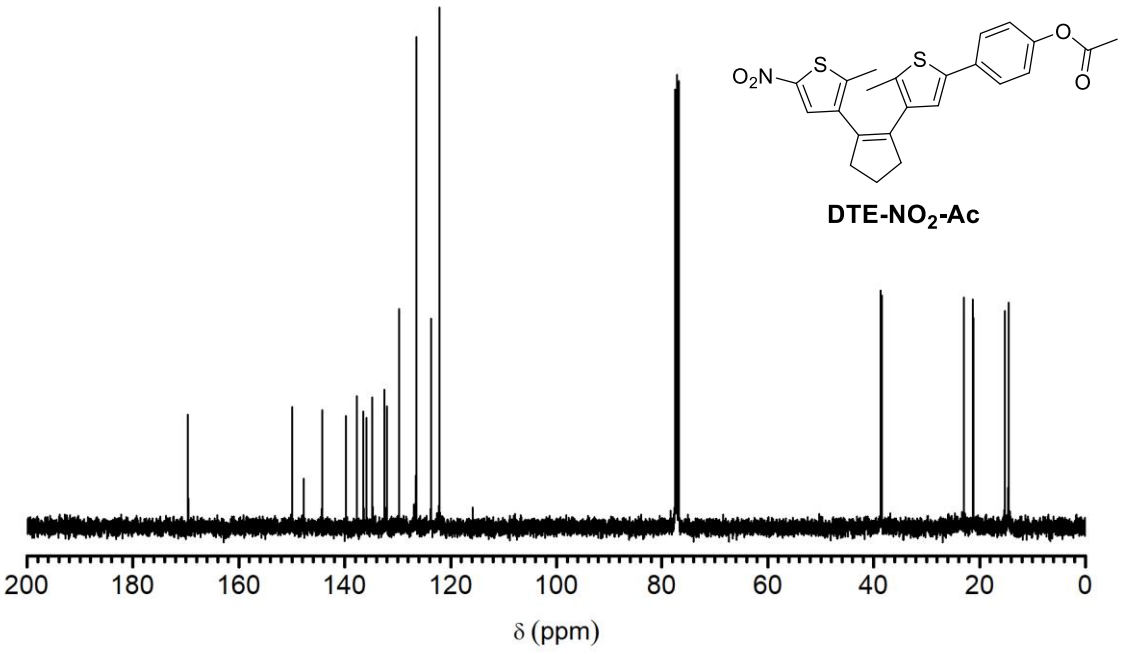

DTE-NO_2-Ac

^{13}C NMR (101 MHz, $CDCl_3$)

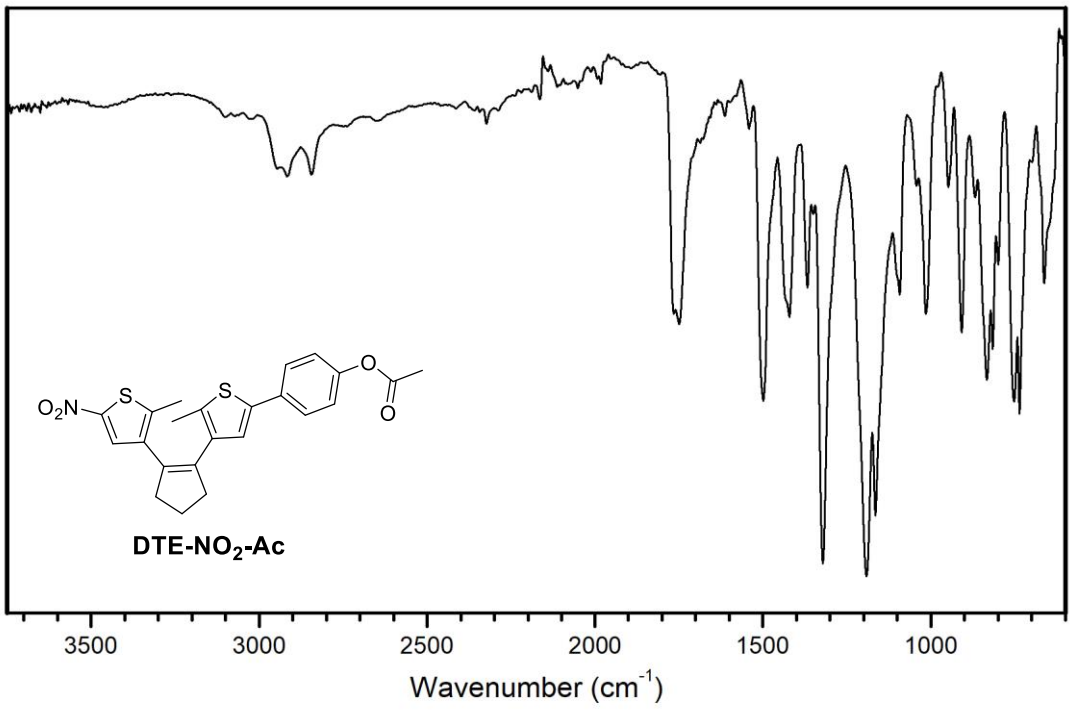

IR (ATR, cm^{-1})

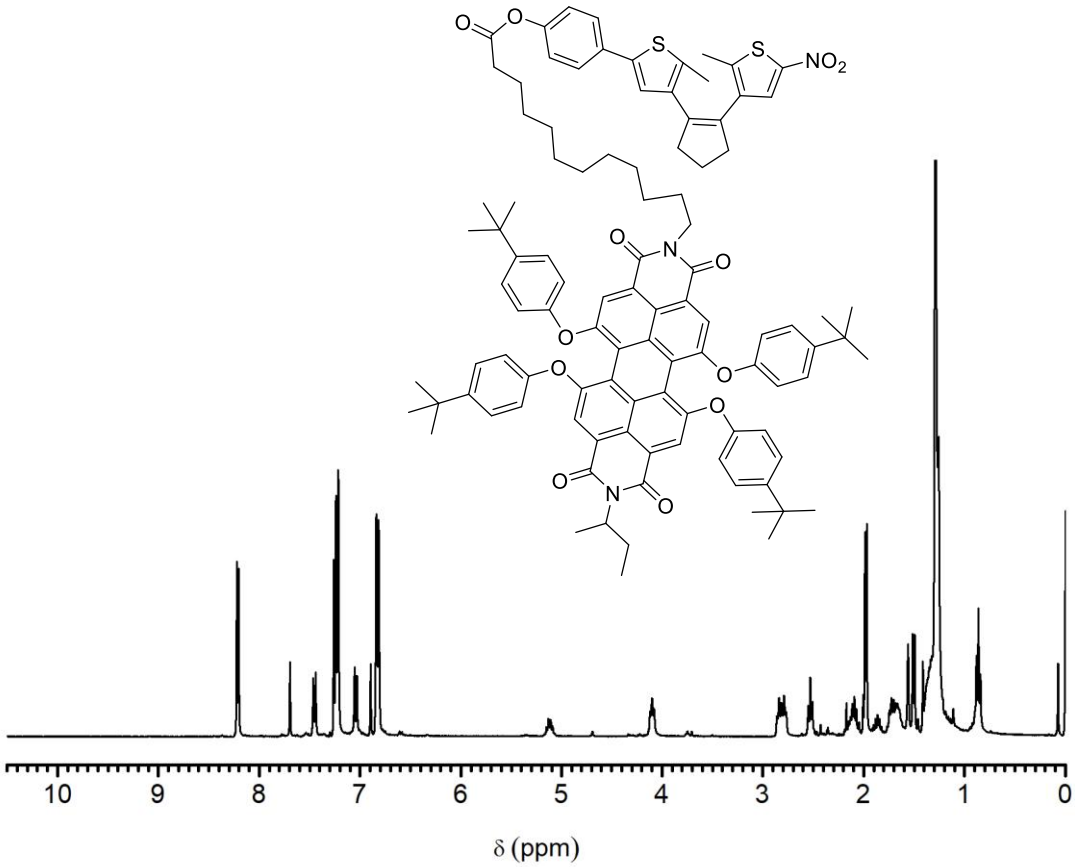

^{1}H NMR (360 MHz, $CDCl_3$)

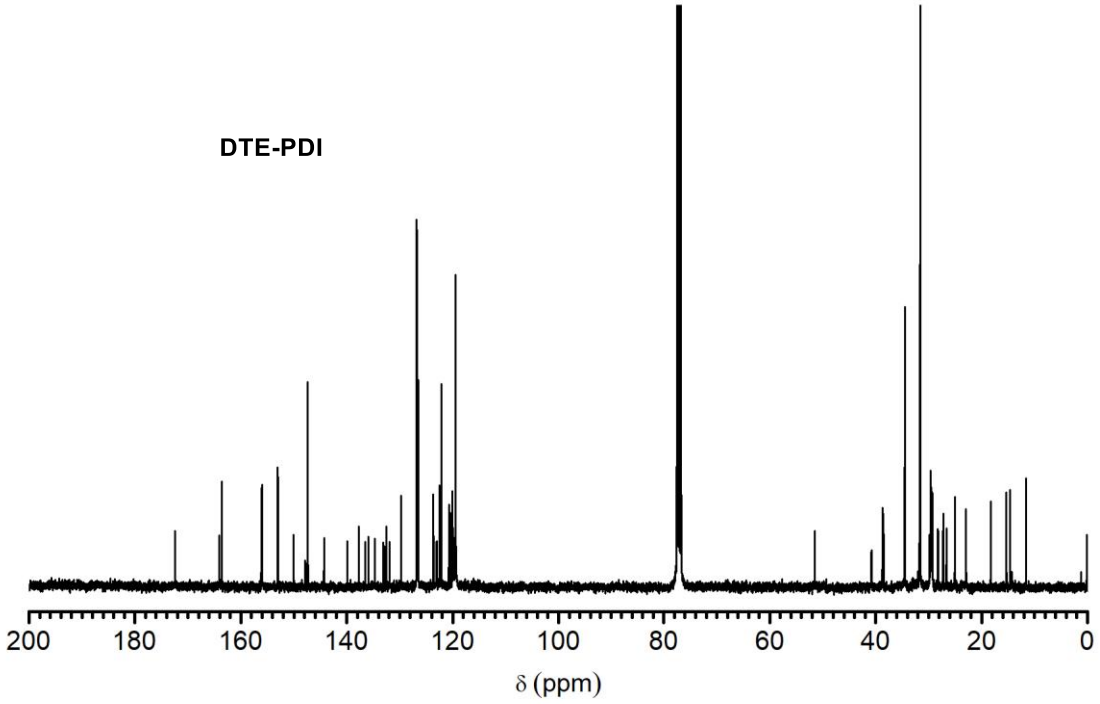

^{13}C NMR (91 MHz, $CDCl_3$)

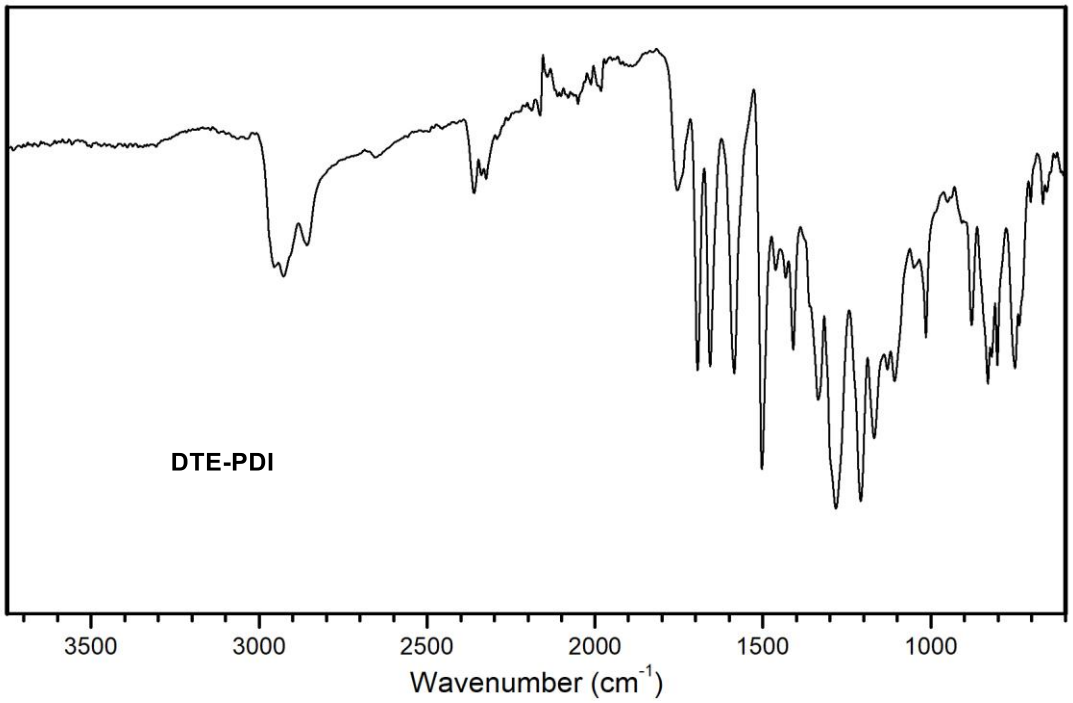

IR (ATR, cm^{-1})

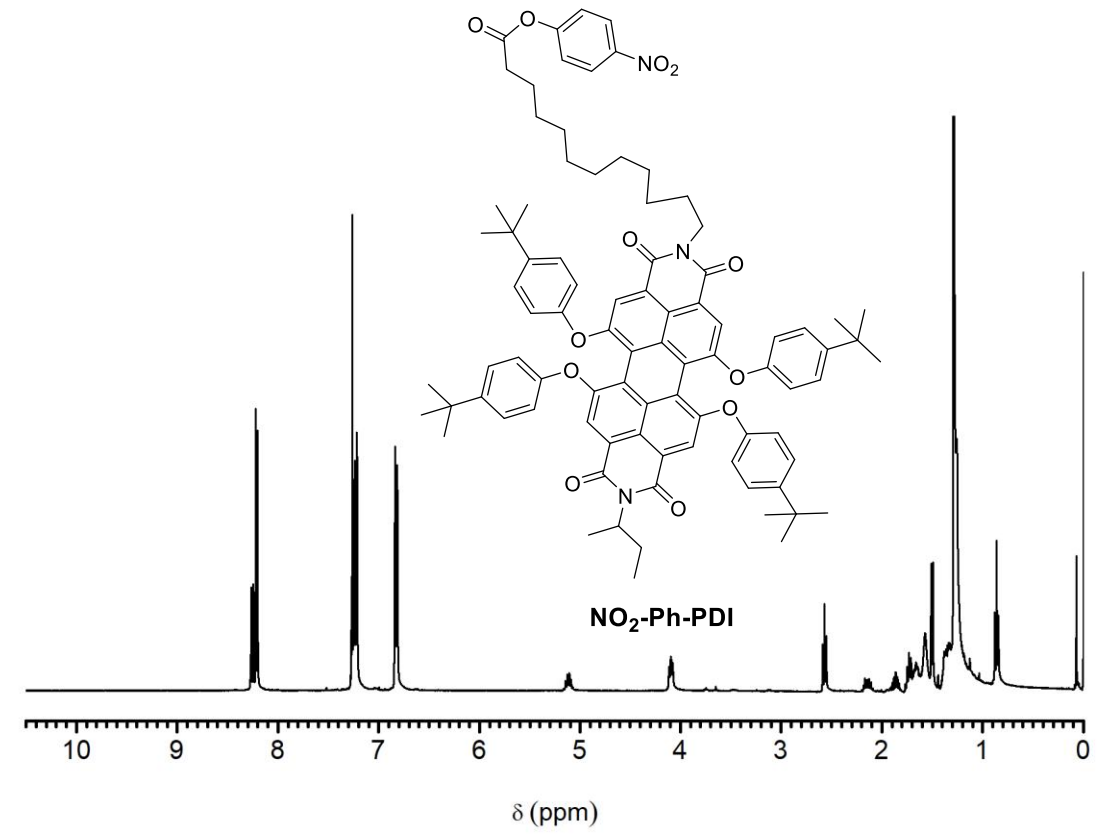

^{1}H NMR (400 MHz, $CDCl_3$)

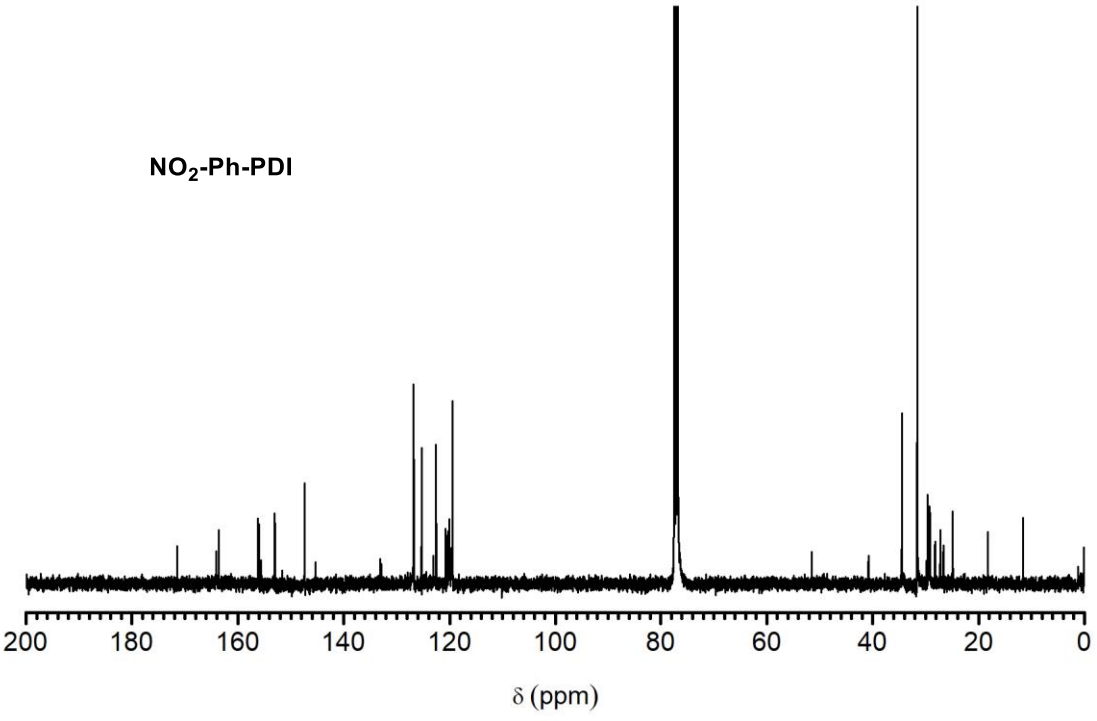

^{13}C NMR (101 MHz, $CDCl_3$)

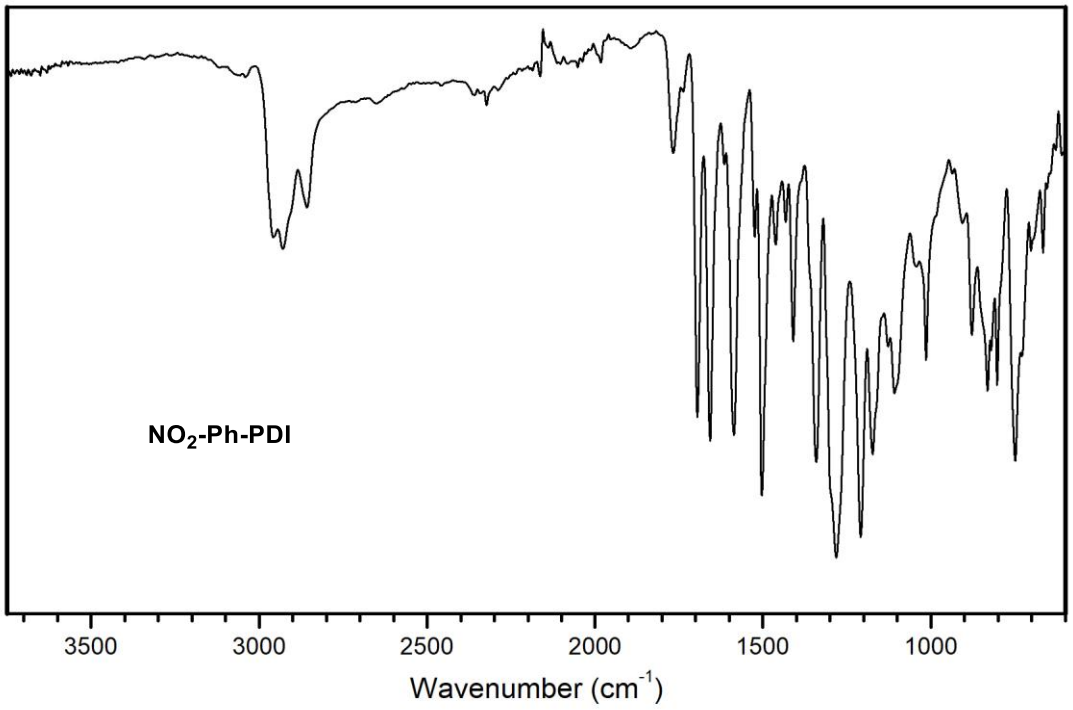

IR (ATR, cm^{-1})

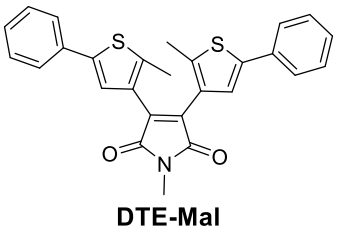

^{1}H NMR (360 MHz, CD_3CN)

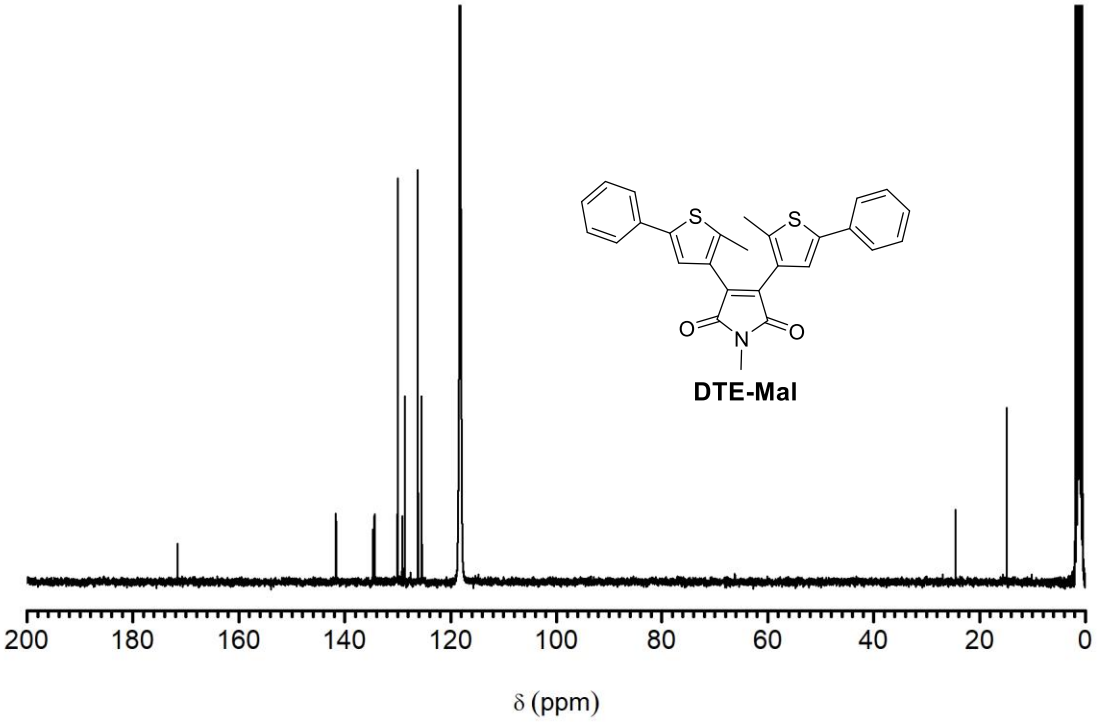

^{13}C NMR (91 MHz, CD_3CN)

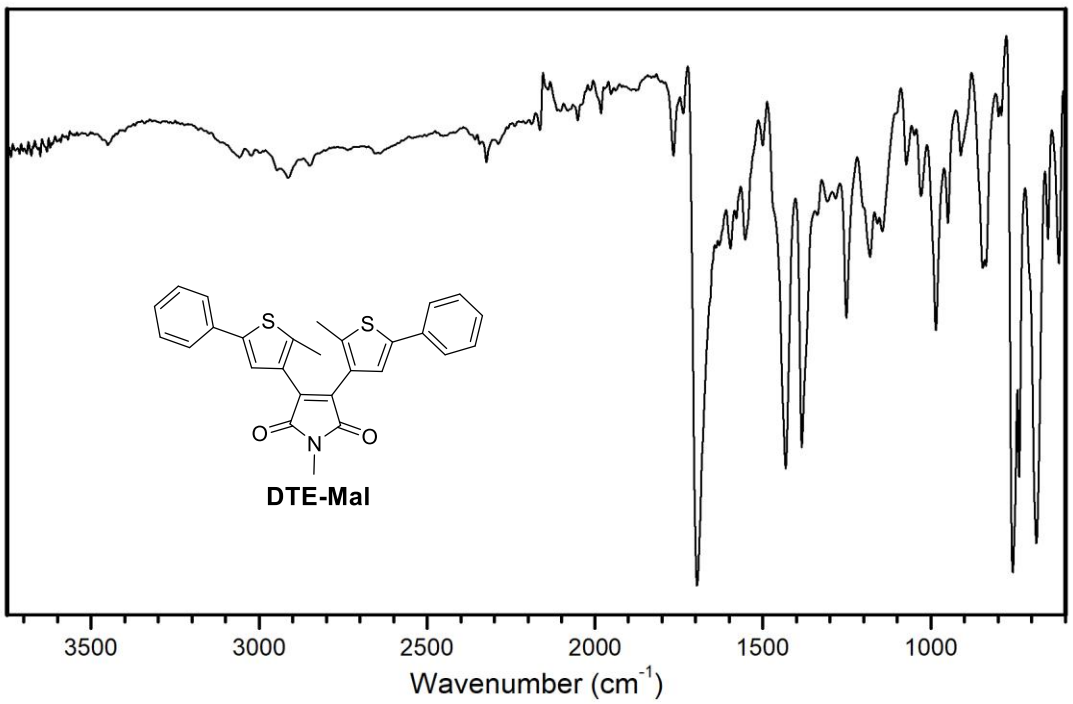

IR (ATR, cm^{-1})

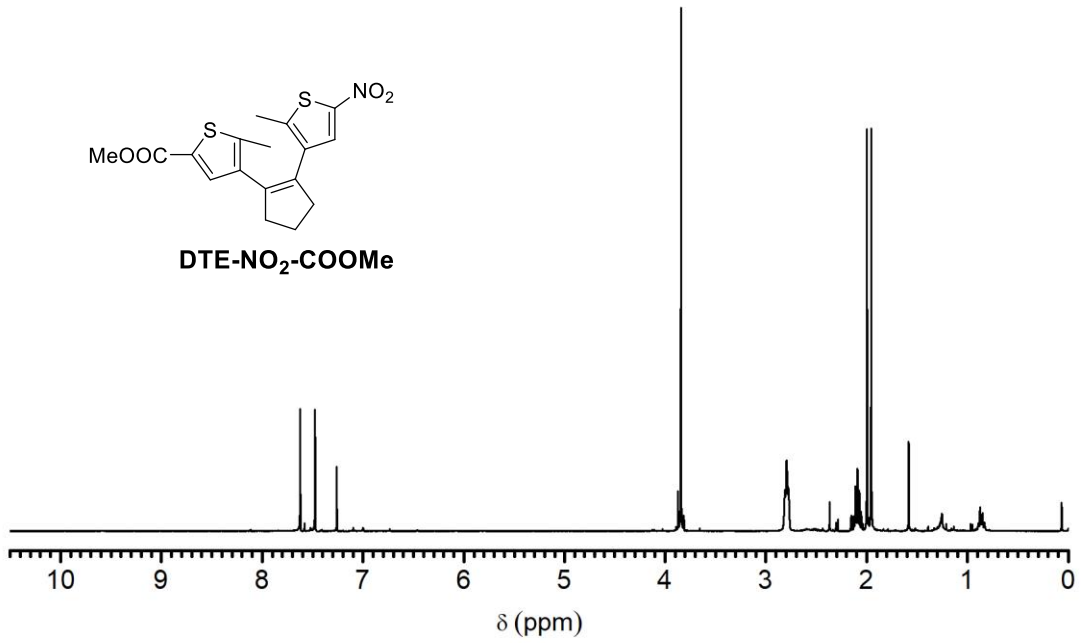

^{1}H NMR (400 MHz, $CDCl_3$)

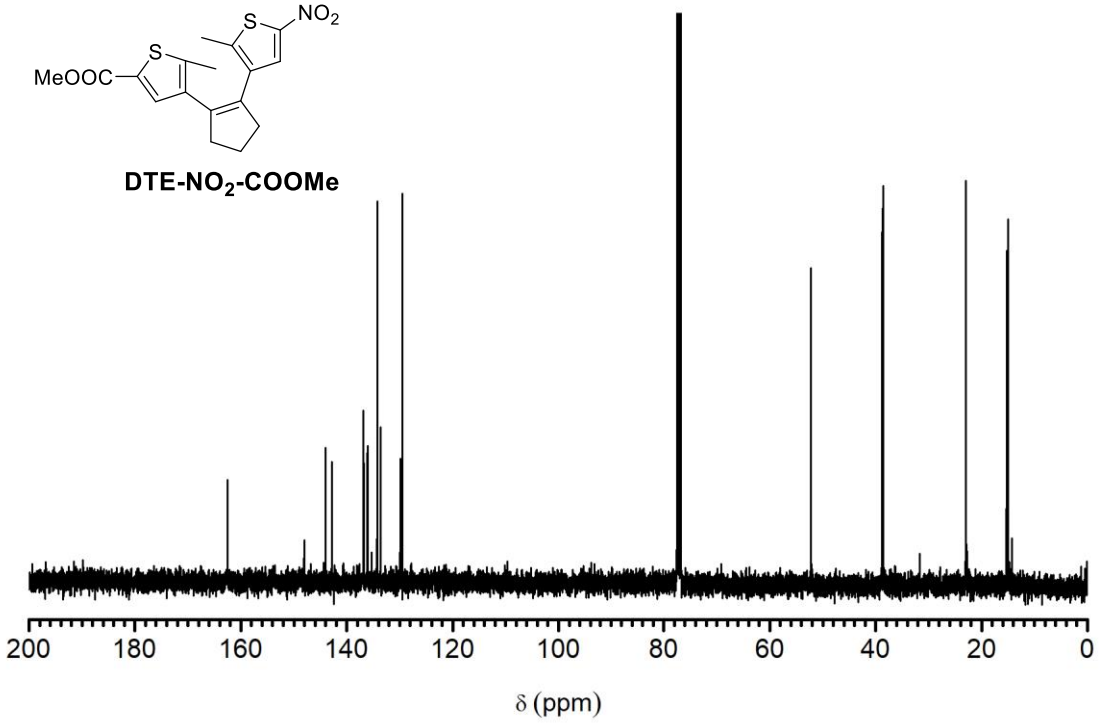

^{13}C NMR (101 MHz, $CDCl_3$)

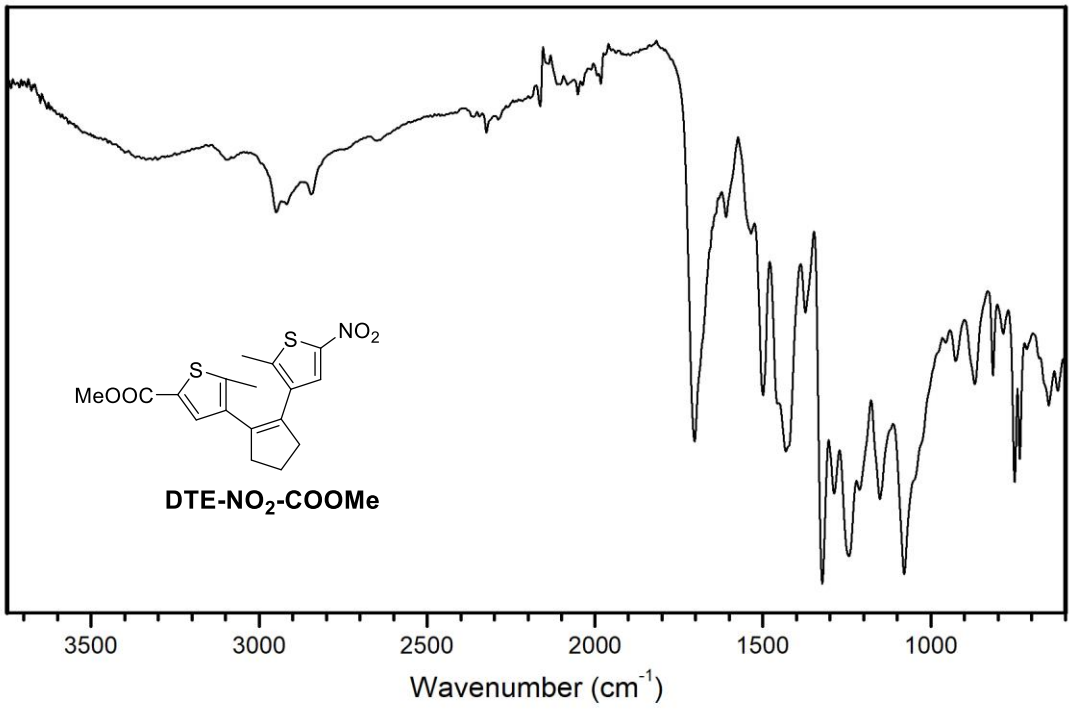

IR (ATR, cm^{-1})

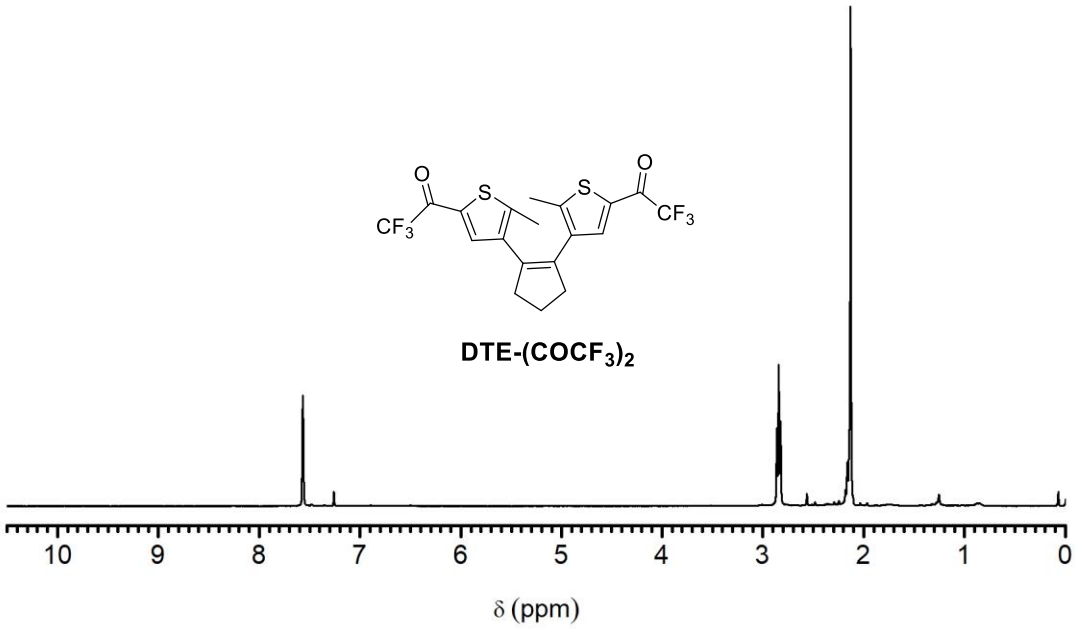

^{1}H NMR (400 MHz, $CDCl_3$)

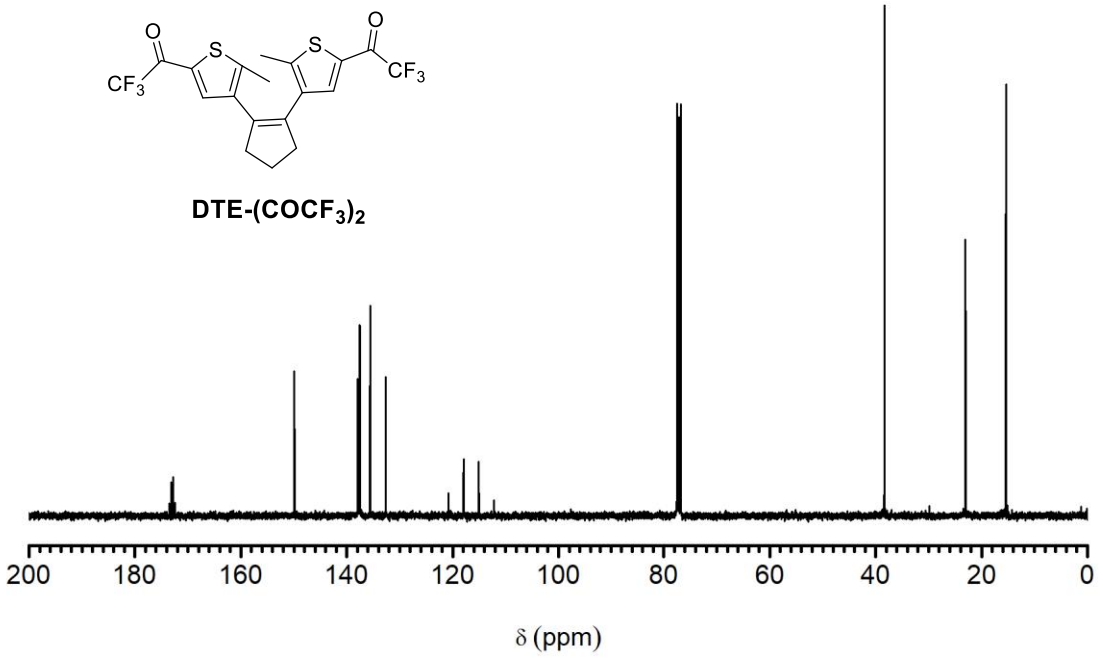

^{13}C NMR (101 MHz, $CDCl_3$)

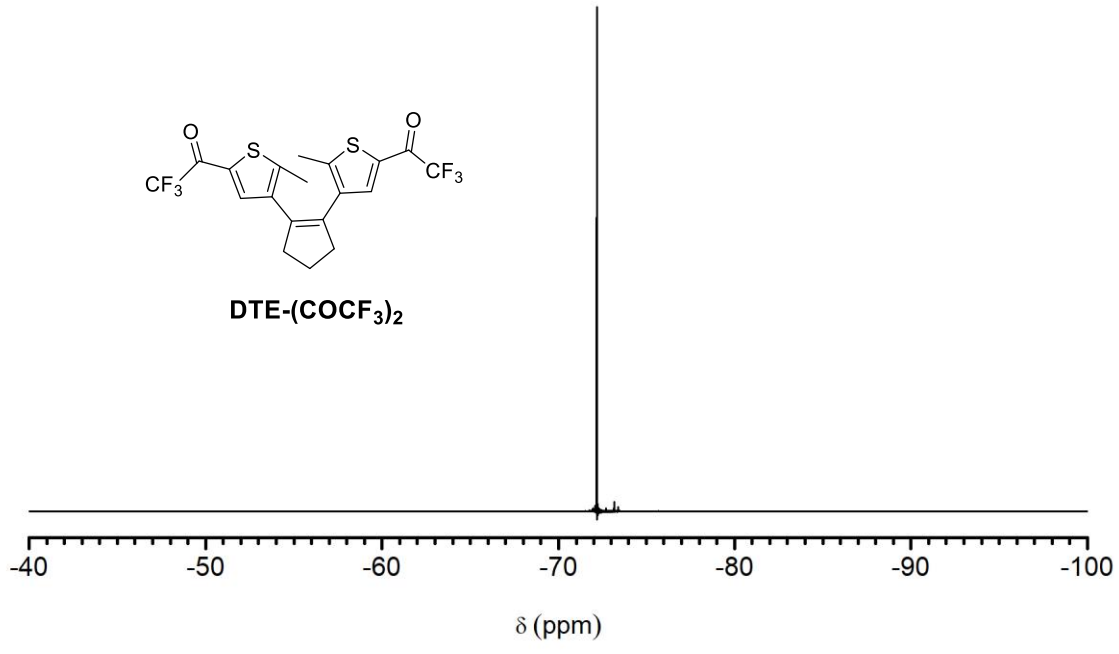

^{19}F NMR (376 MHz, $CDCl_3$)

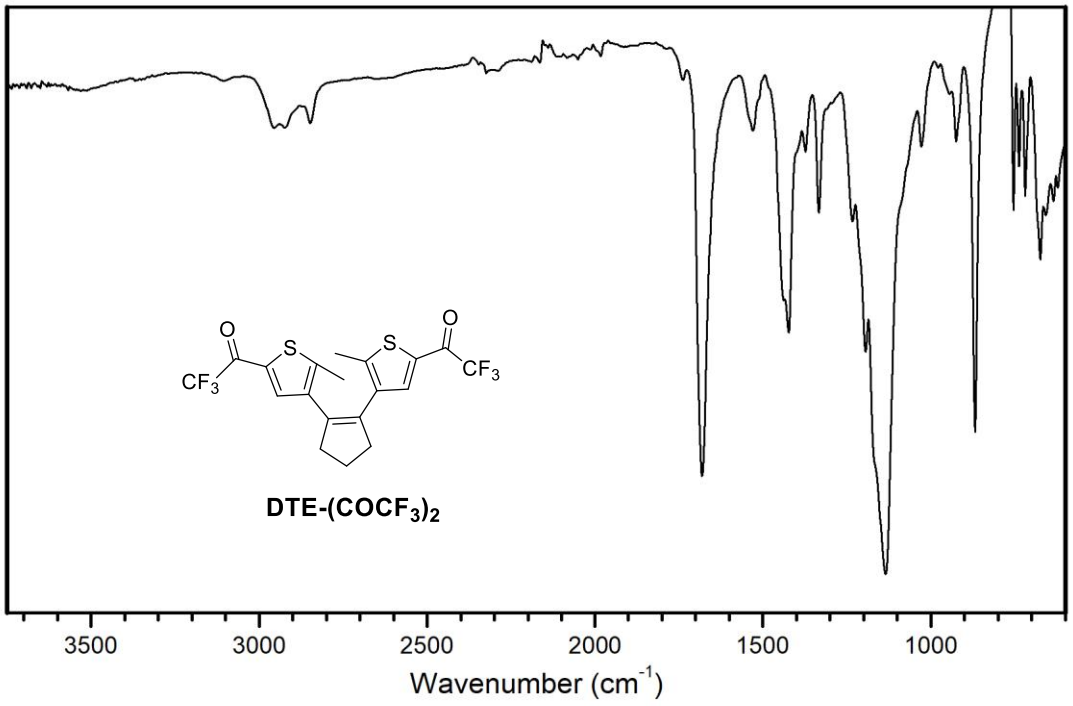

IR (ATR, cm^{-1})

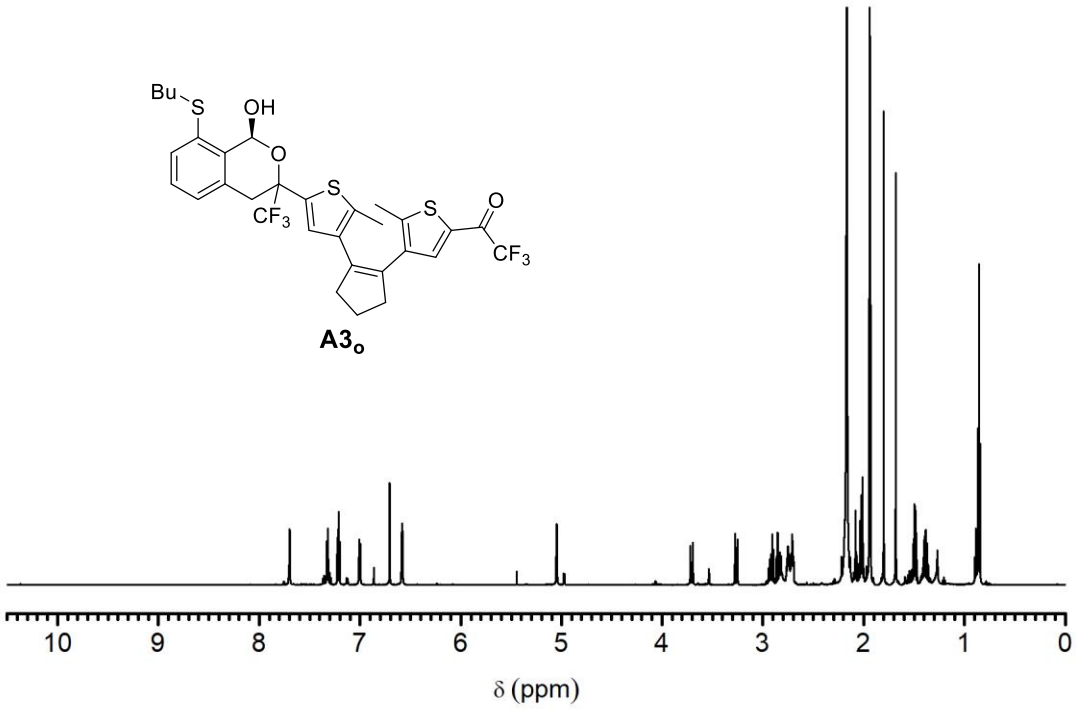

^{1}H NMR (600 MHz, CD_3CN)

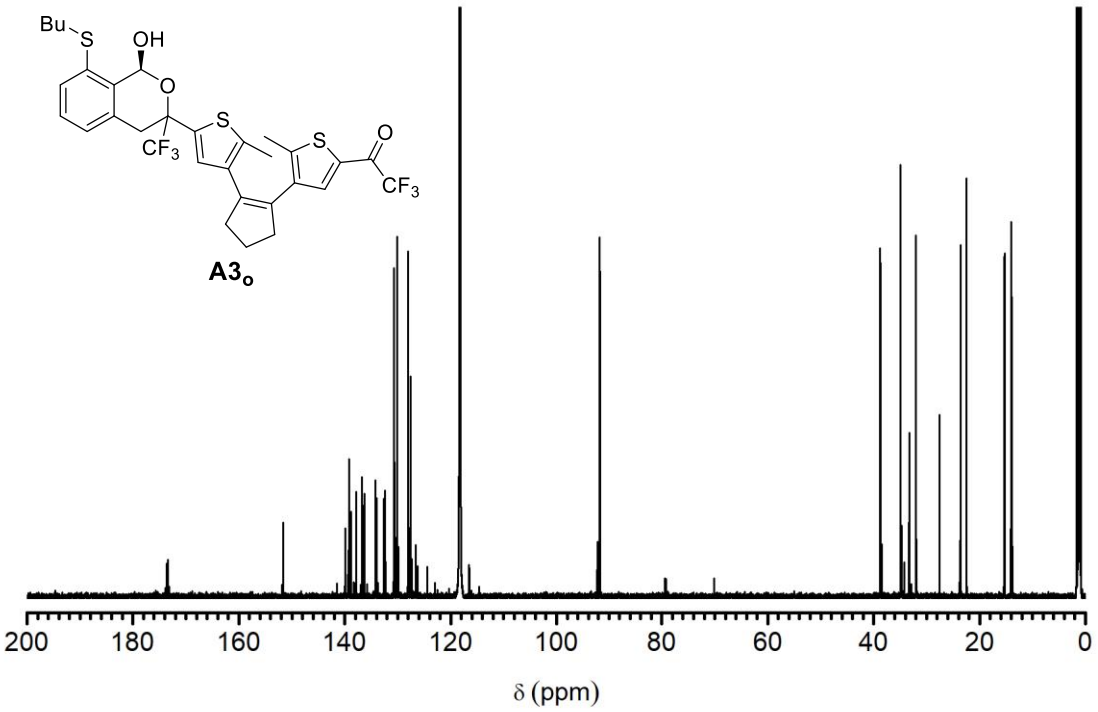

^{13}C NMR (151 MHz, CD_3CN)

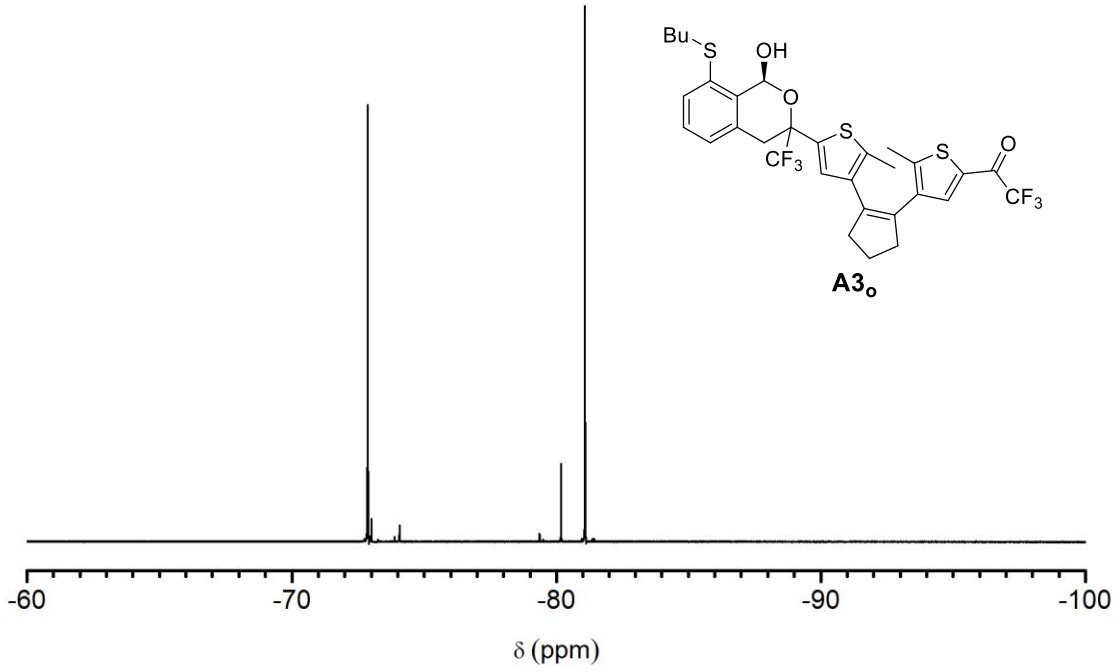

^{19}F NMR (565 MHz, CD_3CN)

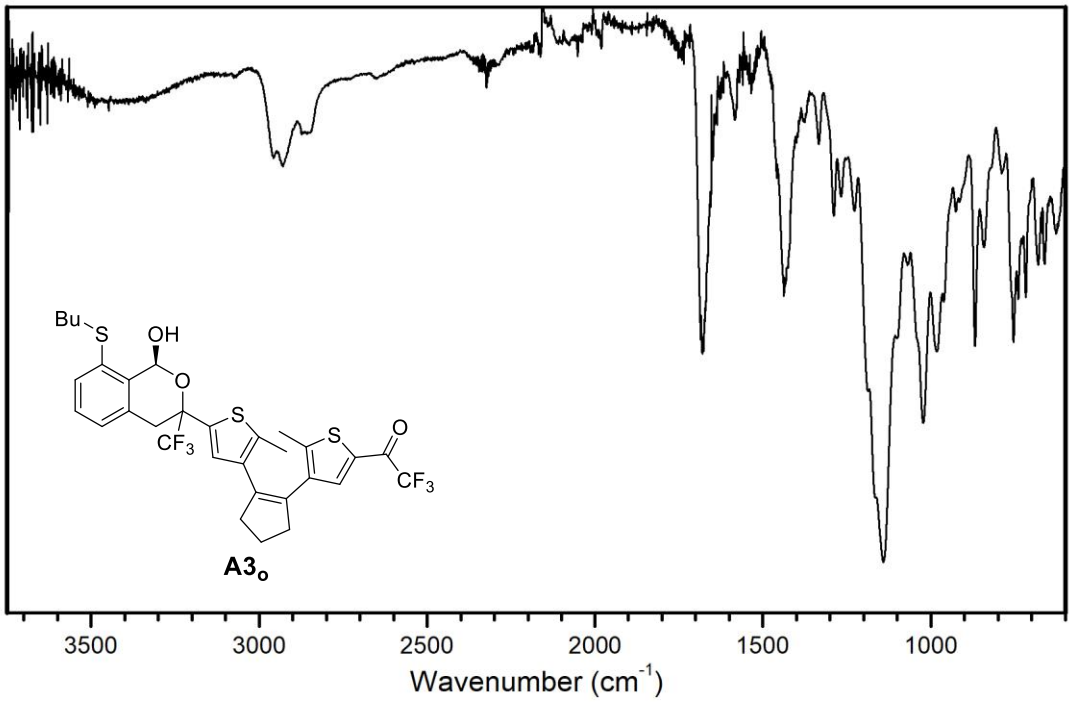

IR (ATR, cm^{-1})

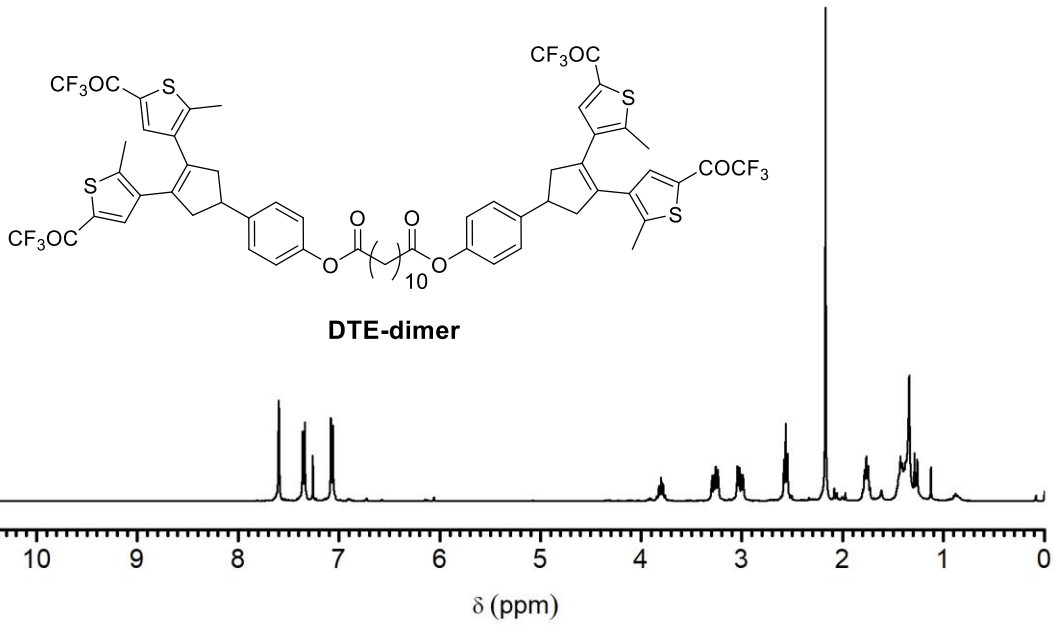

^{1}H NMR (400 MHz, $CDCl_3$)

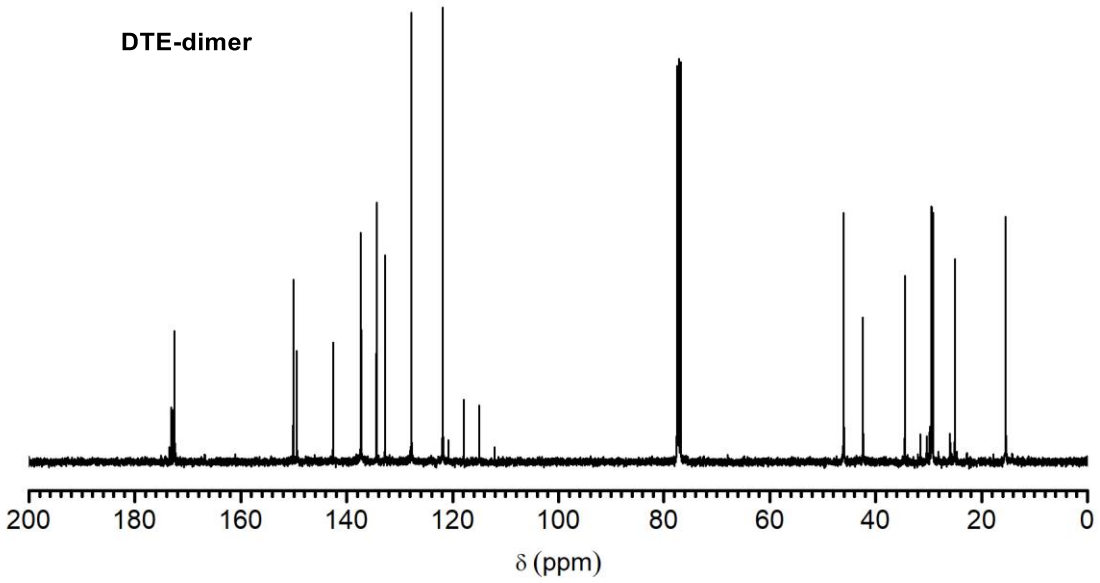

^{13}C NMR (101 MHz, $CDCl_3$)

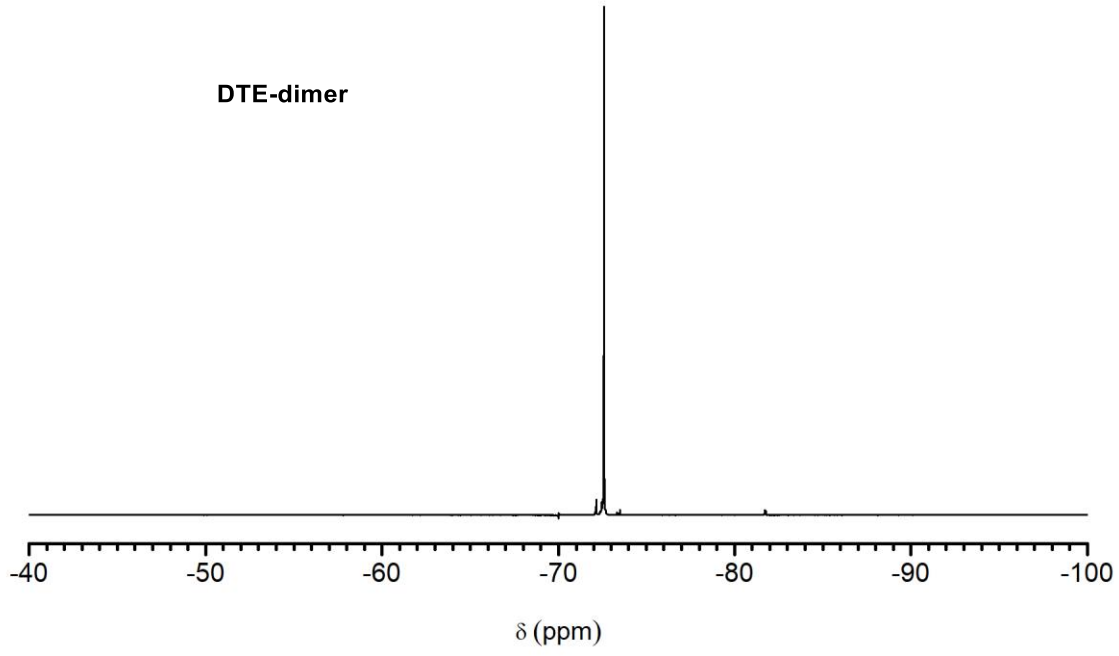

^{19}F NMR (235 MHz, $CDCl_3$)

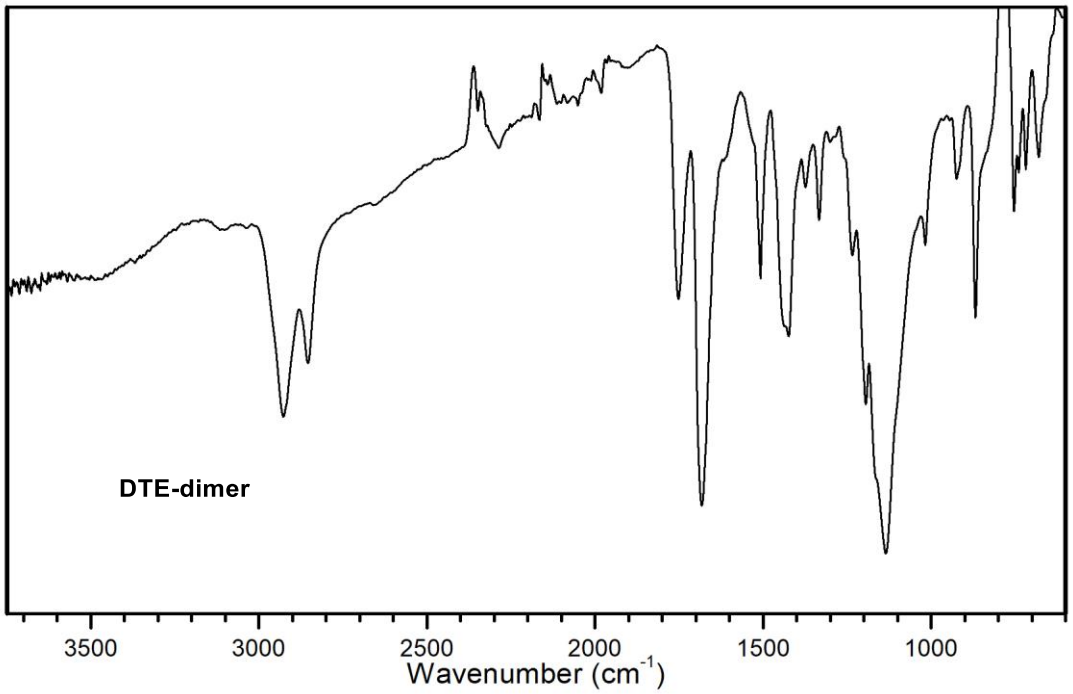

IR (ATR, cm-[1])

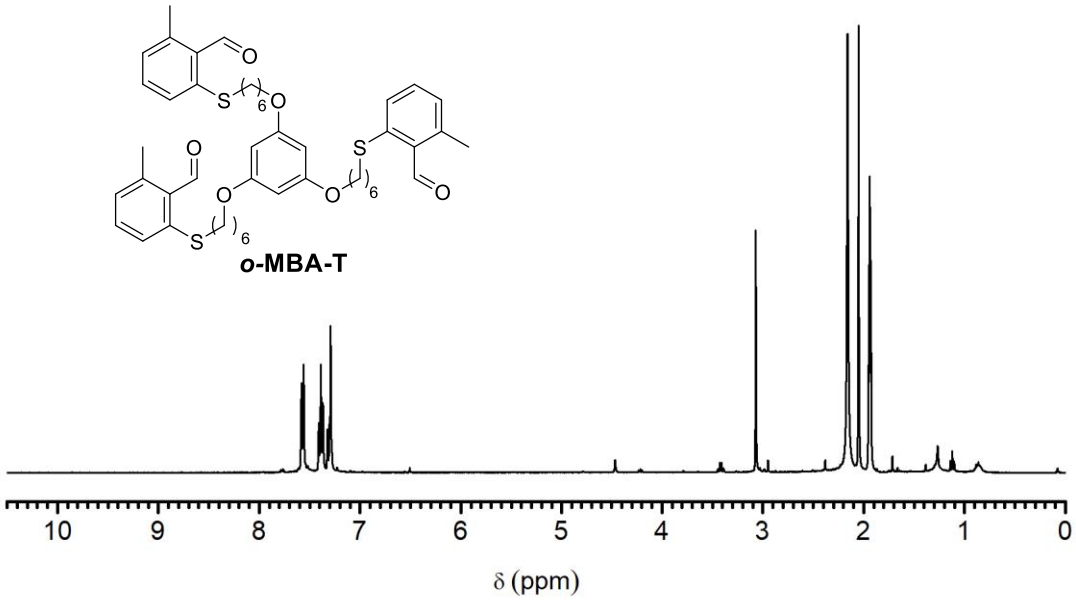

[1]H NMR (250 MHz, $CDCl_3$)

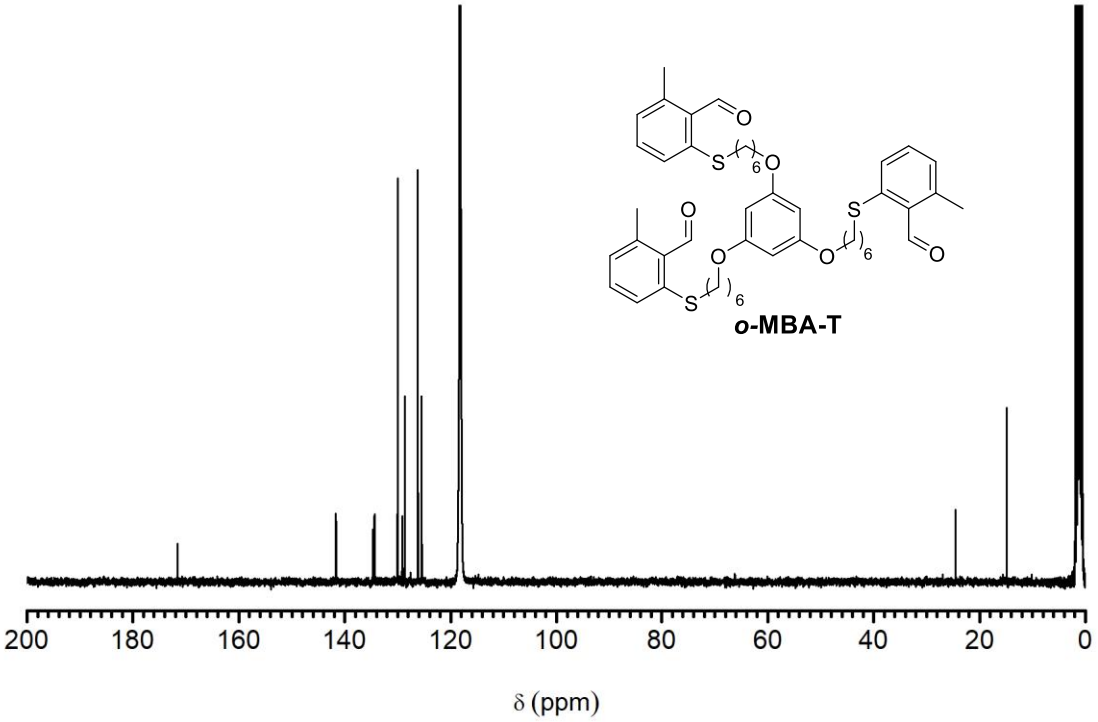

^{13}C NMR (63 MHz, $CDCl_3$)

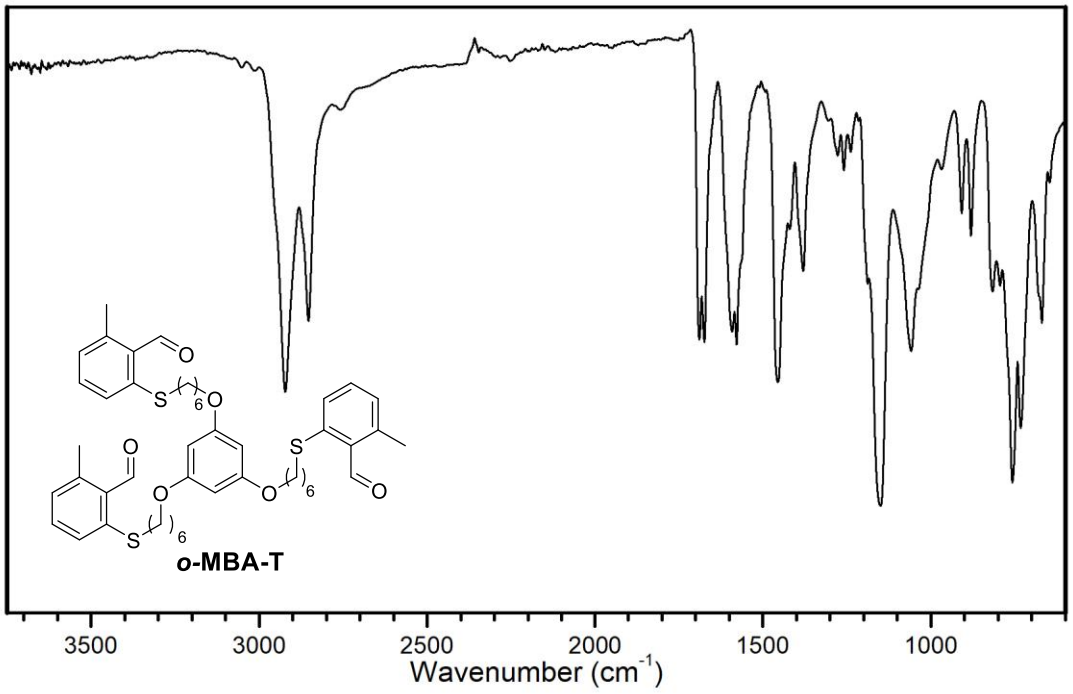

IR (ATR, cm^{-1})